Associated TRNs : IN9201001 - 1100

INIS-mf--13388

DAE SYMPOSIUM ON NUCLEAR PHYSICS

CONTRIBUTED PAPERS VOLUME 34B(1991)

BHABHA ATOMIC RESEARCH CENTRE
BOMBAY

DECEMBER 26 - 30, 1991

Editors : S. Kailas
P. Singh

Organised by

DEPARTMENT OF ATOMIC ENERGY
GOVERNMENT OF INDIA

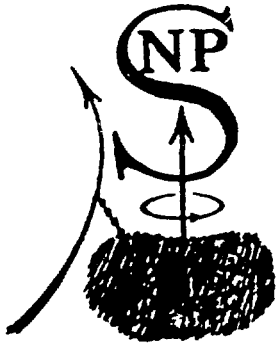

DAE SYMPOSIUM ON NUCLEAR PHYSICS

CONTRIBUTED PAPERS VOLUME 34B(1991)

BHABHA ATOMIC RESEARCH CENTRE
BOMBAY

DECEMBER 26 - 30, 1991

Editors : S. Kailas
P. Singh

Organised by

DEPARTMENT OF ATOMIC ENERGY
GOVERNMENT OF INDIA

DAE SYMPOSIUM ON NUCLEAR PHYSICS 1991

ORGANISING COMMITTEE

Dr. S.S. Kapoor, B.A.R.C. (Chairman)
Dr. S. Kailas, B.A.R.C. (Convener)
Dr. P. Singh, B.A.R.C. (Secretary)

Dr. M.G. Betigeri, B.A.R.C.
Dr. M.A. Eswaran, B.A.R.C.
Prof. Y.K. Gambhir, I.I.T. Bombay
Dr. S.K. Gupta, B.A.R.C.
Dr. B.K. Jain, B.A.R.C.
Dr. S.K. Kataria, B.A.R.C.
Prof. G.K. Mehta, N.S.C. Delhi.
Prof. P. Mukherjee, S.I.N.P.
Dr. D.M. Nadkarni, B.A.R.C.
Prof. S.B. Patel, Bom. University.
Prof. K.G. Prasad, T.I.F.R.
Prof. V.S. Ramamurthy, IP, Bhubaneswar.
Dr. B.C. Sinha, V.E.C.C.
Prof. C.S. Warke, T.I.F.R.

PROGRAMME

THURSDAY, 26 DECEMBER 1991

0930 - 1030	Inauguration
1030 - 1100	TEA / COFFEE
1100 - 1230	Invited talk I1: S.S.KAPOOR
	Heavy ion induced fission and dynamics of nucleus - nucleus collisions
	Invited Talk I2 : J.N.DE
	Stability of nuclei limited by temperature
1230 - 1400	LUNCH
1400 - 1600	Oral Presentation : O1 - O12
1600 - 1700	TEA - Hosted by Director B.A.R.C.
1700 - 1900	Thesis Presentation T1 - T7

FRIDAY, 27 DECEMBER 1991

0930 - 1100	Invited Talk I3 : M.A.ESWARAN Resonant behaviour in heavy-ion nuclear reactions - New nuclear structure in the continuum Invited Talk I4 : S.B.PATEL Co-existence of shapes in nuclei
1100 - 1130	TEA / COFFEE
1130 - 1300	Poster Presentation: P1 - P93
1300 - 1400	LUNCH
1400 - 1600	Oral Presentation: O18 - O29
1600 - 1630	TEA / COFFEE
1630 - 1900	Thesis Presentation T8 - T15

SATURDAY, 28 DECEMBER

(Today the sessions will be at TIFR)

0930 - 1100 Invited Talk I4 : H.ROSSNER

Neutron emission as a probe of fission dynamics

Invited Talk I5 : A.ABBAS

Is nucleon deformed ?

1100 - 1130 **TEA / COFFEE**

1130 - 1300 Oral Presentation: 039 - 051

1300 - 1400 LUNCH

1400 - 1600 SEMINAR : HEAVY ION REACTIONS BELOW AND NEAR THE BARRIER

1. M.DASGUPTA:Cross sections and average angular momenta in fusion reactions near the Coulomb barrier
2. A.K.MOHANTY:L - dependent nuclear potential for heavy ion fusion
3. M.B.CHATTERJEE:Deep inelastic collisions at near barrier energies and search for cold donor - fragment production

1600 - 1645 VISIT to Pelletron Accelerator Facility

1645 - 1730 TEA / COFFEE

1730 - 1830 Evening Lecture : M.K.BANERJEE

A confining quark model of the nucleon

SUNDAY, 29 DECEMBER 1991

0930 - 1100	Invited Talk I7 : R.C.NAYAK Leptodermous expansion studies in finite nuclei Oral Presentation : O35 - O38
1100 - 1130	TEA / COFFEE
1130 - 1300	Poster Presentation: P94 - P177
1300 - 1400	LUNCH
1400 - 1530	Oral Presentation:O13 - O17 and O30 - O34
1530 - 1600	TEA / COFFEE
1600 - 1830	SEMINAR : QUARK GLUON PLASMA

1. C.S.WARKE: (Coordinator) Schwinger's mechanism of Quark - gluon plasma production in ultra - relativistic heavy ion collision
2. N.SARMA:Deconfinement and nuclear collisions
3. Y.P.VIYOGI:Experimental attempts to detect QGP
4. P.R.SUBRAMANIAN: QGP in cosmology

MONDAY, 30 DECEMBER 1991

0900 - 1030	Invited talk I8: P.RING Theoretical description of Giant resonances in hot rotating nuclei Oral Presentation: O60 - O63
1030 - 1100	TEA / COFFEE
1100 - 1300	Oral Presentation:O64 - O75
1300 - 1400	LUNCH
1400 - 1530	Oral Presentation:O52 - O59
1530 - 1600	TEA / COFFEE
1600 - 1700	Concluding Session

C O N T E N T S

I : INVITED TALK

T : THESIS

O : ORAL

P : POSTER

INVITED TALKS/SEMINARS

I1. Heavy ion induced fission and dynamics of nucleus-nucleus collisions
S.S.Kapoor,B.A.R.C.,Bombay

I2. Stability of nuclei limited by temperature
J.N.De,V.E.C.C.,Calcutta

I3. Resonant behaviour in heavy ion nuclear reactions- new nuclear structure in the continuum
M.A.Eswaran,B.A.R.C.,Bombay

I4. Co-existence of shapes in nuclei
S.B.Patel,Bombay University

I5. Neutron emission as a probe of fission dynamics
H.Rossner,HMI,Berlin

I6. Is nucleon deformed ?
A.Abbas,Institute of Physics,Bhubaneswar

I7. Leptodermous expansion studies in finite nuclei
R.C.Nayak,Khallikote college,Berhampur

I8. Theoretical description of Giant resonances in hot rotating nuclei
P.Ring,Technische Universitat Munchen,Germany

S1. Heavy ion reactions below and near the barrier

1. Cross sections and average angular momenta in fusion reactions near the Coulomb barrier
   M.Dasgupta,T.I.F.R.,Bombay

2. L-dependent nuclear potential for heavy ion fusion
   A.K.Mohanty,B.A.R.C.,Bombay

3. Deep inelastic collisions at near barrier energies and search for cold donor- fragment production
   M.B.Chatterjee,S.I.N.P.,Calcutta

S2. Quark gluon plasma

1. Schwinger's mechanism of Quark - gluon plasma production in ultra relativistic heavy ion collision
   C.S.Warke, T.I.F.R., Bombay

2. Deconfinement and nuclear collisions
   N.Sarma, B.A.R.C., Bombay

3. Experimental attempts to detect QGP
   Y.P.Viyogi, V.E.C.C., Calcutta

4. QGP in cosmology
   P.R.Subramanian, University of Madras

THESES

T1. STUDY OF ALPHA INDUCED STRIPPING REACTIONS ON ^{28}Si AT 45 MeV AND SPECTROSCOPIC STRENGTH FOR THE STATES IN MIRROR NUCLEI ^{29}Si AND ^{29}p, V.P.Darshan, Dept. of Physics, Bangalore University, Bangalore-56.

T2. MULTIPARAMETER STUDIES OF NEUTRON EMISSION IN FISSION, M.S.Samant, N.P.D., B.A.R.C., Bombay.

T3. SPECTRAL DISTRIBUTION THEORY AND STRENGTHS OF GAMOW-TELLER AND M1 EXCITATIONS, Sukhendusekhar Sarkar, Saha Inst. of Nucl. Physics, Calcutta.

T4. SOME STUDIES IN THE sdg INTERACTING BOSON MODEL OF ATOMIC NUCLEI, Y.D.Devi, Physics Research Laboratory, Ahmedabad.

T5. STUDY OF HIGH ENERGY NUCLEUS-NUCLEUS INTERACTIONS IN NUCLEAR EMULSIONS, Sudhir Raniwala, Dept. of Physics, University of Rajasthan, Jaipur 302 004.

T6. AN INSIGHT TO RELATIVISTIC NUCLEAR COLLISION BY EMULSION TECHNIQUE, (Ms.) Sharmila Sarkar, Jadavpur University.

T7. ALPHA ANOMALONS - PRIMAL DETECTION AND STUDY IN RELATIVISTIC - HEAVY ION - INTERACTION, Dipak Bandyopadhyay.

T8. SOME STUDIES ON THE INTERACTIONS OF CARBON AND SILICON NUCLEI AT 4.5 GeV/A IN NUCLEAR EMULSION, Tauseef Ahmad, Dept. of Physics, AMU, Aligarh.

T9. SELF-SIMILARITY IN NUCLEAR INTERACTION AT FEW GeV/NUCLEON, Premomoy Ghosh, Jadavpur University, Calcutta.

T10. QUARK-GLUON PLAMS, BARYON-NUMBER DENSITY CONTRAST AND PRIMORDIAL NUCLEOSYNTHESIS, K. Sakthi Murugesan, Dept. of Nucl. Phys., Univ. of Madras.

T11. FISSION, FUSION PROPERTIES AND MOLECULAR CONFIGURATIONS IN CERTAIN EXCITED LIGHT NUCLEI, M.D.Padmini, Phys. Dept., Presidency College, Madras.

T12. STUDY OF NUCLEAR STRUCTURE OF MEDIUM-MASS NUCLEI, H.M.Mittal, Dept. of Phys. & Astrophys., University of Delhi, Delhi.

T13. EQUILIBRIUM AND PRE-EQUILIBRIUM EMISSION IN ALPHA-INDUCED REACTIONS AT MODERATE EXCITATION ENERGIES, B.P. Singh, Dept. of Physics, AMU, Aligarh.

T14. A NEW THEORY OF THE UHE GAMMA RAY PRODUCTION IN CYGNUS X-3, A.K.Mitra, N.R.L., BARC, Srinagar 190006.

T15. SURFACE MODIFICATION OF ALUMINIUM, STAINLESS STEEL AND NIMONIC ALLOY BY ION-IMPLANTATION, A.K. Goel, Dept. of Physic, Kurukshetra University.

a) NUCLEAR STRUCTURE . MODE OF EXCITATION AND RADIOACTIVITY

O1. BAND STRUCTURE IN ^{64}Ge, R.Sahu, Physics Dept., Berhampur University, Berhampur and S.P.Pandya, Physical Research Laboratory, Ahmedabad 380 009. 1

O2. IN BEAM SPECTROSCOPY OF ^{84}Y, S.Chattopadhyay, H.C.Jain, Y.K.Agarwal, M.L.Jhingan and J.A.Sheikh, Tata Institute of Fundamental Research, Bombay. 3

O3. BAND STRUCTURE OF ^{123}I, Ranjana Goswami, B.Sethi, P. Banerjee, Saha Institute of Nuclear Physics, Calcutta and R.K.Chattopadhyay, A.M.College, Calcutta. 5

O4. BAND STRUCTURE AND SIGNATURE EFFECTS IN ODD-Z RARE-EARTH NUCLEI, A.K.Rath* and C.R.Praharaj**, Physical Research Laboratory, Ahmedabad, **Institute of Physics, Bhubaneswar 751 005. 7

O5. HIGH SPIN SPECTROSCOPY OF ^{120}Xe, J.Goswamy, D.Mehta, B.Chand, A.Sharma, N.Singh, P.N.Trehan, Pragya Singh*, R.G. Pilley*, H.G. Devare* and R.K. Bhowmik**, Physics Department, Panjab University, Chandigarh, *TIFR, Bombay. **NSC, New Delhi. 9

O6. STUDY OF Z=64 SUBSHELL GAP SIZE IN N=82 ISOTONES, J.B.Gupta, Ramjas College, Univ. of Delhi, Delhi-7. 11

O7. EVIDENCE OF ALTERNATING PARITY BANDS IN ^{151}Sm, J.M.Chatterjee, Somapriya Basu, K.Kar, D.Banik, Saha Institute of Nuclear Physics, Calcutta and R.K.Chattopadhyay, Ananda Mohan College, Calcutta and R.P.Sharma, S.K.Pardhasaradhi, VECC, Calcutta. 13

O8. E4 STRENGTH DISTRIBUTIONS IN ^{152,154}SM : sdg IBM PREDICTIONS, Y.D.Devi and V.K.B.Kota, Physical Research Laboratory, Ahmedabad 380 009. 15

O9. SIGNATURE INVERSION IN THE 4$^-${5/2[532] p3/2[651]n} BAND IN DOUBLY-ODD ^{152}Eu AND ^{156}Tb, Kiran Jain, A.K.Jain and Alpana Goel, Dept. of Phys., University of Roorkee, Roorkee 247 667. 17

O10. TEMPERATURE DEPENDENT SHAPE TRANSITION IN ^{188}Os, A.Ansari and B.K.Agrawal, Institute of Physics, Bhubaneswar 751 005. 19

O11. THERMODYNAMICS OF SUPERFLUID NUCLEUS, M.Rajasekaran, D.Caleb Chanthi Raj and R.Premanand, Dept. of Phys., Univ. of Madras, Madras 600 025. 21

O12. SPIN CUT-OFF AND OCCUPANCY DENSITIES AND THEIR S-DECOMPOSITIONS : THE NON-INTERACTING PARTICLE CASE, V.K.B.Kota and D.Majumdar, Physical Research Laboratory, Ahmedabad 380 009. 23

O13. RELATIVISTIC MEAN FIELD STUDY OF "ISLAND OF INVERSION" IN NEUTRON-RICH Ne, Na, Mg NUCLEI, S.K. Patra and C.R.Praharaj, Inst. of Physics, Bhubaneswar 25

O14. EXOTIC NUCLEI: RELATIVISTIC MEAN FIELD APPROACH, J.P.Maharana*, J.A.Sheikh+ and Y.K.Gambhir*. *Dept. of Physics, IIT, Bombay 400 076. +T.I.F.R., Bombay. 27

O15. QUANTUM CHAOS IN DINUCLEAR SYSTEM, A.K.Chaudhuri and Santanu Pal, Variable Energy Cyclotron Centre, Calcutta-700 064. 29

O16. PION DRESSING OF NUCLEONS AND NUCLEAR FORCES : A NONPERTURBATIVE APPROACH, P.K.Panda*, R.Sahu**, S.P. Misra*, *Inst. of Physics, Bhubaneswar. **Berhampur University, Berhampur 761 007. 31

O17. ROTATION ALIGNMENT AND BAND CROSSING IN SUPER-DEFORMED BANDS, B.K.Agrawal, Institute of Physics, Bhubaneswar 751 005. 33

P1. SPREADING OF THE $1g_{9/2}$ PROTON STRENGTH IN ^{41}SC, Ramen Majumdar, Vivekananda College, Calcutta 700063. 35

P2. SYSTEMATICS OF THE PAIRING ENERGIES OF EVEN-EVEN NUCLIDES IN THE REGION, Z=4-82, Asok Saha, Dept. of Physics, Univ. College of Science, Calcutta 700 009. 37

P3. STRUCTURE OF K ISOMERIC STATE IN ^{174}Hf AND BREAKDOWN OF K SELECTION RULE, C.R.Praharaj*, A.K. Rath** and J.A. Sheikh+, *Institute of Physics, Bhubaneswar, **Physical Research Laboratory, Ahmedabad, +Tata Inst. of Fund. Research, Bombay. 39

P4. PROTON-DRIP LINE FOR Z=31-40 REGION IN A RELATIVISTIC MEAN FIELD STUDY, S.K.Patra and C.R. Praharaj, Institute of Physics, Bhubaneswar 751 005. 41

P5. RHO-MESON-NUCLEON COUPLING IN RELATIVISTIC MEAN FIELD THEORY, S.K.Patra and C.R.Praharaj, Institute of Physics, Bhubaneswar 751 005. 43

P6. SCISSORS STATES IN EVEN-ODD N=82-126 SHELL NUCLEI: ENHANCEMENT IN B(M1) STRENGTHS DUE TO g-BOSONS, Y.D.Devi and V.K.B.Kota, Physical Research Laboratory, Ahmedabad 380 009. 45

P7. E4 MATRIX ELEMENTS IN ^{198,194}Pt : sdg IBM RESULTS Y.D.Devi and V.K.B.Kota, Physics Research Laboratory, Ahmedabad 380 009. 47

P8. UNITARY DECOMPOSITION OF NUCLEAR INTERACTIONS ALL ACROSS THE PERIODIC TABLE, V.K.B.Kota and D. Majumdar, Physics Research Laboratory, Ahmedabad. 49

P9. QUADRUPOLE MOMENTS AND BAND-MIXING IN TUNGSTEN ISOTOPES IN DPPQ MODEL, J.B.Gupta, Ramjas College, University of Delhi, Delhi 110 007. 51

P10. VARIATION OF ROTATIONAL CONTENT IN E(2_1^+) WITH VALENCE NUCLEON PAIRS, J.B.Gupta and A.K. Kavathekar, Ramjas College, Univ. of Delhi, Delhi-110007. 53

P11. NEUTRON-DEFICIENT NUCLEI NEAR MASS-80 REGION EXCITATION FUNCTION MEASUREMENTS, A.Goswami*, B.S. Tomar*, S.Chattophadhay+, S.K.Saha**, S.K.Basu** and H.C.Jain+. *Radiochemistry Division, BARC, Bombay. +Tata Institute of Fundamental Research, Bombay. **Variable Energy Cyclotron Centre, Calcutta. 55

P12. INTERPLAY OF TRIAXIAL DEFORMATION, ISOSPIN AND TEMPERATURE IN A=90 NUCLEI, A. Mohamed Akbar, S. Veeraraghavan and N. Arunachalam, Dept. of Physics, Govt. Arts College, Tiruvannamalai-606 603. 57

P13. HIGH SPIN STATES IN HOT DEFORMED ZIRCONIUM NUCLEI, S. Veeraraghavan, A. Mohamed Akbar and N. Arunachalam, Dept. of Physics, Govt. Arts College, Tiruvannamalai- 606 603. 59

P14. MODIFIED RVM DESCRIPTION FOR ^{196}Pt ISOTOPE, A.K. Varshney+, K.K.Gupta*, S.P.Sud**, V.P.Varshney++ and D.K.Gupta++, +G.G.D.S.D.College, H.P.University, Baijnath, *Govt. College, Sarkaghat, H.P., **H.P. Univ., Shimla, ++S.V.College, Aligarh, U.P. 61

P15. ANALYSIS OF DEGREE OF RIGIDITY/FREEDOM IN VARIOUS NUCLEI WITH INCREASING ANGULAR MOMENTUM I=3, A.K. Varshney*, K.K.Gupta+, D.K.Gupta++, S.P.Sud+++, R.Prashad and R.K.Tyagi, Applied Physics Deptt., Engg. College, AMU, Aligarh, +Govt. College, Sarkaghat, H.P., +++H.P.University, Shimla, ++S.V. College, Aligarh 202 001. 63

P16. COMPARATIVE STUDY BETWEEN CRANKING METHOD AND LAGRANGIAN MULTIPLIER METHOD, M. Rajasekaran, D.Caleb Chanthi Raj and R. Premanand, Dept. of Nuclear Phys., University of Madras, Madras 600 025. 65

P17. NUCLEONIC SEPARATION ENERGY AS A FUNCTION OF ANGULAR MOMENTUM AND TEMPERATURE, M.Rajasekaran, D.Caleb Chanthi Raj, R.Premanand • and P.Sivakumar, Dept. of Phys., Univ. of Madras, Madras 600 025. 67

P18. AN EMPIRICAL FORMULA FOR NUCLEAR LEVEL DENSITY PARAMETER, M.Rajasekaran, R.Premanand and D.Caleb Chanthi Raj. Dept. of Nucl. Physics, University of Madras, Madras 600 025. 69

P19. GYROMAGNETIC RATIO FOR HIGH SPIN SYSTEMS, M.Rajasekaran, R.Premanand and D. Caleb Chanti Raj, Dept. of Nuclear Physics, Univ. of Madras, Madras. 71

P20. STUDIES OF K-ELECTRON CAPTURE PROBABILITIES IN ^{87}Y, ^{96}Tc AND ^{196}Au, G.Sree Krishna Murty, M.V.S. Chandrasekhar Rao, N.V.S.Vara Prasad,G.Satyanarayana, D.L.Sastry and S.N.Chintalapudi*, Swamy Jnanananda Laboratories for Nuclear Research, Andhra University, Visakapatnam. *Variable Energy Cyclotron Centre, Calcutta. 73

P21. EVIDENCE OF SIGNATURE INVERSION IN Er^{159}, Tripti Mathur and Shanker Mukherjee, Dept. of Physics, Banaras Hindu University, Varanasi. 75

P22. LIFETIME OF THE 113 keV LEVEL AND DIFFERENTIAL ANGULAR CORRELATION OF THE 208-113 keV CASCADE IN 177-Hf, C.C.Dey, B.K.Sinha and R.Bhattacharya, Saha Inst. of Nuclear Physics, Calcutta 700 064. 77

P23. LEVEL DENSITY AT HIGH SPINS FOR THE REACTIONS $^{12}C(^{16}O,1n)^{27}Si$ AND $^{12}C(^{16}O,1p)^{27}Al$, T.R.Rajasekaran, C.R.Ramaswamy and M.P.Sathyavathiamma, Dept. of Physics, Bangalore University, Bangalore 560 056. 79

P24. EFFECT OF TEMPERATURE ON THE SHAPES OF LIGHT NUCLEI, G.Shanmugam, Kalpana Sankar, Arulmozhi.G., Dept. of Physics, Presidency College, Madras 600 005 and K. Ramamurthi, Dept. of Physics, Bharathidasan University, Trichy. 81

P25. MODIFIED SEMI-EMPIRICAL FORMULA FOR NUCLEAR ROTATIONAL STATES, J.S.Batra and Raj K.Gupta, Physics Dept., Panjab University, Chandigarh 160 014. 83

P26. MICROSCOPIC WAVEFUNCTION FOR ^{10}B, Neelam Agarwal and B.B.Srivastava, Meerut University, Meerut 250005. 85

P27. IBM-2 SPECTRA OF 1ν-1π BOSON SYSTEMS IN MICROSCOPIC BASIS, Subrata Sarangi and Jitendra C. Parikh, Physical Research Laboratory, Ahmedabad. 87

P28. MECHANISM OF SHAPE TRANSITION IN DOUBLY EVEN CADMIUM ISOTOPES, S.K.Khosa and P.K.Mattu, Dept. of Physics, Jammu University, Jammu 180 001, India. 89

P29. STUDY OF GROUND STATE SYSTEMATICS IN NEUTRON-RICH PALLADIUM ISOTOPES IN MIROSCOPIC FRAMEWORK, P.K.Mattu and S.K. Khosa, Department of Physics, Jammu University, Jammu 180 001. 91

P30. ROLE OF PROTONS IN THE ONSET OF DEFORMATION IN THE A~100 MASS REGION, Rakesh Kumar Gupta, S.K.Khosa and A.Bharti, Dept.of Physics, Univ. of Jammu, Jammu. 93

P31. INTRINSIC QUADRUPOLE MOMENTS OF ODD-ODD NUCLEI AND SYSTEMATICS OF DEFORMATION PARAMETER, S.D.Sharma, Arvinder Kaur, Arvind Sharma, Dept. of Physics, Panjabi University, Patiala 147 002. 95

P32. SENSITIVITY OF CRANKED NILSSON BCS CALCULATIONS ON INPUT PARAMETERS, Tripti Mathur and Shanker Mukherjee, Dept. of Physics, B.H.U., Varanasi 221005. 97

P33. TENSOR COMPONENTS OF R.I. IN EFFECTIVE INTERACTIONS, M.L.Soni, Madhav Science College, Vikram University, Ujjain. 99

P34. PROBLEM OF SIGN OF THE NEWBY SHIFT, A.K.Jain, Alpana Goel and Kiran Jain, Physics Department, University of Roorkee, Roorkee. 101

P35. TRANSITION CHARGE DENSITIES FOR HEXADECAPOLE EXCITATION IN SOME GERMANIUM NUCLEI, A.J.Singh, S.K. Dhiman, A.S.Raghwa and P.K.Raina, Physics Department, H.P. University, Shimla-5. 103

P36. MOMENT OF INERTIA FOR HOT ROTATING NUCLEI IN STATIC PATH APPROXIMATION, B.K.Agrawal and A.Ansari, Institute of Physics, Bhubaneswar 751 005. 105

P37. GENERATOR COORDINATE METHOD FOR (dtμ) MESOMOLECULE, Meenakshi Aggarwal, B.K.Chikara and V.K.Sharma, Dept. of Physics, Inst. of Advanced Studies, Meerut University, Meerut 250 004. 107

P38. MICROSCOPIC STRUCTURE FOR FIVE NUCLEON SYSTEM, B.K.Chikara, Meenakshi Aggarwal and V.K.Sharma, Dept. of Physics, Inst. of Advanced Studies, Meerut University, Meerut 250 004. 109

P39. K-HARMONICS METHOD APPLIED TO tε AND ^{9}Be, S.R.Sharan* and S.P.Verma+. *Dept. of Physics, T.P.S. College, Patna, +Deptt. of Physics, Science College, Patna. 110

P40. PERTURBATIVE SOLUTION OF INTEGRO DIFFERENTIAL EQUATION, Rakhi Chattopadhyay, Dept. of Physics, Calcutta University, Calcutta 700 009. 113

P41. CHARGE CENTRE DEVIATION IN EXOTIC DECAY, G.Shanmugam and S.I.A.Philomin Raj*, Dept. of Phys., Presidency College, Madras-5, *Dept. of Physics, Madras Christian College, Madras-59. 115

P42. REGULAR, IRREGULAR AND SCARRED WAVEFUNCTIONS IN THE TWO CENTRE SHELL MODEL, Debabrata Biswas, Theoretical Physics Division, BARC, Bombay 400 085 and Santanu Pal and A.K.Chaudhuri, Variable Energy Cyclotron Centre, Calcutta 700 064. 117

P43. STRUCTURE OF $^{178-186}$W FROM THE ARM, S.Sharma, K.S.Sen+ and S.P.Sud+, G.G.D.S.D.College, H.P. University, Rajpur.+Phys. Dept., H.P. Univv., Shimla. 119

P44. NUCLEAR STRUCTURE OF $^{146-154}$Sm IN THE IBM-1, S.Sharma, K.S.Sen+ and S.P.Sud+, G.G.D.S.D.College, H.P. University, Rajpur. +Physics Department, H.P. Univesity, Shimla. 121

P45. TESTS OF RIGID TRIAXIALITY FOR HEAVY Hg-Fm NUCLEI, S.Sharma, K.S.Sen+ and S.P.Sud+, G.G.D.S.D. College (H.P. Univ.,) Rajpur 176 064. + Dept. of Physics, H.P. University, Shimla 171 005. 123

b) LOW AND MEDIUM ENERGY NUCLEAR REACTIONS AND FISSION

O18. EVIDENCE FOR SHAPE ISOMERIC NATURE OF ^{16}O+^{12}C RESONANCES AT 43.8 MeV AND 46.4 MeV IN ^{28}Si OBSERVED THROUGH SELECTIVE ^{8}Be DECAY, Suresh Kumar, M.A. Eswaran, E.T.Mirgule, U.K.Pal, D.R.Chakrabarty, V.M. Datar and N.L.Ragoowansi, N.P.D., B.A.R.C., Bombay. 125

O19. ANGULAR MOMENTUM TRANSFER AND ENERGY LOSS IN THE ^{16}O+^{115}In REACTION AT 100 MeV, B.K.Nayak, S.V. Suryanarayan, D.C.Biswas, L.M.Pant, B.V.Dinesh, V.S. Ambekar, U.Garg*, R.K.Choudhury, N.P.D., B.A.R.C., Bombay. *Notre Dame University, Notre Dame, USA. 127

O20. SPIN DISTRIBUTION BELOW AND NEAR COULOMB BARRIER IN ^{209}Bi(^{10}B,3n) REACTION, P.Mukherjee, I.Mukherjee, B.Sethi and P.Sen, Saha Institute of Nuclear Physics, Calcutta and M.G.Betigeri, B.J.Roy and S.Mythili, Bhabha Atomic Research Centre, Bombay 400 085. 129

O21. ANGULAR - MOMENTUM - DEPENDENT FISSION BARRIERS: FISSION EXCITATION FUNCION OF ^{75}Re^{181} COMPOUND NUCLEUS FORMED BY ^{6}C^{12}+^{69}Tm^{169} AND ^{8}O^{16}+^{67}Ho^{165} REACTIONS, A.K.Pandey, R.C.Sharma, P.C.Kalsi and R.H.Iyer, Radiochemistry Divn, B.A.R.C., Bombay. 131

O22. ALPHA TRANSFER TO CONTINUUM - AN INCOMPLETE FUSION REACTION, B.S.Tomar, A.Goswami, A.V.R.Reddy, S.K.Das, P.P.Burte, S.B.Manohar and Satya Prakash, Radiochemistry Division, BARC, Bombay 400 085. 133

O23. MEASUREMENT OF PRE-SCISSION NEUTRON MULTIPLICITIES FOR $^{12}C+^{232}Th$ AND $^{16}O+^{232}Th$ SYSTEMS, Alok Saxena, R.P.Anand, A.Chatterjee, R.K.Choudhury, S.S. Kapoor, D.M.Nadkarni, B.K.Nayak, L.M.Pant, M.S. Samant and S.V.S.Sastry, Nuclear Physics Division, BARC, Bombay. 135

O24. LIFETIME IN HEAVY ION REACTIONS STUDIED BY CRYSTAL BLOCKING, Vandana Nanal, M.B.Kurup and K.G. Prasad, Tata Institute of Fundamental Research, Bombay 400 005. 137

O25. STUDY OF THE REACTION $^{115}In(^{12}C,^{11}B)^{116}Sn$, B.J.Roy, C.V.Fernandez, M.L.Jhingan*, S.K.Gupta and M.G.Betigeri, Bhabha Atomic Research Centre, Bombay, *TIFR, Bombay. 139

O26. STUDY OF ^{93}Tc AND ^{94}Tc USING THE GDA SET UP AT NUCLEAR SCIENCE CENTRE, S.S.Ghugre, V.P.Salvi, A.M. Narsale and S.B.Patel, Bombay University,Vidyanagari, Bombay 400 098 and S.Muralithar, G.Rodrigues and R.K. Bhowmik, Nuclear Science Centre, New Delhi 110 C67. 141

O27. ELASTIC AND INELASTIC SCATTERING OF ALPHA PARTICLES FROM ^{46}Ti AT $E\alpha$ = 45 MeV, V.Raghunatha Rao, M.Sudarshan, A.Sarma and R.Singh, Physics Dept., NEHU Shillong, 793003 and S.R.Banerjee & S.N.Chintalapudi, Variable Energy Cyclotron Centre, Calcutta. 143

O28. COUPLED CHANNEL ANALYSIS OF THE $^{28}Si(\alpha,^{3}He)^{29}Si$ REACTION AT 45, 65 AND 120 MeV, M.P.Sathyavathiamma, V.P.Darshan, C.R.Ramaswamy and N.G.Puttaswamy, Dept. of Physics, Bangalore University, Bangalore 560 056. 145

O29. POTENTIAL AMBIGUITIES IN HEAVY ION SCATTERING, D.Dutta and Y.K.Gambhir, Dept. of Physics, I.I.T., Bombay 400 076. 147

O30. SPIN DISTRIBUTION FOR THE FUSION OF $^{16}O+^{209}Bi$, S.Kailas, P.Singh and A.K.Mohanty, NPD, BARC, Bombay. 149

O31. A DYNAMICAL APPROACH TO INTERMEDIATE ENERGY NUCLEUS-NUCLEUS COLLISIONS, K.Krishan*, S.Bhattacharya*, P.Wagner+, J.P.Coffin+ and F.Rami+. *Variable Energy Cyclotron Centre, Calcutta. +Centre de Recherches Nucleaires, Strasbourg Cedex, France. 151

O32. ROLE OF DEUTERON SIZE IN ANTIPROTON-DEUTRON ELASTIC SCATTERING, K.Kumar and A.K.Jain, Nuclear Physics Division, BARC, Bombay. 153

O33.EXPLANATION OF e+e- PEAKS IN HEAVY-ION COLLISIONS K.Raja, K.Sakthi Murugesan, G.Janhavi and P.R. Subramanian, Dept. of Nucl.Phys., Madras University, Madras. 155

O34. PHASE-FUNCTION METHOD FOR COMPLEX POTENTIALS, J.Pal, A.K.Jana and B.Talukdar, Dept. of Physics, Visva-Bharati University, Santiniketan 731 235. 157

P46. SCATTERING OF ^{28}Si FROM ^{27}Al AT 70,80,90 AND 100 MeV, S.K.Charagi, Kuldeep, M.G.Betigeri, C.V. Fernandez and S.K.Gupta, Nuclear Physics Division, BARC, Bombay. 159

P47. ELASTIC SCATTERING ANGULAR DISTRIBUTION USING PARAMETER-FREE COULOMB-MODIFIED GLAUBER MODEL, S.K. Charagi and S.K.Gupta, N.P.D., B.A.R.C., Bombay-85. 161

P48. ELASTIC SCATTERING OF ^{12}C ON ^{232}Th, A.K.Mohanty, P.Singh, A.Nijasure, A.Saxena, B.V.John, S.Kailas, S.K.Kataria, A.Chatterjee, S.S.Kapoor and V.S. Ramamurthy*, Nuclear Physics Division, BARC, Bombay. *Institute of Physics, Bhubaneswar. 163

P49. ^{12}C+^{28}Si ELASTIC SCATTERING ABOVE THE COULOMB BARRIER, Yash Pal Singh, Department of Physics, G.K.University, Haridwar 249 404. 165

P50. NUCLEAR FORWARD GLORY IN ^{16}O + ^{16}O SCATTERING, Rajendra Prasad, A.Ostrowski* and H.Voit*, Applied Physics Dept., Z.H.College of Engg. & Tech., A.M.U., Aligarh. *Tandem Laboratory, Physicalisches Institut der Univ. Erlangen-Nuernberg, D-8520 Erlangen, FRG. 167

P51. EXCITATION FUNCTION AT $\theta_{cm} = 90^{o}$ FOR $^{24}Mg(^{24}Mg, ^{24}Mg)^{24}Mg$, Ashok Kumar, K.Eswaraiah, Madhup Seth, Ravi Datt Godiyal, S.R.Verma, R.C.Misra* and B.B. Srivastava**, D.B.S. (P.G.) College, Dehra Dun, *VSSD College, Kanpur. **Meerut University, Meerut. 169

P52. MICROSCOPIC NUCLEAR POTENTIAL FOR $^{16}O+^{24}Mg$ SYSTEM, Ashok Kumar, Madhup Seth, K.Eswaraiah, Ravi Datt Godiyal, P.K.Bhatnagar and Sunita Kumar*, D.B.S. (P.G.) College. *M.K.P. (P.G.) College, Dehra Dun. 171

P53. STUDY OF EXCITATION ENERGY IN VARIOUS FORMS OF NN INTERACTION, R.C.Mishra, Ashok Kumar Sharma and Ashok Kumar*, Dept. of Physics, VSSD College, Kanpur. *Dept. of Physics, DBS College, Dehradun. 173

P54. STUDY OF ANGULAR MOMENTUM IN FUSION REACTIONS, R.C.Mishra, A.K.Sharma and A.Kumar*, Dept. of Phys., VSSD College, Kanpur. *Dept. of Phys., DBS College, Dehradun 248 001. 175

P55. GAMMA RAY EMISSION IN HEAVY ION REACTIONS EXPERIMENTAL SEARCH FOR ENTRANCE CHANNEL EFFECTS, S.P.Das, S.Sen, M.Satpathy, S.Jena, Utkal University, Bhubaneswar, G.V.Raviprasad, R.K.Yadav, L.Satpathy, V.S.Ramamurthy, Institute of Physics, Bhubaneswar and D.Kataria, N. Madhavan, A.Roy, A.Sinha, S.Dutta, Nuclear Science Centre, New Delhi. 177

P56. A SOLVABLE POTENTIAL AND A NEW PENETRABILITY FORMULA FOR NUCLEUS-NUCLEUS FUSION, Zafar Ahmed, Nuclear Physics Division, BARC, Bombay-85. 179

P57. ADIABATIC AND SUDDEN LIMIT APPROXIMATION TO HEAVY ION FUSION POTENTIAL, S.V.S.Sastry, A.K.Mohanty and S.K.Kataria, Nuclear Phys. Divn., BARC, Bombay. 181

P58. USE OF POLARISATION POTENTIAL IN BARRIER PENETRATION MODEL FOR HEAVY ION FUSION, A.K.Mohanty and S.K.Kataria, Nuclear Phys. Divn., BARC, Bombay. 183

P59. HEAVY ION FUSION AT NEAR- AND SUB-BARRIER ENERGIES, S.Kailas, N.P.D., B.A.R.C., Bombay 400 085. 185

P60. MASS EXCHANGE IN HEAVY ION COLLISIONS, M.Rajasekaran, R.Premanand and D.Caleb Chanthi Raj, Dept. of Nucl. Phys., Univ. of Madras, Madras 600025. 187

P61. BARRIER REGION RESONANCE MODEL FOR HEAVY ION RESONANCES, B.Sahu, B.M.Jyrwa, P.Susan and C.S. Shastry, Dept. of Physics, NEHU, Shillong 793 003. 189

P62. THE ROTATION-VIBRATION CHARACTERISTICS OF THE QUASI-MOLECULAR RESONANCES, P.Sarangi and L.Satpathy, Institute of Physics, Bhubaneswar 751 005. 191

P63. ELLIPSOIDAL DEFORMATIONS AND FUSION BARRIER DECREASE, G.Shanmugam and M.D.Padmini*, Presidency College, Madras. *Dept. of Physics, Quaid-E-Millat Govt. College for Women, Madras 600 002. 193

P64. FUSION CROSS SECTION OF SPIN-UNSATURATED NUCLEI, K.C. Panda and T. Patra, Post-Graduate Dept. of Physics, Sambalpur University, Sambalpur. 195

P65. SPIN DENSITY TERMS AND ELASTIC SCATTERING OPTICAL POTENTIAL OF CLOSED j-SHELL NUCLEI, K.C.Panda and T. Patra, P.G. Dept. of Physics, Sambalpur University, Sambalpur 768 109. 197

P66. INTERMEDIATE MASS FRAGMENTS EMISSION IN INTERMEDIATE ENERGY NUCLEUS-NUCLEUS COLLISION, C.Bhattacharya, S. Bhattacharya and K. Krishan, Variable Energy Cyclotron Centre, Calcutta 700 064. 199

P67. NEUTRON SHELL EFFECTS IN THE $^{209}Bi(\alpha,xn)^{213-x}At$ AND $^{197}Au(\alpha,xn)^{201+x}Tl$ REACTIONS, S.S.Rattan and N.Chakravarty, Radiochemistry Division, BARC, Bombay. 201

P68. INVESTIGATION OF PRE-EQULIBRIUM EMISSION IN (α-np) REACTIONS ON $^{128,130}Te$, B.P.Singh, M.G.V. Sankaracharyulu, M.A.Ansari, H.D.Bhardwaj and R.Prasad, Dept. of Physics, A.M.U., Aligarh. 203

P69. ALPHA INDUCED REACTIONS IN YTTRIUM, M.K.Bhardwaj, I.A.Rizvi and A.K.Chaubey, Dept. of Physics, Aligarh Muslim University, Aligarh. 205

P70. MEASUREMENT OF EXCITATION FUNCTIONS AND MEAN PROJECTED RECOIL RANGES OF NUCLEI IN α-INDUCED REACTIONS ON F, Al, V, Co AND Re NUCLEI, M.Ismail, Variable Energy Cyclotron Centre, Calcutta 700 064. 207

P71. INVESTIGATION OF DEUTRON CLUSTER IN ^{6}Li USING 45 MeV ^{6}Li (α,αd) ^{4}He REACTION, Mythili Subramanian, Arun Kumar Jain, Amit Roy* and Ranjan Bhowmik*, Nuclear Physics Division, BARC, Bombay. *Nuclear Science Centre, New Delhi 110 067. 209

P72. GEOMETRICAL EFFECTS ON FINAL STATE INTERACTION IN THREE BODY BREAK-UP EXPERIMENTS, S.Mandal and S.S. Dasgupta, Physics Dept., Burdwan University, Burdwan. 211

P73. HELIUM-ION-INDUCED FISSION EXCITATION FUNCTIONS OF TERBIUM AND YTTERBIUM, A.K.Pandey, R.C.Sharma, P.C.Kalsi and R.H.Iyer, Radiochemistry Division, BARC, Bombay 400 085. 213

P74. KINETIC ENERGY DEPENDENCE OF FISSION FRAGMENT ANGULAR MOMENTUM, T.Datta, S.P.Dange, H.Naik and P.K. Pujari, Radiochemistry Division, BARC, Bombay-85. 215

P75. CHARGE DISTRIBUTION IN LOW ENERGY FISSION OF ACTINIDES, H.Naik, S.P.Dange and T.Datta, Radiochem. Division, B.A.R.C., Bombay 400 085. 217

P76. CHARGE DISTRIBUTION IN 79 MeV 12-C INDUCED FISSION OF 232-Th, A.V.R.Reddy, A.Goswamy, B.S.Tomar, A.G.C.Nair, S.K.Das, S.B.Manohar and Satya Prakash, Radiochemistry Division, BARC, Bombay. 219

P77. PRE-FISSION ALPHA MULTIPLICITIES IN THE ^{19}F+^{181}Ta REACTION, A.Chatterjee, S.Kailas, P.Singh, A.Navin, S.S.Kerekatte, D.C.Biswas, Aruna Nijasure, B.V.John, Alka Karnik and S.S.Kapoor, Nuclear Physics Division, BARC, Bombay 400 085. 221

P78. EFFECT OF PRE-FISSION NEUTRON EMISSION ON THE INTERPRETAION OF FISSION FRAGMENT ANGULAR DISTRIBUTIONS, A.Saxena, S.Kailas, A.Karnik, A. Chatterjee, D.M. Nadkarni and S.S.Kapoor, Nuclear Physics Division, BARC, Bombay. 223

P79. MEASUREMENT OF FISSION FRAGMENT ANGULAR CORRELATION FOR $^{19}F+^{232}Th$ SYSTEM AT 107MeV AND 95MeV, Alok Saxena, D.C.Biswas, D.M.Nadkarni, V.S.Ambekar and B.V.Dinesh, Nuclear Phys. Divn., BARC, Bombay. 225

P80. ANGULAR DISTRIBUTION OF TRANSFER PRODUCTS IN ^{12}C, $^{16}O+^{232}Th$ REACTIONS AT NEAR BARRIER ENERGIES, D.C.Biswas, B.K.Nayak, B.V.Dinesh, L.M.Pant, S.V.S. Sastry, V.S Ambekar, D.M.Nadkarni and R.K.Choudhury, Nuclear Physics Division, BARC, Bombay 400 085. 227

P81. STUDY OF EVAPORATION SPECTRA OF PROTONS AND ALPHA PARTICLES FROM COMPOUND NUCLEI IN MASS REGION=110, Aruna N., B.John, A.Chatterjee, A.Saxena, A.K.Mohanty, P.Singh, K.Kumar, S.Kailas, S.K.Kataria and S.S.Kapoor, Nuclear Phys. Divn., BARC, Bombay. 229

P82. INVESTIGATION OF PRESCISSION NEUTRON EMISSION FROM MASS AND TOTAL KINETIC ENERGY SELECTED FISSION FRAGMENTS IN $^{235}U(nth,f)$; M.S.Samant, R.P.Anand, R.K. Choudhury, D.M.Nadkarni and S.S.Kapoor, Nuclear Physics Division, B.A.R.C., Bombay 400 085. 231

P83. MEASUREMENT OF $^{89}Y(n,\alpha)$ AND $^{109}Ag(n,p)$ REACTION CROSS SECTIONS AT 14.6 MeV, H.M.Agrawal, Dept. of Physics, G.B.Pant University, Pantnagar 263 145. 233

P84. DWIA ANALYSIS OF 200 MeV $^{12}C(\pi^+,\pi^+p)^{11}B$ REACTION USING PERIPHERAL 3-BODY COUPLING MODEL, Arun K.Jain, N.P.D.,Bhabha Atomic Research Centre, Bombay 400 085. 235

P85. PROJECTION OPERATOR FOR CHANNEL SELECTION IN NUCLEAR REACTIONS, G.Ramachandran and M.S.Vidya, University of Mysore, Mysore. 237

P86. ON A NEW METHOD TO DIAGONALIZE NON-ORIENTED SPIN-1 DENSITY MATRICES, A.Sudha Rao, A.R.Usha Devi and G.Ramachandran, Dept. of Studies in Physics, University of Mysore, Mysore. 239

P87. COMPARATIVE STUDY OF ANALYTICAL WAVEFUNCTIONS FOR DEUTERON D-STATE, V.N.Pai* and R.J.Kulkarni, Dept. of Physics, University of Bombay, Bombay-98. *Parle College, Vile Parle (E), Bombay. 241

P88. SHAPE TRANSITION AND LEVEL DENSITY OF HOT NUCLEI IN STATIC PATH APPROXIMATION, B.K.Agrawal and A.Ansari, Institute of Physics, Bhubaneswar 751 005. 243

P89. SUPERSYMMETRIC QUANTUM MECHANICS FOR PHASE-EQUIVALENT POTENTIALS, P.K.Bera and B.Talukdar, Dept. of Physics, Visva-Bharati, Santiniketan 731 235. 245

P90. LEVEL DENSITY DEPENDENT NEUTRON EMISSION SPECTRA AND MULTI-PARTICLE REACTION CROSS-SECTIONS OF Ni-58, Ta-181 AND Bi-209, S.B.Garg, Neutron Physics Divn., Bhabha Atomic Research Centre, Bombay 400 085. 247

P91. DOUBLE DIFFERENTIAL NEUTRON EMISSION CROSS-SECTIONS OF Ni-58 AND Bi-209 AT 14.1 MeV, S.B.Garg, Neutron Physics Division, B.A.R.C., Bombay 400 085. 249

P92. ^{232}Th TOTAL NEUTRON CROSS SECTION FROM 0.1 to 20 MeV, H.M.Jain, Experimental Reactor Physics Section, BARC, Bombay 400 085. 251

P93. COMPUTED EXCITATION FUNCTIONS OF ^{93}Nb FOR 1 TO 20 MeV NEUTRONS, S.L.Bansal and R.K.Mohindra, Physics Dept., Kurukshetra University, Kurukshetra 132 119. 253

c) <u>NUCLEAR MATTER AND NUCLEAR COSMOPHYSICS</u>

O35. MICROSCOPIC CALCULATION OF THE NUCLEON SPIN-ORBIT POTENTIAL, S.M.Saliem and W.Haider, Dept. of Physics, A.M.U., Aligarh 202 002. 255

O36. NUCLEAR COMPRESSIBILITY; AN ANATOMICAL STUDY, V.S.Uma Maheswari, V.S.Ramamurthy and L.Satpathy, Institute of Physics, Bhubaneswar 751 005. 257

O37. HOT NUCLEAR MATTER WITH DENSITY DEPENDENT INTERACTION, C.Das, Physics Dept., Banki College, Cuttack, India, R.K. Tripathi, 13, Natalie DR, Hompton, VA 23600, USA and R. Sahu, Physics Dept., Berhampur University, Berhampur 760 007. 259

O38. MEAN SEPARATION BETWEEN NUCLEATION SITES AND COSMIC QUARK-HADRON PHASE TRANSITION, K.Sakthi Murugesan, G.Janhavi, K.Raja and P.R.Subramanian, Dept. of Nucl. Phys., Univ. of Madras, Madras. 261

P84. BARYON MASS SPECTRA, A.K.Gautam, Rajesh Gaur and A.K.Shiromani, Physics Dept., R.B.S. College, Agra. 263

P95. FINITE TEMPERATURE NUCLEAR MATTER: A FIELD THEORETIC METHOD, H.Mishra, S.P.Misra and P.K.Panda, Institute of Physics, Bhubaneswar and B.K. Parida, Dept. of Phys., Regional College of Education, Bhubaneswar 751 007. 265

P96. SOLAR NEUTRINO PROBLEM AND ASTROPHYSICAL S-FACTOR, Pratibha and V.K.Sharma, Dept. of Physics, Institute of Advanced Studies, Meerut Univ., Meerut. 267

P97. NUCLEAR MATTER RESULTS FOR DENSITY-DEPENDENT M3Y INTERACTION, K.C. Panda, Post-Graduate Dept. Of Physics, Sambalpur University, Jyoti Vihar, Sambalpur 269

d) INTERMEDIATE ENERGY NUCLEAR REACTIONS AND NON-NUCLEONIC DEGREES OF FREEDOM

O39. COULOMB DISSOCIATION OF EXOTIC NUCLEI IN A DIRECT FRAGMENTATION MODEL, R.Shyam, P.Banerjee and G.Baur*, Saha Inst. of Nucl. Physics, Calcutta.* Institute fur Kernphsik, KFA Julich, D-5170 Julich. 271

O40. DETERMINATION OF $^{12}C(p,p')^{12}C^*(1^+)$ INELASTIC SCATTERING AMPLITUDES, A.Sudha Rao, K.S.Mallesh, M.S. Vidya and G. Ramachandran, Univ. of Mysore, Mysore-6. 273

O41. NUCLEON PROPERTIES IN CHIRAL COLOR DIELECTRIC MODEL, Sarira Sahu and S.C.Phatak, Institute of Physics, Bhubaneswar 751 005. 275

O42. SPIN ORBIT N-N INTERACTION FROM COGEP, S.B. Khadkikar and K.B. Vijayakumar, Physical Research Laboratory, Ahmedabad 380 009, India. 277

O43. MULTIPLICITIES OF THE EMITTED NEUTRON AND LIGHT CHARGED-PARTICLES IN MULTIFRAGMENTATION PROCESS, A.Das, L.Satpathy, M.Mishra and M.Satpathy*, Institute of Physics, Bhubaneswar. *Utkal University, Bhubaneswar 751 004. 279

O44. N-N INTERACTION IN CHIRAL COLOUR DIELECTRIC MODEL, Sanjay K.Ghosh, Institute of Physics, Bhubaneswar 751 005. 281

O45. INCLUSIVE $(p,p'\pi^+)$ REACTION, Neelima G.Kelkar and B.K. Jain, Nuclear Phys. Divn., BARC, Bombay. 283

P98. K^+ PRODUCTION IN HEAVY ION COLLISION AT FAR SUBTHRESHOLD BEAM ENERGY, B.Ghosh, Institute of Physics, Bhubaneswar 751 005. 285

P99. BAG MODEL FORMULATION OF HADRON MASSES, Rajesh Gaur, A.K.Gautam and A.K.Shiromani, Physics Dept., R.B.S. College, Agra. 287

P100. ANNIHILATION RANGE, PP SCATTERING PARAMETERS AND COMPLEX POTENTIAL SCATTERING, A.V.Lagu, Physics Department, Banaras Hindu University, Varanasi. 289

P101. DIELECTRIC FUNCTIONAL DEPENDENCE OF GLUONIC EFFECTS IN COLOR DIELECTRIC MODEL, Sarira Sahu, Institute of Physics, Bhubaneswar 751 005. 291

P102. DEPENDENCE OF THE CHARACTERISTICS OF CLUSTERS ON TARGET SIZE IN PARTICLE-EMISSION COLLISIONS, M.Saleem Khan, H.Khushnood and A.R.Ansari, High Energy Physics Lab., Dept. of Phys., Jamia Millia Islamia, N. Delhi. 293

P103. THE SPIN ORBIT FORCE FROM COGEP, K.B.Vijayakumar and S.B. Khadkikar, Physical Research Laboratory, Ahmedabad 380 009, India. 295

P104. TENSOR N-N INTERACTION FROM COGEP, K.B. Vijayakumar and S.B. Khadkikar, Physical Research Laboratory, Ahmedabad 380 009, India. 297

P105. THE EFFECT OF CONFINEMENT OF GLUONS ON N-N SCATTERING : P-P AND N-P DIFFERENTIAL CROSS SECTIONS, S.B.Khadkikar and K.B.Vijayakumar, Physical Research Laboratory, Ahmedabad 380 009. 299

P106. PARITY NON-CONSERVATION IN ATOMS DUE TO NEUTRAL WEAK CURRENTS AND THE NUCLEAR ANAPOLE MOMENT, Swati Bhagwat and B.P.Das, Dept. of Phys., I.I.T., Bombay. 301

P107. BARYONIC MATTER IN THE NONLINEAR MESON FIELD THEORY, Safayet Karim Chowdhury+ and Sasabindu Sarkar Dept. of Theoretical Physics, Indian Association for the Cultivation of Science, Jadavpur, Calcutta-32. 303

P108. SUBNUCLEAR DEGREES OF FREEDOM IN THE DEUTERON, V.K.Sharma, Dept. of Physics, Institute of Advanced Studies, Meerut University, Meerut 250 004. 305

P109. THE p(p,p'π)n REACTION, A.B.Santra and B.K.Jain, Nuclear Physics Division, BARC, Bombay 400 085. 307

P110. INCLUSIVE (P, ++) REACTION, Neelima G.Kelkar and B.K.Jain, Nuclear Phys. Divn., BARC, Bombay-85. 309

P111. SOME CHARACTERISTICS OF PROJECTILE FRAGMENTS PRODUCTS IN ^{28}Si-Em AND ^{12}C-Em INTERACTIONS AT 4.5 A GeV/c, M.Tariq, M.Zafar, S.Ahmad, A.Tufail, Tayyab, A.R.Khan and M.Shafi, Dept. of Physics, AMU, Aligarh. 311

P112. THE EFFECT OF DISPERSIVE /\NN FORCES ON THE SPIN-DEPENDENCE OF N POTENTIAL, Nasra Neelofer and Mohammad Shoeb, Dept. of Physics, AMU, Aligarh-2. 313

e) RELATIVISTIC HEAVY-ION COLLISIONS AND QUARK-GLUON PHASE

O46. THE EFFECT OF DEFORMATION AND COLOUR SINGLETNESS ON QUARK-GLUON DECONFINEMENT PHASE TRANSITION IN THE BAG MODEL, M.G.Mustafa and A.Ansari, Institute of Physics, Bhubaneswar 751 005. 315

O47. QUARK GLUON PLASMA EQUATION OF STATE IN A RELATIVISTIC HARMONIC CONFINEMENT MODEL, S.B. Khadkikar and J.C.Parikh, Physical Research Laboratory, Ahmedabad 380 009. 317

O48. AN IMPROVED QGP MODEL FOR RELATIVISTIC HEAVY ION COLLISIONS, R.S.Kaushal+ and Praveen Akhaury++, Dept. of Physics & Astrophysics, Univ. of Delhi, Delhi. 319
+UGC Research Scientist. ++UGC Junior Research Fellow

O49. EQUATION OF STATE OF QUASI-FREE GLUON GAS, Somenath Chakrabarty+, Debadesh Bandyopadhyay* and Debapriya Syam**, + Saha Inst. of Nucl. Physics, Calcutta. *Goethe-Institut, Steubenstrasse 44, D-6800 Mannheium 1, Germany. **Physics Department, Krishnagar Govt. College, Krishnagar, West Bengal. 321

O50. PHOTONS AND PIONS FROM QUARK-GLUON PLASMA AND HADRONIC MATTER, Subodha Mishra*, Somenath Chakrabarty+, Jan-e Alam**, Dinesh K.Srivastava** and Bikash Sinha**. *Institute of Physics, Bhubaneswar. +Saha Inst. of Nucl. Physics, Calcutta. **Variable Energy Cyclotron Centre, Calcutta. 323

O51. CAN THE HADRONIC GAS SHINE AS BRIGHT AS QUARK-GLUON PLASMA, Somenath Chakrabarty+, Jan-e Alam*, Dinesh K.Srivastava*, Bikash Sinha* and Sibaji Raha#. +Saha Institute of Nuclear Physics, Calcutta-64. *Variable Energy Cyclotron Centre, Calcutta. #Bose Institute, Calcutta 700 009. 325

O52. MODEL DEPENDENT PHASE TRANSITION FROM HADRONIC MATTER TO QUARK-GLUON PLASMA, K.Sakthi Murugesan, G.Janhavi, K.Raja and P.R.Subramanian, Dept. of Nucl. Physics, University of Madras, Madras. 327

O53. TEMPERATURE DEPENDENCE OF BAG CONSTANT USING CHROMOMAGNETISM, N.Meenakumari and M.Rajasekaran, Dept. of Nucl. Phys., Univ. of Madras, Madras 600025. 329

O54. PION COHERENCE ZONE FOR 'HOT' AND 'COLD' EVENTS IN RELATIVISTIC HEAVY ION COLLISION, Dipak Ghosh, Jaya Roy*, Sharmila Sarkar and Ranjan Sengupta, Jadavpur University, Calcutta-32. *RCC, Calcutta-32. 331

O55. EVIDENCE OF SELF-SIMILAR PROTON EMISSION IN NUCLEUS-NUCLEUS COLLISION, Dipak Ghosh, Argha Deb, Premomoy Ghosh, Biswanath Biswas and Jayanta Roychoudhury, Jadavpur University, Calcutta-32. 333

O56. EFFECT OF TEMPERATURE ON COLLECTIVE BEHAVIOUR, B.Singh, H.S. Palsania, V.Kumar, K.B.Bhalla and S.Lokanathan, Dept. of Physics, University of Rajsthan, Jaipur 302 004. 335

O57. HIGH RESOLUTION STUDY OF HELIUM PROJECTILE FRAGMENTS EMITTED IN ^{32}S-EMULSION COLLISIONS AT 200 A GeV ENERGY, (EMU-01 COLLABORATION), Renu Arora, Physics Department, Panjab University, Chandigarh. 337

O58. FORWARD BACKWARD CORRELATIONS EMU - 01 COLLABORATION, Anju Bhasin, Physics Department, University of Jammu, Jammu 180 001. 339

O59. DIFFRACTION DISSOCIATION OF ^{12}C NUCLEI IN NUCLEAR EMULSION, M.S.Ahamad, K.A.Siddiqui and R.Hasan, Dept. of Physics, A.M.U., Aligarh 202 002. 341

P113. EFFECT OF ELECTROWEAK EFFECT AND QCD ON RATIO R, A.K.Gautam, Rajesh Gaur and A.K.Shiromani, Physics Department, R.B.S. College, Agra. 343

P114. ELECTRON-POSITRON ANNIHILATION INTO HADRONS, A.K.Gautam, Rajesh Gaur and A.K.Shiromani, Physics Department, R.B.S. College, Agra. 345

P115. NUCLEAR MASSES FROM QUARK SHELL MODEL, M.Rajasekaran, N.Meenakumari and V.Devanathan, Dept. of Nucl. Phys., Univ. of Madras, Madras 600 025. 347

P116. FINITE SIZE NUCLEONIC EFFECTS IN THE NUCLEAR MEDIUM, M.Rajasekaran and N.Meenakumari, Dept. of Nucl. Physics, University of Madras, Madras 600 025. 349

P117. BOOST NON-INVARIANT FLOW IN ULTRA RELATIVISTIC HEAVY ION COLLISIONS - AN APPROXIMATE METHOD, Jan-e Alam+, Somenath Chakrabarty*, Dinesh K.Srivastava+ and Bikash Sinha+. +Variable Energy Cyclotron Centre, Calcutta. *Saha Inst. of Nucl. Physics, Calcutta-64. 351

P118. BOOST NON INVARIANT HYDRODYNAMICS IN ULTRA RELATIVISTIC HEAVY ION COLLISIONS-AN EXACT METHOD, Dinesh K.Srivastava+, Jan-e Alam+, Somenath Chakrabarty*, Sibaji Raha** and Bikash Sinha+, +Variable Energy Cyclotron Centre, Calcutta. *Saha Institute of Nucl. Physics, Calcutta-64. **Bose Institute, 93/1, APC Road, Calcutta 700 009. 353

P119. CURVATURE RADIATION AND (τ/π^0) SIGNAL OF QUARK-GLUON PLASMA, Somenath Chakrabarty+, Sibaji Raha* and Bikash Sinha**. +Saha Institute of Nuclear Physics, Calcutta-64. *Bose Institute, Calcutta. **Variable Energy Cyclotron Centre, Calcutta 700 064. 355

P120. AN INVESTIGATION OF MANY PION DYNAMICAL CORRELATION IN HEAVY ION INTERACTION, Dipak Ghosh, Sanjib Sen, Madhumita Lahiri, Argha Deb, Biswanath Biswas, Jayanta Ray Choudhury and Jaya Roy*, Jadavpur University, Calcutta. *RCC, Calcutta-32. 357

P121. MULTIPION PRODUCTION IN NUCLEAR COLLISION AND GENERALISED DIMENSION OF FRACTALITY, Dipak Ghosh, Jaya Roy*, Premomoy Ghosh, Argha Deb, Jadavpur University, Calcutta-32. *RCC, J.U., Calcutta-32. 359

P122. COHERENT AND CHAOTIC PIONISATION IN RELATIVISTIC NUCLEAR COLLISION, Dipak Ghosh et.al., Jadavpur University, Calcutta 700 032. 361

P123. EVIDENCE OF SHORT MEAN FREE PATH AND FRACTALITY OF PROJECTILE FRAGMENTS IN HEAVY-ION INTERACTION, D.Ghosh, Jaya Roy*, D.Banerjee, Argha Deb, P.Ghosh, Jadavpur University, Calcutta. *RCC, Calcutta-32. 363

P124. MULTIPLICITY DISTRIBUTIONS OF SECONDARY PARTICLES PRODUCED IN CARBON-AND SILICON-NUCLEUS INTERACTIONS AT 4.5A GeV/c, Tauseef Ahmad, M.Irfan and A.H.Naqvi, Dept. of Phys., A.M.U., Aligarh-2. 365

P125. HOT STABLE STRANGE QUARK MATTER IN THE EARLY UNIVERSE PHASE TRANSITION, K.Sakthi Murugesan and P.R.Subramanian, Dept. of Nucl. Physics, University of Madras, Madras 600 025. 367

P126. THE DECONFINEMENT CRITICAL ENERGY DENSITY DEPENDENCE ON THE HARD CORE RADIUS, S.Karthiyayini and V.Devanathan*, Dept. of Nucl. Physics, Univ. of Madras. *Crystal Growth Centre, Anna Univ., Madras. 369

P127. FRAGMENTATION STUDIES IN ^{40}Ar-EMULSION INTERACTIONS AT 1.8 A GeV, R.R.Joseph*, I.D.Ojha, B.K. Singh and S.K.Tuli, Dept. of Physics, Banaras Hindu Unversity, Varanasi. *Dept. of Phys. & Astrophys., Delhi Unversity, Delhi 110 007. 371

P128. EMISSION OF LOW ENERGY PARTICLES IN ^{32}S-EMULSION INTERACTIONS AT 200 A GeV ENERGY, (EMU-01 COLLABORATION), V.S.Bhatia, Physics Department, Panjab University, Chandigarh 160 014. 373

P129. NON-STATISTICAL FLUCTUATIONS IN RELATIVISTIC HEAVY-ION COLLISIONS EMU - 01 COLLABORATION, Anju Bhasin, Physics Department, Univ. of Jammu, Jammu. 375

P130. MUTIPLICITY CORRELATIONS IN NUCLEUS-NUCLEUS COLLISIONS, K.A.Siddiqui, M.S.Ahmad, R.Hasan, Dept. of Physics, AMU, Aligarh 200 002. 377

f) NUCLEAR INSTRUMENTATION AND EXPERIMENTAL TECHNIQUES

O60. PERFORMANCE OF THE ISOL ION-SOURCE IN THE ON-LINE: SOME NEW AND SURPRISING OBSERVATIONS, A.Chakrabarti, A.Banerjee, S.Chattopadhyay, A.Polley, V.Banerjee, S.Bhattacharya, T.Mukhopadhyay, A.Das, S.K.Pardhasaradhi and R.P.Sharma, Variable Energy Cyclotron Centre, Calcutta. 379

O61. AN ELECTROSTATIC DEFLECTOR FOR FUSION CROSS-SECTION MEASUREMENTS, M.L.Jhingan, H.C.Jain, S.Nagaraj, P.Singh*, Y.K.Agarwal, M.G.Betigeri* and S.Saha, Tata Institute of Fundamental Research, Bombay. *Bhabha Atomic Research Centre, Bombay. 381

O62. BEAM PULSING SYSTEM FOR THE PELLETRON AT TIFR, H.C.Jain and U.T.Raheja, Tata Institute of Fundamental Research, Bombay and P.J.Bhalerao, V.M. Datar and M.Y.Vaze, N.P.D., B.A.R.C., Bombay. 383

O63. POSITION SENSITIVE GAS DETECTORS, D.Kataria, J.Antony and E.T. Subramaniam, Nuclear Science Centre, New Delhi. 385

O64. PULSE HEIGHT DEFECT OF BaF_2 SCINTILLATOR FOR LIGHT CHARGED PARTICLES, Bency V.John, Nuclear Physics Division, BARC, Bombay. 387

O65. GROWTH AND CHARACTERISATION OF BISMUTH GERMANATE SCINTILLATOR, K.Hema Prasad, D.G.Desai, S.C. Karandikar, K.S.Keswani, M.N.Ahuja, Sangeeta and S.C. Sabharwal, Technical Phys. & Prototype Engg. Divn., BARC., Bombay 400 085. 389

O66. A CAMAC CRATE CONTROLLER FOR IBM PC/AT WITH 16BIT DMA INTERFACE, P.S.Arvindakshan, Anita Behere, M.D.Ghodgaonkar and B.R.Bairi, Electronics Division, Bhabha Atomic Research Centre, Bombay 400 085. 391

O67. AN ONLINE DATA ACQUISITION SYSTEM FOR VAX COMPUTER, R.K.Bhowmik, D.K.Goyal and S.Naithani, Nuclear Science Centre, New Delhi. 393

P131. EFFECT OF CURING CYCLES ON ETCHING AND ANNEALING BEHAVIOUR OF CR-39 TRACK DETECTOR, Anupam, S.K.Sharma, S.Kumar and N.Lal, Dept. of Physics, Kurukshetra University, Kurukshetra, India. 395

P132. SOME GAMMA DOSIMETRIC PROPERTIES OF CN-85 AND CR-39, S.L.Sharma, Physics Dept., IIT, Kharagpur,W.B. 397

P133. ^{136}Xe ION TRACK REGISTRATION IN MAKROFOL-KL POLYCARBONATE, Ashavani Kumar, P.J.Jojo and Rajendra Prasad, Dept. of Applied Phys., Z.H.College of Engg. and Tech., A.M.U., Aligarh. 399

P134. DEVELOPMENT OF 8K CHANNEL 100MHZ WILKINSON TYPE ADC, P.K.Mukhopadhyay and K.R.Marballi, Electronics Division, BARC, Bombay 400 085. 401

P135. HEAVY ION REACTION ANALYZER AT NSC, A.K.Sinha, N.Madhavan, J.J.Das, P.Sugathan, E.T.Subramanian, Bishambar Kumar, Rajpal Sharma, D.O.Kataria and Jacob Chako, Nuclear Schience Centre, New Delhi 110 067. 403

P136. THE GENERAL PURPOSE SCATTERING CHAMBER AT THE NUCLEAR SCIENCE CENTRE, N.G.Puttaswamy, N.M.Badiger and M.Raja Rao, Dept. of Phys., Bangalore University, Bangalore and D.K.Avasthi, A.Tripathi, D.Kabiraj and S.Venkataramanan, Nuclear Science Centre, New Delhi. 405

P137. TARGETS OF EXPENSIVE MATERIALS, Jaipal, D.K.Avasthi, S.Gargari, J.Zachrias, Nuclear Science Centre, New Delhi. 407

P138. DEVELOPMENT OF ETCHING AS A TECHNIQUE FOR NUCLEAR TARGETS, S.K.Pardha Saradhi, Md. Eqbal and D.N.Rawat, Variable Energy Cyclotron Centre,Calcutta. 409

P139. THE MAXIMUM ENERGIES FOR MAKING THIN NUCLEAR TARGETS BY ION BEAM DEPOSITION, Arvind Jain, Nuclear Physics Division, B.A.R.C., Bombay 400 085. 411

P140. CANBERRA TO IBM PC INTERFACE FOR DATA ACQUISITION, ANALYSIS, AND STORAGE, S.K.Pal, A.Bandyopadhyay and S.K.De, Variable Energy Cyclotron Centre, Calcutta. 413

P141. A CAMAC INTERFACE FOR SPECTROSCOPY ADCS, B.P.Ajith Kumar, S.Naithani and R.K.Bhowmik, Nuclear Science Centre, New Delhi. 415

P142. A MULTIPLICITY FILTER ARRAY FOR GAMMA RAY SPECTROSCOPY, S.Muralithar, G.O.Rodrigues, R.P.Singh, S.Venkatraman, S.Naithani and R.K.Bhowmik, Nuclear Science Centre, New Delhi. 417

P143. AN ANALYSIS PROGRAM FOR MULTI-DETECTOR ARRAY, R.K.Bhowmik, D.K.Goyal and S.Ghugre*, Nuclear Science Centre, New Delhi.*Student, Bombay University. 419

P144. EFFICIENCY DETERMINATION OF Si(Li) X-RAY DETECTOR IN THE ENERGY RANGE 1-20 KeV, L.C.Tribedi and P.N. Tandon, Tata Institute of Fundamental Research, Bombay 400 005. 421

P145. DETERMINATION OF CARBON ON SURFACE BY PROTON RESONANCE SCATTERING, J.V. Raman, Sanjiv Kumar, V.S. Raju, S.Gangadharan and S.Kailas*, AnalyticalChemistry Division, BARC, Bombay. *NPD, BARC, Bombay. 423

P146. NOVEL TECHNIQUES TO MEASURE ISOTOPE SHIFTS AND HYPERFINE STRUCTURE USING LASER SPECTROSCOPY, S.B.Dutta*, Cyclotron Institute, Texas A&M University; D.L.Clark, Eastman Kodak Research Company, Rochester; T.U. Kuehl, GSI, Darmstadt, Germany; G.D.Sprouse, SUNY, Stony Brook. *Present address: SUNY, Stony Brook. 425

P147. DETECTION OF ^{8}Be USING A SURFACE BARRIER DETECTOR TELESCOPE AND ITS DETECTION EFFICIENCY CALCULATION, Suresh Kumar, M.A.Eswaran, E.T.Mirgule, Nuclear Physics Division, BARC, Bombay. 427

P148. POSITION SENSITIVE GASEOUS DETECTOR FOR HIRA, M.C.Radhakrishna, M.Raja Rao, N.G.Puttaswamy, Dept. of Physics, Bangalore Univesity and D.O.Kataria, A.Roy and A.K.Sinha, Nuclear Science Centre, N.Delhi. 429

P149. PERFORMANCE CHARACTERISTICS OF LARGE AREA POSITION SENSITIVE IONISATION CHAMBER, S.R.S.Murthy, V.S.Ambekar, D.C.Biswas, B.V.Dinesh, L.M.Pant and R.K.Choudhury, Nuclear Phys. Divn., BARC, Bombay. 431

P150. SIMULATION OF ATTENUATION EFFECTS IN THE SAMPLE, N.L.Singh and B.J. Patel, Physics Department, M.S.U., Baroda 390 002. 433

P151. NUCLEAR INSTRUMENTATION FOR RAPID GRADATION OF COAL SEAMS BY NEUTRON TECHNIQUE, N.Raja Sekhar, S.V.S. Ramana Reddy, J.Ramachander Rao, M.Panduranga Rao, A.Venkatappaiah+ and Devaprathap+, Regional Engineering College, Warangal 506 004. *Exploration Division, Singareni Colleries Co.Ltd., Kothagudem. 435

P152. CONTINUOUS SLOWING DOWN APPROXIMATION RANGE OF LOW ENERGY ELECTRONS IN MATTER, Manoranjan Agrawal, Km. Sarita, P.B.Pal*, D.K.Gupta and V.P.Varshney, Dept. of Physics, S.V.College, Aligarh. *Dept. of Physics, Ganjdundwara College, Etah, U.P. 437

P153. CONTINUOUS SLOWING DOWN APPROXIMATION RANGE OF POSITRONS IN THE ENERGY REGION 10-900 KeV, Manoranjan Agrawal, P.B.Pal*, D.K.Gupta and V.P.Varshney, Physics Department, S.V. College, Aligarh. * Dept. of Physics, Ganjdundwara College, Etah, U.P. 439

P154. AN EMPIRICAL STOPPING POWER EXPRESSION FOR 1-4 MeV LITHIUM IONS, Sarita, Manoranjan, P.B.Pal* and V.P.Varshney, Dept. of Physics, S.V.College, Aligarh. *Dept. of Phys., Ganjdundwara College, Etah, U.P. 441

g) ACCELERATORS AND ACCELERATOR BASED INTERDISCIPLINARY RESEARCH

O68. ECR HEAVY ION SOURCE OF VEC, D.K.Bose, G.S.Taki, B.Dasgupta, R.B.Mitra and R.K.Bhandari, Variable Energy Cyclotron Centre, Calcutta. 443

O69. TESTING OF NSC BEAM PULSING SYSTEM, D.K.Avasthi, Vandana Jha, R.Joshi, D.Kanjilal, S.K.Datta, S.Chopra, M.M.Narayanan, A.Tripathi, L.Senapati and A.Mandal, Nuclear Science Centre, New Delhi. 445

O70. MODIFICATIONS INCORPORATED IN THE 16MV PELLETRON FOR BETTER PERFORMANCE, D.Kanjilal, S.Chopra and M.M.Narayanan, Nuclear Science Centre, New Delhi. 447

O71. LOW POWER RF TESTS ON THE RFQ ACCELERATOR, Kavitha Murthy, S.A.Mateen, V.T.Nimje, R.C.Sethi, Nuclear Phys. Divn., BARC, Bombay and S.V.Sadawarte, M.V.Pande, R.D.Luktuke, A.N.Garud, TP&PED, BARC. 449

O72. K-X RAY EMISSION FROM HIGHLY STRIPPED ^{32}S IONS CHANNELED ALONG <100> AXIS IN Si, Vandana Nanal, M.B. Kurup, P.N.Tandon and K.G.Prasad, T.I.F.R., Bombay. 451

O73. STUDY OF EXCITATION FUNCTION AND TRANSITION PROBABILITIES IN Ar IONS, Tapan Nandi, M.B.Kurup and K.G.Prasad, T.I.F.R., Bombay and P.Saraswati, G.Krishnamurthy, P.M.R.Rao and A.P.Mishra, Bhabha Atomic Research Centre, Bombay. 453

O74. K-SHELL VACANCIES AT 25 MeV OXYGEN IONS INSIDE Ti, Fe, Ni AND Gd HOSTS, L.C.Tribedi, R.G.Pillay, K.G.Prasad and P.N.Tandon, T.I.F.R., Bombay 400 005. 455

O75. CHARGE STATE AND TARGET THICKNESS DEPENDENCE OF PROJECTILE X-RAYS FROM 120 MeV $^{32}S^{q+}$ IONS INCIDENT ON C TARGETS, L.C.Tribedi, K.G.Prasad, P.N.Tandon, Tata Institute of Fundamental Research, Bombay 400 005. 457

P155. ENHANCED FOCUSING IN CYCLOTRONS BY RADIAL AND AZIMUTHAL VARIATION IN MAGNETIC FIELD, P.R.Sarma, Variable Energy Cyclotron Centre, Calcutta 700 064. 459

P156. AN ANALYTICAL STUDY OF BEAM TRANSMISSION THROUGH HOLE LENS OF VEC MAGNET, Jane Alam, V.S.Pandit and P.R.Sarma, Variable Energy Cyclotron Centre, Calcutta 461

P157. PC BASED ACCELERATOR CONTROL SYSTEM, B.P.Ajith Kumar, J.Kannaiyan, D.Kanjilal and R.K.Bhowmik, Nuclear Science Centre, New Delhi. 463

P158. DESIGN OF HIGH RESOLUTION LINES FOR VECC, C.Mallik, N.K.Mukhopadhyaya, B.B.Bhattacharya, Variable Energy Cyclotron Centre, Calcutta. 465

P159. DEVELOPMENT OF AXIAL INJECTION SYSTEM AT VECC, G.Pal, C.Mallik, M.H.Rashid, J.Alam, G.S.Taki, D.K.Bose and R.K.Bhandari, VECC, Calcutta. 467

P160. DESIGN OF HIGH POWER DIRECTIONAL COUPLER, S.A.Mateen, Nuclear Physics Division, BARC, Bombay. 469

P161. RELATIVISTIC-QUANTUM PARTICLES FOR BOUND-STATES AND SCATTERED-STATES WAVE SOLUTIONS - SUITABLE FOR HIGH-ENERGY-PARTICLE-ACCELERATORS, J.N.Mohanty and C.B.Samantaray, P.G.Department of Physics, Ravenshaw College, Cuttack 753 003, Orissa. 471

P162. K-SHELL IONIZATION CROSS SECTIONS FOR LOW Z ELEMENTS ($1 \leq Z \leq 22$) BY PROTONS IN THE ENERGY RANGE 0.5 TO 2.5 MeV, L.C.Tribedi and P.N.Tandon, Tata Institute of Fundamental Research, Bombay 400 005. 473

P163. PROTON INDUCED K-IONIZATION CROSS SECTION MEASUREMENTS FOR LOW Z ELEMENTS USING A 400 KeV ION ACCELERATOR, L.C.Tribedi, M.B.Kurup, K.G.Prasad and P.N.Tandon, T.I.F.R., Bombay 400 005. 475

P164. EFFECT OF 100 MeV ^{16}O ION IMPLANTATION ON Pb-DOPED Bi-BASED SUPERCONDUCTORS, S.A.Agnihotry, R.H. Bhavalkar, S.Chandra, National Physical Laboratory, Dr.K.S.Krishanan Road, New Delhi and L.Senapati, D.Kanjilal, G.K.Mehta, Nuclear Science Centre, New Delhi. 477

P165. MEASUREMENT OF THE BREMSSTRAHLUNG RADIATION FROM ELECTRON-ATOM/MOLECULE COLLISIONS, R.Shanker, Atomic Physics Lab., Dept. of Physics, BHU, Varanasi and R.Hippler, Fakultaet fur Physik, Universitat Bielefeld, Germany. 479

P166. MEASUREMENT OF ARGON-RECOIL ION CHARGE STATE DISTRIBUTIONS IN 60-70 MeV $O^{5+,6+}$-Ar COLLISIONS, M.J.Singh, S.K.Goel and R.Shanker, Atomic Physics Lab., Physics Dept., Banaras Hindu Univ., Varanasi, D.O. Kataria, N. Madhavan and A.K. Sinha, Nuclear Science Centre, New Delhi. 481

P167. MICROTRONS AND THEIR APPLICATIONS, H.C.Soni and S.S.Ramamurthi, Centre for Advanced Technology, Indore 452 013. 483

P168 CHARACTERISTICS OF INDUS-1 AND INDUS-2, G.Singh and S.S.Ramamurthi, Centre for Advanced Technology, Indore 452 013. 485

P169. MAGNET FABRICATION TECHNIQUES, S.S. Prabhu, A.M. Puntambekar, K. Sreeramulu, K.A. Hussain and S.S. Ramamurthi, Accelerator Programme, CAT, Indore 487

P170. A COMPACT VERSATILE MAGNETIC BEAM STEERER FOR NSC PELLETRON, G.O.Rodrigues and A.Mandal, Nuclear Science Centre, New Delhi. 489

P171. MOLECULAR BEAMS AND ISOTOPIC BEAMS USING THE NSC 16MV PELLETRON, I.S.Iyer and D.Kanjilal, Nuclear Science Centre, New Delhi 1110 067. 491

P172. MULTIELEMENTAL ANALYSIS OF PANTNAGAR SOIL BY FAST NEUTRON ACTIVATION ANALYSIS, G.C.Joshi and H.M. Agarwal*, Dept.of Phys., G.B.Pant Univ., Pantnagar. 493

P173. HARDENING OF CHROMIUM FILMS BY HIGH ENERGY NICKEL ION IRRADIATION, Amitabh Jain and S.Loganathan I.I.T. Delhi and L.Senapati, Jaipal, D.Kanjilal and G.K.Mehta, Nuclear Science Centre, New Delhi. 495

P174. SURFACE BEHAVIOUR OF N_2^+ ION IMPLANTED AUSTENITIC 302 AND 310 STAINLESS STEELS, S.Aggarwal, A.K.Goel, R.K.Mohindra, P.K.Ghosh*, M.C.Bhatnagar+ and Ami Chand+, Physics Department, Kurukshetra University, Kurukshetra. *WRL, Dept. of Mech. & Indus. Engg., Univ. of Roorkee, Roorkee 247 664. +I.I.T., New Delhi 110 016. 497

P175. UHV FOR SYNCHROTRON RADIATION SOURCE - INDUS-1, M.G. Karmarkar and S.S.Ramamurthi, Centre for Advanced Technology, Indore. 499

P176. MAGNETIC FIELD ANALYSIS FOR SYNCHROTRON MAGNETS, S.P.Mhaskar, R.K.Mishra, R.S.Shinde, Sivakotaiah Y.R.C. Murthi, V.Tomar, Centre for Advanced Technology, Indore. 500

P177. ALPHA INDUCED K-SHELL X-RAY PRODUCTION CROSS-SECTIONS FOR SOME LOW Z ELEMENTS ($8 \leq Z \leq 31$), Anita Rani and N.Nath, Physics Department, Kurukshetra University, Kurukshetra 132 119. 501

INVITED TALKS AND SEMINARS

Heavy Ion Induced Fission and Dynamics of Nucleus-Nucleus Collisions

S.S. Kapoor
Bhabha Atomic Research Centre
Trombay, Bombay 400 085

Heavy ion induced fission and fission-like reactions evolve through a complex nuclear dynamics encountered in the medium energy nucleus-nucleus collisions. In the recent years, measurements of the fragment-neutron and fragment-charged particle angular correlations in heavy ion induced fusion-fission reactions, have provided new information on the dynamical times of nuclear deformations of the initial dinuclear complex to the fission saddle point and the scission point. From the studies of fragment angular distributions in heavy ion induced fission it has been possible to infer the relaxation times of the dinuclear complex in the K-degree of freedom and our recent measurements on the entrance channel dependence of fragment anisitropies have provided an experimental signature of the presence of fissions before K-equilibration. This paper will review recent experimental and theoretical status of the above studies with particular regard to the questions relating to dynamical times, nuclear dissipation and the effect of nuclear dissipation on the K-distributions at the fission saddle in completely equilibrated compound nucleus.

STABILITY OF NUCLEI LIMITED BY TEMPERATURE

J.N. De

Variable Energy Cyclotron Centre
1/AF, Bidhan Nagar, Calcutta-700 064

Hot nuclei are metastable, they release most of their energy by particle emission. Increasing excitation renders them unstable against violent release of energy showing that there is a limit to the temperature that hot nuclei can sustain. We examine these limits in dynamical and statistical model. For dynamics, we first explore the temperature (T) dependence of the interaction potential in the energy density formalism and find that the interaction barrier vanishes at $T \sim 7$ MeV depending on the interacting system. Closely colliding nuclei gain temperature due to nucleon transport (part of the transported nucleons are emitted as preequilibrium particles) and thus the system moves on a complicated dynamical temperature and mass dependent potential energy surface while evolving to a fused composite. Numerical calculations show that fusion cross section then vanishes at energies $E/A \sim 40$ MeV; a dynamical inhibition to the composite temperature beyond 6-7 MeV is thus obtained.[1]

In the statistical model, we assume the hot nuclear drop to be in equilibrium with its own vapour. The pressure and chemical potentials in the liquid and gas phase have then to be equal for stability. A system-dependent limiting temperature $T \sim 6$-8 MeV is then obtained, beyond which the stability criterion no longer holds. Assuming metastable equilibrium with zero pressure, the same limitations are found for normal nuclei. We exploit these ideas to explore the limits of β -stability with the added condition that for stability against nucleon dripping, the nucleon chemical potential must be negative; we then find that nuclei unstable against nucleon

dripping at low temperature may become stable at higher temperature.[2]

References

1. D. Bandyopadhyay, S.K. Samaddar, R. Saha and J.N. De ; Nucl. Phys. A (in press)

2. J.N. De, D. Bandyopadhyay, S.K. Samaddar, and N. Rudra ; Nucl. Phys. A (in press)

RESONANT BEHAVIOUR IN HEAVY ION NUCLEAR REACTIONS - NEW NUCLEAR STRUCTURE IN THE CONTINUUM

M.A. Eswaran
Nuclear Physics Division
Bhabha Atomic Research Centre
Bombay-400 085

The phenomenon of prominent intermediate-width resonances observed in the energy dependence of cross sections of heavy ion reactions at relatively high energies is at present a major line of development in nuclear physics. Experimental identification of these resonances are beset with the difficulty of differentiating them from the statistical fluctuations. Their first observation below the Coulomb barrier prompted models of nuclear molecules and alpha clustering. Later in intensive studies, they were proven to exist well above the barrier and to decay nonstatistically in the particle channels. In spite of intensive studies, this phenomenon is still not fully understood, although there is general agreement that these narrow resonances represent relatively stable highly clustered states in the compound system, indicative of nuclear structure effects in the region of excitation energy and angular momentum where it might have been suspected that all nuclear structure effects would have vanished.

In more recent years, it was suggested that the resonances might be manifestations of shape-isomeric states of the system produced in the super-deformed second well in the potential energy surfaces. Specific experimental observations confirming this interesting surmise are of great interest in the current status of the field. Significant evidences for this from the literature as well as from our recent results on ^{28}Si in the experiments with the Pelletron accelerator will be presented in this talk.

CO-EXISTENCE OF SHAPES IN NUCLEI.

S.B.PATEL
University of Bombay, Vidyanagari, Bombay.

Recent strides in the gamma spectroscopy have revealed spectacular co-existence of shapes in nuclei. For example, transitional nuclei between the double closed shell, Z=64 and N=82 have several interesting properties. At spins below 40 ħ, there is known to be (1,2) a competition among several shapes. This is found to be due to small shifts in the particle alignment frequencies, which produces dramatic difference in band behaviour. For such "soft" nuclei even the neighbours (e.g. isotones) can show strikingly different band structure at high spins. A study of such nuclei using an array of Compton-suppressed Ge detectors leads to interesting physics: mechanism of nuclear shape change, extent to which different shapes co-exist and quenching of pairing correlations with increasing spin.

Some recent studies in the spherical region has revealed a collective behaviour for yrast states in these nuclei (3,4). Deformed, rotational like bands have been observed. Further the rotational inertia was found to remain constant at higher spins, something which is characteristic of good rotors. Much interest is focussed on these aspects.

An axis ratio of 2 to 1 is recognised as corresponding to a Superdeformed shape. A global hunt is on to identify and study superdeformed shape exhibited by nuclei. Pairing forces play a paradoxical role in the description of superdeformed rotational bands (5).

References:
1.F.S.Stephens et al, Phys.Rev.Lett., 54(1985)2584
2.S.B.Patel et al, Phys.Rev.Lett., 57(1986)62
3.D.A.Viggars et al, Phys.Rev.C, 36,3(1987)1006
4.H.Harada et al, Phys.Rev.C, 39,1(1989)132
5.R.R.Chasman, Phys.Lett.B, 242,3(1990)317

NEUTRON EMISSION AS A PROBE OF FISSION DYNAMICS

H. Rossner

H.M.I., Berlin

IS NUCLEON DEFORMED ?

AFSAR ABBAS

Institute of Physics

Bhubaneswar 751005

The surprising answer to the question in the title is : YES ! The evidence comes from a study of the quark model of the single nucleon and when it is found in a nucleus.

It turns out that many of the long standing problems of the Naive Quark Model are taken care of if the nucleon is assumed to be deformed. Only one value of the parameter $P_D \sim 1/4$ (which specifies deformation) fits g_A (the axial vector coupling constant) for all the semileptonic decays of baryons, the F/D ratio, the pion-nucleon-delta coupling constant $f_{\pi N\Delta}$, the double delta coupling constant[1] $f_{\pi\Delta\Delta}$, the M1 transition moment $\mu_{\Delta N}$ and g_1^p the spin structure function of proton[2]. All this gives strong hint that both neutron and protron are deformed. It is important to look for further signatures of this deformation.

When this deformed nucleon finds itself in a nuclear medium its deformation decreases. So much so that in a heavy nucleus the nucleons are actually spherical. We look into the Gamow-Teller strengths, magnetic moments and magnetic transition strengths in nuclei to study this property[3].

1) A.Abbas, Bhubaneswar Preprint, IP/BBSR/91-28.

2) A.Abbas, J. Phys. **G15** (1989) L195.

3) A.Abbas, Phys. Rev. **C36** (1987) R1663.

LEPTODERMOUS EXPANSION STUDIES IN FINITE NUCLEI

Ramesh C.Nayak

Department of Physics,Khallikote College,Berhampur-760001.

Abstract

The use of Leptodermous Expansion (LDE) technique for the study of ground state properties of nuclei has been going on for the last few decades. Here in the present talk the origin and developement of this technique will be reviewed with particular emphasis on how and why this has been applied in nuclear physics in understanding various physical properties of nuclei like binding energy, density distribution, size, shape and radii, and also deformation properties etc. .The relevant techniques, their shortcomings and eventual improvements for understanding these properties in the above model will be discussed.

Particular reference will be made as to how this LDE technique can be used to obtain finite nucleus incompressibility in terms of an anlytical expression involving standard parameters of the nucleus. This expansion involves certain coefficients whose method of calculation will be discussed. This indirectly helps in determining the nuclear matter incompressibility whose value still remains undetermined to a precise extent. Results obtained in this regard in the context of the present model will be finally discussed and compared with those avaialable in other methods.

Theoretical Description
of
Giant Resonances in Hot Rotating Nuclei

P. Ring

Physik Department, Technische Universität München
D-8046 Garching, Federal Republic of Germany

Present theoretical descriptions of the giant resonances in hot rotating nuclei are reviewed. Mean field theory is used as a basis for the description of the hot compound states. Starting from the static solution at finite temperature and with fixed angular momentum small amplitude collective vibrations are calculated in the frame work of finite temperature random phase approximation for quasi-particles. The effect of pairing at low temperatures as well as the effect of rotations on the position of the resonance maxima are investigated. Microscopic and phenomenological descriptions of the damping mechanisms are reviewed. In particular it turns out that fluctuations play an important role in our understanding of the behaviour of the width as a function of the temperature. Motional narrowing is critically discussed.

CROSS-SECTIONS AND AVERAGE ANGULAR MOMENTA IN FUSION REACTIONS NEAR THE COLUOMB BARRIER

M. Dasgupta
Tata Institute of Fundamental Research, Homi Bhabha Road,
Colaba, Bombay 400 005

In recent years there has been an increasing interest in the study of heavy ion collisions near the Coulomb barrier. This has been triggered mainly by the observations of enhancements by factors of about one to two order of magnitude in sub-Coulomb barrier fusion (SBF) cross-sections between medium mass nuclei, as compared to predictions based on one-dimensional barrier penetration model (1-d BPM). Though, a considerable amount of work both theoretical and experimental has been done in this field, a complete understanding of the SBF phenomenon has not yet been achieved.

The relation between fusion excitation function and angular momentum (ℓ) distribution in SBF reactions is a topic of current interest. It is believed that ℓ-distributions provide a more stringent test of SBF models that the excitation functions alone. Simultaneous measurement of ℓ-distribution (or its moments) and fusion excitation function is expected to lead to a better understanding of the relationship between these two qualities. Such information has been obtained in experiments done by our group at BARC-TIFR Pelletron accelerator facility. In the present talk the measurement of fusion cross-sections and the method of determination of average ℓ from partial evaporation residue cross-section will be elaborated. An analysis of the experimental data on the basis of some of the SBF models will be discussed briefly.

L-DEPENDENT NUCLEAR POTENTIAL FOR HEAVY ION FUSION.

A. K. Mohanty
Nuclear Physics Division, BARC, Bom bay-400085.

The most salient features found in the fusion of heavy ion systems are the enhanced sub-barrier fusion and the broadening of the compound nucleus spin distribution around the coulomb barrier which seems to be closely related. Originally it was considered adequate to describe the fusion by penetration of one dimensional potential barrier. In this picture, the potential is considered as a function of the distance between the nuclei where the shape of the reaction partners is assumed to be spherical. However, the substantial enhancement of measured sub-barrier cross sections was found not to be compatible with the predictions of this one dimensional model. The efforts then concentrated on an examination of effects which could influence the nucleus-nucleus potential. The understanding of sub-barrier fusion enhancement was improved by including the influence of orientation of statically deformed reaction partners and of zero point shape fluctuations on the height of potential barrier. In a more general microscopic description sub-barrier enhancement can be explained by including the coupling to the inelastic excitations and also by considering the effect of transfer channel. This becomes cumbersome and impractical if there are a large number of contributing channels. Alternatively, macroscopic model with inclusion of neck degree of freedom can be used which can be thought of treating transfer and inelastic coupling in an average way. It is shown that [1], inclusion of neck dergee of freedom provides an

alternate path for fusion. This effect can be incorporated in the standard one dimensional barrier penetration model (BPM) by replacing the s-wave barrier height with an effective barrier height which depends on bombarding energy. However, to simulate the dynamical effect of channel coupling by BPM model i.e. to explain fusion enhancement as well as broad spin distribution, the effective barrier height should depend on both energy and angular momentum l [2]. The nuclear potential used in BPM model is the real part of the complex nuclear potential used in optical model analysis. The energy and l dependence of real potential suggests that the imaginary potential should also depend on both energy and angular momentum. The l-dependent imaginary potential has been used [3] to obtain fusion cross section from reaction cross section derived from elastic scattering analysis.

In this talk, I will give a brief description of the macroscopic model of nuclear shape evolution, when applied to sub-barrier fusion results in an energy dependent barrier height. To reproduce the spin distribution, in addition to this energy dependence, the need to have the l-dependent real as well as l-dependent imaginary potential will also be discussed.

1.V. S. Ramamurthy et al. Phys. Rev. C41 (1990) 2702
2.A. K. Mohanty et. al Phys. Rev. Lett. 65 (1990) 1096.
3. A. K. Mohanty et. al. Phys. Lett. 247B (1990) 215.

Deep inelastic collisions at near barrier energies and search for cold donor-fragment production.

Mihir B. Chatterjee
Saha Institute of Nuclear Physics, Calcutta-700064.

Deep inelastic collisions in the near barrier energies of the mass asymmetric systems are of importance since controversial results on energy partition are being reported. Energy dissipation and the partition of dissipated energy among the reaction partners are of interest. Search for cold donor-fragment production at near barrier energies were carried out on a mass asymmetric system like Ni + Pb.

Schwinger's Mechanism of Quark-Gluon Plasma Production in Ultra-relativistic Heavy Ion Collision

Warke C.S.

Tata Institute of Fundamental Research, Homi Bhabha Road, Bombay 400 005

ABSTRACT

The ultra-relativistic heavy ion experiments are aimed at observing a new state of hadron matter called quark-gluon plasma (QGP). Various different steps are involved between the nuclear collision process, QGP production and experimentally observed final results. These steps span over the whole range of QGP life history starting from its birth. In this talk, a mechanism of convertion of projectile energy into the production of this new state of matter is discussed.

Schwinger's mechanism of pair production through breakdown of constant electric field is summarized. A new theoretical framework is developed to include confinement and finite spatial dimension effects on pair creation through this mechanism. Its relevance to QGP formation in ultra-relativistic heavy ion collision is pointed out. The qualitative predictions of the theory are compared and contrasted with the others published in the literature.

DECONFINEMENT AND NUCLEAR COLLISIONS

NATARAJA SARMA

Bhabha Atomic Research Centre, Bombay 400 085, INDIA

ABSTRACT

Expensive experiments to detect a deconfined parton phase have been done and are being planned. In these experiments it is hoped that nuclear collisions at relativistic energies will exhibit signals of this new phase. So far all the results may be interpreted in terms of independent nucleon-nucleon interactions. These elementary collisions at very high energies are therefore worth examination since each such collision produces a highly excited entity which emits a large number of hadrons. In the hadronic phase this results in the GS multiplicity distribution. In the parton phase, parton branching results in the popular negative binomial distribution. Though neither the GS nor the NB distribution alone agrees with the data beyond 200 GeV, it is fitted exceedingly well by a weighted sum of the two distributions. Since the negative binomial distribution arises from the branching of partons, we interpret the increase with energy of the negative binomial component in the weighted sum as the onset of a deconfined phase. The rising cross section for the negative binomial component parallels very closely the inclusive cross section for hadron jets which is also considered a consequence of parton branching. The consequences of this picture to nuclear collisions is discussed.

EXPERIMENTAL ATTEMPTS TO DETECT QGP

Y.P. Viyogi
Variable Energy Cyclotron Centre
1/AF Bidhan Nagar, Calcutta 700 064.

Experiments at the CERN SPS; Brookhaven AGS and Fermilab are in progress to study the reaction mechanism in ultra-relativistic N-N and A-A collisions. Some of the proposed signatures of the Quark-Gluon Plasma, e.g. J/ψ suppression, strangeness enhancement etc. have been detected in these experiments but these are not unambiguous. The present results with various experiments will be discussed in detail. Current efforts for the next generation of experiments with truly heavy ions at SPS and AGS will be highlighted. Plans for experiments with RHIC and LHC colliders will be briefly described.

QGP IN COSMOLOGY

P. R. SUBRAMANIAN
Department of Nuclear Physics, University of Madras,
Guindy Campus, Madras 600 025.

The Physics of Quark-Gluon Plasma is a new emerging branch of particle physics, closely connected with nuclear physics, astrophysics and cosmology. In Nature this form of matter has probably existed during the early phases of the Universe and possibly exists even today in some very special form, such as dark matter and strange quark matter in the interior of neutron stars. Cosmology needs a proper candidate to explain theoretically the existence of invisible matter in the Universe. In connection with missing mass and primordial nucleosynthesis, the early Universe quark - hadron phase transition leads to interesting cosmological consequences via the ratio of baryon number densities, R, between the QGP and HRG phases. Treating the QGP phase as a system of interacting relativistic massless particles and by adjusting the QCD scale parameter, we can reduce the value of R in our model with admissible values of the bag constant B. This low value of R at low phase transition temperature or B may be useful to reproduce the light element abundances and to explain the existence of the dark matter in the Universe. The inclusion of the Hagedorn's pressure ensemble correction in the HRG phase and its effect on R has been studied. The end of the QGP era and the beginning of the hadronic era can be calculated using the cosmic quark - hadron phase transition. The early history of a Friedmann Universe can be reconstructed. We conclude that the non-standard big bang theory can explain both PNS and dark matter problems, using the results of the early Universe phase transition from QGP to hadronic phase. Possibility of the formation of strange quark matter will be discussed briefly.

CONTRIBUTED PAPERS

a. NUCLEAR STRUCTURE, MODES OF EXCITATION AND RADIOACTIVITY.

BAND STRUCTURE IN ^{64}Ge

R.Sahu
Physics Department, Berhampur University,
Berhampur-760007,India
and
S.P.Pandya
Physical Research Laboratory, Ahmedabad-380009, India

The N=Z nuclei in the mass region A=60-80 are of special interest since they lie far away from the valley of stability.Shell effects occur simultaneously for both protons and neutrons in these nuclei and play an important role in the understanding of nuclear structure.

Recently Ennis et al.[1] have observed in the self conjugate nucleus 64Ge a ground band extending upto $J=8^+$, a quasi-gamma band and a negative parity K=3 band. We have applied our Deformed Configuration Mixing shell model to the various bands of this nucleus.

We take ^{56}Ni as the inert core and orbits $1p_{3/2}$, $0f_{5/2}$, $1p_{1/2}$ and $0g_{9/2}$ as active configuration space .The spherical energies for these orbits are taken to be 0.0, 0.78, 1.08 and 3.5 MeV, respectively. As in our earlier calculations, we use a modified Kuo interaction. Our theoretical approach is described in ref. [2].

The lowest energy prolate and oblate HF solutions are almost degenerate, the oblate solution being lower by about 0.7 MeV. By making particle-hole excitations, we obtain six lowlying excited intrinsic states. Three of these have $K=0^+$, two have $K=2^+$ and one has $K=4^+$. Since g9/2 orbits lie more than 2.5 MeV higher, they are not expected to contribute to the lowlying positive parity bands. Good angular momentum states are projected from each of these eight intrinsic states and a band mixing calculation is performed to obtain bands of positive parity states.For describing the negative parity band, we make 1p1h excitations to the g9/2 orbit from the lowest prolate and oblate solutions and then perform a tagged HF calculation. We have considered 10 such excited intrinsic states. Of these eight have $K=1^-$ and two have $K=3^-$. Good angular momentum states are projected from each of these intrinsic states and then a band mixing calculation is performed.

The calculated $K=0^+$ ground band agrees quite well with experiment. Except for the $2^+ \text{---} > 0^+$ seperation, the relative

spacing of all the other levels are well reproduced. Our HF approach underestimates the pairing effects. A proper treatment of pairing (as in HFB) would have depressed the lowest 0^+ level somewhat, bringing the $2^+ \rightarrow 0^+$ separation in better agreement with experiment.An analysis of the wave functions of these states shows that there is a good mixing between the prolate and oblate solutions for J=0, 2 and 4. However as we go to higher angular momentum states, the contribution of the oblate solution decreases whereas the $K=2^+$ states and the $K=4^+$ state contribute substantially as J increases. Thus for J > 0 states, there is considerable K-mixing. Ennis et al. [1] have calculated the Total Routhian Surfaces based on the Woods-Saxon cranking model with pairing. Their calculation revealed large triaxiality for this nucleus. We consider only axial symmetric HF states. Hence we can not directly comment regarding the triaxiality of the nucleus. Since there is considerable K-mixing as we go to higher spins, in a way, this suggests that this nucleus is triaxial.

We are able to reproduce the ordering of the $K=2^+$ levels. The wave functions of the low J states have $K=2^+$ as the dominant component. However, there is considerable K-mixing for higher spin states.

Ennis et al. [1] have observed a negative parity band which extends upto $J=13^-$ level. They interprete the 3^- level to be an octupole vibration state. They have also suggested that the structure of this level is different from that of the other negative parity levels, because of very small observed $B(E2,5^- \rightarrow 3^-)$. The 3^- level also decays by E1 transition to the ground band which is forbidden in the absence of isospin mixing. In our calculation all the negative parity levels have a similar structure as they all belong to a $K=1^-$ band predominantly. The energies of the 5^-, 7^-, 9^-, 11^- and 13^- levels agree quite well with experiment. Our calculated 3^- level which is nearly degenerate with the 5^- level should not be compared with the observed 3^- level since we predict large $B(E2,5^- \rightarrow 3^-)$ transition contrary to experiment. Again the decay of 3^- level to the ground band by E1 transition is forbidden in our model. A slight change in the decoupling would make the 3^- level degenerate with or above the 5^- level. If this is so, then the experimentalists would not see this level. Within our model space, it would not be possible to consider octupole vibration states. Hence we can not say whether the observed $J=3^-$ level is a octupole vibration state or not.

[1] P.J.Ennis et al., to be published in Nucl. Phys. A
[2] A.K.Dhar et al. Nucl. Phys. A238(1975)340

IN BEAM SPECTROSCOPY OF ^{84}Y

S.Chattopadhyay, H.C.Jain, Y.K.Agarwal,
M.L.Jhingan and J.A.Sheikh
Tata Institute of Fundamental Research, Bombay-400005

Neutron deficient isotopes of Rb, Sr, Y and Zr with neutron numbers between 40 and 50 show complex interplay of single particle and collective excitations and provide vital information about the interaction of nucleons in the $2p_{1/2}$-$1g_{9/2}$ subshells. Recent spectroscopic studies showed the presence of ground state rotational band with strong deformation in ^{84}Zr with Z=40 and N=44, but low lying levels in ^{84}Sr with Z=38 and N=46 gave indication of only weak deformation in its ground state. The levels in ^{84}Y with Z=39 and N=45 have not been identified so far. In order to explore the dependence of the ground state properties of the mass 84 nuclei on neutron number, the levels in ^{84}Y have been populated through the $^{59}Co(^{28}Si,2pn)$ reaction using 98 MeV ^{28}Si beam obtained from the Pelletron accelerator at T.I.F.R, Bombay. The levels in ^{84}Y were identified initially by studying the excitation functions of the strongest γ-rays in the energy range of 88 to 110 MeV (see fig 1.) The γ-rays with 157 keV and 914 keV energies could not be identified with any of the known reaction channels. These γ-rays belonged to a reaction channel with a peak cross-section around 98 MeV. The position of the peak-cross-section and the shape of the excitation function curve agreed with the predictions of CASCADE calculation for $^{59}Co(^{28}Si,2pn)^{84}Y$ channel. The calculations also predict it to be the strongest channel around 100 MeV in agreement with the experimental observation.

The level scheme of ^{84}Y was built up through a measurement of γ-γ coincidence experiment performed with two different targets-a self-supporting 540μgm/cm^2 ^{59}Co and a 250μgm/cm^2 ^{59}Co evaporated on a 6mg/cm^2 thick gold backing. all together about 60 million coincidences were collected with 5-Compton suppressed HPGe detectors and gated with 2-fold γ-multiplicity measured with 8 NaI(Tl) detectors. Fig 2 shows coincidence spectra obtained with 157 keV and 914 keV gates using backed target. Fig 3 shows the partial level scheme of ^{84}Y as obtained from the present measurements. The lowest 157 keV transition was found to have $\Delta I=2$ character through angular distribution measurement. It was assumed to have a 8^+-6^+ assignment. The 10^+-8^+ assignment for this was ruled out because of the large expected separation between them due to change in seniority for the 8^+ and 10^+ levels. The

spins and parities of the higher excited states have been obtained through the angular distribution and the DCO measurements.

Radioactivity studies[1] indicate that ^{84}Y has a 5^- metastable state at ~ 500 keV with respect to the 1^+ ground state. The possible 6^+-5^- transition was not observed in the present experiment- perhaps because of its low energy. Indeed, shell model calculations[2] with $^{88}_{38}$Sr as the core and with effective interaction of nucleons in the $2p_{1/2}$-$1g_{9/2}$ subshells predict 5^- ground state which is nearly degenerate with 6^+ and 8^+ states in ^{84}Y. The experimental high spin states are in reasonable agreement with calculations provided the 6^+ states are matched. But, there is a discrepency since 1^+ is experimentally the ground state. Perhaps, this situation could be improved upon by including a larger configuration space in the shell model calculations.

References

/1/Nuclear Data Sheets 56 (1989) 561

/2/R.Gross and A.Frankel, Nucl.Phys.A267(1976)85

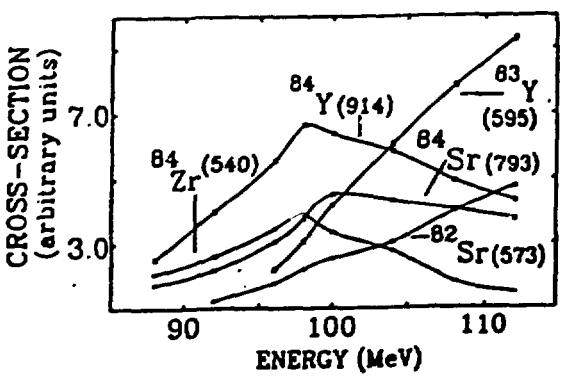

Fig.1 Excitation functions for ^{28}Si+^{59}Co

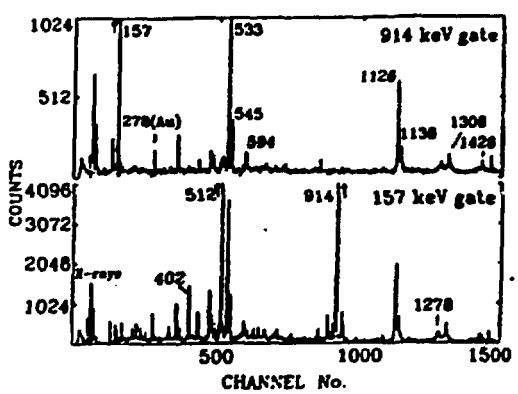

Fig.2 γ-γ coincidence spectra.

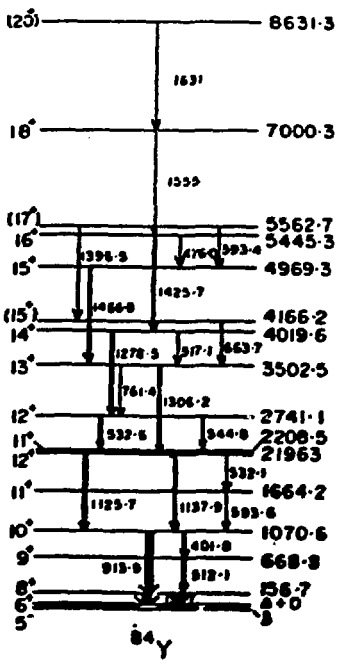

Fig.3 PARTIAL LEVEL SCHEME OF ^{84}Y

BAND STRUCTURE OF ^{123}I

Ranjana Goswami, B. Sethi, P. Banerjee
Saha Institute of Nuclear Physics, Calcutta;
and R. K. Chattopadhyay, A. M. College, Calcutta.

Two collective features observed systematically in odd-proton nuclei with $Z > 50$ are (i) occurrence of $\Delta J = 1$ band characterised by M1 cascade and E2 cross-over transitions, and (ii) $\Delta J = 2$ bands with level-spacings closely following those of the corresponding even-even cores. The levels of these bands are connected by stretched E2 transitions. The $\Delta J = 1$ band has been interpreted as a sequence of rotational states built on a low-lying deformed $g_{9/2}$ proton-hole state. The $\Delta J = 2$ bands, on the other hand, have been explained as arising from the coupling of the odd-proton to the collective motion of the core. In models based on alignment of the orbital angular momentum (j) of the odd-particle with the rotation of the even-even core, the $\Delta J = 2$ bands are predicted with spin-sequences j, j + 2, j + 4, ... (rotation-aligned or decoupled) and j + 1, j + 3, j + 5, ... (partially-aligned or unfavoured). These features have also been explained with fair success considering the coupling of the particle to the vibration of the core.

Experiment

The above mentioned features have been studied in ^{123}I by in-beam gamma-ray spectroscopy in the reaction ^{121}Sb (α, 2n γ) ^{123}I at E = 30 MeV. Gamma-gamma coincidence and gamma-ray angular distributions were measured using HPGe detectors. Experiments were carried out at VECC, Calcutta, using conventional electronics and Norsk Data 560 Computer System for on-line data acquisition.

Results and Discussion

Partial level scheme of ^{123}I based on the present work is shown in Fig. 1. New levels are marked with an asterisk (*). A previously reported uncertain level, but now established in the present work is marked by a triangle (Δ). A few more new levels and transitions observed in the present work are not shown in Fig. 1 due to the complexity of the decay scheme. The level sequences designated by (a), (b) and (c) are the decoupled $\Delta J = 2$ bands based on the $1h_{11/2}$, $2d_{5/2}$ and $1g_{7/2}$ quasi-proton states. The level sequences (d) and (e) have features of the 'unfavoured' bands mentioned above. The connecting transitions in these bands, including the new ones (with the exception of the $(17/2^+) \rightarrow 13/2^+$

transition in band (e) for which the multipolarity assignment was uncertain) are found to be quadrupole from angular distribution measurements. The level sequence (f) is the $\Delta J = 1$ band showing cascade of mixed (M1 + E2) and cross-over E2 transitions. The $J \rightarrow J - 1$ transitions in this band are found to have a positive E2 / M1 mixing ratio, in agreement with previous reports [1,2]. This implies a positive intrinsic quadrupole moment (Q_0) and hence prolate deformation for this band. New high spin member of this band with $J^{\pi} = 19/2^+$, observed in the present work is connected to the lower lying states by two new transitions (cascade and cross-over) as expected for this band. The $19/2^+ \rightarrow 17/2^+$ transition shows a small A_2/A_0 coefficient (close to zero) in its angular distribution. This result is consistent with a positive E2 / M1 mixing ratio and prolate deformation of the $g_{9/2}$ proton-hole state.

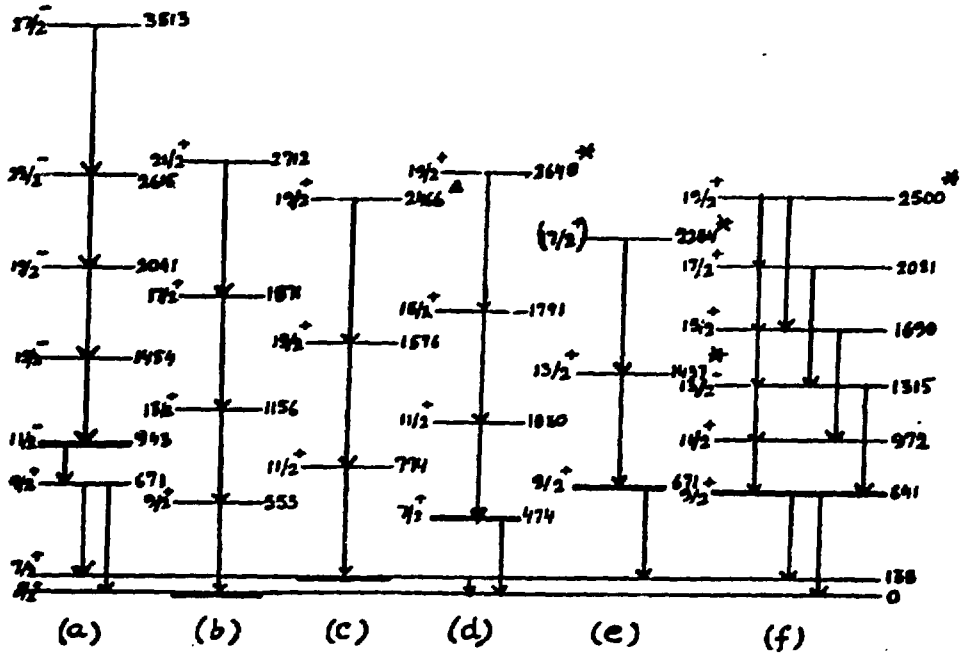

Fig. 1. Partial level scheme of ^{123}I. Band heads are shown by thick lines.

References

[1] U. Hagemann et al., Nucl. Phys. A289, 292 (1977)

[2] R. E. Shroy et al., Phys. Rev. C26, 1089 (1982)

BAND STRUCTURE AND SIGNATURE EFFECTS IN ODD-Z RARE-EARTH NUCLEI

A.K.Rath* and C.R.Praharaj**

*Physical Research Laboratory,Navarangapura,Ahmedabad-380009

** Institute of Physics,Bhubaneswar-751005

Using deformed Hartree Fock and angular momentum projection technique[1] we have studied the band structures and signature effects in ^{147}La,^{149}Pr and ^{151}Pm. For our axially deformed HF calculation we take one major shell each for protons and neutrons outside the ^{132}Sn core. Nilsson single particle energies and surface delta residual interaction are used in our calculation[4]. Angular momentum projected spectra for K=$5/2^-$,$5/2^+$,$3/2^+$ bands compare well with experiment (see Fig.1). The lowest $h_{11/2}$ proton rotational bands in ^{147}La and ^{149}Pr have K=$1/2^-$,$3/2^-$ respectively. In the $h_{11/2}$ proton rotational bands the α=-1/2 branch having more alignment (less collective rotation) is energetically lowered than the α=1/2 signature branch. The energy splitting is maximum for the K=$1/2^-$ band and reduces with increasing K . This is because the nucleon occupying the low Ω high j orbit gets maximally aligned[2] . The charecterstic behaviour of the E2 transitions connecting the two signature branches changes phase (signature inversion) with increasing occupation of the high j orbit. We get signature inversion for the K=$3/2^-$ band in ^{149}Pr(see Fig.2b). Analysis of the aligned angular momenta and the core rotation (see Fig.2a)shows that enhanced transitions are those for which the angular momentum change is in phase with the change in core rotation. Departure from this phase rule leads to signature inversion. It seems that occupation of the Ω=-1/2,3/2 states of the high j orbit inverts the signature dependence.

Signature inversion obtained by Matsuzaki [3] in ^{149}Pr is attributed to gamma vibration. However with axial symmetry we find inversions in the high j ($\pi h_{11/2}$ and $\nu i_{13/2}$ [4]) rotational bands. From our study it appears that signature effects are seen only in the bands based on high j or high j like nucleonic orbits and they represent a major departure from regular rotational behaviour but not that of triaxiality.

1. C.R.Praharaj J.Phys.G14(1988)843,Phys. Lett 119B(1982)17
2. F.S.Stephens Rev.Mod.Phys 47 (1975)43
3. M.Matsuzaki Nucl. Phys. A 491 (1989)133
4. A.K.Rath, Ph.D. Thesis, Utkal University Feb' 1991

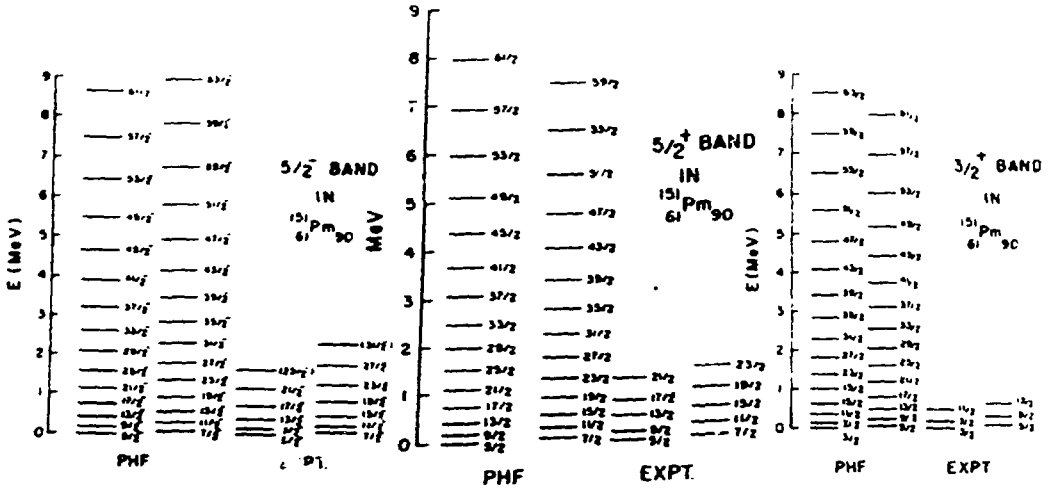

Fig.1 Angular momentum projected (PHF) band structure in ^{151}Pm. Data taken from Phys.lett B 247 (1990)238

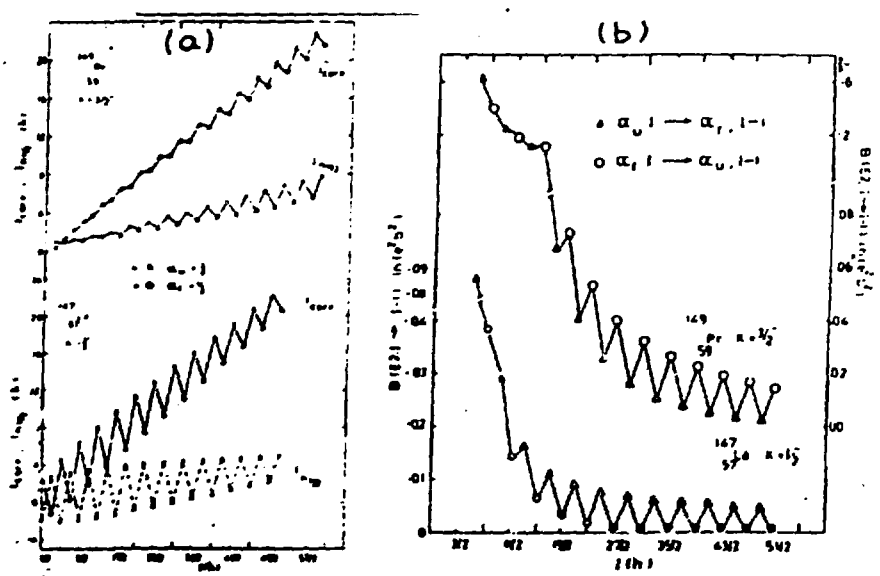

Fig.2: (a) Alignment ($I_{h11/2}$) and core angular momenta (I_{core}) for K=1/2⁻, 3/2⁻ bands of ^{147}La and ^{149}Pr nuclei respectively.(b) Signature dependence in B(E2;I— I-1) values for K=1/2⁻, 3/2⁻ bands of ^{147}La and ^{149}Pr nuclei respectively. b is barn.

HIGH SPIN SPECTROSCOPY OF ^{120}Xe

J.Goswamy, D.Mehta, B.Chand, A.Sharma, N.Singh
P.N.Trehan, Pragya Singh,* R.G. Pilley,* H.G.Devare*
and R.K.Bhowmik.**
Physics Department, Panjab University, Chandigarh
*Tata Institute of Fundamental Research, Bombay
**Nuclear Science Centre, New Delhi.

High spin states of ^{120}Xe were investigated with the $^{107}Ag(^{16}O,p2n)$ reaction. Enriched Ag-107 foil of thickness $\approx$ 1.2 mg/cm^2, rolled onto lead backing (thickness $\approx$ 10mg/cm^2), was used as target. ^{16}O beam of 80 MeV were provided by 14UD Pelletron accelerator at TIFR, Bombay. In the present measurements, five Compton suppressed HPGe detectors, placed in a planar configuration, and multiplicity filter of 8 large size NaI(Tl) detectors were used. A total of 24 million events were collected and sorted into 2k x 2k $E\gamma$-$E\gamma$ matrix after proper gain matching. The γ-ray coincidence relationships were estabilished by setting gates on the photopeaks of individual transitions and projecting the coincident spectra.

The level scheme of ^{120}Xe could be systematised into five bands. The analysis of the data is under process and tentative level scheme is shown in figure 1. The gamma-vibrational band, observed by Loewenich et al [1] alone, was clearly seen in the present analysis with the exception to ordering of few transitions. On the other hand the S-band observed by Rouabah et al [2] but not by Loewenich et al could be identified and characterised in the present analysis. Some of the transitions in the S- band and negative parity band have been corrected for their ordering.

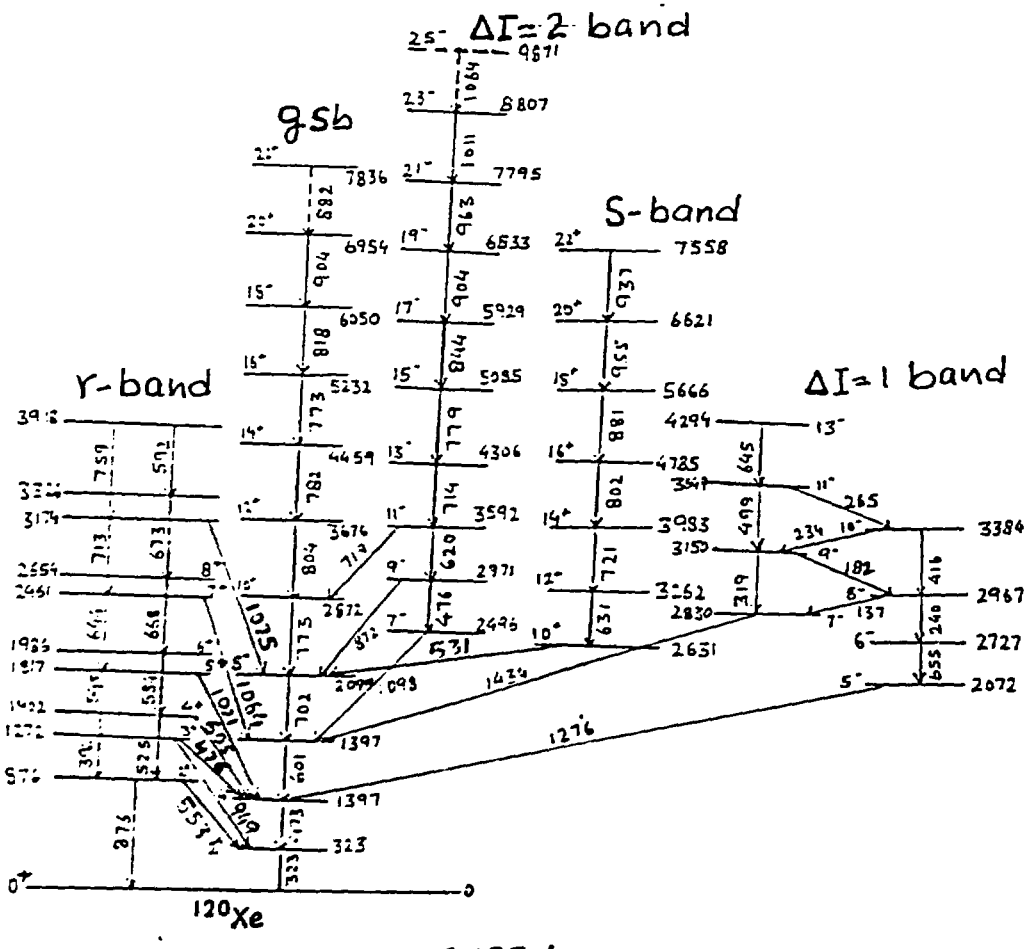

FIGURE 1

Similar experiment has been performed at NSC, Delhi using GDA set up. This data will be used to extend level scheme and to deduce DCO ratios.

Reference :

[1] K.Loewenich et al NPA 460, 361(1986).
[2] M.S.Rouabah et al Z.Phys. A 328, 493(1987).

STUDY OF Z=64 SUBSHELL GAP SIZE IN N=82 ISOTONES

J.B.Gupta
Ramjas College, University of Delhi, Delhi-110007

The low 3^- in ^{146}Gd and the resistance to deformation in Sm and Gd isotopes (N<88) with a drastic shape change at N=90 compared to Ba, Ce and Nd etc. are taken as the typical evidence for the existence of a subshell closure at Z=64 [1]. But a smooth variation in the single particle levels of N=82 isotones and their HFB calculations indicate a gap size of about 2 MeV or less at $d_{5/2}$ orbital from $h_{11/2}$ [2]. Nilsson used a gap of only 1.0 MeV as also adopted by Bohr-Mottelson [3] and Kumar-Baranger [4] in their DPPQ model calculation, as also adopted by other workers [5]. In a surface-Delta interaction study of ^{145}Eu ^{147}Tb, $^{145-147}$Gd, a ΔE_p=0.7 MeV was evaluated recently [6] with a sizable configuration mixing.

In this work we have studied the effect of gap size on the HFB calculation using the DPPQ method for the ^{136}Ba - ^{146}Gd isotones. For each nucleus we calculated the parameters of the Bohr collective Hamiltonian $H_c(V, B_k, \Theta_k)$ (,) for two values of ΔE_p =1.0 and 2.0 MeV. Then we solved H_c and determined appropriate values of the quadrupole strength and the core renormalization factor which reproduced the $E(2_1^+)$ state.

Using these parameters, we again solved the PPQ Hamiltonian for a fixed (=0, =30°) and determined the proton occupation numbers for the orbits above Z=40. Since the occupation number of $g_{9/2}$ orbit was always close to 10, we ignore this here. Then (Z-50) protons occupy the $g_{7/2}$, $d_{5/2}$ and ($h_{11/2}$, $s_{1/2}$, $d_{5/2}$) orbits. Our results are given in Table I, where these are compared with the results of experiment and of Andreozzi et al.[2], who used number conserving pairing method.

With increased energy gap, the occupation numbers of the lower two orbits rise by about one and that of the upper 3 orbits fall by the same amount in better agreement with experiment. But even with larger gap at Z=64 four protons out of 14

in ^{146}Gd occupy the upper orbits. In Ref. [2] a weaker pairing strength gave greater occupation of lower two orbits (Table 1). Our results indicate a sizable configuration mixing due to pairing interaction, in agreement with the results of Ref. [6], and the subshell effect even in N=82 isotones is weak. The 3^- state in N=82 isotones arises from the coupling of $h_{11/2}$ and $d_{5/2}$ orbits which lowers down with increasing protons [7] upto Gd, consistent with our results. Further we note that a much larger quadrupole strength had to be used for reproducing the energy spectrum when the larger gap at Z=64 is used. Thus a smaller gap seems to promote the collective effects more easily in the HFB calculations.

Table 1. Proton spectroscopic factors. Upper row for $g_{7/2} + d_{5/2}$ and lower for $h_{11/2}+d_{3/2}+s_{1/2}$.

Nucleus	PPQ-1	PPQ-2	Expt.	Andreozzi et al
Ba	4.15	4.71	5.Ø (5)	5.31
	1.85	1.28	1.Ø (3)	Ø.7Ø
Ce	5.42	6.17	7.4 (4)	7.ØØ
	2.54	1.76	Ø.6 (4)	Ø.99
Nd	6.61	7.55	8.3(4)	8.61
	3.29	2.32	1.7(5)	1.39
Sm	7.74	8.82	9.9(4)	1Ø.51
	4.12	3.ØØ	2.1(3)	1.48
Gd	8.78	9.93		12.Ø5
	5.Ø5	3.84		1.93

References

1. R.F. Casten, Rev. Mod. Phys. **62** (199Ø) 393
2. F. Andreozzi et al., Phys. Rev. **C41** (199Ø) 25Ø
3. A. Bohr and B.R. Mottelson, Nuclear Structure II (1975)
4. K. Kumar and M.Baranger, Nucl.Phys.**A11Ø**(1968)529
5. M. Saha and S. sen, Phys. Lett.**B252** (199Ø) 181
6. N. R. Walet et al., Zeit Phys. **A332** (1989) 9
7. P.D. Cottle et al. Phys. Rev. **C35** (1987) 1891

EVIDENCE OF ALTERNATING PARITY BANDS IN ^{151}Sm

J.M.Chatterjee, Somapriya Basu, K.Kar, D.Banik.
Saha Institute of Nuclear Physics, Calcutta.
R.K.Chattopadhyay, Ananda Mohan College, Calcutta.
R.P.Sharma, S.K.Pardhasaradhi, VECC, Calcutta.

The observation of the electric dipole transition in transitional nuclei in the actinide region are of great interest in recent years (1,2,3). The observed E1 transition is the manifestation of the intrinsic dipole moment which is interpreted as due to the occurence of the polarisation of the nucleus. In the light transitional nuclei viz. $^{148,150}Sm$. ^{148}Nd and ^{151}Pm, the E1 transitions connecting alternating parity bands were reported (4-6). Our aim was to search such transitions within rotational bands of alternating parity in the odd mass samarium nucleus.

The experiment was carried out at the VECC, Calcutta, via the $^{150}Nd(\alpha,3n\gamma)^{151}Sm$ reaction (enriched ^{150}Nd-96.6%) at E_α=37 MeV. Two large volume HpGe Gamma-X detectors were placed at 90° to the beam direction. A four parameter coincidence data (γ_1,γ_2. time-r.f.) were recorded in list mode on the Norsk Data 560 computer using conventional electronics for subsequent off-line analysis.

Fig.1 shows a partial level scheme of ^{151}Sm. Two bands of alternating parity which are connected by E1 transitions were observed for the first time. The simplex quantum number $s=-I$ can be assigned to the sequence $11/2^+$, $13/2^-$, $15/2^+$, $17/2^-$,.... By means of the I(I+1) rule from the two consecutive negative parity states belonging to the same simplex band, the energy difference δE between the observed level with positive parity and the interpolated level of the same spin but opposite parity in ^{151}Sm as a function of (I-Io) along with that of ^{150}Sm is shown in fig.2 (I, Io being the spin of the excited and g.s. level respectively). For ^{151}Sm investigated in the present work, δE decreases with increasing spin in the same way as it was observed in ^{150}Sm. At low spins the moment of inertia for the band of the opposite parity with respect to the g.s. is larger than its twin band. The spacings of the rotational states vary therefore differently which lead to the apparent decrease of δE.

The rotational properties of the bands of ^{151}Sm i.e. the rotational frequency ω, the ang. momentum I_x along the rotational axis and the effective moment of inertia $\mathcal{J}_{eff}$ were calculated from the energies of the states belonging to these bands using K=11/2 from ref. 7 for the n.p. band and assuming the same value for the positive parity band. The alignment of the nucleons gradually increases with spin, [Fig.3] for both the positive and negative parity bands. At $\hbar\omega$~0.3MeV,it appears that the curves meet, which may suggest a possible shape change of the nucleus [4].The difference of $\mathcal{J}_{eff}$ for the positive and neg. parity bands at lower frequency was interpreted in terms of the

potential energy surface and quadrupole-octupole deformation in ref.2 in the case of ^{221,223}Th . Moreover the experimental routhians E'(MeV)$_{exp}$ calculated for the positive and neg. parity bands shows a similar behaviour as the case of ^{221,223}Th (ref. 2). The existence of alternating parity band observed in the light transitional nuclei and the resemblance of the rotational parameters with those of ^{221,223}Th suggest that ^{151}Sm has an octupole shape at medium spin.

References

(1) W.Bonin *et al*, Z.Phys.,A322 (1986) 59
(2) M.Dahlinger *et al*, Nucl.Phys.,A484 (1988) 337 and refer. therein.
(3) M.E.Debray *et al* Phys. Rev.,C41 (1990) R1895
(4) W.Urban *et al*, Phys. Letts.,B185 (1987) 331
(5) W.J.Vermeer *et al* Phys. Rev.,C42 (1990) R1183
(6) W.Urban *et al* Phys. Letts.,B247 (1990) 238
(7) W.B.Cook *et al* Nucl. Phys.,A259 (1976) 461

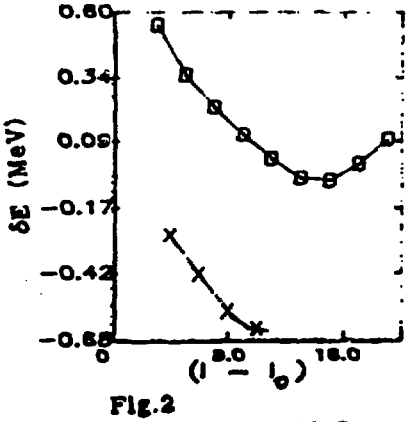

Fig.2

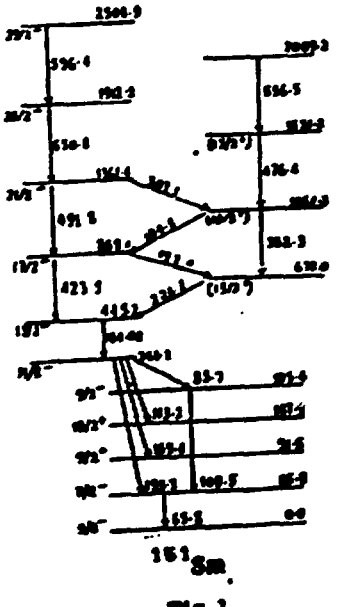

Fig.1

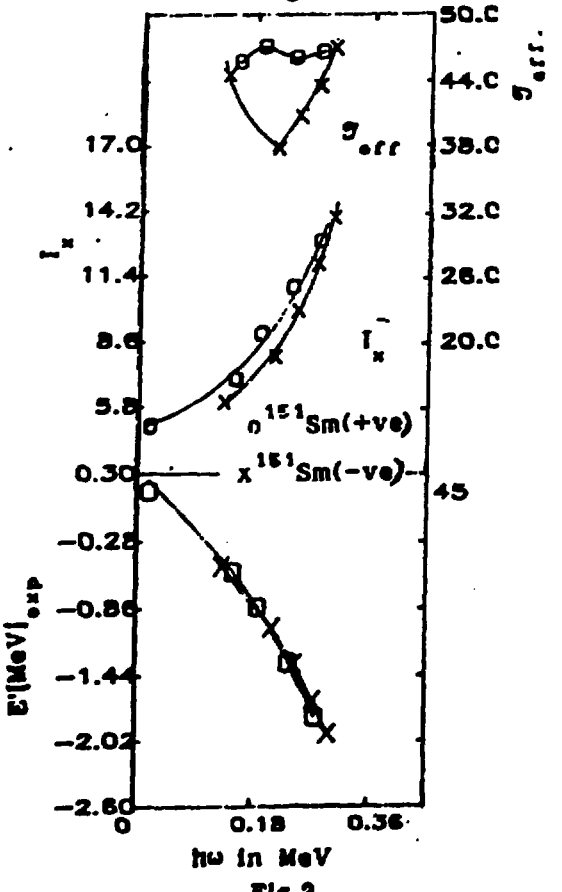

Fig.3

Fig.3 shows the change of I_x, $\mathcal{J}_{eff}$ and E'[MeV] vs. ang. freq.ω

E4 STRENGTH DISTRIBUTIONS IN ^{152,154}Sm : sdgIBM PREDICTIONS

Y.D. Devi and V.K.B. Kota
Physical Research Laboratory, Ahmedabad 380 009

In the past few years considerable amount of experimental data[1,2] on E4 matrix elements and strength distributions has started accumulating. One of the models well suited for the description of E4 data is the sdg Interacting boson model (sdgIBM or simply gIBM). Last year we reported[3] results of gIBM calculations for the various properties (energies, B(E2) and B(E4) values, g-factors, isomer and isotope shifts and two-nucleon transfer (TNT) strengths etc) of 0^+_1, 2^+_1 and 4^+_1 levels in $^{150-158}$Sm. In these calculations, which succinctly bring out the spherical-deformed phase transition, a simple hamiltonian $H = F\,\{\varepsilon_d n_d + \varepsilon_g n_g + \kappa\, Q^2\cdot Q^2\}$ where Q^2 is the gIBM SU(3) quadrupole operator, is employed. However this simple hamiltonian doesnot predict the β,γ band positions very well and with this we cannot reliably predict E4 distributions in Sm isotopes. Therefore we performed detailed spectroscopic calculations in sdg space for ^{152,154}Sm (only for these isotopes some E4 data is available) with the restriction $n_g \leq 2$ (n_g being the number of g bosons) and a hamiltonian that interpolates sdgIBM symmetries $SU_{sdg}(3)$, $SU_{sdg}(5)$, $SU_{sdg}(6)$ and $O_{sdg}(15)$. These calculations reproduce the ground (GS), β- and γ- band levels with r.m.s deviation 49 and 20 keV for ^{152}Sm and ^{154}Sm respectively; Ref. 4 gives the details. All the results obtained by using the simple hamiltonian given in Ref. 3 are kept intact. The ratio $\mathcal{R}$ of sum of the TNT cross-sections to excited 0^+ states to that of the GS 0^+ shows a peak at N=90 for (t,p) and N=88 for (p,t) data. The present calculations together with the ones given in Ref. 3 provide an excellent description of the peak in $\mathcal{R}$; see Fig. 1. Having thus established that we have good wave functions, $B(E4\uparrow) = B(E4;\ 0^+ \longrightarrow 4^+_i)$ are calculated for 4^+ levels below 3 MeV excitation in ^{152,154}Sm and the resulting E4 strength distributions are shown in Fig. 2 (the strength to 4^+_1 has to be multiplied by a factor 6 and 8 for ^{152}Sm and ^{154}Sm respectively). The operator Q^4_{osc} (obtained by taking r^2Y^4 matrix elements in sdg oscillator space),

$$Q^4_{osc;\mu} = e_4 \chi\left[(s^\dagger \tilde{g} + g^\dagger \tilde{s})^4_\mu + \frac{19\sqrt{5}}{28}(d^\dagger \tilde{d})^4_\mu - \frac{5\sqrt{11}}{14}(d^\dagger \tilde{g} + g^\dagger \tilde{d})^4_\mu + \frac{3\sqrt{143}}{28}(g^\dagger \tilde{g})^4_\mu\right]$$

is employed as the E4 transition operator. With $e_4 = 0.034$ eb^2, the observed $B(E4;\ 0^+_{gs} \longrightarrow 4^+_1)$ are predicted very well; the data values are 0.14 ± 0.02 and 0.22 ± 0.02 e^2b^4 and the calculated values are 0.16 and 0.20 e^2b^4 for ^{152}Sm and ^{154}Sm respectively. With the same e_4 effective charge the predicted values for $B(E4;\ 0^+_{gs} \longrightarrow 4^+_\gamma)$ are 0.014, 0.014 e^2b^4 for ^{152}Sm and ^{154}Sm and they are in excellent agreement with the B(IS4) data of Ichihara et al.[1] which gives 0.011 and 0.012 e^2b^4 respectively. With this agreement one is confident of the E4 strength distributions given in Fig. 2 and their experimental confirmation establishes that gIBM is a powerful tool in studying E4 properties of nuclei.

REFERENCES : 1. Ichihara et al, *Phys. Rev.* C36 (1987) 1754; 2. H.C. Wu et al. *Phys. Rev.* C38 (1988) 168; 3. Y.D.Devi and V.K.B.Kota *Sym. Nucl. Phys.* 33B (1990) 09; 4. Y.D.Devi *Ph. D Thesis*, (Submitted to Gujarat University, June 1991).

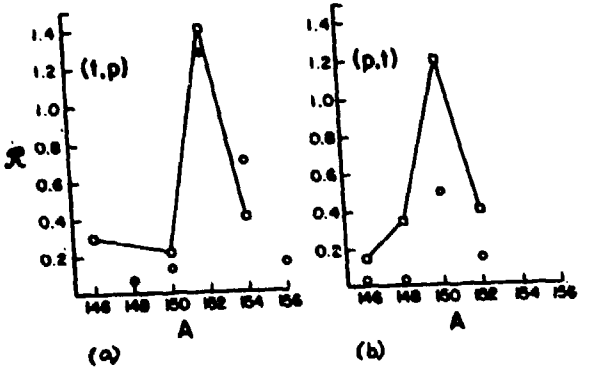

Fig. 1 Comparison of the ratio R of the sum of the cross-sections to the excited 0^+ states to that of the GS 0^+; (a) for (t,p), (b) for (p,t). The circles (O) are calculated values and boxes (□) are from experimental data (ref.4 and references therein). The ratio R is given for the final nucleus A. All the gIBM results (except for $^{152}Sm \rightleftarrows {}^{154}Sm$) are obtained using a simple two parameter interpolating hamiltonian of Ref. 3. For $^{152}Sm \rightleftarrows {}^{154}Sm$ the wave functions obtained by diagonalizing a more general gIBM hamiltonian (see text) are used.

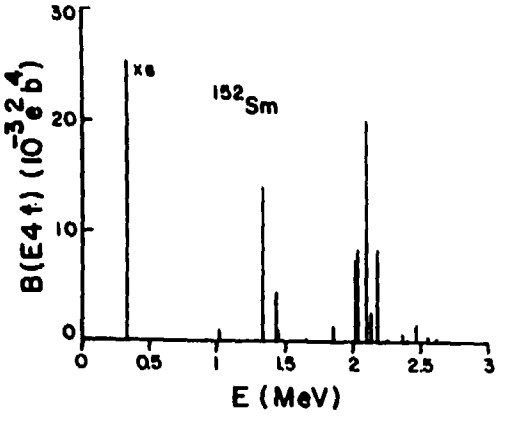

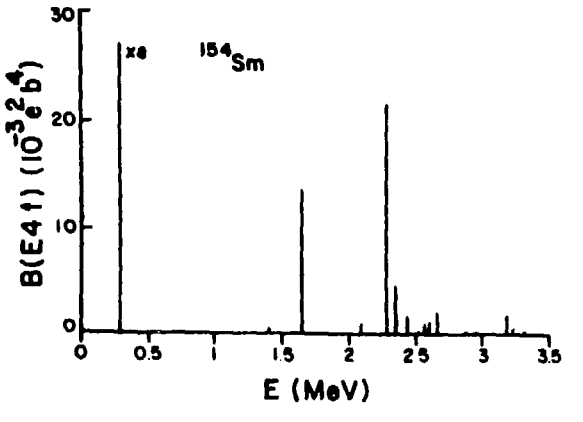

SIGNATURE INVERSION IN THE 4^- {5/2[532]$_p$⊗3/2[651]$_n$} BAND IN DOUBLY-ODD ^{152}Eu AND ^{156}Tb

Kiran Jain, A.K. Jain and Alpana Goel

Dept.of Physics,Univ.of Roorkee,Roorkee-247667,India

The phenomenon of signature inversion /1/ observed in the $K^\pi=4^-$ rotational band in ^{152}Eu and ^{156}Tb is studied in the framework of an axially symmetric two-quasiparticle-plus-rotor model/2/. The configuration assigned to this band is {5/2[532]$_p$⊗ 3/2[651]$_n$} where both are high-j unique parity orbitals. The favoured signature in doubly-odd rotational bands is given by

$$\alpha_F = 1/2(-1)^{j_p-1/2} + 1/2(-1)^{j_n-1/2}$$

which predicts that the even-spin members should be favoured in the $K^\pi=4^-$ band. An analysis of the experimental data in ^{152}Eu and ^{156}Tb suggests that the odd-spin members lie lower in energy in the low-spin region while the theoretically predicted favoured signature is restored in the high-spin region.

To understand the mechanism of the signature inversion, Coriolis coupling calculations with 26 rotational bands have been carried out. The one-quasiparticle configurations involved in the calculations are : Ω=1/2 to 5/2 of $i_{13/2}$-neutron orbital, Ω=1/2 to 7/2 of $h_{11/2}$-proton orbital and Ω=1/2 of $h_{9/2}$-proton orbital. The results of our calculations are shown in Fig.1 where the calculated and the experimental values are shown by solid and dashed lines respectively. We note that a [$h_{11/2}$, $i_{13/2}$] Coriolis coupling fails to reproduce the inversion unlike ^{160}Ho /3/ and, inclusion of $h_{9/2}$ proton orbital plays an important role. It is interesting to note that the $K^\pi=0^-$ (1/2[550]$_p$⊗1/2[660]$_n$) and $K^\pi=0^-$ (1/2[541]$_p$⊗1/2[660]$_n$) bands have opposite phase of staggering and are connected to the 4^- {5/2[532]$_p$⊗3/2[651]$_n$} band through multiple order of couplings. It appears that

the contrasting behaviour of the $K^{\pi}=0^{-}$ bands is being transmitted to the 4^{-} band giving rise to a signature inversion. The results are very sensitive to some of the <j+> matrix elements. Detailed results will be presented elsewhere.

The financial support from CSIR and DAE is gratefully acknowledged.

References:

/1/ I. Hamamoto, Phys. Lett. B235 (1990) 221.
/2/ A.K. Jain *et al.*, Phys. Rev. C40 (1989) 432.
/3/ A.K. Jain and A. Goel, Submitted.

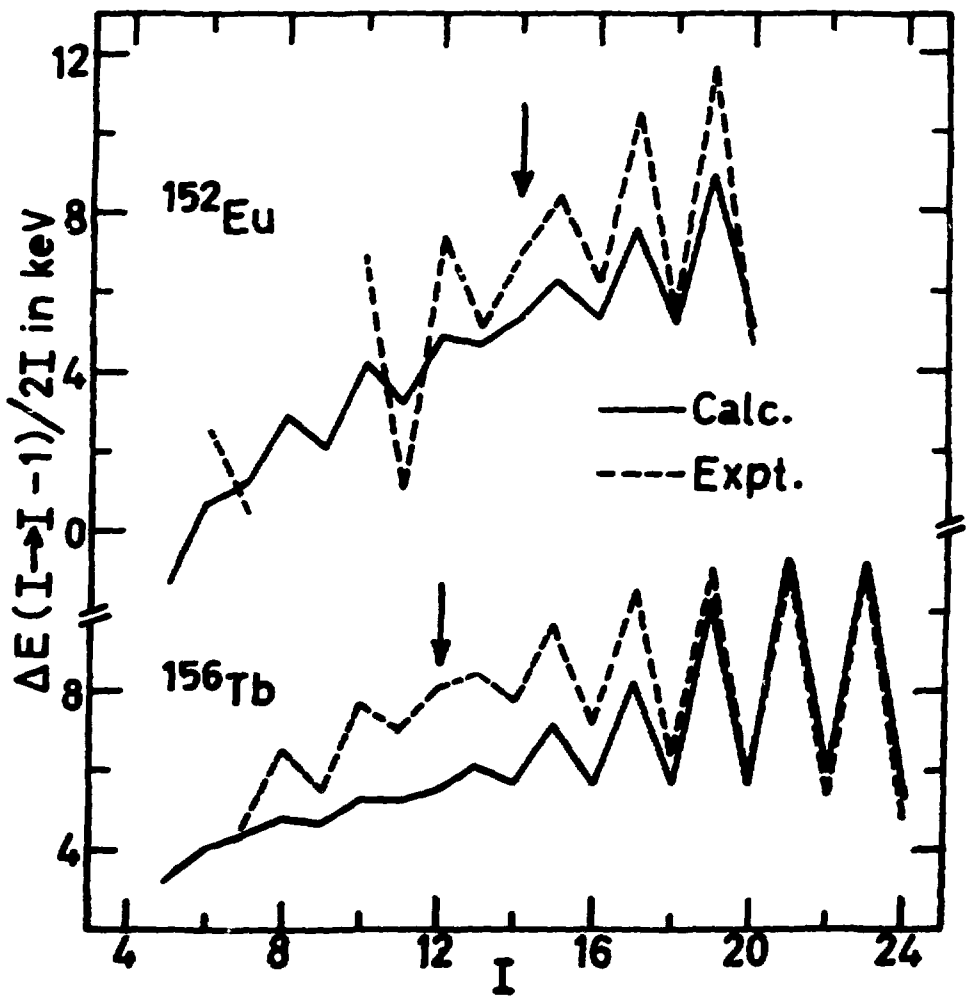

Fig. 1 : Odd-even staggering plots showing signature inversion. Arrows indicate the point of inversion.

TEMPERATURE DEPENDENT SHAPE TRANSITION IN ^{188}Os

A. Ansari and B. K. Agrawal
Institute Of Physics, Bhubaneswar-751005, India

The main structural features of rotational nuclei is more or less understood for the yrast states. Therefore, the interest is now shifting to the study of structure of hot rotating nuclei away from the yrast line where level densities are high.

In the present work we have performed a self-consistent temperature dependent Hartree-Fock-Bogoliubov(HFB) calculation[1] for ^{188}Os to study the effect of temperature on its intrinsic shape parameters. This nucleus has been studied in ref. 1 using a pairing plus quadrupole interaction Hamiltonian of Kumar and Baranger[2]. As elsewhere[3], we would like to point out here that in ref. 1 the set of spherical single particle(sp) energies used is not the correct one. A more appropriate set of sp energy for the Os-Pt region is given in ref. 4. The calculation carried out here is precisely like that in ref. 1 but with the spherical sp energies taken from ref. 4. As will be seen below this has significant consequences. The variation of quadrupole deformation parameter β and proton and neutron pairing gaps, Δ_p and Δ_n, respectively with temperature is displayed in the figure below. In ref. 1 the ground state (T=0) comes out to be triaxial with $\beta = 0.181$ and $\gamma = 22^o$. On the other hand, we get it axially symmetric with $\beta = 0.22$ and $\gamma = 0^o$. In ref. 1 the shape becomes oblate($\gamma = 60^o$) at T=0.6 MeV before becomig spherical at T=1.3 MeV, whereas in the present case it remains prolate throughout with the self-consistent value of γ becoming at most about 5° at T=1.5-1.6 MeV, till finally $\beta \rightarrow 0$. As usual pairing gaps vanish by $T \approx 0.4-0.6$ with a difference that for the lighter rare-earth nuclei Δ_n vanishes before Δ_p.

We would like to mention that our cranked HFB code is now modified to incorporate finite temperature($T \neq 0$) and calculations

for high-spin states are in progress. Our next plan is to include particle number projection and corrections for the $\beta-\gamma$ shape fluctuations.

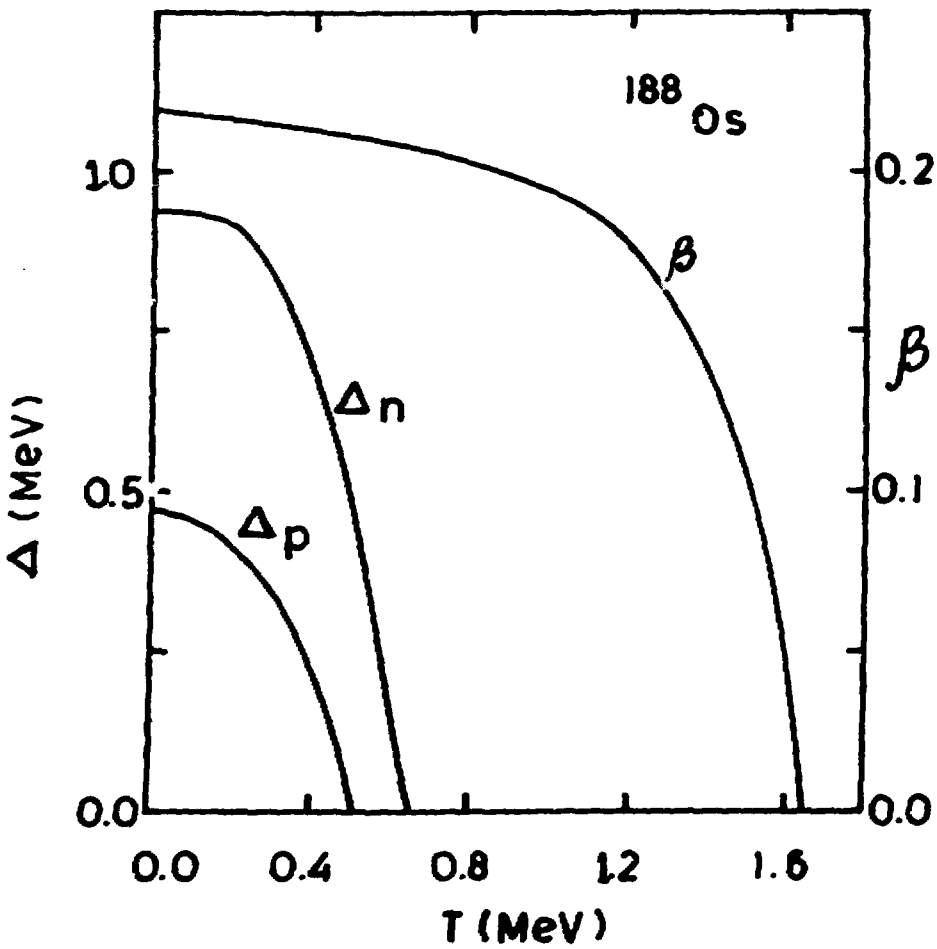

References

1. A. L. Goodman, Phys. Rev. C34 (1986) 1942
2. K. Kumar and M. Baranger, Nucl. Phys. A110 (1968) 529
3. A. Ansari, Phys. Rev. C38 (1988) 953
4. K. Kumar and M. Baranger, Nucl. Phys. A122 (1968) 273

THERMODYNAMICS OF SUPERFLUID NUCLEUS

M. Rajasekaran, D. Caleb Chanthi Raj & R. Premanand
Department of Nuclear Physics, University of Madras,
Guindy Campus, MADRAS 600 025.

In one of our works [1], we analysed Strutinsky's shell correction principle from a thermodynamic viewpoint. We observed that the redistribution of single particle states in the smoothening procedure leads to the creation of entropy S and the corresponding change in energy E and temperature T is very small. We also showed that the area under the T-S curve is equal to the forces of shell structure, and is equal to the shell energy. In this paper, we study the thermodynamical aspects of the superfluid nucleus based on the BCS formalism [2] and obtain the pairing energy from the entropy of the quasi particles and also find the transition temperature T_c from the T-S curve.

The entropy S and temperature T are given by

$$S = -\Sigma_i [n_i \ln n_i + (1-n_i) \ln(1-n_i)] \quad (1)$$

$$T = \partial E / \partial S \quad (2)$$

where $$E = \Sigma_i 2 e_i v_i^2 - \Delta^2/G, \quad (3)$$

and n_i, the occupational probability, is given by

$$n_i = 2v_i^2 = 1 - e_i/\sqrt{(e_i^2 + \Delta^2)} \quad (4)$$

Here $e_i = (\epsilon_i - \lambda)$. ϵ_i's are the Nilsson single particle energy levels, λ the chemical potential of the nucleus and Δ the pairing gap.

The strength of interaction leading to pairing correlation is determined by the interaction strength G. At G = 0, the nuclear state is a normal state. At normal state, S=0, T=0, and the pairing energy is also zero. As G is increased we find that the nucleons tend to remain in the unpaired state till a particular interaction strength is reached, and that a minimum strength of interaction is required for the onset of pairing. Once the pairing

interaction is introduced, we find that entropy is created. The entropy increases while the energy decreases as the pairing strength is increased. As a result the statistical temperature T becomes negative. The plot of T vs S for 154-Dy is shown in fig. (1). The area under the T-S curve is equal to the work done against the forces of pair creation, and we find that this is equal to the pairing energy. The T-S diagram exhibits a normal-superfluid phase transition. The normal phase exists in the region $S < S_1$ and the superfluid phase in the region $S > S_2$. The two phases coexists between S_1 and S_2. The values of S_1 and S_2 are determined by the condition

$$\int_{S_1}^{S_r} TdS = \int_{S_r}^{S_2} TdS \qquad (5)$$

i.e, the shaded area below the critical temperature line T_c is equal to the shaded area above the line. The free energy versus Temperature is shown in Fig. (2). The temperature T_c at which the normal branch and the superfluid branch cross determines the transition between the two phases.

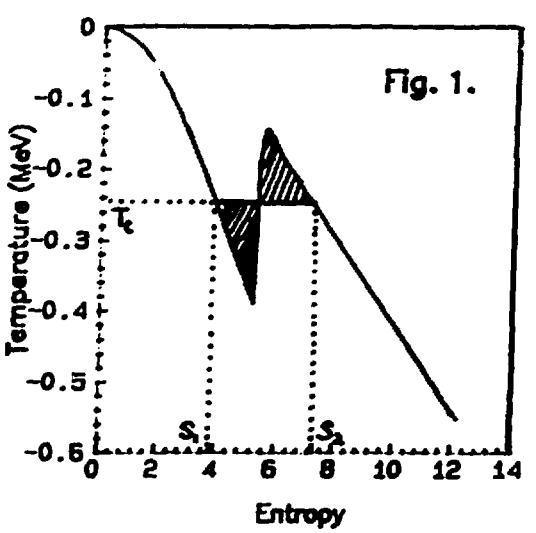

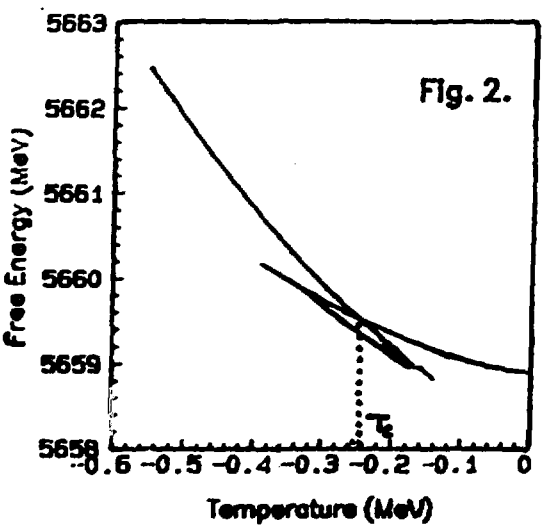

[1] M.Rajasekaran, D.Caleb Chanthi Raj, R.Premanand and V.Devanathan, Phys. Rev. C41 (1990) 394
[2] Belyaev, Mat.-Fys. Medd. 31 (1959) 55

SPIN CUT-OFF AND OCCUPANCY DENSITIES AND THEIR S-DECOMPOSITIONS: THE NON-INTERACTING PARTICLE CASE

V.K.B. Kota and D. Majumdar
Physical Reasearch Laboratory , Ahmedabad 380 009

Spin cut-off factors ($\sigma_J^2(E)=\langle J_z^2\rangle^E$) and occupation numbers ($n_\alpha(E)=\langle \hat{n}_\alpha\rangle^E$, $\hat{n}$ is the number operator for the spherical orbit α) are important quantities in nuclear structure as the former decomposes state densities into observable level densities and the later determines much of the thermodynamic behaviour of the nucleus. It has been suggested recently[1,2] that it is profitable to deal with the density (I(E)) weighted spin cut-off factors and occupancies as the resulting "expectation value densities" are amenable to a moment theory which extends easily to the huge spaces of interest and more importantly to the case with interactions. Given the non-interacting particle (NIP) Hamiltonian $h=\Sigma\varepsilon_\alpha n_\alpha$ (ε_α are single particle energies (s.p.e.)) the state and expectation value ($K=J_z^2$, n_α give $\sigma_J^2(E)$, $n_\alpha(E)$) densities I(E) and $I_K(E)$ respectively and their decompositons are,

$$I^{m,h}(E)=\langle\langle\delta(h-E)\rangle\rangle^m = \sum_m \langle\langle\delta(h-E)\rangle\rangle^m = \sum_m I^{m,h}(E) = \sum_s \Big|\sum_{m\in s} I^{m,h}(E)\Big| = \sum_s I^{s,h}(E) \quad (1)$$

$$I_K^{m,h}(E)=\langle\langle K\delta(h-E)\rangle\rangle^m=\Sigma_m \langle\langle K\delta(h-E)\rangle\rangle^m= \Sigma_m I_K^{m,h}(E) = \sum_s I_K^{s,h}(E) \quad (2).$$

In (1) and (2) $m = \{m_1,m_2,\ldots\}$ defines a configuration with m_1 particles in orbit #1, m_2 particles in orbit #2 etc.; $m=\Sigma m_i$. With m denoting configurations over spherical orbits, by direct counting one can construct I(E) and $I_K(E)$: $\langle K\rangle^E=I_K(E)/I(E)$. Eq. (1) and (2) extend to the unitary configurations $\{m\}=\{\underset{\sim}{m}_1,\underset{\sim}{m}_2,\ldots\}$ defined over unitary orbits $\underset{\sim}{\alpha}$(unitary orbits is a sum of spherical orbits). The smoothed forms for $I^{\{m\}}(E)$ and $I_K^{\{m\}}(E)$ are costructed as Edgeworth corrected Gaussians and hence $I_S(E)$,I(E) and $I_K^S(E)$,$I_K(E)$. With H=h, the fixed {m} densities(also J_z^2 and n_α densities) are convolutions of densities defined over single unitary orbits and the moments (or cumulants) for these densities follow from propagation methods; ref (1,2) give the mathematical details. In order to rigorously test the moment method described above, calculations are carried out for the case of m_p=12, m_n=12 in the spaces {s}, {p}, {sd}, $\{1f_{7/2}\}$, $\{2p_{3/2},1f_{5/2},2p_{1/2}\}$, $\{1g_{9/2},2d_{5/2},1g_{7/2},3s_{1/2},2d_{3/2}\}$, $\{1h_{11/2}\}$, with S=0-4$\hbar\omega$ excitation (here S denotes $\hbar\omega$ excitations) and {} denotes unitary orbits used in the calculations. The s.p.e.(in MeV) used are 0, 8.076, 12.206, 16.388, 20.596, 21.851, 24.752, 29.431, 31.208, 32.201, 33.116, 38.213, 40.383, 41.297, 42.238 and 41.454 respectively. The results in the figure show that there is excellent agreement between moment method and exact results, not only for the total densities but also for the S- decompositions; preliminary calculations of this type are reported in ref. 3,4. The results I(E) and $\sigma_J^2(E)$ are found to fit very well the standard Fermi gas forms[3] upto ~40MeV. The calculated occupancies are seen to have the Fermi form $n_\xi(E)=(2J_\xi+1)/\{1+\exp\beta(E)[\varepsilon-\mu(E)]\}$; β, μ are determined by least square fits.

References: 1)J.B.French and V.K.B.Kota,Phys. Rev. Lett. 51,2183(1983);Report UR-1116 (1989).2)J.B.French,V.K.B.Kota and J.F.Smith, Report UR-1122 (1989).3) J.F.Smith, PhD thesis(University of Rochester,1987). 4)V.K.B.Kota,"Capture Gamma Ray Spectroscopy and related topics"(Asilomar,California,USA,14-19 October,1990).5)J.R.Huizenga and L.G.Moretto,Ann. Rev. Nucl. Sci 22, 427(1972).

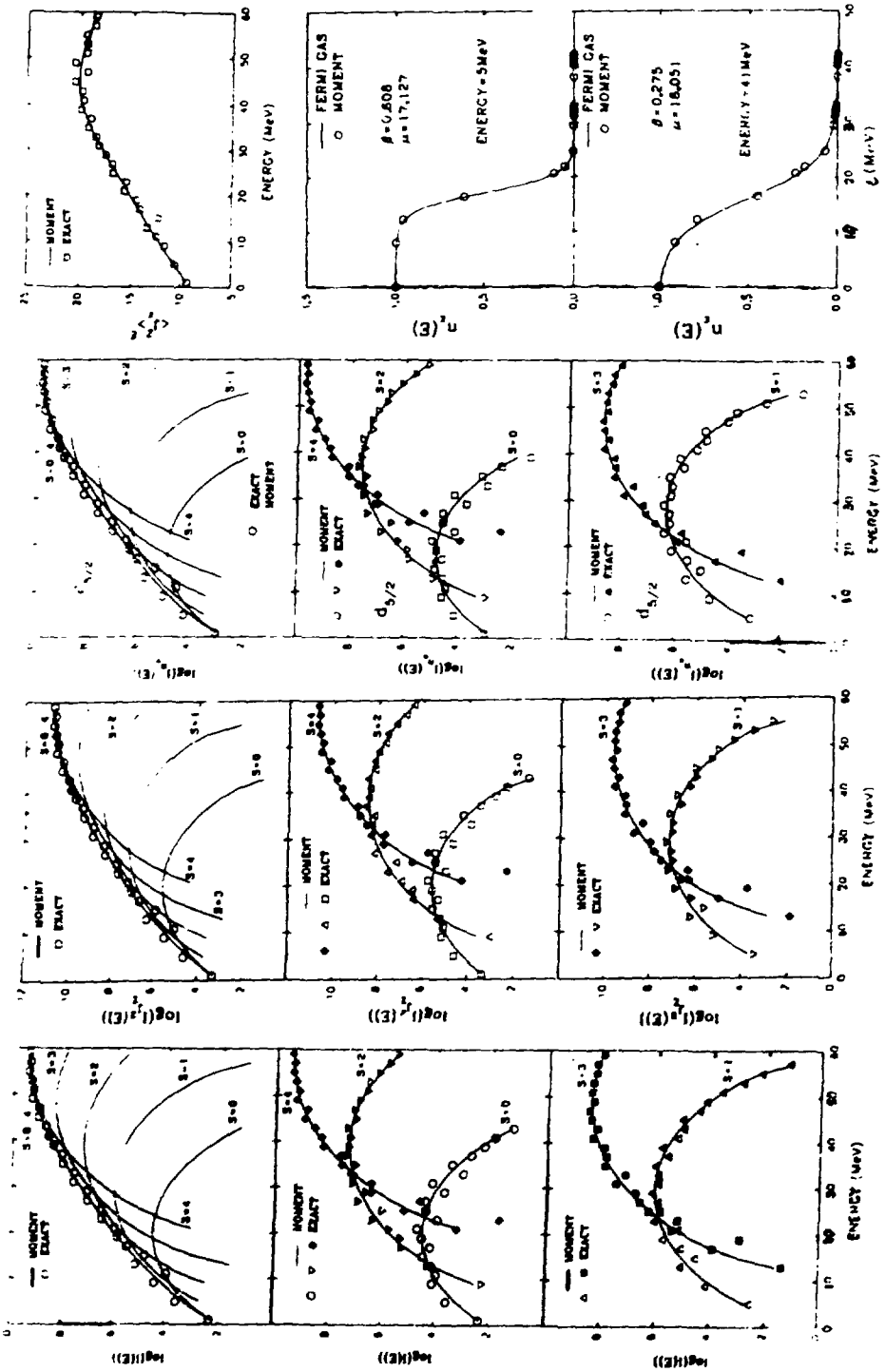
FERMI GAS
MOMENT
β=0.608
μ=17.127
ENERGY=5MeV
β=0.275
μ=18.051
ENERGY=41MeV
n_ℓ(E)
ζ (MeV)
EXACT
ENERGY (MeV)
d5/2

RELATIVISTIC MEAN FIELD STUDY OF "ISLAND OF INVERSION" IN NEUTRON-RICH Ne, Na, Mg NUCLEI

S. K. Patra and C. R. Praharaj
Institute of Physics, Bhubaneswar-751005, India

The binding energies and other properties of the neutron-rich Ne, Na, Mg nuclei are difficult to understand on the basis of existing theoretical models even after allowing for fairly large shell model configuration mixing[1]. It is found [2] that $^{31,32,33,34}Na$ and $^{32,33,34,35}Mg$ have considerably more binding energies than obtained theoretically in spherical shell model studies. It was thus suggested that these nuclei are deformed and form an "island of inversion" having considerably more binding than that obtained from shell model calculations[2]. While in principle a full shell model calculation involving many major shells may be able to account for the binding of these nuclei (provided proper effective interactions are used), such studies are, because of the dimension of the vector space, beyond present day computer capabilities. Even the ground state spins of $^{29,31}Na$ and the other low excitation energy of the 2^+ state in ^{32}Mg are difficult to understand in existing shell model calculations[2].

In this work we present a relativistic mean field (RMF) description of the neutron-rich Ne, Na and Mg nuclei. In the model we have the σ-meson, the ω-meson, the ρ-meson and the photon fields coupled to the nucleons[3]. The isvector ρ-meson is important for neutron-proton asymmetric systems. The photon accounts for the Coulomb repulsion among the protons.

To describe the ground state properties we need static solution of the Lagrangian of ref. [3]. For this case the meson and electromagnetic fields (treated as classical fields) are time independent, whereas the nucleon wavefunctions oscillate with single particle energy E_i. From the above Lagrangian we obtained equations for the fermion and the meson fields and can be found in ref. 3.

The set of partial differential equations are solved by expanding the upper and lower components $f_i^{\pm}$ and $g_i^{\pm}$ of the Dirac spinor ψ_i in terms of a deformed harmonic oscillator potential basis, taking volume conservation into account. The frequencies $\hbar\omega_\perp$ and $\hbar\omega_z$ can be expressed in terms of a deformation parameter in the cylindrical coordinates.

We now present results of our RMF calculations for the binding energies, spins and deformation parameters of the neutron-rich Ne, Na, Mg nuclei.

The difference between the experimentally observed [4] and the RMF and the WBMB binding energies of Ne, Na and Mg nuclei are plotted in fig. 1. It is quite clear from table 1 and figure 1 that the

present RMF calculations are closer to experiment than shell model calculations[2] in limited model space. The most severe cases of underbinding in neutron-rich Na and Mg nuclei in shell model analysis have been studied in the Relativistic Mean Field model. The binding energies obtained are much closer to the experiment. The ground state spins of ^{29}Na and ^{31}Na are correctly given as $\frac{3}{2}^+$ in the RMF model. We are able to use a large model space and to incorporate the deformation effects. In RMF studies we find that the neutron-rich Ne, Na and Mg nuclei are highly deformed [fig. 2] which helps to explain the binding energies and other properties of these nuclei reasonably well. A further improvement in binding energies is possible if the rho-meson-nucleon coupling strength is slightly reduced from previous value (see dot-dash curve in fig. 1).

References

[1] X. Campi et al, Nucl. Phys. A251 (1975) 193.
[2] E. K. Warburton et al, Phys. Rev. C41 (1990) 1147.
[3] Y. K. Gambhir et al, Ann. Phys. (N.Y.) 198 (1990) 132.
[4] A. H. Wapstra and G. Audi Nucl. Phys. A432 (1985) 1.

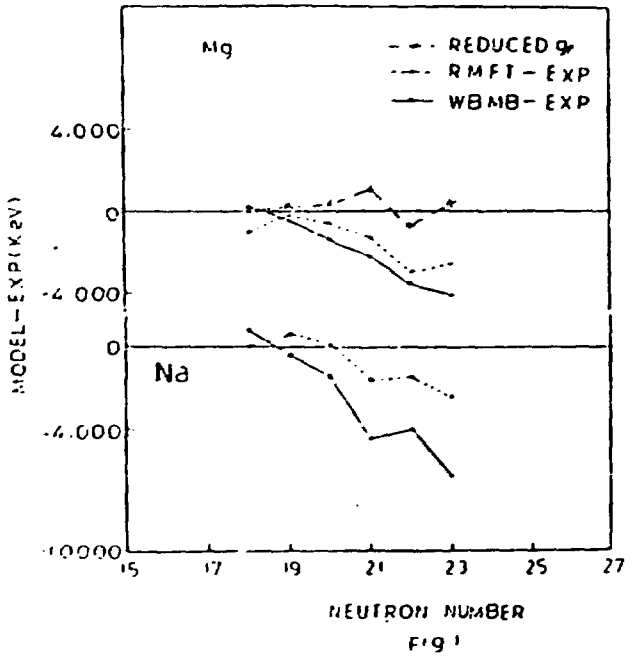

Fig 1

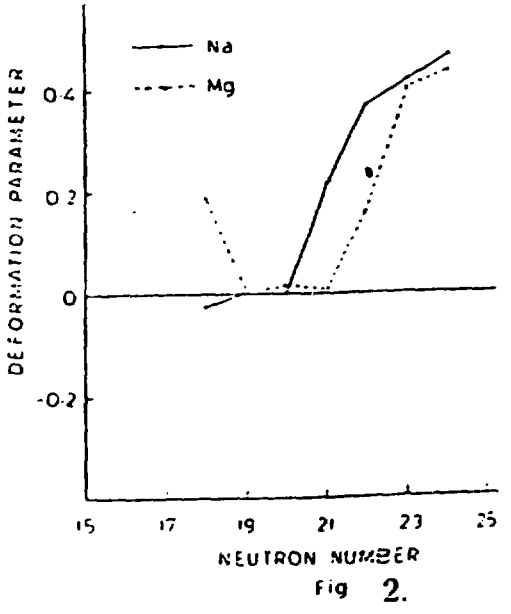

Fig 2.

EXOTIC NUCLEI : RELATIVISTIC MEAN FIELD APPROACH

J.F. Maharana[a], J.A. Sheikh[b] and Y.K. Gambhir[a]
a:Department of Physics, I.I.T. Bombay 400 076
b:T.I.F.R., Colaba, Bombay 400 005

In recent years highly neutron rich (deficient) nuclei far away from the stability line are being produced in various research laboratories. The study of these so called Exotic Nuclei reveal several interesting features e.g. large deformations, abrupt changes in rms radii, shape co-existence etc. The 28-50 nuclear range is of particular interest because here both neutron rich as well as neutron deficient nuclei can be produced and the nucleus N=Z show large deformations. For example ^{80}Zr till todate is the known highly deformed N=Z nucleus ($\beta \simeq 0.5$).

Here we analyse these Exotic Nuclei in the 28-50 region using the Relativistic Mean Field (RMF) Theory. The RMF equations are solved self consistently by expanding separately the Dirac spinors and the meson fields for Sigma (σ), Omega (ω), Rho (ρ) mesons in terms of Harmonic Oscillator (HO) basis (for details see ref.1).

The masses and the coupling constants of the respective meson fields with the Dirac nucleon spinor fields are taken from the earlier work and correspond to the highly successful parameter set NL1. The explicit values of these parameters are:

Masses(MeV):			The coupling constants:	
Nucleon:	m_N	= 938.0	g_σ	= 10.14
Mesons :Sigma	m_σ	= 492.5	g_w	= 13.29
Omega	m_w	= 795.36	g_ρ	= 4.98
Rho	m_ρ	= 763.0	Photon α	= 1/137

In addition Sigma (σ) meson is considered to move in nonlinear potential with cubic and quartic terms having coupling constants $g_2 = -12.17$ and $g_3 = -36.27$ respectively.

The pairing is taken into account in the constant gap approximation. The required gap parameters Δ_n (Δ_p) for neutrons (protons) are obtained either from the observed odd-even mass differences where available or from the empirical relation $12/\sqrt{N(Z)}$.

Some of the representative results arranged in the table show the following features:

1. The results are in good agreement with the experiment where ever available .
2. Slightly deformed (near spherical; β=very small) solutions in general appear slightly lower in energy ($\Delta E \simeq 1.5$Mev) as compared to the corresponding spherical (β=0.)solutions .
3. The deformed and spherical solutions appear very close to each other for ^{74}Sr, ^{76}Sr, ^{76}Zr, ^{78}Zr and ^{80}Zr with energy differences ΔE -1.7, -1.6, 0.01, 0.01 and 1.6 Mev, respectively. Thus indicating a possible shape co-existence very near to the ground state for these systems .
4. The charge (proton rms) radius decrease with the decrease with the addition of neutrons from ^{74}Sr to ^{76}Sr .

Nucleus		Δ_n	Δ_n	E/A	r_c	r_{rms}	β
^{74}Sr	(Sph)	2.0	1.95	-8.20	4.34	4.15	0.
	(Def)	2.0	1.95	-8.23	4.31	4.17	.432
^{76}Sr	(Sph)	1.95	1.95	-8.37	4.31	4.17	0.
	(Def)	1.95	1.95	-8.39	4.24	4.12	.008
	(Def)	1.95	1.95	-8.40	4.32	4.20	.467
^{76}Zr	(Sph)	2.0	1.9	-8.02	4.41	4.20	0.
	(Def)	2.0	1.9	-8.04	4.31	4.14	.001
	(Def)	2.0	1.9	-8.02	4.38	4.22	.433
^{78}Zr	(Sph)	1.95	1.9	-8.22	4.40	4.22	0.
	(Def)	1.95	1.9	-8.24	4.31	4.17	.0001
	(Def)	1.95	1.9	-8.22	4.39	4.25	.466
^{80}Zr	(Sph)	1.9	1.9	-8.38	4.37	4.23	0.
	(Def)	1.9	1.9	-8.40	4.31	4.12	.0004
	(Def)	1.9	1.9	-8.36	4.38	4.21	.466

References :

1. Y.K. Gambhir et.al.; Ann Phys. 198, 132(1990) and references quoted therein .

QUANTUM CHAOS IN DINUCLEAR SYSTEM

A. K. Chaudhuri and Santanu Pal
Variable Energy Cyclotron Centre, I/AF Bidhan Nagar
Calcutta 700 064, India

With a view to study chaos in a dinuclear system, the nearest neighbour level spacing distributions (LSD) of the single particle states were analysed. The energy levels of the dinuclear system consisting of two potential pockects with full spin-orbit potential and neck degrees of freedom were obtained for various separations. The physical process we have in mind is that of dissipative deep inelastic heavy ion collisions ,where concepts such as markovian or fast relaxation of intrinsic motion are invoked hinting a fast spreading in phase space or onset of chaos. Details of the model can be found in ref. [1,2]. In fig.1, the potential of the dinuclear system is shown. To study the fluctuating properties of the single particle energy levels, we use the integrated density of states as [3],

$$N(E) = \sum_i \theta (E-E_i) \qquad (1)$$

The staircase function (1) was unfolded to obtain a new sequence with mean spacing unity. The LSD were studied in terms of P(s) the probability of obtaining a mean spacing s. It is now known that for a integrable,i.e. non-chaotic system, the LSD is given by the Poisson distribution, $P(S) = \exp(-S)$, whereas for a non-integrable i.e. a chaotic system, the LSD follows the Wigner /Gaussian Orthonormal Ensemble (GOE) distribution, $P(S) = (32/\pi^2)S^2 \exp(-4S^2/\pi)$.

In fig 2 the LSD in the form of histograms are shown for two separations of the dinuclear system. At R=0 fm, the dinuclear system coaleases to form a single nucleus acquiring additional symmetry (rotaional) and the LSD is characteristic of Poisson distribution. At an intermediate separtion of 7 fm, the LSD changes to Wigner type distribution showing the chaotic component in the system. We introduce a 'chaos' parameter 'a' such that,

$$P(S) = a\, P_{Wigner}(S) + (1-a)\, P_{Poisson}(S) \qquad (2)$$

The variation of the chaos parameter 'a' with R, obtained by fitting histogram is shown in fig.3. This figure portraits the onset and subsequent diminishing effect of chaos in a dinuclear system. The present study demonstrates the importance of the neck degree of freedom in a dinuclear system, which in addition to allowing particle and momenta to be exchanged also make them irreversible.

References:
[1] B.Milek,W.Norenberg and P.Rozmej,Z. Phys. A334(1989)233.
[2] S.Pal and A.K.Chaudhuri, Nucl.Phys. A(in press)
[3] T.A. Brody et al, Rev. Mod. Phys.53((1981)385.

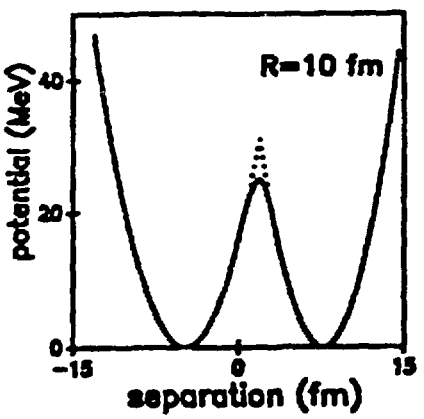

Fig.1

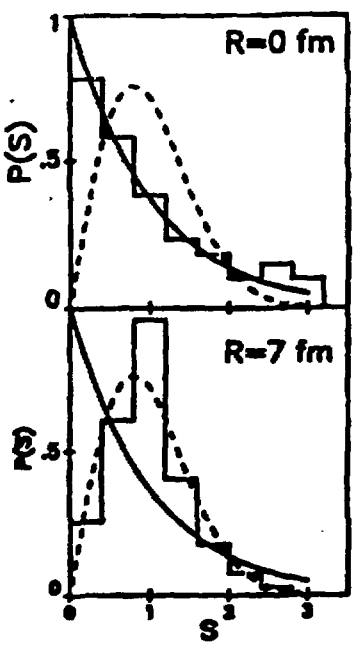

Fig.2

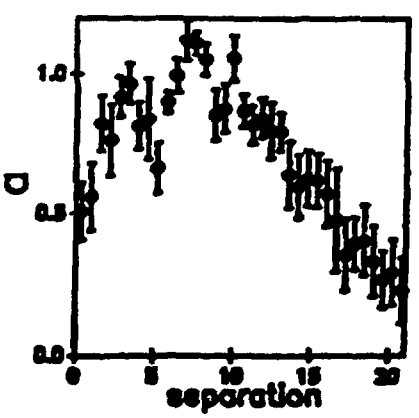

Fig.3

PION DRESSING OF NUCLEONS AND NUCLEAR FORCES: A NONPERTURBATIVE APPROACH

P.K. Panda*, R. Sahu**, S.P. Misra*
* Institute of Physics, Bhubaneswar-751005, India,
** Berhampur University, Berhampur-761007, India.

Pion nucleon interaction is known to be a strong interaction, where perturbative analysis fails. Recently in field theory a nonperturbative approximation scheme with coherent states has been proposed to study nuclear matter [1]. We shall here consider a state for a physical nucleon with off mass-shell coherent cloud of scalar isoscalar pion pairs. The pion pairs simulate the effect of σ-mesons. The coherent states corresponds to the quantum picture of classical fields of Walecka model [2].

We define a 'dressed' single nucleon state of momentum $\vec{p}$ as

$$|\vec{p},\alpha>=\frac{1}{(2\pi)^{3/2}}\int e^{i\vec{p}\cdot\vec{x}}\psi_\alpha(\vec{x})^\dagger U(\vec{x})d\vec{x}|vac>$$

where

$$U(\vec{x})=exp\left(\frac{1}{2}\int f(\vec{x};\vec{z}_1,\vec{z}_2)a_i(\vec{z}_1)^\dagger a_i(\vec{z}_2)^\dagger d\vec{z}_1 d\vec{z}_2-h.c.\right)$$

which describes the dressing of pions. The energy expectation value of the nucleon at zero momentum for the interacting nucleon is given as

$$h(f)\delta_{\alpha'\alpha}=(2\pi)^3<\vec{0},\alpha'|\mathcal{H}(\vec{z})|\vec{0},\alpha>$$

where $\mathcal{H}(\vec{z})$ is the effective Hamiltonian density of the system including nucleons, pions and interactions which was derived in Ref. 1. The above energy expection value is a functional of the meson dressing f. We then consider the single nucleon with pion dressing as determined through energy minimisation.

Next we consider two nucleon bound system. For this purpose we write the deuteron state of zero momentum as

$$|D^m(\vec{0})>=$$
$$\frac{1}{2\sqrt{2}}\frac{1}{(2\pi)^{3/2}}\int\psi_I(\vec{x}_1)^\dagger U^{mn}(\vec{x}_1-\vec{x}_2)\sigma_n\tilde{\psi}_I(\vec{x}_2)U(\vec{x}_1,\vec{x}_2)d\vec{x}_1 d\vec{x}_2|vac>,$$

with $\tilde{\psi}_I=\sigma_2\tau_2\psi_I^\dagger$ as the charge conjugate of ψ_I. We also substitute for $U^{mn}(\vec{r})$, with $\vec{r}=\vec{x}_1-\vec{x}_2$,

$$U^{mn}(\vec{r})=[\delta^{mn}u_s(\vec{r})cos\alpha+p^{mn}(\hat{r})u_d(\vec{r})sin\alpha]$$

where

$$p^{mn}(\hat{r}) = \frac{1}{\sqrt{2}}(3\hat{r}^m\hat{r}^n - \delta^{mn}),$$

and $U(\vec{x}_1, \vec{x}_2) = U(\vec{x}_1)U(\vec{x}_2)$, with $U(\vec{x})$ as defined earlier. In the above u_s and u_d are s- and d- wave functions respectively and α is the mixing angle. The energy expectation value

$$h(f)\delta^{mn} = (2\pi)^3 < D^m(\vec{0})|\mathcal{H}(\vec{z})|D^n(\vec{0}) > .$$

This will include both the effects of the nucleon wave function and of the meson dressing. We consider here one pion exchange and ω-repulsion in addition to dressing through pion pairs. We then minimise the energy. The minimisation gives the binding energy of deuteron to be 2.2603 MeV which is in good agreement with the experimental value of 2.2 MeV. We get the d-state probability to be 8.87 % and the average meson number is found to be 1.157×10^{-4}. We also calculate magnetic moment, the r.m.s. radius and and quadrupole moment and obtain $\mu_d = 0.834$ nm, $< r^2 >^{1/2} = 2.74$ fm and $Q = 9.2 \times 10^{-27}$ cm^2 which may be compared with the experimental values $\mu_d = 0.857$ nm, $< r^2 >^{1/2} = 1.95$ fm and $Q = 2.82 \times 10^{-27}$ cm^2.

The analysis, defacto replaces scalar isoscalar potential in nuclear physics by multipion condenasates and yields approximately correct results.

REFERENCES

[1]. A. Mishra, H.Mishra and S.P.Misra Int. J. Mod. Phys. A5 17 (1990) 3391.

[2]. J.D. Walecka, Ann. Phys. 83 (1974) 491.

ROTATION ALIGNMENT AND BAND CROSSING IN SUPERDEFORMED BANDS

B. K. Agrawal

Institute Of Physics, Bhubaneswar -751005

A new superdeformed(SD) region with mass number $A \approx 100$ was discovered with the observation of SD bands in $^{104,105}Pd$[1], a couple of years ago. The dynamical moment of inertia $\Im^{(2)}$ for SD bands in these nuclei show large variation as compared to almost constant moment of inertia for SD bands in rare-earth[2] nuclei. The increase in $\Im^{(2)}$ at rotational frequency $\hbar\omega$ nearly equal to 1 MeV indicates the existence of band crossing in the SD bands, which was observed for the first time in SD bands. Later on, such a crossing was observed also in SD bands for ^{146}Gd[3]. It has been interpreted that the SD bands in $^{104,105}Pd$ are built on highly rotation aligned configuration which involves the neutrons as well as protons in $h_{11/2}$.

We report here the axially deformed ($\gamma = 0$) Hartree-Fock (DHF) and angular momentum projection calculation for ^{104}Pd. The configuration space consists of all the orbits up to $h_{11/2}$ above the core with N=50 and Z=28. In the figure 1, we have shown the DHF orbits for prolate deformed ^{104}Pd. Each of these orbits is labelled by

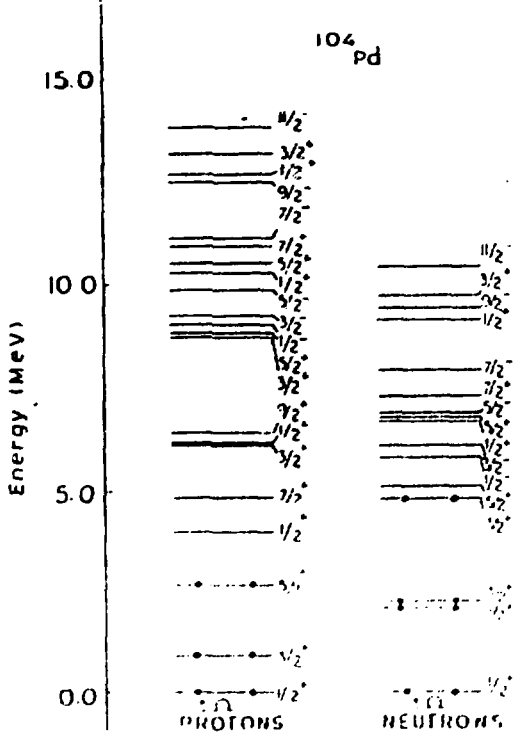

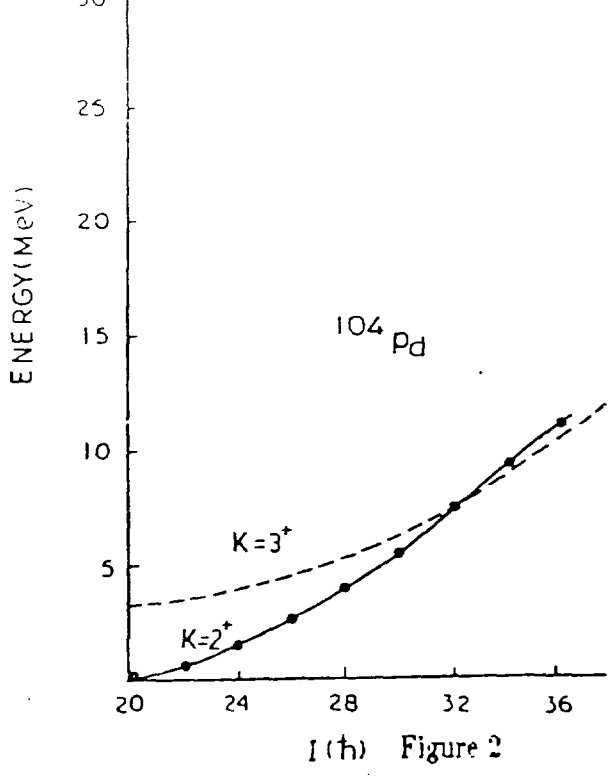

Figure 2

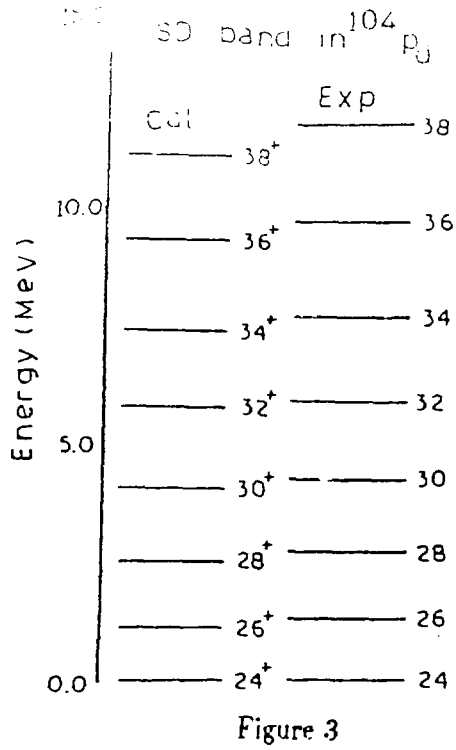

Figure 3

its intrinsic quadrupole deformation q_o in units of eb^2 and the quantum number $k = \Omega^\pi$, where Ω is single-particle angular momentum component along symmetry axis in the body fixed frame. We note that the DHF orbits for protons or neutrons just below the Fermi surface(shown by dotted line) are either weakly prolate($q_o > 0$) or strongly oblate($q_o < 0$) deformed. On the other hand, there are orbits above the Fermi surface which can cause more deformation as well as considerably large rot ation alignment. We have considered two such configurations which are (a) $K = 2^+$ and (b) $K = 3^+$. In figure 2. we show the band crossing between the bands built on these configurations. The band with $K = 2^+(\beta_o = .33)$ corresponds to $(h_{11/2})^{2n}(h_{11/2})^{2p}$ and $K = 3^+(\beta_o = .35)$ corresponds to $(h_{11/2})^{2n}(h_{11/2})^{2p}(g_{7/2})^{2p}$. The value of the intrinsic deformation(β_o) is very close to the observed value which is nearly equal to .4. To compare our results with the experiment as shown in figure 3, we compare our result with the observed spectrum. consider only yrast states. Therefore, the angular momentum states with spin upto $32\hbar$ belog to $K = 2^+$ band.and higher ones correspond to $K = 3^+$ band. We find that overall trend of the spectrum obtained is in quite close agreement with the observed SD band in ^{104}Pd.

References

1. A. O. Macchiavelli et al, Phys. Rev. C38, 1088 (1988).
2. P. J. Twin et al Phys. Rev. Lett. 57 811 (1986).
3. M. A. Riley et al Nucl. Phys. A520 59 (1991)

SPREADING Of THE $1g_{9/2}$ PROTON STRENGTH IN ^{41}SC

Ramen Majumdar,Vivekananda College,Cal.700063.

The distribution of the $1g_{9/2}$ proton strength functions of ^{41}Sc can be explained on the basis of the core polarisation effect on the proton states in the doubly magic nucleus ^{40}Ca. The broad fragmented pattern of this high spin state of ^{41}Sc that has been revealed through the recent experimental results based on $(^3He,d)^{40}Ca$ reaction[1] arises because of the strong interaction of the proton states with the collective vibrational states of ^{40}Ca.The energy of the $1g_{9/2}$ state can be known from the solution of the Schrodinger eqn. with the relevant potential parameters for ^{40}Ca[2].This energy coincides with the particle coupled vibrational mixed configurations of ^{41}Sc *and this is the prime reason for the loss of shell* model identity of the $9/2^+$ proton state of ^{40}Ca.Our theoretical calculations are based on the model that has been explained in our recent works of ^{207}Pb[3].

A few fragmented states are shown below.

E(Mev)		Sp.factor	
Theo.	Exp.	Theo.	Exp.
4.0		0.45	
11.8		0.004	
12.4	2.0-12.4	0.004	=0.84
13.6		0.003	
14.9		0.020	
16.7		0.032	

Ref.

1.J.Guillot et.al. Phys.Letts.258(1991)271

2.O.Olsson et.al. Nucl.Phys.A513(1990)205

3.R.Majumdar Phys.Rev.C42(1990)631

SYSTEMATICS OF THE PAIRING ENERGIES OF EVEN-EVEN NUCLIDES IN THE REGION, Z = 4 - 82

Asok Saha
Department of Physics, University College of Science, 92, A.P.C. Road, Calcutta-700009

It is well-known that nuclear binding energy consists of at least five different components, viz. (i) volume energy, (ii) surface energy, (iii) coulomb energy, (iv) symmetry energy and (v) pairing energy. Although contributing only a small part of the total nuclear binding energy, pairing energy explains why even-even (E-E) nuclei are more stable than the adjacent odd-odd (O-O) nuclei or even-odd (E-O)/odd-even (O-E) nuclei /1/. Although the magnitude of pairing energy is known to decrease with increasing A, attempts to predict it in terms of A or Z have not met with much success /2,3/.

The author has computed the pairing energies of the even-even nuclides of all the elements in the mass range 8-208 (Z=4 to 82), using the mass tables of Wapstra and Audi /4/. Pairing energies of several even-odd and odd-even nuclides in this range were also computed. The following generalisations could be made :-

1. Pairing energy ($P_{(E-E)}$) of any given E-E nuclide in the above-noted mass range is more than double those of the adjacent E-O and O-E nuclides.
2. The nuclides of any given element (i.e. same Z), follow, with few exceptions, the relationship, $P_p(E-E) > P_n(E-E) > P_p(E-O) > P_n(O-E)$, P_p and P_n being proton and neutron pairing energies respectively.
3. Pairing energy values of nuclides of the same Z against the A's show a convex-upward distribution with the highest value being at N=Z (for $Z \leqslant 28$).
4. The arithmetic mean pairing energies for even-even nuclides ($\bar{P}_{(E-E)}$) shows good fit (96.83%), with the relationship $\bar{P}_{(E-E)} = 17.7\ Z^{-\frac{1}{2}}$ MeV; however, $\bar{P}_{(E-E)}$s for Z = 12-20 and Z = 48-50 are

appreciably lower and higher than this best fit relation respectively (Fig.A).

5. The degree 2 residuals of $\bar{P}(E-E)$ values against Z show a sigmoid distribution with a minimum at Z = 12-20 and maximum at Z = 40-50 (Fig.B).

6. Except for the high pairing energy of the single-closed shell nuclei of Sn (Z=50), correlation between pairing energy and shell closures is absent.

References

/1/ M.K.Pal, Theory of Nuclear Structure, Aff. East-West Press (1982) p.148.

/2/ A.H.Wapstra, G. Audi and R. Hoekstra, Nucl. Phys., A432 (1985) 195.

/3/ T.Von Egidy, et al, Nucl. Phys., A481(1988) 189.

/4/ A.H.Wapstra and G.Audi, Nucl. Phys., A432 (1985) 55.

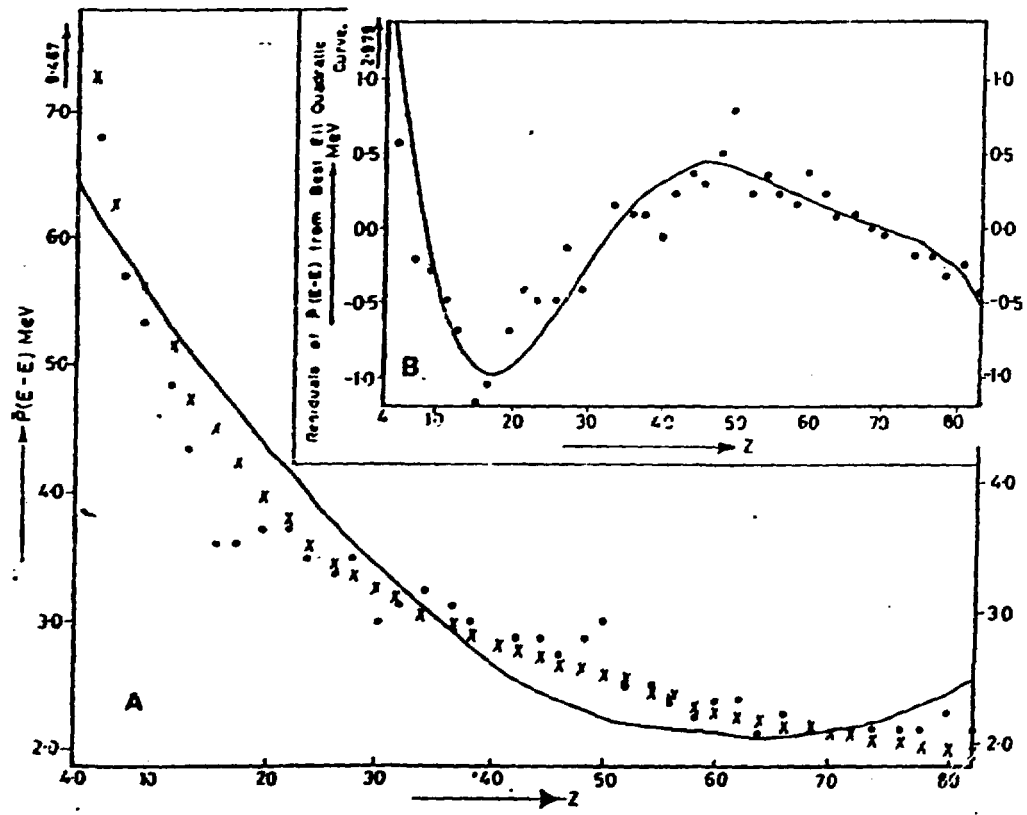

Fig. A. $\bar{P}$ (E-E) vs Z plot (in dots) in the range Z = 4-82, showing also (a) Degree 2 best-fit polynomial curve and (b) values (in crosses) based on equation $\bar{P}(E-E) = 17.7\ Z^{-\frac{1}{3}}$ MeV.
B. Degree 2 polynomial residuals of $\bar{P}$ (E-E) plotted against Z with a best-fit (96.5%) degree 5 polynomial curve.

STRUCTURE OF K ISOMERIC STATE IN ^{174}Hf AND BREAKDOWN OF K SELECTION RULE

C. R. Praharaj*, A. K. Rath**
and
J. A. Sheikh***
*Institute of Physics, Bhubaneswar;
** Physical Research Laboratory, Ahmedabad;
***Tata Institute of Fundamental Research, Bombay

Walker et al [1] have found experimentally a remarkable case of violation of K selection rule in the electromagnetic decay of $K = 14^+$ 3.7 μs isomer in ^{174}Hf. They have identified twelve different lowlying bands (including the $K = 0^+$ ground band and the $K = 1^+$ rotation-aligned band) to which the 14^+ isomer decays with probabilities which are usually large.

We have studied the structures of some of these bands by deformed Hatree-Fock and angular momentum projection calculation. A surface delta interaction has been used as the interaction among nucleons [2,3]. The deformed Hartree-Fock orbits are given in the figure. The negative parity proton deformed orbits originate from $h_{11/2}$ and $h_{9/2}$ states. The positive parity neutron orbits belong to $i_{13/2}$ shell. One can have one-particle-one-hole $(-\frac{9}{2}^-)^{-1}(\frac{7}{2}^+)^1$ proton excitation and one-particle-one-hole $(-\frac{5}{2}^-)^{-1}(\frac{7}{2}^+)^1$ neutron excitation near the Fermi surfaces giving a $K = 14^+$ band. The $K = 1^+$ s-band is obtained by angular momentum projection from $(-\frac{5}{2}^-)^{-1}(\frac{7}{2}^-)^1$ neutron excitation configuration.

Two-body interaction mixes many of these bands and bandmixing can explain the electromagnetic transitions. For example the $K = 0^+$ ground band and the $K = 14^+$ band can mix by proton-neutron interaction in the projection kernel $< \Phi_{14+} \mid V_{pn} \exp(-i\beta J_y) \mid \Phi_{0+} >$.

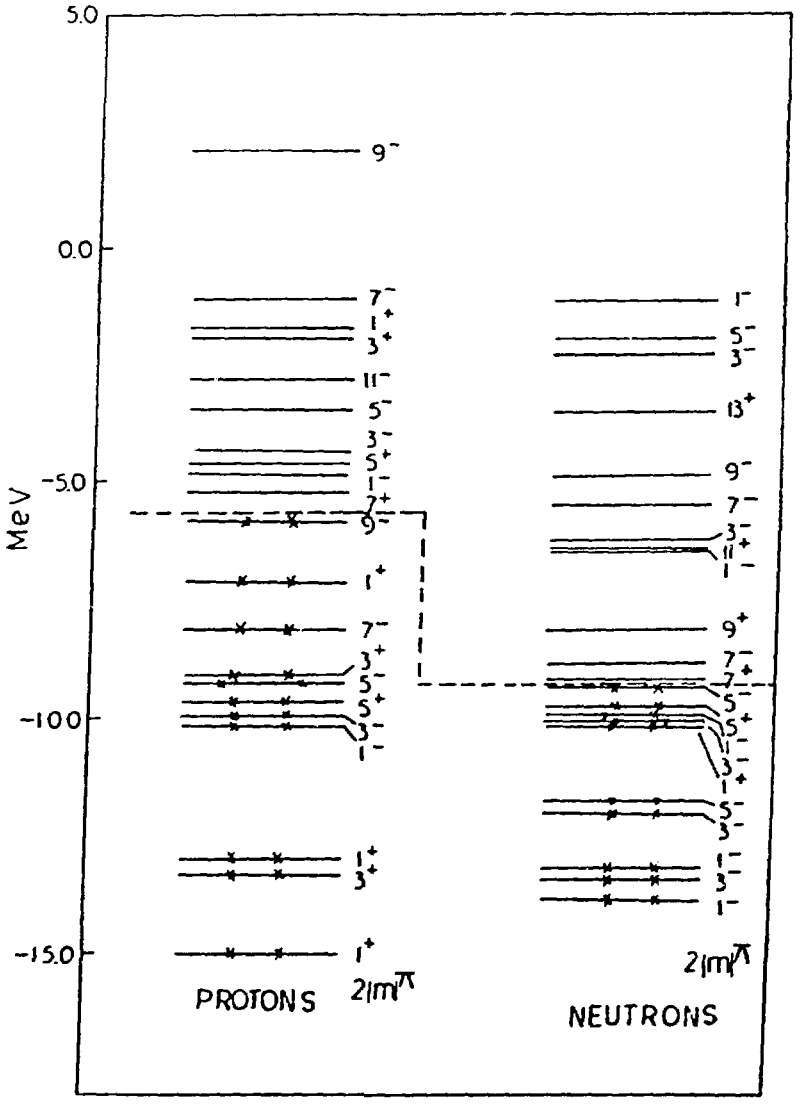

References

[1] P. M. Walker et al, Phys. Rev. Lett. **65** (1990) 416.
[2] C. R. Praharaj and J. A. Sheikh, J. Phys. **G17** (1991) L33.
[3] A. K. Rath, Ph. D. Thesis, Inst. of Physics, Bhubaneswar (1991).

PROTON-DRIP LINE FOR Z=31-40 REGION IN A RELATIVISTIC MEAN FIELD STUDY

S. K. Patra and C. R. Praharaj
Institute of Physics, Bhubaneswar-751005, India

Recently six new isotopes near the limits of stability of proton-rich nuclei in the Ga through Sr region have been discovered by the MSU Group [1]. These isotopes, in particular ^{65}As and ^{69}Br, are important in providing a path for the synthesis of nuclei in the 60-80 mass region due to the astrophysical rapid proton (rp) capture process [2]. Wallace and Woosley [3] have conjectured rapid proton capture process in accreting matter from nearby companion stars onto the surface of a neutron star and this provides a way of synthesising very neutron-deficient nuclei close to the proton-drip line [2] in $A \approx 60 - 80$ region. The existence of these new highly neutron-deficient isotopes is a delicate balance between the attractive nuclear force and repulsive electromagnetic force in atomic nuclei. Thus there is a limit to the excess number of protons one can have in a nucleus. This situation is further aggravated by the electromagnetic Coulomb repulsion among protons which strives to break the nucleus apart. The limits to the number of protons are known as the proton drip lines.

In this work, our aim is to study the proton-drip line of the recently discovered nuclei of Ga, Ge, As, Br, Sr and neighbouring nuclei on their proton-drip line side using (NL1 parameters set) deformed relativistic mean field (RMF) formalism [4], involving interacting mesons and nucleons. In view of the importance of these nuclei near the proton-drip line in astrophysical rapid-proton (rp) capture process [2], we emphasise their properties and compare our results with experiment and nuclear mass models, wherever possible. In our calculations, we see the proton separation energies of the isotopes can be known from the calculated binding energies of two neighbouring nuclei

$$\epsilon^{p}_{separation} = BE(N, Z+1) - BE(N, Z) \qquad (1)$$

The proton separation energies decrease with decrease of mass number of the proton-rich nuclei. The point at which the proton separation energy becomes negative marks the proton-drip line. The proton-drip line for various nuclei (i.e. the stable isotope having the minimum number of neutrons) in our calculations are presented in figure 1. Also we have made a comparison of our results for the proton-drip line with the mass formula of Janecke-Masson [5].

In the case of Ga, As, Se, Br, Rb, Sr and Y the RMF theory predicts more stable isotopes than the prediction of Janecke-Masson [5] mass formula, whereas the mass formula of Janecke and Masson predicts one and

two more isotopes for Ge and Kr respectively (figure 1). The experimentally observed nuclei ^{65}As and ^{69}Br are found to be proton unstable in Janecke-Masson mass formula, whereas these nuclei are well-bound in RMF model with proton separation energies 1.324 and 1.682 MeV respectively. The large proton separation energies imply that these two nuclei should be included in constructing the path for nuclear synthesis [1] by rp process.

In our RMF calculations, ^{70}Kr is proton unstable, while ^{69}Kr and ^{70}Kr are proton-stable in Janecke-Masson mass formula. Therefore the RMF results imply a different path for nuclear synthesis (arrow of figure 1) than the prediction of Mohar et al [1].

References

[1] Mohar M. F. et al, Phys. Rev. Lett. **66** (1991) 1571.
[2] Mathews G. J., Nature **351** (1991) 348.
[3] Wallace R. K. et al, Astrophys. J. Suppl. **45** (1981) 389.
[4] Gambhir Y. K. et al, Ann. Phys. **198** (1990) 132.
[5] Janecke J. et al, Atomic Data and Nucl. Data Tables **39** (1988) 265.

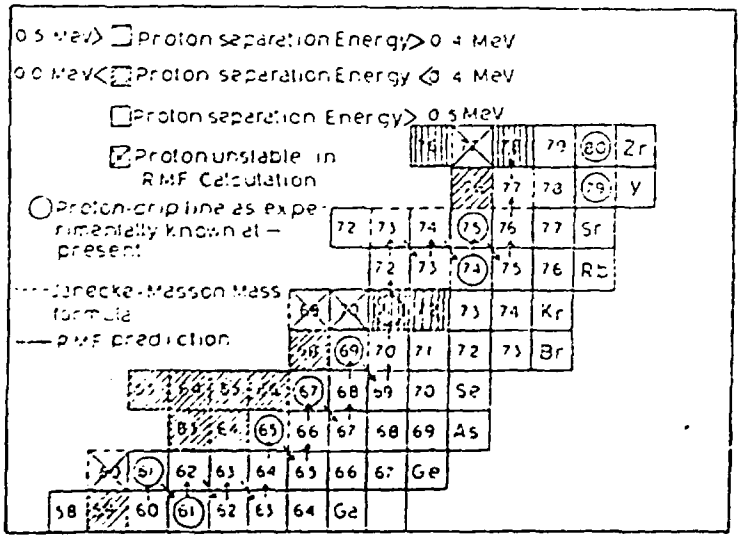

Figure 1

RHO-MESON-NUCLEON COUPLING IN RELATIVISTIC MEAN FIELD THEORY

S. K. Patra and C. R. Praharaj
Institute of Physics, Bhubaneswar-751005, India

One of the successful theories in describing nuclear properties is the Relativistic Hartree theory proposed by Walecka[1] and developed by Walecka and others[1-4]. The Relativistic Mean Field (RMF) approach gives a good description of the ground state properties of finite nuclei throughout the mass table near the stability line[4]. However the parameter sets of RMF have not been optimised for nuclei away from the stability line. In this RMF theory the proper spin-orbit interaction is obtained in the Dirac equation for nucleons through interaction with the scalar meson sigma (σ) and vector meson omega (ω). The isospin asymmetry is generated by the coupling of the ρ-meson to the isospin current in the Lagrangian density, so that the contribution of ρ-mesons to the binding energies of nuclei becomes increasingly important for large isospin asymmetry.

In this work, we have studied various observables of nuclei with the best parameter set available in the literature, namely the set NL1 of Reinhard et al[3] for proton-neutron asymmetric systems. We find that although the parameter set NL1 is quite good near the stability line, it is unable to reproduce the experimental observables for the nuclei on the neutron-rich side. This has to do with the coupling strength of the ρ-meson used in NL1. Our aim in this work is to find out a more accurate value of the ρ-meson-nucleon coupling strength to improve the results, without changing the other couplings and parameters. The ρ-meson-nucleon coupling constant g_ρ is crucial for the neutron-rich side.Ω We use the equations of motion for the various fields derived from the Lagrangian [3,4]. The equations for the nucleons and mesons are solved self-consistently by expansion of the Dirac spinors and the meson fields in a cylindrical oscillator basis with the number of major shells $N_F=8$ and $N_B=12$ for nucleons and bosons respectively. The non-linear sigma model gives[3] binding energies much closer to the experimental bindings. It will thus be useful to study the effect of variation of ρ-meson coupling on properties of nuclei in the context of a non-linear sigma model using the general deformed RMF formalism. Also a fine variation of the ρ-meson coupling strength can lead to a closer agreement between the binding energies obtained in RMF calculations and the experimental binding energies. This is of importance for very neutron-rich exotic nuclei, because the parameter set NL1 of Reinhard et al[3] was chosen keeping in view nuclei near the stability line. In fact we shall see that there is a significant improvement in the binding energies even in the

case of non-exotic nuclei like ^{116}Sn, ^{124}Sn and ^{208}Pb when g_ρ is reduced from 4.9755 to 4.75.

Although the parameter set NL1 reproduces the experimental observables quite well, it still gives underbinding for heavy nuclei by several MeV. There is thus a need for improving on this parameter set, without destroying the agreement obtaining in this set for the nuclear matter properties and properties of light mass nuclei near the stability line. The most obvious quantity in the Lagrangian which can accomplish this is the ρ-meson-nucleon coupling constant. Examining the NL1 parameter set of Reinhard et al[3], it is observed that the uncertainties in the σ and ω-coupling constants are negligible, whereas there is a large error bar in the ρ-meson coupling strength. Here, we have found a more accurate value of the ρ-meson coupling constant by calculating a number of observables such as binding energies, rms radii and quadrupole deformation parameters. We have carried out calculations for a large number of nuclei in different regions of the periodic table with NL1 parameter set without and with changing of the ρ-coupling constant g_ρ. From fig. 1, we observe an overbinding in Sn nuclei by changing the original value of g_ρ from 4.9755 to a new value g_ρ=4.60. This clearly shows that the actual value of g_ρ lies between 4.9755 and 4.60. It is found that a reasonably more accurate value of the ρ-meson coupling constant is 4.75 (fig. 1). We have also calculated the isotopic chains of O, Ca, Ni, Cd, Dy, Pb using NL1 with g_ρ =4.9755 and g_ρ=4.75. In all of these chains of isotopes the binding energies improve significantly when the value g_ρ=4.75 is used. It is also found in our calculations that the deformation parameters do not change significantly with the variation of the rho-meson coupling constant. The rms radii are even less sensitive to the ρ-coupling strength. Thus the ρ-meson coupling g_ρ=4.75 is a more reasonable value than the strength used previously in the NL1 parameter set. By changing this values of g_ρ from 4.9755 to 4.75 the bulk asymmetry energy coefficient improves a little (i.e. $a_{asym} \approx 41.930$ MeV).

References

1. J. D. Walecka, Ann. Phys. (N. Y.) 83 (1974) 491.
2. B. D. Serot and J. D. Walecka, Adv. Nucl. Phys. 16 (1986) 1.
3. P. G. Reinhard et al, Z. Phys. A323 (1986) 13.
4. Y. K. Gambhir, P. Ring and A. Thimet, Ann. Phys. (N. Y.) 198 (1990) 132.

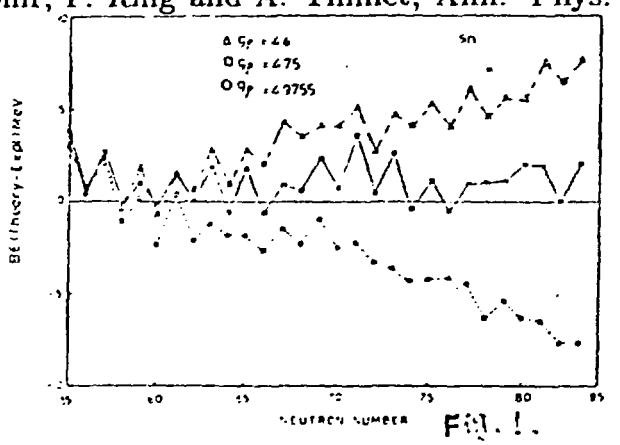

Fig. 1.

SCISSORS STATES IN EVEN-ODD N=82-126 SHELL NUCLEI: ENHANCEMENT IN B(M1) STRENGTHS DUE TO g-BOSONS

Y.D. Devi and V.K.B. Kota
Physical Research Laboratory, Ahmedabad 380 009

The discovery of M1 excited 'scissors' 1^+ state in ^{156}Gd in 1984 lead to large number of studies[1] on M1 states in even-even nuclei. The proton-neutron interacting boson model (pnIBM) provides a simple description of the scissors states[2]. Recently attention is being paid to the question of scissors states in odd-A nuclei[3]. In ref.4), employing the SU(3) ⊗ U(2) limit of IBFM with g(ℓ=4) bosons (gIBFM) the classification of M1 excited scissors states and their B(M1) strengths to ground state (GS) are given in sd and sdg models for the even-odd nuclei in the N=82-126 shell, taking the M1 operator to be $T^{M1}=g_\pi L_\pi+g_\nu L_\nu$ which behaves as a (11) tensor w.r.t SU(3) group. Due to the presence of g-bosons there will be enhancement in B(M1) strengths by a factor 2 as $2N \to 4N$, $2N_\pi \to 4N_\pi$ and $2N_\nu \to 4N_\nu$ (N, N_π and N_ν are the total, proton and neutron boson numbers respectively). In addition there will be a non-trivial enhancement as general M1-operator in gIBFM contains(with four g-factors) a piece that behaves as a (33) tensor of SU(3)

$$T^{M1} = \sum_{\rho=\pi,\nu}\sqrt{10}\left\{g_{2,\rho}(d_\rho^\dagger\tilde{d}_\rho)^1 + \sqrt{6}\, g_{4,\rho}(g_\rho^\dagger\tilde{g}_\rho)^1\right\}$$

$$= \sum_{\rho=\pi,\nu}\left\{ A_{1,\rho}\, T_\rho^{\{21^3\}(11)1} + A_{3,\rho}\, T_\rho^{\{21^3\}(33)1}\right\} ; \; A_{1,\rho} = \sqrt{10/7}\,(g_{2,\rho}+6g_{4,\rho}),\quad A_{3,\rho} = \sqrt{60/7}\,(g_{4,\rho}-g_{2,\rho});$$

$$T_\rho^{\{21^3\}(11)1} = \sqrt{1/7}\,(d_\rho^\dagger\tilde{d}_\rho)^1+\sqrt{6/7}\,(g_\rho^\dagger\tilde{g}_\rho)^1;\; T_\rho^{\{21^3\}(33)1}=-\sqrt{6/7}\,(d_\rho^\dagger\tilde{d}_\rho)^1+\sqrt{1/7}\,(g_\rho^\dagger\tilde{g}_\rho)^1.$$

In the SU(3) ⊗ U(2) limit of gIBFM the GS, scissors states are labelled $|(4N,0)\otimes(40)\ (\lambda_{GS}\mu_{GS})KLJ\rangle$ and $|(4N-2,1)\otimes(40)\ (\lambda_s\mu_s)K'L'J'\rangle$, with $(\lambda_{GS}\mu_{GS})$ = (4N+4-2r,r), $(\lambda_s\mu_s)$ = (4N-2r-k+3,r+2k-1); k = 0,1 for N=82-126 shell nuclei. Using the pseudo-Nilsson scheme[5] the even-odd nuclei in N=82-126 shell can be classified into three classes with $(\lambda_{GS}\mu_{GS})KLJ$ = (4N-2,3)11J, (4N-2,3)33J and (4N,2)00J; (^{187}Os,^{189}Os), (^{177}Hf,^{173}Yb) and (^{171}Yb) are the only stable nuclei that belong to the three classes respectively (hence the scissors states are accessible to conventional (e,e'),(p,p') and (γ,γ') probes). The M1 reduced matrix elements connecting GS to scissors states are of the form $[(A_{1\pi} - A_{1\nu})X^{(11)} + (A_{3\pi} - A_{3\nu})X^{(33)}] = \bar{A}_1X^{(11)} + \bar{A}_3X^{(33)}$. The results for $X^{(11)}$ and $X^{(33)}$ are shown in the tables. The g-factor data for ground and γ- bands in Yb-Hf-W-Os isotopes give $\bar{A}_1 \approx 5\mu_N$ and $-5\mu_N \le \bar{A}_3 \le -2\mu_N$ (see ref. 4 for details). From the tables one can see that $X^{(11)}$ and $X^{(33)}$ are of opposite sign and then with the above $\bar{A}_1$, $\bar{A}_3$, the (33) tensor contribution adds to the (11) tensor contribution and enhances the later by a factor 2-4. With this enhancement one has scissors states with B(M1) ~ 2-3μ_N^2 and hence they should be observed in experiments.

REFERENCES: 1. A.Richter, *Nucl. Phys.* A522 (1991) 139c; references therein; 2. O.Scholten et al., *Nucl. Phys.* A438 (1985) 41; 3. A.A.Raduta and D.S.Delion, *Nucl. Phys.* A513 (1990) 11, P.Van Isacker and A.Frank, *Phys Lett.* 225B (1989) 1; 4. Y.D.Devi and V.K.B.Kota (to be published), Y.D.Devi, *Ph. D Thesis* (Submitted to Gujarat University, June 1991); 5 R.Bijker and V.K.B.Kota, *Ann. Phys. (N.Y)* 187 (1988) 148.

TABLE : M1 Reduced Matrix Elements for Scissors States in sdgIBM for Even-Odd Nuclei in N=82-126 Shell

$(\lambda_S,\mu_S)K_L^{\prime}$	$L^{\prime}$	$J^{\prime}$	E(MeV)	$\langle(\lambda_S,\mu_S)K_L^{\prime}L^{\prime}J^{\prime}\|T^{(\lambda_0,\mu_0)1}\|(\lambda_{GS},\mu_{GS})K_L^{\prime}LJ\rangle$			
				^{187}Os:(4N-2,3)111/2		^{189}Os:(4N-2,3)111/2	
				$X^{(11)}$	$X^{(33)}$	$X^{(11)}$	$X^{(33)}$
(4N-4,4)0	0	1/2	2.71	0.29	-0.26	0.40	-0.36
	2	3/2	2.81	0.20	-0.18	-0.09	0.08
		5/2	2.82	——	——	0.26	-0.24
2	2	3/2	2.81	0.43	-0.39	-0.19	0.17
		5/2	2.82	——	——	0.56	-0.51
(4N-3,2)0	1	1/2	3.29	0.29	-0.26	-0.20	0.18
		3/2	3.30	0.20	-0.19	0.44	-0.41
2	2	3/2	3.36	-0.25	0.23	0.11	-0.10
		5/2	3.37	——	——	-0.32	0.30
				^{173}Yb:(4N-2,3)335/2		^{177}Hf:(4N-2,3)335/2	
				$X^{(11)}$	$X^{(33)}$	$X^{(11)}$	$X^{(33)}$
(4N-4,4)2	2	3/2	2.85	0.47	-0.42	——	——
		5/2	2.48	-0.13	0.11	0.53	-0.47
	3	5/2	3.05	-0.27	0.24	-0.06	0.05
		7/2	2.54	0.06	-0.05	-0.30	0.26
	4	7/2	3.30	0.10	-0.09	0.02	-0.02
		9/2	2.65	——	——	0.11	-0.10
4	4	7/2	3.30	1.14	-1.02	0.21	-0.18
		9/2	2.65	——	——	1.23	-1.09
(4N-3,2)2	2	3/2	3.08	0.82	-0.73	——	——
		5/2	2.74	-0.22	0.20	0.92	-0.82
	3	5/2	3.28	-0.47	0.42	-0.10	0.09
		7/2	2.77	0.11	-0.09	-0.52	0.46
	4	7/2	3.53	0.18	-0.16	0.03	-0.03
		9/2	2.88	——	——	0.19	-0.17
				^{171}Yb:(4N,2)001/2			
				$X^{(11)}$	$X^{(33)}$		
(4N-2,3)1	1	1/2	2.36	0.43	-0.38		
		3/2	2.46	0.61	-0.54		
(4N-1,1)1	1	1/2	3.56	-0.30	0.27		
		3/2	3.66	-0.43	0.39		

The M1 matix elements whose magnitude is smaller than 10^{-2} are not shown. Note that $B(M1;J \longrightarrow J') = \frac{3}{4\pi}(2J+1)^{-1}(\bar{A}_1 X^{(11)} + \bar{A}_3 X^{(33)})^2$.

E4 Matrix Elements in ^{198,194}Pt : sdgIBM Results

Y.D. Devi and V.K.B. Kota
Physical Research Laboratory, Ahmedabad 380 009

Recently E4 transition matrix elements for the decay of the first three 4^+ levels to ground state (GS) are measured[1] in ^{198,194}Pt and their theoretical description is a challenging problem. The Pt isotopes are known to be γ-soft ($O_{sd}(6)$ of sd interacting boson model (sdIBM)) with $SU_{sd}(3)$ (rotational) or $U_d(5)$ (vibrational) admixtures[2]. Both sd and sd $\times$ 1g (with[1] and without[3] mixing between the sd and g(ℓ=4) spaces) calculations fail to explain consistently the spectra, E2 and E4 data in ^{198,194}Pt. Therefore we performed calculations in sdgIBM with $n_g \leq 2$ (n_g being the number of g bosons) restriction and employing a hamiltonian and E2 and E4 transition operators that interpolate sdgIBM symmetries[4],

$$H = \varepsilon_d \hat{n}_d + \varepsilon_g \hat{n}_g + \alpha_1\left[H(SU_{sdg}(3))\right] + \alpha_2\left[H(SU_{sdg}(6))\right] + \alpha_3\left[H(O_{sd_2}(15))\right] + \alpha_4\left[H(O_{sd}(6))\right] + \alpha_5\left[H(O(3))\right] \quad (1)$$

$$T^{E2} = \alpha\left[Q^2_\mu(s) + \beta\, I^2_\mu\right];\quad Q^2_\mu(s) = 4[7/15]^{1/2}(s^\dagger\tilde{d}+d^\dagger\tilde{s})^2_\mu - 11[2/21]^{1/2}(d^\dagger\tilde{d})^2_\mu + [36/105](d^\dagger\tilde{g}+g^\dagger\tilde{d})^2_\mu - 2[33/7]^{1/2}(g^\dagger\tilde{g})^2_\mu;\quad I^2_\mu = (s^\dagger\tilde{d}+d^\dagger\tilde{s})^2_\mu \quad (2)$$

$$T^{E4} = \zeta\left[I^4_\mu + \eta\, Q^4_{esc:\mu}\right];\quad I^4_\mu = (s^\dagger\tilde{g}+g^\dagger\tilde{s})^4_\mu;\quad Q^4_{esc:\mu} = \left[(s^\dagger\tilde{g}+g^\dagger\tilde{s})^4_\mu + \frac{19\sqrt{5}}{28}(d^\dagger\tilde{d})^4_\mu - \frac{5\sqrt{11}}{14}(d^\dagger\tilde{g}+g^\dagger\tilde{d})^4_\mu + \frac{3\sqrt{143}}{28}(g^\dagger\tilde{g})^4_\mu\right]. \quad (3)$$

H(G) with G = $SU_{sdg}(3)$, $SU_{sdg}(6)$, $O_{sdg}(15)$, $O_{sd}(6)$ and O(3) are defined in ref. 4. With (N,n_d,n_g) being $(5,\geq1,\leq2)$ and $(7,\geq2,\leq2)$ the model space dimensions do not exceed 27 and 53 for ^{198}Pt and ^{194}Pt respectively; the n_g restriction derives from the occupation numbers in $O_{sd}(6)$ and $SU_{sd}(3)$ limits. The low-lying levels (below ~2MeV) in ^{198}Pt and ^{194}Pt are reproduced with r.m.s deviation ~94 keV and 143 keV respectively. The resulting wavefunctions are used in calculating the E2 and E4 matrix elements and the results are shown in Tables-1,2. Besides E2 and E4 matrix elements large number of B(E2)'s are also well reproduced[4]. As seen from the Tables, the three pieces of E4-data are well reproduced with two and one parameters in the E4-operator for ^{198}Pt and ^{194}Pt respectively. It is worth mentioning that g-boson occupancy $\langle n \rangle$ for 4^+_1, 4^+_2 and 4^+_3 are (0.05,0.62,0.95) and (0.03,0.03,0.99) for ^{198}Pt and ^{194}Pt respectively. The results of the present claculation establish that one can reliably predict E4 properties with $n_g \leq 2$ restriction in sdgIBM.

REFERENCES : 1. A.Sethi et al. *Nucl. Phys.* A518 (1990) 536; 2. R.F.Casten and J.A.Cizewski *Nucl. Phys.* A425 (1984) 653; 3. Y.D.Devi and V.K.B.Kota *J. Phys. G: Nucl. Part. Phys.* 17 (1991) 465; 4. Y.D.Devi *Ph. D Thesis*, (Submitted to Gujarat University, June 1991); 5. H.H.Bolotin et al. *Nucl. Phys.* A370 (1981) 146; 6. A.E.Stuchberry et al. *Nucl. Phys.* A365 (1981) 317; 7. G.J.Gyapong et al. *Nucl. Phys.* A258 (1986) 165; 8. C.Baktash et al. *Phys. Rev.* C18 (1978) 131.

TABLE - 1

E2 AND E4 MATRIX ELEMENTS FOR ^{198}Pt

$L_i \longrightarrow L_f$	$\lvert\langle f\rVert T^{E2}\rVert i\rangle\rvert$ (eb)		
	Expt	gIBM[a] (2g)	sd x 1g[b]
$0_1^+ \longrightarrow 2_1^+$	1.02 ± 0.04[b] 1.01 ± 0.05[c]	1.18	1.07
$0_1^+ \longrightarrow 2_2^+$	0.039 ± 0.005[b] 0.034 ± 0.012[d]	0.08	0.12
$2_1^+ \longrightarrow 2_1^+$	0.55 ± 0.16[e]	0.81	0.51
$2_1^+ \longrightarrow 2_2^+$	1.16 ± 0.08[c]	1.14	1.12

$L_i \longrightarrow L_f$	$\lvert\langle f\rVert T^{E4}\rVert i\rangle\rvert$ (eb^2)	
	Expt	gIBM[a] (2g)
$0_1^+ \longrightarrow 4_1^+$	0.144 ± 0.003[b]	0.147
$0_1^+ \longrightarrow 4_2^+$	0.124 ± 0.006[b]	0.124
$0_1^+ \longrightarrow 4_3^+$	0.094 ± 0.007[b]	0.085

The parameters used in the E2 operator (see eq(2)) are κ = 0.01eb and β = 10/3. For the E4 operator (see eq(3)) the parameters are ζ = 0.09eb^2 and η = -2/3.

[a] present calculation [b] ref. [1] [c] ref. [5] [d] ref. [6] [e] ref. [7].

TABLE - 2

E2 AND E4 MATRIX ELEMENTS FOR ^{194}Pt

$L_i \longrightarrow L_f$	$\lvert\langle f\rVert T^{E2}\rVert i\rangle\rvert$ (eb)		
	Expt	gIBM[a] (2g)	sd x 1g[b]
$0_1^+ \longrightarrow 2_1^+$	1.18 ± 0.05[b] 1.27 ± 0.006[c]	1.31	1.42
$0_1^+ \longrightarrow 2_2^+$	0.098 ± 0.004[b] 0.09 ± 0.002[c]	0.20	0.21
$2_1^+ \longrightarrow 2_1^+$	0.79 ± 0.04[c]	1.03	0.81
$2_1^+ \longrightarrow 2_2^+$	1.46 ± 0.03[c]	1.22	1.47

$L_i \longrightarrow L_f$	$\lvert\langle f\rVert T^{E4}\rVert i\rangle\rvert$ (eb^2)	
	Expt	gIBM[a] (2g)
$0_1^+ \longrightarrow 4_1^+$	0.132 ± 0.003[b]	0.121
$0_1^+ \longrightarrow 4_2^+$	0.066 ± 0.011[b]	0.079
$0_1^+ \longrightarrow 4_3^+$	0.159 ± 0.004[b]	0.124

The parameters used in the E2 operator (see eq(2)) are κ = 0.052eb and β = 0. For the E4 operator (see eq(3)) the parameters are ζ = 0.16eb^2 and η = 0.

[a] present calculation [b] ref. [1] [c] ref. [8]

UNITARY DECOMPOSITITON OF NUCLEAR INTERACTIONS ALL ACROSS THE PERIODIC TABLE

V.K.B. Kota and D. Majumdar
Physical Research Laboratory, Ahmedabad 380 009

In the French-Kota theory[1] for nuclear level densities and partition functions, proton-neutron space under consideration is first decomposed into distant configurations according to harmonic oscillator excitations characterised by S ($S\hbar\omega$, S=0,1,2,....); for heavy nuclei the definition of S has to be somewhat modified. Then S subspaces are decomposed into unitary configurations and these in turn are decomposed into spherical configurations (see ref. 2 for definitions of unitary and spherical orbits and configurations). A similar unitary decomposition of the Hamiltonian, H = h + V, is sought. The non-interacting particle Hamiltonian h being a 1-body operator, is decomposed into 0 and 1 body parts with respect to the chosen spaces (it is scalar with respect to spherical configurations). Prior to unitary decomposition of V it is first divided into two parts; one is S conserving (i.e. $\Delta S=0$) and the other is not ($\Delta S \neq 0$). The S preserving part (we call it $V_{\Delta=0}$) is decomposed into two parts : the scalar parts with respect to configurations (call it $V^{[0]}$) and a tensor part ($V^{[\Lambda]}$); $V^{[0]}$ generates centroids of the spherical configurations and $V^{[\Lambda]}$ causes the spreading of the spikes. Thus $V_{\Delta=0} = V^{[\Lambda]} + V^{[0]}$. Now $V^{[0]}$ being a 2-body operator can be decomposed into 0,1 and 2 body parts with respect to the unitary group defined by the chosen space and thus $h + V^{[0]}$ can now be written as $h + V^{[0]} = h^0 + h^1 + V^{0,[0]} + V^{1,[0]} + V^{2,[0]}$. The 1- body part $V^{1,[0]}$ shifts the NIP spikes and the 2-body part $V^{2,[0]}$ causes the shift of the centroids not representable by a NIP Hamiltonian. In order to have a measure for the strength of these various parts, unitary norms ($|O|$ denotes norm of O)can be used. The definitions and procedures of calculating these norms are already available (ref. 1). This exercise (unitary decompositions and calculation of norms) has been carried out for various interactions (references to the various interactions given in the table and the single particle energies used can be had from the authors) all across the periodic table and the results for norms are shown in the table. Also shown in the tables is the error in the norm of $h + V^{[0]}$ when $V^{2,[0]}$ is dropped. This comes out to be less than 2% in all regions of the periodic table; similar results for a few interactions are obtained earlier[1]. Thus, irrespective of the region of periodic table and the interaction one is using, the $V^{2,[0]}$ can always be neglected. Moreover one can see the renormalization (norm of $V^{1,[0]}$) of h is important. Thus at this stage of $h + V^{[0]}$, one has a renormalized NIP Hamiltonian and this result is valid independent of the region of the periodic table as established by the results given in the table. The NIP theory and results given in ref. 2,3 can be used to deal with the $h + V^{[0]}$ part in level density calculations.

References :

1) J.B.French and V.K.B. Kota, Phys. Rev. Lett. **51**, 2183(1983); University of Rochester Report UR-1116 (1989). 2) V.K.B. Kota and D. Majumdar in this proceedings. 3) J.B.French, V.K.B. Kota and J.F.Smith, UR-1222 (1989).

Table : Norms of various tensor parts of $h + v^{[0]}$

Space	interaction	(m_p, m_n, s)	$\|h^1\|$	$\|v^{1,[0]}\|$	$\|H^1\|$	$\|v^{2,[0]}\|$	Error
(2s,1d) [a]	PW	(4,6,0)	5.75	4.55	10.01	1.66	1.37%
		(8,8,0)	5.58	7.33	12.55	1.55	0.77%
	UNIV-SD	(4,6,0)	6.36	1.65	7.16	1.16	1.32%
		(8,8,0)	6.17	2.51	7.50	1.02	0.93%
	BONN-SD	(4,4,0)	5.58	1.42	6.94	1.43	2.13%
		(6,8,0)	5.75	2.76	8.41	1.53	1.65%
	Pairing+Q.Q	(4,4,0)	5.58	0.58	5.50	0.43	0.30%
		(4,6,0)	5.75	0.75	5.66	0.41	0.26%
(1f,2p) [a]	MWH2	(6,6,0)	8.12	0.63	8.72	1.24	1.01%
		(10,10,0)	8.86	1.20	9.99	1.49	1.11%
	RMFP6	(6,6,0)	8.15	2.45	8.66	0.76	0.39%
		(8,8,0)	8.71	3.48	9.59	0.85	0.39%
	RMFP13	(6,6,0)	7.79	1.23	8.74	1.21	0.96%
		(10,10,0)	8.50	2.18	10.21	1.38	0.92%
#1 [a]	KBB	(4,6,0)	3.53	1.97	5.23	0.89	1.44%
		(8,8,0)	4.08	3.78	7.43	1.21	1.32%
(s,p,sd,fp) [b]	KUO	(6,6,2)	6.15	3.73	9.73	1.33	0.94%
	10-orbit	(6,6,4)	6.60	3.99	10.28	1.48	1.04%
		(12,12,0)	5.58	6.08	11.66	1.66	1.01%
		(12,12,2)	6.73	6.76	13.31	1.86	0.97%
(s,p,sd,	KUO	(22,22,0)	5.09	3.76	8.63	0.51	0.18%
fp,sdg) [c]	15-orbit	(22,22,1)	6.02	4.41	10.14	0.70	0.24%
		(22,22,2)	6.74	4.95	11.32	0.91	0.33%
		(22,22,3)	7.33	5.40	12.24	1.11	0.41%
		(22,22,4)	7.81	5.79	12.98	1.29	0.49%
#2 [a]	SDI	(14,10,0)	4.74	0.00	4.74	0.04	~0.00%
		(22,24,0)	4.94	0.00	4.94	0.04	~0.00%
	Pairing+Q.Q	(14,10,0)	4.74	0.14	4.87	0.09	0.02%
		(24,25,0)	4.80	0.27	5.04	0.09	0.02%
#3 [a]	SDI	(8,16,0)	6.33	0.00	6.33	0.03	~0.00%
		(10,21,0)	6.77	0.00	6.77	0.03	~0.00%
	Pairing+Q.Q	(8,16,0)	6.33	0.12	6.41	0.08	0.01%
		(13,21,0)	7.00	0.16	7.12	0.09	0.01%

#1 : $(2p_{3/2}1f_{5/2}2p_{1/2}1g_{9/2})$; #2 : $(1g_{7/2}2d_{5/2}2d_{3/2}1h_{11/2}3s_{1/2})^{m_p}$, $(1h_{9/2}2f_{7/2}2f_{5/2}3p_{3/2}3p_{1/2}1i_{13/2})^{m_n}$; #3 : $(1h_{9/2}2f_{7/2}2f_{5/2}2p_{3/2}2p_{1/2}1i_{13/2})^{m_p}$, $(1i_{11/2}2g_{9/2}2g_{7/2}3d_{5/2}3d_{3/2}4s_{1/2}1j_{15/2})^{m_n}$ a) s = 0; b) s = 0+1+2+3; c) s = 0+1+2+3+4. m_p and m_n are proton and neutron numbers.

QUADRUPOLE MOMENTS AND BAND-MIXING IN TUNGSTEN ISOTOPES IN DPPQ MODEL

J.B.Gupta
Ramjas College, University of Delhi , Delhi-7

The $^{182-184}W$ isotopes, having deformed g-bands with nearly constant $R_4 (=E_4/E_2)$, but overlapping γ- and β-bands varying fast with N, present quiet a challenge to nuclear theory [1-5]. Using Dynamic Pairing-Plus-Quadrupole model Kumar-Baranger [1] predicted the shape transitions from prolate to asymmetric-oblate-spherical in W-Os-Pt nuclei, which were supported by later experiments. However, they also predicted strong $\gamma-\beta$ band mixing, yielding small E2 quadrupole moments of the $K^{\pi}=2^{+}_{2}$ states in $^{182-186}W$, decreasing to lowest value in ^{182}W. This trend was partially supported by the Coulomb excitation results of Ref. [2] for $^{184-186}W$, but disagreed with those of others [3]. Recent experimental data [4] on the quadrupole moments of $^{182-184}W$ removes this anomaly in experiment, indicating weak band coupling. In H_{IBM} with 6 free parameters, the γ-band structure was reproduced, and with same χ_ν of Q operator, reasonable B(E2), $Q(2_1)$ and $Q(2_2)$ values were obtained [6]. In 4-parameter IBM-1, we have obtained similar satisfactory results.

Using the improved parameter free version of the dynamic deformation theory, employing the modified Nilsson potential with strutinsky shell correction, Veskovic et al. [5] have reproduced these small band mixing features. In view of the wide success of the DPPQ model for the Nd-Sm-Gd-Dy isotopes in the A= 150-160 region, we have re-examined the predictions of the model for the $^{182-186}W$ isotopes.

From the original version of the DPPQ model [1], several improvements have been made in the calculation technique [7], which version has been used in our work. The spherical s.p. levels as in [1] have been used, but the wave functions are now expanded in terms of some analytic functions, enabling the reduction in matrix size and better numerical accuracy. Our partial results are given in Table 1 for

Table 1. Some E2 moments in $^{182-186}$W in DPPD model.

Quantity		^{182}W	^{184}W	^{186}W
I=0 comp in 2^+_1		99.7 %	98.7	94.4
	2^+_2	93.4	14.9	10.5
	2^+_3	94.3	84.5	90.1

	Exp	Theo	Exp	Theo	Exp	Theo
B(E2, $0-2_1$)	4.1% [1]	3.43	3.73 [7]	3.32	3.50 [6]	3.03
B(E2, $0-2_2$)	0.134 [6]	0.097	0.14 [1]	0.14	0.15 [1]	0.12
B(E2, $0-2_3$)	0.028 [2]	0.122	0.03	0.08	6×10^{-4}	0.04
$Q(2_1)$ e.b	-1.85 [2]	-1.45	-1.75	-1.45	-1.68 [2]	-1.12
$Q(2_2)/Q(2_1)$	-0.92 [2]	-0.48	-1.19 [7]	-0.87	-0.8 [3]	-0.91
DDM [5]		-0.91		-0.93		-1.02

the K-components of the 2^+ states, their quadrupole moments and B(E2) values.

The present results of the DPPD model broadly agree with experiment. The K=2 component mixing is smaller than obtained previously, conforming to small band mixing, and decreasing towards ^{186}W, though it is still larger than the 10 % mixing obtained in the DDM calculation [5]. The $Q(2_2^+)$ value is positive and decreases in magnitude as N is increasing, and $|Q(2_2)/Q(2_1)|$ varies 0.7 to 0.9, instead of only 0.08 given earlier [1]. The fall in $E(2_2)$ towards ^{186}W is also obtained but energy values are low. The fall of the $K=0_2$ band is not obtained and the B(E2, 2_3-2_1) values are larger by a factor of 3-8. Thus the present DPPD results represent an improvement, but need further study of the role of spherical single particle levels adopted as in [1].

References

1. K. Kumar-M. Baranger, Nucl. Phys. A122 (1968) 273
2. J.J. O' Brien et al., Nucl. Phys. A291 (1977) 510
3. F.K. McGowan et al. Nucl. Phys. A289 (1977) 253
4. C.Y. Wu et al., Phys. Rev. C40 (1989) R3
5. M. Veskovic, W.D. Hamilton and K.Kumar, Phys. Rev C41 (1990) R1
6. P.D.Duval & B.R.Barret, Phyd. Rev. C23 (1981) 493
7. K. Kumar, Nucl. Phys. A231 (1974) 189

VARIATION OF ROTATINAL CONTENT IN $E(2_1^+)$ WITH VALENCE NUCLEON PAIRS

J.B.Gupta and A.K.Kavathekar
Ramjas College, University of Delhi, Delhi-110 007

Treating the energy of $I^\pi = 2_1^+$ state in even Z - even N nuclei as a sum of rotational energy (ROTE) $bI(I+1)$ and vibrational energy aI plus R-V interaction energy $cI^2(I+1)$, called shape fluctuation energy (SFE), the evaluation of shape transition with increasing nucleon (or hole) pairs product (N_pN_n) is studied. A correspondence of ROTE and B(E2, $0^+ - 2^+$) versus the N_pN_n product is illustrated. The constancy of the $E(2_1^+) \times B(E2)\uparrow$ which is a measure of the partial E2 transition strength (Energy Weighted Sum Rule) EWSR at low excitation energies is thus made more transparent.

In earlier work of Gupta et al.[1], the variation of ROTE and SFE with N_pN_n product was studied. However, with increasing deformation of a nucleus, both ROTE and SFE fall, so that a realistic picture of the rotational content in a collective state (say 2_1^+) is not given. Here we illustrate the variation of ROTE/$E(2_1^+)$ versus the N_pN_n product, which shows an exponential growth in the Z=50-82, N=82-126 region and almost linear rise in the Xe-Gd, N<82 region. As earlier, the energy equation

$$E(I) = bI(I+1) + aI + cI^2(I+1) \qquad (1)$$

was used to determine the coefficient a,b,c by a least square fit to the known energies of $I^\pi \leq 12^+$ states for each nucleus. Then ROTE in 2_1^+ was evaluated. The exponential growth ROTE is illustrated by a LS fit to the theoretical curve given by

$$Y = \text{ROTE}/E(2_1^+) = B + A[1 - e^{-C(X - X_o)}] \qquad (2)$$

where $X = N_pN_n$. The LS fit equations here were solved by a special method, wherein one has to input approximate values of A, B, C, X_o obtained by hand fit. Then defining $A = A_o + \alpha$ etc., the values of α, β, γ are determined by using the residuals

$$r_i = Y_i(calc) - Y_i(expt) \qquad (3)$$

in the equation

$$d_i = r_i + \alpha\left(\frac{\partial Y_i}{\partial A}\right)_o + \beta\left(\frac{\partial Y_i}{\partial B}\right)_o + \gamma\left(\frac{\partial Y_i}{\partial C}\right)_o \qquad (4)$$

and solving Eq.4 by the standard LS fit method.

Again, the Z = 50-82, N = 82-126 space was divided into 4 quadrants by the mid Z=66, N=104 values so that the space of particle pairs is distinct from that of hole pairs. For the three regions: Ba-Gd (N<82), Dy-Pt (N<104) and Yb-Hg (N>104), data was fit to exponential growth curve (2) with the values of constants as listed below.

Region	B	A	C	X_o
I	0.195	0.833	0.131	5
II	0.04	1.053	0.114	15
III	0.415	0.67	0.167	10
β_2/β_{sp} [2]	0.605	3.175	0.012	0

The variation in these growth constants reveal the underlying physical differences in the three regions.

In a hydrodynamic description, the rotation and vibration represent the 2 branches of a single surface wave motion on a liquid drop. The smooth N_pN_n dependence exhibits the macroscopic deformation effects and the intimate relation of the two branches. Systematic deviations from smooth curve represent the underlying microscopic effects.

Raman et al. [2] plotted the B(E2)↑ and (β_{def}/β_{sp}) versus the N_pN_n product for the Z=50-82, N=82-126 regions on a single plot and obtained a fit to Eq. 2. Their values of A,B,C are similar to our values. Thus a rise in B(E2)↑ corresponds to the rise of ROTE in 2_1^+ state. The constant $E(2_1^+)$ x B(E2)↑ and EWSR implies a falling vibrational component and the rise in B(E2)↑ comes from the increase in rotational content which represents a coherent motion.

References

1. J.B. Gupta et al., Phys. Scripta 41 (1990) 660
2. S. Raman et al., Phys. Rev. C37 (1988) 805

NEUTRON-DEFICIENT NUCLEI NEAR MASS-80 REGION
I. EXCITATION FUNCTION MEASUREMENTS

A. Goswami[1], B. S. Tomar[1], S. Chattopadhay[2], S. K. Saha[1,3], S. K. Basu[3] and H. C. Jain[2]

1 Radiochemistry Division, B. A. R. C., Bombay.
2 Tata Institute of Fundamental Research, Bombay.
3 Variable Energy Cyclotron Centre, Calcutta.

The neutron-deficient nuclei near mass-80 region have drawn considerable attention in the recent years. These nuclei exhibit several interesting features, such as, the presence of large ground state quadrupole deformations, coexistence of different shapes at low excitation and rapid variation in the shape as a function of N and Z. According to PES calculations/1/, it is expected that Nb (Z=41) and Zr (Z=40) isotopes are prolate deformed (β_2~0.4) for A≤82 ; oblate deformed(β_2~-0.2) for 83<A<85 and weakly deformed for A≥86. The systematic data for light Zr isotopes/2/, indeed, demonstrate a jump in collectivity between N=86 and 84. Similar studies on Nb isotopes are, therefore, important for a better understanding of this transition region. A survey of the literature indicates that very little information is available on the excited states of Nb (A=84-87). The present work on excitation function measurements is initiated with a view to choose the proper reaction and projectile energies for a detailed spectroscopic studies of some of those Nb isotopes.

The nuclei of interest were produced by bombarding self-supporting rolled (~500 μgm/cm**2) enriched (99.9%) Ni-58 targets with Si-28 (E_{lab}= 85-120 MeV) and S-32 (E_{lab}= 110-132 MeV) beams respectively, from the BARC-TIFR Pelletron Accelerator. Prompt gamma-rays were detected with two HPGe detectors, one with rectangular BGO anti-compton shield, placed at 90° and the other without a shield, placed at 45° to the beam direction.

On the basis of the latest information available/3,4/, the dominant reaction channels from the two reactions have been identified and their absolute production cross-sections were deduced after proper normalisation and efficiency correction. Typical excitation function curve for Ni + S reaction is displayed in Fig. 1. The dominant channels in the case of Ni + Si reaction are found to be channels like, (4p), (3p), (α2p) etc. and neutron channels are very

much inhibited, in agreement with the available data.We have definitely observed prompt gamma-rays from Nb-87 (3p), Nb-86(3pn) and Nb-84(αpn) besides other known channels. From beam-off spectra, short-lived activities pertaining to the ground and isomeric state decays of the said Nb nuclei have been observed. Theoretical estimates of cross-sections for various observed channels have been done with the code "CASCADE" and were found to be in good agreement with the experimental data. Detailed gamma-gamma and gamma-x spectroscopy is planned in the next step.

References:

1. P. Moller and J. R. Nix, AT&NDT 26, 165 (1981)
2. C. J. Lister et al., PRL 59, 1270 (1987)
3. W. Gelletly et al., PL B253, 287 (1991)
4. B. J. Min et al., NP A530, 211 (1991)

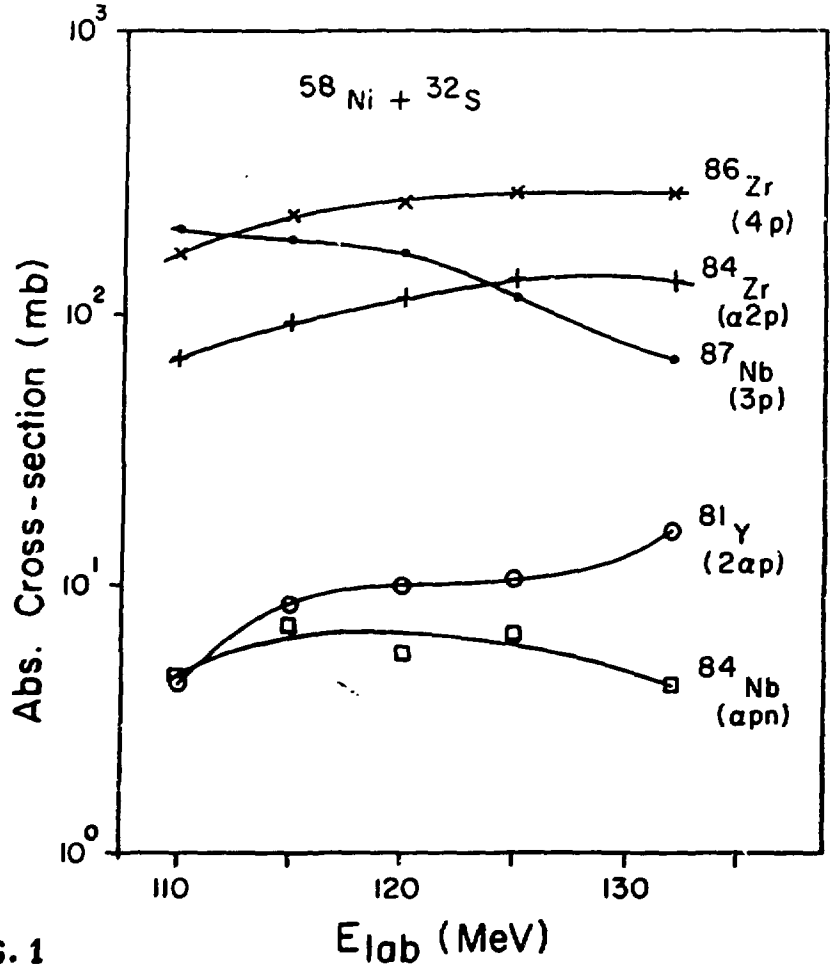

FIG. 1

INTERPLAY OF TRIAXIAL DEFORMATION, ISOSPIN AND TEMPERATURE IN A = 90 NUCLEI

A.Mohamed Akbar, S.Veeraraghavan† and N.Arunachalam
Department of Physics, Government Arts College, Tiruvannamalai 606 603

The statistical theory of hot nuclei /1,2/ is used to extract the nuclear parameters such as the asymmetry parameter, single particle level density parameter etc. as functions of isospin, temperature and triaxial deformation in the case of Zr. The isospin induced shape transitions of this nucleus at various temperatures are studied.

The triaxial deformation is introduced into the picture by using the triaxial Nilsson Hamiltonian

$$H = \frac{p^2}{2m} + \frac{m}{2}(\omega_x^2 x^2 + \omega_y^2 y^2 + \omega_z^2 z^2) + C\,l\cdot s + D(l^2 - \langle l^2 \rangle) \quad (1)$$

where the oscillator frequencies and the deformation parameters used are as in /3/.

The grand canonical partition function for a system of A nucleons at a temperature $T = 1/\beta$ is

$$\Omega_0(\alpha, \beta, \gamma) = \sum_{\epsilon_i, N_i, \tau_i} \exp(\alpha N_i - \beta E_i + \gamma \tau_i) \quad (2)$$

where the Lagrangian multipliers α, β and γ conserve the particle number, total energy and z component of total isospin. The corresponding conservation equations in terms of the single particle energies are

$$\langle N \rangle = A = \sum n_i^+ + \sum n_i^- \quad (3)$$

$$\langle E \rangle = \sum (n_i^+ + n_i^-)\,\epsilon_i \quad (4)$$

$$\langle \tau \rangle = \sum n_i^+ \tau_z^+ + \sum n_i^- \tau_z^- \quad (5)$$

where n_i^+ and n_i^- are the occupation probabilities for neutrons and protons with isospin projections $+\frac{1}{2}$ and $-\frac{1}{2}$ respectively.

The asymmetry parameter is given by /2/

$$\alpha_{asy} = \frac{AT}{8\left(\frac{\partial \tau}{\partial \gamma}\right)} \quad (6)$$

where

$$\frac{\partial \gamma}{\partial \tau} = -\left[\sum n_i^+(1-n_i^+)\tau_z^{+2} + \sum n_i^-(1-n_i^-)\tau_z^{-2}\right]^{-1} \quad (7)$$

The equilibrium deformation parameters δ and θ corresponding to the minimum total energy for ^{90}Zr are tabulated for various temperatures. At T = 0.3 MeV the nucleus is prolate for isospins from 0 to 3, spherical for isospins from 4 to 6, oblate for the isospin 7

Equilibrium deformation of ^{90}Zr at different isospins and temperatures.

Isospin	T=0.3 MeV		T=0.6 MeV		T=1.1 MeV	
	δ	θdeg.	δ	θdeg.	δ	θdeg.
0	0.2	-120	0.2	-120	0.0	-180
1	0.1	-120	0.1	-120	0.0	-180
2	0.1	-120	0.1	-120	0.0	-180
3	0.1	-120	0.0	-180	0.0	-180
4	0.0	-180	0.0	-180	0.0	-180
5	0.0	-180	0.0	-180	0.0	-180
6	0.0	-180	0.0	-180	0.0	-180
7	0.1	-180	0.0	-180	0.0	-180
8	0.1	-160	0.0	-180	0.0	-180
9	0.1	-140	0.0	-180	0.0	-180
10	0.1	-140	0.0	-180	0.0	-180

and tries to become prolate at higher isospins.These deformation fluctuations vanish at a high temperature of about T = 1.1 MeV, because of the vanishing isospin and shell effects at this temperature.

The variation of asymmetry parameter for ^{90}Zr as a function of total isospin and temperature is depicted in Fig.1.This parameter is obtained after minimising the total energy of the system with respect to deformation for each temperature.This asymmetry parameter shows a maximum at all temperatures for $\tau = 5$ corresponding to the stable neutron number N=50 and proton number Z=40.It is obvious from the figure that higher temperatures cause a decrease in the maximum at the isospin $\tau = 5$.

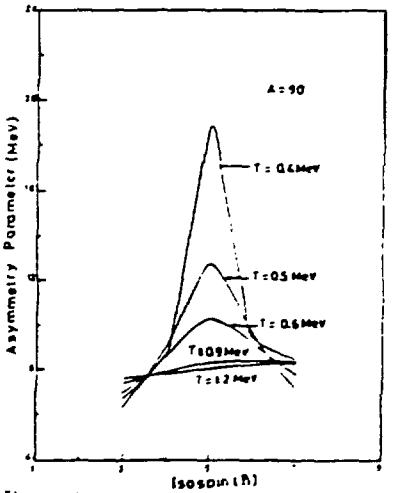

Fig.1. Variation of asymmetry parameter with isospin at various temperatures in the case of A = 90 for minimised total energy with respect to deformation.

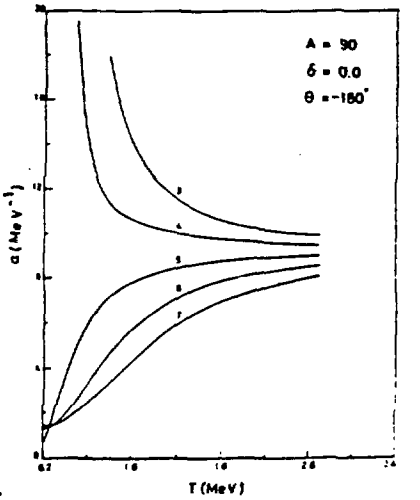

Fig.2. Variation of the single particle level density parameter with temperature for various isospins of the isobar A = 90.The numbers on the curve refer to the isospin of the system.

Fig.2.shows the variation of the single particle level density parameter with temperature for various isospins of ^{90}Zr. This parameter is minimum for the isospin $\tau = 5$ at $T = 0.3$ MeV indicating the higher stability of this isospin. The effect of isospin is less significant at higher temperatures and the curves converge to the predicted value of $a \approx A/10$.

Further work is in progress to detect Yrast traps in the excitation energy versus isospin plane by drawing constant entropy lines.

References

/1/ C.Bloch,in Proceedings of the statistical properties of nuclei edited by Garg (Plenum,NewYork,1977), pp.379 and 403; Phys.Rev.93 (1954) 1094.

/2/ M.Rajasekaran,N.Arunachalam, T.R.Rajasekaran and V.Devanathan Phys.Rev.C 38, (1988) 1926.

/3/ M.Rajasekaran,N.Arunachalam,and V.Devanathan Phys. Rev.C 36 (1987)1860.

†Deparment of Physics,Sacred Heart College,Tirupattur, 635 601,Tamil Nadu.

HIGH SPIN STATES IN HOT DEFORMED ZIRCONIUM NUCLEI

S.Veeraraghavan,A.Mohamed Akbar and N.Arunachalam
Department of Physics,Government Arts College,Tiruvannamalai.606603

Recently Bloementhal et al. [1] have analysed experimentally the nuclear structure effects in Zirconium nuclei and it is our aim to study the properties of this nucleus in detail within the framework of the statistical theory.Triaxial deformation, rotation in angular momentum space and temperature degrees of freedom are included in the study.The variation of single particle level density parameter with temperature and rotation, the nature of particle distribution near the Fermi level and the behaviour of excitation energy with rotation are analysed.

The grand canonical partition function for a system of N neutrons and Z protons in a state of total angular momentum M along the rotation axis is [2]

$$Q(\alpha_z,\alpha_N,\beta,\gamma)=\Sigma\exp(-\beta E_i+\alpha_z Z_i+\alpha_N N_i+\gamma M). \quad (1)$$

The Lagrangian multipliers α_z, α_N, and γ conserve the proton number, neutron number and total angular momentum M along the z axis for a given temperature $T=1/\beta$. The corresponding equations in terms of single particle energies ϵ_i and spin projections m_i are

$$\langle Z\rangle=\Sigma n_i^z=\Sigma\left[1+\exp(-\alpha_z+\beta\epsilon_i^z+\gamma m_i^z)\right]^{-1} \quad (2)$$

$$\langle N\rangle=\Sigma n_i^N=\Sigma\left[1+\exp(-\alpha_N+\beta\epsilon_i^N+\gamma m_i^N)\right]^{-1} \quad (3)$$

$$\langle E\rangle=\Sigma n_i^N\epsilon_i^N+\Sigma n_i^z\epsilon_i^z \quad (4)$$

$$\langle M\rangle=\Sigma n_i^N m_i^N+\Sigma n_i^z m_i^z \quad (5)$$

The excitation energy E of the system for an angular momentum state M is given by

$$E^*(\delta,\theta,M,T)=\left|\Sigma n_i^z\epsilon_i^z-\Sigma\epsilon_i^z\right| \quad (6)$$

with a similar equation for protons. The single particle level density parameter a is found using the relation

$$a(\delta,\theta,M,T)=\frac{S^2(\delta,\theta,M,T)}{4E^*(\delta,\theta,M,T)} \quad (7)$$

where the entropy S is calculated using

$$S=-\Sigma\left[n_i\ln n_i+(1-n_i)\ln(1-n_i)\right] \quad (8)$$

Figure 1 shows the occupation probability n_i^z of neutrons in ^{90}Zr as a function of ϵ_i for different spins at temperatures T = 0.3 MeV and T = 1.2 MeV. It is seen from the curves that as the nucleus rotates faster the particles near the Fermi level tend to shift to higher levels and this effect is more pronounced for higher spins. An increase of nuclear temperature also plays the same role in shifting more particles to higher levels.

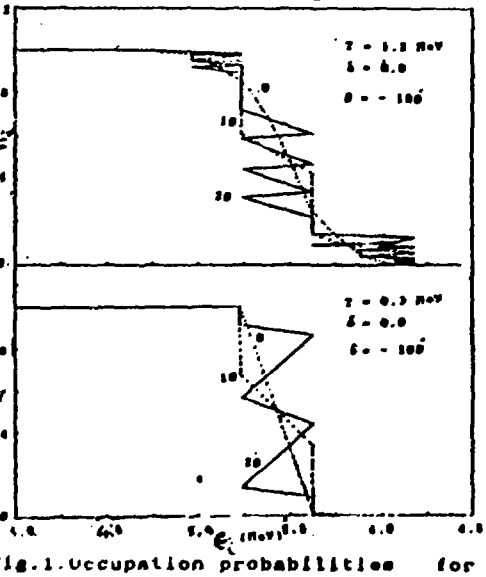

Fig.1.Occupation probabilities for neutrons as functions of the single particle energies for A = 90. The numbers on the curve refer to the z component of the total angular momentum of the system.

The variation of single particle level density parameter for ^{90}Zr as a function of temperature and angular momentum is depicted in Fig.2. The effect of rotation on the single particle level density parameter is very much pronounced at low temperatures as the shell structure plays a major role at these temperatures. The single particle level density parameter fluctuations are different for different angular momentum states of the nuclei at low temperatures. As the temperature increases to sufficiently high values, the value of the parameter a tends to reach the empirical value of A/10 for all spins.

Constant temperature lines are drawn in the excitation energy versus the total angular momentum plane for A = 90, 94, and 96 in Fig.3. These lines are drawn by minimising the total energy of the system with respect to triaxial deformation at temperature T = 0.9 MeV. The curve for A = 96 exhibits a backbending at spin M = 12 $\hbar$ while the curve for A = 94 has a backbending at spin M = 14 $\hbar$. However for the magic number nuclei A= 90 no such effects are observed even upto a spin of 22 $\hbar$.

The inclusion of pairing correlations into the picture may give the true state of affairs of the system and calculations are in progress towards this end.

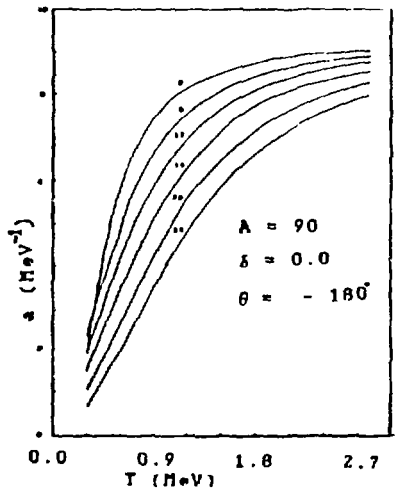

Fig.2. Variation of the single particle level density parameter with temperature for A = 90. The numbers on the curve refer to the z component of the total angular momentum of the system.

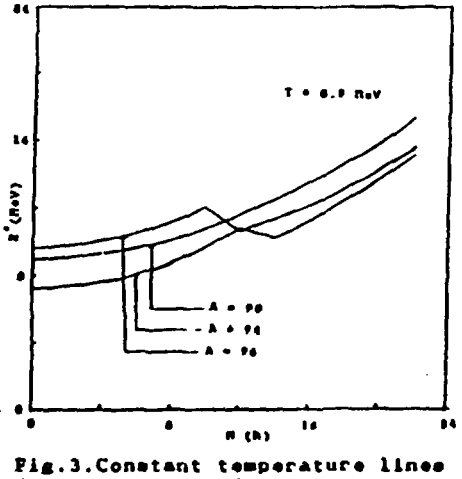

Fig.3. Constant temperature lines for isotopes of Zirconium

References

/1/ D.J.Bluementhal et al.Phys.Rev.Lett.66,3121(1991).

/2/ M.Rajasekaran, T.R.Rajasekaran and N.Arunachalam,Phys.Rev.C37,307(1988).

†Department of Physics,Sacred Heart College,Tirupattur, 635601,Tamil Nadu.

MODIFIED RVM DESCRIPTION FOR 196 Pt ISOTOPE

A.K.Varshney[+], K.K.Gupta[*], S.P.Sud[**], V.P.Varshney[++] and D.K.Gupta[++]

+ G.G.D.S.D.College,(H.P. Univ.), Baijnath-176125,(H.P.) * Govt.College, Sarkaghat (H.P.).**H.P.Univ.,Shimla (H.P.). ++ D.V.College, Aligarh-202001(U.P.)

The Platinum groupe of isotopes which lies on the boundary of the strongly deformed rare earth nuclei has becomes a subject of great interest both experimentally and theoretically. Platinum nuclei are neither good roters nor good vibrators but lie in between rotational and vibrational cases. The nucleus 196 Pt is one of the most interestin structures in the heavy mass tranisition region. It has become a focus of much theoretical and experimental work /1,2/.

We performed the Rotation Vibration Model (RVM) calculations with three band mixing (RVM-3). These calculations failed badly in reproducing the observed energy spectrum, B(E2) values and branching ratios. We modified the three band mixing rotation vibration modle (RVM-4) by introducing two more parameter under the assumption of different mass parameters for rotation, beta-vibration and gamma-vibration. The energy levels, B(E2)'s and branching ratios have been calculated for 196 pt using the relations given in reference /3,4/. The Boson Expansion Technique (BET) results are given for comparison only.

It is observed that the RVM-4 predictions in almost all cases are close to the experimental ones. The large variations of BET results in $2_3 \rightarrow 4_1/2_1$ and $2_3 \rightarrow 4_1/2_2$ ratios have been found to be reduced significantly in the present work. This is fascinating here to see that the assumption of a different physical picture of generating the beta-vibrational band /2/ could not reproduce the experimental rates for the decay of 2_3^+ level while the RVM results which assume 2_3^+level to be the second member of the beta-vibrational band are in closer agreement.

Table:- B(E2)'s and Branching ratios in ^{196}Pt (in units of e^2b^2)

TRANSITION	EXP*	RVM-4	RVM-3	BET*
$2_1 \rightarrow 0_1$	0.294(14)	0.298	0.312	0.294
$4_1 \rightarrow 2_1$	0.425(15)	0.397	0.464	0.502
$2_2 \rightarrow 0_1/2_1$	1×10^{-5}	0.010	0.03	0.019
$4_2 \rightarrow 2_2/4_1$	0.92	3.09	0.597	1.35
$2_3 \rightarrow 2_1/0_2$	0.01	0.076	0.06	0.003
$2_3 \rightarrow 4_1/2_1$	2.18	1.42	6.06	14.11
$2_3 \rightarrow 2_2/0_2$	0.1	0.084	0.08	0.02
$2_3 \rightarrow 2_2/2_1$	9.09	1.27	1.21	5.88
$2_3 \rightarrow 4_1/2_2$	0.24	1.1	5.0	2.4
$2_3 \rightarrow 4_1/0_2$	0.024	0.094	0.40	0.048

* from reference 2 and 5

References

/1/ Nucl. Phys. A 270, 317 (1976).
/2/ Phys. Rev. C 22, 888 (1980).
/3/ Phys. Rev. C 27, 872 (1983).
/4/ Nuovo Cimento A 99, 1 (1988) and reference cited there in.
/5/ Nucl. Phys. A 196, 369 (1972).

ANALYSIS OF DEGREE OF RIGIDITY/FREEDOM IN VARIOUS NUCLEI WITH INCREASING ANGULAR MOMENTUM I=3

A.K.Varshney*, K.K.Gupta+, D.K.Gupta++, S.P.Sud+++, R.Prasad and R.K.Tyagi.
Applied Physics Deptt., Engg.College, A.M.U.,Aligarh-202002 (U.P.)+Govt.College., Sarkaghat,(H.P.).++S.V. College,Aligarh-202001. +++ H.P.Univ. Shimla-5 H.P.

The study of E2 transitions from the 2^+ state of the gamma-vibrational band has previously been made by Gupta et.al./1/. In this study, it is oberved that the DF (rigid) model /2/ values are closer to the experimental ones and the DR (dynamic) model /3/ keeps comparatively a large number of nuclei outside its rigime than the DF model. And further for the nuclei which lie beyond the approach of both the models it is found that experimental values are closer to the DF model than to the DR predictions. This supremacy of DF (rigid) over DR (dynamic) estimates observed by Gupta et.al./1/ leads to the suggestion that this study strongly supports the adiabatic approximation of 2^+ state of the gamma-vibrational band and favours the rigid shape of the nucleus at this spin.

The ratio $B(E2;3^+ \rightarrow 2^+/4^+)$, in which the experimental values are available for a large number of nuclei /4,5/ has been considered for studying the validity of the Asymmetric Rotor Model (ARM) (DF (rigid) and DR (dynamic) models) and to check the usefulness of asymmetry at energy exceeding 1 Mev i.e. 3^+ state of the gamma-vibrational band. The enhancement/hindrence factor (F) has been computed authentically in both the models. It is observed, in general, that the DR (dynamic) model factor (F_D) is closer the unity and less than the DF (rigid) model factor (F_R).

The nuclei in which F_R is nearer to unity and F_D is more but within the limit of acceptability of model (i.e. $.2 \leq F \leq 5$)/6/ it indicates that the nuclei at 3^+ state spin areless rigid than the 2^+ state spin of the same band and want some freedom, though the variation of degree of freedom can not be said exactly. It, therefore, has been confirmed that the nucleus is not so rigid at 3^+ state as it was at 2^+

state of the gamma-vibrational band. However there are few exceptions 104 Pd, 106 Pd, 108 Cd, 110 Cd, 156 Gd and 160 Er.

Further, for most of the nuclei in which F_R and F_D are nearly equal to unity, we find that γ(non-axiality parameter) $\leq 15°$. Basically these nuclei do not come in the range of the ARM and therefor can easily be explained by any of the models. Exceptions are 102 Ru, 150 Sm, 156 Er, 178 Er and 186 W. However we can not estimate the exact shape of the nucleus and especially the degree to which β -and γ -freedom is existing.

Table:- Enhancement/Hindrence Factor (F) values for $B(E2;7^+ \rightarrow 2^+/4^+)$ ratio

NUCLEUS	γ	F_R	F_D	NUCLEUS	γ	F_R	F_D
98 Mo	26.2	2.88	1.39	160 Er	15.0	0.87	0.70
100 Ru	24.3	2.44	1.12	162 Er	13.2	1.01	3.10
102 Ru	25.5	1.59	0.74	164 Er	12.9	1.65	0.98
104 Ru	24.5	2.47	1.10	166 Er	12.7	2.82	1.62
104 Pd	25.0	0.05	4.13	168 Er	11.3	2.72	1.30
106 Pd	26.5	0.01	4.50	170 Er	11.4	3.21	1.45
108 Cd	24.3	0.16	0.72	164 Yb	14.8	1.71	1.35
110 Cd	26.0	0.03	3.25	166 Yb	13.0	1.76	1.07
150 Sm	20.5	1.42	0.82	168 Yb	11.7	2.54	1.23
152 Sm	13.2	1.57	0.81	170 Yb	10.8	2.47	2.14
154 Sm	9.5	2.23	0.59	172 Yb	9.5	4.80	1.10
152 Cd	21.5	2.14	1.12	174 Hf	10.8	3.01	0.84
154 Cd	14.0	1.35	1.19	176 Hf	10.2	3.28	0.95
156 Gd	11.0	0.53	0.21	182 W	11.4	3.44	1.51
158 Gd	10.3	6.20	1.81	184 W	13.1	2.15	1.46
158 Dy	12.7	1.72	1.22	186 W	15.8	1.51	1.08
160 Dy	11.7	2.19	1.06	186 Os	16.5	2.62	1.67
162 Dy	12.0	2.53	1.28	188 Os	19.2	2.26	1.33
156 Er	23.5	1.67	1.02	190 Os	22.5	2.82	1.15
158 Er	18.7	1.79	1.01	230 Th	10.5	3.19	1.67

Referenc-es

1. Nuovo Cimento B 58,101 (1980): J.Phys.Soc.Jpn. 40,4(1980).
2. Nucl. Phys. 8,257 (1958).3. Nucl.Phys. 60,529(1964).
4. Nucleus 2, 1(1987). 5. J.Fiz.Mal.8, 35 (1937).
6. Nucl.Phys. A 231,189 (1974).

* Present Address: Physics Deptt., H.P.S.S.S.College, DALHOUSIE-176125 (H.P.)

COMPARATIVE STUDY BETWEEN CRANKING METHOD AND LAGRANGIAN MULTIPLIER METHOD

M. Rajasekaran, D. Caleb Chanthi Raj and R. Premanand
Department of Nuclear Physics, University of Madras,
Guindy Campus, MADRAS 600 025.

In the cranked Nilsson model [1], the rotational part of the Hamiltonian wJ_z, where w is the rotational frequency, is diagonalised using the oscillator basis. The effect of wJ_z is to split states with spin projections $\pm m_z$, which are degenerate in the case of axially symmetric nuclei. The matrix elements of wJ_z generates angular momentum.

In our earlier work [2], we prescribed a single particle density function which includes the rotational part αJ_z for axially symmetric nuclei and showed that by treating α as the lagrangian multiplier, it is possible to generate angular momentum.

The present study is to analyse the above methods and establish the connection between the rotational frequency w and the lagrangian multiplier α. In the former, the term corresponding to collective rotation wJ_z is incorporated in the Hamiltonian of the system itself, while in the later, single particle levels are used and angular momenta are generated from the particle spin projections m_z through the lagrangian multiplier α.

Our calculations show that the rotational frequency w and the lagrangian multiplier α are identically equal for axially symmetric shapes This is because the single particle spin projections along the symmetry axis of an axially symmetric nuclei is a good quantum number and that their matrix elements of different spin projections do not mix. This is after all anticipated since the structure of the Hamiltonian of axially symmetric cases allows us the freedom of adding the rotational part separately to the eigen values of H_0. However, for triaxial deformations the single particle spin projections m_z ceases to be a good quantum number because the matrix elements of the Hamiltonian of a triaxially deformed nuclei connects states of different m_z. Hence, for a triaxially deformed nuclei, $\alpha \neq w$.

In the cranking method, the increasing w of the nucleus is accomplished by the rearrangement in the set of occupied states and consequently, if the required a priori value of I does not overlap with angular momentum value occurring in the step function I(w) mentioned above, equation I = I(w) cannot be solved. This problem

has been encountered in the course of the calculations by many groups. So to get quantities like shell correction, for a given angular momentum , they interpolated between two given I values. Through the lagrangian multiplier method, however, we are to get all angular momentum states.

Calculations were done by the cranking method [1] and quantities like shell correction, rotational energy were calculated for the optimal spin states. These quantities for other spins were got by interpolation. Calculation were also performed by the lagrangian method and the same quantities obtained for all spin states. It is observed that the quantities obtained by both the method are equal.

We shall now bring out some interesting common features of the lagrangian multiplier method and the slanted fermi surface method. In the slanted fermi surface method , the excited configurations can be found by tilting the straight line corresponding to the fermi surface , and they are denoted as the optimal states at the given deformation. The intermediate spins are obtained from particle-hole excitations across the sloping fermi surface.

In the present method, the angular momentum states are built through the lagrangian multiplier α. The lagrangian multiplier is varied, which in turn alters the occupational probability such that $\Sigma\, n_i m_i = I$. The occupational probability obtained by solving the simultaneous equations in Ref.2. is either 1 or 0 for the optimal configurations of the sloping fermi surface method. In fact, the orbitals depopulating and populating are also the same. The occupational probability of the other angular momentum states are not equal to 0 or 1 but intermediate between them. In the cranking model, for intermediate spins, interpolating techniques are used which may not be dependable when the shell structure changes drastically with spin.

In conclusion we say that the present formalism avoids interpolation technique of mathematical origin and is able to build all angular momentum states. The occupational probability are obtained in a natural way in the present approach which proves to be a good test for the method so that it can be confidently applied for other configurations as well.

[1] R. Bengtsson et al, Phys. Lett. 57B (1975) 301.
[2] M. Rajasekaran and D. Caleb Chanthi Raj, Nucl. Phys. Symp. (India) 32B (1989) 98.

NUCLEONIC SEPARATION ENERGY AS A FUNCTION OF ANGULAR MOMENTUM AND TEMPERATURE

M. Rajasekaran, D. Caleb Chanthi Raj, R. Premanand & P. Sivakumar

Department of Nuclear Physics, University of Madras, Guindy Campus, MADRAS 600 025.

The formation and subsequent de-excitation of a fused compound system is an interesting problem in view of the several degrees of freedom involved, particularly the stability against fission, particle emission and shape changes.

A new formula for the neutron separation energy at high energy and high spins was derived by us [1] using statistical theory. Here we theoretically analyse the compound nucleus and its decay by particle emission from a macroscopic-microscopic point of view. Such a picture is consistent with the classical model of heavy ion reaction, where one visualises the nucleus as a liquid drop with shell effects added to it from microscopic calculations.

The energy of the rotating nucleus is given by

$$E = U_{LD} + (\hbar I)^2 / 2\mathcal{I} \qquad (1)$$

For the liquid drop energy U_{LD} we use the Moller et. al. [2] version of LDM. We bring in the shell effects by invoking the microscopic moment of inertia $\mathcal{I}$, calculated from the statistical theory [1]. The lagrangian multiplier of the statistical theory generates the total angular momentum I, energy E for various temperatures T of the compound system. The energy Eq. (1) of the rotating nucleus now has got the classical tendencies hidden in the first term and the shell effects in the second term. The moment of inertia is obtained from the expression

$$\mathcal{I} = \hbar^2 I \, (\partial E_{rot}/\partial I)^{-1} \qquad (2)$$

where $E_{rot} = E(I,T) - E(0,T)$

The separation energies of neutron (S_n) and proton (S_p) from the compound nucleus is given by

$$S^{I_i}(N_i,Z_i,N_f,Z_f) = B^{I_i}(N_i,Z_i,B_j^i) - B^{I_f}(N_i-N_f,Z_i-Z_f,B_j^i)$$

(Z_f, N_f) = (1,0) for neutrons
(0,1) for protons

Here B^{I_i} and B^{I_f} represent the binding energy of the initial and final nuclei at spins I_i and I_f respectively.

Separation energies of neutron and proton are calculated as a function of total angular momentum of Hg-194 compound nucleus for different temperatures. Results of the behaviour of S_n and S_p as a function of angular momentum at T = 0.5, 1 & 2 MeV are shown in Figure.

We observe that S_p is almost 1.5 times smaller than S_n. This effect results from the larger neutron deficiency in the parent nucleus Hg-194 [3].

The separation energy curves corresponding to T = 0.5 MeV shows a fluctuating behaviour. This is due to shell effects. Increase in temperature of compound system removes the shell effects as can be seen from the figure. Increase in temperature also increases the probability for particle emission.

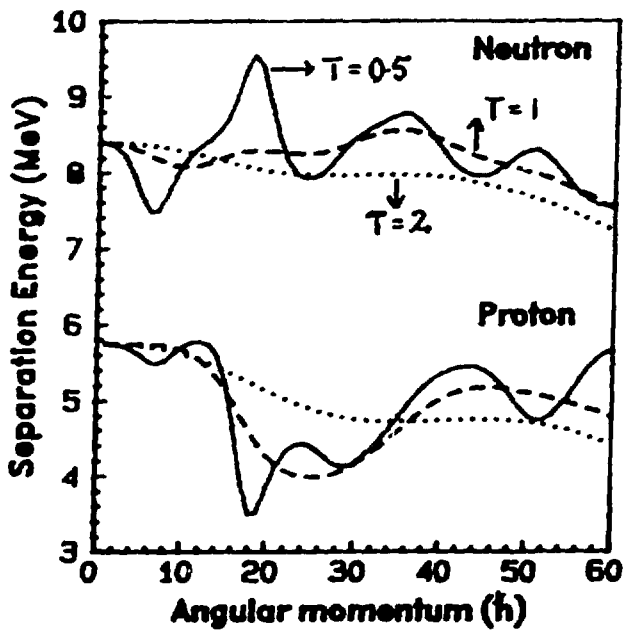

1. M.Rajasekaran et al, Phys.Rev. Lett. 61 (88) 2077
2. P.Moller et.al. Atomic data and Nuclear data Tables 39 (1988) 225
3. M. Faber et al, Z. Phys. 291 (1979) 337

AN EMPIRICAL FORMULA FOR NUCLEAR LEVEL DENSITY PARAMETER

M. Rajasekaran, R. Premanand & D. Caleb Chanthi Raj
Department of Nuclear Physics, University of Madras,
Guindy Campus, Madras 600 025.

The evaluation of the level density parameter 'a' is important since it plays a major role in the determination of the nuclear level density, which is a basic ingredient in statistical analysis of nuclear reactions. It has been a subject of many investigations at low and high excitation energies, both for experimentalists and theoreticians.

Experimentally, information on the level density parameter $a = A/K$ is obtained from the nuclear resonances and from the analysis of evaporation spectra. Theoretically, the level density parameter 'a' is obtained from the Fermi gas model, and is given by [1]

$$a = \pi^2 g(\epsilon_F)/6, \qquad (1)$$

where ϵ_F is the Fermi energy, $g(\epsilon)$ is the single particle level density. The inverse level density parameter $K = A/a$ obtained using Eq. (1) has the value 16 MeV as compared with the empirical value of $K \sim 8$ MeV. This discrepancy led to many theoretical works on 'a' involving effects of finite size, deformation and angular momentum dependence, pairing and shell effects.

Here we propose a new empirical formula for 'a' which fits very well with the experimentally derived 'a' values.

We know the nuclear level density parameter 'a' is roughly proportional to the mass number A of the system. Other than A, we make 'a' dependent on the surface, Coulomb and asymmetric energies of the nucleus and write 'a' in the form

$$a = c_1 A + c_2 Z^2 + c_3 (A-2Z)^2 + c_4 A^{2/3} \qquad (2)$$

where the coefficients c_1, c_2, c_3 and c_4 are

obtained by fitting Eq.(2) with experimental 'a' values.

The 'a' vs. 'A' graph would show dips in and near closed shell nuclei and humps in mid shell nuclei because of shell effects. This trend is accounted for by adding a term proportional to shell correction to the level density parameter given by

$$\Delta a = a_{shell} - \bar{a}. \qquad (3)$$

$\bar{a}$ can be obtained the Strutinsky's approach [2] and a_{shell} can be calculated by counting the number of levels above and below the Fermi energy with the energy difference of 1 MeV.

First, we group the available data, ranging from A = 25 to 245, in three different regions as (1) Light and medium nuclei (A = 25-140), (2) Rare earth nuclei (A = 141-177) and (3) Actinide nuclei (A = 230-245). The plot 'a' vs A for the light and medium mass nuclei region shows a good fit with the experimental data.

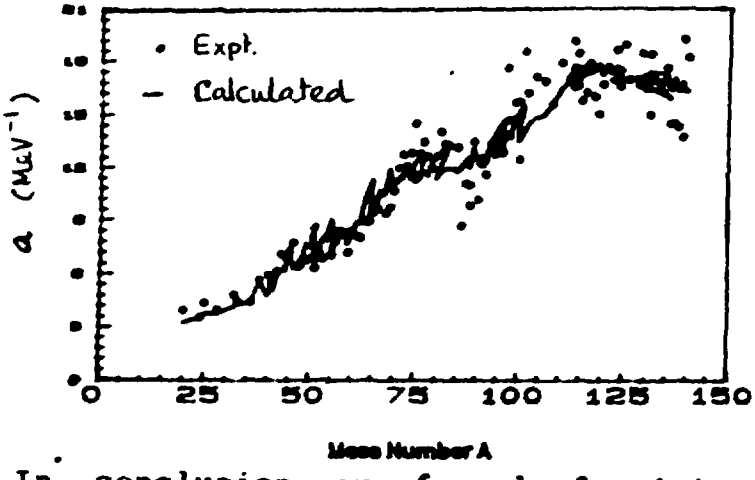

In conclusion, our formula for 'a' takes into account the effects of surface, Coulomb and neutron-proton asymmetry and is in good agreement with the experimental values.

References:

[1] A. Bohr and B.R. Mottelson, Nuclear Structure, Vol. I, (Benjamin, Reading, MA, 1969).

[2] V.M. Strutinsky, Nucl. Phys. A95 (1967) 420.

[3] H. Baba, Nucl. Phys. A159 (1970) 625.

Work supported UGC-COSIST under SAP.
R.P. thanks Govt. of Tamilnadu for the fellowship.

GYROMAGNETIC RATIO FOR HIGH SPIN SYSTEMS

M. Rajasekaran, R. Premanand & D. Caleb Chanthi Raj
Department of Nuclear Physics, University of Madras,
Guindy Campus, Madras 600 025.

The gyromagnetic ratio g_R is a collective nuclear parameter which measures the magnetic properties associated with nucleonic flow. In the simplest versions of nuclear collective models, the gyromagnetic factor of collective states are expected to be of the order of Z/A, with the assumption that all protons and neutrons take part equally in the collective motion. But the accuracy of the experimental information was in general not good enough to test this property. Theoretically, there are many methods to calculate the g-factors like i) pairing-plus quadrupole approach, the projected Hartree-Fock (PHF) method, the cranked Hartree-Fock-Bogolyubov (CHFB), Interacting boson approximation (IBA), etc. In the present work, we calculate the g-factor by statistical method involving pairing correlation. We calculate g for high spins for various temperatures.

In the BCS formalism the equations for particle number, energy, and angular momentum are [1]

$$N = \Sigma_i \{1-(\epsilon_i-\lambda)\tanh[\beta(E_i-\gamma m_i)/2]/2E_i\}, \quad (1)$$

$$E = \Sigma_i \epsilon_i\{1-(\epsilon_i-\lambda)\tanh[\beta(E_i-\gamma m_i)/2]/2E_i\} - \Delta^2/G, \quad (2)$$

$$\& \; I = \Sigma_i \{m_i/[1+\exp\beta(E_i-\gamma m_i)]\}, \quad (3)$$

where $E_i = \sqrt{[(\epsilon_i-\lambda)^2+\Delta^2]}$ are the quasi-particle energies, ϵ_i and m_i are the single particle energies and spin projection, G is the pairing strength, Δ is the gap parameter, β is the reciprocal of the temperature T and λ is the chemical potential. The parameters γ, $/\backslash$ and λ are fixed by solving equations (1-3) along with the gap equation

$$\Sigma_i \tanh[\beta(E_i-\gamma m_i)/2]/2E_i = 2/G. \quad (4)$$

The moment of inertia is given as

$$\mathcal{J} = \hbar^2 \, I \, (\partial E_{rot}/\partial I)^{-1}, \qquad (5)$$

where the rotational energy $E_{rot}(I) = E(T,I)-E(T,0)$. The gyromagnetic ratio is given by [2]

$$g_R = \mathcal{J}_p/(\mathcal{J}_p+\mathcal{J}_n). \qquad (6)$$

In this work, we have calculated the gyromagnetic ratio for ^{186}Os nucleus upto the angular momentum states of 20 h for different values of the temperature T = 1.5 to 2.0 MeV. In the figure given below we plot g-factor vs Angular momentum I for various temperatures. The $g_2(I=2)$ value for ^{186}Os is well reproduced with the experimental value. Further works on the osmium isotopes and rare-earth region are under way.

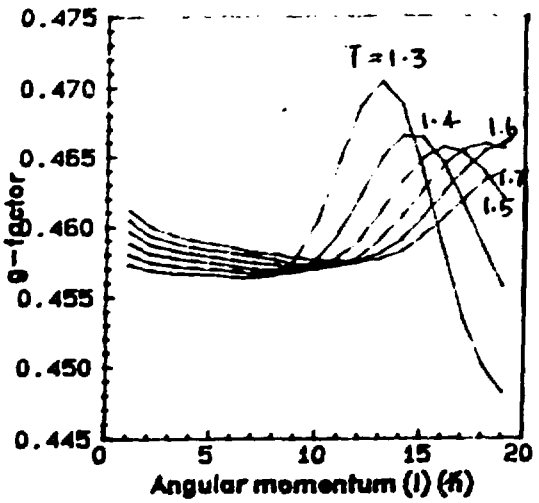

References:

[1] L.G. Moretto, Nucl. Phys. A216 (1973) 1.

[2] J.M. Eisenberg and W. Greiner, Microscopic theory of the nucleus, (North-Holland, Amsterdam, 1975) p.383.

Work supported UGC-COSIST under SAP.
R.P. thanks Govt. of Tamilnadu for the fellowship.

STUDIES ON K- ELECTRON CAPTURE PROBABILITIES IN ^{87}Y, ^{96}Tc AND ^{196}Au

G. Sree Krishna Murty, M.V.S. Chandrasekhar Rao, N.V.S. Vara Prasad, G.Satyanarayana, D.L. Sastry and S.N.Chitalapudi[†]

Swamy Jnanananda Laboratories for Nuclear Research, Andhra University, Visakhapatnam.

[†]Variable Energy Cyclotron Centre, Calcutta.

Experimental studies on K- electron capture probability and EC/β^+ offer a good tool in nuclear spectroscopy to assign the level parameters, nature of the β - transitions and check the validity of different theories based on varying assumptions. We have reported earlier[1-3] K & L capture probabilities measured in the decay of ^{105}Ag, ^{167}Ta, ^{161}Ho, ^{125}I and ^{131}Ba employing the X-γ sum-peak method. These measurements were carried out using a high resolution HpGe detector coupled to an ADCAM 100 data acquisition system in a close geometry. As an extension of these studies K-electron capture probabilities were measured for the first time in ^{87}Y, ^{96}Tc and ^{196}Au. The results of the present investigations are reported in this paper.

^{87}Y ($T_{1/2}$ = 80.3h) : Produced via $^{85}Rb(\alpha,2n)$ reaction at an energy of 26 MeV at VECC. The P_K value of the $1/2^- \longrightarrow 3/2^-$ electron capture transition and to the 873 keV level in the daughter ^{87}Sr was measured using the same technique. The relevant X -, γ- and sum spectrum is shown in figure 1. The sum peak and γ - intensities were determined after applying usual corrections. The following expression was used to determine the experimental P_K value.

$$N_{484.8+K_\alpha} = f_{K_\alpha}\ \omega_K\ \varepsilon_{K_\alpha}\ P_K\ N_{484.8}$$

The experimental P_K value thus obtained is given in Table 1 together with the theoretical value. The theoretical value was computed using the formula of Behrens and Janacke[1-2].

^{96}Tc ($T_{1/2}$ = 4.3d): Produced via the reaction $^{93}Nb(\alpha,n)$ at a beam energy of 24 MeV. The experiment was performed as in the case of ^{87}Y. The experimental P_K value was determined for the EC decay of ^{96}Tc to the 2448.6 keV level in the daughter ^{96}Mo. The P_K experimental and theoretical values are given in Table 1.

^{196}Au ($T_{1/2}$ = 6.18d) : Produced via ^{197}Au (α,2p3n) at a beam energy of 50 MeV. The experimental and theoretical P_K values were determined as in the case of ^{87}Y and ^{96}Tc and the same are given in Table 1.

From Table 1 it may be concluded that the present experimental P_K values are in good agreement with the theory within experimental uncertainties.

REFERENCES :

1. G.Sree Krishna Murty et al, J. of Phys. G16(1990)1095
2. M.V.S. Chandrasekhar Rao et al, Z.Phys. A335(1990)25
3. G.S.Krishna Murty et al, DAE Symp. 33B(1990)5

TABLE 1

ISOTOPE	TRANSITION	LEVEL ENERGY (keV)	P_K VALUE	
			EXP.	THEORY
^{87}Y	$1/2^- \longrightarrow (3/2^-)$	873	0.811 ± 0.035	0.878
^{96}Tc	$7^+ \longrightarrow 6^+$	2440.6	0.866 ± 0.039	0.870
^{196}Au	$2^- \longrightarrow 2^+$	688.7	0.776 ± 0.038	0.805
	$2^- \longrightarrow 2^+$	355.7	0.847 ± 0.051	0.813

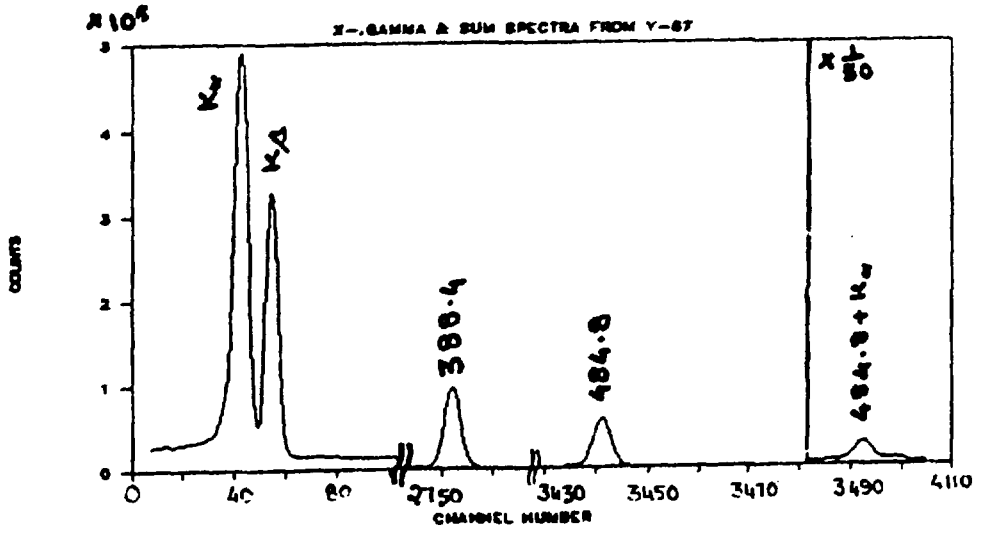

EVIDENCE OF SIGNATURE INVERSION IN Er^{159}

Tripti Mathur and Shanker Mukherjee,
Department of Physics,
Banaras Hindu University, Varanasi - 221005.

For odd A nuclei, the rotational bands built on a unique parity high j orbit splits into two branches, such that each branch is specified by a particular signature quantam number

$$\alpha_I = \frac{1}{2} \text{ for } I = \frac{1}{2}, \frac{5}{2}, \frac{9}{2}, \ldots$$

and $$\alpha_I = -\frac{1}{2} \text{ for } I = \frac{3}{2}, \frac{7}{2}, \ldots$$

Generally, the $I = j \pmod 2$ branch is energetically favoured, while $I = j + 1 \pmod 2$ branch is shifted upward in energy. However, it was found that for a few odd A nuclei, the dependence of energy on signature is reversed for $I > I_c$, where I_c is the angular momentum at which first band crossing takes place.

Recent experimental data for Er^{159} shows signature inversion (fIG. 1) just after $Ic = \frac{21}{2}$ and it exists there for a wide range of spin.

Since the experimental Routhians (Ref.1) shows that the signature splitting is normal below the band crossing frequency and is inverted above it, therefore we expect that the theoretical Routhians should also give signature inversion. However, calculations within the frame work of CSM with pairing[1] for axilly symmetric nucleus does not show any signature inversion

Many authors[2-4] believe that the signature inversion is an indication of the γ deformation or γ - vibration of the nucleus. There are two approaches to understand this phenomena, one is CSM model with pairing taking $\gamma \neq 0^o$, and the other is the rotor particle model, taking a permanent γ deformation or γ - vibration.

The effect of non-axiallity on signature inversion will be reported.

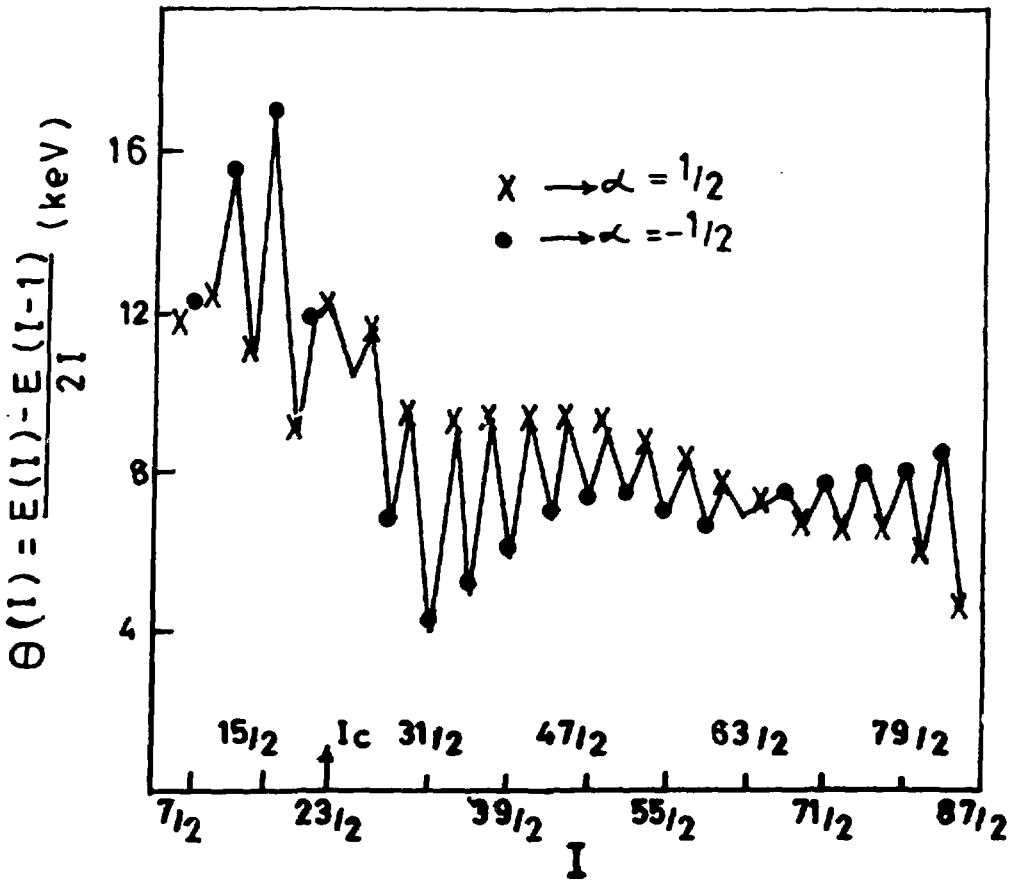

Reference -

1. R. Bengtsson and S. Frauendorf, Nucl.Phys. A 327 (1979) 139
2. A. Ikeda and Takafuni Shimano. Phy. Rev. Lett. 63 (1989) 139
3. A. Ikeda and Takafuni Shimano. Phy. Rev. C 42 (1990) 149
4. R. Bengtsson et al. Nucl. Phys A 415 (1984), 189

LIFETIME OF THE 113 keV LEVEL AND DIFFERENTIAL ANGULAR CORRELATION OF THE 208-113 keV CASCADE IN 177-Hf

C. C. Dey, B. K. Sinha and R. Bhattacharya
Saha Institute of Nuclear Physics
1/AF, Bidhannagar, Calcutta - 700 064

The 113 keV $9/2^-$ level of ^{177}Hf is known to be a member of the $7/2^-$ rotational band. The measured values of half-life of this level range from 320-540 ps [1]. However, the accepted value is $T_{1/2}$ = 490 ± 15 ps [2], measured by Holmberg et al. [1] at a time resolution of 1.1 ns, much longer than the half-life measured. In the measurement of magnetic moment of a level by the IPAC method an accurate value of half-life of the level is required. Using the value $T_{1/2}$ = 490 ± 15 ps for the 113 keV level, the magnetic moment has been reported as $\mu(9/2^-)$ = 1.082 ± 0.042 nm [3] which is different from the value predicted by Matthias et al. [4] (μ = 0.82 ± 0.15 nm) from theoretical considerations. Therefore, it seems useful to remeasure the half-life with a BaF_2-BaF_2 set up, producing subnanosecond time resolution [5,6]. Using such an ultrafast set up, it is also useful to study the differential angular correlation of the 208-113 keV cascade. From this study it is possible to find the value of $A_2(0)$ of this cascade and thus to find the mixing ratio of the 113 keV γ-transition more correctly. The 208 keV transition is known to be a pure E2 γ-transition.

The half-life and angular correlation measurements have been performed using two BaF_2 detectors (38-x 25-mm each). The BaF_2 crystals are coupled to Phillips XP2020Q photomultiplier tubes. The measurement of differential angular correlation has been performed for the first time at a time resolution of 620 ps. The source used is in the form of $LuCl_3$ in HCl, obtained from BRIT, Bombay.

The delayed coincidence spectrum of the 208-113 keV cascade has been analysed using the programme DBLCON [7] and a value of $T_{1/2}$ = 583 ± 6 ps has been obtained. This value of the half-life is in disagreement with all the values

found from earlier measurements. Taking the value of the half-life from our measurement and the value of $g\tau = 0.170 \pm 0.004$ from the report of Hûble et al. [8], a new value of magnetic moment for the 113 keV level is found to be $\mu(9/2^-) = 0.91 \pm 0.02$ nm. This value of μ is close to the predicted value [4].

The results of the differential angular correlation measurement are: $A_2(0) = -0.162 \pm 0.004$, $\lambda_2 = (6.4 \pm 2.6) \times 10^7\ s^{-1}$. The corresponding value of the E2/M1 mixing ratio of the 113 keV γ-transiton is found to be $\delta(113) = -4.85 \pm 0.05$. Thus it is seen that there is small but finite attenuation of the angular correlation in the liquid chloride source and the value of the mixing ratio found from $A_2(0)$ can be considered as more accurate. Other results of the mixing ratio obtained from integral measurements on the 208-113 keV cascade are listed in table 1.

Table -1

Results of angular correlation measurements on the 208-113 keV cascade of 177-Hf

Authors	Value of $A_2/A_2(0)$	$\delta(113)$
Holmberg et al.[1]	-0.157 ± 0.001	-4.9 ± 0.1
Hrastnik et al.[9]	-0.208 ± 0.012	-3.7 ± 0.3
Agnihotry et al.[10]	-0.192 ± 0.007	-3.99 ± 0.25
Present work	-0.162 ± 0.004	-4.85 ± 0.05

References:

1. *Holmberg et al., Phys. Scr. 6, 177 (1972)*
2. *Nucl. Data Sheets 16, 135 (1975)*
3. *Raghavan, At. Data & Nucl. Data Tables 42, 189 (1989)*
4. *Matthias et al., Ark. Fys. 22, 139 (1962)*
5. *Laval et al., Nucl. Instr. and Meth. 206, 169 (1983)*
6. *Sinha et al., Nucl. Instr. and Meth. A276, 237 (1989)*
7. *Warburton, Comput. Phys. Commun. 13, 371 (1978)*
8. *Hubel et al., Phys. Rev. C12, 2013 (1975)*
9. *Hrastnik et al., Z. Phys. 239, 25 (1970)*
10. *Agnihotry et al., Phys. Rev. C9, 336 (1974)*

LEVEL DENSITY AT HIGH SPINS FOR THE REACTIONS $^{12}C(^{16}O,1n)^{27}Si$ AND $^{12}C(^{16}O,1p)^{27}Al$*.

T.R. Rajasekaran, C.R. Ramaswamy and
M.P. Sathyavathiamma
Department of Physics, Bangalore University,
Bangalore - 560 056.

The study of the nuclear level density (ρ) at high spins is important since it decides the phase space available for the excited nuclei. The recent study[1,2] of the reaction $^{92}Zr(^{64}Ni,1n)^{155}Er$ at high spins has established the dependence of the level density on the single-neutron emission probability.

In this paper, the structural effects due to spin, and temperature on the level density has been studied theoretically, using the statistical model, for reactions $^{12}C(^{16}O,1n)^{27}Si$ at excitation energy E^* 40MeV and $^{12}C(^{16}O,1p)^{27}Al$ at E^* 60MeV. The existence of super-deformation[3] for ^{28}Si is studied through dependence of angular momentum (M) on moment of inertia ($\mathcal{I}$).

The logarithm of partition function is given by

$$\ln Q = \Sigma \ln[1+\exp\{\alpha - \beta\varepsilon_i(\omega)\}].$$

The conservation equations of number, M & energy are

$$\langle N\rangle = \Sigma n_i = \Sigma[1+\exp\{-\alpha + \beta\varepsilon_i(\omega)\}]^{-1},$$

$$M = \Sigma n_i m_i \quad \text{and} \quad E = \Sigma \varepsilon_i(\omega) n_i + \hbar\omega \Sigma m_i n_i.$$

The single particle levels $\varepsilon_i(\omega)$ with spin projection m_i are obtained by diagonalizing the cranked Nilsson Hamiltonian. The internal excitation energy of the residual nucleus is $U = E - S - \mathcal{E} - E_{rot}$ where S is the neutron/proton separation energy, $\mathcal{E}$ is the kinetic energy of the outgoing neutron/proton and E_{rot} is the rotational energy of the residual nuclei. $\rho(U)$ is obtained using the relation:

$$\rho(U) = \frac{(\hbar^2/2\mathcal{I})^{3/2}}{12(U+T)^2}\sqrt{a}(2M+1)\exp(2\sqrt{aU})$$

where moment of inertia $\mathcal{I} = \hbar^2 M(\partial M/\partial E_{rot})$.

* Work supported in part by grant received from UGC.

Fig. 1 shows $\mathcal{J}$ versus for M T=1 MeV. The fluctuations with M represent the shape transitions from g.s.-oblate (upto M = 13ħ) to triaxial shape (upto M = 20ħ) and to prolate shape (after M=20ħ, stable super-deformation). Figs. 2 & 3 depict ρ as a function of M for various U values for neutron and proton emissions respectiveiy. The decrease in ρ for M=15ħ and 20ħ compared to the spinless case (M=0ħ) is due to the shape transition and also due to the increase in the rotational energy of the system at higher spins.

We thank Drs. M. Rajasekaran and N.G. Puttaswamy for many useful discussions.

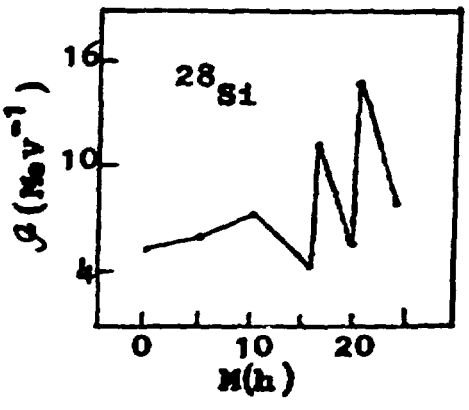

Fig. 1

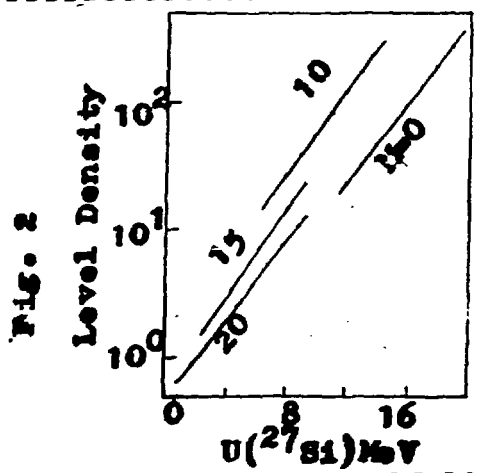

Fig. 2

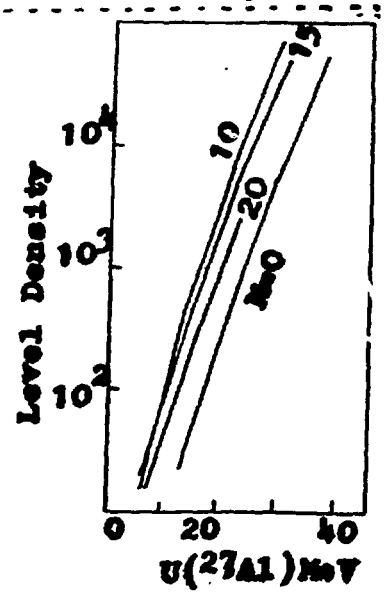

Fig. 3

References:
1. M. Rajasekaran and T.R. Rajasekaran, Phys. Rev. Lett. 61, 2077 (1988); Nuclear Physics (DAE) 33A, 209 (1990).
2. S. Henss et al., Phys. Rev. Lett. 60, 11 (1988)
3 J.J. Kolata et al., Phys. Rev. Lett. 61, 1187 (1988).

EFFECT OF TEMPERATURE ON THE SHAPES OF LIGHT NUCLEI

G.Shanmugam, Kalpana Sankar, Arulmozhi.G
Department of Physics, Presidency College, Madras - 5.
and
K.Ramamurthi
Department of Physics, Bharathidasan University, Trichy.

Growing experimental information is presently becoming available on the shapes and properties of highly excited nuclei, formed in heavy-ion reactions. To perform such a study theoritically and to analyse the nuclear shape transitions with temperature, some version of mean-field approximation is always used. One either uses the strutinsky's method(1) or the summation method(2) for such a study. But these mean field theories ignore the statistical thermal fluctuations in the order parameters of hot nuclei. For the light nuclei with a small number of particles, such fluctuations can be so large as to produce average values for the order parameters which could be qualitatively different from mean-field equilibrium values.

Recently(3) we have been attempting to obtain the shapes of hot light nuclei in the s-d shell region using both the summation and strutinsky's method, but taking into account the important effect of thermal fluctuations. The required formulae for such calculations have already been given in our earlier work(3). In the present calcualtions we have also included pairing (which is usually neglected) when we determine the shapes of such light nuclei at T=0, I=0.

The potential energy surfaces obtained by us for the case of ^{20}Ne without and with thermal fluctuations in the summation and strutinsky's method are shown diagramatically. It is clearly seen from the diagrams that thermal fluctuations do change the shapes of light nuclei and both the methods qualitatively yield same results.

References:

(1) Y.Alhassid, J.Zingman and S.Levit Nucl.Phys. A4 69, 205 (1987).

(2) G.Shanmugam and M.Thiagasundaram, Phys. Rev.C, in press
(3). G.Shanmugam, K.Ramamurthi and Kalpana Sankar, Nucl.Phys. (India) 33B, 65 (1990)

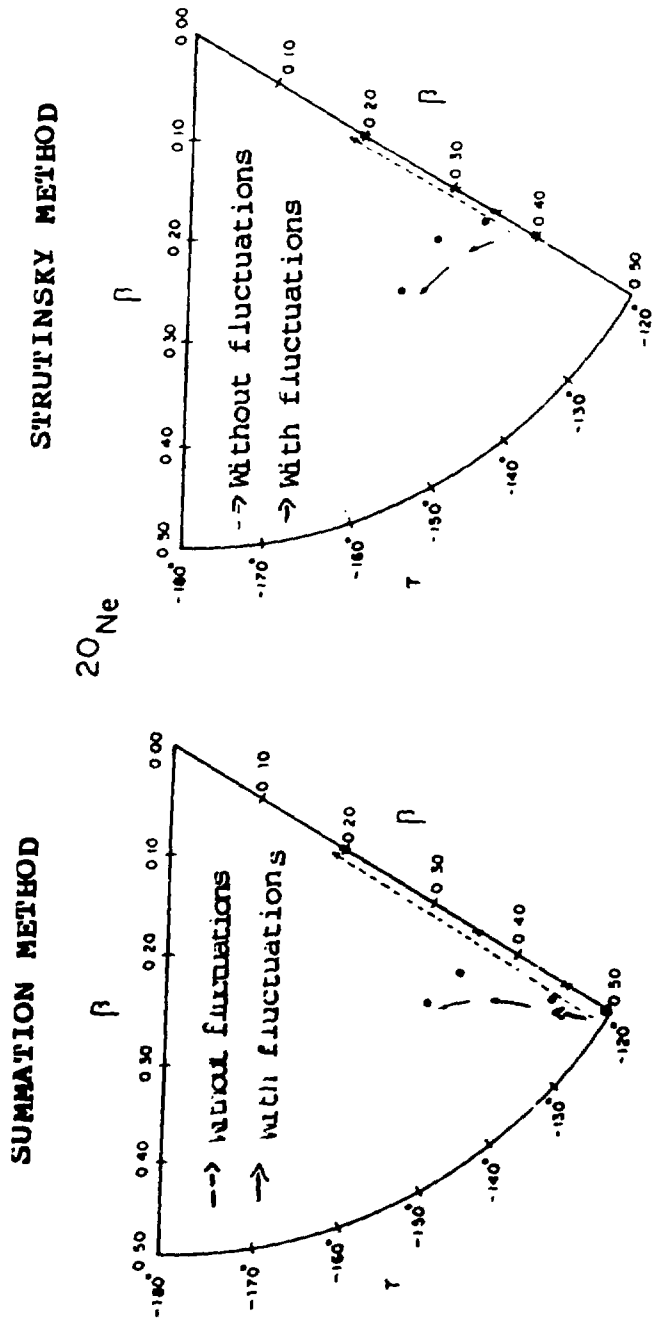

Modified Semi-empirical Formula for Nuclear Rotational States

J.S. Batra and Raj K. Gupta
Physics Department, Panjab University,
Chandigarh-160014, India.

In his, so-called, semi-empirical formula (SEF), Sood/1/ summed up the infinite series in J(J+1):

$$E_J = AJ(J+1) - BJ^2(J+1)^2 + CJ^3(J+1)^3 - DJ^4(J+1)^4 + \cdots \quad (1)$$

by assuming

$$\frac{C}{B} = \frac{D}{C} = \cdots\cdots\cdots = N\,\frac{B}{A} \quad (2)$$

and obtained

$$N = 2.85 - 0.05\,I = a - b\,I \quad (3)$$

for the best fit to the rare-earth nuclei data. The SEF is also applied recently/2/ to some actinides with different a and b values for different nuclei. In this paper, we show that the straight line expression for N is obtained in a natural way if the nuclear softness (NS) model of one of us/3/ is introduced in the summation proceedure of Sood. This makes B/A also dependent on J.

In the NS model/3/, we make Taylor series expansion of the moment-of-inertia $\mathcal{I}_J$ ($A = \hbar^2/2\mathcal{I}_J$) about its ground-state value $\mathcal{I}_0$ for $J = 0$. We obtain

$$\mathcal{I}_J = \mathcal{I}_0\,(1 + \sigma_1 J + \sigma_2 J^2 + \sigma_3 J^3 + \cdots) \quad (4)$$

with $\sigma_n = \frac{1}{n!\,\mathcal{I}_0}\,\frac{\delta^n \mathcal{I}_0}{\delta J^n}$, called the nuclear-softness parameters. For B/A, we use the Bohr-Mottelson expression/4/ and write it again in terms of ground-state value B_0/A_0:

$$\frac{B}{A} = 4A^2\left(\frac{1}{(\hbar\omega_\gamma)^2} + \frac{3}{(\hbar\omega_\beta)^2}\right) = \frac{1}{(1+\sigma_1 J+\sigma_2 J^2+\cdots)}\,\frac{B_0}{A_0} = M(J)\frac{B_0}{A_0} \quad (5)$$

This modifies Sood's assumption (2) as:

$$\frac{C}{B} = \frac{D}{C} = \cdots\cdots = k\,\frac{B}{A} = k\,M(J)\frac{B_0}{A_0} = N'(J)\,\frac{B_0}{A_0} \quad (6)$$

which gives the modified Semi-empirical formula

(MSEF), first order softness as

$$E_J = \frac{A_0}{1+\sigma_1 J} J(J+1) \left(\frac{1 + (N'-M)\frac{B_0}{A_0} J(J+1)}{1 + N'\frac{B_0}{A_0} J(J+1)} \right) \quad (7)$$

We obtained the Sood's SEF for $\sigma_1 = 0$, $M = 1$ and $N' = N$. However, the new parameter (since $\sigma_n << 1$) of MSEF is

$$N'(J) = k\, M(J) = \frac{k}{(1+\sigma_1 J+\sigma_2 J^2+ \text{---})^2} = k(1-2\sigma_1 J) = a - bI \quad (8)$$

which has exactly the form (3) used in SEF.

For an overall comparison with the experimental data we consider the energy ratio $E(J)/E(2)$ thus elimination of the scale parameter $A_0 (= \hbar^2/2\mathcal{J}_0)$. The other parameter B_0/A_0 is determined in terms of the energy ratio $E4^+/E2^+$. There by reduces MSEF to only interms of two parameters. Calculations using the MSEF is presented for one nucleus (U^{232}) and its comparision with the SEF is also discussed. The rest of nuclei will be presented later on.

Nucleus	J	$R_{J2}(=\frac{E_{4^+}}{E_{2^+}})$(Expt)	R_{J2} (Abzouzi)	R_{J2} (Ours)
^{232}U	04	3.2827	3.2865	3.2813
	06	6.7747	6.7614	6.7418
	08	11.3654	11.3023	11.2603
	10	16.9315	16.7851	16.7225
	12	23.3573	23.0972	23.0373
	14	30.5524	30.1412	30.1408
	16	38.4243	37.8334	37.9937
	18	46.9059	46.0992	46.5758
	20	55.8792	54.8681	55.8792

Where as for this nuclei k=2.85 and $\sigma_1 = 0.000848$. Here our formulation MSEF gives better results then SEF and similarly for other nuclei which will be published elsewhere.

References:

1. P.C. Sood, Phys. Rew., 161(1967)1063.
2. A. Abzouzi and M.S. Antony, Phys. Rew., C37(1988)401.
3. R.K. Gupta, Phys. Lett., 36B(1971)173.
4. A. Bohr and B.R. Mottelson, Kgl. Danske Videnskab. Selskab. Mat.-Fys. Medd., 27(1953)16.

(MICROSCOPIC WAVEFUNCTION FOR ^{10}B)

Neelam Agarwal and B.B.Srivastava
Meerut University, Meerut-250005

The 10 body system i.e. ^{10}B is a complicated system as the coexistance of shell structuresand cluster structure exist in light nuclei, also the physical interpretation of R.G.M[1] (Resonating Group method) and CGCT (Complex Generator Coordinate method is strongly reminiscent to this idia recently.

The nucleus 10_B is considered as aα-α-d cluster system.[2] The trial wavefunction for 10_B has been formulated using cluster model ideas and harmonic oscillator shell model representation and then it is transformed into an antisymmetrized product of ten single particle wavefunction then it can be written in the form of 10X10 siater determinant. Using such techniques the normalization constant for this transformed wavefunction has been calculated. Next the method for the calculation of the expectation value of various terms in the 10_B Hamiltonian using this wavefunction has been described.

An up to date literature survey[3] has been made for theoretical and experimental studies of elastic scattering of low energy(<10 MeV) nucleons from 10_B.

The trial wavefunction of 10_B may be written as

$$\phi_{3,3} = A\left[\phi(\alpha_1)\phi(\alpha_2)\chi_{00}(\vec{R}_{\alpha_1}-\vec{R}_{\alpha_2})\chi_{\ell,m_\ell}\left(\frac{\vec{R}_{\alpha_1}+\vec{R}_{\alpha_2}}{2}-\vec{R}_d\right)\phi_{1,M_d}(\alpha)\right]$$

Here $\phi_{1,M_d}(\alpha)$ contains spin-isospin of deutron and

$R_\alpha = (\vec{r}_9 + \vec{r}_{10})/2$

Now the cluster model wavefunction can be represented as by applying different transformations.

$$\phi_{3,3} = N\left(\frac{4}{5\pi^2}\right)^3 \int A \prod_{j=1}^{4}\prod_{k=5}^{8}\prod_{i=9}^{10} \xi_{\alpha_1}\xi_{\alpha_2}\xi_d \exp\left[\frac{-\alpha}{2}\left\{\vec{r}_j - \frac{i}{2\alpha}(\vec{A}''+\vec{B}'')\right\}^2\right].$$

$$\exp\left[\frac{-\alpha}{2}\left\{\vec{r}_K - \frac{i}{2\alpha}(\vec{A}''-\vec{B}'')\right\}^2\right] \exp\left[\frac{-\beta}{2}\left\{\vec{r}_i + i\left(\frac{2\vec{A}''}{\beta}+\frac{4i(\alpha-\beta)}{5\beta}\vec{R}_2''\right)\right\}^2\right].$$

$$\chi_{00}(\vec{R}_1'')\,\chi_{22}(\vec{R}_2'')\exp\Big[-\frac{1}{\alpha}A''^2-\frac{2A''^2}{\beta}-\frac{1}{\beta}B''^2+\alpha R_1''^2-2i\vec{R}_1''\cdot\vec{B}''+$$

$$R_2''^2\Big\{\frac{-4\alpha}{5}-\frac{16\beta}{25}+\frac{8\alpha^2}{25\beta}\Big\}+\vec{R}_2''\cdot\Big\{\frac{-28i\vec{A}''}{5}-\frac{8i\alpha\vec{A}''}{5\beta}\Big\}\Big]\cdot d\vec{R}_1''\,d\vec{R}_2''\cdot d\vec{A}''\,d\vec{B}''$$

Where N is the normalization constant and I have calculated the value of N which is in a big expresion.

This is all of interest since so far no microscopic theoretical studies have been done for the 10_B system. Apart from demonstrating the range of applicablity of RGM for 11 nucleon scaltering system this study will also indicate the extent to which the formulated cluster model wavefunction is a good representation of the ground state of 10_B nucleus.

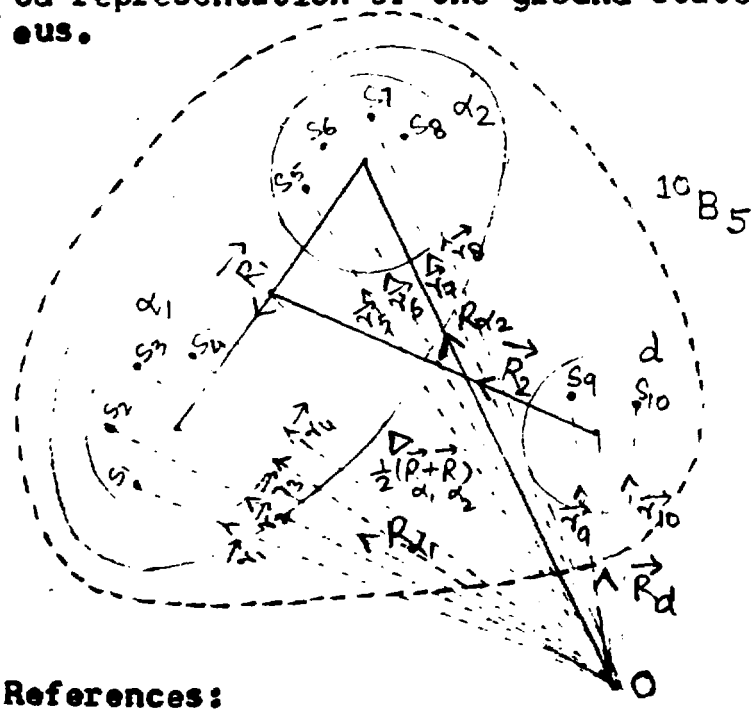

References:

1. J.A.Wheeler, phys.Rev.52(1937) 1083,1107.
2. Y.C.Tang, M.Lemere, phys.Rep.C-47(1978)167.
3. N.Agarwal, B.B.Srivastava project Report 1990.

IBM-2 SPECTRA OF $1\nu - 1\pi$ BOSON SYSTEMS IN MICROSCOPIC BASIS

Subrata Sarangi and Jitendra C. Parikh
Physical Research Laboratory,Navrangapura, Ahmedabad-380009.

We present here, in continuation of our work reported at Madras last year[1], the results of IBM-2 calculations of some $1\nu - 1\pi$ boson systems, e.g., Ti^{44}, Ne^{20}, Zn^{60} and Mo^{94}. This has been achieved by (1) deriving and calculating single fermion pair energy(s.f.p.e.) and two fermion pair matrix elements(t.f.p.m.e.) (2) equating the Hamiltonian defined by them to IBM-2 Hamiltonian through Marumori mapping.

The fermion coupled pair states $\mid B^{\rho}_{J}\rangle (\rho = \nu \text{ or } \pi)$ are projected good angular momentum J=0,2,4 (for S,D and G pair) states from the HF orbits $C_{j^{\rho}_{k}}$ in the chosen SM basis space $\{j^{\rho}_{k}\}$

$$\mid B^{\rho}_{J0}\rangle = \mathcal{N}^{\rho}_{J} \sum_{j^{\rho}_{k}, j^{\rho}_{l}; k \le l} (-1)^{j^{\rho}_{l} - \frac{1}{2}} \sqrt{1+\delta_{kl}}\,(2-\delta_{kl}) \langle j^{\rho}_{k}\, \tfrac{1}{2}\, j^{\rho}_{l}\, -\tfrac{1}{2} \mid j^{\rho}_{k} j^{\rho}_{l} : J0\rangle\, C_{j^{\rho}_{k}}\, C_{j^{\rho}_{l}} \mid (j^{\rho}_{k} j^{\rho}_{l})J\rangle \quad (1)$$

Adopting a concise notation, we define the curly-C coefficients $\mathcal{C}^{\rho}_{(kl)J}$ such that

$$\mid B^{\rho}_{J}\rangle = \sum_{(\rho; kl); k \le l} \mathcal{C}^{\rho}_{(kl)J} \mid (\rho; kl)J\rangle \quad (2)$$

The s.f.p.e. of $\mid B^{\rho}_{J}\rangle$ is the expectation value of 1+2 body fermion Hamiltonian H_J with T=1 in the state $\mid B^{\rho}_{J}\rangle$. The t.f.p.m.e., $\langle (B^{\nu}_{J_1}\, B^{\pi}_{J_2})J \mid \mathcal{V}_{\nu\pi} \mid (B^{\nu}_{J_3}\, B^{\pi}_{J_4})J\rangle$ alongwith eqn. (2), is given by the sum over four curly-C coefficients multiplied by the basic matrix element $\langle((\nu; k_1 l_1)J_1, (\pi; k_2 l_2)J_2)J \mid \mathcal{V}_{\nu\pi} \mid ((\nu; k_3 l_3)J_3, (\pi; k_4 l_4)J_4)J\rangle$. The basic matrix element is calculated by employing techniques by French *et al*[2]. The operator $\mathcal{V}_{\nu\pi}$ is the (fermion) two body interaction, used for the HF calculations, in $\nu - \pi$ formalism.

The Marumori mapping of 1 and 2 S^{ρ}, D^{ρ}, G^{ρ} states onto the 1 and 2 s^{ρ}, d^{ρ}, g^{ρ} boson space is straight forward. The IBM-2 Hamiltonian is equal to the one defined by the s.f.p.e. and t.f.p.m.e. of the fermion pair states. The spectra of Ti^{44}, Ne^{20}, Zn^{60} and Mo^{94} generated by the IBM-2 Hamiltonian are plotted in figs.(1), (2), (3) and (4). The fermion t.b.m.e. of Ti^{44} in $\{f_{\frac{7}{2}}\}$ shell are taken from Skouras *et al*[3] (table 1). In fig(1), 'model-2' label is for the sdgIBM-1 result of Skouras *et al* for Ti^{44}. For Ne^{20} and Zn^{60}, we have chosen the Wildenthal's universal sd interaction and Koops and Glaudemans'[4] ASDI respectively. The protons of Mo^{94} are in $\{g_{\frac{9}{2}}\}$ orbit and neutrons in $\{d_{\frac{5}{2}}, s_{\frac{1}{2}}, d_{\frac{3}{2}}, g_{\frac{7}{2}}, h_{\frac{11}{2}}\}$ with s.p. energies 0.0, 1.0, 2.5, 3.0, 3.6 MeV respectively. The t.b.m.e. is SDI with strength $A_{T=0} = 0.6 MeV$ and $A_{T=1} = 0.35 MeV$. However, as discussed by Elliott *et al*[5], in case of light nuclei with protons and neutrons filling the same major shell, the IBM-2 Hamiltonian does not conserve T-symmetry. This occurs in our calculations for Ti^{44}, Ne^{20} and Zn^{60}. But, in the g.s. band of these nuclei the T-mixing is minimal(of order 10^{-2} or less) ensuring the good agreement

with the expt. and SM results seen in figs.(1),(2) and (3). Their excited bands, with either T=1 or T=0 and 2 mixed, are pushed up. In case of Ti^{44}, the inclusion of the I pair to S,D and G pairs restores the T-symmetry and exactly reproduces the SM results. Mo^{94} having protons and neutrons in inequivalent shells gives good T-states. So the excited bands also come in agreement with the experiment as seen in fig (4).

1. Subrata Sarangi and Jitendra C. Parikh, DAE Symp. on Nucl. Phys. Vol.(33B) (1990) 19
2. J.B. French *et al*, *Complex Spectroscopy*, Adv. in Nucl. Phys. Vol 3. 193
3. L.D. Skouras *et al*, Nucl. Phys. A516 (1990) 255
4. J.E. Koops and P.W.M. Glaudemans, Z. Phys. A280 (1977) 181
5. J.P. Elliott *et al*, Nucl. Phys. A469 (1987) 51

We would like to thank Professors S.P.Pandya and V.K.B.Kota for very valuable suggestions and discussions. We also thank Prof. V.K.B.Kota for providing us with Wildenthal's interaction.

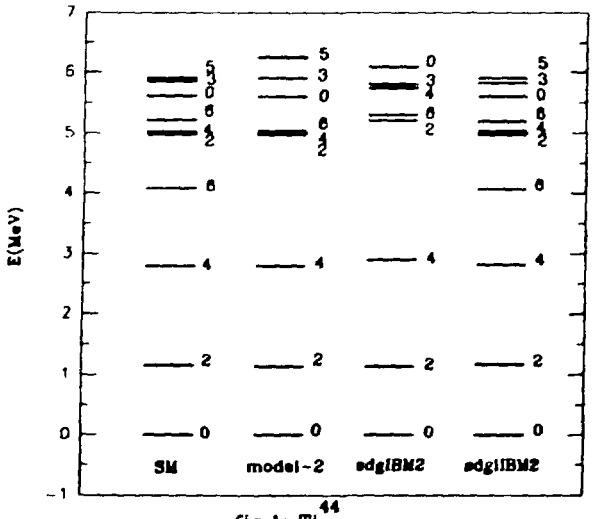

fig.1: Ti^{44}

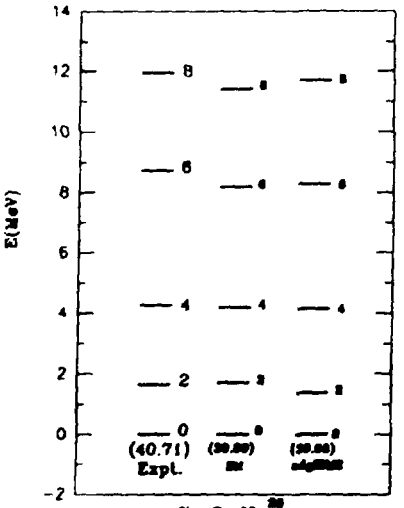

fig.2: Ne^{20}

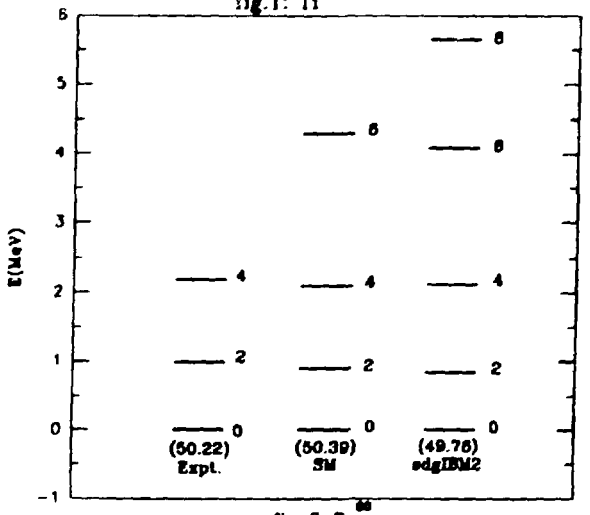

fig. 3: Zn^{66}

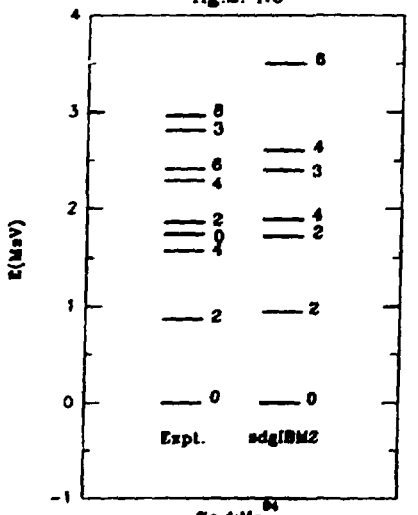

fig.4:Mo^{94}

MECHANISM OF SHAPE TRANSITION IN DOUBLY EVEN CADMIUM ISOTOPES

S.K. Khosa and P.K. Mattu
Department of Physics, Jammu University
Jammu-180 001, India.

In this paper we report on the calculations of the high-spin yrast spectra of the doubly even nuclei $^{98-110}$Cd. Apart from the energy spectra we shall also discuss the results of the calculations of the reduced transition probabilities for E2 transitions for the yrast states. The calculations presented here are carried out in the VAP - framework employing pairing-plus-quadrupole-quadrupole effective interaction. The details of the input parameters of our model and the valence space used, are the same as those employed in our earlier work.[1]

In Fig. 1 we have presented the observed as well as the theoretical yrast spectra resulting from the VAP method. It is seen that the VAP yrast spectra in the nuclei $^{98-110}$Cd are in reasonably good agreement with the experiments. In table 1 we present a comparison of the observed $B(E2; 0^+ \longrightarrow 2^+)$ values with the ones computed by using the prescription employed by Ripka.[2] It is satisfying to note that the calculated B(E2) estimates are in good agreement with the experiments provided one chooses $e_{eff} = 0.15$. It therefore turns out that the VAP prescription, in conjuntion with the pairing plus quadrupole-quadrupole interaction, provides a fairly accurate microscopic description of the observed high-spin yrast spectra in the nuclei $^{98-110}$Cd.

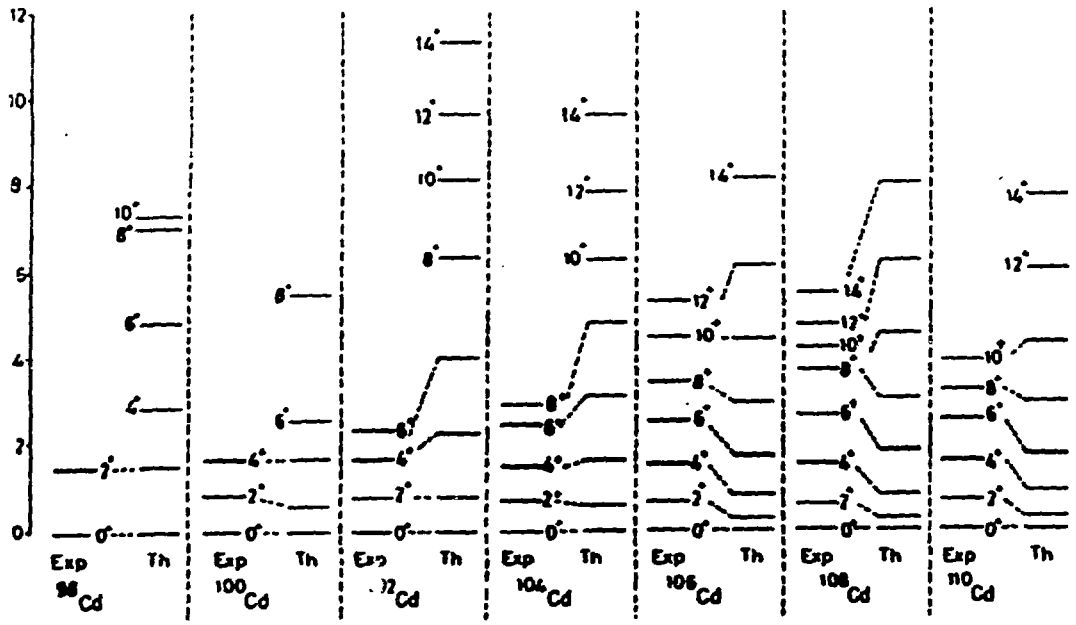

FIG. 1. Comparison of the observed (exp) as well as the calculated (th) yrast spectra in the nuclei $^{98-110}$Cd.

TABLE 1. Comparison of the calculated and the observed B(E2; $0^+ \longrightarrow 2^+$) values in some Cd isotopes.

Nucleus	B(E2; $0^+ \longrightarrow 2^+$) X 10^{-48} e^2Cm^4			
	Calculated			
	e_{eff} = 0.1	e_{eff} = 0.15	e_{eff} = 0.2	Expt
^{106}Cd	0.368	0.434	0.50	0.410
^{108}Cd	0.386	0.457	0.629	0.430
^{110}Cd	0.400	0.475	0.557	0.450

References

1. P.K. Mattu and S.K. Khosa, Phys. Rev. C 39, 2018 (1989).

2. G. Ripka, in Advances in Nuclear Physics, edited by M. Baranger and E. Vogt (Plenum, New York, 1968), Vol. 1.

STUDY OF GROUND STATE SYSTEMATICS IN NEUTRON-RICH PALLADIUM ISOTOPES IN MICROSCOPIC FRAMEWORK

P.K. Mattu* and S.K. Khosa
Department of Physics, Jammu University
Jammu-180 001, India

In this paper we report on the calculations of the high-spin yrast spectra of the doubly even nuclei $^{100-112}$Pd. Apart from the energy spectra we shall also discuss here the results of the calculations of the reduced transition probabilities for E2 transitions for the yrast states. The calculations presented here are carried out in the VAP - framework employing pairing - plus - quadrupole - quadrupole effective interaction. The details of the input parameters of our model and the valence space used, are the same as those employed in our earlier work.[1]

In Fig. 1 we have presented the observed as well as the theoretical yrast spectra resulting from the VAP method. It is seen that the VAP yrast spectra in the nuclei $^{100-112}$Pd are in reasonably good agreement with the experiments. Besides this the observed backbending in ^{104,106}Pd also seems to be qualitatively reproduced.[1]

We next consider the reduced transition probabilities for E2 transitions $B(E2; 0^+ \longrightarrow 2^+)$ in Pd isotopes. In table I we present a comparison of the observed $B(E2; 0^+ \longrightarrow 2^+)$ values with the ones computed by using the prescription employed by Ripka.[2] It is satisfying to note that the calculated B(E2) estimates are in good agreement with the experiments. Further our results on subshell occupation numbers indicate that the observed shape transition around A = 108 in the Palladium region can be understood in terms of strong deformation producing tendency of n-p interaction operating between valence particles in the spin-orbit partner orbits.

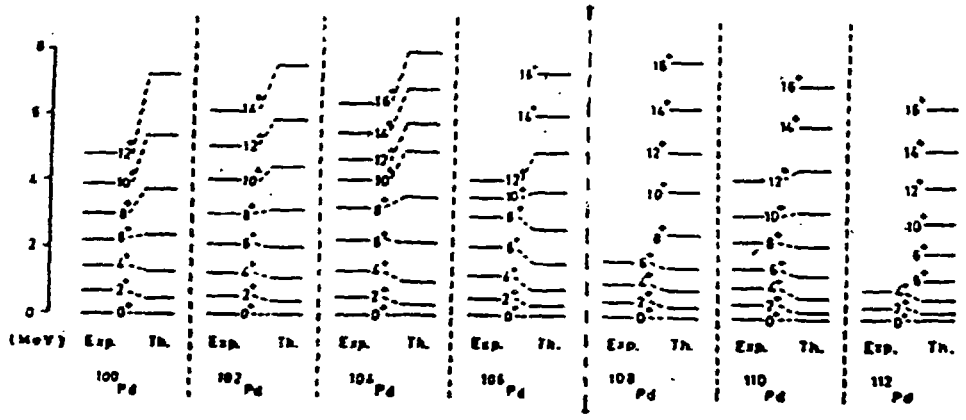

Fig. 1. Comparison of the observed (exp.) as well as the calculated (th.) yrast spectra in the nuclei $^{100-112}$Pd.

Table 1. Comparison of the calculated and the observed $B(E2; 0^+ \longrightarrow 2^+)$ values in some Pd isotopes.

Nucleus	$B(E2; 0^+ \longrightarrow 2^+) \times 10^{-48}$ e^2Cm^4 Calculated			Expt.
	e_{eff}=0.30	e_{eff}=0.35	e_{eff}=0.40	
^{102}Pd	0.35	0.40	0.46	0.46±.03
^{104}Pd	0.50	0.58	0.66	0.51±0.05
^{106}Pd	0.61	0.70	0.80	0.61±0.06
^{108}Pd	0.65	0.75	0.85	0.70±0.07
^{110}Pd	0.67	0.78	0.88	0.82±0.08

References

1. S.K. Khosa and P.K. Mattu, Phys. Rev. C 38, 1498 (1988).

2. G. Ripka, in Advances in Nuclear Physics, edited by . Baranger and E. Vogt (Plenum New York, 1968), Vol. 1.

ROLL OF PROTONS IN THE ONSET OF DEFORMATION IN THE A≃100 MASS REGION

RAKESH KUMAR GUPTA, S.K. KHOSA AND A.BHARTI DEPTT. OF PHYSICS, UNIVERSITY OF JAMMU, JAMMU.

The region of deformation among neutron rich nuclei with A 100 exhibits some interesting features including (i) an abrupt transition from nearly spherical to highly deformed ground state in the Sr and Zr isotopic chains at N=60 and there is evidence for co-existence of spherical and deformed shapes[1] near the shape transition in these nuclei.

In this paper, we have attempted to examine the observed sharp and sudden spherical to deformed prolate shape transitions by carrying out a Nilsson Model Calculations using the new macroscopic mass formula of moller and mix with a Nilsson type of potential for the shell corrections. In the fig. 1a and 1b we present the results of our calculations, Our results indicate that energy difference between spherical and deformed minima in $^{88-100}$Sr and $^{90-102}$Zr go on decreasing with increasing neutron number with the exception of ^{94}Sr and ^{96}Zr. In ^{98}Sr and ^{90}Zr the energy gap between spherical and deformed minima is 5.03 Mev and 6.4 Mev where as in ^{96}Sr and ^{98}Zr it is 0.26 Mev and 0.53 Mev. Thus in this mass region our results indicate the possibility of co-existence of spherical to deformed shapes. Our results also indicate that the sudden onset of deformation at N = 60 in Sr and Zr nuclei arises due to two factors. Firstly due to sudden occupation of low components of $(g7/2)_\nu$ and $(h_{11/2})_\nu$ - orbits and secondly due to sudden polarisation of the $(P_{3/2})_\pi$ and $(f_{5/2})_\pi$ proton shells.

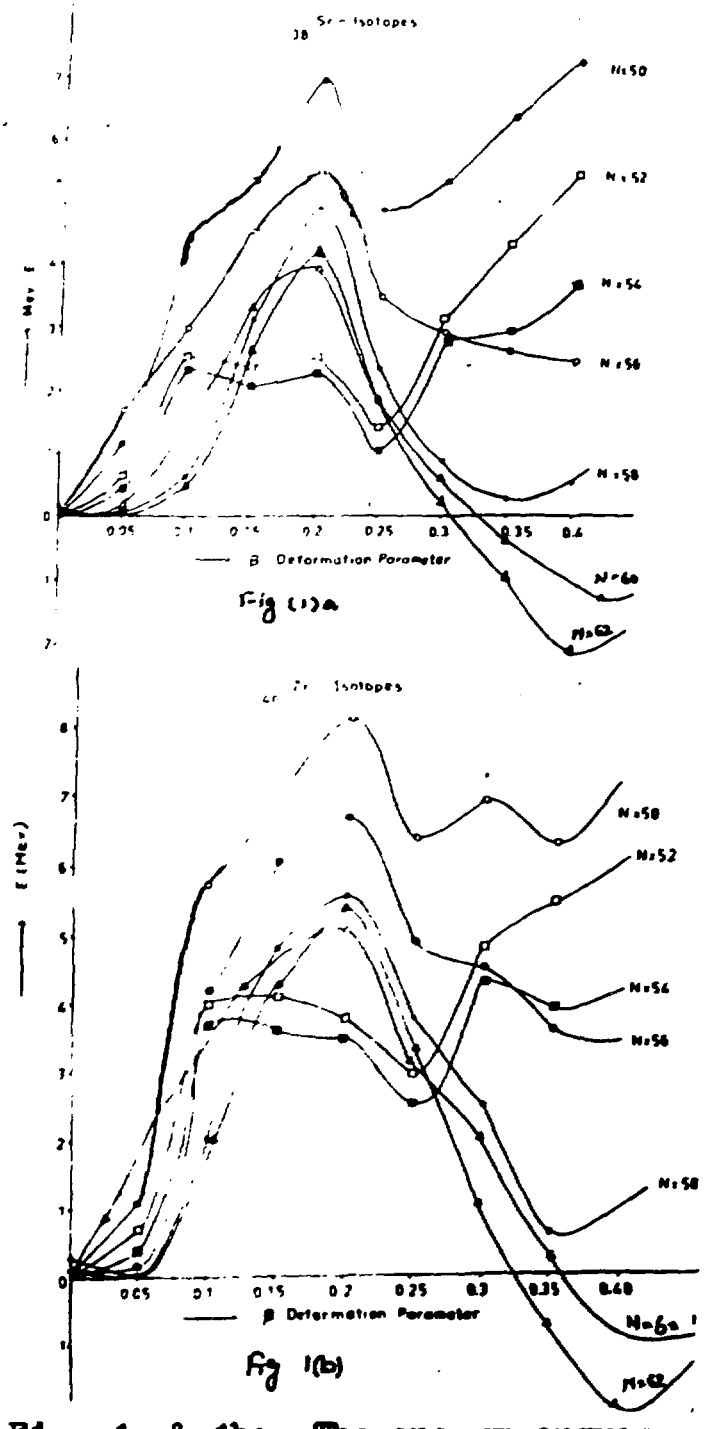

Fig. 1a & 1b:- The energy curves as a function of deformation paramater (β) for Sr and Zr isotopes. Ref:1.H.Mach at al., Phys.Lett.B230,21 (1989).

INTRINSIC QUADRUPOLE MOMENTS OF ODD-ODD NUCLEI AND SYSTEMATICS OF DEFORMATION PARAMETER

S.D.SHARMA, ARVINDER KAUR, ARVIND SHARMA
Department of Physics, Punjabi University, Patiala-147002, India.

INTRODUCTION: The systematics of deformation parameter throughout periodic table has already been studied [1,2], on the basis of quadrupole moments of Even-Even and odd A nuclei. Now there is enough data on quadrupole moments of odd-odd nuclei. It is worthwhile to study the systematics of deformation throughout the periodic table in order to view the variation on going from odd-odd to odd Z nuclei. In this paper an attempt to study the variation of deformation throughout periodic table is made.

THEORY:

The expression for Intrinsic quadrupole moment without any configuration mixing in the ground state i.e. K = I is given by,

$$q_c = \frac{Q}{\sqrt{\frac{16\pi}{5}\frac{I(2I-1)}{(I+1)(2I+3)}}} - q_p\left(N_p+\tfrac{3}{2}\right)\sqrt{\frac{5}{4\pi}}\left\{\frac{\Omega_p(\Omega_p+1)-3\Lambda_p^2}{4\Omega_p(\Omega_p+1)}\right\}$$

where Q is the experimentally reported value of quadrupole moment

But, $q_c = 3Z R_0^2 \beta/4\pi = 3{\cdot}438\times10^{-3} Z A^{2/3}\beta$ barns

$$\text{or } \beta = q_c/3{\cdot}438\times10^{-3} Z A^{2/3} = \frac{q_c \times 290{\cdot}86678}{(Z-1)A^{2/3}}$$

The deformation parameter is calculated using the above relation for both odd-odd and odd-Z nuclei.

RESULTS AND DISCUSSION:

From the tabulated results in (Table I), it is clear that the value of deformation parameter β in the prelanthanide region ($40 < Z < 57$) builds up to .06. So it is not significantly deformed. In the lanthanide region, it is found that the value of β builds upto .32. So it is concluded that lanthanide region is quite deformed one.

In case of nearly doubly magic nuclei i.e. $^{51}_{23}V_{28}$ (near magic nos 20 & 28) and $^{141}_{59}Pr_{82}$ (near magic nos 50 and 82) etc. deformation becomes -ve where as in case of single magic nuclei (as can be seen from Table) the deformation as expected may not become negative.

It may be remarked that the results for best fit value of β in neighbouring odd-Z and odd-odd nuclei is almost the same. The value of β changes in a systematic manner on going from neighbouring Z nuclei.

Thanks are due to Professor H.S.SAHOTA and Professor M.SINGH for encouragements and the facilities provided for this work.

TABLE I

Deformation Parameter in Neighbouring Odd-Z and Odd-Odd Nuclei:

S.No.	Odd-Z Nucleus ${}^{A}_{Z}X_{N}$	Deformation Parameter β	Odd-Odd Nucleus ${}^{A}_{Z}X_{N}$	Deformation Parameter β
1.	${}^{11}_{5}B_{6}$	1.05	${}^{10}_{5}B_{5}$	1.11
2.	${}^{51}_{23}V_{28}$	-.029	${}^{50}_{23}V_{27}$	.04
3.	${}^{55}_{25}Mn_{30}$	.26	${}^{54}_{25}Mn_{29}$	.275
4.	${}^{59}_{27}Co_{32}$	.18	${}^{60}_{27}Co_{33}$	0.20
5.	${}^{71}_{31}Ga_{40}$	.08	${}^{72}_{31}Ga_{41}$	.21
6.	${}^{79}_{35}Br_{44}$	.22	${}^{80}_{35}Br_{45}$	.30
7.	${}^{81}_{35}Br_{46}$	.21	${}^{80}_{35}Br_{45}$	.28
8.	${}^{85}_{37}Rb_{48}$	.10	${}^{86}_{37}Rb_{49}$	.11
9.	${}^{113}_{49}In_{64}$	.01	${}^{112}_{49}In_{63}$	.07
10.	${}^{123}_{51}Sb_{72}$	-.05	${}^{122}_{51}Sb_{71}$	.11
11.	${}^{133}_{55}Cs_{78}$	.01	${}^{134}_{55}Cs_{79}$	.05
12.	${}^{135}_{55}Cs_{80}$	.02	${}^{136}_{55}Cs_{81}$	.04
13.	${}^{137}_{57}La_{80}$	.04	${}^{138}_{57}La_{81}$	.06
14.	${}^{139}_{57}La_{82}$	.02	${}^{140}_{57}La_{83}$	.01
15.	${}^{141}_{59}Pr_{82}$	-.03	${}^{142}_{59}Pr_{83}$	.01
16.	${}^{159}_{65}Tb_{94}$	.28	${}^{158}_{65}Tb_{93}$	.32

SENSITIVITY OF CRANKED NILSSON BCS CALCULATIONS ON INPUT PARAMETERS

Tripti Mathur and Shanker Mukherjee,
Department of Physics,
Banaras Hindu University, Varanasi - 221005.

In this work we examine the sensitivity of the cranked shell model (CSM) calculation with respect of parameters (Δ, λ), one obtained by solving the BCS eq. and the second obtained from the neutron seperation energy[1], to solve the quasi particle equation.

In addition to this, the critical frequency, w_c, at which the backbend occurs and the aligned angular momentum, i, relative to the ground state band are determined from the experimental rotational bands for Mo^{100}, these quantities are then compared with the theoritical ones obtained using the CSM. The result are summarized in the following Tables :

Table : Experimental and theoretical estimates of critical frequency and parameters used in the analysis.

S.N.	Method	Critical frequency, w_c, (Mev)
1.	$\frac{2\vartheta}{\hbar^2}$ vs $(\hbar w)^2$ curve	0.40
2.	Expt. Routhian with $\vartheta_0 = 4.26\hbar^2$ Mev^{-1}, $\vartheta_1 = 80\hbar^4$ Mev^{-3}	0.37
3.	Theoritical Routhians with	
	(i) $\Delta_n = 0.150\hbar w_0$, $\lambda_n = 5.141\ \hbar w_0$	0.44(BCS)
	(ii) $\Delta_n = 0.148\hbar w_0$, $\lambda_n = 4.853\hbar w_0$	0.39 (expt. neutron seperation energy)

Table 2 : Comparison of experimental and theoretical alignments

S.N.	Methods	Alignment 'i'
1.	Experiment (using Harris parameters)	6.7 $\hbar$
2.	Theory (from the slopes of the theoritical Routhians)	6.45 $\hbar$

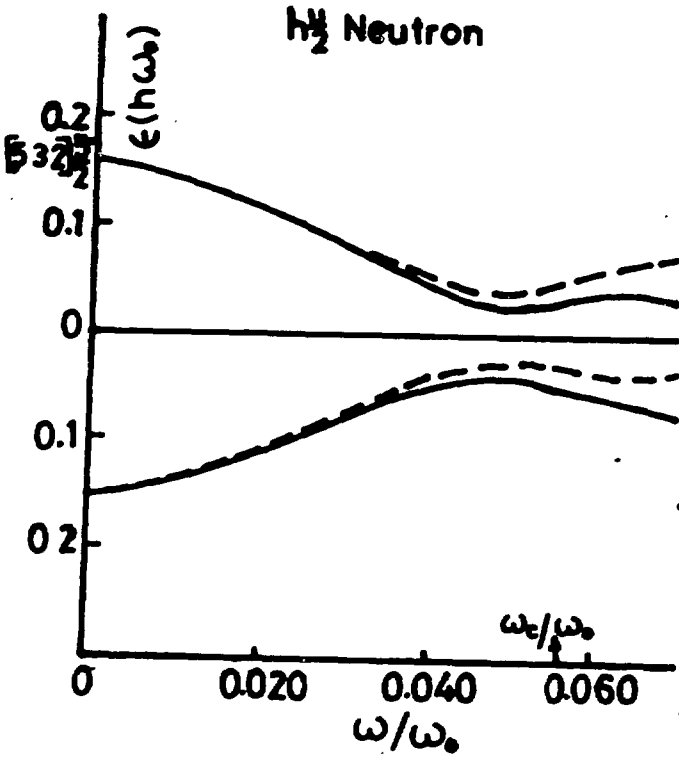

Fig 1. Vp energies vs ω (Table 1/s.No 3 i)

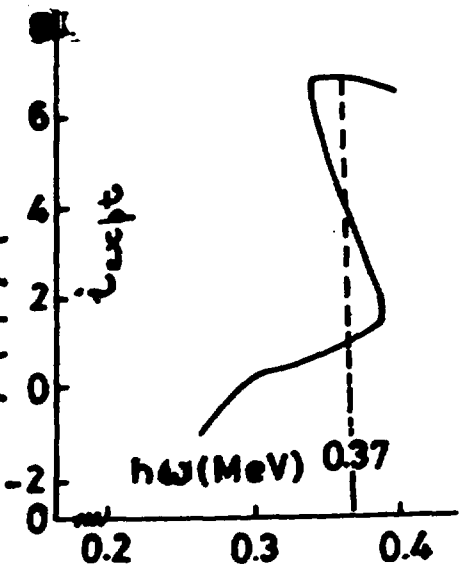

Fig 2. $i_{expt.}$ vs $\hbar\omega$
See Table 2./s.No. 1

We see that the effect of the change in the pairing energy, is to change the band crossing frequency. But within the limitations of the CSM approach, the agreement between theory and experiment is reasonable. The choice of the parameter λ_n, also plays an important role in determining the lowest quasi particle level.

Reference - 1. Tripti Mathur and Shanker Mukherjee, Phy. Rev. C 44, 1991

TENSOR COMPONENTS OF R.I. IN EFFECTIVE INTERACTIONS

M.L.Soni
Madhav Science College, Vikram University
Ujjain

The effective interaction depends sensitively on the choice of the configuration space. Various effective interactions in s-d and the truncated s-d regions have been studied in terms of TBME. Each TBME has pooled together in it contributions from the various spin tensor ranks and from the component spin angular momenta states weighted by suitable geometri-weight factors.

Thus it is possible to see the nature of the interaction more transparently through the proper study of R.I. We have determined the contributions of the various tensor components of R.I. to the full effective interactions. The results are compared in table shown for the various effective interactions.

Kulkarni & Pandya//1/ have reported that all radial integrals I_{nl} have progressively reducing strengths for higher and higher value of l and for $l \geq 2$ the values of R.I. practically reduces to zero. As per expectations we find RI Op,1p,Of and 1pOf have diminishing strengths in tensor force. Further it is a common belief/2/ that the odd state tensor force is repulsive in nature and even tensor force is attractive. The attractive odd tensor force in Chiange et al A and in PR are exceptions. In this connection it is well to remember that Schiffer & True interaction/3/ extracted from experimental data, has a weak attractive tensor force potential of -6.1 Mev(range 1.415 F) which was enhanced to a value -25.48 Mev by Han et al in order to explain the energy spectra of nuclei with $18 < A < 20$ and $36 < A < 38$ in lower and upper s-d shell. Though this anomaly of the difference arises partly because of the relatively insensitivity of the nuclear properties on the interaction components. Except SRCH B all interactions have attracting strengths of RI Of.

Tensor Components of RI's in iso-spin triplet state.

Interaction	Op	1p	Of	1pOf
Kuo	.679	0.645	-0.043	-0.001
K, 12FP	.557	0.468	-0.021	-0.250
H/2nd/	.579	0.101	-0.054	-0.133
H/PR/	1.008	-.405	-0.086	0.317
H/AVPR/	.540	0.205	-0.017	-0.147
H/Gupta/	.545	0.200	-0.017	-0.143
H/SRCHA/	.560	0.261	-0.117	-0.201
H/SRCHB/	.532	0.283	0.125	-0.159
Chiang A	-0.316	-0.771	0.952	-0.116
Chiang B	0.738	0.780	-0.095	0.103

Similarly all interactions except PR are attractive in RI 1pOf of tensor force in iso-spin triplet states. Here one can see the wide difference in the nature ofChiange A and B interactions which is a very contrary nature in all the RI of the tensor forces.

REFERENCES

/1/ D.R. Kulkarni and S.P.Pandya, Nuovo Cimento 60 B (1969) 199

/2/ K.P.Joshi and Y.R.Waghmare, Phy.Rev. C7 (1973) 874

/3/ J.P.Schiffer and W.W.true,Rev. Mod Phys. 48 (1976) 191

PROBLEM OF SIGN OF THE NEWBY SHIFT

A.K. Jain, Alpana Goel and Kiran Jain

Physics Dept., Univ. of Roorkee, Roorkee-247667, India

A longstanding problem in deformed odd-odd nuclei is the lack of explanation of the sign and magnitude of the Newby shifts from the n-p residual interaction calculations. An n-p interaction of purely central character, which is fitted to reproduce the G-M (Gallahager-Moszkowski) splittings, gives the wrong sign for the Newby shift in triplet configurations ($\Sigma=1$) whereas a correct sign is obtained in singlet ($\Sigma=0$) configurations but the magnitude becomes too large [1,3]. Sood and Ray [2] overcame this problem by introducing an arbitrary phase factor $(-1)^{\Sigma}$ and taking a modulus of the Wigner and the spin-dependent matrix elements rather than the actual signs. However, no basis was given for using these assumptions. In this paper, we argue that the sign change between triplet and singlet cases might follow from the transformation properties of the single particle states in the asymptotic limit of large deformation.

The wavefunction for a K=0 band is written as

$$|IMK=0,\alpha\rangle=(2I+1/32\pi^2)^{1/2}D^{I}_{M0}\{|K=0,\alpha\rangle+(-1)^{I}R_i|K=0,\alpha\rangle\},$$

where R_i is the rotation operator $exp(-i\pi J_y)$ with eigenvalues $j_\alpha=\pm1$ and

$$|K=0,\alpha\rangle=1/\sqrt{2}\{|\rho_p\Omega\rangle|\rho_n-\Omega\rangle-j_\alpha|\rho_p-\Omega\rangle|\rho_n\Omega\rangle\}.$$

The K=0 band thus splits into two sequences: $j_\alpha = +1$ ($I=0,2,..$) and $j_\alpha = -1$ ($I=1,3,..$). In the asymptotic limit of large deformation, the single particle wavefunction may be written for the singlet case as

$$|K=0,\alpha\rangle=1/\sqrt{2}\left\{Y^{\ell_1}_{-\Lambda_1}\chi_{-\Sigma_1}\cdot Y^{\ell_2}_{\Lambda_1}\chi_{\Sigma_1}- j_\alpha\, Y^{\ell_1}_{\Lambda_1}\chi_{\Sigma_1}\cdot Y^{\ell_2}_{-\Lambda_1}\chi_{-\Sigma_1}\right\},$$

and for the triplet case

$$|K=0,\alpha\rangle=\frac{1}{\sqrt{2}}\left\{Y^{\ell_1}_{-\Lambda_1}\chi_{-\Sigma_1}\cdot Y^{\ell_2}_{\Lambda_1+2\Sigma_1}\chi_{-\Sigma_1}-j_\alpha Y^{\ell_1}_{\Lambda_1}\chi_{\Sigma_1}\cdot Y^{\ell_2}_{-\Lambda_1-2\Sigma_1}\chi_{\Sigma_1}\right\}$$

Note that the R^2 operator leaves the orbital angular momentum functions unchanged. However, the same is not true for the spin wavefunctions which transform like spinors. Therefore, using the transformation properties of spinors, we get

$$R_i|K=0,\alpha\rangle=\frac{1}{\sqrt{2}}(-1)^{\ell_1+\ell_2+1}\left\{Y^{\ell_1}_{\Lambda_1}\chi_{\Sigma_1}\cdot Y^{\ell_2}_{-\Lambda_1}\chi_{-\Sigma_1}-j_\alpha Y^{\ell_1}_{-\Lambda_1}\chi_{-\Sigma_1}Y^{\ell_2}_{\Lambda_1}\chi_{\Sigma_1}\right\}$$

for the singlet case, and

$$R_i|K=0,\alpha\rangle=\frac{1}{\sqrt{2}}(-1)^{\ell_1+\ell_2}\left\{Y^{\ell_1}_{\Lambda_1}\chi_{\Sigma_1}\cdot Y^{\ell_2}_{-\Lambda_1-2\Sigma_1}\chi_{\Sigma_1}-j_\alpha Y^{\ell_1}_{-\Lambda_1}\chi_{-\Sigma_1}Y^{\ell_2}_{\Lambda_1+2\Sigma_1}\chi_{-\Sigma_1}\right\}$$

for the triplet case. Clearly, a sign difference arises between the singlet and the triplet case. This explains the phase factor $(-1)^2$ introduced in reference [3]. It appears that the spin part of the wavefunction is 'decoupled' and should be trated rather independently. Further investigations continue.

Financial support from D.A.E. and C.S.I.R. is gratefully acknowledged.

References:

1. J. P. Boisson, R. Pipenbring and W. Ogle, Phys. Rep. C26 99 (1976).
2. P. C. Sood and R. S. Ray, Pramana-J. Phys. 27 537 (1986)
3. A. Goel, A. K. Jain, R. W. Hoff and R. K. Sheline, Pramana- J. Phys. 36 105 (1991).

Transition Charge Densities for hexadecupole excitation in some Germanium Nuclei.

A. J. Singh S. K. Dhiman A.S.Raghwa and P. K. Raina.
Physics Department, H. P. University Shimla-5.

Inelastic electron scattering experiments on nuclei to large momentum transfers (up to $3fm^{-1}$) has become one of the interesting field for the study of nuclear structure. One of the main reasons which make this study important is the possibility of translating the scattering cross section data in to transition charge density (TCD) via Fourier-Bessel expansion method.

The medium mass nuclei are under continuous study by various experimental groups like Mainz, Saclay[1] and Hampshire[2]. Theoretical groups are also engaged in explaining and predicting the possible underlying structure by looking at the interactions and the behaviour of the core in these nuclei. The calculation of transition charge densities for different excitations acquires the importance due to its dynamic nature . In other words, one looks at the properties of two states involved in the transitions to a deeper extent, as a function of radial distance.

The results of quadrupole excitations for $^{70,72,74,76}Ge$ as seen by Saclay group are a real challenge for any theoretical approach trying to reproduce collective properties of these nuclei. The observed anomalous behavior in $0^+ \rightarrow 2_2^+$ transition in ^{70}Ge has been attempted in IBM framework[2] and the explaination of qualitative behaviour has also been seen through variational calculation[3].

The successful calculation of TCD for quadrupole excitation[4] has made us look into the hexadecupole excitation of these nuclei and here we presented the results of $0^+ \rightarrow 4^+$ excitation for $^{70,72,74,76}Ge$ nuclei. The calculations have been done in the HFB frame work[4] using the interactions proposed by Tripathi and Sharma[5].

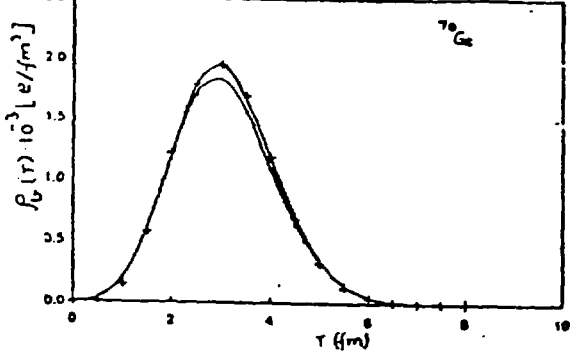

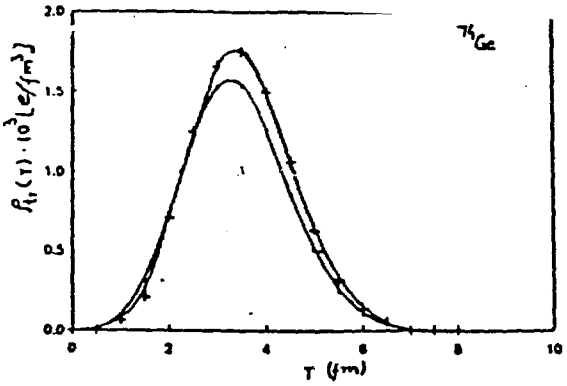

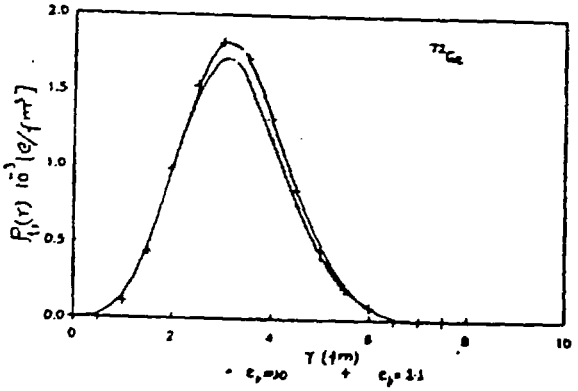

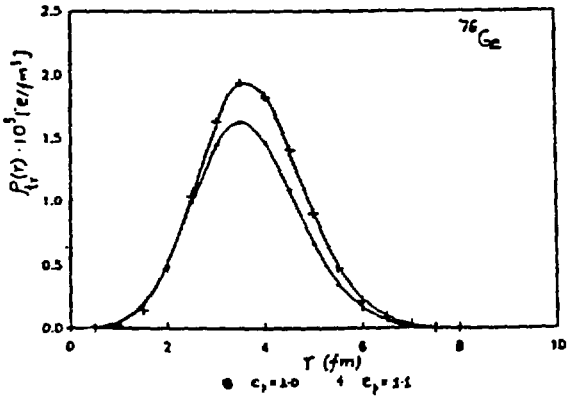

From the graphs one can notice one broad peak at r=3.0 - 3.5 fm. The comparison of results[3] for quadrupole excitation to these results show that hexadecupole results do not show any anomalous behaviour in contrast to the quadrupole excitation.

Two of the authors (ASR and PKR) would like to thank DST for the grants under project no. SP/YS/P13/89 and IIT Kanpur for allowing the use of computer.

References

1. J. P.Bazantay at al. Phys Rev. letts. 54 (1985) 643.
2. T.E.Milliman et al. Phys. Rev. C41 (1990) 2586.
3. G.Mukherjee, S.K.Sharma, P.K.Raina DAE symposium on nuclear Physics, December 1989, Aligarh (Submitted to Phys. Rev.C)
4. P.K. Raina and S.K. Sharma Phys. Rev. C37 (1988) 1427
5. P.N.Tripathi and S.K.Sharma Phys. Rev. C34 (1986) 1081

MOMENT OF INERTIA FOR HOT ROTATING NUCLEI IN STATIC PATH APPROXIMATION

B. K. Agrawal and A. Ansari
Institute Of Physics, Bhubaneswar, India-751005

Recent experiments are providing new informations on properties of hot nuclei formed in heavy ion fusion reactions. Experimental tools involve measurement of $\gamma-$ray spectra and light particles emitted by the compound nucleus duing its cooling process. Of the special interest here is the study of structural changes in hot rotating nuclei using static path approximation[1,2](SPA) which includes nuclear shape fluctuations. We have applied this approximation to the cranking Hamiltonian and studied a softly deformed nulcleus, ^{64}Zn.. In cranking model the moment of inertia is given as:

$$\Im = \frac{< J_x >}{\omega} \tag{1}$$

where $< J_x >$ is the expectation value of J_x and ω is the cranking frequency.

The partition function for grand canonical ensemble in SPA is given as:

$$Z(\mu_p, \mu_n, 1/T, \omega) = 4\pi(\frac{\alpha}{2\pi T})^{5/2} \int_0^\infty \beta^4 d\beta \int_0^{\frac{\pi}{3}} sin3\gamma d\gamma e^{\frac{-\alpha\beta^2}{2T}}$$

$$\times Tr e^{-(\hat{H}^\omega - \mu_p N_p - \mu_n N_n)/T} \tag{2}$$

where α is a parameter related to the interaction strength[1] and $\hat{H}^\omega$ is a cranked Nilsson type deformed one body Hamiltonian with statandard notations:

$$\hat{H}^\omega = \hat{H}_o - M\omega_o^2 \beta r^2 (cos\gamma Y_{2,0} + \frac{1}{\sqrt{2}} sin\gamma (Y_{2,2} + Y_{2,-2})) - \omega j_x \tag{3}$$

Using Eq. (1) and (2) we have obtained the moment of inertia for hot rotating ^{64}Zn as shown in figure below. At temperature T=0.5 MeV the moment of inertia shows an upbending around $\hbar\omega = 1 MeV$. As temperature increases this upbending disapppears gradually and moment inertia becomes almost constant, corresponding to the $\Im_{rigid}$ for more or less spherical shape.

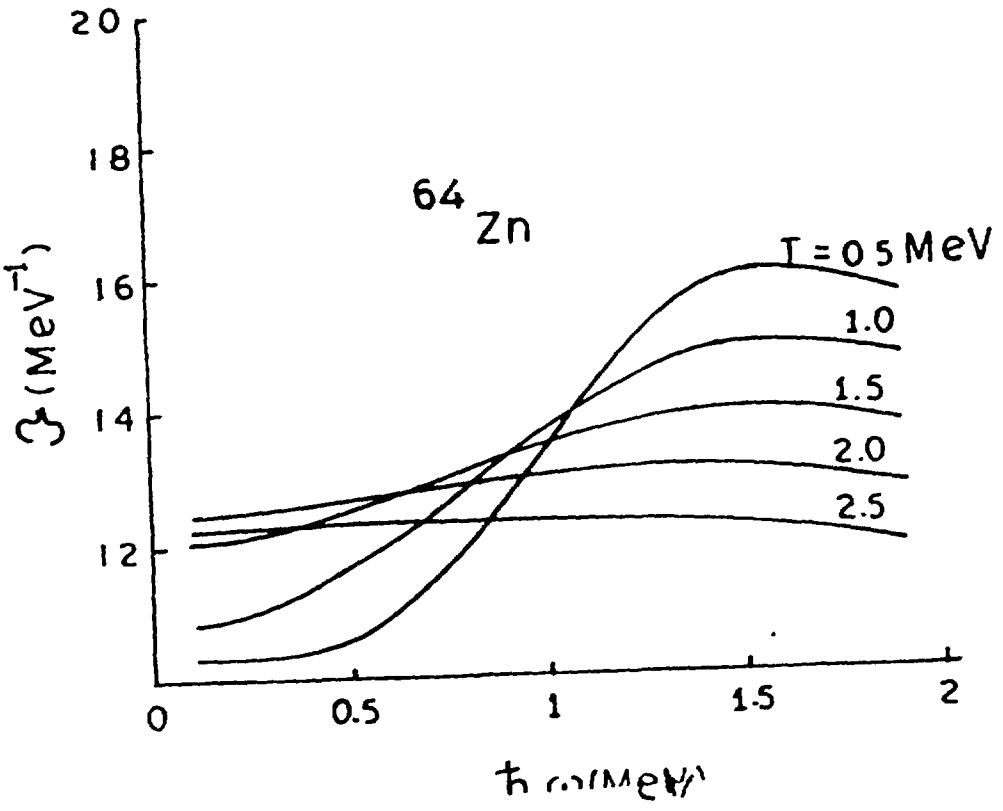

References

1. B. Lauritzen and G. Bertsch, Phys. Rev. C39, 2412 (1989)
2. P. Arve, G. Berstch, B. Lauritzen and G. Puddu, Ann. Phys. 183, 309 (1988)

GENERATOR COORDINATE METHOD FOR ($dt\mu$) MESOMOLECULE

MEENAKSHI AGGARWAL, B.K.CHIKARA and V.K.SHARMA
Department of physics, Institute of Advanced Studies
Meerut university, Meerut 250004, India

Muon-catalyzed fusion of deuterium-tritium has recently become a topic of widespread interest, as a new journal "MUON CATALYZED FUSION" was started in 1987. The most crucial and perhaps the most fascinating aspect of the muon catalysis is the role played by the resonant formation of the $dt\mu$ molecule [1] which occurs due to the existence of a very weakly bound J=v=1, by only ~0.65 eV, excited state in the $dt\mu$ mesonic molecule.

The experiments on muon catalyzed fusion are particularly relevant for the study of mesomolecular formation rate, which is sensitive to the mesomolecular energy spectrum. The sufficiently sharp estimate of mesomolecular energy levels are due to Dubna group, which considered the mesomolecule as a pure Coulomb three-body problem and obtained the energy levels using Born-Oppenheimer approximation.

For the calculation of actual mesomolecular levels to the desired degree of accuracy, unlike other recent calculations[2,3] one should take into account the nuclear interactions and nuclear size effects. In the present investigation we propose a new technique to include nuclear interactions within the framework of three-centre generator coordinate method[4].

The hamiltonian for $dt\mu$ system as three-centre GCM is given by[4]

$$H = \left[-\frac{\hbar^2}{2m}\sum_{i=1}^{5}\nabla_i^2 - T_{c.m.}\right] - \frac{\hbar^2}{2M_\mu}\nabla_\mu^2 + \sum_{i<j}^{5} V_{ij}^N + \sum_{i<j}^{5} V_{ij}^C + \sum_{i=1}^{5} V_{\mu i}^C \qquad (1)$$

The GCM wavefunction of $dt\mu$ molecule is a superposition of three-centre GC function with

respect to relative Jacobi coordinates $\vec{S}_{dt}$ and $\vec{S}_{dt\mu}$ as[5]

$$\Psi^{GCM}_{dt\mu}(\vec{X}) = \int d\vec{S}_{dt}\, d\vec{S}_{dt\mu}\, f(\vec{S}_{dt}, \vec{S}_{dt\mu})\, \Phi_{dt\mu}(\vec{X}, \vec{S}_{dt}, \vec{S}_{dt\mu}) \qquad (2)$$

where GC amplitude 'f' satisfy the following GHW equation

$$\int d\vec{S}'_{dt}\, d\vec{S}'_{dt\mu}\left[H(\vec{S}_{dt}, \vec{S}_{dt\mu}; \vec{S}'_{dt}, \vec{S}'_{dt\mu}) - E\,N(\vec{S}_{dt}, \vec{S}_{dt\mu}; \vec{S}'_{dt}, \vec{S}'_{dt\mu})\right] \cdot f(\vec{S}'_{dt}, \vec{S}_{dt\mu}) = 0$$

with

$$\begin{Bmatrix} H(\vec{S}_{dt}, \vec{S}_{dt\mu}; \vec{S}'_{dt}, \vec{S}'_{dt\mu}) \\ N(\vec{S}_{dt}; \vec{S}_{dt\mu}; \vec{S}'_{dt}, \vec{S}'_{dt\mu}) \end{Bmatrix} = \left\langle \Phi(\vec{X}, \vec{S}_{dt}, \vec{S}_{dt\mu}) \begin{Bmatrix} H \\ I \end{Bmatrix} \Phi(\vec{X}, \vec{S}'_{dt}, \vec{S}'_{dt\mu}) \right\rangle \qquad (3)$$

(4i)

The GHW equation (3) can be solved exactly and energy eigen value can be obtained accurately[3]. To compare with Dubna group in Born-Oppenheimer approximation we can solve (3) as

$$E(S_{dt}, S_{dt\mu}) = \frac{H(S_{dt}, S_{dt\mu}; S_{dt}, S_{dt\mu})}{N(S_{dt}, S_{dt\mu}; S_{dt}, S_{dt\mu})} \qquad (4)$$

which is comparable to the energy levels given by

$$E_{JV} = E(S_0) + \omega(V + \tfrac{1}{2}) + \frac{J(J+1)}{2M_0 S_0^2} \qquad (5)$$

where S_0 is the value of S_{dt} at which $E(S_{dt}, S_{dt\mu})$ is minimum and M_0 reduced mass of dt-system. The advantage of the present technique over others[2,3] is to get sufficient accuracy with few generator coordinates.

REFERENCES

1. S.S GERSTEIN and L.I. PONOMAREV. Phys.Lett. **72B** (1977) 80.
2. CHI-YU HU. Phys.Rev. **A36** (1987) 4135;
   V.I. KOROBOR et al. Phys.Lett.**196B**(1987)272;
   K. SZALEWICZ et al. Phys.Rev.**A36**(1987)5494.
3. M. KAMIMURA. Phys.Rev. **A38** (1988) 621.
4. MEENAKSHI AGGARWAL. M.Phil.Thesis (1990) Meerut University.
5. V.K. SHARMA and M.A. NAGARAJAN.J.Phys.G:Nucl. Phys. **10** (1984) 1703.

MICROSCOPIC STRUCTURE FOR FIVE NUCLEON SYSTEM

B.K.CHIKARA, MEENAKSHI AGGARWAL and V.K.SHARMA
Department of Physics, Institute of Advanced Studies
Meerut University, Meerut 250004, India

Microscopic theories for the structure of light nuclei is, in general, based on the nuclear properties ranging from single-particle features to many different kinds of collective features. Among these the generator coordinate method (GCM) and the resonating group method (RGM) have been widely used for the structure of light nuclei. In both these methods, the centre-of-mass motion is treated properly and Pauli principle is exactly taken into account. Recently it has been shown that the GCM has a physical interpretation as the coexistence of shell-model and cluster aspects-a unique feature in light nuclear system.

Here we present the GCM for the structure of five nucleon systems i.e. the mirror nuclei ^{5}He and ^{5}Li each of which has two different kinds of possible cluster structures allowed by Pauli principle. We have considered ^{5}He and ^{5}Li as two possible kinds of configurations due to energy break up threshold [1]. ^{5}He has (α+n) and (t+d) configurations whereas the possible configurations for ^{5}Li are (α+p) and (h+d) systems.

The two-centre GCM wavefunction of the nucleus A(^{5}He or ^{5}Li) can be simplified and the c.m. dependence can be factored out easily if we consider that the oscillator width parameters of clusters are equal [2]. The GCM wavefunction belonging to a definite total angular momentum J, its z-component M and parity π in projected basis as

$$^A\psi^{JM\pi}(x) = \sum_\beta \int_0^\infty ds\, f_\beta^{J\pi}(s)\, \Phi_\beta^{JM\pi}(x,s) \qquad A = {}^5He \quad \beta = (\alpha+n),\ (t+d) \qquad (1)$$

$$A = {}^5Li \quad \beta = (\alpha+p),\ (h+d)$$

where GC amplitudes satisfy the following coupled GHW equations:

$$\sum_{\beta,\beta'} \int_0^\infty ds' \left[H^{J\pi}_{\beta\beta'}(s,s') - E N^{J\pi}_{\beta\beta'}(s,s') \right] f^{J\pi k}_{\beta'}(s') = 0 \qquad (2)$$

The hamiltonian and normalization matrix are given by

$$\left\{ \begin{matrix} H^{J\pi}_{\beta\beta'}(s,s') \\ N^{J\pi}_{\beta\beta'}(s,s') \end{matrix} \right\} = \left\langle {}^{A}\Phi^{J\pi}_{\beta}(\vec{x},s) \left| \begin{matrix} H \\ I \end{matrix} \right| {}^{A}\Phi^{J\pi}_{\beta'}(\vec{x},s') \right\rangle \qquad (3)$$

The values of various channels are defined as in eq.(1). The hamiltonian matrix elements are calculated and it is found that the K.E. and nuclear interaction matrix elements are same for mirror nuclei with similar channels. The Coulomb matrix elements are different for various nuclei and configurations. Some of these are given as [3]

$$H^{J\pi}_{\beta\beta'} = T^{J\pi}_{\beta\beta'} + {}^{N}V^{J\pi}_{\beta\beta'} + {}^{C}V^{J\pi}_{\beta\beta'} \qquad (4)$$

$$T^{J\pi}_{\lambda_1,\lambda_2} = \left[\frac{3\hbar^2\beta}{m} - \frac{\hbar^2\beta^2}{10m}(s^2+s'^2) \right] N_L(s,s') + \frac{3\hbar^2\beta^2}{10m} 4\pi \sum_{\Lambda} \langle L100|\Lambda 0\rangle^2$$
$$N_L(s,s') + \frac{\hbar^2\beta^2}{200m} e^{-\frac{\beta}{5}(s^2+s'^2)} \cdot 4\pi \left[34 \sum_{\Lambda} i_\Lambda(2/5\,\beta ss') \langle L100|\Lambda 0\rangle^2 \right.$$
$$\left. +16 \sum (-)^{\Lambda} i_\Lambda(\beta/10\, ss') \langle L100|\Lambda 0\rangle^2 \right] \qquad (5)$$

$$N V^{J\pi\Lambda}_{\lambda_1,\lambda_2} = e^{-\beta/5(s^2+s'^2)} \left[3q(0,0)(\omega+m)\, i_L(2/5\,\beta ss') + f(x)\left[4\omega - 2H \right.\right.$$
$$+2\beta - m)\, i_L\left\{ \left(\frac{2\beta}{5} - \gamma_i/4\right) ss' \right\} - (2\beta - 4m - 2H + \omega)\, i_L\left\{ \left(\frac{\gamma_i}{2} - \frac{\beta}{10}\right) \right.$$
$$\left.\left. ss' \right\} - (3\omega + 5m)(-)^L i_L(\beta/10\, ss').\left(e^{\gamma_i/4 s^2} + e^{\gamma_i/4 s'^2} \right) \right] \right] \qquad (6)$$

$$\text{with } f(x) = K_x \exp\left[-\gamma_i/4 (s^2+s'^2) \right], \quad K_x = \sum_{i=1}^{2} V_x q_i^2 \gamma_i^{3/2}, \quad x \equiv (q,\gamma)$$

$${}^{C}V^{J\pi}_{\lambda_1,\lambda_2} = f'(x)\, q_{00}(0,0)\, N_L(s,s') \qquad f'(x) = \frac{e^2}{4\pi\epsilon_0} \beta^{1/2} \frac{2}{\sqrt{\pi}} \sum_{n=1}^{6} Y_{0n} \qquad (7)$$

REFERENCES

1. F.C. BARKER and C.L. WOODS, Aust. J. Phys. 38 (1985) 563.
2. V.K. SHARMA in the DEVELOPMENTS OF NUCLEAR CLUSTER DYNAMICS, World Scientific (1989) 50
3. MEENAKSHI AGGARWAL, M.Phil. Thesis (1990) Meerut University.

K-HARMONICS METHOD APPLIED TO t_Σ AND $^9_\Sigma Be$

S.K.Sharan[1] and S.P.Verma[2]
1. Deptt. of Physics, T.P.S. College, Patna
2. Deptt. of Physics, Science College, Patna.

The method of hyperspherical harmonics (K-harmonics) has been used to study the ground state of Σ-hypernuclei in a three-particle model. The method developed by Simonov[1] and applied by Verma and Sural[2] utilises -s expansion of the three-particle wave function in a complete set of angular functions in six dimensional hyperspace.

The three particles are represented by the Jacobi coordinates

$$\vec{\eta} = \sqrt{\frac{m_1 m_2}{(m_1+m_2)\mu}}\left(\vec{r}_1 - \vec{r}_2\right) \qquad (i)$$

$$\vec{\xi} = \sqrt{\frac{(m_1+m_2)m_3}{(m_1+m_2+m_3)\mu}}\left(\frac{\vec{r}_1+\vec{r}_2}{2} - \vec{r}_3\right) \qquad (ii)$$

Where $\mu = (m_1+m_2+m_3)/3$.

The Schrodinger equation for the three body system is

$$\left[-\frac{1}{2\mu}\left(\nabla^2_{\vec{\xi}} + \nabla^2_{\vec{\eta}}\right) + \hat{V}^{(12)} + \hat{V}^{(13)} + \hat{V}^{(21)} - E\right]\psi(\vec{\xi},\vec{\eta}) = 0 \qquad (iii)$$

Where $\hat{V}^{(ij)}$ are the pair-potentials. The three body wave functions is expanded as

$$\psi(\vec{\xi},\vec{\eta}) = \sum_{K,\nu} \rho^{-2}\chi_K^\nu(\rho)\, U_K^\nu(\Omega_\rho) \qquad (iv)$$

where $\rho = \sqrt{\xi^2+\eta^2}$ and Ω_ρ are the five angular variables. Substituting (iv) in (iii) and integrating over the angular variables we get a system of coupled differential equation, which in turn is converted into coupled integral equations for

$$\chi_K^\nu(\rho) = \int_0^\infty I_{K+2}(R\rho_<)\, K_{K+2}(k\rho_>) \times \sum_{K'\nu'} U_{KK'}^{\nu\nu'}(\rho')\,\chi_{K'}^{\nu'}(\rho')\, d\rho' \qquad (v)$$

Here $k=\sqrt{-2\mu\epsilon}$ and $U_{\kappa\kappa'}^{\nu\nu'}$ are the m.e. of the two body pair interaction.

We have taken two-body central potentials of Gaussian shape and numerically solved the integral equation (v) for the ground state energies using Gauss-quadrature formula.

For Σ-hypertriton (t_Σ) in $(\Sigma-n-n)$ model the n-n potentials are those fitted to n-n scattering length and effective range data. The n Σ interaction range has been chosen to be $\beta_{n\Sigma} = 1.834$ fm and results have been obtained for two sets of ($n\ \Sigma$) potential strengths : Set A ($V_{n\Sigma} = -29.54$ MeV) and set B ($V_{n\Sigma} = -65.63$ MeV) which desinates the threshold of formation and the b.e. limit of hyperdeutron for the lowest K-harmonics (i.e. K=0) the results compares will with the Faddeev calculation[3].

	Kharchenko et al(MeV)	our results (MeV)
Set A	1.85	1.72
Set B	28-29	27.35

For $^{5}_{\Sigma}$Be treated in ($\alpha-\alpha-\Sigma^{\circ}$) model we have used one term Gaussian $\alpha-\alpha$ potential of Buck et al[4] and found that $V_{\alpha\Sigma^{\circ}} = -65.54$ MeV, $\beta_{\alpha\Sigma^{\circ}} = 1.355$ fm. gives results in a ground state energy 3.52 MeV which is close to Jibuti et al[5] calculation. Further work for inclusion of higher K-harmonics is in progress.

1. Yu.A.Simonov,Sov.Jour.Nucl.Phys. 3 ,755(1966)
2. S.P.Verma and D.P.Sural,Phys.Rev.C22,229(1980); J.Phys.G.8 ,73(1982);P.Kumar et al,Proc.Nucl. Phys.Symp.BARC.30B, 170(1987).
3. V.F.Kharchenko and V.E.Kuzmichev,Nucl.Phys. A386 ..... (1982).
4. B.Buck et al,Nucl.Phys. A275 , 246(1977).
5. R.I.Jibuti et al. Few Body Prob. in Phys.Proc. ninth Europ.Conference,USSR,World Scientific (1985), p. 284.

PERTURBATIVE SOLUTION OF INTEGRO DIFFERENTIAL EQUATION

Rakhi Chattopadhyay

Dept of Physics. Calcutta University. 92,A.P.C Road,Cal-700009

Fabre and his collaborators/1/have derived an Integro Differential Equation (IDE) involving two variables for a many boson system interacting through two body interactions in which all correlations higher than two body correlations are disregarded. This has the same structure and degree of complexity for all A (=no. of particles). This makes the IDE a powerful tool for calculation of a many body system. But difficulties arise during solving it numerically. We solve the IDE by perturbation method. IDE for a system of A identical bosons (mass m) interacting through two body potential $V(r_{ij})$ has the form,

$$\left[\frac{\hbar^2}{m}\left\{\frac{\partial^2}{\partial r^2} - \frac{\lambda(\lambda+1)}{r^2} + \frac{4}{r^2}\frac{1}{\omega_\ell(z)}\frac{\partial}{\partial z}(1-z^2)\omega_\ell(z)\frac{\partial}{\partial z}\right\} + E - V_0(r)\frac{A(A-1)}{2}\right] P_\ell(z,r)$$

$$= \left[V\left(r\sqrt{\frac{1+z}{2}}\right) - V_0(r)\right]\left[P_\ell(z,r) + \int_{-1}^{+1} f_\ell(z,z')P_\ell(z',r)\,dz'\right] \quad \cdots (1)$$

where, $\lambda = \ell + (3A-6)/2$, $\alpha = (3A-8)/2$, $\beta = \ell + \frac{1}{2}$,

$$V_0(r) = \frac{1}{h_0^{\alpha\beta}}\int_{-1}^{+1} V\left(r\sqrt{\frac{1+z}{2}}\right)\omega_\ell(z)\,dz \quad \cdots (2)$$

ℓ is total orbital angular momentum, $P_K^{\alpha\beta}(z)$, $h_K^{\alpha\beta}(z)$ and $\omega_\ell(z)$ are respectively Jacobi polynomial, its norm and weight function. The function $f_\ell(z,z')$ is given by Fabre/1/.

$$f_{K\ell}^{2} = 1 + \left[2(A-2)\left(-\tfrac{1}{2}\right)^{\ell} P_K^{\alpha\beta}\left(-\tfrac{1}{2}\right) + (A-2)(A-3)/2\, P_K^{\alpha\beta}(-1)\delta_{\ell,0}\right]/P_K^{\alpha\beta}(1)$$

$$\cdots (3)$$

Subtraction of hypercentral potential/1/ $V_0(r)$ makes

the convergence factor and right side of equation (1) small and is taken as the perturbing term. We express E and $P_l(z,r)$ as, $E = E^{(0)} + \lambda E^{(1)} + \lambda^2 E^{(2)} + \cdots$ (4) and $P_l(z,r) = P^{(0)}(z,r) + \lambda P^{(1)}(z,r) + \lambda^2 P^{(2)}(z,r) + \cdots$ where $E^{(n)}$, $P^{(n)}$ refer to nth order perturbation .

The zeroth order equation is separable in hyper radial and angular part . Solution of angular part is just the Jacobi polynomial $P_K^{\alpha\beta}(z)$ and solution $f^{(0)}_{K\mu}(r)$ of radial part is done numerically. We expand 1st and 2nd order wave functions in terms of complete set of zeroth order wave function.

$$P^{(n)}(z,r) = \sum_{K,\mu} a^{(n)}_{K\mu} P^{(0)}_{K\mu}(z,r) = \sum_{K\mu} a^{(n)}_{K\mu} f^{(0)}_{K\mu} P_K^{\alpha\beta}(z) ; \quad (n = 1, 2 \cdots) \qquad \cdots\cdots (5)$$

First and second order perturbed energy terms are obtained as,

$$E^{(1)} = \frac{f^2_{K_0 l}}{h^{\alpha\beta}_{K_0}} \left\langle f^{(0)}_{K_0\mu_0} \middle| V_{K_0K_0}(r) \middle| f^{(0)}_{K_0\mu_0} \right\rangle \cdots\cdots (6)$$

where $f^{(0)}_{K_0\mu_0}(r)$ is the ground state radial part of the wave equation and

$$V_{KK_0}(r) = \int_{-1}^{+1} P_K^{\alpha\beta}(z) \left[V\left(r\sqrt{\frac{1+z}{2}}\right) - h_0^{\alpha\beta} V_0(r) \right] P_{K_0}^{\alpha\beta}(z)\, dz \cdots\cdots (7)$$

For $K = K_0 = 0$, $E^{(1)} = 0$ (see Eq.(2)). So there is no 1st order energy shift for ground state .The 2nd order perturbed energy term is found to be,

$$E^{(2)} = \sum_{K'\mu'}{}' \left(\frac{f^2_{K_0 l}}{h^{\alpha\beta}_{K_0}}\right) \left(\frac{f^2_{K' l}}{h^{\alpha\beta}_{K'}}\right) \frac{\left\langle f^{(0)}_{K_0\mu_0} \middle| V_{K_0K'}(r) \middle| f^{(0)}_{K'\mu'} \right\rangle \left\langle f^{(0)}_{K'\mu'} \middle| V_{K'K_0} \middle| f^{(0)}_{K_0\mu_0} \right\rangle}{\left(E^{(0)}_{K_0\mu_0} - E^{(0)}_{K'\mu'}\right)}$$

$K' \neq 0$ $\qquad\qquad\qquad

CHARGE CENTRE DEVIATION IN EXOTIC DECAY

G.Shanmugam and S.I.A.Philomin Raj ⊕
Department of Physics, Presidency college, Madras-5
⊕ Dept. of Physics, Madras Christian College, Madras-59

In exotic decay(1-3), it is observed that the coulomb energy calculated at the touching distance is always much higher than the experimental barrier height. To overcome this discrepancy, inclusion of either finite range attraction term in the coulomb energy expression or proximity term is generally in vogue. But a new concept of charge centre deviation had been introduced in our previous paper(4) to explain this discrepancy qualitativ _/ , whereas in the present work the quantity of the charge centre deviation has been derived from the giant dipole resonance (GDR) analogy.

When the daughter and fragment nuclides are just touching (fig.1), the proton fluids will be shifted away from the point of contact due to electrostatic repulsion, whereas the chargeless neutron fluids will remain touching at their common tangent T. As a result, the charge centres will be shifted away from the centres of mass. Thus, while touching, the centre of mass distance is r_t whereas the distance between charge centres is $d > r_t$. Thus the coulomb barrier height is given by

$$V(r_t) = \frac{Z_1 Z_2 e^2}{d} - Q \quad \ldots\ldots\ldots(1)$$

From fig.1, $d = x_1 + x_2 + r_t$ $\ldots\ldots\ldots(2)$

Where $x_1 = F/k_1$ and $x_2 = F/k_2$ with $F = Z_1 Z_2 e^2/r_t^2$

The nuclear force constants k_1 and k_2 (see fig.2) are $k_1 = m_1 w_1^2$, $k_2 = m_2 w_2^2$ where $m_1 (m_2)$ is the effective mass of $Z_1 (Z_2)$ protons assumed to be concentrated at C_1' (C_2'). w_1 and w_2 are the natural frequencies of the proton fluids assumed to be harmonic. In GDR, the proton fluid displacement is caused by incident gamma ray, whereas in this case the displacement is due to coulomb repulsion between the two proton fluids. The binding nature

prcduces the restoring force. The angular frequencies are determined from the relation $\hbar\omega = BA^{-1/6}$ established from GDR studies. Using this concept, the calculated barrier heights are in agreement with the experimental ones within 2 MeV. (see Table). Also the calculated (4) branching ratios are in good agreement with the experimental ones.

PARENT	FRAGMENT	BARRIER HEIGHT		Log (T/T_α)	
		Present	Exptl.	Present	Exptl.
Fr-221	C-14	30.34	28.44	12.87	13.10
Ra-221	C-14	29.86	27.95	12.71	12.90
Ac-225	C-14	32.26	30.48	12.55	12.40
Pa-231	Ne-24	33.76	32.39	11.15	11.22
Ra-223	C-14	30.33	28.39	9.11	9.20
U -234	Mg-28	34.37	33.99	25.50	25.75
Pu-238	Mg-28	34.61	34.64	25.66	25.70
Pu-238	Si-32	33.03	33.25	24.91	25.30

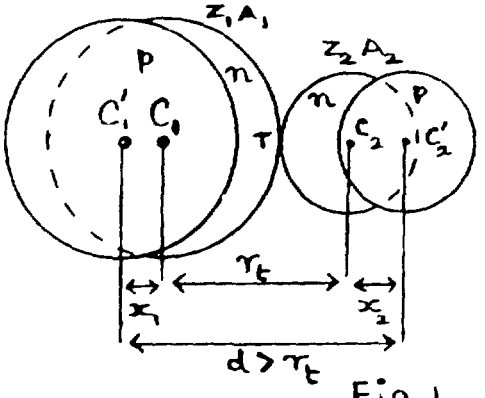

Fig.1

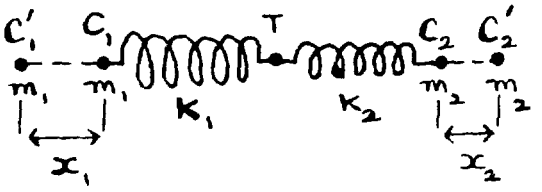

Fig.2

REFERENCES:

(1) D.N.Poenaru and M.Ivascu, J.Phys.45(1984)1099

(2) G.Shanmugam and B.Kamalaharan, Phy.Rev. C38 (1988) 1377

(3) Y.J. Shi and W.J.Swiatecki, Nucl. Phys-A438, (1985) 450

(4) G.Shanmugam and S.I.A. Philomin Raj, DAE Symp. on Nucl. Phys., 33B (1990) 59

REGULAR, IRREGULAR AND SCARRED WAVEFUNCTIONS IN THE TWO CENTRE SHELL MODEL

Debabrata Biswas
Theoretical Physics Division, Central Complex, B.A.R.C.
Bombay 400 085

Santanu Pal and A.K. Chaudhuri
Variable Energy Cyclotron Centre,1/AF Bidhan Nagar
Calcutta 700 064

The single particle motion of a nucleon in a dinuclear system plays an important role in low energy nucleus-nucleus reactions. One normally considers here either the classical 'window' formula or a rigorous quantum mechanical 'one-body' mechanism. As the underlying assumptions of both the approaches share some common features (e.g. 'never come back' vs. 'markovian') , we would be interested here in manifestations of classical motion in single-particle wave functions.

The basic idea is that of associating a ray of a classical trajectory to the normal direction on wave fronts. For this purpose, single-particle eigen wave functions are calculated in a two-centre shell model [1]. The nodal lines of a given eigenfunction are obtained on the (ρ,z) plane using a cylindrical co-ordinate system. A typical example of nodal patterns for different separations (R) between the two potential centres is shown in fig.1. The outer line in each plot defines the classically allowed region of the particular state.

It is immediately ovserved that the patterns are regular at large or very small separations, whereas they are irregular at intermediate (near touching) configurations. This 'chaotic' nature of the single-particle states corroborates to the 'never come back' assumption. However, it is important to recognize that here it happens due to the very nature of the neck potential without invoking any two-body collision.

Fig.2 shows the nodal pattern as well as the contour lines of a special kind of orbits, called 'scarred' states. Such a state essentially corresponds to a classical periodic motion (along z-direction in this case) and stands out among neighbouring irregular states. A full account of such states will be given elsewhere [2].

References:

[1] S.Pal and A.K. Chaudhuri, Nucl.Phys.A (in press)
[2] D. Biswas, S.Pal and A.K. Chaudhuri (to be published)

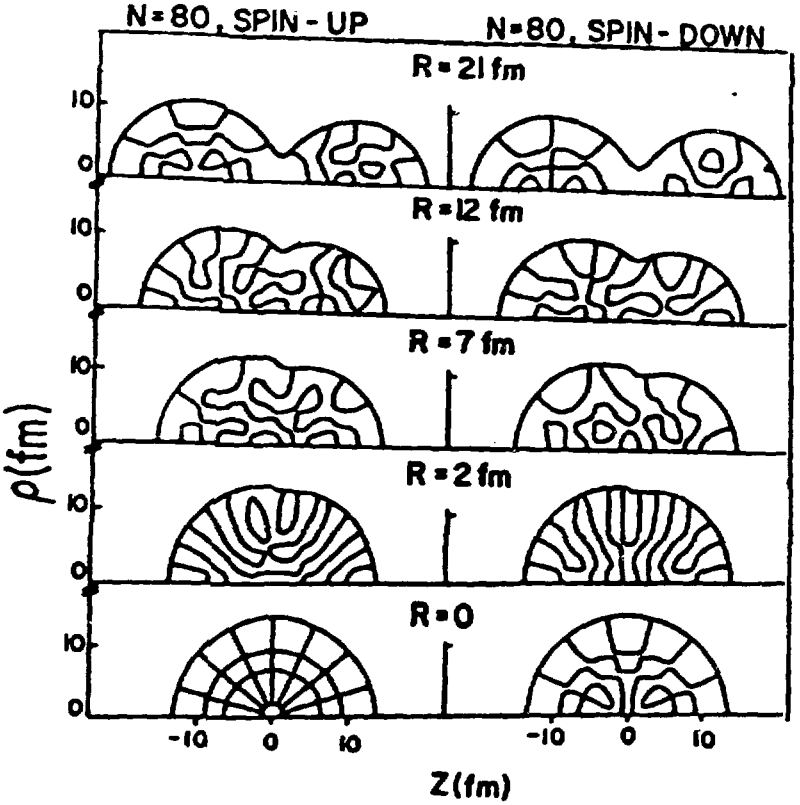
N=80, SPIN - UP
N=80, SPIN - DOWN
R=21 fm
R=12 fm
R=7 fm
R=2 fm
R=0
ρ(fm)
10
0
-10
0
10
Z(fm)

Fig.1

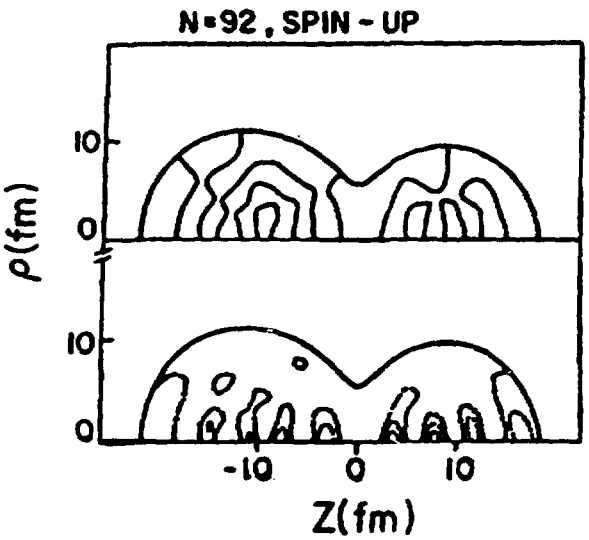
N=92, SPIN - UP
ρ(fm)
10
0
10
0
-10
0
10
Z(fm)

Fig.2

STRUCTURE OF 178-186 W FROM THE ARM

S.Sharma, K.S.Sen+ and S.P.Sud+
G.G.D.S.D College (H.P. University) Rajpur-176064
+Physics Department, H.P.University, Shimla-171005

178-186 W isotopes lie on shape phase transition from well deformed to spherical region and have challenging features. Kumar and Baranger /1/ had applied DPPQ model to explain the complex structure of these isotopes. Recently Sahu/2/ used pairing-plus-quadrupole-quadrupole-interaction (PPQQI) model to explain energy spectrum, B(E2) values and B(E2) ratios for 180-186W . These models /1,2/ are unable to explain the variation of $B(E2 ; 2_\gamma - 0_g/2_g)$ ratio with N (figure will be presented).

Asymmetric rotar model (ARM)/3/ is applied to explain energy spectrum, B(E2) values and B(E2) ratios for (γ-g) transitions. The valuesof asymmetry parameter(γ) are obtained using the values of energies of 2^+_γ and 2^+_g states. Our results are as follows:-

1. The values of γ are12.2,12.1,11.4,13.8& 15.9 for 178-186W isotopes respectively.
2. Calculated energy spectrum is satisfactory with standard deviation, σ = 70.5,31.9,13.6,31.1 & 59.3 KeV for 178-186W respectively.
3. Interband and intraband B(E2) values from ARM are close to the experimental data (see Table1)
4. B(E2) ratios for (γ-g) transitions from ARM lie between the VM and RM limit and quite close to the experimental data. Theoretical results are compared with the PPQQI /2/ and experimental data/4/.

References:- /1/ Nucl.Phys.A 110 (1968)429; A122(1968)273
/2/ Can.J.Phys.67(1989)479
/3/ Nucl.Phys.8 (1958)237
/4/ At.Data & Nucl.Data Table 36 (1987)1; 31 (1984)369; Table of Isotopes(1978); Nucl.Data sheets 14 (1975)559; 11(1977)1; 13 (1974)267; 13 (1974)549; 52 (1987)127.

Table: [illegible] B(E2) values & B(E2) ratios

Transition	178W		180W			182W			184W			186W		
	Expt.	ARM	Expt.	ARM	PPQQI	Expt.	ARM	PPQQI	Expt.	ARM	PPQQI	Expt	ARM	PPQQI
2'-0/2	2.9	.5	.52(4)	.45	2.8	.51	.48	1.76	.53(5)	.41	.48	.41	.33	.47
2'-2/4	0.3	10		10.1	14.0	210	10.1	12.3	11.3(32)	8.4	9.8	6.4	7.1	7.5
3'-2/4		1.12	1.95(76)	1.1	1.6	1.98	1.1	1.56	1.6 (2)	.8	1.1	0.79	.61	.72
3'-2/2'		.04		.04	.03							.0024	.06	.059
4'-2/4		.12	.21(9)	.12	.2	.26	.12	.19	.19	.07	.13	.11	.03	.05
4'-2/2'		.02		.02	.02		.02	.02	.02	.02	.02	.05	.01	.016
4'-2'/3'		.65		.45	.15		.45	.45	.7	.5	.5			
4'-2/2-0		1.44		1.44	1.45		1.44	1.46	1.38(3)	1.45	1.48	1.29(11)	1.46	1.52
4'-0/2-0		0.04		.04	.03		.04	.03	.04	.05	.04	.043(4)	.06	.06
2-0			0.84(5)	.84	1.06	.83(2)	.83	.98	.69(1)	.69	.7	.7	.7	.7
2'-0				.03	.03	.025(1)	.03	.03	.030(2)	.041	.041	.030(2)	.042	.041
2'-2						.047(3)	.06	.05	.069(4)	.124	.112	.069 (4)	.124	.112
2-3'				.08	.08		.07	.07		.104	.105		.1	.11
2-4				2.17	2.76	2.08(15)	2.2	2.6	1.6(1)	1.8	1.9	1.6(4)	1.8	1.9
3'-4				.05	.04		.04	.03		.12	.1		.124	.104
4-4'				.09	1.6		1.4	1.7		1.1	1.2		.14	.14

NUCLEAR STRUCTURE OF $^{146-154}$Sm IN THE IBM-1

S.Sharma, K.S.Sen+ and S.P.Sud+
G.G.D.S.D.College (H.P.University) Rajpur-176064
+Physics Department, H.P.University, Shimla-171005.

The Sm isotopes lie on a shape transitional region and provides a challenge for nuclear theory in correlating and deseribing a wide variety of experimental data. These isotopes have been studied extensively, experimentally/1/and theoretically /2/. Scholten etal/3/used the IBM-1 Hamiltonian with ELL, EPS, QQ and PP interaction parameters, to explain the complex nuclear structure of these isotopes and obtained a partial success in explaining the energy spectrum of g, β and γ bands, B(E2) values and B (E2) ratios for (β -g) transitions with large deviations for (γ -g) transitions. Castanos et.al./4/ used effective H_{IBM} and obtained a common set of nine interaction parameters by including the all known energy levels of all isotopes and partial success have been obtained to explain energy spectrum. Chuu et.al/5/ performed effective IBM calculation for N=88 and 90 isotones and their results are not in agreement.

The B(E2) ratios for (γ -g) and (β -g) transitions depend sensitively on rotational & vibrational interaction and it requires a delicate balance of quadrupole and pairing interation in IBM Hamiltonian. Such delicate balance have been obtained in the DPPQ model calculation by Gupta/6/.

In the present calculation we have included all known energy level in the PHINT program and obtained appropriate balance among QQ, LL, PP and EPS interaction forces of H_{IBM}. These parameters are usedto calculate B (E2) values and B(E2) ratios for transition from β, γ and higher bands. The theroretical results are compared with the experimental data and DPPQ model calculation (See Table 1 for ^{150}sm and results will be presented for other isotopes).

Conclusion:- A delicate balance of the pairing and quadrupole force is obtained to remove most of the discrepancies between experimental and theoretical

B(E2) values and B(E2)ratios. The results of present study are in agreement with the experimental data for energy spectra of g, β, γ and higher bands B(E2) values and B(E2) ratios.

References-- /1/ Nuclear Data Sheets 41(1984) 195;59(1990)392;48(1986)345;58(1989)93;52(1987)1
/2/F.Iachello and A.Arima,The Interacting Boson model,cambridge University Press,(1987).
/3/C.Scholten et.al,Ann.Phys.(N.Y.)115 (1978)325
/4/O.Castanos et.al,Nucl.Phys.A379 (1982)61
/5/ Cnuu et.al,Phys.Rev.C30 (1984)1300;42 (1990)280
/6/J.B.Gupta,Phys.Rev.C28 (1983)1829

Table1. B(E2) ratios for ^{150}Sm

$I_i - I_f / I_f$	Ex /1/	IBM	BFQ/6/
$2_\beta - 0_g / 2_g$	.012(2)	.06	.04
$2_\beta / 4_g$	.39(25)	.38	1.8
$0_2 / 0_1$	145(45)	45	41
$0_2 / 4_g$	1.0(6)	1.0	
$4_\beta - 2_\beta / 2_g$	6.6(3)	6.6	9.1
$2_\gamma - 2_g / 4_g$	1.3(2)	.31	.5
$0_\beta / 2_g$	.33(3)	.07	.53
$0_2 / 0_g$	5.2(17)	27	0.4
$0_2 / 4_g$	2.2(11)	0.6	
$3_\gamma - 2_g / 4_g$	.38(2)	.44	
$2_\beta / 2_g$	3.3(3)	7.3	9.5
$2_\gamma / 2_g$	17.9E	33.7	13
$4_\gamma - 2_g / 4_g$	.05(1)	.13	.26
$2_\beta / 2_\gamma$	2.9(9)	4.3	.02
$2_\gamma / 2_g$	61(10)	80	
$5_\gamma - 4_g / 6_g$	.17(1)	.03	
$4_g / 4_\gamma$	≥.04	.03	
$3_\gamma / 4_g$	43(3)	35	
$0_3 - 2_\beta / 2_g$	165(32)	137	
$2\beta_2 - 2_\beta / 2_g$	80(12)	3.7	
$4\beta_2 - 2_g / 4_g$	.33(4)	.04	
$4_g / 6_g$	.43(3)	1.6	
$2_\beta / 4_\beta$	.36	.32	
$2_\beta / 2_g$	8.3(5)	70	
$2_\gamma / 2_g$	12.3(3)	14	
$2_{\beta_1} / 2_g$	283(15)	8135	
$2_{\beta_1} / 2\beta_1$	34(10)	116	
$2_{\beta_2} / 2_\gamma$	23(8)	506	
$2_{\beta_2} / 3_\gamma$	14(5)	4.1	
$3_\gamma / 2_g$	21(1)	1980	

Acknowledgment : We are grateful to Dr. Olaf Scholten U.S.A. for providing the PHINT Package.

TESTS OF RIGID TRIAXIALITY FOR HEAVY Hg - Fm NUCLEI

S. Sharma, K.S. Sen+ & S.P. Sud
G.N.D. S.D. College (H.P. University) Rajpur - 176064 (H.P.)
+Department of Physics, H.P. University, Shimla-171005

Recently Gupta- Sharma/1/ and Mittal - Sharma-Gupta/2/ carried out an extensive survey of all available data on interband (γ-g) B(E2) ratios of rare earth(Nd-Hg) and light mass (Te-Sm) nuclei and checked the internal consistency in the predictions of the Davydov-Filippov (DF) model/3/. They/1,2/ reported that the B(E2,2_γ-0_g/2_g) and B(E2,3_γ-2_g/4_g) do have some relationship with asymmetry parameter(γ), but others (γ-g)B(E2) ratios are not related to γ. Here we extended the above test for the heavy Hg-Fm ($202 \leq A \leq 266$) nuclei.

The experimental B(E2) ratios for (2_γ-0_g/2_g), (2_γ-2_g/4_g), (3_γ-2_g/4_g), (4_γ-2_g/4_g), (2_γ-0_g/2_g-0_g) and (4_g-2_g/2_g-0_g) transitions have been collected from the recent available data in Nuclear Data sheets and Table of Isotopes. These B(E2) ratios are plotted Vs γ for six transitions and show the following trends :

I. All these nuclei have $\gamma \geq 7.8^\circ$ as determined from the ratio R_γ ($=E_{2_\gamma^+}/E_{2_g^+}$) where,

$$\gamma = (I/3)\ \mathrm{Sin}^{-1}\left[(9/8)\left\{1-\left(\frac{R-I}{R+I}\right)^2\right\}\right]^{1/2}$$

2. The DF B(E2) ratios for (2_γ-0_g/2_g) and (3_γ-2_g/4_g) fall monotonically with increasing γ from 0° to 30°. Data points do lie on such a DF curve, but for the same γ in different nuclei B(E2) ratios often differ through large factor.

3. For (2_γ-2_g/4_g) transition data points are available only for $7.8^\circ \leq \gamma \leq 17.2^\circ$ region and lie between the rotational limit(RL) and DF trend.

4. Experimental B(E2) ratios for (2_γ-0_g)/(2_g-0_g) transition are available for $8^\circ \leq \gamma \leq 17.2^\circ$ region and lie between 0 to 0.02. These values are close to the SU(3) limit of 1/4 - I/4/.

5. B(E2,4_γ-2_g/4_g) data points lie between RL and VM limit. DF trend has no support.

6. Most of the data points for transition (4_g-2_g)/(2_g/0_g) lie on the DF curve.

Conclusion :Out of six B(E2) ratios studied here, data for $(2_\gamma - 0_g/2_g)$, $(3_\gamma - 2_g/4_g)$ and $(4_g - 2_g)/(2_g/0_g)$ follow the theoretical DF trend.

References :

/1/ J.B. Gupta and S. Sharma, Physica Scripta 39 (1989) 30

/2/ H.M. Mittal, S. Sharma and J.B. Gupta, Physica Scripta 43 (1991) 358

/3/ A.S. Davydov and G.F. Filippov, Nucl.Phys. 8 (1958) 237

/4/ F. Iachello and A. Arima, The Interacting Boson Model, Cambridge University Press, Cambridge (1987)

Fig.1.

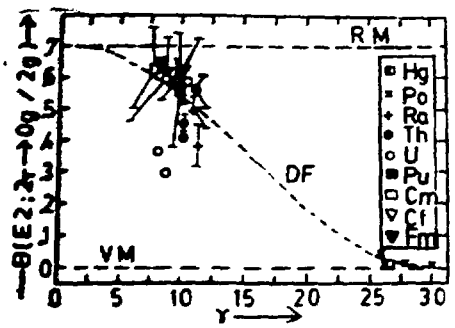

Fig.2.

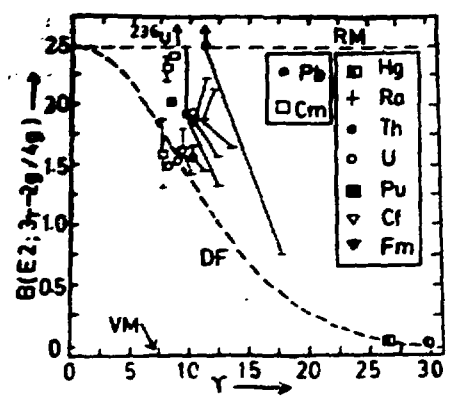

b. LOW AND MEDIUM ENERGY NUCLEAR REACTIONS AND FISSION.

EVIDENCE FOR SHAPE ISOMERIC NATURE OF $^{16}O + ^{12}C$ RESONANCES AT 43.8 AND 46.4 MeV IN ^{28}Si OBSERVED THROUGH SELECTIVE ^{8}Be DECAY

Suresh Kumar, M.A. Eswaran, E.T. Mirgule, U.K. Pal
D.R. Chakraborty, V.M. Datar and V.L. Ragoowansi
Nuclear Physics Division, B.A.R.C., Bombay-400085.

In extending our earlier study of heavy ion resonances[1] in the system $^{16}O + ^{12}C$, we report in the present work experimental evidence for the heavy ion resonances to be superdeformed shape isomeric states in the shell model secondary minimum in ^{28}Si.

A beam of ^{16}O from Bombay Pelletron and a natural carbon target of thickness 104 $\mu g/cm^2$ were used. For ^{8}Be detection ΔE and E detectors of 30 μm and 2000 μm thickness were used at 9° to the beam with a large solid angle of 5.3 msr so that the two alpha particles from decay of ^{8}Be are detected with reasonable efficiency which is numerically calculated. For alpha detection, two more telescopes were used at 6° and 16°. Some of the excitation function measurements obtained are shown in the figure 1(a) to (e) for bombarding energy range $E(^{16}O)$ = 60 to 90 MeV. For the alpha channels the excitation functions shown are average over the data of all three angles recorded at 6°, 9° and 16°.

From these measurements the striking result emerges that at $E(^{16}O)$ = 63 and 69 MeV there are two resonances corresponding to E_{cm} = 27.0 and 29.6 MeV (Ex= 43.8 and 46.4 MeV in ^{28}Si) which decay dominantly to ^{24}Mg, 20.25 MeV state by alpha emission and to quartet states[2] near 6.7 to 7.8 MeV in ^{20}Ne by ^{8}Be emission and not to ground state and other lower lying non-quartet states of ^{20}Ne. The cross correlation at these two resonances are indicated by vertical dashed lines in the figure. Figure (f) and (g) also show the cross correlation coefficient between excitation functions (a) and (c) and between (b) and (c) respectively. The cross sections observed for the alpha channel shown in the figure (c) and (d) are an order of magnitude larger than expected from statistical model calculations.

It is well established[3] that the quartet states of 7.2 MeV (0^+) and 7.82 MeV(2^+) are 8p-4h states which are super deformed shape isomeric states

in the shell model secondary minimum in ^{20}Ne. Hence our observation of decay of the two resonances at 43.8 and 46.4 MeV in ^{28}Si to these quartet states in ^{20}Ne, provide direct evidence for the resonances to

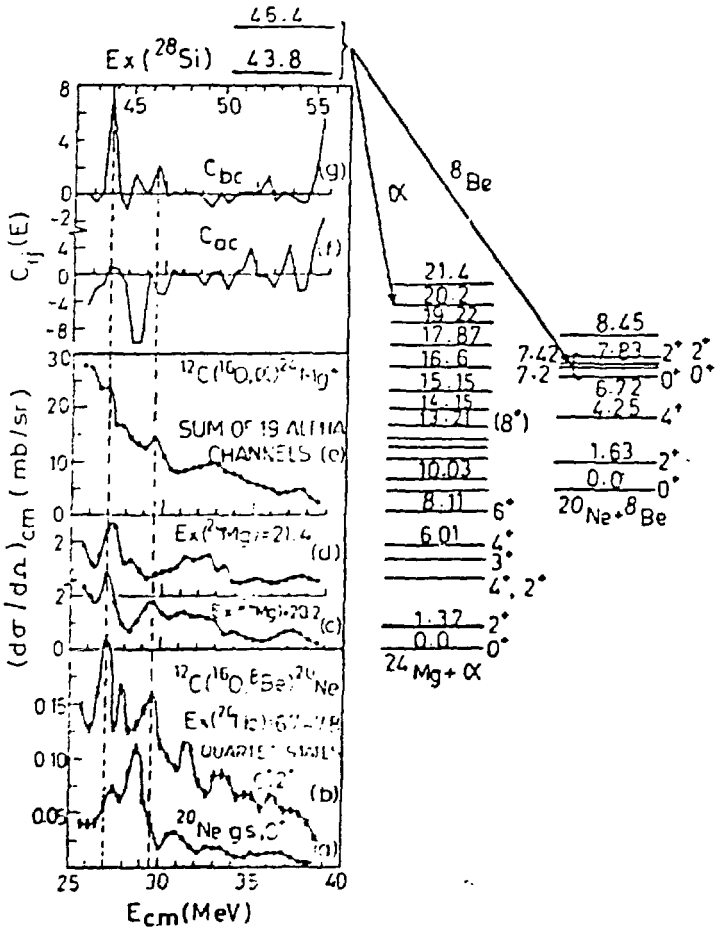

be superdeformed shape isomeric states in ^{28}Si. The existence of such states is also predicted in the potential energy calculation of Leander and Larsson[4] with an excitation of one quartet from 1p shell to 2p-1f shell.

1) Suresh Kumar et.al., Nucl.Phys.Symp.(DAE), Aligarh, (1989) 029 and Madras,(1990) 103.; M.A. Eswaran et.al., Phys. Rev.C39 (1989) 1856.
2) H. Voit et.al., Phys. Rev.Lett. 30 (1979) 564.
3) R.J. Ledoux et.al., Phys. Rev. C30 (1984) 866.
4) G.Leander & J.E.Larsson,Nucl.Phys. A239 (1975) 93.

ANGULAR MOMENTUM TRANSFER AND ENERGY LOSS IN THE $^{16}O + ^{118}Sn$ REACTION AT 100 MeV.

B.K.Nayak, S.V.Suryanarayan, D.C.Biswas, L.M.Pant, B.V.Dinesh, V.S.Ambekar, U.Garg*, R.K.Choudhury
Nuclear Physics Division, BARC, Bombay - 400085.
* Notre Dame University, Norte Dame, USA.

Heavy ion reactions at energies around coulomb barrier are characterized by main reaction channels such as elastic scattering, inelastic excitations, transfer of one or few nucleons, deep-inelastic reactions and fusion. In the past above reactions have been extensively investigated and main features of the reaction mechanism have been generally understood. However there are still some interesting aspects to study like the angular momentum and energy transfer correlation, the evolution of angular momentum transfer distribution in different reaction channels and the coupling between different reaction channels, Which will provide further information about reaction mechanism and to test some of the model predictions.

In the present investigation we have taken up $^{16}O + ^{118}Sn$ reaction at E_{Lab}=100 MeV. We measured γ-ray mutiplicity emitted by the outgoing nuclei in coincidence with projectile like fragments (PLF). For this purpose a multiplicity filter, consisting of 15 hexagonal (57cmX63cm) BGO scintillators, was operated in coincidence with a ΔE-E telescope consisting of ΔE(50μm) and E(500μm) Si detectors.

The first three moments of the γ-ray multiplicity distribution were calculated from the data. **Fig.1a** shows the measured <M> as a funtion of total kinetic energy loss (TKEL) for outgoing PLF with Z=7,6,5 at θ_{Lab}=45°. In all these PLF channels in the region of low TKEL, <M> increases with TKEL but in the region of higher TKEL (>45 MeV) <M> show a decreasing trend. The decrease in the <M> can be understood as loss in the angular momentum due to

particle emission for higher TKEL. The variation of widths of the γ-ray multiplicity distribution ($\sigma_M=\mu_2^{1/2}$) is shown in **Fig.1b.** It is seen initially for lower values of TKEL the width remains more or less constant but for higher TKEL (>45 MeV) it shows a higher width , which seems to be correlated with shape evolution of the angular momentum distribution taking place for highly damped processes. **Fig.2** shows the γ-ray multiplicity distribution obtained by a β-distribution function such that it reproduces first two moments of each PLF channels.

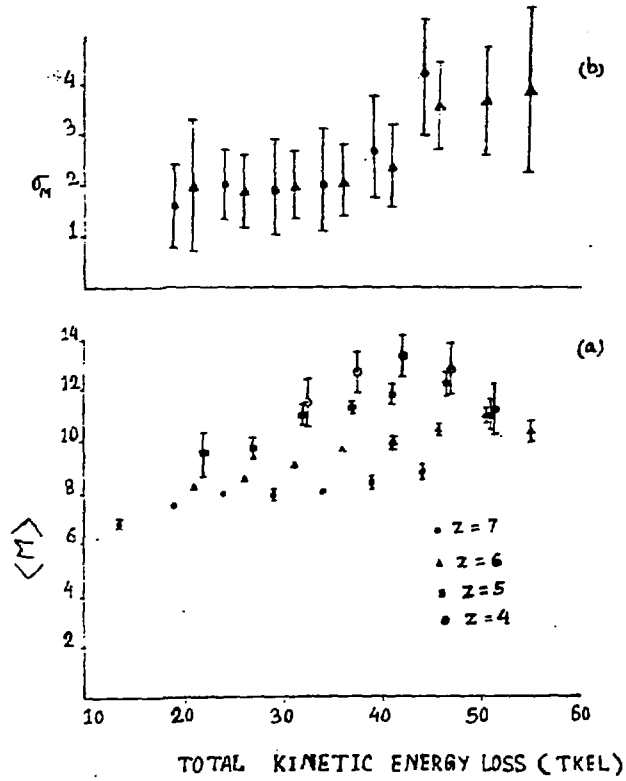

Fig.1

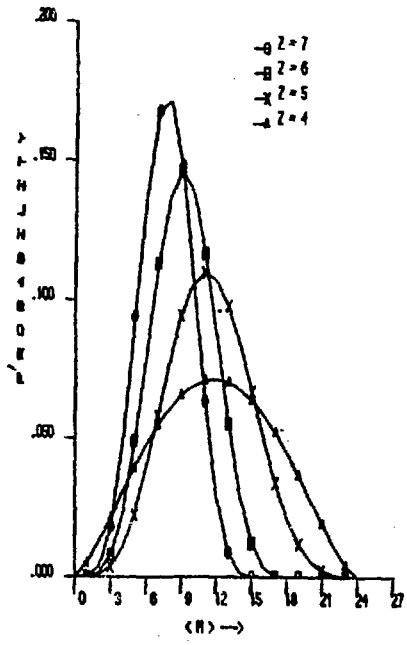

Fig.2

REFERENCES:

1. C. Agodi et. al.,Nucl.Phys.**A515**(1990)525-540
2. Z.Phys,**A334**,55-72(1990)

SPIN DISTRIBUTION BELOW AND NEAR COULOMB BARRIER IN ^{209}Bi (^{10}B,3n) REACTION

P. Mukherjee, I. Mukherjee, B. Sethi and P. Sen
Saha Institute of Nuclear Physics, Calcutta 700 064
M.G. Betigeri, B.J. Roy and Mythili S.
Bhaba Atomic Research Centre, Bombay 400 085

The importance of channel coupling effects on heavy ion fusion cross section at projectile energies near the coulomb barrier is known for nearly one decade. However there have been very few experimental studies on the spin distribution in sub barrier fusion reaction[1]. Spin distribution in the evaporation residue ^{216}Ra is measured by us at several incident projectile energies for the reaction ^{209}Bi (^{10}B,3n). The experiment was done at the BARC-TIFR Pelletron facility.

Eight 5 cm dia x 7.5 cm long NaI detectors packed closely around the target form a multiplicity filter. The channels were identified with a single Ge detector placed at 90^0 with respect to the beam. Very clean fold pattern was obtained up to N=6 fold.

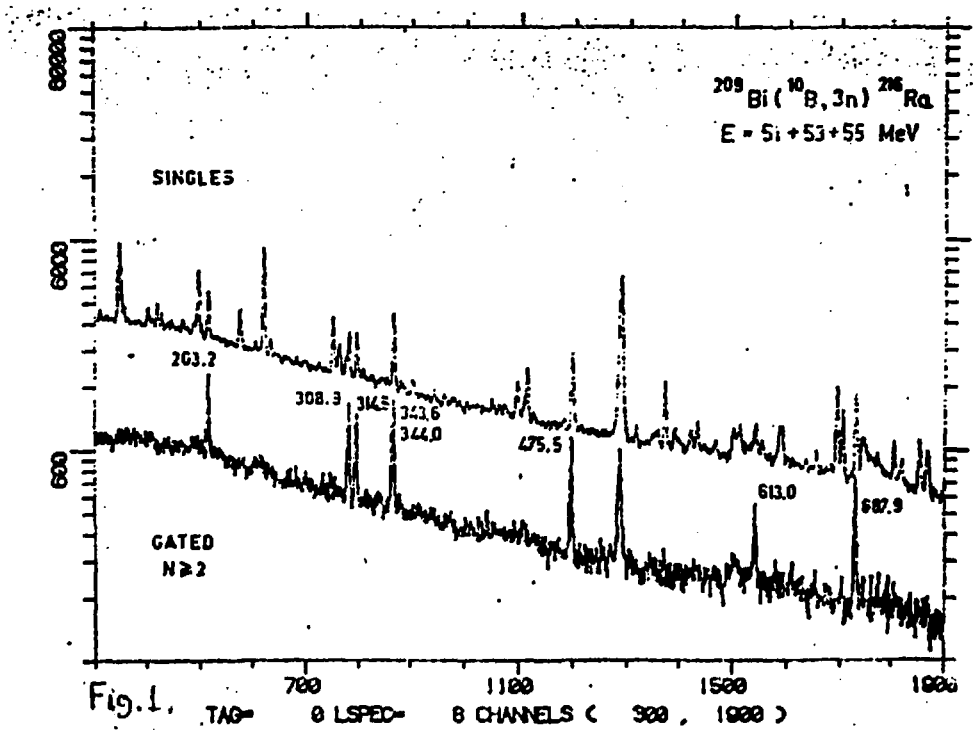

Fig.1.

In figure 1 the spectra are shown for the ungated and $N \geqslant 2$ gate condition. A remarkable enhancement of the 3n channel enabled us to follow the excitation of high spin states in ^{216}Ra even when the fusion cross section is very small. The decay scheme of ^{216}Ra has been established by us in a sperate work based on ^{209}Bi (^{11}B,4n) reaction where the 613.0 keV transition is identified with the transition $12^+ \rightarrow 10^+$. The yield of this gamma ray in (^{10}B,3n) reaction gives the spin population probability, P_J. The result is listed in Table 1 together with the theoretical estimates based on barrier penetration model[2].

Table 1. Spin excitation probability P_J for $J=12^+$

E(MeV)	51	53	55	58
P_J(Expt)	.003	.017	.025	.028
P_J(Theo)	.002	.020	.031	.030

In the barrier penetration model calculation the following parameters are used : $\hbar\omega_\circ = 4.0$ MeV, $R_B = 11.37$ f and $\gamma = 5.12$.

References :

1) A.H. Wuosmaa, et.al., Phys.Lett. 263B, 23 (1991).

2) P.J. Nolan, et.al., Phys.Rev.Lett. 54,2211(1985).

ANGULAR - MOMENTUM - DEPENDENT FISSION BARRIERS : FISSION EXCITATION FUNCTION OF $_{75}Re^{181}$ COMPOUND NUCLEUS FORMED BY $_{6}C^{12}+_{69}Tm^{169}$ AND $_{8}O^{16}+_{67}Ho^{165}$ REACTIONS

A.K. Pandey, R.C. Sharma ,P.C.Kalsi and R.H.Iyer
Radiochemistry Division, BARC.
Bombay-400085.

The availability of heavy ions of moderate energies at the BARC-TIFR 14 UD Pelletron facility provides unique opportunities to investigate systems of high angular momentum and to test theoretical models for their adequacies in interpreting and quantifying the experimental data . With a view to understanding the effect of angular momentum on fission barrier and fragment anisotropy we have measured the fission cross sections and fragment angular distributions of the $_{75}Re^{181}$ compound nucleus produced by $_{6}C^{12}+_{69}Tm^{169}$ and $_{8}O^{16}+_{67}Ho^{165}$ reactions at several bombarding energies above the fusion barriers . In particular , we have chosen lower energies where no experimental data are available and where the average angular momentum of the $O^{16}+Ho^{165}$ systems is lower than that of the $C^{12}+Tm^{169}$ system (Fig.1) the cross over occurring at an excitation energy of about 57.6 MeV and $\langle l \rangle_{av}$ about 27.5 $\hbar$.

Experimental details are given in some of our related publications[1,2]. Briefly , targets of Ho^{165} & Tm^{169} oxides of0.5-1.0 mg/cm^2 thickness deposited on high purity silver foils were used .Fission fragments recoiling in the backward hemisphere with respect to the heavy ion beam (90^0-165^0 Lab angle) were detected in a cylindrical Lexan detector .

Statistical model fits to the experimental excitation functions are shown in Figs.2&3. We have included some experimental values at higher energies from Sikkeland[3]. The calculations were performed by using angular-momentum-dependent fission barriers $E_f(J)$ from RLDM[4] and from the rotating finite range model RFRM of Sierk[5] at differnt $\langle l \rangle_{av}$ values (Fig.4). Evaporation residue cross sections σ_{ER} rather than total reaction cross sections σ_R (optical model) were used to get Γ_f/Γ_n values . σ_{ER} for $C^{12}+Tm^{169}$ were taken from Ref.6 and that for $O^{16}+Ho^{165}$ was computed by assuming similar σ_{ER}/σ_R ratios for both systems . The a_f/a_n ratio was floated ; the best fit was found to be 1.00. Another parameter i.e. the ratio of rotational energy at saddle to equilibrium R^0_s/R^0_e was also floated ; the best value was found to be 0.75 . It is seen that best fits to the experimental data are provided by using the $E_f(J)$ from RFRM . The predicted cross sections are much smaller with $E_f(J)$ from RLDM (Figs.2-3).

Our data are consistent with RFRM $E_f(J=0)$ value of 19.2 MeV for Re^{181}.The RLDM $E_f(J=0)$ value of 22 MeV is high and is inconsistent with the experimental data .Another noteworthy observation is the excellent correspondence between the variation of $\langle l \rangle_{av}$ of $C^{12}+Tm^{169}$ and $O^{16}+Ho^{165}$ (Fig.1) and the Γ_f/Γ_n values (Fig.5) with excitation energy.The cross-over point (E=57.6 MeV and $\langle l \rangle_{av}$27.5 $\hbar$) represents a true compound nucleus with out any entrance channel effects . Further measurements of σ_f and $d\sigma/d\Omega$on the Re^{181} and other systems at excitation energies close to the cross-over region are in progress.

1-R.H.Iyer,A.K.Pandey,P.C.Kalsi& R.C.Sharma,Proc.Nucl.Phys.Symp.,0-24,33B(1990),Madras.
2-R.H.Iyer,A.K.Pandey,P.C.Kalsi and R.C.Sharma,Phys.Rev.,C44,No.5(1991) .
3-T.Sikkeland,Phys.Rev.,135.B669(1964).
4-S.Cohen et.al ,Ann. phys.,82,557 (1974).
5-A.J.Sierk,Phys.Rev.,C33,2309(1986).
6-F.Plazil et.al, Phys.Rev.,C29,1145(1984).

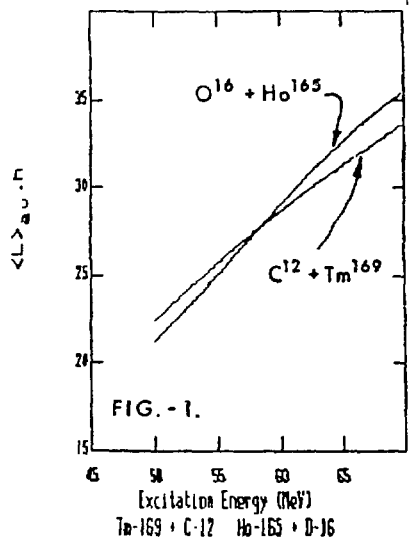
O^{16} + Ho^{165}
C^{12} + Tm^{169}
FIG.-1.
Excitation Energy (MeV)
Ta-169 + C-12 Ho-165 + O-16

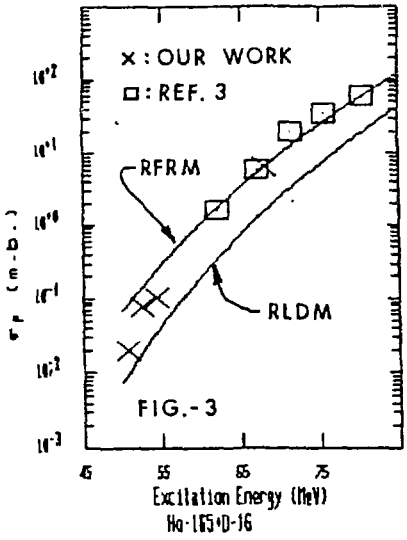
×: OUR WORK
□: REF. 3
RFRM
RLDM
FIG.-3
Excitation Energy (MeV)
Ho-165+O-16

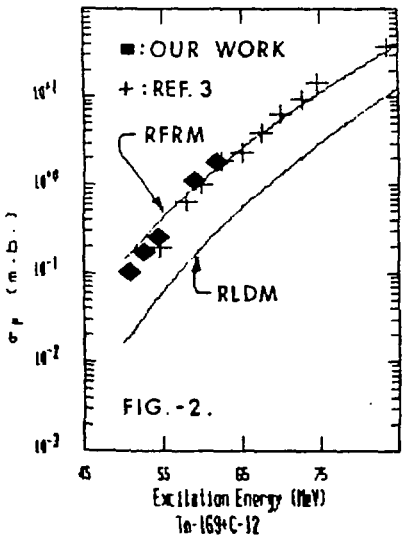
■: OUR WORK
+: REF. 3
RFRM
RLDM
FIG.-2.
Excitation Energy (MeV)
Ta-169+C-12

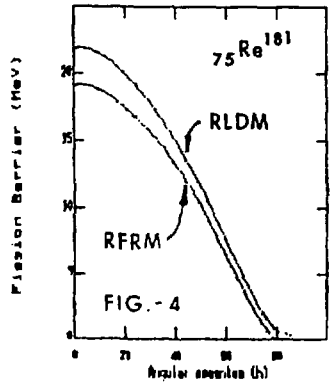
$_{75}Re^{181}$
RLDM
RFRM
FIG.-4

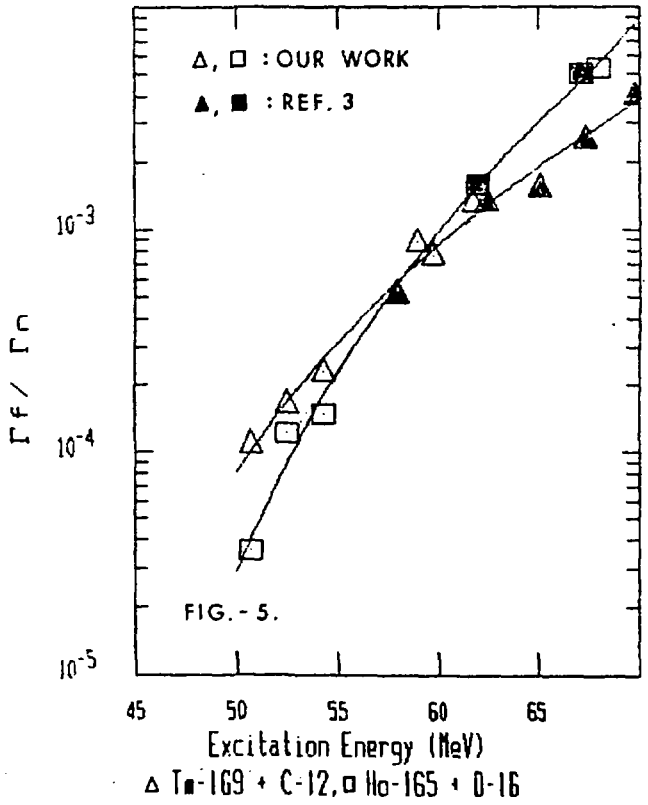
Δ, □ : OUR WORK
▲, ■ : REF. 3
FIG.-5.
Excitation Energy (MeV)
Δ Ta-169 + C-12, □ Ho-165 + O-16

ALPHA TRANSFER TO CONTINUUM - AN INCOMPLETE FUSION REACTION

B.S.Tomar, A.Goswami, A.V.R.Reddy, S.K.Das, P.P.Burte, S.B.Manohar and Satya Prakash
Radiochemistry Division, B.A.R.C. Bombay 400 085

The coincidence measurements between the high energy ejectiles and prompt gamma rays of evaporation residues by Inamura et al (1) led to the identification of incomplete fusion reactions (ICF) in which only a part of the projectile fuses with the target while the remaining part escapes with the beam velocity. Wilczynski et al(2) explained these reactions in terms of their sum rule model. These processes are common in the projectile energy range of 10-20MeV/amu. However recent observations(3) indicate that such processes can occur at lower projectile energies also. In order to investigate this aspect, we determined the excitation functions for the technitium and niobium isotopes produced in the ^{12}C +^{93}Nb and ^{16}O + ^{89}Y reactions covering a projectile energy range of 45-80 MeV for ^{12}C and 55-95MeV for ^{16}O. These products can be produced either by evaporation of multiple alpha particles from the compound nucleus or by transfer of an alpha particle from projectile to target. The experiments were carried out using BARC - TIFR pelletron facility. Self supporting targets of Nb/Y (2.5mg/cm^2) separated by aluminium foils (2mg/cm^2) were irradiated with $^{12}C/^{16}O$ beams in a stack of three targets per irradiation. The cross sections were determined by off-line gamma spectrometric technique.

The excitation functions for the $^{94-96}Tc$ are shown in figure 1. The largest error on a cross section data is 15% which is the propagated error on counting statistics, uncertainty in target thickness, particle intensity and detector efficiency. The solid line is an eye guide to the experimental points. The figure also shows the predictions of the CASCADE code for the evaporation residues. The dashed lines are for ^{12}C + ^{93}Nb system while the dot-dashed lines are for ^{16}O + ^{89}Y system. The figure shows that the excitation functions for $^{95,96}Tc$ in ^{12}C + ^{93}Nb are much higher than those in

^{16}O + ^{89}Y. Further they are also much higher than CASCADE predictions. Similar observation is also obtained for ^{92m}Nb in ^{16}O + ^{89}Y. These observations indicate significant amount of alpha transfer from projectile to target in both the reactions.

These alpha transfer reactions can be termed as ICF reactions as the alpha particle brings in sufficient excitation energy to the resultant nucleus so that it can emit one or two neutrons and the products of such reactions resemble the fusion products. Further they are found to take place even at the projectile energy equal to 4MeV/amu contrary to the predicted threshold of 10MeV/amu for ICF reactions. How much the alpha cluster structure of the projectiles (^{12}C, ^{16}O) would enhance these reactions is however a subject to be investigated. Studies on range measurement of evaporation residues and particle - gamma coincidences would help in understanding the mechanism of such reactions.

References:

1.T.Inamura et al Phys. Lett 68B, 51 (1977)
2.J.Wilczynski et al Nucl.Phys. A373, 109 (1982)
3.D.J.Parker et al. Phys. Rev. C35, 161 (1985)

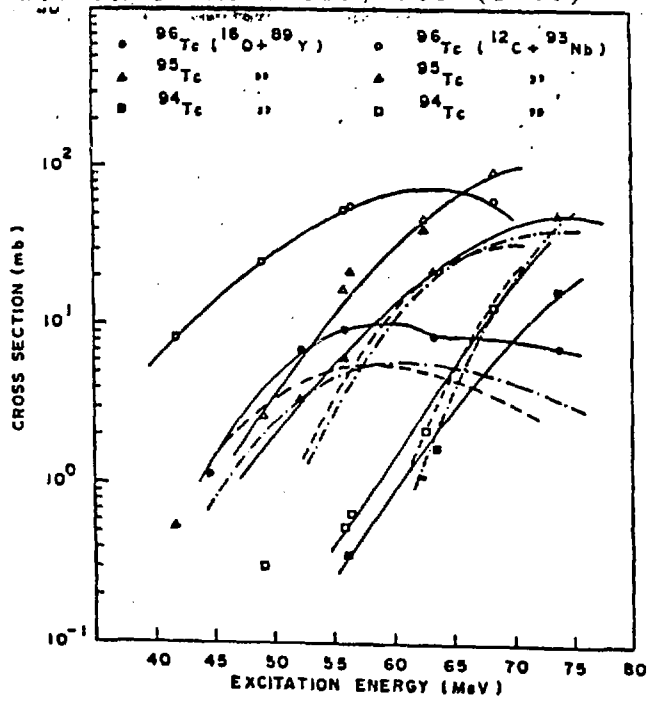

Figure 1. Excitation functions for $^{94-96}Tc$ in ^{12}C + ^{93}Nb and ^{16}O + ^{89}Y with CASCADE predictions.

MEASUREMENT OF PRE-SCISSION NEUTRON MULTIPLICITIES FOR $^{12}C+^{232}TH$ AND $^{16}O+^{232}Th$ SYSTEMS

Alok Saxena, R.P.Anand, A.Chatterjee, R.K.Choudhury, S.S.Kapoor, D.M.Nadkarni, B.K.Nayak, L.M.Pant, M.S.Samant and S.V.S.Sastry
Nuclear Physics Division, B.A.R.C, Bombay 400 085

Neutron emission in fusion-fission reactions has been found to be a sensitive probe of dynamics and time scales of the fission process [1,2]. The measured pre-scission multiplicities are found to be much larger than that expected from statistical model predictions. These data led to the realisation that the large-scale collective modes involved in fission must have a significant relaxation time ($>10^{-20}$sec) implying highly damped motion of nuclear fluid. It was shown in an earlier work[3] on fission fragment angular distributions that the fusion dynamics exhibits an abrupt transition at liquid drop Businaro-Gallone (BG) point in the entrance channel mass/charge asymmetry. The Systems of $^{12}C+^{232}Th$ and $^{16}O+^{232}Th$ were seen to lie on either side of the BG point. In the present work, we have measured pre-scission neutron multiplicities for these two systems at two different bombarding energies. Fission fragments were detected by two surface barrier detector at 105^0 and 165^0 with respect to the beam direction and the neutron energy spectra were measured at 0^0 and 90^0 with respect to two fission detector by the time of flight method using two NE213 detectors. The observed neutron energy spectra, after efficiency correction were fitted with pre-scission and post-scission components. The measured neutron spectra along with the two component fits are shown in fig.1. The deduced parameters are shown in the table. The statistical calculations of ν_{pre} are found to be .84 and .35 for $a_f=a_n=A/10$ in this region of excitation energies and are not sensitive to the change in excitaion energy whereas the measured ν_{pre} values increase with the increase in the excitation energies. The discrepancy is somewhat larger for the ^{16}O induced reaction as compared to

the ^{12}C induced reaction. These results are discussed to deduce the magnitude of time by which fission is delayed and the possible entrance channel effects.

REFERENCES:
1.J.O.Newton,Pramana 33 (1989) 175
2.S.S.Kapoor, Proceedings of Consultants Meeting on Physics of Neutron Emission in Fission, Mito City,Japan, May, 1988, INDC(NDS)220(1989)p221
3.V.S.Ramamurthy et al, Phys. Rev. Lett. 65 (1990) 25

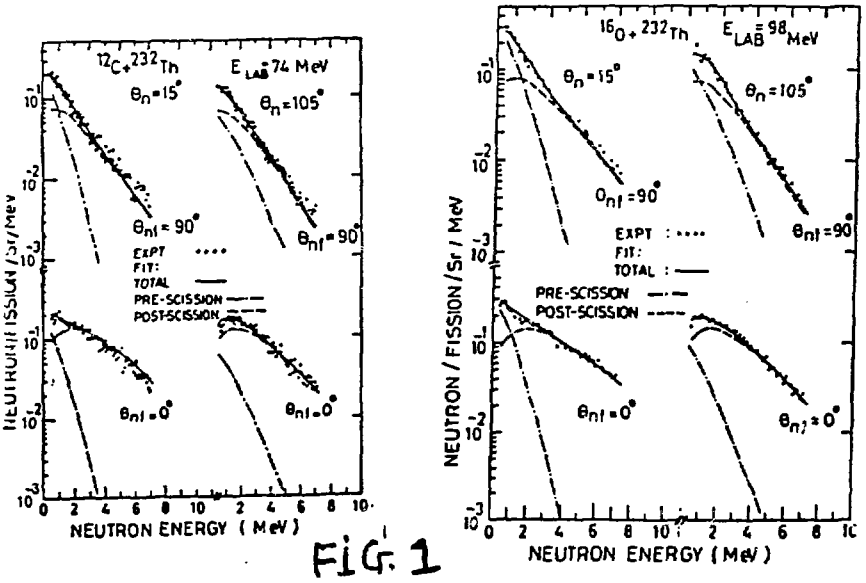

FIG. 1

$^{12}C + ^{232}Th$

E_{lab} (MeV)	E_x (MeV)	θ_n (Deg)	ν_{post}	T_{post} (MeV)	ν_{pre}	T_{pre} (MeV)
80	53	15°	2.05±.3	1.5±.2	1.9±.2	.55±.2
80	53	105°	2.35±.3	1.35±.2	1.8±.2	.8±.2
74	47	15°	2.01±.3	1.35±.2	1.36±.2	.5±.2
74	47	105°	2.15±.3	1.4±.2	1.5±.2	.9±.2

$^{16}O + ^{232}Th$

E_{lab} (MeV)	E_x (MeV)	θ_n (Deg)	ν_{post}	T_{post} (MeV)	ν_{pre}	T_{pre} (MeV)
98	55	15°	2.3±.3	1.5±.2	2.1±.2	.5±.2
98	55	105°	2.5±.3	1.4±.2	1.9±.2	.8±.2
92	49	15°	2.3±.4	1.3±.2	1.8±.3	.6±.2
92	49	105°	2.65±.4	1.5±.2	1.5±.3	.5±.2

LIFETIME IN HEAVY ION REACTIONS STUDIED BY CRYSTAL BLOCKING

Vandana Nanal, M.B.Kurup, K.G.Prasad
Tata Institute of Fundamental Research, Bombay 5.

In Rutherford scattering experiments, if the target is a single crystal and a detector is placed along the crystallographic direction then scattered particles are blocked from reaching the detector. If a $2-d$ position sensitive detector is used, one gets an image of the crystal showing various planes and the axis. The blocking technique is used for measuring compound nuclear life-times and reaction times in the range 10^{-15} - 10^{-19} sec., provided charge particles are emitted in the process.

A semiconductor detector having an active area of $24 \times 24mm^2$ was used in the experiment. The detector gives both X and Y position along with energy information. The position calibration was done using a grid pattern. Central $10 \times 10mm^2$ portion of the detector shows good linearity and gives position resolution better than $1mm$.

A $1.25\ \mu m$ $< 100 >$ natural Si single crystal target was mounted on a double axes goniometer. The detector was placed at 20° to the beam, at a distance of $35.6cm$ and $56cm$ from the target, giving an angular resolution of 0.16° and 0.1° respectively. ^{16}O beam of 3-5 MeV/amu and ^{28}Si beam of 2-4 MeV/amu from pelletron accelerator were used for the experiment. Fig. 1 shows the $< 100 >$ blocking pattern for Rutherford scattering of 54 MeV ^{16}O beam. The blocking dip is constructed from linear region of this $2-d$ pattern by circular integration around the minimum. In case of ^{28}Si beam, dip width varies as $1/\sqrt{E}$ whereas for ^{16}O this variation is masked by angular resolution of the detector. The minimum yield values agree well with those obtained from channeling experiment[1].

In $^{16}O + {}^{28}Si$ reaction, ^{44}Ti is formed which then decays by emission of particles such as protons, α-particles etc. The preliminary analysis of blocking pattern for α-particles in the energy range 8-18 MeV show the significant time delay effects (see fig.2). Blocking dip for these particles is very shallow and wide as compared to that of elastically scattered particles. Assuming complete fusion, we can estimate the decay time for multiple particle emission(τ_{MP}) using the relation,

$$\Delta\chi_{min} = 2CN\pi dv^2\tau_{MP}^2$$

where C is a constant ($C \simeq$ 2-3), N is the no. of atoms per unit volume, d is the interatomic distance along the crystal axis and v is the recoil velocity of compound nucleus. For 54 MeV ^{16}O beam (excitation energy 45.3 MeV) change in the minimum yield($\Delta\chi_{min}$) is about 40% ($\pm$ 6%). From this we can estimate τ_{MP} as $\simeq (8\pm2)$ x 10^{-16} sec.

Besides the change in the minimum yield, decay times also affect the width of the blocking dip. This is due to variations in the emission times in the different channels as well as the distribution in energy of emitted particles. Thus, it is crucial to study the scaling of the blocking dip as a function of energy and atomic number, so as to measure changes in the dip parameters properly. Further, the variation of lifetimes as a function of excitation energy is also of much interest. A detailed study of these aspects is planned for the near future.

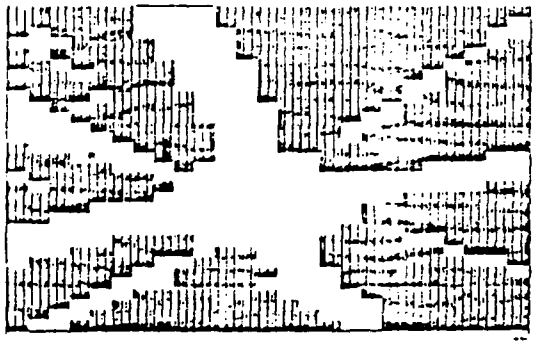

Fig. 1

←

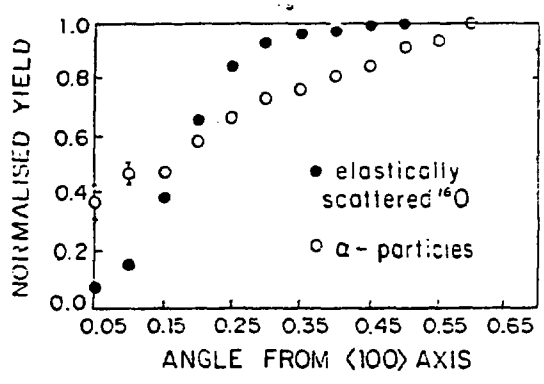

Fig. 2

→

Reference:

1. V.S.Nanal et.al. Proc. of DAE Symp. on Nucl. Phys.,1990, O63.

STUDY OF THE REACTION ^{115}In (^{12}C, ^{11}B) ^{116}Sn

B.J.Roy, C.V.Fernandes, M.L.Jhingan*
S.K.Gupta and M.G.Betigeri
Bhabha Atomic Research Centre, Trombay, Bombay-85.
*Tata Institute of Fundamental Research, Bombay-5

One particle one hole excitations form a very important class of fundamental modes of nuclear excitation. Whereas the coherent participation of many p-h configuration is characteristic of a giant resonance, high spin 1p-1h states are often extremely simple and contain only a few shall model configurations. Recent calculations[1] on ^{116}Sn nucleus describe the excited states in terms of neutron quasi particle (2qp) and proton 1p-1h excitation. The proton space is spanned by holes in one of the orbitals in 20-50 shell and the particle can occupy one of the next major shell 50-82; the gap between the two is about 4 MeV. All excitations below 4 MeV are essentially neutron excitations. Recent experiments [2,3] involving light ion induced proton transfer reactions on ^{115}In indicate that the high spin states based on ($1g_{9/2}$ ' $1g_{7/2}$) and ($1g_{9/2}$ ' $1h_{11/2}$) configurations are split into two distinct groups centred about 4.2 and 5.8 MeV excitation energy in ^{116}Sn. Since the high spin states are selectively excited in heavy ion induced reactions, the motivation for the present experiment was two-fold: a) to locate the centre of energy and strengths of 1p-1h states and b) extend the studies to higher excitation energies to locate other 1p-1h states not reported earlier.

The present study consists of two parts: 1) study of angular distributions of states excited in the present reaction at an incident energy of 84 MeV (which is about twice the Coulomb barrier); 2) study the variation of cross-sections for the high spin states as a function of incident energy. This has been done at E_{lab} = 66, 72, 80 and 84 MeV. Three surface barrier counter telescopes were set up to locate the transfer channel at three angles simultaneously. Fig.1 shows the spectrum. The usual characteristics of Q_{max} and high spin excitation are all present. Over and above, the high spin states are riding on a background suggestive of a break-up spectrum for ^{12}C -- ^{11}B + P peaking at the expected energy . Fig.2 shows the excitation function study and clearly show the nature of the two groups of states around 4.57 and 6.2 MeV involving proton transfer angular momenta corresponding to

l=4 and 5. Fig.3 shows the angular distributions for the structures observed in the present study. DWBA calculations to obtain strength information are in progress

References

1) M.Waroquier et al. Phys.Rep. 148 (1987) 250
2) S.Y.Van der Werf et al. Phys.Lett. 166B(1986) 372
3) J.M.Schippers et al. Nucl.Phys.A510(1990) 70

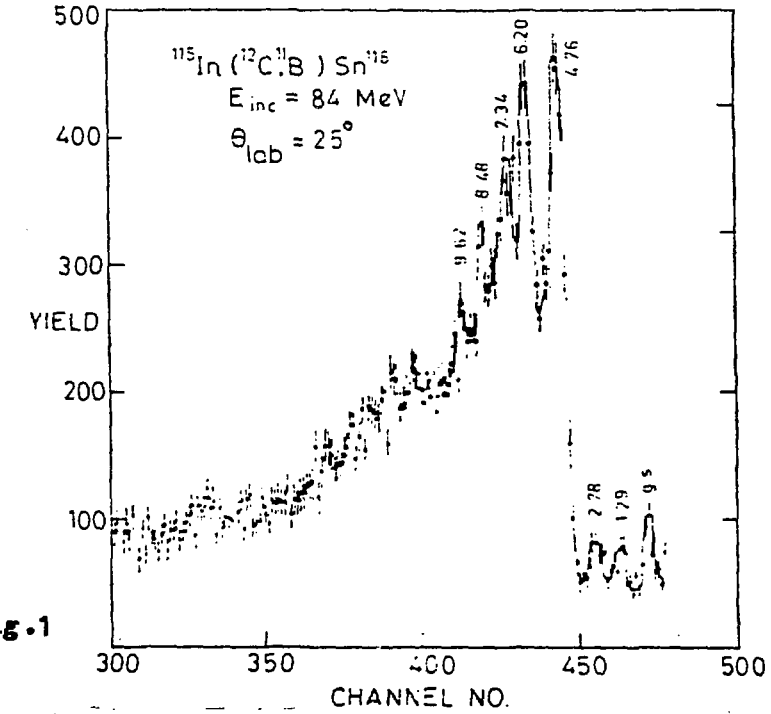

fig.1

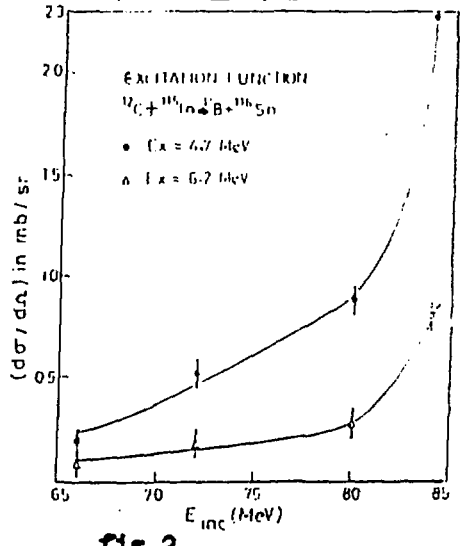

fig.2

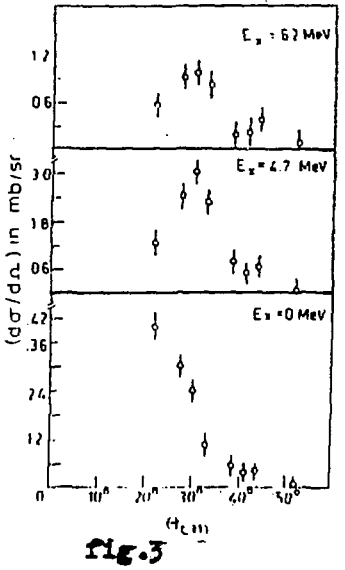

fig.3

STUDY OF ^{93}Tc AND ^{94}Tc USING THE GDA SET UP AT NUCLEAR SCIENCE CENTRE

S.S.Ghugre, V.P.Salvi, A.M.Narsale and S.B.Patel,
Bombay University, Vidyanagari, Bombay 400098
and
S.Muralithar, G.Rodrigues and R.K.Bhowmik
Nuclear Science Center, JNU Campus, New Delhi 110067

Evidence for collective properties of some isotopes of Sn nucleus, which has a closed proton shell, was found recently [1,2]. Interestingly a cascade of quadrupole transitions was observed in Sn nuclei suggesting a collective behaviour for yrast states in these nuclei. These deformed bands in the spherical region are called "Intruder Bands". Rotational inertia was found to be almost constant at 0.4 MeV < hw < 0.6 MeV implying a good rotor. Microscopic understanding of these aspects is not satisfactory [3].

We are studying the N = 50 and near magic nuclei, 93Tc and 94Tc using the Gamma Detector Array (GDA) at the NSC, New Delhi which consists of six Compton-Suppressed HPGe detectors and a 14 element BGO multiplicity filter. Levels of 93Tc and 94Tc were populated by the 66Zn(31P,2p2n)93Tc and 66Zn(31P,2pn)94Tc reactions at the energy of 115 MeV. Target used was 99% enriched 1.2 mg/cm^2 foil of 66Zn backed by 20 mg/cm^2 Pb.

The typical gamma-gamma coincidence rate was 150 cps. In all 25 million events were collected on mag tape. Data have been sorted into a large dimension (1k x 1k) matrix for the gamma energies in coincidence from which one dimensional histograms for gamma energy in one detector gated by a suitable transition in the other detector can be generated.

In an earlier study of ^{93}Tc via ^{6}Li + ^{90}Zr reaction [4], a +ve and a -ve parity band have been established with stretched E2 interband transitions. These measurements have been extended to higher

spins by gating on known members of these bands. A number of new transitions in ^{93}Tc have been obsrved (figs 1,2). Attempts are being made to place these in the level scheme. Analysis of the transitions in neighbouring nuclei is in progress.

The help of Ms.P.Singh in making the target is acknowledged. We thank the NSC Pelletron staff for making available a high quality ^{31}P beam to us and Mr. B. Choubisa for help in the experiment.

1) D.A.Vigars et al. Phy.Rev.C 36 (1987) 1006.
2) H.Harada et al. Phy.Lett.B 207 (1988) 17.
3) K.Heyde et al. Phy.Lett.B 155 (1985) 303.
4) B.A.Brown et al. Phy.Rev.C 13 (1976) 1194.

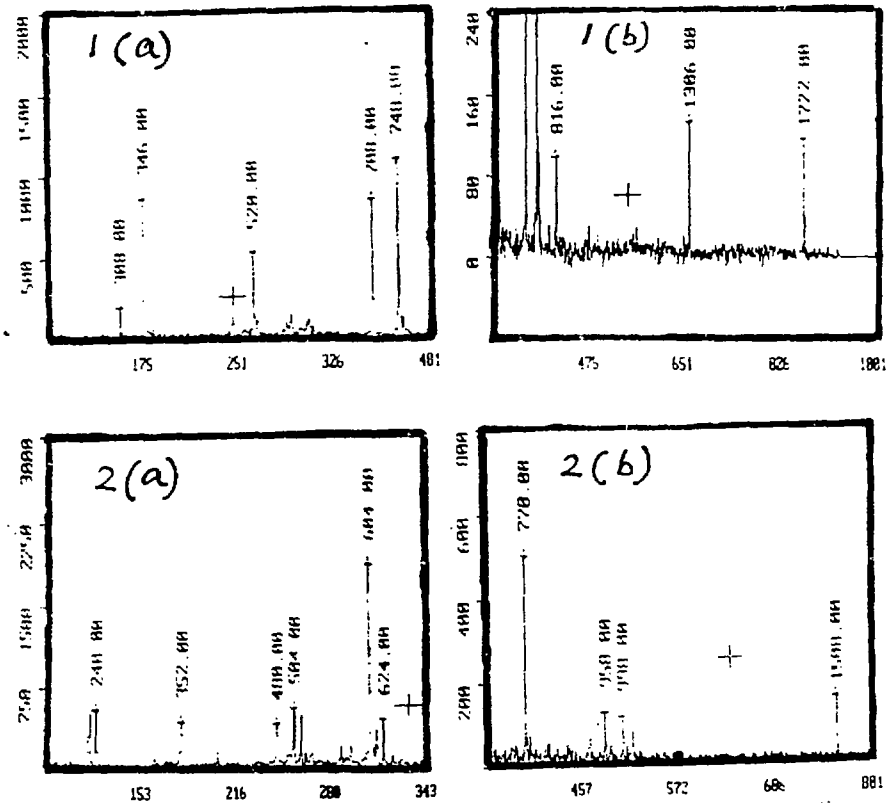

Energy Levels of ^{93}Tc gated by 1434 KeV (+ve band) and 1095 KeV (-ve band)

ELASTIC AND INELASTIC SCATTERING OF ALPHA PARTICLES FROM ^{46}Ti AT E_α = 45 MeV

V.Raghunatha Rao, M.Sudarshan, A.Sarma and R.Singh
Physics Department, NEHU Shillong-793003.
S.R.Banerjee and S.N.Chintalapudi
VEC(BARC), 1/AF Bidhan Nagar, Calcutta-700064.

In this contribution we present the results of our measurement of differential cross sections for elastic and inelastic scattering of 45 MeV α-particles from 46-Ti. The experiment was performed at the VECC, Calcutta, where an unanalysed alpha beam from the 224 cm cyclotron was focussed onto a self supporting target of 46-Ti(thickness=1.080 mg/cm^2, enrichment = 81.02%) mounted at the centre of the 91.5 cm diameter scattering chamber. The measurement covered the laboratory angular range from 10^o to 135^o in 2.5^o steps. The overall errors in the cross sections due to uncertainties in the target thickness, integrated charge, solid angle and counting statistics ranged from about 6 to 10%.

A detailed optical model analysis of the elastic data was carried out using Woods-Saxon, and Woods-Saxon squared radial dependences for real as well as imaginary parts of the potential as given below

$$V(r)=V_c(r, R_c)-V_R[f(r, r_R, a_R)]^m-i\ V_I[f(r, r_I, a_I)]^n$$

and $f(r, r_x, a_x) = [1 + \exp\{(r-R_x)/a_x\}]^{-1}$,

where all the symbols have their usual meanings and the form factor powers m and n can assume values 1 and/or 2. We attempted various combinations of m and n and found that the experimental angular distribution was best described with m=2, n=1 combination. A similar analysis of the 35 MeV data [1] resulted in the same values of m and n for the best representation of the experimental angluar distributions. Figure 1. shows a comparison of the optical model calculations for various combinations of m and n with the data. The potential parameters with the form factors (m,n) used are also listed in the same figure.

The most sensitve region of the potential in

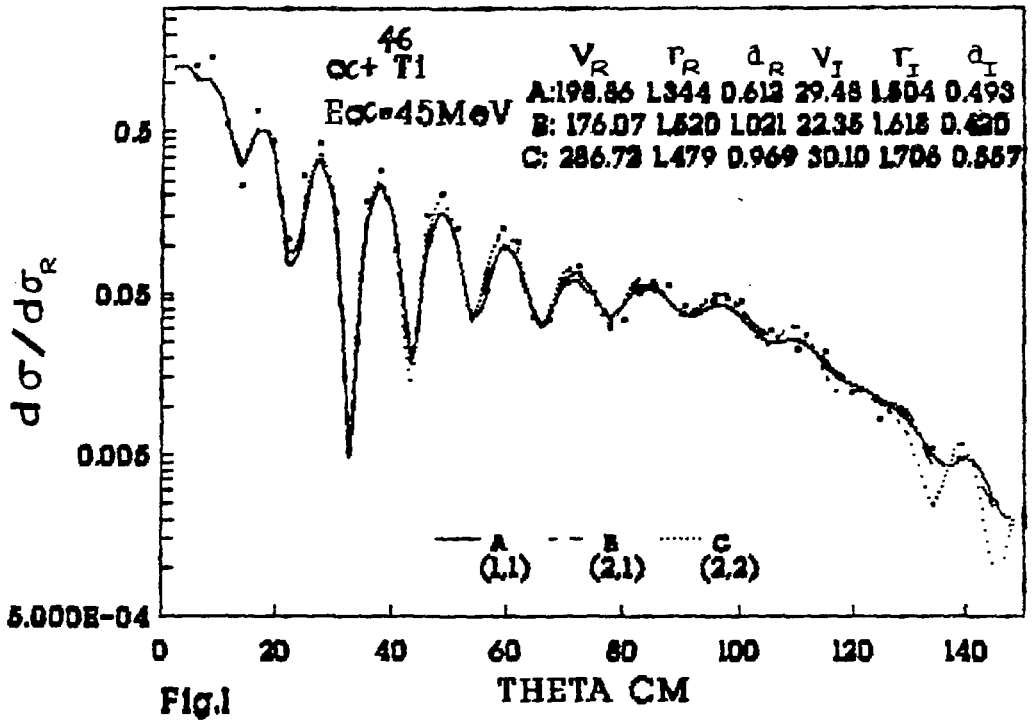

Fig.1

predicting the elastic scattering cross sections was also determined using a notch perturbation test [1,2]. The chi square maximum occurs at ~ 5.65 fm for the real part and at ~ 5.9 fm for the imaginary part. From this test it is inferred that 46-Ti nucleus appears effectively black to 45 MeV α-particles within first 4 fm of the radius.

The inelastic scattering angular distribution to the first excited state (0.889 MeV, 2^+) was analysed in terms of collective model using the distorted wave Born approximation(DWBA). The distorted waves were generated by the optical potential (m=n=1) deduced from the elastic data. The DWBA calculations, carried out by DWUCK4, [3] agreed well with the data.

AKNOWLEDGEMENTS

The authors wish to thank the staff of the VECC(BARC), Calcutta for providing the beam and other facilities for carrying out these measurements. Financial assistance from the UGC, New Delhi is gratefully acknowledged.

REFERENCES

1. Rao V R *et al.*J.Phys.G:Nucl.Part.Phys.(In Press)
2. Cramer J G and DeVries R M 1980 Phys.Rev.C22 91
3. Kunz P D 1982 Univ. of Colorado (Unpublished)

COUPLED CHANNEL ANALYSIS OF THE $^{28}Si(\alpha, ^{3}He)^{29}Si$ REACTION AT 45, 65 AND 120 MeV

M.P. Sathyavathiamma, V.P. Darshan, C.R. Ramaswamy and N.G. Puttaswamy
Department of Physics, Bangalore University, Bangalore 560 056.

The $^{28}Si(\alpha, ^{3}He)^{29}Si$ reaction has been studied experimentally at incident energies of 45 MeV[1], 64.9 MeV[2] and 120 MeV[3]. The fits to experimental angular distributions deduced using a direct one-step process are satisfactory only for the 1.27-MeV $3/2^+$ state and the 3.62-MeV $7/2^-$ state; however, the fits to the $1/2^+$ ground state, $5/2^+$ 2.03 MeV state, $3/2^+$ 2.43 MeV state and the $5/2^+$ 3.02 MeV state are poor.

We have therefore analysed the experimental data using coupled-reaction-channel (CRC) approach[4]. The amplitude and sign of the coupling strengths are taken from quasi-particle-core-coupling (QPCC) calculations[4].

As an example, the couplings used to describe the transition to the $1/2^+$ ground-state are shown in fig.1.

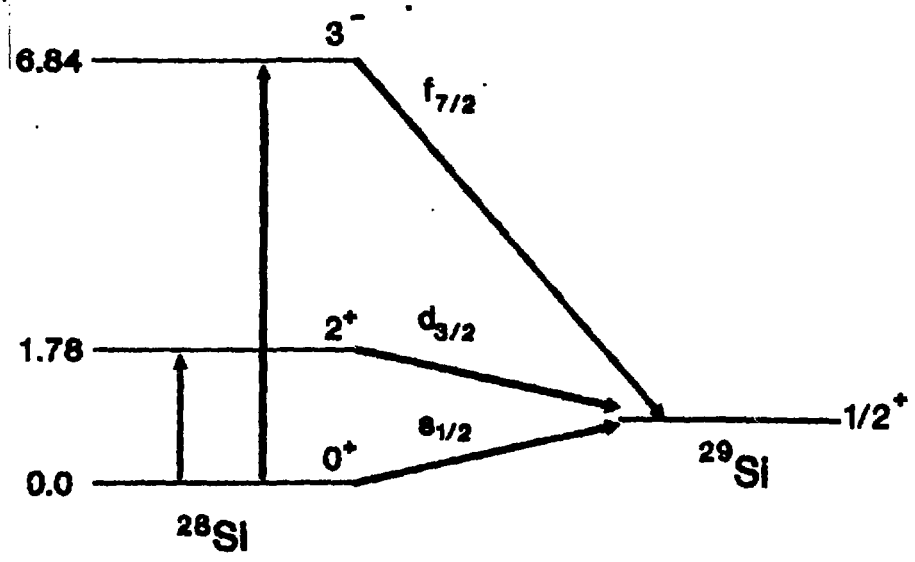

Fig 1. Schematic diagram showing the coupling scheme.

The fits to experimental data shown in fig.2 indicate that the coupled-channel effects are important. The fits to the other states also improved when CRC calculations were done for the states in ^{29}Si.

This work has been supported in part by a research grant from the University Grants Commission.

References:-

1. V.P. Darshan, Ph.D. Thesis, Bangalore University, 1991.
2. M. Yasue et al., INS Annual Report (1983) p 23.
3. J. Van der Plicht et al., KVI Annual Report (1976) p 17.
4. P.D. Kunz, Computer code CHUCK3, 1984.

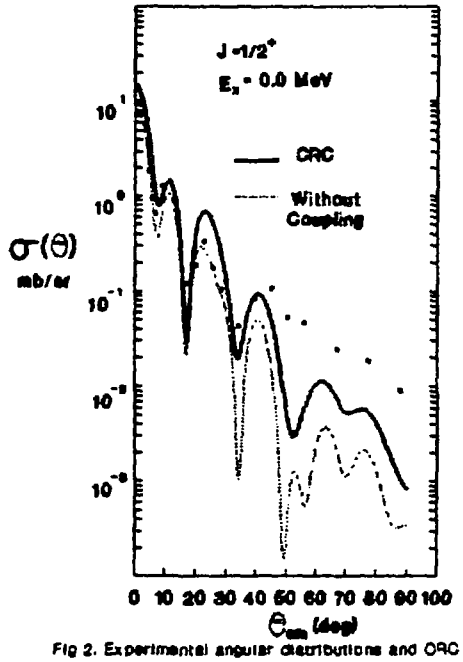

Fig 2. Experimental angular distributions and CRC Predictions

POTENTIAL AMBIGUITIES IN HEAVY ION SCATTERING

D. Dutta and Y.K. Gambhir
Department of Physics, I.I.T., Bombay 400 076

Heavy ion reactions are one of the most widely studied scattering processes, and the optical model of elastic scattering is the most widely used method of analysis. Many ambiguities are known to exist for such optical model potentials, e.g. inner region insensitivity. We have studied such ambiguities and report here a few representative results for heavy and light ions.

Using the Jost function formulation[1], we arrive at $1-\eta_l^2 = \sum_{i=0}^{\infty} \varkappa_r(\lambda, r_i, \Delta)$; $r_{i+1} = r_i + \Delta$, $r_0 = 0$

where

$$\varkappa_r(\lambda, r_i, \Delta) = 4k\ \mathrm{Im}\left[\frac{\phi(\lambda,k,r)}{F(\lambda,-k)} \cdot \frac{(\phi^*(\lambda,k,r)}{F^*(\lambda,-k)}\right]\Bigg|_{r_i}^{r_i+\Delta}$$

$$\sigma_r = \sum_{i=0}^{\infty} \sigma_r^{(i)}(r_i, \Delta)\ ;\ \sigma_r^{(i)}(r_i, \Delta) = \sum_{l=0}^{\infty} \frac{\pi}{k^2}(2l+1)\varkappa_r(\lambda, r_i, \Delta)$$

Here $\phi(\lambda,k,r)$ is the regular solution of the Schrodinger equation with nuclear optical model potential k^2 is energy and $\lambda = l+1/2$. $F(\lambda,\pm k)$ are the Jost functions, η_l is the reflection function for the l^{th} partial wave and σ_r is total reaction cross-section.

The commonly used Woods-Saxon type of optical potential (listed below in obvious units) with surface absorptive and volume absorptive terms was employed. The spin-orbit term was neglected as we studied even-even nuclei only.

System	Energy	V	W_o	r_o	r'_o	a	a'	r_c
$^{12}C+^{208}Pb$	1450	20	123.4	1.06	.98	1.17	.95	1.30
$^{16}O+^{24}Mg$	35	25	5.65	1.35	1.35	.47	.30	1.25
	50	32.5	7.90	1.35	1.35	.47	.30	1.25

Some of the representative results are displayed in Figs.(1)-(4).

The systematics observed are:

-For heavy ion reactions (fig.1) all contributions to α_{gr} arise mostly from the surface region.
-For light and medium ions (fig.2) the α_{gr} is oscillatory and $l \leq l_{crit.}$ partial waves probe the inner region to some extent. However they peak at the surface and major contribution is still from the surface region.
-At higher energies and for volume absorptive potentials low l values for medium and light ion penetrate deep into the inner regions and the oscillations are now suppressed. However, the major contribution is still from the surface region. For heavy ions however all partial waves are confined to the surface. This holds also for volume absorptive potential and for high energies.
-It appears that the Coulomb barrier is partially responsible for confining the partial waves to the surface.

Reference:

1. C.S. Shastry et al., Phys. Rev. C28,1109 (1983)
2. J.Y. Hostachy et al., Nucl. Phys. A490,441 (1988)
3. H.T. Fortune et al., Phys. Rev. C20,648 (1979)

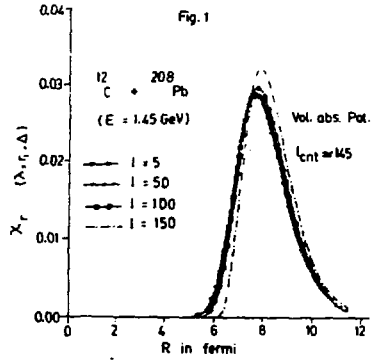

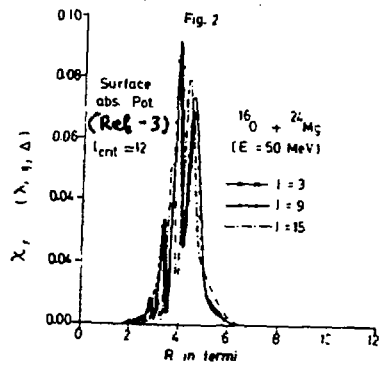

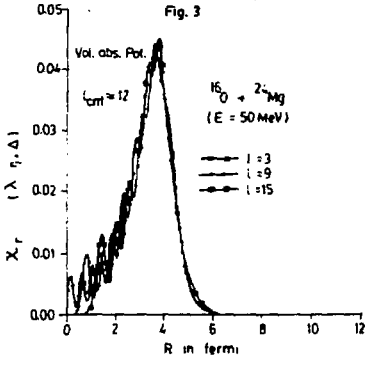

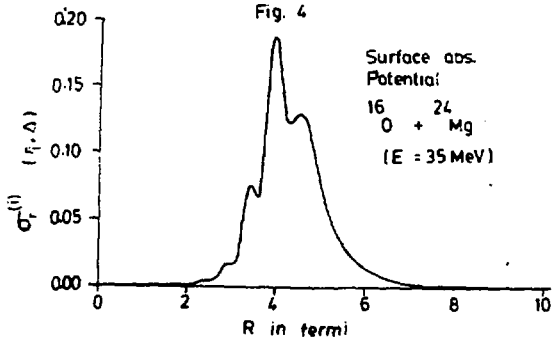

SPIN DISTRIBUTION FOR THE FUSION OF $^{18}O+^{209}Bi$

S. Kailas, P. Singh and A.K. Mohanty
Nuclear Physics Division, B.A.R.C., Bombay-400 085

It is a continuing challenge to explain simultaneously the various phenomena which take place at near- and sub-barrier energies. Several approaches/1/ including the coupled channels(CC) analysis /2/, the optical model analysis/3/ and the use of dispersion corrected energy dependent barrier parameters/4/ have been successful in explaining not only fusion but also elastic scattering at the same time. In the present work, we have applied the above three methods to explain the fusion excitation and the $< l^2 >$ over the energy range $V_B-4<E<V_B+15$ MeV for the system $^{18}O+^{209}Bi$. The data are from Ref.5. The CC calculations performed included coupling to the low lying $2^+, 3^-$ and 5^- states. For $E_{c.m.}$=83.5 and 89.0 MeV using the $<l^2>$ from CC calculations and the measured fission fragment anisotropies, the K_0^2 values have been deduced. For lower energies, these K_0^2 values have been scaled down as $\sqrt{Ex}$. With these K_0^2 values and measured anisotropies, the experimental $< l^2 >$ values have been deduced. The optical model parameters required for Udagawa approach have been taken from Ref.6. The fusion radius has been varied to fit σ_F and hence obtained $< l^2 >$. For the analysis using dispersion relation correction has been applied not only at the most sensitive radius (12.5fm) but also for a range of r values and hence the barrier parameters V_B, R_B and hw which are now energy dependent have been obtained. With these parameters as inputs both σ_F and $< l^2 >$ have been calculated. Overall the agreement between the experiment and the calculations is good (Fig.1) over the entire energy range. It is concluded that $< l^2 >$ data for this system, in contrast to that found for $^{18}O+^{208}Pb$, can be explained satisfactorily (Fig.2).

References:
/1/G.R. Satchler, Phys.Rep. 199,147(1991)
/2/C.H.Dasso et al. Nucl.Phys. A405,381 (1983)
/3/T. Udagawa et al. Phys.Rev. C32,124 (1985)
/4/I.J. Thompson et al. Nucl.Phys. A505,84 (1989)
/5/E. Vulgaris et al. Phys.Rev. C33,2017 (1986)
/6/P. Singh et al. -to be published (1991)

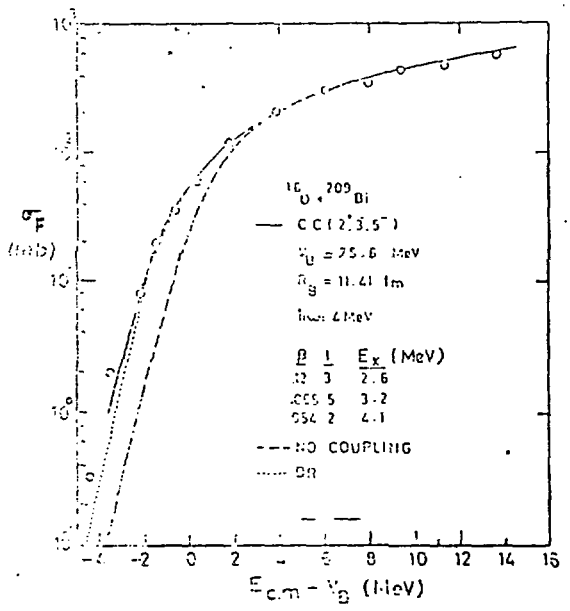

Fig.1

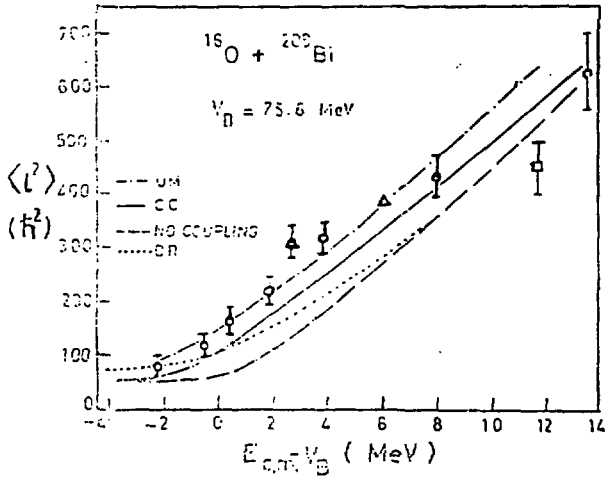

Fig.2

A DYNAMICAL APPROACH TO INTERMEDIATE ENERGY NUCLEUS-NUCLEUS COLLISIONS

K.Krishan[a], S.Bhattacharya[a], P.Wagner[b], J.P.Coffin[b] and F.Rami[b]

a) Variable Energy Cyclotron Centre, 1/AF Bidhan Nagar, Calcutta - 700 064

b) Centre de Recherches Nucleaires, B.P.20, F-67037 Strasbourg Cedex France

Dynamical evolution of nucleus-nucleus collisions in the Fermi energy domain is followed from the point of interaction to the evaporation residues on event by event basis by Monte -Carlo simulation technique. The complete reaction process comprises two phases, (*i*) the preequilibrium phase and (*ii*) the evaporation phase. The initial preequilibrium phase leads to the formation of an incompletely fused composite after the emission of preequilibrium nucleons. Subsequently, this composite decays leading to the final residues. The preequilibrium phase of the reaction is simulated in the Promptly Emitted Particle model [1] and the later stage, forming the same event , is simulated using the Binary Sequential Decay model[2]. The calculations are parameter free. The trajectory calculation for the preequilibrium phase is carried out up to the time when there is no further preequilibrium emission. After this time the composite formed is assumed to be fully thermalised. This time is typically of ~ 50 fm/c. We have applied this model to study the exclusive proton and alpha energy distributions and other physical observables (measured in coincidence with the residues) for the representative reaction 40Ar + 13C at 1100 MeV. Fig. 1 depicts the average nucleon loss from the projectile and the target versus time along the trajectory in the preequilibrium phase of the reaction. It is evident from fig. 1 that there is no further nucleon loss through preequilibrium emission after 50 fm/c. In fig.2 the calculated exclusive energy distributions of α-particles for 15° and $\pm 30^{\circ}$ angles, in coincidence with residues at 5°, are displayed along with the experimental data [3]. Fig.3 shows the calculated exclusive proton energy distributions for forward and backward angles, in coincidence with the residues along with the experimental data[3]. Positive/negative angles refer to the particle detector on the same/opposite side of the fragment detector with respect to the beam direction. The calculated results for α and proton agree well with the respective experimental data. The

high energy tail in the exclusive α energy spectra, however, can not be reproduced in our model as the preequilibrium emission of α's and complex particles is not considered here.

References:

[1] S. Bhattacharya, K. Krishan, J. N. De and S. K. Samaddar; Phys. Rev. C37 (1988) 2916

[2] J. Richert and P. Wagner; Nucl. Phys. A517 (1990) 399

[3] M. Zahar et al.; Z. Phys. A339 (1991) 465

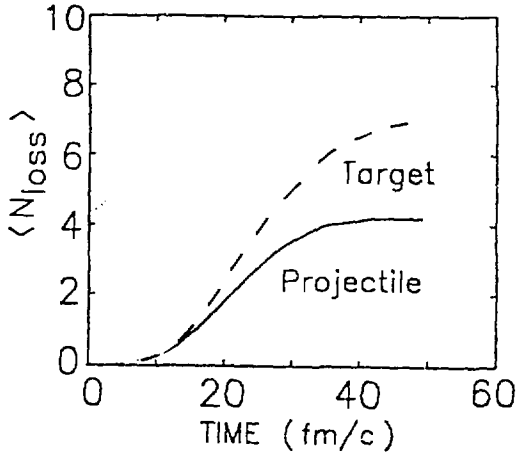

FIG. - 1

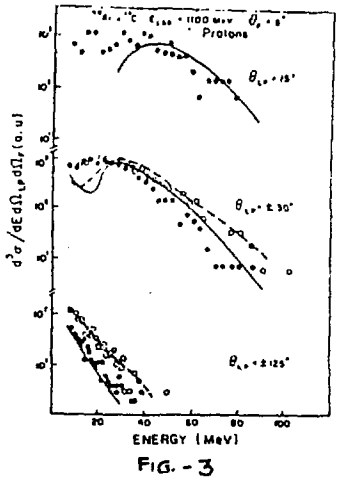

FIG. - 3

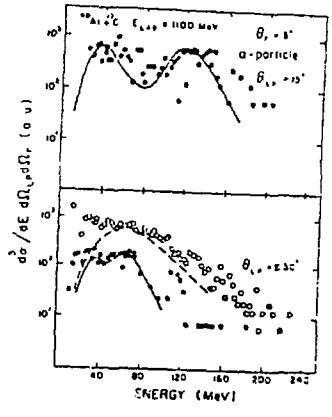

FIG. - 2

ROLE OF DEUTERON SIZE IN ANTIPROTON- DEUTERON ELASTIC SCATTERING

K. Kumar and A. K. Jain
Nuclear Physics Division, BARC, Bombay-4000 85

The interaction of antinucleons with nuclei are expected to reveal the nature of the interaction in $\bar{N}N$, which have large annihilation component. Earlier studies[1] on knockout reaction with ^6Li target have indicated that the deuteron cluster in ^6Li may be shrunk. In the present work the differential cross section for $\bar{p}d$ elastic scattering is calculated using Glauber formalism[2], where deuteron cluster of various sizes has been used. As the main contribution to scattering cross section comes from the region of small momentum transfers[2], the effect of the size of the deuteron on the cross sections could be dramatic. The differential cross section can be written as[3] :

$$d\sigma/dt=\{1+R^2\exp[b_p t(R-1)]+2*RS(t)\exp[.5*b_p t(R-1)]$$

$$-R^2\sigma_p\exp[b_p t(R-1)]\phi_n(t)/2\pi - R\sigma_p\phi_p(t)/2\pi$$

$$+R^2\sigma_p^2/(64.*\pi^2 b)\exp[-b_p t/(R+1)]\phi\}d\sigma_{\bar{p}p}/dt \quad ...(1)$$

where $t= -q^2$ and $b= 0.5b_p(R+1)$; $R = \sigma_n/\sigma_p$, ϕ_n, ϕ_p, ϕ are the various integrals[3]. The form factor of the deuteron $S(q)$ is written in an approximate way as:

$$S(q)=C_1\exp(-\gamma_1 q^2)+C_2\exp(-\gamma_2 q^2) \quad ...(2)$$

Since the ground state wave function of the deuteron is not known very accurately, particularly for small neutron-proton separations, the deuteron size effects on the elastic cross section are obtained by varying the γ_1 parameter in eq(2).

The differential cross section $d\sigma_{\bar{p}p}/dt$ in eq(1) is written as:

$$d\sigma_{\bar{p}p}/dt= \sigma_p^2 \exp(b_p t)/16\pi$$

where the values of σ_p, b_p and R are taken from Ref3.

Elastic cross sections are calculated for antiproton energies of 57.4, 124.1 and 170.5 MeV. Fig 1 shows the cross sections as a function of momenta $t(GeV/c)^2$ for various deuteron sizes r_d=1.82 (free size), 1.5 and 2.3 fm. For low values of t(=20 units) the cross section increases by $\sim$ 35% at all energies if r_d is reduced by~15% , while for larger t(60 units) it increases by~25% . However the shape of the distribution does not change as shown in the fig 1. These results would be useful in calculating $\bar{p}^6$Li elastic cross setions, where ^{6}Li could be described as α+d cluster model[4].

References

1. A. K. Jain and N. Sarma; Nucl. Phys. 233(1974)145.
2. V.Franco and R.J.Glauber; Phys. Rev. 142(1966)1195.
3. L.A.Kondratyuk et al.;Sov.J.Nucl.Phys. 33(1981)413.
4. Y. C.Tang and K.Wildermuth;Phys.Rev. 123(1961)548.

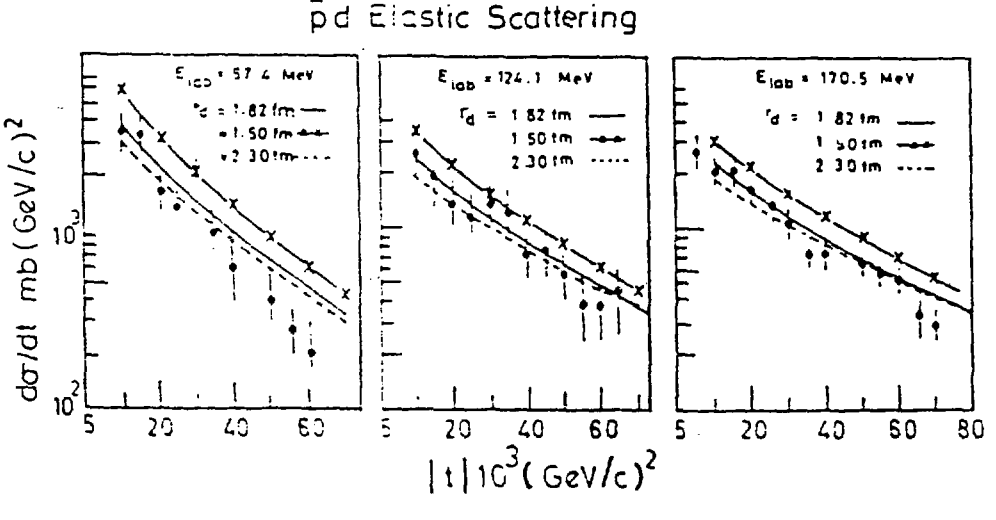

EXPLANATION OF e+e- PEAKS IN HEAVY-ION COLLISIONS

K. Raja, K. Sakthi Murugesan, G. Janhavi, and
P. R. Subramanian
Department of Nuclear Physics, University of Madras,
Guindy Campus, Madras 600 025.

We calculate the kinetic energies of positrons and electrons produced in heavy-ion collisions using our **Neutral Nuclear Dust (NND) hypothesis** [1], wherein we assume that atleast one neutral boson (of mass $\sim 2m_e$) is bound to each nucleon inside the nucleus. The NND consists of an e+ and an e-.

Production of e+e- in heavy-ion collisions is a three step process, viz., NND affinity resonance, nuclear electrostatic, and nuclear magnetic interactions. The affinity resonance arises due to the interaction of the corresponding dust paricles in the projectile and the target nuclei. Now these dust particles are polarised by the intense nuclear electric field E which is of the order of 10^{21} Vm^{-1}. The polarised positrons and electrons are within the combined superstrong nuclear magnetic field [2] B ($\sim 10^{11}$ T) at the peripheral distance 'a' equal to 1.875 fm. The new born e+ and e- from the NND are lifted and ejected by this field from the colliding system as a two-directional e+e- gun. This can account for the back-to-back emission of the correlated e+e- coincidence events. Now the kinetic energy of positrons or electrons ϵ_k is given by

$$\epsilon_k = (N_d + 3/2)\ B\ e\ v\ a, \qquad (1)$$

where N_d is the 3-D harmonic oscillator energy level quantum number which takes the values from 0 to 6, e the electronic charge and v the velocity of the projectile ion. Multiple peaks (discreteness [3]) arise due to the decay of NND from different shells of the nucleus. In our calculations we found the 320 keV prominent peak arising due to the decay of dust particles from the sixth shell (N_d = 5) of the nucleus (see Table I). This shell is almost in the periphery of the nucleus having more number of nucleons than its inner ones.

References [4] and [5] (the non-conservation of mass and the Q value of the elastic or quasi-elastic scattering) are highly in favour of NND hypothesis, showing that the GSI spectrum is triggered by nuclear effects. The calculated values of kinetic energies of positrons or electrons agree very well with the experimental values. Our hypothesis can explain the origin of e+ peaks with independent of Z_u and back-to-back emission of e+e- in heavy-ion collisions.

Table I. Calculated kinetic energies (in keV) of positrons (or electrons) for different colliding systems comprising five supercritical (cols. 2 to 6) and three sub-critical (cols. 7 to 9). N_d varies from 0 to 6. BE/u = Binding energy per nucleon.

BE/u MeV	6.07	6.02	5.8	5.83	5.75	5.9	5.9	5.7
Z_u	188	186	184	182	180	171	165	164
N_d								
0	79	78	75	75	74	78	75	71
1	132	130	125	125	123	130	126	118
2	184	182	175	175	172	183	176	166
3	237	234	225	225	222	235	227	213
4	290	286	275	275	271	287	277	260
5	343	338	326	325	320	340	328	308
6	396	390	376	375	370	392	378	355

References

[1] K. Raja, K. Sakthi Murugesan, G. Janhavi, and P. R. Subramanian, submitted to Phys. Rev. Lett.

[2] J. Reinhardt and W. Greiner, in *Treatise on Heavy-Ion Science*, edited by D. A. Bromley (Plenum, New York, 1985), Vol.5, p. 81.

[3] A. Chodos and L. C. R. Wijewardhana, Phys. Rev. Lett. 56, 302 (1986).

[4] E. Berdermann et al., in *GSI Report* 90-1 p.161, (1991) (unpublished); ibid., O. Frohlich et al., p. 163; ibid., H. Tsertos et al., p. 164.

[5] H. Bokemeyer, in *Selected Topics in Nuclear Structure*, edited by J. Styczen *et al.* (World Scientific, Singapore, 1990), Vol.2, p.332.

PHASE-FUNCTION METHOD FOR COMPLEX POTENTIALS

J.Pal, A.K.Jana and B.Talukdar
Department of Physics, Visva-Bharati University
Santiniketan-731 235, West Bengal, India

We consider the scattering problem for absorptive interactions within the framework of phase function method [1]. A Green's function approach is used to derive the phase equations for calculating the real and imaginary parts of the scattering phase shifts. As a case study we apply these algorithms on a shallow potential, the real and imaginary parts of which have been deduced from experimental data [2].

In figure 1, we portray Re and Im as a function of the centre of mass energy E for the partial waves l= 0, 2 and 4. The imaginary part of the phase shifts for the S-wave vary smoothly with E . This is true for D and G waves only after E = 22 MeV. In the low-energy region Im and Im exhibit some rapid fluctuations. One would be tempted to acknowledge them as symptomatic of sharp resonances. But we know that no such resonances do exist in the low-energy region for the scattering. Thus great care must be taken while dealing with scattering on a complex potential. During the course of our computation we found that remarkable smooth and systematic behaviour of the real part of the phase shift was destroyed in the energy regions where Im fluctuated rapidly. However, the real part of the phase shifts above and below these narrow ranges joined smoothly leaving no trace on the cross section.

The alpha-particle is tightly bound such that at least 20 MeV of energy is required in its centre of mass to loosen this "robust" object. Thus, upto about this energy of the system, the scattering is elastic and the introduction of an imaginary potential may appear aesthetically unpleasing. but the present case study refers to the following.

The alpha particle is beleived to be an important substructure of the more complex nuclei and the cluster model of nuclei and hypernuclei is of considerable interest. Such models involves two or more alphas and one needs to use an potential that is in accord with fundamental studies and scattering results. In this case external excitation will be feasible even at low energies and our model calculation refers to such a physical situation.

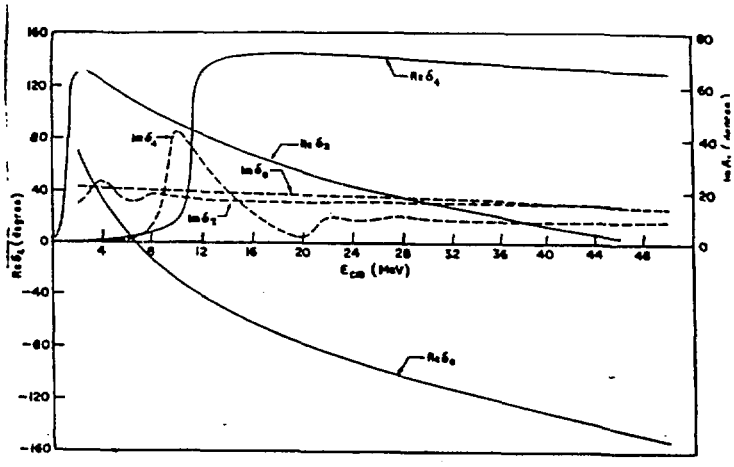

Fig.1 : The real and imaginary part of the phase shifts as a function of E .

References

[1] F. Calogero, Variable Phase Approach to Potential Scattering (Academic Press, New-York 1967)

[2] P. Darriulat, G. Igo, H. G. Pugh and H.D.Holmgren Phys. Rev. 137 315 (1965)

SCATTERING OF ^{28}Si FROM ^{27}Al AT 70,80,90 AND 100 MeV

S.K.Charagi, Kuldeep, M.G.Betigeri, C.V.Fernandez
and S.K. Gupta
Nuclear Physics Division, B.A.R.C., Bombay 400 085.

The elastic scattering angular distribution has been measured for $^{28}Si+^{27}Al$ system using a silicon beam from 14UD pelletron on Aluminium target. The Al target was a self supporting film of ~45 $\mu g/cm^2$ thickness prepared by the vacuum evaporation technique. The scattered particles were detected with a μ200 m thick silicon surface barrier detector each subtending a solid angle of 0.129 msr. The angular offset of the chamber was less than 0.1 degree. The ratio of elastic to Rutherford cross section have been plotted in the fig.1 as a function of angle. The measured data show characteristic Fresnel oscillations at forward angles followed by an exponential fall. The data have been analysed using various models.

Within the framework of the Generalised Fresnel Model (GFM) /1/ the parameters Δ and l_g were varied to get the best fit to the data. These results have also been analysed within the framework of the parametrized phase shift model (PPSM) using the three parameter Frahn-Venter parametrization /2/ of the form given below for the phase shift

$$\delta_l^o = \left\{1 + \exp\left[(l_g - l)/\Delta\right]\right\}^{-1} + i\mu \frac{\partial}{\partial l}\left\{1+\exp\left[\frac{(l_g - l)}{\Delta}\right]\right\}^{-1} \quad (1)$$

The fit to the elastic angular distribution data using the PPSM is also indicated in fig.1. Table 1 shows the values of l_g, Δ, μ and χ^2 values using GFM and PPSM.

Energy MeV(lab)	Method Used	l_g	Δ	μ	χ^2
	PPSM	20.78	.564	.001	0.75
70	GFM	20.05	1.286	-	1.107
	PPSM	26.60	1.168	1.203	1.44
80	GFM	26.55	1.573	-	1.483
	PPSM	31.47	1.760	1.437	1.25
90	GFM	31.31	1.973	-	1.08
	PPSM	35.70	1.623	2.170	0.61
100	GFM	36.02	2.593	-	2.47

Table I

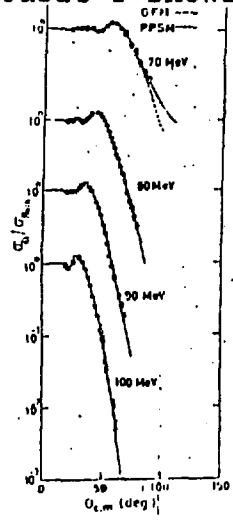

Fig.1 →

Fig.2 gives the fit to the elastic scattering angular distribution data using the Optical Model with the Woods-Saxon form of the potential /3/ and the Coulomb-modified Glauber Model (C.M.G.M) /4/.

Table 2 gives the parameters of optical potential of Woods-Saxon form at different energies.

Lab Energy(MeV)	V_R (MeV)	r_R (fm)	a_R (fm)	V_I (MeV)	r_I (fm)	a_I (fm)
70	54.03	1.15	0.63	23.50	1.15	0.63
80	59.44	1.15	0.63	31.15	1.15	0.63
90	61.85	1.15	0.63	36.75	1.15	0.63
100	70.02	1.15	0.63	31.24	1.15	0.63

Table II

The total reaction cross-sections were calculated using the scattering matrix elements determined from the elastic scattering analysis. Table 3 gives the comparison of the total reaction cross section (σ_R) values in milibarn using various models.

Total Reaction Cross Sections (mb)

Energy	PPSM	GFM	C.G.M.	OPTICAL
70	664	669	653	650
80	962	1004	929	919
90	1224	1245	1139	1192
100	1364	1505	1303	1345

Table III

References:

1. Frahn, W.E., Phys.Rev. 26, 568 (1971).
2. Venter, R.H., Frahn, W.E., Ann.Phys.(N.Y) 27, 401 (1964).
3. J.Raynal, ECIS 79: A Coupled Channel Computer Code (Unpublished).
4. S.K.Charagi, S.K.Gupta, Coulomb-modified Glauber model, Nucl.Phys. Symp. (1989).

Fig.2 →

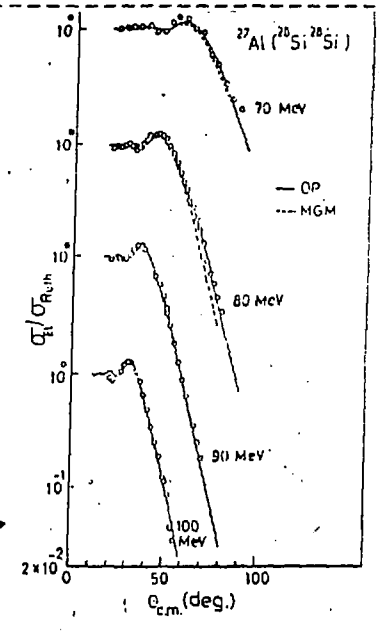

ELASTIC SCATTERING ANGULAR DISTRIBUTION USING PARAMETER-FREE COULOMB-MODIFIED GLAUBER MODEL

S.K.Charagi and S.K.Gupta
Nuclear Physics Division, B.A.R.C, Bombay 400-085

The Glauber model modified for the effect of the Coulomb field has been used to analyse a large amount of heavy-ion elastic scattering data with considerable success/1/. The input to the model is the nucleon-nucleon cross section, nuclear densities and α_{NN} the ratio of real and imaginary parts of the forward N-N scattering amplitude. Earlier we had used α_{NN} as free parameter/1/. In this paper we have given a prescription for its calculation at low energies upto ~15 MeV/nucleon. The model is thus parameter free and has the predicting power. The quantity α_{NN} has been obtained using the S wave results for N-N scattering. σ_{pp}, α_{pp}, σ_{nn}, α_{nn} and σ_{np}, α_{np} for singlet and triplet state is

$$\sigma_{pp} = 4\pi/k^2(1+\alpha_{pp}^2), \quad \alpha_{pp} = \frac{1}{k}\left(-\frac{1}{a_{pp}} + \frac{r_{op}k^2}{2}\right)$$

$$\sigma_{nn} = 4\pi/k^2(1+\alpha_{nn}^2), \quad \alpha_{nn} = \frac{1}{k}\left(-\frac{1}{a_{nn}} + \frac{r_{on}k^2}{2}\right) \qquad (1)$$

$$\sigma_{np1} = \pi/k^2(1+\alpha_{np1}^2), \quad \alpha_{np1} = \frac{1}{k}\left(-\frac{1}{a_{np1}} + \frac{r_{onp1}k^2}{2}\right)$$

$$\sigma_{np3} = 3\pi/k^2(1+\alpha_{np3}^2), \quad \alpha_{np3} = \frac{1}{k}\left(-\frac{1}{a_{np3}} + \frac{r_{onp3}k^2}{2}\right)$$

The scattering length and range parameters are/2/

$a_{pp} = -7.828$, $a_{nn} = -17.1$, $a_{np1} = -23.75$, $a_{np3} = 5.424$

$r_{op} = 2.80$, $r_{on} = 2.84$, $r_{onp1} = 2.75$, $r_{onp3} = 1.759$

Then α_{NN} is calculated as

$$\alpha_{NN} = \frac{\alpha_{pp}\sigma_{pp}Z_pZ_t + \alpha_{nn}\sigma_{nn}N_pN_t + (\alpha_{np1}\sigma_{np1} + \alpha_{np3}\sigma_{np3})(N_pZ_t + Z_pN_t)}{\bar{\sigma}_{NN}A_pA_t} \qquad (2)$$

where $\bar{\sigma}_{NN}$ is the average nucleon-nucleon cross section,

$$\bar{\sigma}_{NN} = \frac{\sigma_{nn}N_pN_t + \sigma_{pp}Z_pZ_t + (\sigma_{np1} + \sigma_{np3})(N_pZ_t + Z_pN_t)}{A_pA_t} \qquad (3)$$

$$k = 0.10975\sqrt{E_{lab}}$$

The phase shift in eikonel model approach is given by

$$\delta_l = \bar{\sigma}_{NN}(\alpha_{NN} + i)\Omega_l/2 \qquad (4)$$

and the overlap integral of the nuclear densities Ω_ℓ for a Gaussian density distribution of type

$$\rho_i = \rho_i(0)\ \exp(-r^2/a_i^2)$$

can be written as/3/

$$\Omega_\ell = \left[\frac{\rho_T(0)\,\rho_P(0)}{2}\cdot\pi^2\cdot\frac{a_T^3\,a_P^3}{(a_T^2+a_P^2+r_0^2)}\right]\exp\left[\frac{-b_\ell'^2}{(a_T^2+a_P^2+r_0^2)}\right] \quad (5)$$

where $\rho_P(0)$, $\rho_T(0)$ and a_P, a_T the parameters of Gaussian distribution are adjusted to reproduce the experimentally determined nuclear surface texture/3/ and r_0 is the nuclear range parameter. The distance of closest approach is given as

$$k\,b_\ell' = \left\{\eta + \left[\eta^2 + \left(\ell + 1/2\right)^2\right]^{1/2}\right\} \quad (6)$$

$$\eta = Z_P Z_T e^2/\hbar v$$

The scattering amplitude

$$f(\theta) = f_c(\theta) + \frac{1}{2ik}\sum (2\ell+1)\,P_\ell(\cos\theta)\,e^{2i\sigma_\ell}\left(e^{2i\delta_\ell} - 1\right) \quad (7)$$

is then evaluated using δ_ℓ given by Eq 4 and the Coulomb phase shift is calculated using the standard expression. In fig.1 the solid line shows the predictions of elastic angular distribution by this model for ^{16}O + ^{40}Ca system. The data points in this figure are taken from ref/4/. The reasonablly good agreement between the data and our calculations demonstrates the predictive power of the model at energies as low as 2.5 Mev/nucleon

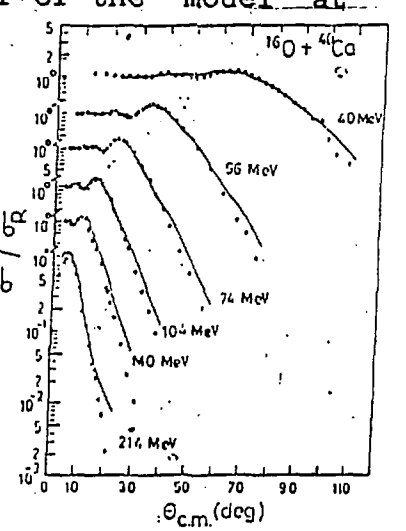

References.

1. S.K.Charagi and S.K.Gupta: Nucl.Phys.Symp ,A.M.U(1989)
2. Londergan.J: Proc of SERC school in Nucl Phy , Jaipur (1987)
3. S.K.Charagi and S.K.Gupta: Phys.Rev. C 41 (1990)
4. G.R.Satchler ,Phys Reports 55,183 (1979).

Fig.1 →

ELASTIC SCATTERING OF ^{12}C ON ^{232}Th

A. K. Mohanty, P. Singh, A. Nijasure, A. Saxena, B. V. John, S. Kailas, S. K. Kataria, A. Chatterjee, S. S. Kapoor and V. S. Ramamurthy.*

Nuclear Physics Division, BARC Bombay 400085

* Institute of Physics, Bhubaneswar 751004

The conventional optical model with real and imaginary potentials whose values are dependent on the bombarding energy have been used to explain the elastic scattering and reaction cross section data. Recently we have shown [1] that using the same elastic scattering parameters but l-dependent imaginary potential, one can also explain the fusion cross section. In this model, fusion cross section can be obtained from reaction cross section provided potential parameters for elastic scattering are known. Therefore, we have measured elastic scattering angular distribution for ^{12}C on ^{232}Th at energies 65, 67, 72, 75 and 82.5 MeV in the angular range 30^0 to 160^0 using 14 UD BARC-TIFR Pelletron accelerator. The elastically scattered ^{12}C ions were detected by means of three 1mm surface barrier detectors and one telescope mounted 10^0 apart in a scattering chamber.

It is seen in recent years [2] that around the Coulomb barrier the strength of real optical potential increases while the strength of the imaginary potential decreases due to channel couplings. Similiar effect are also expecied in the present analysis. However, in case of ^{232}Th, the measured angular distribution is the sum of elastic and inelastic events as experimentally it is not possible to seperate them due to many low lying levels. It was shown earlier [3] that when the data is sum of elastic and inelastic scattering, the optical model still can be applied to fit this quasi elasic data and the deduced reaction cross section is consistent with the value obtained from the coupled channel calculation where this inelastic channels are considered explicitly.

Therefore, we have performed optical model analysis using Woods-Saxon and double folding potential (with standard M3Y interaction) . For imaginary part Woods-Saxon form factors were used. The potential parameters were obtained by minimising the χ^2 . The fitted value along with the experimental data are shown in fig 1. It is observed that, even though the fits are good, the potential parameters (at some energies) show anomalous behaviour due to presence of in-elastic components. The contribution from inelastic channel becomes dominant at backward angle. The effect of inelastic contribution on the potential parameters is shown in fig 2. The lower curve is obtained fitting the data up to 125^0 for which the normalisation factor of real potential is 1.0. the upper curve is obtained after fitting all the points up to 155^0 and it results with a normalisation factor of .4 which is unphysical. Therefore, to obtain any unambigous potential parameters, it is essential to include dominant in-elastic channels while fitting the quasi-elastic data.

1. A. K. Mohanty et. al. Phys. Lett. 247b (1990) 215.
2. M.A Nagarajan et.al.Phys. Rev. Lett 54 (1985) 1136
3. Deschler H. et al. Nucl. Phys. A436 (1979) 463

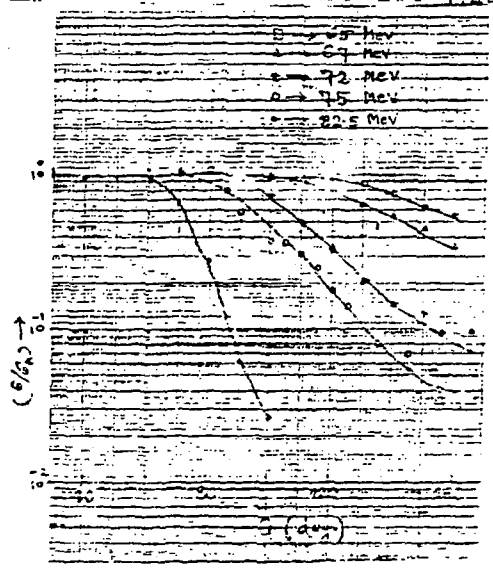

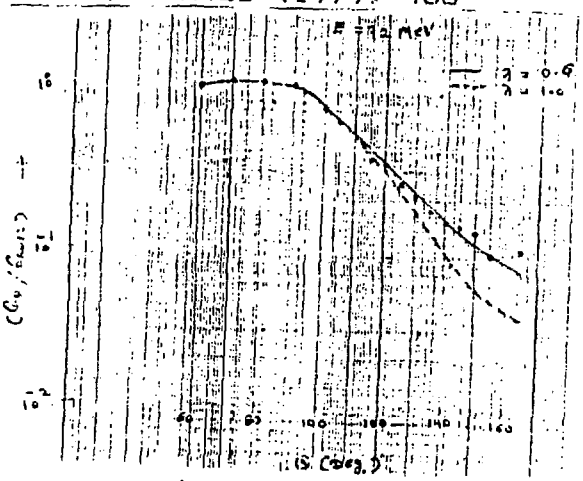

12C+28Si ELASTIC SCATTERING ABOVE THE COULOMB BARRIER.

Yash Pal Singh, Department of Physics, G.K.Universi -ty,Haridwar-249404.

Elastic heavy-ion scattering is sensitive to the tail region of the ion-ion potential because of the strong absorption. Alarge number of the investigations of non-symmetrical system C+Si have a particular importance in heavy-ion study because both nuclei are of complex nature and backward angle observations could also be made. For this purpose,a simplified microscopic theory is applied to study C+Si elastic scattering at ELAB=74.0 MeV which is more than three times the coulomb barrier energy at which nuclear potential and absorption phenomenon both become significant. Here the effective interaction between the two ions is taken to be the sum of complex nuclear potential,coulomb potential and the cetrifugal potential. The Coulomb and Centrifugal potentials are calculated easily by familiar techniques. However,the complex nuclear potential,which is made up of real and imaginary parts,is evaluated with great difficulty.The real part is microscopically derived using the equivalence of Resonating Group Method(RGM) and Generator Coordinate Method(GCM) in double folding modle/1/.RGM calculations in this case become quite cumbersome as Carbon nucleus has incomplete p-shell and Silicon nucleus exhibits oblate and prolate configurations. Due to incomplete shell of carbon, its microscopic wavefunction has to be projected on a 0+ state describing the ground state of the carbon nucleus/2/. On the other hand, due to two shapes of Silicon nucleus, the real part of the nuclear potential is taken as an averege of nuclear potentials obtained for C+Si (oblate) and C+Si (prolate) configurations/3/. The imaginary part of the nuclear potential, which accounts for absorption effect, is described by a simple phenomenological picture. Here, it is constructed in the form of real nuclear potential divided by a dimensionless strength parameter chosen to have the

value 2.17 for C+Si system/4/. The exchange effects are crudely compensated by adjusting the parameter "u" as 1.1 in the analytic form of the real part of nuclear potential. The scattering cross-sections are computed from complex nuclear phase shift and the Coulomb phase shifts. In Fig. 1, the full line curve represents the results of the presents approach. There is close agreement between the results of present theory and expermental data of Satchler et al. over full angular range/5/.

References:

/1/ M.Kamimura and T.Matsuse, Prog. Theor. Phys. 51 (1974) 438.

/2/ O.D.Sharma and B.B.Srivastava, J.Phys. G. Nucl. Phys. 6(1980) 209.

/3/ Yash Pal Singh, D.Phil. Thesis (Garhwal University) 1986 (Unpublished).

/4/ B.Behera et al., Phys. Rev. C21 (1980) 1883.

/5/ G.R.Satchler, M.L.Halbert, R.G.Stokstad, R.M. De Vries, D.A. Goldberg and J.G. Cramer, Nucl. Phys. A 346 (1980) 179.

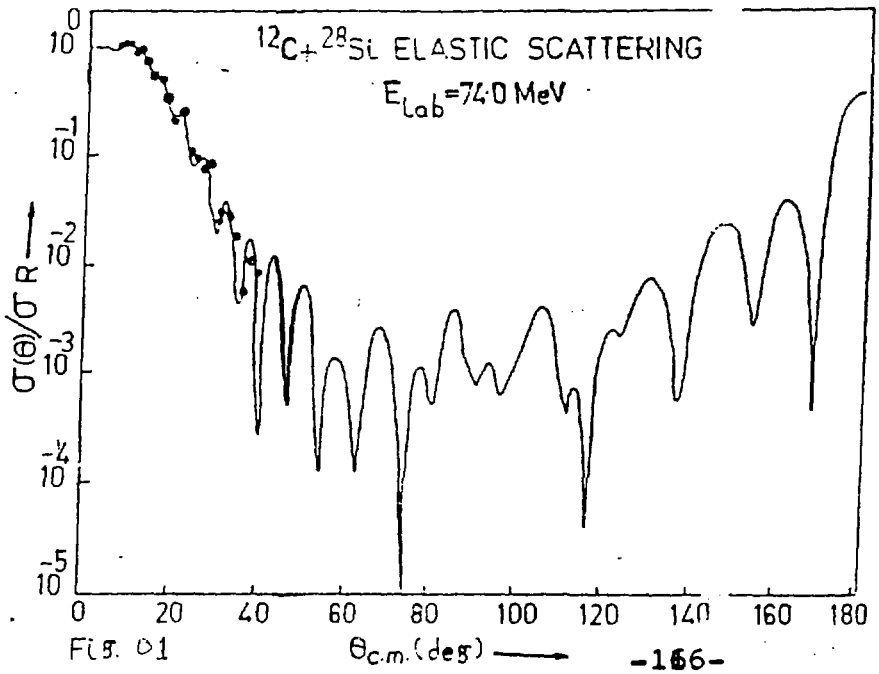

Fig. 01

NUCLEAR FORWARD GLORY IN $^{16}O + ^{16}O$ SCATTERING

Rajendra Prasad, A. Ostrowski* and H. Voit*
Applied Physics Department, Z.H.College of Engg. and Technology, A.M.U. Aligarh, 202002
*Tandem Laboratory, Physicalisches Institüt der Universität Erlangen-Nürnberg, D-8520 Erlangen, FRG

Glory scattering is a well known optical phenomenon and is also expected in atom-atom and nucleus-nucleus collision. The forward glory is characterised by the enhancement of cross sections at forward angles. It was predicted to exist in heavy ion interactions[1-3] and first experimental evidence was given by Ostrovski etal.[4] in $^{12}C + ^{12}C$ scattering. The existence of forward nuclear glory is strongly related to the ability of determination of nuclear scattering amplitude $f_N(\theta)$ at small scattering angle θ. $f_N(\theta)$ exhibits an undulating envelope at forward angles. Moreover a large value of $|f_N(\theta)|$ as compared to total cross section is expected. General Optical Theorem (GOT) for charged particles can provide model independent determination of $f_N(\theta)$ if the sufficient accurate experimental data at very forward angles are obtained.

The measurable quantity $\sigma_{SOD}(\theta)$, called as sum of difference cross section for identical particles is given as[2,3]

$$\sigma_{SOD}(\theta) = \sigma_R - (4\pi/k)\,|\hat{f}_N(\theta)|\,[\sin\hat{\phi}_N(\theta) - 2\sigma_0] + 2\cos(\hat{\phi}_N(\theta) - 2\sigma_0 + \eta \ln\tfrac{1}{2}\theta) \times \sin(\eta \ln\tan\tfrac{1}{2}\theta) \quad \ldots (1)$$

with $|\hat{f}_N(\theta)|\exp[i\hat{\phi}_N(\theta)] = f_N(\theta) - f_N(\pi-\theta)$ being the symmetrized nuclear scattering amplitude. σ_0 and η are the s-wave Coulomb phase shift and the Sommerfield parameter respectively. The term $C(\theta)$ becomes negligibly small θ values[5,6]. For $\theta \to 0$ equation becomes

$$\sigma_{SOD}(\theta) = \sigma_R - (4\pi/k)\,|\hat{f}_N(0)| \times \sin(\hat{\phi}_N(0) - 2\sigma_0 + 2\eta \sin\tfrac{1}{2}\theta) \quad \ldots (2)$$

In this case σ_{SOD} oscillates with constant amplitude $(4\pi/k)\,|\hat{f}_N(0)|$ symmetrically with respect to σ_R.

Fig. 1 shows $\sigma_{SOD}(\theta)$ for $^{16}O + ^{16}O$ system at E(CM) =16 MeV calculated by eq. 2 by means of a synthetic $^{16}O + ^{16}O$ angular distribution which was generated with nuclear phases from the phase shift analyses of $^{16}O + ^{16}O$ data at E(CM) = 16 MeV in the angular range θ(CM) = 30-90°. The oscillations predicted by eq.2 occurs symmetrically with respect to σ_R for angles less than 3°. It also shows that measurements should be made in small angular steps.

The glory experiment was performed with the ^{16}O beam from EN tandem accelerator at Erlangen, W.Germany. The main feature of specially designed experimental set

up is the large distance (145cm) between target and detector which enables the measurements at very small angles and in small angular increments. The detector used is a position sensitive proportional counter consisting of U shaped cathode in which a resistive wire (62cm long, 7.5μm dia. and 12 Ωm^{-1} sp. resistence) is spanned. The slit system of movable frame consisting of 36 very precise slits made through electron beam erosion was mounted in front of the detector. The angular distance between subsequent slits is 0.4^{o}. With such a set-upan angular distribution could be measured between θ(lab) = 1.4 and 17^{o} in 68 angular steps of 0.2^{o} in two runs. Isobutan gas is filled in the detector at 40 torr. The detector chamber is separated from the scattering chamber by a 66X1.6 cm^2 window covered with a 1.5 μm thick mylar foil. The target used was a gas target and also specially made thin target(≈ 10 $\mu g/cm^2$) of Al_2O_3.

Fig. 2 shows σ_{SoD} as obtained from the experimental data for E(CM) = 16 MeV. It exhibits pronounced oscillations which occur with almost constant amplitude in the most forward angular range. The oscillations are very similar to those showing up in σ_{SoD} resulting from synthetic elastic scattering data.

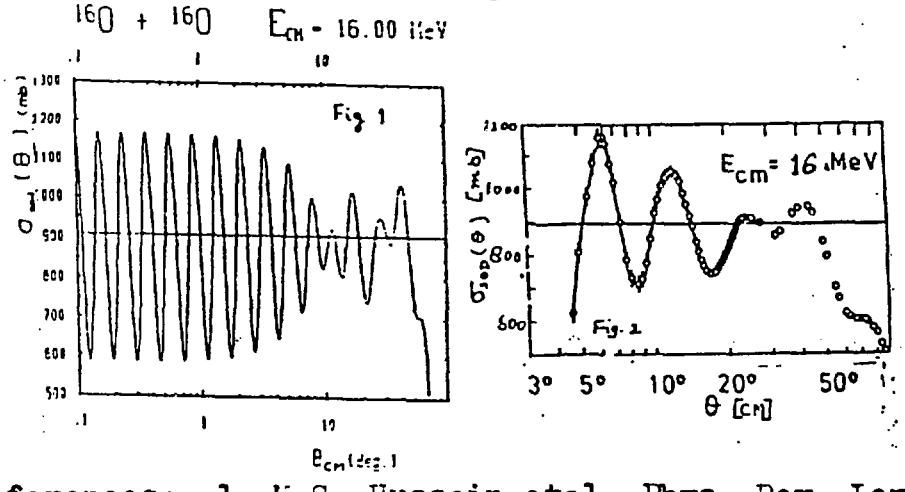

References:- 1. M.S. Hussain etal., Phys. Rev. Lett. 52(1984)511.
2. J. Barrette and N. Alamanos, Nucl. Phys.A 441(1985)511.
3. W. Tiereth etal., Nucl. Phys. A 464(1987)125.
4. A. Ostrowski etal., Phys. Lett. B232(1989)46.
5. C. Marty, Z.Phys. A309(1983) 261.
6. R. Lipprheide, Nucl. Phys. A469(1987)190.

EXCITATION FUNCTION AT $\theta_{cm} = 90°$ FOR $^{24}Mg(^{24}Mg,^{24}Mg)^{24}Mg$

Ashok Kumar, K. Eswaraiah, Madhup Seth, Ravi Datt Godiyal, S.R. Verma, *R.C. Misra and **B.B. Srivastava, D.B.S. (P.G.) College, Dehra Dun, *V.S.S.D. College, Kanpur, **Meerut University, Meerut.

A full scale microscopic calculation of the excitation function for 24Mg(24Mg,24Mg)24Mg at 90° is rather impractical due to large number of nucleons involved, deformed shape of 24Mg and absorption effect. Hence, in the present investigation a simple microscopic method that accounts for these features in a good approximation has been applied to calculate the excitation function for 24Mg-24Mg elastic scattering at energies above the coulomb barrier. Here, one starts with scattering amplitude, $f(\theta)$, as

$$f(\theta) = f_C(\theta) + f_N(\theta) \qquad (1)$$

where, $f_C(\theta)$ is the Coulomb scattering amplitude and $f_N(\theta)$ is the nuclear scattering amplitude containing both Coulomb and nuclear phase shifts. The Coulomb shifts are computed by familiar technique. The significant nuclear phase shifts corresponding to l=0 to l_{max} are computed by the numerical solution of the partial wave differential equation neglecting the exchange effects. The differential equation requires the effective potential which consists of complex nuclear potential, the Coulomb potential and the centrifugal potential. It is resonable to conceive a simple picture of the complex nuclear potential as /1/.

$$V_N(R) = \lambda_R V_R(R) + i \lambda_I V_R(R) \qquad (2)$$

where, λ_R and λ_I are the dimensionless strength parameters and their values are selected for different energies. The shape of the imaginary potential is taken to be the same as that of real potential. To make calculation simple λ_R is chosen to 1 and only λ_I is varied. The real nuclear poten-

tial $V_R(R)$ is taken to be the direct potential of the single channel Resonating Group Method (RGM) and is microscopically evaluated by double folding method as described in Refs. /2,3/. The exchange mixture parameter 'u' which appears in nucleon-nucleon potential is varied around 1 and adjusted to a value 0.8 in the present calculation for getting best possible results. All the parameters used are compiled in the Table. The ideal situation of getting parameter-free potentials is not yet reached but it is encouraging to have free parameters only two. In the figure, the excitation function σ_E is calculated at 90° for five energies (hollow big circles) compared with the experimental data (solid circles) /4/. The agreement is fairly good thus demonstrating the utility of the present simple theory.

References

/1/ V.K. Bhatnagar, Doctoral Thesis, Garhwal University, (1988) (unpublished).

/2/ Ashok Kumar et al, Int. Symp. on Structure and Reactions of unstable Nuclei, Niigata, Japan, (1991) 40.

/3/ Ashok Kumar et al, DAE Symp. on Nucl. Phys. (India) (1991) (communicated).

/4/ H. Emling et al. Nucl. Phys. A239 (1975) 172.

TABLE

E_{cm} (MeV)	λ_R	u	λ_I	l_{max}
22.5	1	0.8	0.20	24
25.0	1	0.8	0.50	30
27.5	1	0.8	0.25	34
30.0	1	0.8	0.50	38
33.0	1	0.6	0.66	42

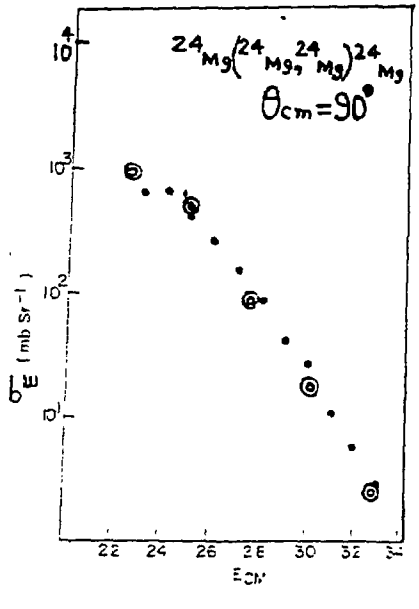

MICROSCOPIC NUCLEAR POTENTIAL FOR $^{16}O+^{24}Mg$ SYSTEM

Ashok Kumar, Madhup Seth, K. Eswaraiah, Ravi Datt Godiyal, P.K. Bhatnagar and *Sunita Kumar, D.B.S. (P.G.) College, *M.K.P. (P.G.) College, Dehra Dun.

Experimental cross sections for Heavy-ion collisions are generally analysed on the basis of phenomenological potentials, in which many parameters are adjusted by the comparison between calculation and experiment. However, the experimental data do not determine this type of potential uniquely and also it contains no theoretical foundation for the potential shape. Beyond these models there are a number of microscopic descriptions, which are based on a realistic or effective nucleon-nucleon interaction and on the structures of the nuclei involved. In these models, many-body Schrödinger equation leads to a highly non-local, energy dependent and non-Hermitean nucleus-nucleus potential and calculations become impractical when absorptive part is also included. Hence, a simplified microscopic method is desirable. One such approach is the Resonating Group Method (RGM) /1/. In the RGM a system of two fragment ions or 'clusters' is described by a completely antisymmetrized many-nucleon wave function,

$$\Psi = \tilde{A}[\phi_1(\xi_1)\ \phi_2(\xi_2)\ \phi(x)] \qquad (1)$$

The internal states of the ions are described by the internally antisymmetrized wave functions ϕ_1, ϕ_2 which depend on the translationally invariant internal coordinates ξ_1, ξ_2 respectively. The wave function ϕ of the relative motion depends on the separation x of the centre-of-mass of the ions. The operator $\tilde{A}$ is the rest-antisymmetrizer which takes into account all possibilities of exchange nucleons between the two ions. The Hamiltonian of the RGM consists of a simple direct part H_d and a complicated exchange part H_{ex}. The direct part contains the kinetic energy of relative motion T_{rel} and a direct real potential $V_d(R)$ which for a local nucleon-nucleon potential, is local and identical to the folding potential $V_R(R)$ given by,

$$V_R(R) = \left\langle \phi_1(\xi_1)\ \phi_2(\xi_2) \left| \sum_{\substack{i\in 1 \\ j\in 1}} V_{ij} \right| \phi_1(\xi_1)\ \phi_2(\xi_2) \right\rangle_{R} \quad (2)$$

The equivalence relation between RGM and generator coordinate method (GCM) is used for solving Eq.(2) /2/. Here ^{16}O ion is a doublly magic while ^{24}Mg is deformed. The natural dynamical generalization of the filling approximation is used by considering 2/5 magnitude of the unfilled 1d shell of ^{24}Mg to make it spherically symmetric /3/. Using eq. (2), the microscopic nuclear potential for $^{16}O+^{24}Mg$ is analytically calculated and computed as shown in figure. This RGM folding potential is quite deep at small separations and decreases fast as desired /4/. Thus, it avoids the ambiquities of the assumed form and it is expected to work satisfactorily for explaining the elastic scattering data as evident from Ref. /5/.

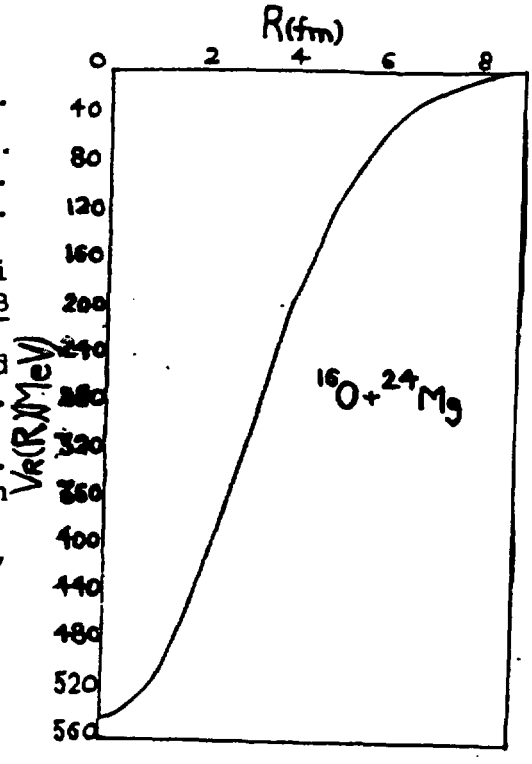

References

/1/ H. Friedrich, Phys. Rep. 74(2) (1981) 209.

/2/ Ashok Kumar and B.B. Srivastava, Can, J. Phys. 66 (1988) 813.

/3/ V. Maruhn - Rezwani et al, Phys. Lett 67B (1977) 134.

/4/ G.R. Satchler and W.G. Love, Phys. Rep. 53 (1979) 183.

/5/ Ashok Kumar et al. Fourth Int. Conf. on Nucleus-Nucleus-Collisions, Kanazawa, Japan, (1991) 155.

STUDY OF EXCITATION ENERGY IN VARIOUS FORMS OF NN INTERACTION

R.C.Mishra, Ashok Kumar Sharma and *Ashok Kumar
Deptt. of Physics, V.S.S.D. College, Kanpur-208 002
* Deptt. of Physics, D.B.S. College, Dehradun-248 001

We made a comparative study of variation of excitation energy at the various instants of collision event for various forms of NN interaction in case of $^{12}C + ^{12}C$ reaction. The two forms of NN interaction are obtained by putting m = 1 and m = 2 in the following relation, /1/

$$V_{ij}^{(N)} = - V_e \left(1 - \frac{C}{r_{ij}} \right) \exp - \left(\frac{r_{ij}}{r_e} \right)^2$$

In the above expression, V_e, C and r_e are the depth parameter, repulsive core radius and range parameter of NN interaction.

The form of NN interaction changes by changing the value of m. The above potential becomes highly repulsive for internucleon distances which are less than C. Parameters of the choosen form of NN interaction are adjusted so as to reproduce the experimental binding energy and rms radius of ^{12}C nucleus /2/. Table below shows the values of parameters and calculated binding energy and rms radius for the two choosen forms of NN interaction.

The colliding systems($^{12}C + ^{12}C$) are fired from a distance where the nuclear interaction is completely ineffective with given value of bombarding energy and angular momentum. The motion of each pair of nucleons is controlled by Newton's equation of motion. In this classical microscopic approach each nucleon is taken as a classical spinless point particle and zero point motion is not taken into account /3/. The colliding nuclei in the centre of mass frame are bombarded with E_{cm} = 28.20 MeV. The peak of fusion cross section curve is obtained at this energy. The impact parameter responsible for fusion determines the value of initial angular momentum. The value of impact parameter in both the cases of NN potential is 5.2 fm.

The excitation energy at any instant is calculated by substracting the energy of the centre of mass of the system in the total kinetic energy given to the system. The difference of energy goes for exciting the nucleons. The excitation energy is calculated from the initial stage i.e. when the nuclei were bombarded upto fusion event at the regular interval of one NS (10^{-23} sec.). The results are shown in the figure. In case of m = 1 NN interaction the nuclei are not in excited state upto T = 5 NS but they are highly excited at T = 8 NS. Oscillatory nature of excitation energy reveals that the nucleons are in the chaotic state. The peak of excitation is observed at T = 22 NS. For m = 2 NN interaction the excitation of nucleons starts from the very beginning of the collision event. The peak of excitation in this case is obtained at T = 26 NS. The oscillatory nature of excitation curve starts from T = 3 NS and it continues till fusion.

Acknowledgement : One of us (RCM) is thankful to UGC, New Delhi and D.A.E., Govt. of India for providing financial assistance to carry this work.

Table 1

M	V_o (MeV)	C (fm)	r_o (fm)	Calculated - BE (MeV)	Calculated RMSR (fm)	Experimental - BE (MeV)	Experimental RMSR (fm)
1	38.2×10^5	2.10	0.2	92.695	2.370	92.16	2.460
2	10500	2.145	1.0	91.52	2.476		

References :

/1/ H.S. Koehler and Y.R.Waghmare, Nucl. Phys. 66 (1965) 261: Y.R.waghmare, Phys. Rev. B136 (1964), 1261.
/2/ R.C.Mishra & Y.R.Waghmare Proc ICNRM 1989, SINP Calcutta.
/3/ S.S.Godre & Y.R.Waghmare, Phys. Rev. C36 (1987) 1632.

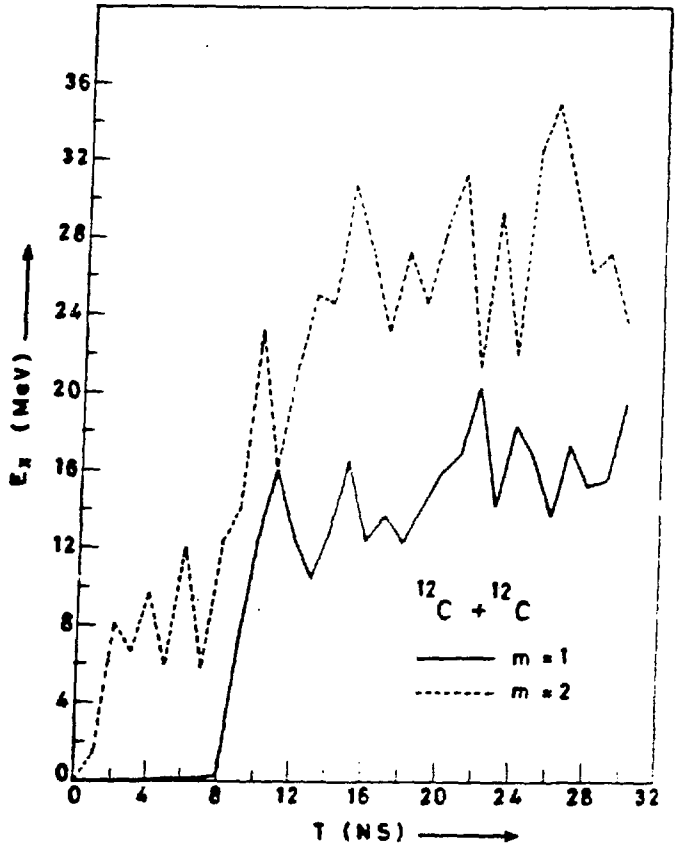

STUDY OF ANGULAR MOMENTUM IN FUSION REACTIONS

R.C.Mishra, A.K.Sharma & *A.Kumar
Deptt. of Physics, V.S.S.D. College, Kanpur-208 002
*Deptt. of Physics, D.B.S. College, Dehradun-248 001.

In peripheral collisions, angular momentum is the important parameter. We made a comparative study on the variation of angular momentum with respect to collision time for two different cases of NN interaction. The light mass heavy-ion system $^{12}C + ^{12}C$ is choosen for the above study. The NN interactions are obtained by changing the value of parameter m in the following relation /1/,

$$V_{ij}^{(N)} = -V_0 \left(1 - \frac{C}{r_{ij}}\right) \exp - \left(\frac{r_{ij}}{r_0}\right)^m$$

We have choosen m = 1 and 2 for our study. For m = 1 (M1 form) the tail of NN interaction is of exponential nature and for m = 2 (M2 form) it is of gaussian nature. Parameters V_0, C and r_0 are adjusted to reproduce the binding energy and rms radius of ^{12}C nucleus in the ground state, very close to experimental value for each form of NN interaction /2/. Table given elsewhere /3/ shows the values of binding energy and rms radius.

$^{12}C + ^{12}C$ nuclei placed in centre of mass frame are initially bombarded with Ecm = 28.20 MeV and a given value of angular momentum (impact parameter). The corresponding value of velocity of nucleons is 1.5 fm/NS. There are three initial parameters given to the colliding nuclei. These are energy (velocity), impact parameter and initial relative random orientation of the colliding nuclei. All the three parameters remain same for the choosen forms of NN interaction. Therefore, starting with the same initial conditions we calculate angular momentum at different instants (NS) of collision event for the choosen form of NN interaction. The velocity and position of individual nucleons is calculated at the end of every NS. This calculation is made in classical equation of motion approach /2/.

In CEOM appraoch necleons are treated as classical spinless particles interacting via suitable two body potential. The angular momentum is calculated with the above calculated values of velocity and position of individual nucleons.

Results : In the figure angular momentum of one of the colliding nuclei is plotted at the various instants of collision event. For both the potentials the value of angular momentum is same from T = 0 NS to T = 6 NS. M2 form of potential shows peak and dip of angular momentum curve at T = 18 NS and 21 NS respectively while the behaviour of M1 form of potential is vice versa. Moreover peak and dip are not so prevalent in this form of potential. The nature of angular momentum curves is oscillatory in both cases of NN interaction during 6th. and 30th. NS.

References : /1/ H.S.Koehler and Y.R.Waghmare, Nucl. Phys. 66 (1965) 261;. Y.R.Waghrare, Phys. Rev. B136 (1964), 1261.
/2/ R.C.Mishra and Y.R.Waghmare, Proc. ICDR 1989, Banglore University.
/3/ R.C.Mishra, A.K.Sharma & A.KUmar, the other paper submitted to D.A.E. Sympo 1991.

Acknowledgements : One of us (PCM) is thankful to UGC, New Delhi and D.A.E., Govt. of India for the financial help provided for the above work.

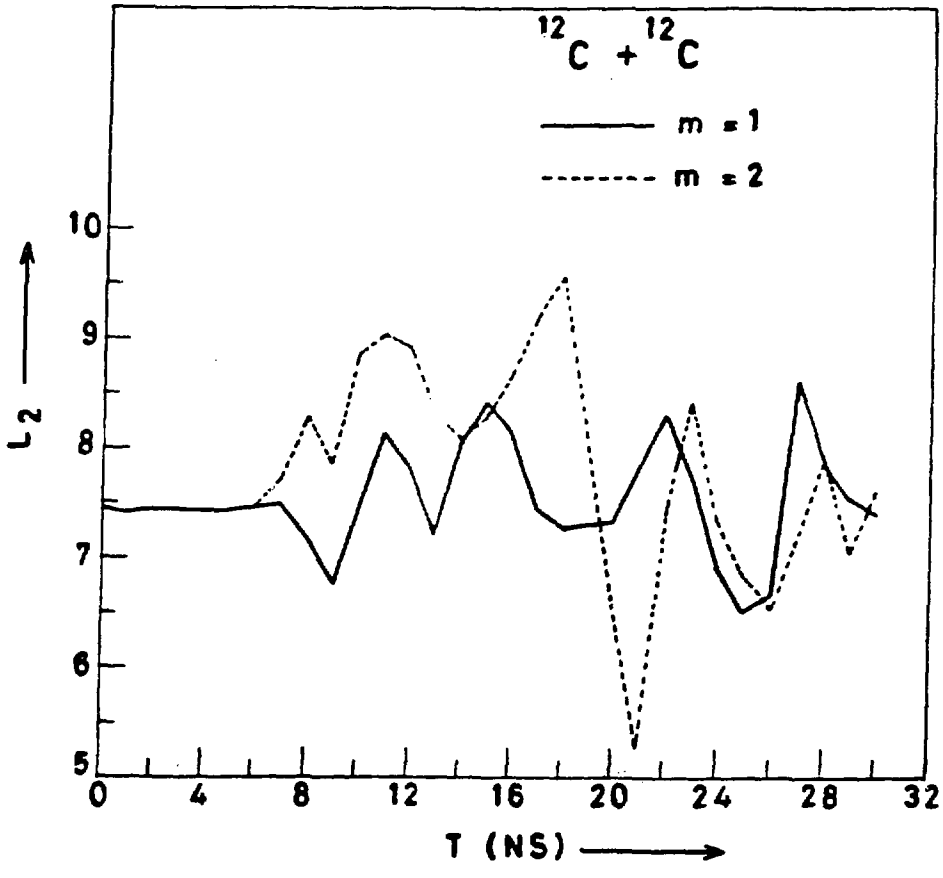

GAMMA RAY EMISSION IN HEAVY ION REACTIONS - EXPERIMENTAL SEARCH FOR ENTRANCE CHANNEL EFFECTS

S.P.Das,S.Sen,M.Satpathy,S.Jena,Utkal University,Bhubaneswar.
G.V.Raviprasad,R.K.Yadav,L.Satpathy,V.S.Ramamurthy
Institue of Physics, Bhubaneswar.
D.Kataria,N.Madhavan,A.Roy,A.Sinha,S.Dutta
Nuclear Science Centre,NewDelhi.

Recent experiments [1,2] on gamma ray spectra in the energy region 8-12 MeV and neutron multiplicities in heavy ion induced fission reactions indicate an enhanced emission of GDR gamma rays from the fused composite nucleus and prefission neutrons over the predictions of the standard statistical model of the decay of excited compound nuclei. These have been interpreted in terms of a retardation of the fission process in relation to the other competing decay modes of the compound nucleus. Weidenmuller and collaborators[3] have shown that the presence of friction in the nuclear collective dynamics during the passage over the fission barrier results in an apparent retardation of fission decay. On the otherhand, Ramamurthy[4] has recently argued that, in heavy ion fusion reactions, since there is a long dynamical path between capture of the projectile by the target and compound nucleus formation, the enhanced GDR gamma ray emission from the fused composite system and prefission neutron emission could indeed be signatures of the entrance channel dynamical details of the fusion process. It would therefore be very interesting and important to establish experimentally whether these enhanced emissions of GDR gamma rays and prefission neutrons arise due to the post-compound nucleus or the pre-compound nucleus dynamics. Ramamurthy has also proposed that for a direct experimental test of whether a measurement carries a signature of the entrance channel dynamics, one should make a study of its dependence on the entrance channel mass/charge asymmetry across the Businaro-Gallone critical asymmetry since the fusion dynamics is expected to change abruptly across this point. The importance of entrance channel dynamics on the fragment angular distributions in heavy ion induced fission reactions has already been established recently[5]. We have therefore

carried out a measurement of the gamma ray energy spectra in fission induced by ^{12}C and ^{16}O on ^{209}Bi target.

Carbon and Oxygen beams from the 15UD Pelletron accelerator of the Nuclear Science Centre, NewDelhi was used to bombard self-supporting bismuth targets.Gamma rays in the energy interval 3-20 MeV were detected using a 5"x5" **NaI(Tl)** detector placed at distance of about 80 cm from the target. Time of flight method was used to eliminate neutrons with the zero time obtained from the RF pick up of the beam pulsing system. Unlike the earlier measurements, no fission detection was included since fission is the predominant decay channel in the reactions studied here. Electronic pileup rejection was also incorporated in the experiment. The measured spectra exhibit the well known exponential fall off characteristic of statistical gamma rays below 8 MeV and the GDR bump from fragment emission around 14 MeV. Deviation from an exponential around 8MeV is also visible in the spectra. Detailed analysis of the spectra are in progress to extablish whether there is an entrance channel dependence as expected around 8-12 MeV characteristic of GDR emission from the fused composite system.

References

1. M.Thoennessen et al, Phys. Rev.Lett.59(1987)2860
2. A.Gavron et al, Phys. Rev.C35(1987)579
3. H.A.Weidenmuller, Prog. in Part. and Nucl. Phys.3(1980) P.Grange et al Phys. Rev.C27(1983)2063
4. V.S.Ramamurthy, Int.Conf.on NUclear Reaction Mechanism, Calcutta,World Scientific 1989
5. V.S.Ramamurthy et al, Phys.Rev.Lett.65(1990)25

A SOLVABLE POTENTIAL AND A NEW PENETRABILITY FORMULA FOR NUCLEUS-NUCLEUS FUSION

Zafar Ahmed, Nuclear Physics Division, BARC, Bombay-85

In the calculation of the nucleus-nucleus fusion rates, as per the one-dimensional barrier penetration method (1D-BPM), we suggest that the standard fusion barriers which are generally expressible as (D_1 is left free; c_1 and c_2 are to be taken from ref.[1], $b=1.333fm^{-1}$)

$$V_l(r)=Z_1Z_2e^2/r + \hbar^2 l(l+1)/(2mr^2)+Dc\exp[b(c_1+c_2-r)] \quad (1)$$

should be parametrized using a solvable barrier

$$V_l(r)=V_1[1-[(1-\exp(x))/(1-C_1\exp(x))]^2] \quad (2)$$

where $x=(R_1-r)/[d_1(1-C_1)]$, $\hbar^2/(2md_1^2)=(\hbar\omega_1)^2/4V_1$. Note that the relevant parameters are: V_1, $\hbar\omega_1$ and C_1. Figs.1 and 2 show the close fits of the fusion barriers for several partial-waves, for $^{16}O+^{13}C$ and $\alpha+^{238}U$, respectively. Fig.(3) shows the fits of s-wave barriers for the heavier ($^{58}Ni+^{58}Ni$, $^{16}O+^{208}Pb$) systems. In fig. 3 dots are due to the actual potential(1), solid lines are due to eq.(2) and the dashed lines are the parabolic fit.

Recently [2], using the exact and the WKB penetrability of another branch of the potential barrier (2), we have analytically demonstrated that the barrier penetration in nucleus-nucleus fusion is inherently and fairly a semi-classical event. The potential barrier (2) entails a singularity at negative energies, however, it being away from the turning points allows a legitimate use of the WKB approximation; denoting $B_1=1/C_1$, $\epsilon_1=\mathrm{sgn}(C_1-1)$ and $\Delta_1=(\hbar\omega_1)^2(1-C_1)^2/(4V_1)$, we get $T_l(E)=[1+\exp(2\pi\epsilon_1K_1)]^{-1}$, where

$$K_1=[\sqrt{(E/\Delta_1)}-\sqrt{[E/\Delta_1+(B_1^2-1)V_1/\Delta_1]}+(B_1-1)\sqrt{(V_1/\Delta_1)}] \quad (3)$$

Fig.4 displays the s-wave penetrability for $^{16}O+^{13}C$ and $^{16}O+^{208}Pb$, using HW, WKB (employing (1)) and the present formula (3). The good agreement between solid and dashed line indicates the goodness of our parametrization of the fusion barriers. We have calculated the fusion rates for $^{16}O+^{13}C$(fig.5), $\alpha+^{238}U$(fig.6), $^{16}O+^{208}Pb$ and $^{58}Ni+^{58}Ni$, and observed that when $\xi(1/\sqrt{MeV})=\sqrt{V_0}/\hbar\omega_0$ is less than unity or close to it the present formula renders true 1D-BPM estimates(solid line) which agree well with the experimental data (circles)[3,4]. The squares in these figures denote the numerical subbarrier-WKB results using the actual potential(1). The instances where ξ deviates much from unity ($^{16}O+^{208}Pb$ $\xi=1.90$; $^{58}Ni+^{58}Ni$ $\xi=2.52$) all the three methods yield similar results indicating the genuine failure of the rationale of 1D-BPM. Further, it is interesting to note the WKB-tunnelling time of the present barrier

$$\tau(E)=[2\pi\hbar\xi/(\sqrt{E}(1-C_0))][1-[1-(B_0^2-1)V_0/E]^{-1}] \quad (4)$$

indicates that the subbarier tunnelling is slower than that of over the barrier tunnelling. Larger the value of ξ slower will be the tunnelling, whereupon the other degrees of freedom are required and the 1D-BPM fails.

REFERENCES:[1]-J.Blocki et al. Ann.Phys.105 (1977) 427,[2]-Z.Ahmed (1991) to be submitted to Phys.Rev.C,[3]-B.Dasmahapatra et al. Nucl. Phys. A394 (1983) 301,[4]-H.Friesleben and J.R.Huizenga Nucl.Phys. A224 (1974) 503.

I am grateful to Dr.S.K.Kataria for suggesting the problem.

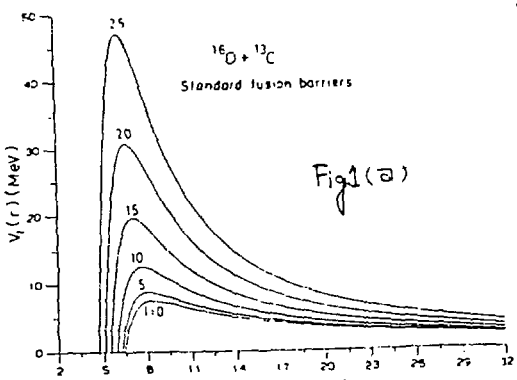

Fig 1(a)

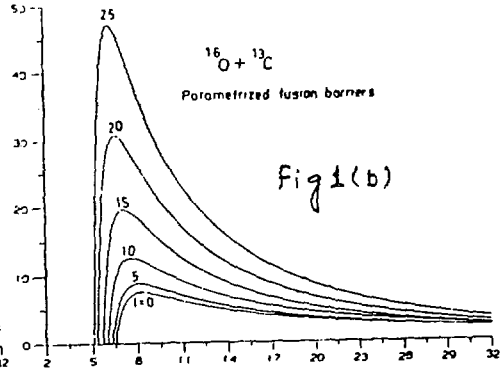

Fig 1(b)

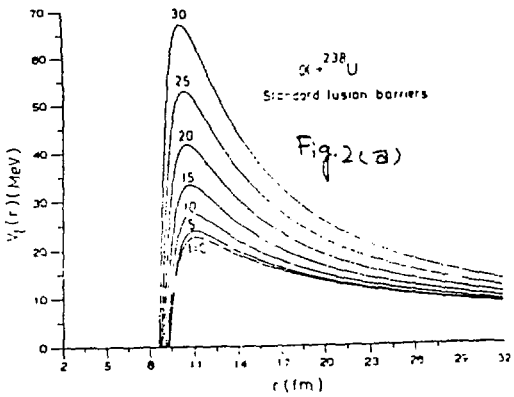

Fig 2(a)

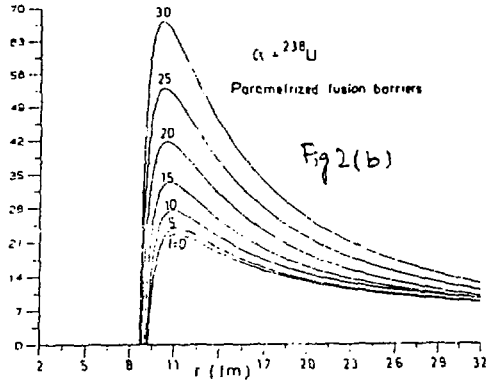

Fig 2(b)

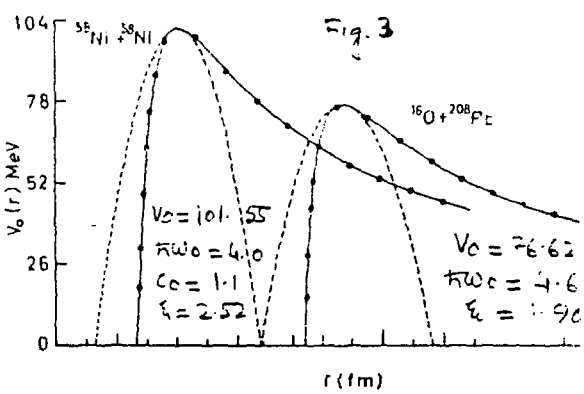

Fig. 3

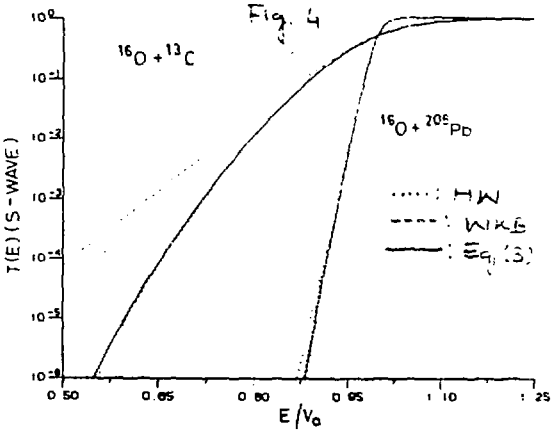

Fig. 4

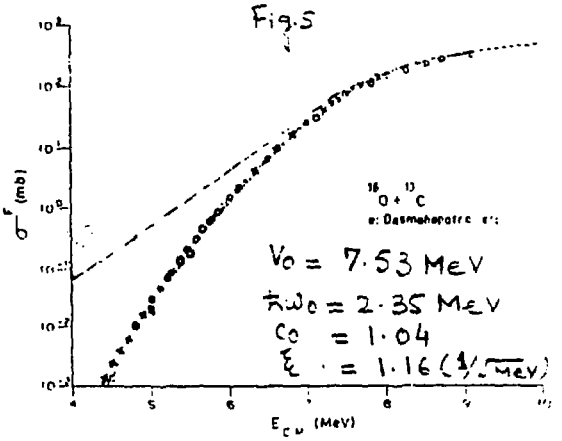

Fig.5

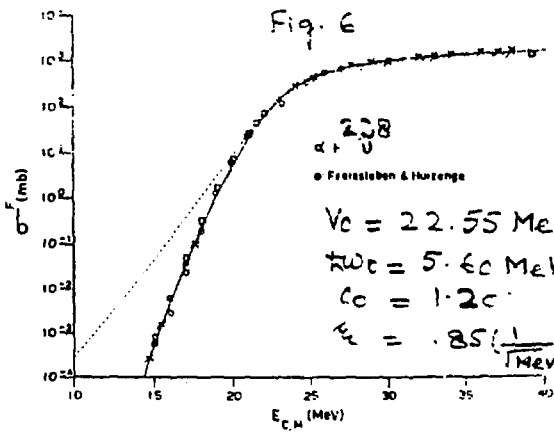

Fig. 6

ADIABATIC AND SUDDEN LIMIT APPROXIMATION TO HEAVY ION FUSION POTENTIAL.

S.V.S. Sastry, A.K.Mohanty and S.K.Kataria.
Nuclear Physics Division, B.A.R.C., Bombay 400085.

Fusion excitation functions of two heavy ions and compound nucleus spin distributions are not yet understood fully inspite of extensive work in this field . Various models have been used to understand the enhancement of fusion cross-sections and broadening of spin distributions at energies near and below the coulomb barrier. It is seen that, when energy approaches the coulomb barrier, other degrees of freedom such as coupling to various low lying levels as well as nucleon transfers or neck formation become quite important in giving rise to sub-barrier fusion enhancement. However, a common feature of all these processes is that the fusing system finds an energy dependent barrier. In order to reproduce both fusion cross section and the compound nucleus spin distribution, we have proposed [1] a modified BPM where the fusion barrier depends on the effective kinetic energy (which is defined as $\epsilon = E - E_R$ where E_R is the rotational energy at the interaction barrier R_B) rather than on E alone. Therefore, we parametrise fusion barrier in a simple way as follows:

$$\begin{aligned} &\text{if } \epsilon > E_2 && \text{then } V_0 = V_2 \\ &\text{if } E_1 \leq \epsilon \leq E_2 && \text{then } V_0 = \beta\epsilon + C \\ &\text{if } \epsilon < E_1 && \text{then } V_0 = V_1 \end{aligned}$$

When ϵ is high enough, the fusing system does not have much time for any nucleon rearrangements and it passes through a sudden barrier. In the 2nd case, the barrier height linearly depends on ϵ. In the third case, ϵ is low enough to allow full relaxation of all degrees of freedom and the system sees the lower limit of the barrier also known as the adiabatic limit. Using this simple model, we have fitted fusion cross-section for several systems and derived average spin values <l>. Out of six parameters, V_1, V_2, E_1, and E_2 , R_B and $\hbar\omega$, we choose V_2 , R_B and $\hbar\omega$ from proximity potential. We have varied remaining three parameters V_1 , E_1 and E_2 to get best fits to fusion cross-sections. We have observed that V_1 and E_1 has a nice linear relationship given by $E_1 = .98\ V_1 - .11$. The adiabatic potential V_1 , can be fixed by fitting deep sub barrier cross

sections. We have also seen that E_2 has linear dependence on V_2 . Although this helps as a guide line to choose E_2 , we have chosen it as a free parameter for obtaining best fit to the experimental data. Using the χ minimisation procedure we have fitted fusion excitation function for 20 H.I. systems in the mass range 20<A<240. The systematics of adiabatic barrier V_1 shows a linear dependence on $Z_1 Z_2$ parameter and also has significant shell-structure effects.

Fig.1, shows a plot of the difference $\Delta V=(V_2 - V_1)$ versus $Z_1 Z_2$ parameter. As can be seen, the ΔV is large for heavier system, where the subbarrier enhancement is rather large. In fig. 2, we have shown a plot of ratio of <l> values calculated using 1dimensional BPM and the present model results as a function of $(E - V_0)$ for Ni+Mo system. In the vicinity of the coulomb barrier, this quantity shows a well developed peak, implying that average <l> in our model enhanced strongly in the narrow energy region, and in agreement with general trends in the experimental data. This can be interpreted as the manifestation of threshhold anomaly (TA) in spin distribution like the TA which is seen in elastic scattering analysis where the real nuclear potential becomes more attractive at the coulomb barrier.

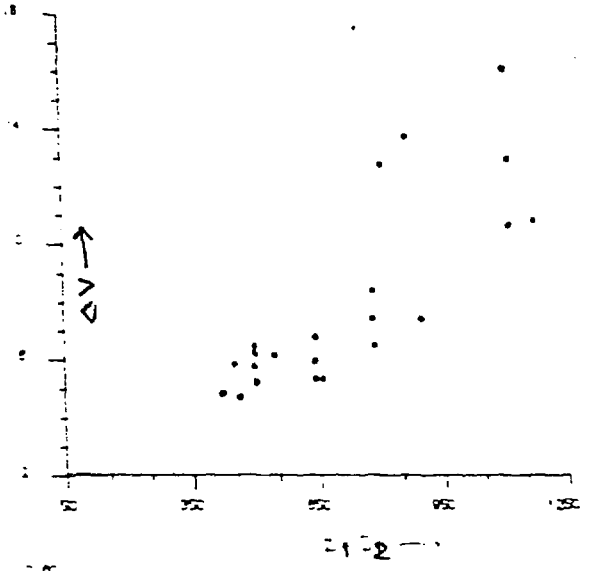

FIG 1

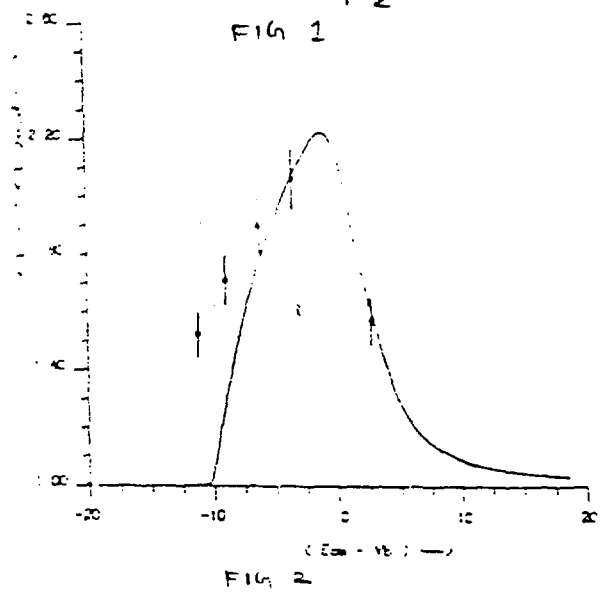

FIG 2

1. A. K. Mohanty et. al. Phys. Rev. Lett. V65 (1990) 1096.

USE OF POLARISATION POTENTIAL IN BARRIER PENETRATION MODEL FOR HEAVY ION FUSION.

A.K.Mohanty and S.K.Kataria.
Nuclear Physics Division, BARC, Bombay 400085

Fusion cross-sections and spin distributions have been studied for $^{32}S+ ^{64}Ni$ system in the framework of a new barrier penetration model(BPM) including the contribution of dynamical polarisation potential. The significant contribution of the polarisation potential at the vicinity of the coulomb barrier energy V_0(known as thereshold anomaly) has been well recognised in recent studies [1]. In the BPM studies, this polarisation potential ΔV is added to fusion barrier height V_0 to get correct fusion cross-section. The ΔV can be obtained from the energy dependence of the imaginary potential by use of dispersion relation. So ΔV can be written as

$$\Delta V(E,r) = \Delta V(E) f(r)$$

where the radial dependence of the polarisation potential f(r) has the same radial dependence as that of imaginary potential. It has been realised that in order to reproduce both fusion cross-section and spin distribution, it is necessary to include both energy as well as radial dependence of the polarisation potential. Recently Satchler et. al.[2] has shown that large <l> value can be obtained by taking f(r) as the derivative of Wood-Saxon form in optical model calculation. We have tried to get the same effect in BPM model using $\Delta V(E,r)$ where the radial dependence has the surface peaked form which is an extreme limit. However, we do not find much improvement in spin distribution.

In our earlier study of $^{16}O+^{208}Pb$ system using Optical Model for H.I. fusion[3], we had proposed that the strength of imaginary potential W, should be written in terms of available kinetic energy ϵ in the relative separation co-ordinate. As a result of this new appraoch the polarisation potential ΔV also becomes a function of energy ϵ in place of the beam energy E as is generally used in the literature. In the present work, we have carried out B.P.M.calculations using W.K.B. approximation for barrier penetration model for $^{32}S + ^{64}Ni$ system for which experimental data on elastic scattering, fusion excitation function and average spin values have been measured. BPM calculations for fusion excitation function and average spin values <l> were carried out for the following cases:

i) Using bare fusion barrier V_0

ii) Using $V_0 + \Delta V(E, R_B)$ where $\Delta V(E, R_B)$ is the Polarisation Contribution obtained from elastic scattering analysis at given R_B and E.

iii) Using $V_0 + \Delta V(\epsilon, R_B)$ where $\Delta V(\epsilon, R_B)$ is the polarisation contribution obtained from $W(\epsilon, R_B)$.

Fig.1. shows the plot of <l> versus E for the three cases along with experimental data. As can be seen from the figure, only case III results are in agreement with experimental data where we calculated the E and l-dependent polarisation potential ΔV in terms of effective energy ϵ in the radial separation co-ordinate. The r-dependence of $\Delta V(E,R)$ as suggested earlier is rather too weak to fit the l-values for $^{32}S + ^{64}Ni$ system. The C.C-calculations l-distribution of fusion cross-sections are also well reproduced by case III. Therefore, it can be concluded that BPM calculations are best carried out using polarisation component which are E and l dependent.

1. G. R. Satchler, Phys. Reports 199 (1991) 147
2. G. R. Satchler et. al. Phys. Rev. C 41 (1990) 1869.
3. A. K. Mohanty et al. Phys. Lett. B 247 (1990) 215.

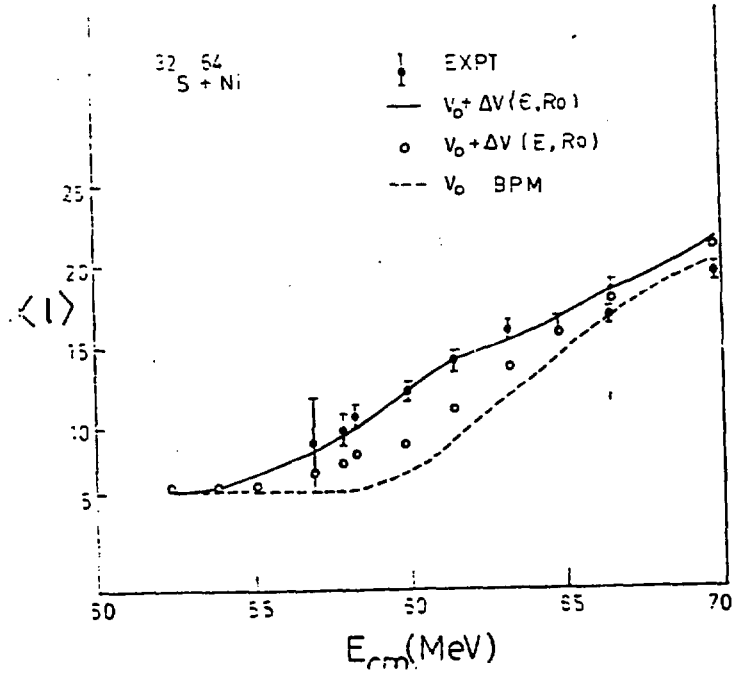

Heavy Ion Fusion at Near- and sub-barrier energies

S.Kailas
Nuclear Physics Division, B.A.R.C., Bombay 400 085

Several models have been proposed to explain heavy ion fusion at near- and sub-barrier energies/1/. In Stelson's method /2/ the neck formation initiated by exchange of nucleons when two ions interact is an important ingredient and the the cross section in the above range is given as

$$\sigma(E) = \pi R^2 (E-T)^2 / [4(B-T)E] \quad \text{-----(1)}$$

and the first moment of the spin distribution as

$$\langle \ell \rangle = \frac{2}{15}\left[\frac{2\mu R^2}{\hbar^2}(E-T)\right]^{1/2} \quad \text{-----(2)}$$

Here B, R = barrier height and radius T = the lowest barrier below which effects due to deformation etc. will show up. According to ref.2 the T value is sensitively dependent on the neutron separation energy of the target and will exhibit a strong isotopic dependence. The three parameters B,T,R are determined by them from a fit to fusion data. It is also possible to identify the B and T values respectively with the 'sudden' and the 'adiabatic' barriers/3/.

In the present work, the B and R values have been calculated using the prescription of KNS/4/which is successful in explaining the nuclearmasses, fusion, fission data. The T values have been calculated using the procedure of ref.3 with the following modifications: the nuclear masses from Moller and Nix/5/, the γ parameter(surface tension coefficient)as

$$\gamma = 1.25\left[1 - 2.3\left((N-Z)/A\right)^2_{CN}\right]$$

which is consistent with r = 1.16 used in nuclear mass calculation. With these values of B,T,R and expressions (1) and (2), we have calculated σ_F and $\langle l \rangle$ for a number of systems. In the figure the (B-T) values calculated are compared with the values obtained from fits to fusion data. The values are plotted as a function of ϵ defined as/6/ $\epsilon = 4Z_1Z_2/[A_1^{1/3}A_2^{1/3}(A_1^{1/3}+A_2^{1/3})]$ The prediction assuming only neck degree of freedom is also shown(neck). Also shown is the comparison between $\langle l \rangle$ calculated with

the experimental values. Overall the agreement between the experiment and the calculation is satisfactory. Using this parameter free approach we have been able to bring out not only the isotope dependence seen for the Sm isotopes but also lack of it in the case of the Sn isotopes.

/1/ G.R.Satchler, Phys.Rept.199,147 (1991)
/2/ P.Stelson et al.Phys.Rev.C41,1584 (1990)
/3/ J.Wilczynski etal.Nucl.Phys.A511, 429 (1990)
/4/ H.J.Krappe,et al.Phys.Rev.C20,992(1979)
/5/ P.Moller and J.R.Nix,At.Nuc.Dat.Tab.39,213(1988)
/6/ C.E.Aguiar et al Nucl.Phys.A500,195(1989)

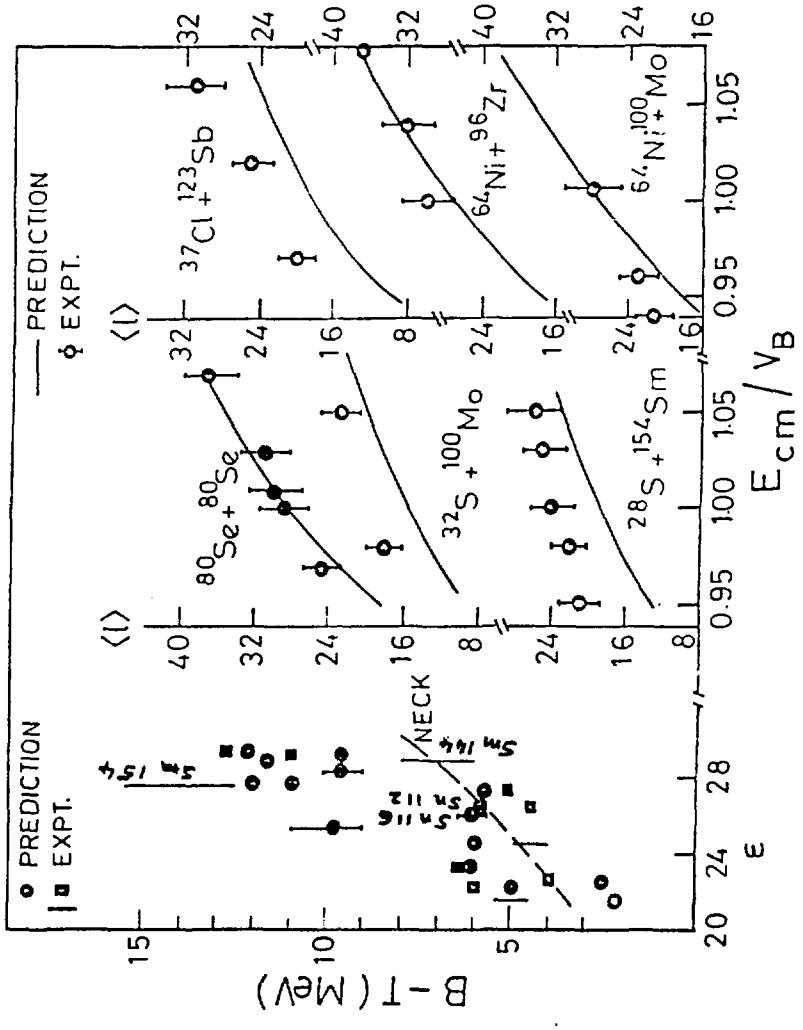

MASS EXCHANGE IN HEAVY ION COLLISIONS

M. Rajasekaran, R. Premanand & D. Caleb Chanthi Raj
Department of Nuclear Physics, University of Madras,
Guindy Campus, Madras 600 025.

We propose a classical treatment of mass exchange between heavy ions in collisions at energies around Coulomb barrier. We treat the reduced mass of the collision partners as a dynamical variable and obtain classical trajectories from which the cross-section could be obtained. However, barrier penetration effects beyond the classical region have to be included to obtain more meaningful results.

We start with the classical equation for the relative velocity angular velocity [1]

$$\dot{r} = \sqrt{\frac{2}{\mu}\left[E-V(r)-\frac{l^2}{2\mu r^2}\right]} \quad , \qquad (1)$$

$$\dot{\theta} = l/\mu r^2 \quad , \qquad (2)$$

where $\mu(r)$ is a function of r, is given by

$$\mu(r) = \frac{A_1(r)\ A_2(r)}{A_1(r) + A_2(r)} \quad , \qquad (3)$$

for which we have used a simple Wood-Saxon form as

$$A_1(r) = A_p - \frac{\Delta M}{1+\exp[(r-r_o)/a]}$$

$$A_2(r) = A_p + A_T - A_1(r)$$

The value of ΔM is varied from 0 to 4.

The classical equation for cross-section is given by

$$\frac{d\sigma}{d\Omega} = \frac{b}{\sin\theta}\left(\frac{db}{d\theta}\right) \qquad (4)$$

Here we consider the scattering of ^{19}F on ^{232}Th at E_{lab} = 110 MeV for five different ΔM values. Fig.1 shows the deflection functions with the real Wood-Saxon potentials (V_o = 3 MeV) in addition to the Coulomb potential [$V(r) = V_N(r)+V_C(r)$]. As ΔM increases the rainbow scattering occurs at larger angles and saturates (backward rainbow angle) at ΔM = 2, but the forward rainbow angle decreases. The peaks in differential cross section (ratio of elastic to the Rutherford) are widely spread for $\Delta M > 2$ than the peaks for $\Delta M < 2$ (Fig. 2).

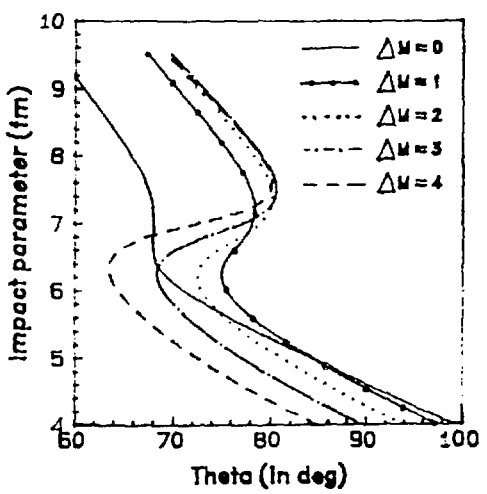

Fig. 1

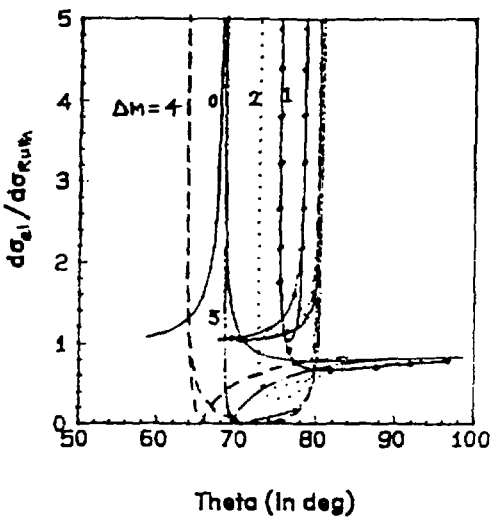

Fig. 2

[1] W. Nörenberg and H.A. WeidenmÜller, Introduction to the Theory of Heavy ion collisions, Lecture notes in Physics, Vol.51, Springer-Verlag, 1976.

Work supported UGC-COSIST under SAP.
R.P. thanks Govt of Tamilnadu for the fellowship.

BARRIER REGION RESONANCE MODEL FOR HEAVY ION RESONANCES

B.Sahu,B.M.Jyrwa,P.Susan and C.S.Shastry
Department of Physics,N.E.H.U.
Shillong-793 003,Meghalaya.

Using an explicit analytical expression of the s-wave S-matrix for the short range repulsive Eckart potential barrier we correlate the classical orbiting and corresponding quantum mechanical barrier states.These are compared with the results of earlier works [1,2] on this problem and some additional interesting features such as dependence of width of barrier states on height of the barrier and spacing between the levels of the barrier region resonances are pointed out [3].Based on the results of the above potential we give the following four-parameter (a,b,c,d) semiempirical formula for resonance energy $E(n,l)$ for the analysis of barrier region resonance states in nucleus - nucleus collisions.

$$E(n,l)=V_B^{(l)}+ a + bl + dl^2 - c(n+3/4)^2 ,$$

$$n = 0,1,2,.... \qquad (1)$$

where $V_B^{(l)}$ is the height of the nucleus-nucleus effective potential for the l^{th} partial wave.Large number of resonances observed in the $^{12}C + ^{12}C$ and $^{12}C + ^{16}O$ systems are explained satisfactorly (see **Fig.1** and **Fig.2**) using the above formula.In developing our model the following aspects are considered.Below a critical l the effective real nucleus-nucleus potential between two heavy ions is characterised by a Coulomb barrier region and a potential pocket.Such potential generates resonance states.However,these states may originate not only from the potential pocket but also from the barrier top region provided absorption is not large in the barrier region and the barrier is reasonably flat.These states corresponding to barrier top is usually termed as barrier top resonances and resonances associated with orbiting etc.The above conditions of a barrier for generating reso-

nance states are fullfilled in the case of heavy ion systems where one can assume the imaginary part of the potential to be large in the pocket region and small in the barrier region.

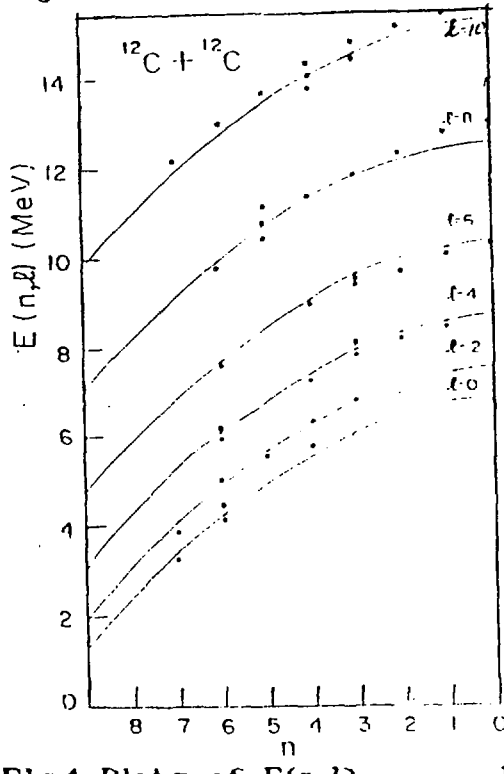

Fig.1 Plots of E(n,l) against the assumed values of n for the $^{12}C+^{12}C$ system [Eq.(1)].The parameters are a=0.5985 MeV, b = 0.02119285MeV, c = 0.060085 MeV, and d = -0.008393 MeV.

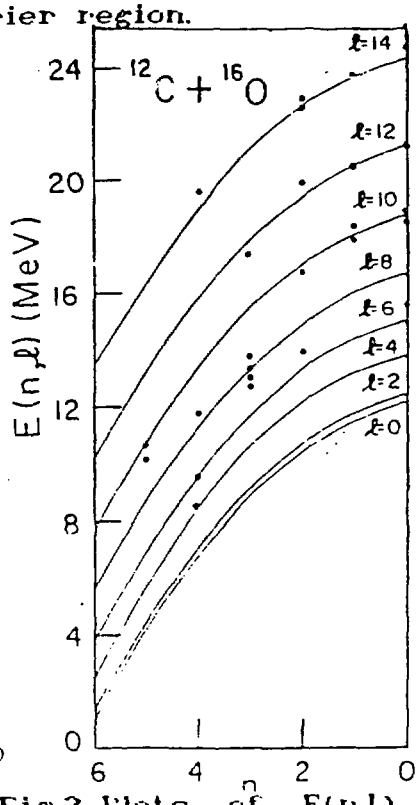

Fig.2 Plots of E(n,l) against the assumed values of n for the $^{12}C+^{16}O$ system [Eq.(1)].The parameters are a=4.15049 MeV, b = 0.1942653 MeV, c = 0.2453 MeV, and d = -0.012391 MeV.

References:-

[1]W.A.Friedman and C.J.Goebel, *Ann.Phys.*,**104**,145 (1977)

[2]D.M Brink and N.Takigawa, *Nucl.Phys.*,A279,159 (1977)

[3]B.Sahu, B.M.Jyrwa, P.Susan and C.S.Shastry, *Phys.Rev.*C,(To appear).

THE ROTATION-VIBRATION CHARACTERISTICS OF THE QUASI-MOLECULAR RESONANCES

P.Sarangi and L.Satpathy
Institute of Physics, Bhubaneswar-751005

Understanding of the quasi-molecular resonances has been a challenging problem since the discovery of this phenomenon in 1960 by Bromley et. al. in the $^{12}C + ^{12}C$ reaction. Recently, we have attempted [1,2] to describe the states in terms of rotational-vibrational excitation similar to those observed in diatomic molecule. The dipole degrees of freedom characterised by the distance R, between the two nuclei, is supposed to play the important role. Observing the analogy between heavy-ion potential and Morse potential, we had proposed that a combination of a constant and the Morse potential will be a good approximation for the potential for this phenomenon. We have developed a method to determine the parameters of this potential following a two-body quantum mechanical description of the resonance data. We have shown that the rotation-vibration characteristics naturally emerges in our description without pre-supposing such a picture.

The rotation-vibration characteristics in usual nuclear spectra have been recognised since very early days of nuclear physics. The origin of these states are quadrupole degrees of freedom. How good are the manifestation of the rotation and vibration modes can be judged from the smallness of the ratio of the characteristics rotational to vibrational energy $\epsilon_{rot}/\epsilon_{vib}$. In the case of quasi-molecular states, the rotation-vibration are of di-pole origin. From the study of $^{12}C + ^{12}C$, $^{12}C + ^{16}O$ and $^{16}O + ^{16}O$ systems using our above model we calculate [1-3] these ratios. In the following table, we present the depth, the range, of the potential obtained by us, along with the ratio $\epsilon_{rot}/\epsilon_{vib}$ for these systems.

Table

Systems	Depth (MeV)	Range (fermi)	$Ratio \epsilon_{rot}/\epsilon_{vib}$
$^{12}C + ^{12}C$	7.0	15	0.05
$^{12}C + ^{16}O$	16.7	16	0.03
$^{16}O + ^{16}O$	22.8	16	0.02

It can be seen that the ratios are quite small to justify the rotation-vibration picture emerging from our study. These may be compared

with the familiar low-lying nuclear states where quadrupole degrees of freedom give rise to rotation-vibration spectra. For ^{188}Os and ^{190}Os, where the rotation-vibration picture is applicable, the ratio is 0.04 and 0.05 respectively. From the ratios of three systems, it may be calculated that rotational-vibrational characteristics are more strongly pronounced in $^{12}C+^{16}O$ and $^{16}O+^{16}O$ systems compared to $^{12}C+^{12}C$ system. Thus these characteristics are very well manifested in the dynamics of quasi-molecular resonances. So the diatomic-like molecular picture proposed by us in on a firm ground.

References:

1. L.Satpathy, P. Sarangi and A.Faessler, J.Phys. G:Nucl. phys. **12** (1986) 201.
2. L. Satpathy and P. Sarangi,*J. Phys. G: Nucl. Part. Phys.***16** (1990) 469.
3. L. Satpathy, Pradip k. Sahu and P. Sarangi (Submitted to Jr. of Phys. G)

ELLIPSOIDAL DEFORMATIONS AND FUSION BARRIER DECREASE

G.SHANMUGAM & M.D.PADMINI*
Department of Physics, Presidency College, Madras 600 005.

*Department of Physics, Quaid-E-Millat Govt. College for Women, Madras 600 002.

An important condition for forming a compound nucleus in a heavy ion collision is that the dynamical path of the fusing system should pass inside the fission saddle point in a multidimensional deformation space. For certain lighter nuclear system and low angular momentum the fission saddle point lies outside the point of contact in heavy ion reactions and the required condition is automatically satisfied once a one dimensional interaction barrier is overcome. But for heavier nuclear systems and high angular momentum the fission saddle point lies inside the contact point and the centre of mass bombarding energy should exceed the maximum in the one dimensional interaction barrier by an amount ΔB inorder to form a compound nucleus.

Aguiar et al /1/ recently have given a method to calculate the effective barrier decrease ΔB for a variety of projectile target combinations and have shown that

$$\Delta B = \alpha \left(\frac{Z^2}{A}\right)^{\beta}_{eff} \qquad \text{where } \alpha = .0016 \text{ MeV}; \quad \beta = 2.5$$

$$\text{and} \quad \left(\frac{Z^2}{A}\right)_{eff} = \frac{4Z_1Z_2}{A_1^{1/3}A_2^{1/3}\,(A_1^{1/3}+A_2^{1/3})}$$

The aim of the present work is to calculate this barrier decrease at different spins by actually introducing ellipsoidal deformation degree of freedom in the elliptic lenniscatoid parametrization for the fusion of two colliding light nuclei /2/.

Assuming volume conservation, the path of the two ellipsoidally deformed colliding nuclei is expressed in terms of a single dimensionless parameter ζ which is the ratio between the transverse and radial semi axes and the centre of mass distance (r). The region of

practical interest in the two dimensional potential surface calculation is limited to $0.4 \leq S \leq 1.6$ and $2^{2/3} \leq \frac{r}{p} \leq 2.8$. Here $(2^{2/3})R_o$ is the distance for two touching spheres, R_o being the radius of the eventual compound nucleus.

The required potential curve can now be obtained by calculating the total energy of the system comprising of surface, coulomb, proximity and rotational energies and minimising it at each spin with respect to S for each centre of mass separation. By comparing this with the corresponding curve obtained without including deformation one can obtain the barrier energy decrease.

The table below gives the fusion barrier energy and its position without and with ellipsoidal deformations for three illustrative reactions at zero spin. The last two columns of the table show the barrier decrease ΔB calculated by Aguiar et al and our results. Our results are found to agree fairly well with the results derived from the empirical formula of Aguiar et al.

Reaction	Two spheres		Two ellipsoids		ΔB	
	E_f	R_f	E_f	R_f	Aguiar et al	Our results
$^{12}C+^{12}C$	4.8	7.6	4.8	7.6	0.14	0
$^{24}Mg+^{24}Mg$	19.1	8.8	18.6	9.5	0.79	0.5
$^{28}Si+^{28}Si$	25.8	9.3	25.2	9.6	1.17	0.6

Not much change is produced in ΔB values at higher spins for these cases.

/1/ Aguiar C.E., Barbosa V.C., Canto L.F. and Donangelo R Nucl.Phy.A472, 571 (1987).

/2/ Royer G., Piller C., Mignen J and Raffray Y. J.Phys.G Nucl.Part Phys. 16, 1077 (1990).

FUSION CROSS SECTION OF SPIN-UNSATURATED NUCLEI

K C Panda and T Patra
Post-Graduate Department of Physics
Sambalpur University, Jyoti Vihar
Sambalpur - 768019

It is well known that the fusion process is sensitive to the position and height of the interaction barrier which is situated some 1-1.5 fm inwards of the strong absorption radius D_{sa}. Therefore, the calculation of fusion cross section ^{sa} of spin unsaturated nuclei will further show the effect of the spin density terms of Skyrme energy density on the calculated real part V of their optical potential deeper than D_{sa}. This is reported in the present paper.

The fusion cross section σ_F in terms of the partial wave expansion is obtained as,

$$\sigma_F = \pi\lambda^2 \sum_{L=0} (2l + 1)P_L \qquad (1)$$

where P_L is the transmission coefficient derived by approximating the nuclear potential V_E as a parabola near the barrier D_B.

$$P_L = \left[1 + \exp\left[2\pi\left(\mu/\hbar^2 |V''(R_B)|\right)^{1/2}(V(R_B) - E_{cm})\right]\right]^{-1} \qquad (2)$$

V is the sum of nuclear V_E, coulomb and centrifugal potential, and L is orbital angular momentum of the incident partial wave and λ is its de-Broglie wave length.

To compute the fusion cross sections around the position of interaction barrier of spin-unsaturated nuclei, we have first calculated the energy dependent real part V_E of their optical potential using the Skyrme energy density[1]. We have

also calculated the potential V_N excluding both the spin density terms from the Skyrme energy density. Our preliminary results for the system $^{40}Ca + ^{48}Ca$ show that the difference between the potential $V_E(D_B)$ and $V_N(D_B)$ is within 0.4% at the barrier D_B.

Potentials in MeV	E_{cm} (MeV)			
	55	60	65	70
$V_N(D_B)$	55.8	55.7	55.5	55.1
$V_E(D_B)$	55.6	55.5	55.4	54.8

The fusion cross section σ_F (equation (1)) obtained from these calculated potentials V_N and V_E are presented below.

Potentials	σ_F (mb)			
E_{cm} (MeV) =	55	60	65	70
V_N	30	230	400	570
V_E	31	234	408	578

It is seen that the spin density terms affect the fusion cross sections within 2% only in contrast to the earlier conclusion of Das and Satpathy.[2]

References :

1. K C Panda and T Patra J. Phys. G: Nucl. Part. Phys. 16, 593 (1990).
2. B K Das and R K Satpathy J. Phys. G: Nucl. Part. Phys. 16, 221 (1990).

SPIN DENSITY TERMS AND ELASTIC SCATTERING OPTICAL POTENTIAL OF UNCLOSED j-SHELL NUCLEI

K C Panda and T Patra
Post-Graduate Department of Physics
Sambalpur University, Jyoti Vihar
Sambalpur - 768019

The effect of the spin density terms $\frac{1}{16}(t_1-t_2)(\vec{J}_n^2+\vec{J}_p^2)$ and $-\frac{1}{2}W_o(\rho\vec{\nabla}.\vec{J}+\rho_n\vec{\nabla}.\vec{J}_n+\rho_p\vec{\nabla}.\vec{J}_p)$ of the complex Skyrme energy density[1]

$$\begin{aligned}H_c(\rho,\tau,\vec{J}) &= \frac{\hbar^2}{2m}\tau+(1+i\tau)\left[\tfrac{1}{2}t_o\left[(1+\tfrac{1}{2}x_o)\rho^2-(x_o+\tfrac{1}{2})(\rho_n^2+\rho_p^2)\right]\right.\\ &+\tfrac{1}{4}(t_1+t_2)\rho\tau+\tfrac{1}{8}(t_2-t_1)(\rho_n\tau_n+\rho_p\tau_p)+\tfrac{1}{16}(t_2-3t_1)\rho\nabla^2\rho\\ &+\tfrac{1}{32}(3t_1+t_2)(\rho_n\nabla^2\rho_n+\rho_p\nabla^2\rho_p)+\tfrac{1}{4}t_3\rho_n\rho_p\rho\\ &+\left.\tfrac{1}{16}(t_1-t_2)(\vec{J}_n^2+\vec{J}_p^2)-\tfrac{1}{2}W_o(\rho\vec{\nabla}.\vec{J}+\rho_n\vec{\nabla}.\vec{J}_n+\rho_p\vec{\nabla}.\vec{J}_p)\right] \quad (1)\end{aligned}$$

on the optical potential and elastic scattering cross sections of spin unsaturated unclosed j-shell nuclei such as $^{18}O+^{58}Ni$ at E_{lab}=63 MeV is investigated in the present paper.

To this end we have derived[2] the spin densities $\vec{J}_n$ and $\vec{J}_p$ of ^{18}O and ^{58}Ni and used these expressions alongwith the densities $\rho=\rho_n+\rho_p$ obtained from shell model wave function in the EDM integral to calculate the energy dependent real V_E and imaginary W_E parts of the optical of $^{16}O+^{58}Ni$ at E_{lab} = 63 MeV.

$$V_E(D,E_{cm})+iW_E(D,E_{cm})=\int[H_c(\rho,\tau,\vec{J})-H_c(\rho_1,\tau_1,\vec{J}_1)-H_c(\rho_2,\tau_2,\vec{J}_2)]\,d^3R \quad (2)$$

We have also excluded both the spin density terms from the complex Hamiltonian density H_c (equation(1)) and calculated the corresponding potentials V_N and W_N.

Our results presented in a table show that at the strong absorption radius D_{sa} the potentials V_E and W_E

$-V_E(D_{sa})$ (MeV)	$-V_N(D_{sa})$ (MeV)	$-W_E(D_{sa})$ (MeV)	$-W_N(D_{sa})$ (MeV)
1.88	2.01	1.27	1.44

differ from V_N and W_N by 6.9% and 13.4% respectively. This difference is also manifested in the computed elastic scattering cross sections of $^{18}O+^{58}Ni$. The results are presented in another table.

Potential	$\sigma_{el}(\theta)/\sigma_R(\theta)$						
θ(deg)≈	20	25	30	35	40	45	50
V_E+iW_E	1.02	0.95	1.16	1.06	0.60	0.27	0.106
V_N+iW_N	1.20	0.98	1.24	1.12	0.65	0.31	0.12

It is found that the ratios of the elastic σ_{el} to Rutherford σ_R cross sections obtained from the potential V_E+iW_E predicts the experimental data nicely in the entire angular range whereas the cross sections obtained from the potential V_N+iW_N differ from their experimental values. Thus we conclude that the spin density terms of unclosed j-shell spin unsaturated nuclei have appreciable contribution towards the surface part of the real and imaginary potential and consequently have some effect on the elastic scattering cross sections unlike the case of closed j-shell spin unsaturated nuclei.[1]

References

1. K C Panda and T Patra J. Phys. G: Nucl. Part. Phys. 16, 593 (1990).
2. R K Puri, P. Chattopadhyay and R K Gupta Phys. Rev. C 43, 315 (1991).

INTERMEDIATE MASS FRAGMENTS EMISSION IN INTERMEDIATE ENERGY NUCLEUS-NUCLEUS COLLISION

C. Bhattacharya, S. Bhattacharya and K. Krishan
Variable Energy Cyclotron Centre, Bidhan Nagar, Calcutta-64

Intermediate mass fragments (IMF, $3 \leq Z \leq Z_{total}/2$) emission in intermediate energy nucleus-nucleus collisions is a subject of intensive theoretical and experimental studies at the present time. At high bombarding energies (in excess of total nuclear binding energies), there are indications that the excited composite undergoes multifragmentation - which essentially means that the final states involve "instantaneous" emission of two or more IMFs [1]. However at lower bombarding energies (~10-50 MeV/u), it has been fairly well established that the reaction processes responsible for IMF emission are predominantly binary in nature [2]. In this energy regime, the main contribution to the IMF emission comes from one or more of the follwing processes; (i) quasi elastic (QE) or few particles transfer reactions, (ii) deep inelastic collisions(DIC) or massive transfer reactions, and (iii) decay of hot incompletely fused composite (IFC). Thus, it is essential to estimate the contributions of all these processes to have a proper insight of the reaction mechanisms undelying IMF emission, which, to our knowledge, have not been systematically done in the past. Here, we report a systematic calculation of the contributions of each of the three processes and show that total IMF emission cross-sections over the whole range of mases can be fairly well explained by combining the contributions of the three above mentioned processes.

The details of the calculation will be discussed elsewhare and is given in brief. We calculate the collision trajectories for each impact parameter by solving Euler-Lagrange equations with conservative Coulomb and proximity potentials and the non conservative friction forces are generated by stochastic nucleon exchange [3]. The calculation has been done on event by event basis using Monte-Carlo simulation technique and at each stage of its time evolution, the emission of promptly emitted particles have been taken care of. The QE and DIC processes are further differentiated with a velocity cutoff *ie*, if the velocity of the IMF is greater than $x * V_{in}$ (V_{in} being the incident

velocity), it falls in QE category, otherwise it belongs to DIC. The factor x has been typically chosen to be ~ 0.8. Slight variation of x does not affect the cross sections significantly. For fusion trajectories, the IFC formed after the emission of preequilibrium particles is allowed to decay and the cross sections for the IMFs are calculated using statistical binary fragmentation model [4]. The results of the calculation for the representative system Ne + Ag at 20,40 MeV/u are shown in the figure alongwith the respective experimental data [5]. It is seen that heavier fragments are very well explained by the decay of IFC, whereas the lighter fragments (upto projectile) are predominantly emitted in the DIC process. The QE contribution in the present case is not significant since the measurements [5] were done at angles larger than the grazing angle. Thus it is seen that the emission from DIC and decay of IFC can explain the whole range of IMF emission data.

References:

[1] S.J.Yennello et. al., Phys. Rev. Lett. 67 (1991) 671

[2] L.G.Moretto and G.J.Woznick, LBL-25631 (1988)

[3] S.Bhattacharya, K.Krishan, J.N.De and S.K.Samaddar, Phys. Rev. C37 (1988) 2916

[4] C.Bhattacharya and S.Bhattacharya, Phys. Rev. C43 (1991) 1491

[5] N.H.Papadakis et. al. , Phys. Lett. B240 (1990) 317

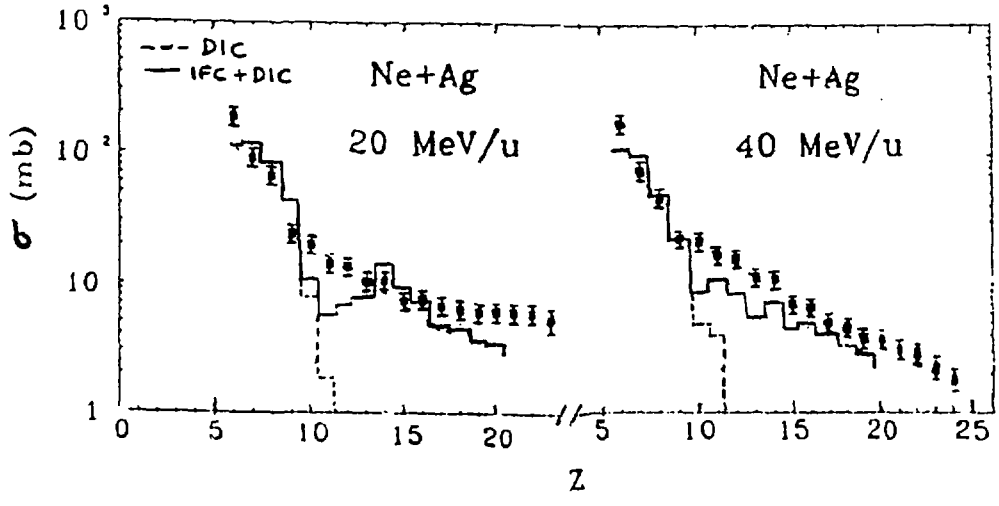

NEUTRON SHELL EFFECTS IN THE 209Bi(α,xn)213-xAt AND 197Au(α,xn)201-xTl REACTIONS.

S.S. Rattan and N. Chakravarty.
Radiochemistry Division, Bhabha Atomic Research Centre, Bombay-85

For a broad range of nuclei, proton shell and sub-shell effects in the production cross sections of 14 MeV (n,p) reactions have been observed [1]. Neutron shell effects have not been seen or quantitatively investigated so far for spallation reactions induced by charged particle projectiles. The stimulus for this work therefore was to see whether such mean field effects show up in the integral cross sections for the 209Bi(α,xn)213-xAt and 197Au(α,xn)201-xTl reactions at moderate bombarding energies.

The reaction cross sections were obtained by the 50 and 60 MeV a particle bombardments on 197Au and 209Bi targets of nuclear grade purity. The cross sections were obtained by off line γ-spectrometric assay of the residues. Details of the experiment and data reduction are given elsewhere [2,3]. The measured cross sections were supplemented with those obtained from literature. Meaningful systematics from the (α,xn) cross sections (σ(α,xn)), of a given target can be extracted if the σ(α,xn) are compared at the same available energy of the residual (Eav) where,

$$Eav = E\alpha(cm) + Q(x) \qquad (1)$$

Eα(cm) being the α particle energy in the centre of mass frame and x the neutron multiplicity. Corresponding to the Eα values resulting from the Eav values of 1,2,3,4,5 and 6 MeV, the σ(α,xn) were read off from the excitation functions for the 209Bi and 197Au targets individually.

Figs.1 and 2 show the variation of σ(α,xn) with the N of the residual. The distribution for 201-xTl (fig.2) is very nearly symmetrical displaying the stationary centroid of a typical statistical distribution. There is a larger yield of the products with lower N for both 209Bi and 197Au targets because the Eαs corresponding to the same Eav value for these products is higher leading to a higher absorption cross section. The striking feature of fig.1 however, is that the distributions at the Eav values of 1,2,3 and 4 MeV are skewed towards higher N with the centroid at N=126 which gradually shifts to a lower N value at higher Eav. This clearly shows the importance of the 126 neutron shell in determining the 209Bi(α,xn)213-xAt yields at low Eav. As the Eav and correspondingly Eα is raised, the shell effect is washed away and the distribution acquires a greater symmetry. A relatively low Eav e.g. 4 MeV nonetheless corresponds to an Eα of as high as ~56 MeV for the 209Bi(α,6n)207At reaction. This work suggests that mean field effects still retain sufficient influence at these elevated energies to affect the course of the reaction. A quantitative analysis of the observations in terms of the statistical nuclear reaction model is underway.

References

1. A. Chatterjee, Nucl. Phys. 60, 273 (1964).
2. N. Chakravarty, S.S. Rattan, R.J. Singh, S.M. Sahakundu, Satya Prakash and S.K. Ghosh, Radiochim. Acta 48, 1 (1989).
3. S.S. Rattan, N. Chakravarty, A. Ramaswami and R.J. Singh, Radiochim. Acta (Accepted)

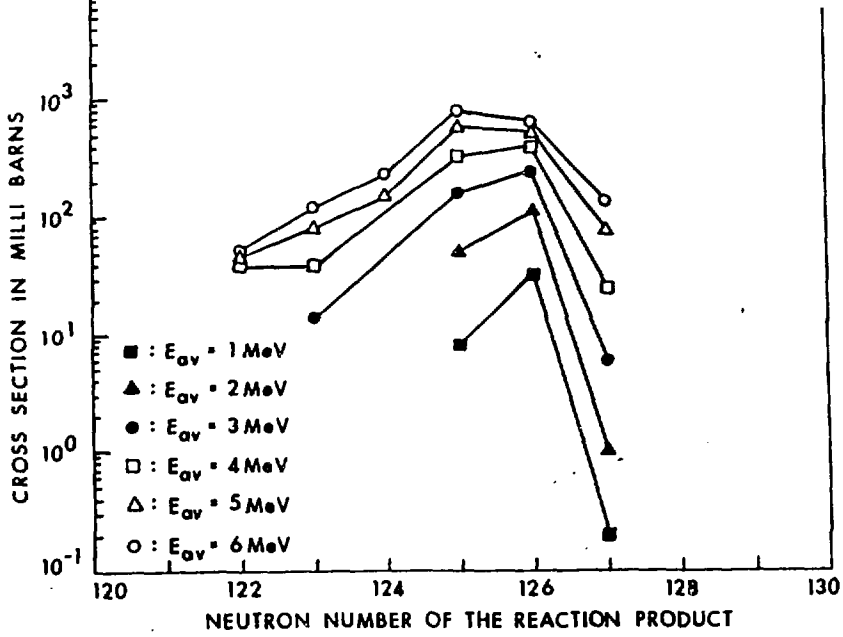

FIG.-1. EXPERIMENTAL PRODUCTION CROSS SECTION FOR REACTION PRODUCTS IN $^{209}Bi(\alpha, xn)^{213-x}At$ AS A FUNCTION OF NEUTRON NUMBER OF THE REACTION PRODUCT AT DIFFERENT AVAILABLE ENERGIES (E_{av}).

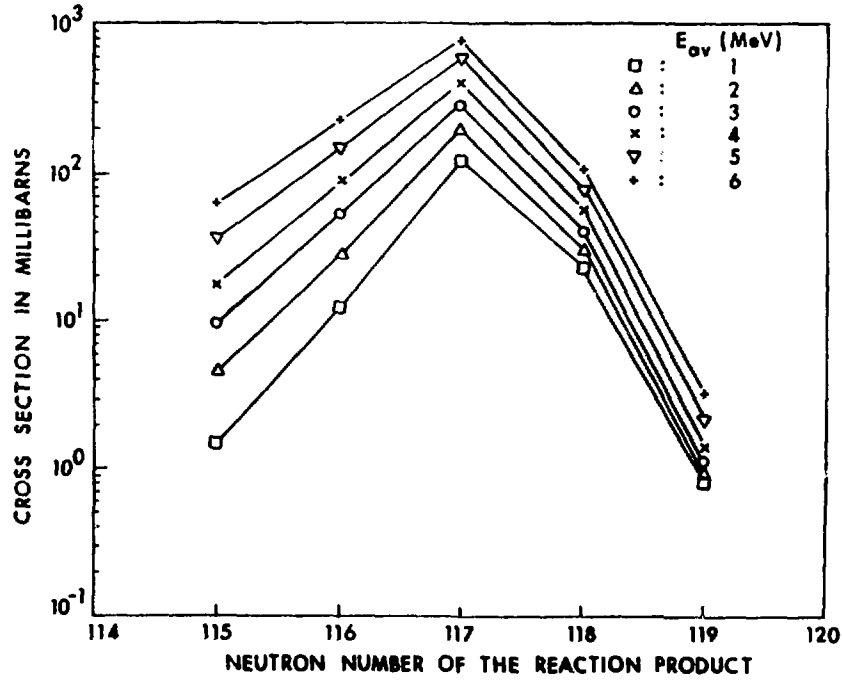

FIG.-2. INTERPOLATED EXPERIMENTAL PRODUCTION CROSS SECTION FOR REACTION PRODUCTS IN $^{197}Au(\alpha, xn)^{201-x}Tl$ AS A FUNCTION OF NEUTRON NUMBER OF THE REACTION PRODUCT AT DIFFERENT AVAILABLE ENERGIES (E_{av}).

INVESTIGATION OF PRE-EQUILIBRIUM EMISSION IN (α, np) REACTIONS ON ^{128,130}Te

B. P. Singh, M. G. V. Sankaracharyulu, M. A. Ansari, H. D. Bhardwaj* and R. Prasad
Department of Physics, A. M. U. Aligarh-202002
*D. S. N. College, Unnao (U. P)

Recent experiments have clearly indicated that the equilibrium statistical model underestimates the probability of emission of particles with higher kinetic energies. The so called "hard component" of the particle spectra and the "high energy tails" of the experimental excitation functions cannot be reproduced by equilibrium models. It is quite possible that the emission of particles may take place even before the establishment of thermodynamic equilibrium of the CN. This reaction mechanism is termed as pre-equilibrium (PE) emission/1/.

With a view of studying PE-emission, we have undertaken a programme of precise measurement of excitation functions for α-induced reactions on different nuclei covering the whole range of periodic table. As part of this programme excitation functions for the reactions ^{128}Te(α,np)^{130}I, ^{130}Te(α,np)^{132}I and ^{130}Te(α,np)^{132m}I have been measured using stacked foil technique and enriched isotopes. To the best of our knowledge excitation functions for these reactions have been measured for the first time. Samples have been prepared from the enriched isotopes of ^{128}Te(83%) and ^{130}Te(61%). The stacks were irradiated using the α-particle beam of Variable Energy Cyclotron of VECC, Calcutta. Beam currents during the irradiations were kept ≈ 100 nA. Post-irradiation analysis has been performed using Ge(Li) detector. Excitation function for ^{128}Te(α,np) reaction has been measured upto ≈ 45 MeV, while, excitation functions for ^{130}Te(α,np) reactions have been measured upto ≈40 MeV.

Excitation functions have also been calculated theoretically using CN model with and without the inclusion of PE-emission. The CN calculations have been performed using Hauser-Feshbach model/2/, while

PE-emission has been simulated employing exciton model (EM) of Griffin/3/. As expected/4/ inclusion of PE-emission based on EM calculations gives satisfactory agreement with measured excitation functions. In all the calculations the values of level density parameter 'a', fictive ground state energy 'Δ' and effective moment of inertia were taken consistently from the table of Dilg et al/5/. Theoretical calculations give satisfactory agreement with experimental data when the initial exciton number n_o=6(5p+1h) alongwith parameter FM=430 MeV^3 of square of two-body residual interaction matrix element were chosen.

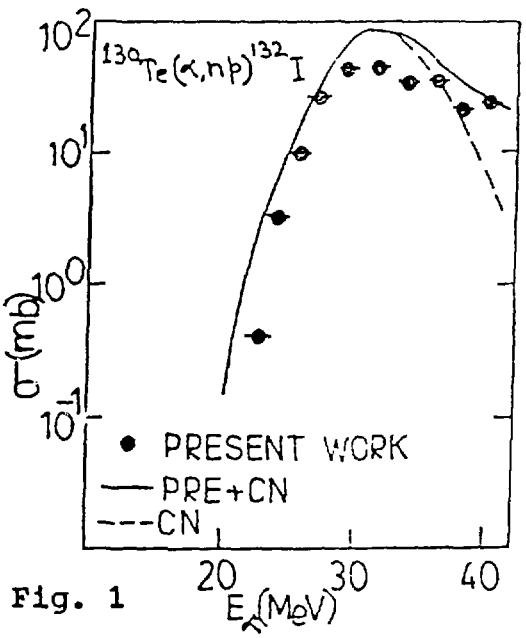

Fig. 1

The reaction Te(α,np) may proceed via reaction paths (α,np) and (α,pn). Calculations were performed for both these paths and the calculated cross-section is the sum of these two. As a representative case presentaly measured and theoretically calculated excitation function for the reaction ^{130}Te(α,np)^{132}I is shown in fig.1. It may be seen from this fig., and also in general sound agreement is found between experimental and theoretical excitation functions. The PE-fraction FR, which is the measure of relative strength of PE-component has also been calculated and as expected found to be energy and mass number dependent.

1. M.Blann, Ann. Rev. Nucl. Sci., 25(1975)133
2. W.Hauser and H.Feshbach, Phys. Rev. 87 (1952)366
3. J.J.Griffin, Phys. Rev. Lett. 17(1966)478
4. B.P.Singh et al., Nuovo Cim. 104A(1991)475
5. W.Dilg et al., Nucl. Phys. A217(1973)269

ALPHA INDUCED REACTIONS IN YTTRIUM

M.K. Bhardwaj, I.A. Rizvi and A.K. Chaubey
Department of Physics, A.M.U. Aligarh.

The study of excitation function of the nuclear reactions is very useful because they are basic data for yield calculations in radioisotope production. This also helps in testing of models of nuclear reaction. The high energy tail portion of the excitation function is of major interest as it leads to reaction mechanisms other than equilibrium (compound) one.

In the present work, we have studied the excitation function for (α,n), (α,3n) (α,4n) reactions in Y-89. Stacked foil activation technique was followed. The targets were made by depositing the Yttrium powder on alluminium sheet of 1 mil thickness, by centrifugal method in target division of variable Energy Cyclotron Centre (VECC), Calcutta. Thickness of the target foil was 50 ug/cm^2. The bombarding energy of the α-beam was ranging from 60 to 18 MeV. During the irradiation of the stack, the counting of incoming α-particles was done from integrated beam charge. Using this charge, the flux was calculated. For checking the flux, the copper foil was used as a flux monitor and a good agreement was found with less than 10% discrepancy.

The multiple scattering at small angles increases path length of stopping material. However in case of α-particle, the path length correction is very small/1/ and hence neglected.

The theoretical excitation function calculations were done using the compound nucleus model with and without the inclusion of PE

emission of particles. For analysing the equilibrium part, the compound nucleus model of Weisskopf-Ewing/2/ was adopted. The contribution from the pre-equilibrium process has been included at the first step of the evaporation. The GDH model was used for analysing the PE part. The theoretical calculations have been done for n_o = 4,5,6 with different configurations but it is found that n_o = 4 (2n + 2p + oh) gives the best fit to our experimental data.

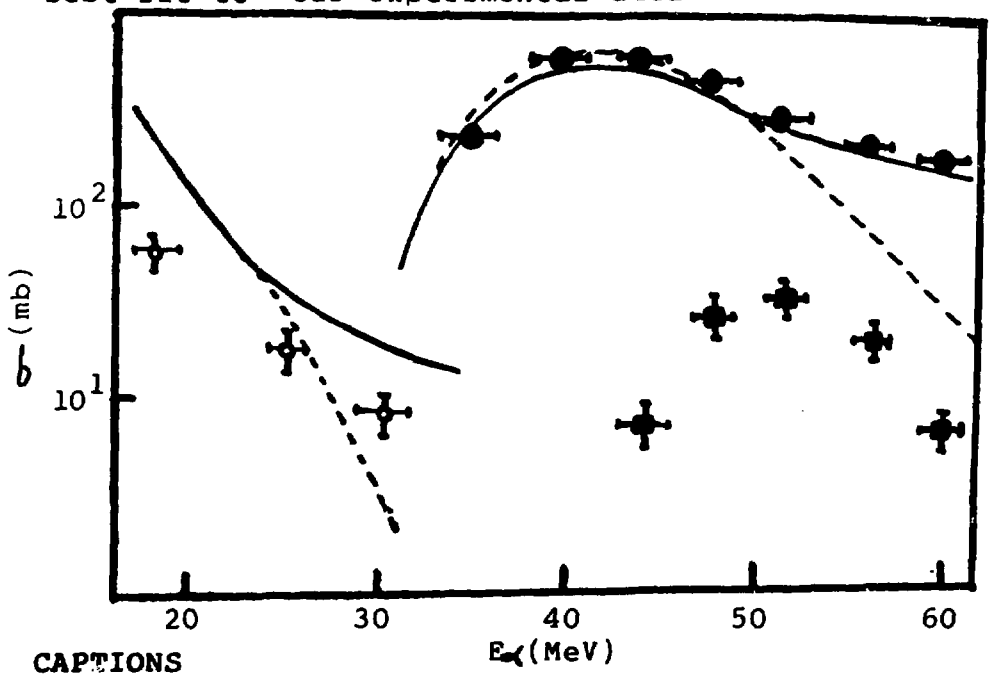

CAPTIONS

○ $^{89}Y(\alpha,n)\ ^{92}Nb$ Reaction

● $^{89}Y(\alpha,3n)\ ^{90}Nb$ Reaction

■ $^{89}Y(\alpha,4n)\ ^{89}Nb^g$ Reaction

REFERENCES

1. U. Fano. Ann. Rev. Nucl. Sci. 13, 1, (1963).
2. V.F. Weisskopf and D.H. Ewing. Phys. Rev. 57, 472 (1940).

MEASUREMENT OF EXCITATION FUNCTIONS AND MEAN PROJECTED RECOIL RANGES OF NUCLEI IN α -INDUCED REACTIONS ON F, Al, V, Co AND Re NUCLEI. M.Ismail, V.E.C.C.,I/AF, Bidhan Nagar Calcutta-700 064

Excitation function and mean projected recoil ranges of nuclei produced in the α-particle induced reactions on F,Al,V,Co and Re targets were measured by conventional thick target thick recoil catcher technique for bombarding energies $E\alpha \leq 65$ MeV. The measured cross-sections are compared with calculations considering equilibrium as well as pre-equilibrium reaction mechanism according to the hybrid and geometry dependent hybrid model of Blann using the code Alice/85/300. High energy part of the excitation functions are dominated by pre-equilibrium reaction mechanism whereas the low energy parts are dominated by evaporation with its characteristic peak. In this paper emphasis will be placed on the GDH model, for it provides a potentially better description of the physical process i.e., a higher probability of peripheral collisions to undergo precompound decay than for central collisions. Geometry Dependent Model with initial exciton number no= 4 (nn=2, np=2, nh=0) gives better fits compared to Hybrid Model with same initial exciton configuration and mfp parameter k=1.0 for α-induced reactions on F,V,Co and Re. Whereas for α-induced reaction on Al comparitively large initial exciton configurations (8/4/4/0) or (10/5/5/0) were required to fit the excitation functions reasonably well.

The work reported here also relates the measurements of the recoil ranges of nuclei produced with a view of getting experimental information about the momentum transfer associated with specific final nuclei. Recoil ranges were converted into recoil momentum using Lindhard, Scharff and Schiott (LSS) and Blaugrund theories. These theories were also used to calculate projected recoil ranges for full momentum transfer pertaining to fusion reactions. The linear momentum transfer characteristics of reactions supplement

the energy partitioning characteristics of the reactions. The aim was to seek clues about some aspects of the interaction from the trends and magnitudes of the observed ranges. During the last few years considerable effort has been devoted to studies of the linear momentum transfer in light and heavy-ion induced reactions . The average linear momentum transfer characterises the global features of the projectile-target interaction. Whereas the recoil momentum distribution of the residual nuclei provides a convenient indication of the reaction mechanism, it will be greatest for complete fusion reactions and reduced for direct, pre-equilibrium and break-up processes in which much of the incident momentum is carried away by the fast particles in the early stages of the reaction. In the present work the linear momentum transfer characteristic in the α-induced reactions on 59-Co and 51-V, were obtained employing the classical method of thick-target thick-catcher recoil range measurements. One of the representative fig for the excitation function fo the reaction 51-V(α,3n)52-Mn is shown below along with [illegible] model (solid line) and Hybrid model (-pts) fits. Recoil range data are also shown in the same Fig.

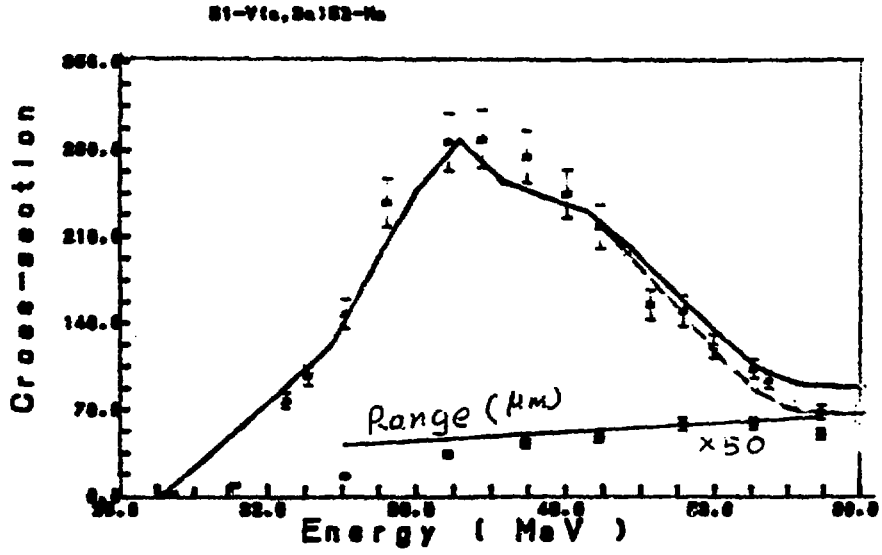

INVESTIGATION OF DEUTRON CLUSTER IN ^{6}LI USING 45 MEV ^{6}LI (α,αd) ^{4}HE REACTION

Mythili Subramanian, Arun Kumar Jain, Amit Roy*,
& Ranjan Bhowmik
Nuclear Physics Division, B.A.R.C., Bombay-400085
* Nuclear Science Centre, New Delhi-110067.

Coincidence measurements of alpha and deutron in the knockout reaction of ^{6}Li bombarded by the alpha beam of 45 MeV was done at VECC. The alpha and deutron particles were detected in surface barrier telescopes. Angular correlation was done and data collected for seven angle pairs was analysed off-line.

However in the reaction ^{6}Li(α,αd) there is contamination from intermediate states formed viz. ^{8}Be and ^{6}Li. ^{8}Be can be formed and excited to its resonance states and subsequently decay into two αs, one of which is detected in coincidence with the deutron emitted earlier. Similarly ^{6}Li could also be excited to states above its particle breakup threshold and decay from its excited state as a α+d pair- in this case the deutron is in coincidence with the alpha scattered earlier. From kinematics it was found that the decay from these resonances (11.4, 16.6, 16.92 in ^{8}Be and 4.31 and 5.65 in ^{6}Li) would contribute in the same energy region as our reaction for certain angle pairs. Hence it was necessary to remove the contribution from these resonances before comparing the experimental cross-section to the cross-section yielded by the DWIA model incorporating the peripheral-3-body approximation[1].

Since five resonances (3 in ^{8}Be and 2 in ^{6}Li) are to be fitted, a χ^2 procedure was adopted. The resonances were fitted with either a Gaussian(11.4 MeV) or a Briet-Wigner form. The width of the resonances was converted to corresponding widths in alpha energy ; from kinematics the alpha energy corresponding to the resonances were extracted. These energies and widths were then used for fitting. The experimental data was corrected for these resonances and then the experimental $|\phi(q)|^2$ distribution thus obtained was compared to that predicted by the DWIA

model incorporating the (a) Kinematic Coupling Approximation (KCA) and (b) Peripheral-3-Body approximation (P3BCM).From Fig.1 it is clear that the P3BCM fits the data better than the KCA. The data corresponds to θ_{cm}=60 where the spectator alpha takes no momentum at all.

The better fit from the P3BCM approximation leads to certain results.While the differential cross-section ($d\sigma/d\Omega$)is predicted to be nearly flat by the KCA approximation , P3BCM predicts an increase in cross-section with angle (Fig.2).The experimental cross-section has a deeper minimum than that predicted by KCA - hence a smaller deutron cluster size is incorporated into the calculation to fit the data[2]. However, with the P3BCM the deeper minimum is predicted - one does not need a shrunk deutron cluster size in this model to fit the data.

References.

(1). A.K.Jain Phy.Rev C ,in print
(2). Proc. DAE Symposium 28B(1985)24

Fig. 1

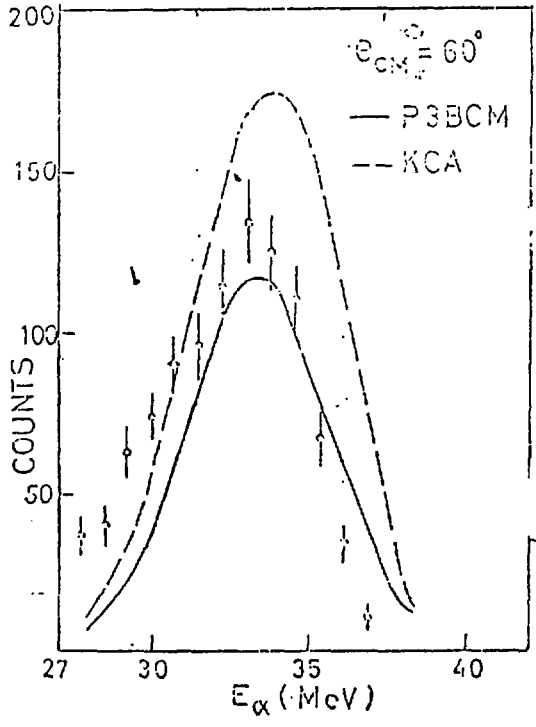

Fig. 2

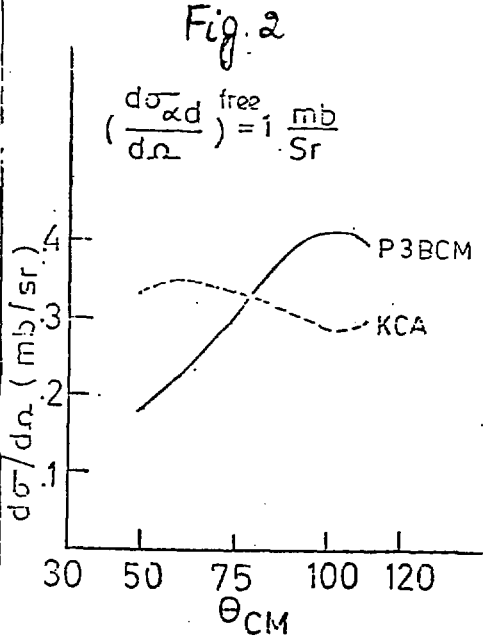

GEOMETRICAL EFFECTS ON FINAL STATE INTERACTION IN THREE BODY BREAK-UP EXPERIMENTS

S. Mandal. & S. S. Dasgupta
Physics Department, Burdwan University
Burdwan - 713 104

Two body final state interaction is an important thing in three body break-up experiment. The two body final state interaction can populate bound states (ground state as well excited states) or virtual states of different nucleus. The excitation energy and width of the state can be deduced. A great deal of effort has been spent in performing such experiments 1). The energy spectrum of these nucleus may lead to a study of a clear forces. Since there are several phase pace factor in three body break-up experiment , it is difficult to calculate actual interaction cross-section . Often geometrical effects enough to introduce large errors in experimentally obtained cross-sections. Usually, two dimensional locii between energies of outgoing particles are analysed 2). Finite dimension of the detectors in a coplanar setup causes geometrical effects which disturbs the symmetry around central kinemetric locus and causes the spreading of data. The assymetry along arc is large enough and most of the cases the peak overlaps on f.s.i peak 3). To extract actual events one have to seperate the effect due to geometrical factor unless the angular resolution of the detector is guite good, so that all events seem to be projected on central kinemetric locus 1). There is no existing method to calculate the said phase space factor along arc. We have developed the method of calculation by computation. Preleminary results are obtained for alpha induced deuteron break-up at incedent energy of 45 Mev for several pair of angles (Fig.) .

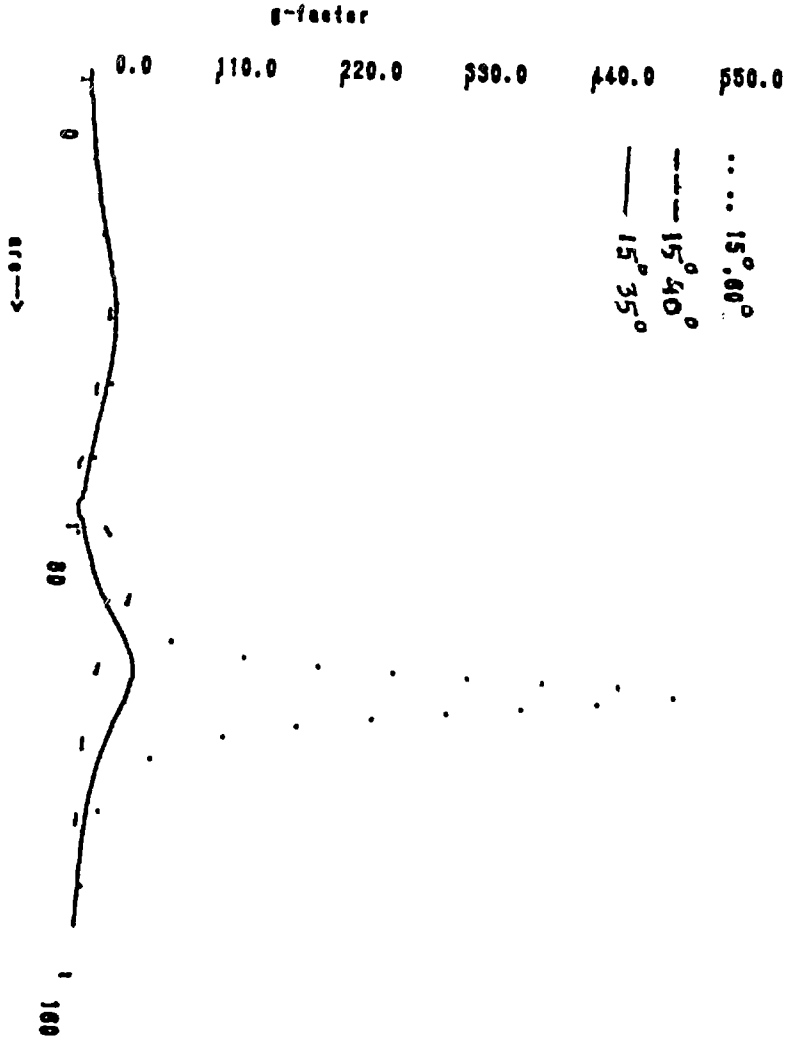

References :-

1) N. Arena , Seb. Cavallaro , A. D. Arrigo , G. Giadira , A. Italiane , M. Herman. & M. Lombardi . Phys. Rev. C 40 (1989).
2) G. G. Ohlsen NIM 37 (1965) 240 .
3) M. Bruno , F. Cannanta , M. D'Agastino , M. L. Fiandri , G. Vannini , M. Lombardi & Y. Koike .
4) S. S. Dasgupta , R. J. Slobodrian , R. Roy , C. Rioox and F. Lahlou . Phy. Rev. C 22 (1980) .
5) S. Mandal and S. S. Dasgupta D.A.E. (1989) .

HELIUM-ION-INDUCED FISSION EXCITATION FUNCTIONS OF TERBIUM AND YTTERBIUM

A.K. Pandey, R.C. Sharma, P.C. Kalsi and R.H. Iyer
Radiochemistry Division, B.A.R.C.
Trombay, Bombay-400 085.

SUMMARY

Excitation functions for the helium-ion-induced fission of Tb(Z=65) and Yb(Z=70) in the energy range 34-65 MeV have been measured using Lexan polycarbonate plastic as the fission fragment track detector. The data were analysed in terms of the statistical model expression for Γ_f/Γ_n, the ratio of the fission width to neutron emission width to get the fission barriers and the level density parameters. The measured fission barriers compare very well with the theoretical barriers obtained by Liquid drop model, shell corrected liquid drop barriers, finite-range models of Sierk and Mustafa et.al

INTRODUCTION

As part of a systematic program of work on the fission properties of low Z(Z<80) elements induced by light and heavy ions, we have measured the fission cross sections of Tb(Z=65) and Yb(Z=70) induced by helium-ions in the energy range 34-65MeV from the VECC, Calcutta.

EXPERIMENTAL

Experimental details are given in our recent publication[1] and are described here briefly. Targets were prepared from highly purified Tb_2O_3 and Yb_2O_3 on high purity silver foils in the form of deposits 1-2mg/cm^2 thickness by a method developed by us[1]. Fission events recoiling in the backward direction were recorded using a cylindrical Lexan detector. Typical He-ion beam currents were 1-2μAh per experiment. After irradiation, the detector was etched in 6N NaOH. The fission cross sections were calculated by comparing the number of fission tracks in a specified area in the detector from the sample with the number of tracks in the same area from a standard (in this case gold and lutetium) irradiated under the same experimental conditions.

RESULTS AND DISCUSSION

The excitation energies were calculated by assuming full momentum transfer and a weighted av. Q value of -2.2 MeV for Ytterbium and -0.7 MeV for Terbium. The excitation functions were analysed in terms of the statistical model expression[2]. A least square fitting procedure was used to fit the experimental Γ_f/Γ_n values to the theoretical equation to get

the 'best fit' values for E_f, a_f, a_n and a_f/a_n. The fitted curves corresponding to $a_f = A/8$ and $A/20$ (reasonable upper and lower limits) are shown in figs. 1 and 2. The values of E_f, a_f and a_n for Ho^{163} (i.e. $He^4 + Tb^{159}$) and $Hf^{177.1}$ (i.e. $He^4 + Yb^{173.1}$) are 31.4 ± 3.5 MeV, 13.58 MeV^{-1}, 13.45 MeV^{-1} and 23.9 ± 3.0 MeV, 14.76 MeV^{-1}, 14.33 MeV^{-1} respectively. The experimental fission barriers compare very well with the theoretical values based on the non-rotating liquid drop[3] shell corrected liquid drop[4] finite-range models of Sierk[5] and Mustafa et.al.[6] A systematic trend is observable with regard to the a_f/a_n values in the lighter element region. As one moves away from the closed shell region the af/an values tend to decrease and reach a value close to unity. The a_f/a_n values of 1.35, 1.18, 1.17, 1.11, 1.08, 1.03, 1.04, 1.03 and 1.01 for gold, Iridium, Rhenium, Lutetium, Thulium, Erbium, Holmium, Terbium and Ytterbium respectively (Present work) very clearly demonstrate this trend.

REFERENCES

1. R.H.Iyer, A.K.Pandey, P.C.Kalsi and R.C.Sharma, Phys.Rev. C44, No. 5 (1991).
2. R.Vandenbosch and J.R.Huizenga, Nuclear Fission, Academic Press, NewYork (1973).
3. S.Cohen, F.Plazil and W.J.Swiatecki, Ann.Phys. 82, 557 (1974)
4. W.D.Myers and W.J.Swiatecki, Report No. UCRL-16489 (1966).
5. A.J.Sierk, Phys.Rev. C33, 2309 (1986).
6. M.G.Mustafa, P.A.Baisden and H.Chandra, Phys.Rev. C25, 2524 (1982).

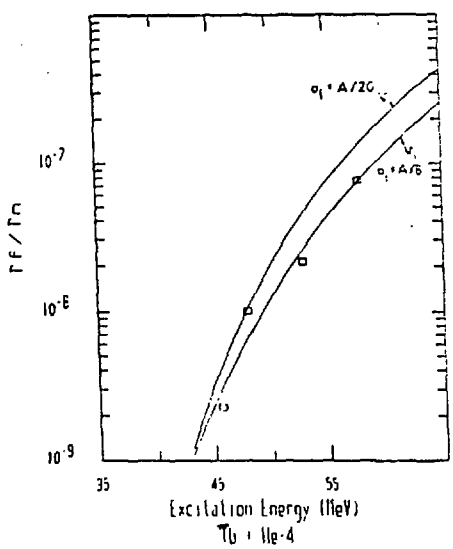

FIG.-1.

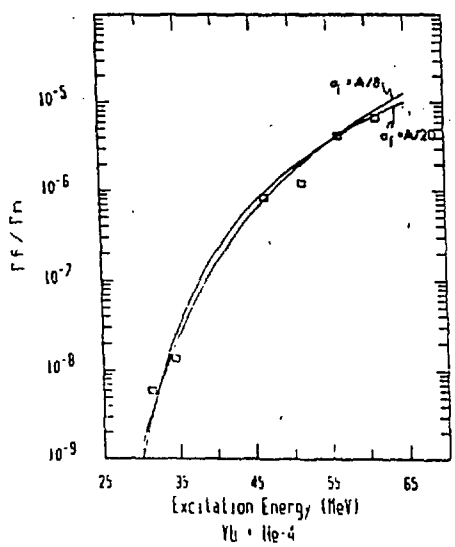

FIG.-2.

KINETIC ENERGY DEPENDENCE OF FISSION FRAGMENT ANGULAR MOMENTUM

T.Datta, S.P.Dange, H.Naik and P.K.Pujari
Radiochemistry Division, Bhabha Atomic Research Centre,
Trombay, Bombay-400 085.

Investigations on fragment angular momentum in medium energy fission provide insight into the roles of various collective degrees of rotation. Such investigations free from averaging over fragment mass/charge, emission angle[1] and kinetic energy bring out specific details regarding influence of various collective and intrinsic degrees on the rotational modes. So far kinetic energy dependence of fragment angular momentum has been studied[2] in $^{235}U(n_{th},f)$ and it is worthwhile to carry out such studies in medium energy fission in view of higher input angular momentum and temperature. In this paper we present the preliminary significant results on variation of fragment J_{RMS} for ^{132}I with average kinetic energy in $^{232}Th(\alpha,f)$ at 35.5 and 39.1 MeV alpha particle energies.

The experiments were carried out using thin target-thick catcher technique and electrodeposited (<200 $\mu g/cm^2$) Th targets, covered with 0.3 and then 1.0 mil aluminium catcher foils, employing stack-foil technique. Irradiations were carried out at the 88" variable energy cyclotron, Calcutta using 40 MeV alpha beam for appropriate times. The stack-foil assembly was placed such that for the 39.1 MeV alpha beam fragments were collected in forward direction and in backward direction for 35.5 MeV alpha beam. Activities of ^{132}Te and $^{132}I^{m,g}$ were monitored in each of the 0.3 and 1.0 mil foils gamma spetrometrically using a high resolution HPGe detector coupled to a 4K MCA, with a resolution of 2.0 keV at 1332 keV. Ratios of all the activities in 0.3 and 1.0 mil foils were determined in each case and the independent isomeric yield ratios for ^{132}I in each of 0.3 and 1.0 mil foils were determined from the observed activities using appropriate equations and after correcting for precursor contribution. Fragment J_{RMS} for ^{132}I in the individual 0.3 and 1.0 mil foils at each energy were deduced from the observed yield ratios and spin analysis using the code GROGI2[1] and are given in table-1.

It was seen that in the case of 39.1 MeV bombardment the ratio of activities of ^{132}Te in 1.0/0.3 mil foils is 0.73±

0.06 for forward collection while for 35.5 MeV bombardment the activity ratio in 1.0/0.3 mil foils is 0.38±0.03 for backward collection. Such large difference in the 1.0/0.3 mil activity ratios in the two cases is due to the difference in the forward and backward range or kinetic energy (KE) of a given fragment on account of the centre-of-mass velocity. Calculations carried out invoking the angular distribution function in range-energy treatment[3] of thermal fission show excellent agreement with kinetic energy data in $^{235}U(n_{th},f)$ system indicating insignificant change of kinetic energy with excitation energy of the present system.

It is generally expected that 0.3 mil foil adjacent to the target attenuates larger proportion of the lower KE fragments while higher KE fragments reach the distant 1.0 mil foil. Table-1 clearly shows that in 1.0 foils or at high KE region low J_{RMS} is obtained. This is due to lower temperature and deformation for a given fragment (constant Q value) at high KE when higher J-levels are not highly populated statistically, at both 35.5 and 39.1 MeV bombardment energies. Further, J_{RMS} in 35.5 MeV alpha induced fission are lower than in the case of 39.1 MeV due to lower temperature and orbital momentum at the entrance channel at 35.5 MeV. Significantly low J_{RMS} at high KE is seen at 35.5 MeV compared to 39.1 MeV due to more stringent attenuation of low-medium range KE fragments in 0.3 mil foil in the backward direction.

ACKNOWLEDGEMENTS:- The authors acknowledge the keen interest shown by Dr. P.R. Natarajan Head, R.Ch.D. and Dr. R.H. Iyer. The VECC crew are also acknowledged for their assistance.

Table-1: Fragment J_{RMS} variation with KE domains in $^{232}Th(\alpha,f)$

Eα(MeV)	Activity Ratio (1.0/0.3) mil	Fragment $J_{RMS}(\hbar)$ 0.3 mil	1.0 mil
39.1	0.73±0.06	15.6±1.2	9.5±0.5
35.5	0.38±0.03	11.6±1.4	7.8±0.6

References:

1. T. Datta et.al. Z. Phys.A- 330, 103 (1988); T. Datta et.al. Phys. Rev. Lett. (To be published).
2. H.O. Denschlag et.al., Proc. IAEA Symp. on Phys. and Chem. of Fission, Julich, Vol-II, 249 (1979).
3. J.M. Alexander, M.F. Gazdik, Phys. Rev. 120, 874 (1960).

CHARGE DISTRIBUTION IN LOW ENERGY FISSION OF ACTINIDES

H. Naik, S.P. Dange and T. Datta
Radiochemistry Division, Bhabha Atomic Research Centre
TROMBAY, BOMBAY 400 085

The experimental investigation of charge distribution in low energy fission provide important information on (i) influence of nuclear structure effect and (ii) dynamics of descent in the potential energy surface. The structural effects are inferred generally from the isobaric yield distributions in terms of certain parameters e.g. most probable charge (Z_p) and its deviation from that based on unchaged charge distribution Z_{UCD} i.e. charge polarization (Z) as well as width parameter (σ_Z) of the Gaussian distributio [1] comprise these parameters. On the other hand dynamical aspect of fission was studied by Nifeneker et.al.[2] by interpreting odd-even effect as a function of fissility parameter (Z^2/A) and excitation energy above second saddle point (E^*-B_0). In order to investigate these aspects, in the present work fractional cumulative yield (FCY) of two nuclides namely ^{128}Sn and ^{131}Sb were determined in thermal neutron induced fission of ^{233}U, ^{235}U, ^{239}Pu, ^{241}Pu and ^{245}Cm.

Electrodeposited target of ^{233}U(100μg), ^{235}U(100μg), ^{239}Pu(100μg), ^{241}Pu(25μg) and ^{245}Cm(2μg) covered with superpure aluminium foils (25 um thick) were irradiated for approriate times in the reactor APSARA at a flux of $1.2*10^{12}n\cm^2\sec$. After each irradiation the catcher foil was counted on an efficiency calibrated 80 cc HPGe detector coupled to a 4K channel analyser having resolution 2.0 keV at 1332.0 keV. The areas of of the photopeaks of interest were calculated after subtracting the linear Compton contribution. From the activities of ^{128}Sn and ^{131}Sb cumulatives yields were calculated using ^{135}I as a monitor and usual decay-growth equations. FCY values were determined from the cumulative and the chain yields as given in the table-1 along with the literature data of $^{250}Cf^*$[3]

Table-1 shows that the FCY of both the nuclides (^{128}Sn and ^{131}Sb) decreases with increase of Z^2/A of the fissioning system with slight fluctuation at $^{234}U^*$ and $^{242}Pu^*$. The observed decreasing trend is expected on the basis of change in the Z_p and σ_Z with intrinsic excitation energy [4]. The intrinsic excitation energy is likely to increase in turn with increase in the fissionability parameter on account of sharply increasing Q-value and higher viscosity. It is difficult to evaluate the intrinsic excitation energy quantitatively though the major fraction (~ $3/4^{th}$)of the energy above the second saddle point goes into intrinsic degrees as is known from the comparison of neutron

yield and kinetic energy between spontaneous fission and neutron induced fission [5]. Table-1 shows a very good correlation of FCY of the above two nuclides as a function of excitation energy above the second saddle point with slight deviation only at $^{234}U^{*}$. It is also observed from the table-1 that the FCY of both the nuclides are close in the fissioning nuclei pairs $^{236}U^{*}$: $^{242}Pu^{*}$ and $^{234}U^{*}$:$^{240}Pu^{*}$ This may be due to the close resemblance in their N/Z ratios. Besides these, using the FCY value of one more nuclide from literature the Z_p (and thus ΔZ) and σ_Z were evaluated independently. The ΔZ and σ_Z values obtained are also given in Table-1 showing that the ΔZ value for ^{128}Sn is lower than in the case of ^{131}Sb. This may be due to the presence of spherical 50 proton shell in the former indicating the effect of shell closure proximity. This is further supported from the very low σ_Z valuein the case of ^{128}Sn compared to ^{131}Sb.

Thus the above observations indicate that charge distribution is closely associated with the Z^2/A, N/Z and E^*-B_0 of the fissioning nucleus. Further it also depends on nuclear structural effect.

Acknowledgement: Authors sincerely thank Dr.P.R.Natarajan, Head, Radiochemistry Division for his keen interest in the work.

References:

1. A.C.Wahl et.al.Proc.of IAEA Symp.on Phys.and Chem. of Fission, Vienna,813(1969).A.C.Wahl At.Data. Nucl.Data Table 39,1(1988).
2. H.A.Nifnecker,et.al. Proc. of IAEA Symp. on Phys. and Chem. of Fission Julich, (1979).
3. J.K. Dickens and J.W. McConnel Phys. Rev. c-24,192(1981)
4. B.D. Wilkins et.al. Phys. Rev. C-14, 1832 (1976).
5. R.Vandenbosch and J.R.Huizenga,"Nuclear Fission" 1973.

Table-1.

Fissioning System	234-U	236-U	242-Pu	242-Pu	246-Cm	250-Cf
FCY of 128-Sn	0.787	0.945	0.852	0.930	0.748	0.590
	+0.056	+0.035	+0.055	+0.016	+0.03	+0.051
Z_p	50.23	49.92	50.13	49.90	50.23	50.40
σ_Z	0.36	0.36	0.38	0.38	0.38	0.38
ΔZ	-0.258	-0.117	-0.238	-0.049	-0.152	-0.263
FCY of 131-Sb	0.566	0.797	0.649	0.784	0.646	0.421
	+0.038	+0.01	+0.019	+0.028	+0.028	+0.056
Z_p	51.25	50.93	51.20	50.97	51.23	51.90
σ_Z	0.55	0.55	0.57	0.57	0.60	0.60
ΔZ	-0.333	-0.349	-0.376	-0.217	-0.395	-0.292
Z^2/A	36.171	35.867	36.817	36.512	37.463	38.413
E^*-B_0 in MeV	1.343	1.015	1.463	1.206	2.156	3.023

CHARGE DISTRIBUTION IN 79 MeV 12-C INDUCED FISSION OF 232-Th

A.V.R.Reddy, A.Goswami, B.S.Tomar, A.G.C. Nair, S.K.Das, S.B.Manohar and Satya Prakash, Radiochemistry Division, BARC, Trombay, BOMBAY 400 085.

INTRODUCTION : Studies of charge and mass distribution in heavy ion induced fission of actinides at moderate energy give unique opportunity to understand the mechanism of the reaction compared to the low energy fission, due to absence of shell and pairing effects, although compound nuclei in these reactions will have excitation energies around 50 MeV and above leading to multichance fission. Studies on charge distribution in heavy ion induced fission of actinides are scarce and few measurements indicated the possible presence of two peaked distributions(1,2), one centered around neutron deficient products and the other centered around neutron rich products. It was attributed that neutron rich products were formed from non-equilibrium process and the neutron deficient products were formed from normal low energy fission process. The widths of these two distributions showed dependence on the excitation energy. In view of these interesting observations, systematic studies on the determination of the independent yields of different elements in the heavy ion induced fission of actinides were initiated and yields of antimony and iodine isotopes in the 79 MeV 12-C induced reaction of 232-Th are reported in this paper.

EXPERIMENTAL: Self supporting target of thorium (2.5 mg/cm^2) was covered with 6.75 mg/cm^2 aluminium foil and bombarded with 79 MeV 12-C ions at BARC-TIFR pelletron facility, TIFR, Bombay. Duration of bombardment was kept around 20-30 min for the short lived products and 5-6 hours for long lived products. Current on the target was around 30 particle nA which was measured using an electron suppressed Faraday cup. After appropriate cooling, the catcher foils were dissolved and antimony and iodine were separated using standard radiochemical separation procedures(3). 125-I and 125-Sb were used as tracers for determination of radiochemical yields. The radioactivity of iodine and antimony isotopes in separated samples were assayed using high resolution gamma spectrometry.

RESULTS AND DISCUSSIONS: The standard decay-growth relations and the measured photo-peak areas were used to calculate the yields of different isotopes, details of which are given

elsewhere(4). Yields obtained in the present investigations are given in table 1. Isotopic yields of each element are fitted to a gaussian to obtain the distribution parameters, width of the distribution (σ_A) and the most probable mass (Ap). We did not observe two-peaked distribution indicating that cross-section for fission following the direct reactions is negligible compared to that for fusion-fission. The widths of the distribution for both antimony (Z=51) and iodine (Z=53) are higher compared to those observed in the low energy fission. The broadening of widths could be due to higher nuclear temperature and multichance fission. Ratios of most probable mass to charge for both antimony and iodine are nearly same which indicates that the fission follows Unchanged Charge Distribution (UCD). These ratios were used to arrive at the average fissioning system mass and the total number of neutron emitted in this reaction as 235.8+0.7 and 8.2+0.7 respectively.

ACKNOWLEDGEMENTS: The authors are thankful to Dr.P.R. Natarajan, Head, Radiochemistry Division,BARC for his keen interest in this work and to the operation crew of the pelletron machine for their cooperation.

REFERENCES:

1)Y.W. Yu etal., Phys. Rev. C 36,2396 (1987).
2) M. de Saint Simon etal., Phys. Rev. C 2(,2447 (1982)
3) K. Flynn, Report ANL-75-24 (1976).
4) A.V.R. Reddy, Ph. D Thesis, S.V. University (1986).

Table 1. Isotopic yields of antimony and iodine

Isotope	yield	Isotope	yield
122-Sb	1.744	128-I	0.54
124-Sb	5.022	130-I	1.00
126-Sb	2.449	131-I	1.40
127-Sb	4.801	133-I	0.62
128-Sb	1.00	134-I	0.33
129-Sb	1.00	135-I	0.32

Table 2. Charge distribution parameters

Z	σ_A	σ_A*	Ap	Ap/Z
51	2.79+0.34	2.197	124.9+0.5	2.449
53	2.24+0.07	2.210	130.6+0.1	2.464

* Width calculated taking into account of nuclear temperature effect and UCD hypothesis.

PRE-FISSION ALPHA MULTIPLICITIES IN THE $^{19}F+^{181}Ta$ REACTION

A.Chatterjee, S.Kailas, P.Singh, A.Navin, S.S.Kerekatte, D.C.Biswas, Aruna Nijasure, B.V.John, Alka Karnik and S.S.Kapoor
Nuclear Physics Division, B.A.R.C., Bombay-400 085

Comparison of the data on pre-fission neutron multiplicities, ν_{pre} in heavy-ion reactions [1] with the statistical model indicate overdamped motion of the nuclear fluid with time scales $\gtrsim 30\times10^{-21}$ s. Measurements of pre-fission alpha (α_{pre}) and proton (π_{pre}) multiplicities can be used to verify these time-scales. However, contradictory results have been reported recently. In one case [2], α_{pre}, π_{pre} and ν_{pre} from $^{192,195,198}Pb$ compound nuclei are explained with a combined pre-saddle delay of $t_d=10\times10^{-21}$ s and post-saddle delay, $t_{ssc}=50\times10^{-21}$ s; whereas another group reports [3] that α_{pre} values for $^{19}F+^{197}Au$ can be reproduced without considering delayed fission.

We have measured α_{pre} for $^{19}F+^{181}Ta$ at 110MeV. The target was 2mg/cm^2 self-supporting Ta. Two NaI detectors(45mm dia) were used to detect α-particles employing pulse-shape discrimination to distinguish between γ, α and p. Fission fragments were detected in a gas ionisation chamber at 130° to the beam and subtending a solid angle of 376msr. The spectra of alpha particles at 30° and 75° in coincidence with fission were measured. The detectors were covered by Al-foil (14mg/cm^2) to stop elastically scattered particles. The spectra were calibrated using a ^{228}Th alpha source. The pre- and post-fission components in the measured spectra can be separated by virtue of the difference in the Coulomb barrier in addition to the kinematic focussing effect. A simultaneous fit of the two spectra was made with calculated spectra from the code PACE2 incorporating pre- and post-fission emission.

In agreement with ref 3 we find that the experimen

tal spectra are shifted to 2MeV lower than calculated. A comparison of the measured α_{pre} and ν_{pre} from the literature [1] with PACE2 calculations (using $a_\nu = A/10\ MeV^{-1}$, $a_f/a_\nu = 1.00$) is shown in the figure.

The measured $\alpha_{pre} = (1.33 \pm 0.3) \times 10^{-3}$ at 110MeV is larger than predicted, which can be taken to imply delayed fission. However it is neccessary to measure α_{pre} over a range of bombarding energies before arriving at a definite conclusion.

[1] J.O.Newton, Pramana 33 (1989) 175.
[2] J.P.Lestone et al, Phys.Rev.Lett. 67(1991)1078.
[3] H.Ikezoe et al, Phys.Rev. 42(1990)342 and R1187.
[4] D.J.Hinde et al, Nucl. Phys. A452(1986)550.

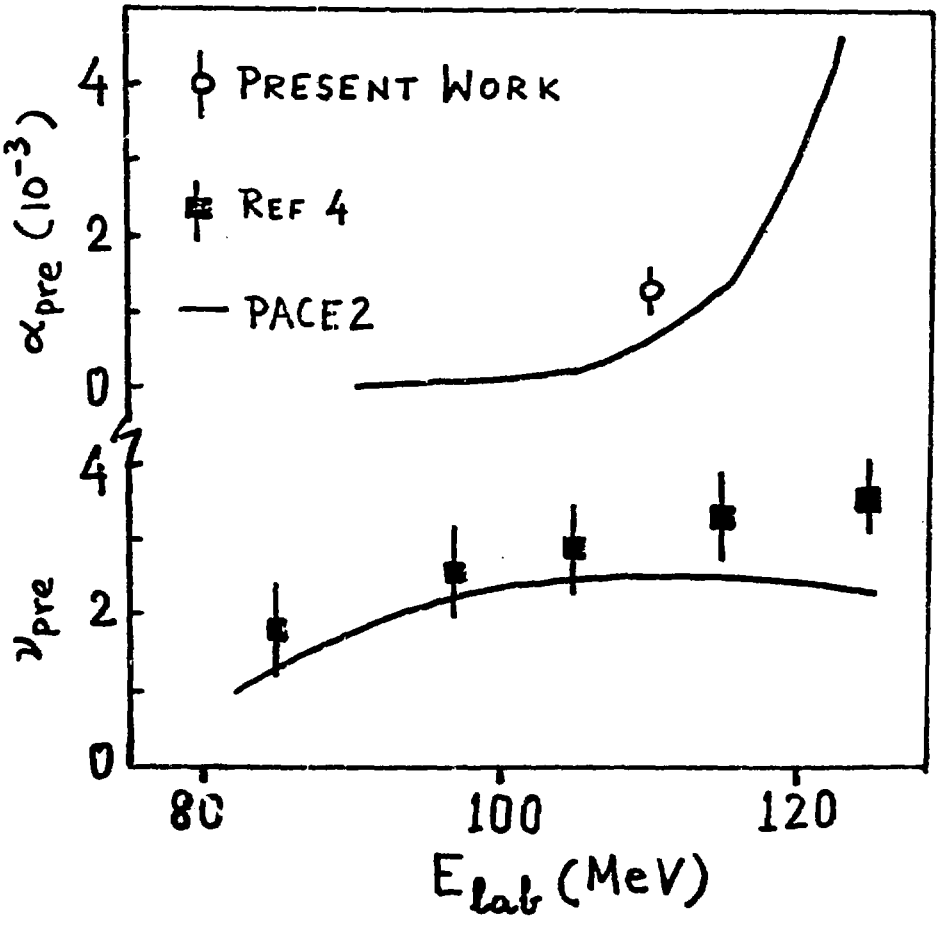

EFFECT OF PRE-FISSION NEUTRON EMISSION ON THE INTERPRETATION OF FISSION FRAGMENT ANGULAR DISTRIBUTIONS:

A.Saxena,S.Kailas,A.Karnik,A.Chatterjee,D.M.Nadkarni and S.S.Kapoor
Nuclear Physics Division,B.A.R.C.,Bombay-400 085

In several cases of heavy-ion fusion-fission reaction, the fission fragment angular distributions have been found to be anomalous. In an earlier work[1], it was shown that fission fragment anisotropies exhibit an abrupt transition with respect to the entrance channel mass/charge asymmetry. In the present work we have investigated the effects of pre-fission neutron emission on the interpretation of fission fragment angular distributions. Neutrons evaporated before the saddle-point configuration reduce the excitation energy at the transition state. The effect of higher chance fission therefore increases the calculated anisotropy according to the standard saddle point statistical model. In the earlier work, K_0^2 was calculated from α-induced fission data[2] for the same compound nucleus after scaling it with Ex using the relation,

$$K_0^2 = J_{eff}\sqrt{(Ex/a)}/\hbar^2$$

However, as the experimental information on pre-fission neutron emission in α-induced fission is not available for various systems studied here. We have corrected for compound nucleus excitation energy and spin change due to evaporation of neutrons in K_0^2 for different values of $\nu_{pre}(\alpha)$ for the α-induced reaction; whereas for heavy-ion induced fission excitation energy and the spin was corrected using the data available[3,4]. Fig. 1 shows the influence of this neutron emission in α-induced fission as well as heavy-ion induced fission. It is shown that for $\nu_{pre}(\alpha)<2$, ^{10}B, ^{12}C induced fission of ^{232}Th and ^{237}Np are normal and ^{16}O and ^{19}F induced fission are anomalous for all the values of $\nu_{pre}(\alpha)$. This confirms the earlier conclusion[1] regarding entrance channel dependence of fission fragment anisotropies is unaltered even after correction for pre-fission

neutron emission.

REFERENCES:

1.V.S.Ramamurthy et. al. Phys.Rev.Lett 65(1990)25
2.R.F.Reising et. al. Phys.rev. 141(1966)1161
3.J.O.Newton,Pramana 33(1989)175
4.A.Saxena et. al.DAE Symposium (1991)(this proceedings)

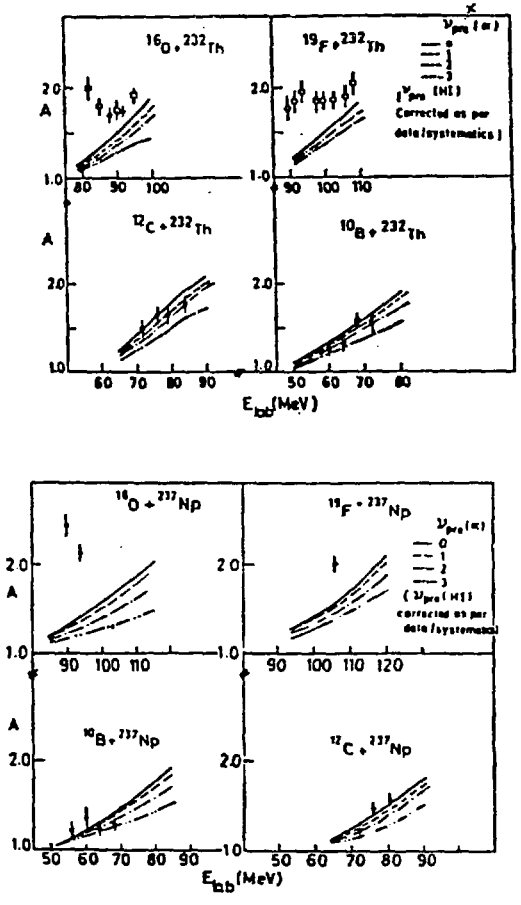

FIG 1

MEASUREMENT OF FISSION FRAGMENT ANGULAR CORRELATION FOR $^{19}F+^{232}Th$ SYSTEM AT 107 MeV AND 95 MeV.

Alok Saxena, D.C.Biswas, D.M.Nadkarni, V.S.Ambekar and B.V. Dinesh.
Nuclear Physics Division,B.A.R.C.,Bombay-400 085

P.Bhattacharya, P.Basu, S.Bhattacharya, and M.L.Chatterjee,
Saha Institute of Nuclear Physics, Calcutta-700064.

Fission fragment folding angle is related to the linear momentum transferred from the projectile to the fissioning nucleus. At incident energies close to the coulomb barrier, the contribution from incomplete momentum transfer come from peripheral collisions which include the inelastic scattering or transfer reactions. It is important to know their contributions for the quantitative analysis of the fission fragment angular distribution. In an earlier experiment for the ^{19}F + ^{232}Th system at 104.4 MeV, it was shown that the most probable peak of measured folding angle distribution corresponds to about 95±3% of the full momentum transfer (Ref.1). In the present work we have measured the folding angle distribution for ^{19}F + ^{232}Th system using ^{19}F beam of 107 and 95 MeV at BARC-TIFR Pelletron accelerator facility. A self-supporting target of 1.8 mg/cm^2 was used. Two MWPC's of active areas (7 cm x 5.2 cm)and (14.5 cm x 5.2 cm)were kept in back to back geometry and both of them were operated using Isobutane at a pressure of 3.3 Torr. One surface barrier detector was kept behind the smaller MWPC. Details of the MWPC have been given in Ref.2. The angle calibration of the MWPC could be obtained from the position of nylon wires. In the present work data measured with surface barrier detector and large MWPC have been reported. The fragment angular correlation spectrum for 107 MeV is shown in the figure along with the gaussian fit.

The most probable peak is compared with the expected one for complete fusion in the following table.

E_{LAB}	ϑ_{SB}	Measured ϑ_{ff}	Calculated ϑ_{ff}	FWHM
107 MeV	90°	156.6°±0.5°	156.8°	8.1°
95 MeV	90°	160.5°±0.8°	158°	7.1°
95 MeV	119.6°	164.1°±0.5°	162.4°	6.0°

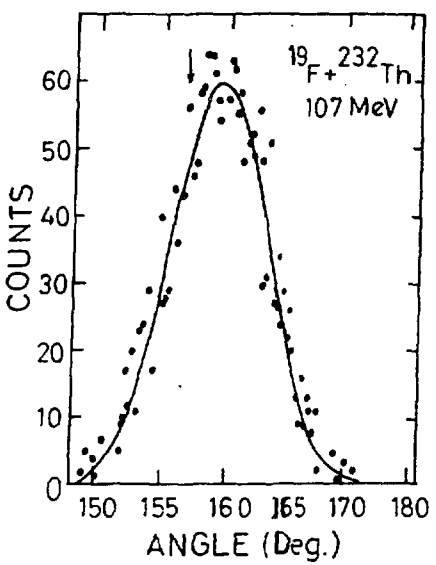

The most probable peak for both the energies is consistent with 90 ± 3 % of the full momentum transfer and the folding angle distribution is broadened for 107 MeV compared to 95 MeV.

References:
1.Alok Saxena etal,DAE Symposium of Nuclear Physics NP 33B(1990) 117
2.P.Bhattacharya etal. NIM A276(1989) 585-587.

ANGULAR DISTRIBUTION OF TRANSFER PRODUCTS IN $^{12}C,^{16}O+^{232}Th$ REACTIONS AT NEAR BARRIER ENERGIES.

D.C. Biswas, B.K. Nayak, B.V. Dinesh, L.M. Pant, S.V.S. Sastry, V.S. Ambekar, D.M. Nadkarni and R.K.Choudhury.
Nuclear Physics Division, B.A.R.C, Bombay-400 085.

The entrance channel mass asymmetry plays a significant role in the dynamics of nuclear reactions near the liquid drop Businaro- Gallone point. In a previous work it was observed that the transfer reactions exhibit common properties which depend mainly on the number of transferred nucleons rather than the specific nature of colliding ions and at higher energies the probablity of many nucleon transfer increases relative to few nucleon transfer at the grazing angle [1]. In order to study the effects of entrance channel mass asymmetry in transfer reaction, earlier we measured the yields of projectile-like fragments over the angular range 70 deg to 110 deg for 78.6 MeV $^{12}C+^{232}Th$ and 87.2 MeV $^{16}O+^{232}Th$ reactions. The present work investigates the dependence of angular distribution of projectile like fragments on bombarding energy and entrance channel mass asymmetry. Beams of ^{12}C(E_{lab}=83,80,76 and 72 MeV) and ^{16}O(E_{lab}=96 and 88 MeV) from the 14 UD BARC-TIFR Pelletron accelerator were used to bombard self supporting ^{232}Th target of 1.8 mg/cm^2 thickness. Yields of various reaction products were measured by using a ΔE gas and E-surface barrier detector telescope[3]. Another similar telescope was used to measure the fission fragments at fixed angle (90 deg) for normalization purpose. The details of experimental procedure is described earlier[2].

Relative yields for both the system at different lab angles are obtained after normalization to the fission counts and is plotted in fig.1 and 2 for different projectile energies. At the higher energies the angular distribution is nearly bell shaped for both the systems and the angular distribution becomes broader and slightly forward peaked with increasing nucleon transfer. As the

barrier energy is approached the angle corresponding to maxium yield (grazing angle) moves towards back angle resulting in a flatter distribution. Yields of $^{232}Th(^{12}C,Be)$ is relatively more than that of $^{232}Th(^{12}C,B)$ at angles smaller than grazing angles for higher energies and at all angles as the beam energy approaches the barrier energy. Analysis based on statistical models incorporating nucleon exchange and cluster transfers are being carried out to understand the striking difference in the particle transfers in the two systems.

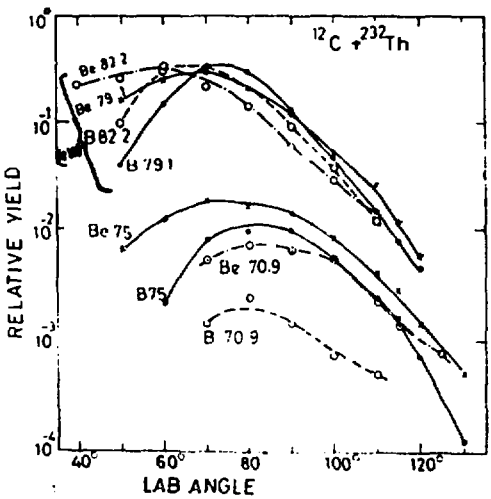

Fig.1.

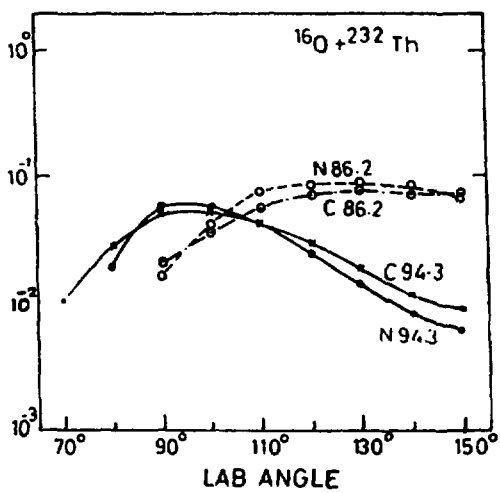

Fig.2

References:
1) J.S. Karp et al, Phys. Rev C25(1982)P1838.
2) D.C. Biswas etal Proc. NP Symp 1990, Madras.
3) D.C. Biswas, M.N. Rao and R.K. Choudhury, Nucl. Instr. Meth.B53(1991)P251.

STUDY OF EVAPORATION SPECTRA OF PROTONS AND ALPHA PARTICLES FROM COMPOUND NUCLEI IN MASS REGION=110

Aruna N., B. John, A. Chatterjee, A. Saxena,
A.K. Mohanty, P. Singh, K. Kumar, S. Kailas,
S.K.Kataria, S. S. Kapoor
Nuclear Physics Division, B.A.R.C., Bombay 400085.

It has been reported earlier [1,2] that light charged particle (p,α) spectra evaporated from compound nuclei formed during heavy ion reactions can be fitted only if evaporation barriers for these particles are lowered substantially as compared to their fusion barriers which are used for fitting inverse reaction cross-sections.

In order to study the phenomenon in detail, we have recorded proton and alpha spectra at various backward angles between 110° to 170° in case of the following reactions:

$^{12}C + ^{89}Y \rightarrow ^{101}Rh$ (50, 80 MeV)
$^{19}F + ^{107,109}Ag \rightarrow ^{126,128}Ba$ (96 MeV)
$^{7}Li + ^{107,109}Ag \rightarrow ^{114,116}Sn$ (34 MeV)
$^{19}F + ^{93}Nb \rightarrow ^{112}Sn$ (70,85,96,103 MeV)

Solid state detector telescopes of thicknesses (15 μm,1 mm), (25 μm,2 mm), (40 μm,2 mm) have been used in order to record these spectra. The calibration of these detectors has been done using recoil protons from a Mylar target as well as with alpha particles from a ^{229}Th source. Each spectrum has been normalised by using Rutherford scattering data obtained from a monitor detector placed at a fixed forward angle. Some of the above spectra have been re-recorded with different detectors and also with different experimental set-ups. Each of these laboratory spectra has been converted into centre of mass specrum, which is then fitted with an asymmetric Gaussian distribution:

$$\frac{N_1}{\sigma_1\sqrt{2\pi}} \exp\left[-\frac{1}{2}\left(\frac{x-\mu}{\sigma_1}\right)^2\right] \qquad \text{for } x \leq \mu$$

$$\frac{N_2}{\sigma_2\sqrt{2\pi}} \exp\left[-\frac{1}{2}\left(\frac{x-\mu}{\sigma_2}\right)^2\right] \qquad \text{for } x > \mu$$

It has been observed that the peak position obtained in different measurements varies by + 0.5 MeV at the same angle. This indicates the uncertainties in the determination of spectral shapes.

Various statistical model codes use different approximations. Hence, the experimentally obtained spectra have been compared with those obtained from the statistical model codes ALICE, PACE and CASCADE. Same input fusion cross-sections and level density parameters have been used in case of all the three codes. Fig. 1 and Fig. 2 show the typical experimental p and α spectra respectively, in case of F+Nb (103 MeV) along with the code calculations. The disagreement between all these codes is clearly seen. Multiplicities of p and α as obtained from these codes are given in Table 1. Further investigations into the comparison of different codes and selection of a proper code is under progress.

Table 1

Code	Multiplicities		
	neutrons	protons	alphas
Alice	4.64	1.17	0.18
Pace	3.58	0.80	0.65
Cascade	3.52	0.81	0.66

Ref.1. J.M.Alexander et al. ,Z. Phys. A 305, 313-318 (1982)
2. Moses et al. ,Z. Phys. A 320, 229-236(1985)

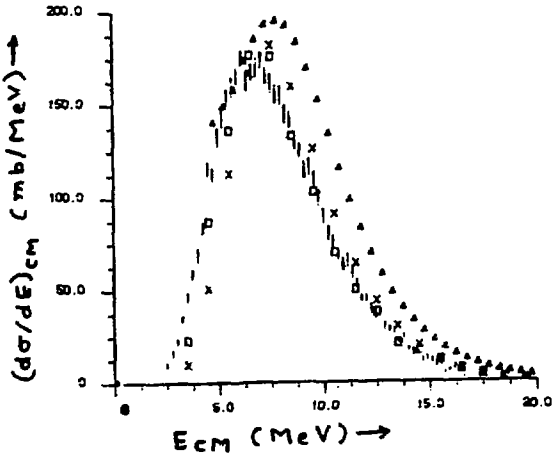

FIG. 1

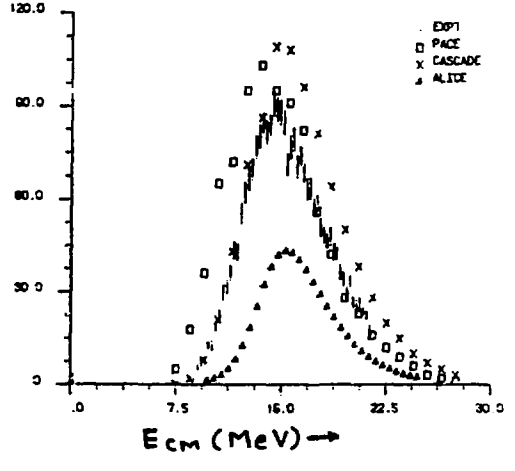

FIG. 2

INVESTIGATION OF PRESCISSION NEUTRON EMISSION FROM MASS AND TOTAL KINETIC ENERGY SELECTED FISSION FRAGMENTS IN $^{235}U(n_{th}, f)$

M.S.Samant, R.P.Anand, R.K.Choudhury, D.M.Nadkarni and S.S.Kapoor,
Nuclear Physics Division, B.A.R.C., Bombay 400085.

Prompt neutron emission in thermal neutron induced fission of ^{235}U and $^{252}Cf(sf)$ has been studied in great detail/1/ to study the yield of prescission (ν_{pre}) neutrons. The analysis of the recently measured angular distributions/2,3/ for the case of $^{252}Cf(sf)$ has led to the conclusion that the yield of prescission component is less than 5%. The question of whether or not the prescission neutron component is present, is answered by comparison of the experimental neutron-fragment angular correlations with those calculated from the kinematical considerations assuming neutron emission from fully accelerated fragments. The calculated neutron angular distribution is however, very sensitive to the emission spectrum of neutrons in the rest frame of fragments. In earlier analysis the emission spectra have been obtained from model calculations and any uncertainty in this would effect the conclusions on ν_{pre}.

In the present work we have measured the angular distributions of neutrons emitted in ^{235}U (n_{th},f) as a function of fragment mass and total kinetic energy (TKE) bins. The neutron spectra were measured using a (2" x 2") NE213 liquid scintillator detector by using the time of flight technique, the energy and angle of both the fission fragments were measured using a 4 π back-to-back gridded ionisaton chamber. The details of the experimental set-up have been described in ref./4/. The selfconsistent model independent Monte-Carlo calculations were carried out using the experimentally measured neutron multipilcities and neutron emission spectra for different fission fragment mass and TKE groups, assuming neutron emission from fully accelerated fragments. A comparison of the measured and the calculated neutron anisotropies then gives the value

of the prescission neutron component. Fig.1.shows the ν_{pre} values obtained as a function of total kinetic energy for different mass pairs, it is seen that the ν_{pre} values increase as the TKE increases. These results on the prescission neutron component can give important insight into saddle to scission dynamics and the timescale of the fission process.

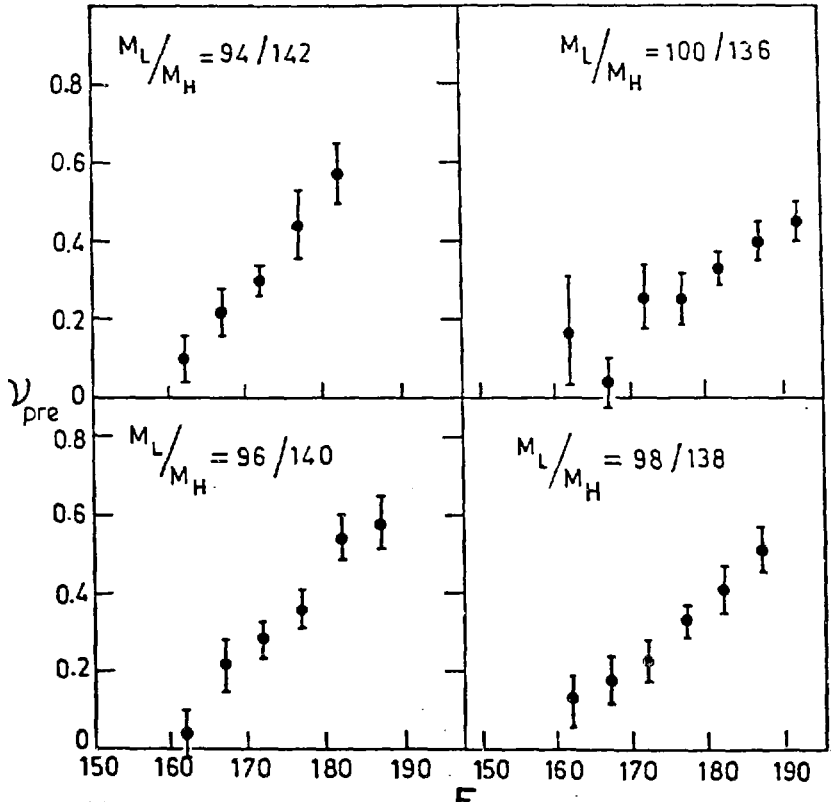

Fig.1

1.H.Marten et al.,Proc.Int.Conf.on Nuclear Physics, Nuclear Fission,Gaussing,1985; Zfk-592 (1986) 1; and ref. given therein

2.H.Marten & D.Seeliger, Proc.Int.Conf.on Nucl.Data for basic and applied science, Santa Fe, USA, May, 13-17, 1985

3.C.Buldtz Jorgensen & H.H.Knitter, Nucl.Phys. A490 (1988) 307

4.M.S.Samant et al.,DAE Symp.on Nucl.Phys., Madras 33B (1990) p.129

MEASUREMENT OF $^{89}Y(n,\alpha)$ AND ^{109}Ag (n,p) REACTION CROSS-SECTIONS AT 14.6 MeV

H.M. AGRAWAL*
Department of Physics
G.B. Pant University, PANTNAGAR 263 145

The activation method has been used to measure 14 MeV cross-sections for $^{89}Y(n,\alpha)$ and ^{109}Ag (n,p) reactions which are important to the designing concepts of future fusion reactors and have emerged new requests in the world request list of nuclear data (WRENDA 87/88 Report). These reactions lead to short-lived activities and therefore a fast sample transfer and analysis system of neutron generator KORONA /1/ is best suitable for these measurements. Cyclic activation and measurement are possible with a minimum cycle period of 5 sec. By means of the computer controlled sample transfer system, values of t_i (irradiation time), t_d (decay time), t_m (measurement time) and t_r (time between measurement and next irradiation) and thus p (cyclic period) can be achieved which are constant within less than 1%.

Samples of Ag pure metallic foils and of Y in powdered form having purity better than 99% were used for irradiation at KORONA. The resulting γ-activities of the sample were measured by calibrated Ge(Li) detector. During the first few seconds of short livesd nuclide analysis, the counting rate can easily exceed 2.10^5 cps. Therefore, a special electronic unit determines the pile up and dead time losses and corrects the registered pulses in the memory of the multichannel analyser by incremenating not one but a variable, loss dependent weighting factor /2/.

Employing the well known excitation functions of reactions [$^{90}Zr(n,2n)$, $^{93}Nb(n.2n)$] and [$^{58}Ni(n,p)$, $^{58}Ni(n,2n)$] the neutron energy at the centre of the cylindrical target of KORONA was determined to a median at 14.6 MeV and a FWHM of 0.6 MeV /3/. For the neutron flux monitoring, a long-counter is used. The long counter has been calibrated via the well known cross-section of the reaction $^{27}Al(n,\alpha)$. The time dependent fluctuations of flux were corrected for cyclic activation and measurement with the code ZYKLA.

The results are given as follows:

Reaction	Half life (sec.)	E_γ (KeV) I_γ (%)	Measured cross section (mb)	Literature value (mb)
$^{89}Y(n,\alpha)^{86m}Rb$	61 sec	556(98.2%)	1.78±0.06	1±.04
$^{109}Ag(n,p)^{109m}Pd$	4.69min	188.9(55.7%)	4.6±0.8	9.4±1.3

Our value for first reaction is higher than the recommended value of Qaim /4/ and for second reaction it is lower than his value. We feel that in view of short half lives of products, cyclic activation must be applied to get accurate results as has been done in the present work.

References

/1/ H.U. Fanger et al., J. Radioanal. Chem. 61,(1981) 147

/2/ R. Pepelink et al. Nucl. Instrum. Meth. 226, (1984) 411

/3/ H.M. Agrawal and R. Pepelink (under publication)

/4/ S.M. Qaim, 14 MeV Neutron Activation cross-sections in Handbook of Spectroscopy, Vol 3 CRC Press, Florida (1981).

* It is a great pleasure for me to thank Dr. R. Pepelnik (GKSS Research Centre, West Germany) for his keen interest throughout this work during my stay there as a guest scientist.

DWIA ANALYSIS OF 200 MeV $^{12}C(\pi^+,\pi^+p)^{11}B$ REACTION USING PERIPHERAL 3-BODY COUPLING MODEL

Arun K. Jain
Nuclear Physics Division,
Bhabha Atomic Research Centre, Bombay-400 085.

There has been a renewed interest in the proton knockout reaction using pi-mesons[1]. The interpretation is normally done in the impulse approximation using distortions in the incident as well as emergent channels. Since the pi-meson is a strongly interacting as also strongly absorbed particle in the nucleus one expects large distortion effects. this restricts the reaction more to the surface of the nucleus. It has been shown earlier[2] that when distortion effects are large one should use a proper treatment of the 3-body coupling term in the final state. It has also been demonstrated[2] that the conventional kinematic coupling approximation(KCA) which treats the 3-body coupling term by replacing it by its asymptotic plane wave kinematic value is not good in the surface region. Moreover when one of the two outgoing particles is relatively weakly distorted by optical potentials then a Peripheral 3-Body Coupling Model (P3BCM) is most suitable[3] where the coupling term $T_{coup} \equiv -\frac{\hbar^2}{m_B}\vec{\nabla}_{\pi B}\cdot\vec{\nabla}_{pB}$ is replaced by

$$T_{coup}(P3BCM) = -\frac{\hbar^2}{m_B}\left\{ i\vec{\nabla}_{\pi B}\cdot\vec{k}_{pB} + i\vec{k}_{\pi B}\cdot\vec{\nabla}_{pB} + \vec{k}_{\pi B}\cdot\vec{k}_{pB}\right\}$$

where $\vec{k}_{\pi B}$ and $\vec{k}_{pB}$ are the momenta conjugate to $\vec{r}_{\pi B}$ and $\vec{r}_{pB}$ relative coordinates. Using this form of the coupling term also one can still separate the 3-body final state Schroedinger equation into two 2-body Schroedinger equations.

In the present paper this P3BCM formalism has been used to analyse the 200 MeV s-wave proton in ^{12}C knockout data of Ziock et al.[4]. The calculations are made using the bound wave function from Elton and Swift for the s-wave proton. The π-mason distorted waves are calculated using modified Kisslinger type potential[5] in the Klein Gordon equation . For the proton distorted waves optical potential parameters of Nadasen et al have been employed . The final-energy prescription has been used for the π-p scattering cross section which enter the calculations through the impulse approximation where on-shell cross sections are normally used.

The calculated results using plane waves (PW), kinematic coupling approximation (KCA) and Peripheral 3-Body Coupling Model (P3BCM) are compared with the experimental data in fig. 1. It is seen that the shape of the energy sharing distribution is better reproduced by the P3BCM formalism than the KCA formalism. The shapes are normalized to the experimental data so as to produce an appealing visul fit. This is done because the KCA curve is slightly shifted to larger pi-meson energy for which the peak position does not match. The normalization factors or the spectroscopic factors have been found to be close to the theoretical predictions of Cohen and Kurath [6].

These calculations indicate that for the analysis of knockout data where strongly interacting particles are participating one should employ the P3BCM formalism for the proper description of the 3-body final state.

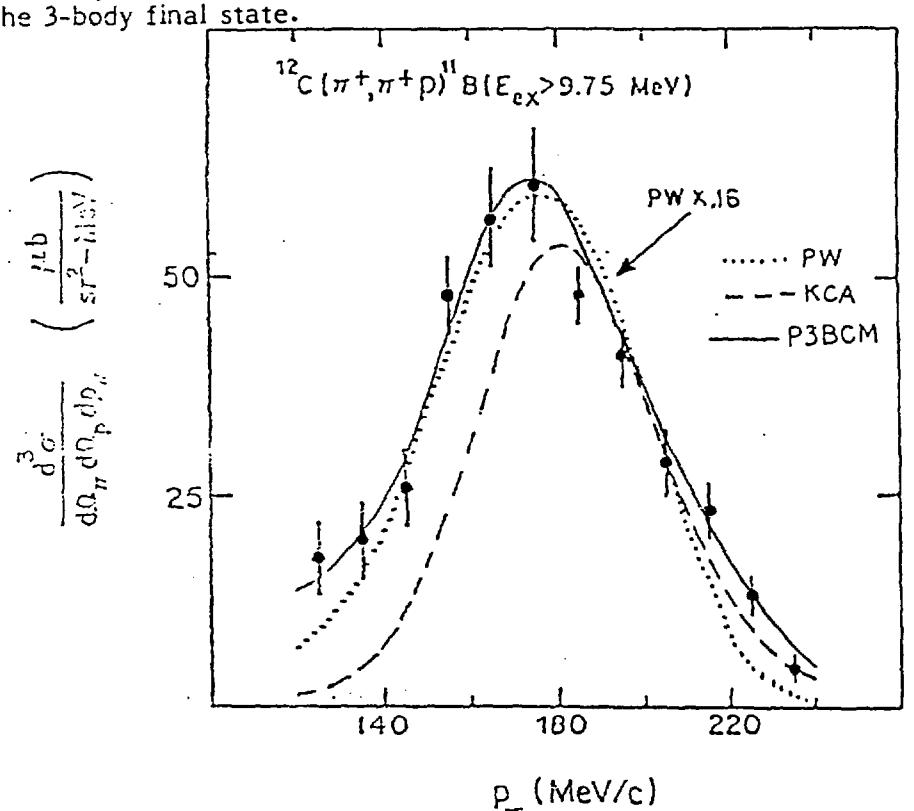

1. S. H. Yoo et al Phys. Rev. Lett. 63 (1989) 739
2. A. K. Jain, Phys. Rev. C42(1990)368
3. A. K. Jain, Phys. Rev. C under publication.
4. H. J. Ziock et al, Phys. Rev. C24 (1981) 2674
5. E. H. Auerbach et al., Phys. Rev. 162 (1967) 1683
6. S. Cohen and D. Kurath, Nucl. Phys. A101 (1967) 1

PROJECTION OPERATOR FOR CHANNEL SELECTION IN NUCLEAR REACTIONS

G.Ramachandran and M.S.Vidya
University of Mysore, Mysore

Abstract: The projection operator capable of selecting specified states of total angular momentum (Isospin) in reactions involving particles with arbitrary spins (isospins) is presented.

In view of the considerable progress made in producing polarized beams and targets with spin $> \frac{1}{2}$, it is of interest to consider the spin structure of the reaction amplitude for a+b→ c+d with arbitrary spins s_a, s_b, s_c, s_d respectively. Blatt and Biedenharn/1/ have outlined a general method of phase shift analysis for particles with arbitrary spins. In the well-known case of NN scattering, itself, the connection between the Wolfenstein/2/ amplitudes and the phase shifts is highly involved /3/ and consequently the emphasis has shifted to determine directly the amplitudes from experiments/4/ In simple cases like π-N scattering the channel selection with well defined total angular momentum J or isospin I is elegantly achieved through the use of appropriate projection operators/5/. So also in the case for singlet and triplet states of spin (or isospin) in N-N scattering. Such a technique for higher spins when the resulting angular momentum channels number more than 2 appear to be unknown. We present here the answer to this basic problem.

Consider in general a situation where a system consists of two angular momenta j_1 and j_2, the projection operator $\Pi_j(j_1, j_2)$ for the total angular momentum j is obtained in the form

$$\Pi_j(j_1, j_2) = \sum_k (T^k(j_1) . T^k(j_2))(-)^{j_1+j_2-j} [j]^2 \times W(j_1 j_1 j_2 j_2; kj) / [j_1][j_2] \qquad (1)$$

where the summation over k extends from 0 to $2j_2$,

if we make the convention to denote the smaller of the two angular momenta by j_2, and $T^k_q(\vec{J})$ are irreducible tensor operators constructed out of the angular momentum operator J and is normalised through

$$\langle jm' | T^k_q(\vec{J}) | jm \rangle = C(jkj;mqm')/k/ \qquad (2)$$

It is readily seen that(1) will reduce in special cases to the well known projection operators. Moreover, it is obvious that $\pi_j(l,s)\,\pi_s(s_1,s_2)$ is the projection operator for channel selection with total angular momentum j when particles with spin s_1 and s_2 have relative orbital angular momentum l. It is also obvious that(1) is adequate to handle isospin projection.

References

/1/ J.M.Blatt and L.C.Biedenharn, Revs. Mod. Phy. 24, 258 (1952)

/2/ L.Wolfenstein, Ann. Rev. Nucl. Sc. 6, 43(1956)

/3/ M.H.MacGregor, M.J.Moravcsik and H.P.Stapp, Ann. Rev. Nucl. Sc., 10, 291 (1960)

/4/ C.R.Schumacher and H.A.Bethe, Phys. Rev. 121, 1534 (1961)
G.R.Goldstein and M.J.Moravcsik, Phys. Rev. Lett., 53, 1885 (1984)
G.Ramachandran and V.Ravishankar, Phys. Rev. C37, 553 (1988)
G.Ramachandran and S.N.Sandhya, Mod. Phys.Lett., A3, 1113 (1988)
S.N.Sandhya, A.Sudha Rao and G.Ramachandran, J. Phys. G16, L95 (1990)
S.N.Sandhya, Phys. Rev. C41, 378 (1990)

/5/ G.Giacomelli, Rev. Nuov. Cim., 2, 297 (1971)
G.Hohler et al., Handbook of Pion-Nucleon Scattering, Karlsruhe (1979).

ON A NEW METHOD TO DIAGONALIZE NON-ORIENTED SPIN-1 DENSITY MATRICES

A Sudha Rao , A.R. Usha Devi and G. Ramachandran
Department of Studies in Physics, University of Mysore
Mysore -6.

Abstract: It is shown that the diagonalization of the density matrix for a non-oriented spin-1 system can in general be achieved in an elegant manner by using the SU(3) representation.

A representation for the density matrices, for nuclei with spin $s > \frac{1}{2}$ in terms of the generators of the group SU(n) where n=2s+1 was suggested by Ramachandran and Murthy (1). As a consequence ρ can be viewed as a vector in a n^2-1 dimensional real linear vector space and its domain is restricted to the inside of a regular polyhedra with n vertices in a (n-1) dimensional vector space. In particular, since a spin-1 system provides the simplest example of non-oriented spin systems(2), we outline here a general method which is applicable when both the vector and tensor polarization are non-zero.

We write the density matrix in the Lakin frame (where the z-axis is chosen parallel to the vector polarization and the basis states are the $|jm\rangle$ states defined with respect to that z-axis) and express in terms of the SU (3) parameters ($h^R_{\alpha\beta}$, $e^{(\gamma)R}_{\alpha\beta}$)

Then we make a unitary transformation $U_1 = e^{-i\frac{\sqrt{3}}{2}E^{(2)}_{13}\pi/4}\, e^{+i(\frac{1}{\sqrt{3}}H_1+\frac{1}{\sqrt{12}}H_2)\delta}$ such that ρ reduces to the following form:

$$\rho^{U_1} = U_1 \rho^R U_1^+ = \frac{Tr\rho}{3}\left[I + H_1 h_1^{U_1} + H_2 h_2^{U_1} + E^{(1)}_{12} e^{(1)U_1}_{12} + E^{(1)}_{13} e^{(1)U_1}_{13} + E^{(2)}_{13} e^{(2)U_1}_{13}\right]$$

Another unitary transformation of the form $U_2 = e^{-i\sqrt{3}H_2\varphi}$ is required to send ρ^{U_1} into real

symmetric form : $\rho^{u_2} = \frac{Tr\rho_0}{3}[I + H_1 h_1^{u_2} + H_2 h_2^{u_2} + E_{12}^{(1)} e_{12}^{(1)u_2} + E_{13}^{(1)} e_{13}^{(1)u_2}]$

which can then be readily diagonalized by a principal axis transformation (3). The method outlined above finds a ready application to the diagonalization of the density matrix describing a spin -1 system like, ^{2}H or ^{14}N exposed simultaneously to an external magnetic field, and also an electric quadrupole field. Needless to say it also finds application in the context of NQR.

ASR and ARU thank UGC(India) for financial assistance.

References:

(1) G. Ramachandran and M.V.N. Murthy, Proc. Nucl. and solid state phys. symp. pune 20B (1977).

(2) G. Ramachandran, Invited talk at the MAT SCIENCE conference on 'The Discrete and the continuum in physics ' held at Mysore in March (1983), unpublished; G. Ramachandran, Invited talk at the international symp. on ' Perspectives in Nuclear Physics',Journal of Madras University, section B,50, No.1(1987).

(3) G. Ramachandran, K.S. Mallesh and V. Ravishankar J. Phys. G: Nucl. Phys.10(1984) L163 -L166. G. Ramachandran, V. Ravishankar, S.N. Sandhya and Swarnamala Sirsi, J.Phys. G: Nucl.Phys 13(1987) L271-L273.

COMPARATIVE STUDY OF ANALYTICAL WAVE-FUNCTIONS FOR DEUTERON D- STATE

V N Pai* and R J Kulkarni

Dept.of Physics, University of Bombay, Bombay-98

Recently, the study of the simplest nucleus deuteron has become prominent and various model wave functions have been employed in the calculations of reactions involving the deuteron. In this paper we have used three different analytical wave function for the deuteron D- state in the calculations of the tensor analyzing power in backward (p, d) elastic scattering:

i) the realistic McGee wave function (1966)/1/ given by: $U(r) = N\left(e^{-\alpha r} + \sum_{j=1}^{4} C_j e^{-\epsilon_j r}\right)$

$W(r) = N\left[\alpha r\, h_2(i\alpha r) + \sum_{j=1}^{5} C_j \epsilon_j' r\, h_2(i\epsilon_j' r)\right]$

where $x h_2(ix) = e^{-x}\left(1 + \frac{3}{x} + \frac{3}{x^2}\right)$, $\alpha = 0.2338\ fm^{-1}$, $N = 0.8896\ fm^{-1/2}$

Remaining parameters are as in /1/.

ii) the wave function of Adler et al. (1977)/2/ given by: $W(r) = \eta N (1 - e^{-\gamma r})^5 e^{-\beta r}\left(1 + \frac{3}{\beta r} + \frac{3}{\beta^2 r^2}\right)$ where $\gamma = 0.2316\ fm^{-1}$, $\gamma = 1.09\ fm^{-1}$, $N = 0.885\ fm^{-1/2}$, $\eta = 0.025$ and $\beta = 5.98\gamma = 1.385\ fm^{-1}$.

We have used here the Hulthén Wave function for the S-state.

iii) the CMM wave function of Anton-Certov et al (1987)/3/:

$U(r) = \sum_{i=1}^{7} C_i e^{-m_i r}$; $W(r) = \sum_{i=1}^{7} D_i e^{-m_i r}\left[1 + \frac{3}{m_i r} + \frac{3}{(m_i r)^2}\right]$,

where the parameters in the wave- functions are given in Table 1 of ref./3/. We have used the specific wave function ψ_{LS}^{8A} with 8% P_D .

It is well known that the deuteron D-Wave is absolutely essential for the understanding of the tensor analyzing power $T_{20}^{ONE}(180°)$ in the one-nucleon-exchange (ONE) mechanism of Nakamura et al/4/:

$$T_{20}^{ONE} = \frac{1}{\sqrt{2}} \frac{(2\sqrt{2} R_0 - R_2) R_2}{(R_0^2 + R_2^2)}$$

where,

$$R_0(Q) = \sqrt{\frac{2}{\pi}} \int U(r) j_0(Qr) r\, dr, \quad R_2(Q) = -\sqrt{\frac{2}{\pi}} \int W(r) j_2(Qr)\, r\, dr.$$

---

* PARLE COLLEGE, Vile Parle (E) Bombay 400057.

$Q=\frac{1}{2}(q-p_f)$ is the relative momentum of nucleons inside the initial deuteron. u(r) and w (r) are the S- and D- wave functions; and $j_0(Qr)$, $J_2(Qr)$ are the spherical Bessel functions.

We have evaluated the integrals and then calculated T_{20}^{ONE} using the above wave functions. The numerical integrations were carried out using the IMSL subroutine DCADRE, based on Ramberg qadrature, with a cut-off value at r= 15 fm. The results are tablulated below:

Q	McGee			Adler			A.Certov.		
fm^{-1}	R_0	R_2	T_{20}^{ONE}	R_0	R_2	T_{20}^{ONE}	R_0	R_2	T_{20}^{ONE}
0·5	1·9863	−0·2309	−0·2389	0·980	−0·237	−0·2004	1·891	−0·234	−0·254
1·0	0·437	−0·1735	−0·7822	0·246	−0·187	−0·810	0·396	−0·177	−0·671
1·5	0·105	−0·1153	−1·434	0·079	−0·124	−1·269	0·108	−0·111	−1·364
2·0	0·0027	−0·0755	−0·5728	0·043	−0·078	−0·721	0·027	−0·069	−1·289
2·5	−0·018	−0·0487	0·0387	0·007	−0·047	−0·442	0·003	−0·043	−0·822
3·0	−0·012	−0·0309	0·0319	0·006	−0·028	−0·302	−0·002	−0·027	−0·559
3·5	−0·004	−0·0197	−0·246	0·005	−0·021	−0·112	−0·0014	−0·018	−0·546
4·0	−0·005	−0·013	0·0276	−0·004	−0·017	0·001	−0·0013	−0·011	−0·463

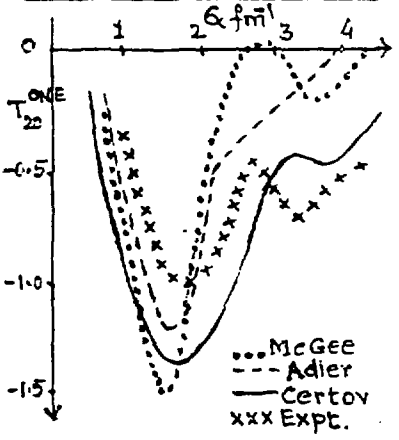

The figure shows the variation of $T_{20}^{ONE}(180^\circ)$ with Q. It is observed that all the three wave function almost reproduce the gross characteristics of the experimental features/5/. However, the wave function of Certov et al seems better suited for the purpose as it reproduces the first exptl. minimum at T_p =250 MeV fairly well and also indicates the second exptl. minimum at around T_p =700MeV

REFERENCES:

/1/ McGee I.J., Phys. Rev. 151 (3), 772.

/2/ R.J.Adler et al, Phys.Rev.C 16(1977),1231.

/3/ Certov A.et al, Phys.Rev.C 36(5),(1987),2040

/4/ A. Nakamura, L.Satta , Nucl, Phys,A 445(1985) 706

/5/ Arvieux J. et al, Phys. Rev.Lett, 50(1983) Nuel, Phys A 431 (1984)613.

SHAPE TRANSITION AND LEVEL DENSITY OF HOT NUCLEI IN STATIC PATH APPROXIMATION

B. K. Agrawal and A. Ansari
Institute Of Physics, Bhubaneswar, India-751005

The nuclear level density is a basic ingredient required to study statistical properties (e.g. nuclear reaction) of a nucleus. On the other hand, the nuclear shape describes its internal symmetries which are directly related to the physical observables. Therefore, the study of these at finite temperature has been of considerable interest. Since nucleus is a finite system, the statistical fluctuations at higher temperatures can play a significant role. Such fluctuations are not included in a Hartree-Fock type mean field approximation. The so called static path approximation[1,2] (SPA) method includes fluctuating mean field in nuclear collective space. We have applied this method to study the level density parameter and the quadrupole deformation in softly deformed Zn isotopes at finite Temperatures.

The partition function for the grand canonical ensemble is given as:

$$Z = Tre^{-(\hat{H}-\mu_p N_p-\mu_n N_n)/T} \tag{1}$$

If the Hamiltonian $\hat{H}$ consists of a simple quadrupole-quadrupole interaction term then in SPA

$$Z(\mu_p,\mu_n,1/T) = 4\pi(\frac{\alpha}{2\pi T})^{5/2}\int_0^\infty \beta^4 d\beta \int_0^{\frac{\pi}{3}} sin3\gamma d\gamma e^{\frac{-\alpha\beta^2}{2T}} \times Tre^{-(\hat{H}'-\mu_p N_p-\mu_n N_n)/T} \tag{2}$$

where, α is a parameter related to the interaction strength[1] and $\hat{H}'$ is a Nilsson type deformed one body Hamiltonian with statandard notations:

$$\hat{H}' = \hat{H}_o - M\omega_o^2\beta r^2(cos\gamma Y_{2,0} + \frac{1}{\sqrt{2}}sin\gamma(Y_{2,2}+Y_{2,-2})) \tag{3}$$

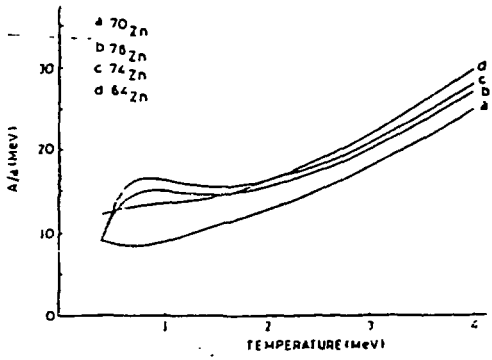

Figure 1

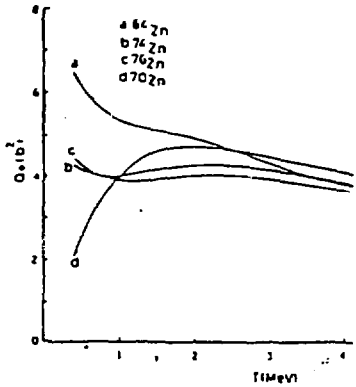

Figure 2

Using equation (2) we have computed the nuclear level density parameter 'a' and the average mass quadrupole deformation Q_o in units of square of oscillator length parameter, b for Zn isotopes at various temperatures ranging from 0.2 to 5 MeV as shown in figures 1 and 2, respectively. In all the cases the transition from deformed towards spherical shape is very gradual as temperature increases, in contrast to the sharp transition in a mean field approximation. It is seen that except for ^{70}Zn other neighbouring isotopes show similar trend in level density parameter as well as average deformation. The unique behaviour of ^{70}Zn is essentially due to neutron shell closure at N=38.

The work is in progress to study hot rotating nuclei using a cranking Hamiltonian within SPA.

References

1. B. Lauritzen and G. Berstch, Phys. Rev. C39, 2412 (1989)
2. P. Arve, G. Berstch, B. Lauritzen and G. Puddu, Ann. Phys. 183, 309 (1988)

SUPERSYMMETRIC QUANTUM MECHANICS FOR PHASE-EQUIVALENT POTENTIALS

P. K. Bera and B. Talukdar
Department of Physics
Visva-Bharati, Santiniketan
731 235
INDIA

In this paper we shall work within the framework of supersymmetric quantum mechanics [1], develop an analytical approach to construct phase-equivalent partners for (i) Morse and (ii) Hulthen potentials and try to gain some physical weight for the problem in the context of few-body dynamics.

The three-parameter (D,d,r_1) Morse and two parameter (V_0,a) Hulthen potetials are given by

$$V_0^M(r) = D\, e^{2(r_1-r)/d} - 2D\, e^{(r_1-r)/d} \qquad (1)$$

and

$$V_0^H(r) = -V_0 \frac{e^{-r/a}}{(1 - e^{-r/a})} \qquad (2)$$

respectively. Using supersymmetric transformations we have obtained phase-equivalent potentials $V_2^M(r)$ and $V_2^H(r)$ for (1) and (2). The subscript 2 indicate that we have used two supersymmetric transformations to arrive at our results . The auxiliary potentials needed for the purpose are

$$V_1^M(r) = V_0^M(r) + \frac{\alpha_1}{d^2} \exp\left[\frac{r_1 - r}{d}\right] \qquad (3)$$

and

$$V_1^H(r) = V_0^H(r) + \frac{e^{-r/a}}{a^2 (1 - e^{-r/a})^2} \qquad (4)$$

In Fig. 1 we plot the values of the reduced potentials $V_0^M(r)$, $V_1^M(r)$ and $V_2^M(r)$ as a function of r for the $^1S_0$ nucleon-nucleon scattering [2]. The potential $V_1^M(r)$ just misses the bound state at 2.218 MeV while $V_2^M(r)$ is altogether repulsive and far more singular at the origin. By calculating the interaction Green's functions $G^{(+)M}(k,r,r')$ and $G^{(+)M}(k,r,r')$ we have found that $V^M(r)$ tends to trigger the Efimov effect [3] but this effect is not observed for $V_2^M(r)$. Considering $V_0^H(r)$ as a screened Coulomb potential we portray in Fig. 2 the variations of $V_0^H(r)$, $V_1^H(r)$ and $V_2^H(r)$ as a function of r for a = 50 a. u. of length. The corresponding Coulomb results are also shown here. Hulthen curves exhibit some anomaly in respect of their Coulomb limit. The potential $V_2^H(r)$ misses the 1S state. Thus it may be of some interest in the study of electron scattering by Li^+ ion.

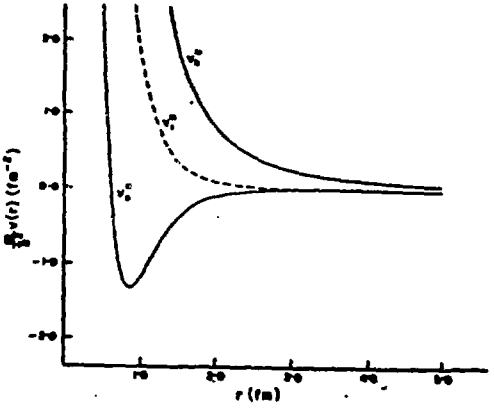

Fig.1 The Morse potential

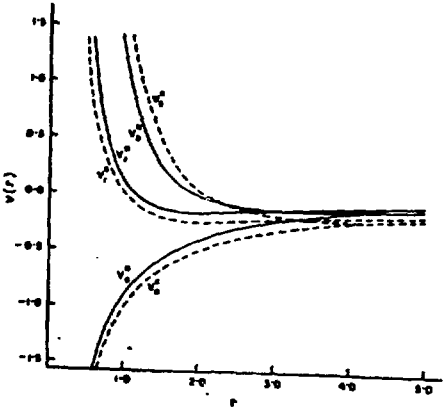

Fig.2 The Hulthen potential

References
1. E. Witten, Nucl. Phys. B 188, 513(1987)
2. M. G. Fuda, Phys. Rev. C 1, 1910(1970)
3. V. Efimov, Phys. Lett. 33B, 563(1970)

LEVEL DENSITY DEPENDENT NEUTRON EMISSION SPECTRA AND MULTI-PARTICLE REACTION CROSS-SECTIONS OF Ni-58, Ta-181 AND Bi-209; *S.B. Garg, Neutron Physics Division, Bhabha Atomic Research Centre, Trombay, Bombay 400 085*

Neutron emission spectra and multi-particle reaction cross-sections are determined for Ni-58, Ta-181 and Bi-209 at 14.1 MeV for fusion and dosimetry applications in the framework of geometry dependent hybrid model /1/ which describes pre-equilibrium decay products followed by the statistical decay of the excited nucleus calculated with the evaporation model. The following level density prescriptions are employed in the statistical energy region: a) Fermi-gas (FG) model /2/ b) Kataria-Ramamurthy-Kapoor (KRK) model /3/ and c) Ignatyuk-Smirenkin-Tishin (IST) model /4/.

In the Fermi-gas model the level density parameter is determined by matching the calculated and measured (n,2n) and (n,3n) cross-sections over a wide energy range and it is fixed at A/9 for Ni-58, A/13 for Ta-181 and A/20 for Bi-209. In the KRK and IST models shell dependent level density is used. The pairing energy corrections adopted for the FG model are $11/\sqrt{A}$; for the KRK model - those of Gilbert and Cameron /5/ and for the IST model these are taken as $4/A^{1/2}$ and suitaby applied by taking into consideration the even-even, odd-even and odd-odd nature of the nuclide.

The computed cross-sections are (n,n), (n,2n), (n,p), (n,pn), (n,alpha), total neutron, proton and alpha-emission and the energy spectra of the outgoing neutrons. A few of the salient cross-sections are given below to bring out the impact of the level density options:

Mat	L.D. Option	n,2n	n,p	n-em	p-em	x-em
28-Ni-58	Fermi	62.7	296	1130	955	85.4
	KRK	9.0	622	724	1030	97.8
	IST	174.0	91.5	1520	991	17.0
73-Ta-181	Fermi	2120	14.4	4450	15.2	0.13
	KRK	2130	14.4	4460	15.2	0.60
	IST	2120	14.3	4440	15.1	0.0
83-Bi-209	Fermi	2360	12.1	5020	13.9	0.41
	KRK	2400	12.0	5050	13.8	0.03
	IST	1950	12.0	4600	13.8	0.0

It is noted that for the singly closed shell nuclide Ni-58 all the three level density options produce different results, FG results being close to the measured data. In the case of Ta-181 there is a perfect agreement among the various except for the alpha channel and in Bi-209 (n,2n) and neutron emission cross-sections are suppressed in the IST by about the same magnitude with the alpha-channel closed. Charged particle emission in heavy nuclides is generally minimal due to large Coulomb potential barrier and any discrepancy in alpha-emissions is not likely to be of any consequence from the application point of view, Figs. 1 and 2 represent the neutron emission spectra in Ni-58 and Bi-209 where curves 1,2 and 3 depict the FG, KRK and IST model results. It is noted that the FG data reproduces the measured spectra upto about 8 MeV of neutron outgoing energy. Above this energy direct reaction mechanism is to be considered to reproduce the experimental data. In the case of Ta-181 the KRK data struck a better agreement.

Based on this limited study it may be observed that the KRK and IST level density models may be employed in heavy nuclides for data prediction. The IST model parameters may need a review for meaningful applications. The FG model is, of course, quite satisfactory.

REFERENCES: 1. M. Blann and H.K. Vonach; Phys. Rev. C28, 1475 (1983); M. Blann; Lawrence Livermore National Laboratory Report UCID-20169 (1984)
2. H.A. Bethe; Phys. Rev. 50, 332 (1936)
3. S.K. Kataria, V.S. Ramamurthy and S.S. Kapoor; Phys. Rev. C18, 549 (1978)
4. A.V. Ignayuk, G.N. Smirenkin and A.S. Tishin; Sov. J. Nucl. Phys. 21, 485 (1975)
5. A. Gilbert and A.G.W. Cameron; Can. J. Phys. 43, 1446, (1965)

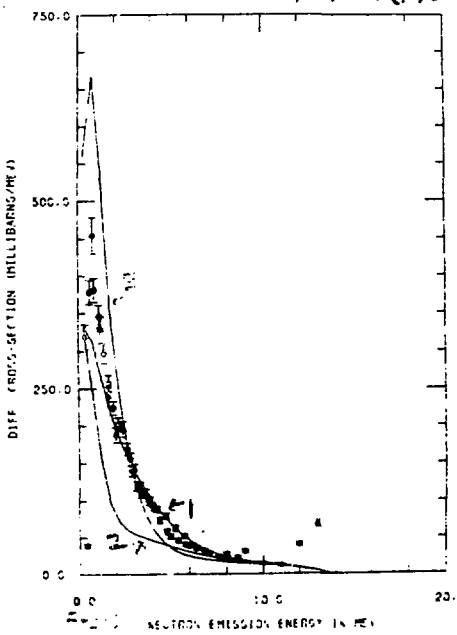

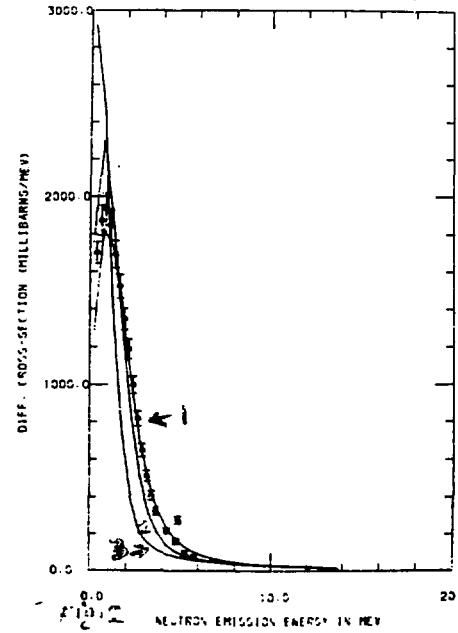

DOUBLE DIFFERENTIAL NEUTRON EMISSION CROSS-SECTIONS OF Ni-58 AND Bi-209 AT 14.1 MeV; *S.B. Garg, Neutron Physics Division, Bhabha Atomic Research Centre, Trombay, Bombay 400 085*

Angle-energy correlated double differential neutron emission cross-sections (DDX) play a significant role in determining the neutronics of a system based on fusion or fission process by providing anisotropic scattering data of the outgoing neutrons. In this investigation, double differential neutron emission cross-sections of Ni-58 and Bi-209 are determined at the primary neutron energy of 14.1 MeV using the following recipes:

(1) Systematics of Kalbach /1/ based on a variety of experimental data abbreviated as KS in the text and (2) Method of folding the nucleon-nucleon scattering kernel /2/ abbreviated as FKM in the text.

The objective is to determine which one of the above two methodologies is better suited to reproduce the experimental DDX so that it may be adopted as a tool to predict data at those energies and angles where measurements are not available or where measurements are difficult to perform.

In this study cross-sections for the various reaction products in the pre-equilibrium stage are determined with the geometry dependent hybrid model and in the equilibrium stage with the evaporation model. The pre-equilibrium decay cross-section is estimated by including surface effects, gamma-ray competition, energy dependent transition rates for individual particles based on the considerations of optical model potential and nucleon-nucleon interactions and the energy dependent single particle level densities. In the equilibrium stage, the level density parameter is determined as A/9 for Ni-58 and A/20 for Bi-209 by matching their measured and calculated (n,2n) and (n,3n) cross-sections over a wide energy range.

Figs. 1 and 2 represent DDX's for Ni-58 and Bi-209 at 100° and 102° respectively together with the measured data taken from references /3,4/. In these figures curve 1 is obtained with the KS and curve 2 with the FKM. It is noted that in the case of Ni-58 the KS data are depressed and in the case of Bi-209 the KS data are enhanced over a wide energy range of neutron emission in comparison with the FKM data. At several

emission energies the calculated results are within the experimental deviations in these two medium and heavy nuclides. At 8 MeV or higher energies of neutron emission the calculated and measured data show discrepancies. This is due to the fact that direct reaction mechanism is not included in the computations. It appears from this study that DDX obtained with the KS is marginally superior to that calculated with the FKM. It is, however, to be noted that the FKM data are obtained purely from the theoretical considerations without adjusting many model parameters and with some refinement it may serve as a predictive model for DDX.

REFERENCES: 1. C. Kalbach; Phys. Rev. C37, 2350 (1988)

2. M. Blann, W. Schobel and E. Plechaty; Phys. Rev. C30, 1493 (1984)

3. N. Yabuta, Private Communication (1987)

4. A. Takahashi et al; OKTAVIAN Report A-87-01, Volume II (1987).

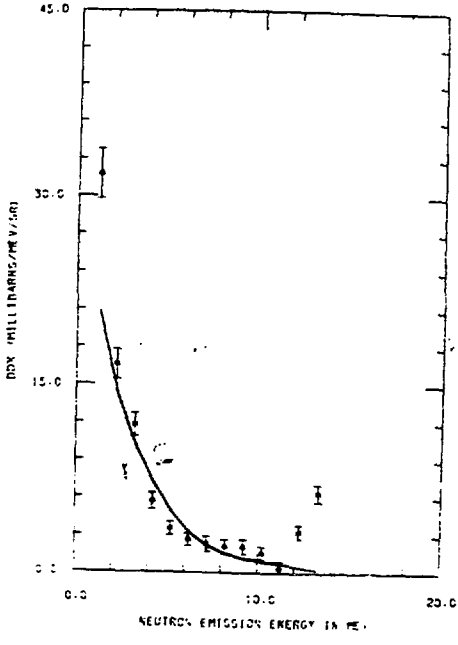

FIG. DDX AT 100 FOR [illegible] AT 14.1 MEV NEUTRON ENERGY WITH KALBACH SYSTEMATICS AND BLANN'S EDH MODEL

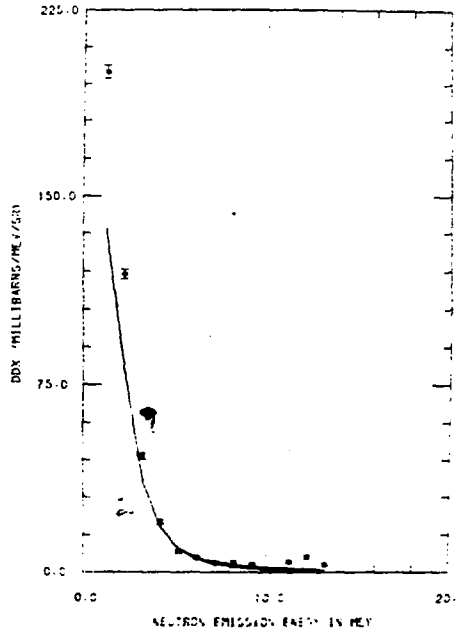

FIG. DDX OF BI-209 AT [illegible] MEV WITH KALBACH SYSTEMATICS AND BLANN'S EDH MODEL

^{232}Th TOTAL NEUTRON CROSS SECTION FROM 0.1 TO 20 MEV

H.M. Jain
Experimental Reactor Physics Section, B.A.R.C.

To predict the neutron cross sections (n ,nn',nf), H - F statistical model based computer program HAUSER-V is being used by us for nuclear data evaluation for ^{232}Th-^{233}U fuel cycle. It needs spherical optical model (SOM) parameters as input or when default options is given then it used the Willmore and Hodgson (WH) SOM parameters built-in input. The computer program HAUSER-V was modified by us to calculate the total cross section also. This modified program was checked by performing ^{238}U total cross section calculation using the SOM parameters given in Ref.1 and the calculated values agree with their results. For ^{232}Th the calculations were performed using the conventional SOM parameters of Jary (6), MY (1), MY (2) (Madland and Young and WH (4) from the Table I of Ref.2.

Also the recently measured data of nine authors (total number of data points 529 from 0.050 to 20 MeV) were fitted with computer program SPLINE. It is a weighted least square fitting program based on cubic spline curve. Weights are taken as the inverse of square of errors assign to measured data points. For two authors the reported errors were increased because there were large number of data points with fine energy interval but poor in quality and they were reduced to small number by averaging them.

The theoretical predicted values by HAUSER-V program using the default option i.e., WH (4) SOM parameters are in complete disagreement with SPLINE fitted values, while the calculated values with Jary (6) and MY (2) SOM parameters are in good agreement with the SPLINE output. Similar differences were observed for ^{238}U total cross section also.

This exercise was done to select a suitable SOM parameters set for ^{232}Th to perform further calculations using HAUSER-V program and to improve the evaluation based on model based calculations for interpolating the cross sections where measurements do not exist. Total cross section measured data are easily available and with better accuracy and should be used for checking the input SOM parameters. The default option should not be used directly so that total cross section calculated comes out be same as sum of the partial cross sections for consistency even if they are calculated with diff-

erent computer programs.

Acknwoledgement

The author would like to acknowledge thanks to Dr.S.K. Gupta, NPD for the helpful discussion to modify the HAUSER_V program for total cross section calculation.

References

1. A. Smith et.al., "Evaluation of the ^{238}U Neutron Total Cross Section", ANL/NDM_ 74 (1982).

2. P.E. Hodgson, "The Neutron Optical Model in the Actinide Region", Report 101/61, Oxford University.

COMPUTED EXCITATION FUNCTIONS OF ^{93}Nb FOR 1 TO 20 MeV NEUTRONS

S.L. BANSAL and R.K. MOHINDRA
Physics Department, Kurukshetra University,
Kurukshetra-132 119.

Excitation functions of ^{93}Nb for (n,p), (n,α), (n,d), (n,t), (n,He^3), (n,2n) and (n,3n) reactions induced by 1-20 MeV neutrons have been computed. These computations are based on evaporation model considering the pre-equilibrium emission[1,2] under some approximations. The excitation functions of ^{93}Nb for different reactions have been shown in the fig. along with the available experimental values[3-5] at some energies for comparison and results are in fairly good agreement . For (n,p) and (n,d) reactions, the measured cross-section values are not available. The (n,t) reaction cross-section values are multiplied by three for the proper presentation of their variation with energy. In the shown experimental values of (n,t) and (n,He^3) reaction cross sections, the spread in energy is also depicted due to angle of emission, and deutron energy loss in the Ti(T) target. The charged particle data of neutron induced reactions are of great importance for design of fission and fusion reactors, shielding problems and in the design of other nuclear devices, when such cross-sections are not amenable to exprimental measurements.

References:

1. Zhang Zin, Zhou Delin and Cai Dunjiu, The Systematics of (n,2n) and (n,3n) cross-sections, NEA Data Bank, France (1987).
2. Zhao Zhixiang and Zhou Delin, Systematics of Excitation Functions for (n, charged particle) Reactions, NEA Data Bank, France (1986).
3. E. Gadioli and P.E. Hodgson, Rep. Prog. Phys. 52 (1989) 247.
4. S.M.Qaim, R. Wolfle and H. Liskien, Phys. Rev. C 34, No.2 (1986)489.
5. P.E.Hodgson, Contemp. Phys. Vol.29, No.5,(1988) 457.

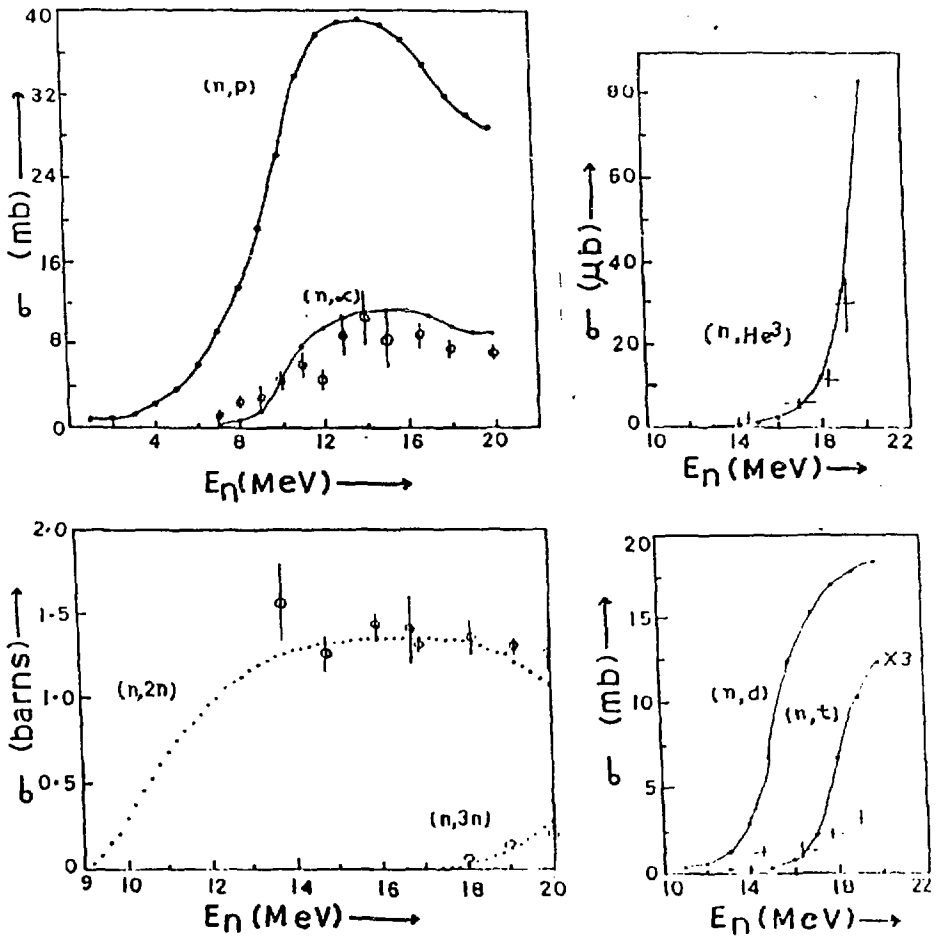

Fig. : Computed Excitation Functions of ^{93}Nb for the Reactions (n,p), (n,α), (n,d), (n,t), (n,He^3), (n,2n) and (n,3n) along with the Experimental data whereable available are depicted. The (n,t) cross-sections have been multiplied by three for their proper presentation.

c. NUCLEAR MATTER AND NUCLEAR COSMOPHYSICS.

MICROSCOPIC CALCULATION OF THE NUCLEON SPIN-ORBIT POTENTIAL

S.M. Saliem and W. Haider
Department of Physics, A.M.U., Aligarh-202002

The spin-orbit part of nucleon optical potential has in the past /1-2/ been calculated in the Brueckner's theory. However, using the short range nature of the effective NN spin-orbit potential these calculations invoked the Zero Range Approximation (ZRA) for both the direct and exchange terms. In the present work, we include the Finite Range Effect (FRE) only in the direct part while still using the ZRA for the calculation of exchange term. Furthermore, we also investigate the energy dependence of the direct and exchange terms.

The direct term of the spin-orbit potential, without applying ZRA is :

$$V_{so}^{D}(r_1,E) = -\pi \int_0^{\infty}\int_{-1}^{1} dx\,dz\, \frac{x^3 z}{r_1}\, \rho(\sqrt{r_1^2+x^2+2r_1xz})\, t_{so}^{D}(x;\rho(r_1),E)\, \vec{L}_1\cdot\vec{S}_1 \qquad \ldots (1)$$

We have calculated the spin-orbit potential for p- ^{40}Ca elastic scattering at 30 and 200 MeV using eq. (1) within the framework of Brueckner's theory. The results of our calculation are shown in fig (1). Curves I and II correspond to the ZRA calculation of the real part of the direct term at 30 and 200 MeV respectively, whereas III and IV correspond to that of exchange term at the same energies. Curves V and VI correspond to our exact calculation of the real part of the direct term.

Our results indicate the following: Firstly, the inclusion of finite range effect makes a significant reduction ($\approx$ 20% at both 30 and 200 MeV) in the direct term of spin-orbit potential. Secondly, in ZRA, the real part of the direct term seems to be energy independant, whereas all the energy dependence seems to come from the exchange part. Finally, the imaginary parts of direct and exchange terms are so small that their energy

dependence can not be predicted with any certainty. The effects of these changes to the prediction of proton polarisation data are being studied.

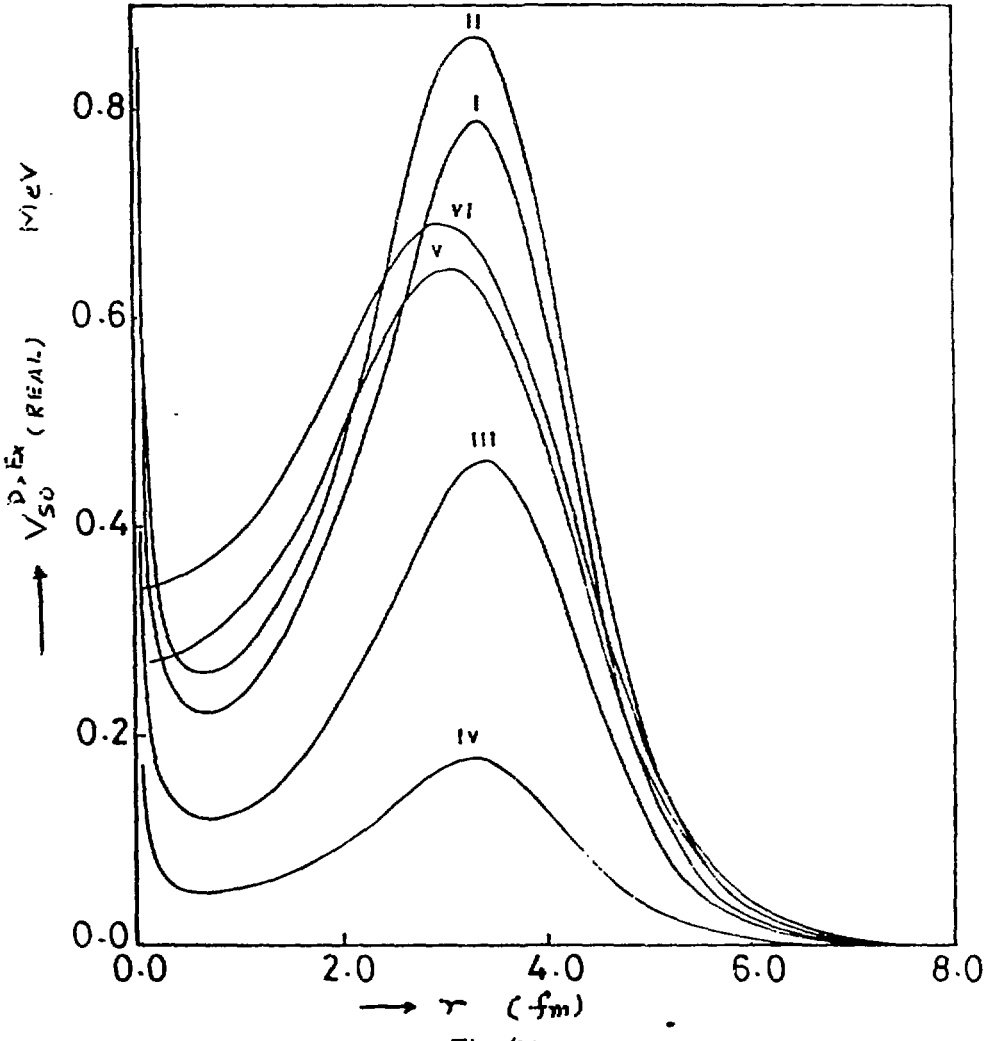

Fig (1)

References :

/1/ R.R. Scheerbaum, Nucl.Phys. A 257 (1976) 77.

/2/ F.A. Breiva and J.R. Rook, Nucl. Phys. A297 (1978) 206.

NUCLEAR COMPRESSIBILITY; AN ANATOMICAL STUDY

V.S. Uma Maheswari, V.S. Ramamurthy and L. Satpathy
Institute of Physics, Bhubaneswar - 751005

The nuclear compressibility coefficient plays an important role in the modelling of several astrophysical phenomena, as well as in high energy heavy-ion collisions. Recent experimental determination[1] of the breathing-mode energies(E_{GMR}) suggests, rather a high value for the surface coefficient K_s. This value is in total disagreement with the theoretical predictions. The procedure adopted by Sharma et.al., to deduce the volume K_v and surface K_s coefficients is as follows. First, they define a reduced quantity $\overline{K}_A$, given as

$$\overline{K}_A = K_v + K_s A^{-1/3} \tag{1}$$

where $\overline{K}_A = K_A - K_c A^{-2/3} - K_\Sigma \beta^2 - K_z Z^2 A^{-4/3}$. Here K_A is derived from the experimental E_{GMR}. On the other hand, the Coulomb K_z, the asymmetry K_Σ and the curvature K_c contributions are borrowed from theoretical calculations. Then by a straight line fit to eqn.(1), they obtain K_v and K_s. In this work, we try to figure out the factors responsible for the apparent discrepancy in K_s. Here we mainly focus on the curvature effects through an analytical study. We performed ETF[2] calculations for a symmetric system, using a Skyrme force, and neglecting the Coulomb effects. This is done using the energy density functional formalism, where the total energy is given by $E = \int \epsilon[\rho(\vec{r})] d^3r$, subject to the number conservation $A = \int \rho(\vec{r}) d^3r$, and parametrising the density as a Fermi-like function. Then, by making a scaling transformation, $\vec{r} \longrightarrow \lambda\vec{r}$, one obtains the so-called *scaling compressibility*,

$$K_A^{sca} = \frac{d^2 E/A}{d\lambda^2} \mid_{\lambda=1}$$

. Using this scaling model, we derive analytical expressions for the various compressibilty coefficients. However, these quantities depend on the finite nuclei saturation density ρ_o. By Taylor expanding around its nuclear matter value ρ_∞, we obtain expressions for K_v, K_s and K_c. Here, we find that the curvature effect is much more significant than the semi- infinite ($SINM$) estimation. Although SINM limit is good enough for surface estimation, it largely underestimates the curvature effect. This is mainly due to two reasons; First, the leptodermous nature of the nuclei and Second, the finite-size effects. Because of these effects, apart from the pure curvature effect, one has contributions from volume and surface to the order of $A^{-2/3}$. This *effective curvature*,K_c^{eff}, is very large and negative, (*about* -1500 MeV for SKM* force), compared to the value enforced by Sharma et.al., i.e. +375 MeV. From the eqn.(1), it is clear that the extraction of K_s very much depends upon K_c. For the sake of simplicity we studied a symmetric and a no Coulomb system. For real systems, it can be shown that these two effects, in particular, Coulomb force further complicates the extraction procedure.

In conclusion, we have shown that the extrapolation from K_A to its nuclear matter value is not that straight forward, as the finite-size effects significantly modify the various compressibility coefficients. By this simplistic, yet realistic study, we have tried to emphasize the importance of "curvature" effects, and this may be one of the reasons for the disagreement in K_s between the theoretical and experimental values.

References

1. M.M. Sharma et.al., Nucl.Phys.A504(1989)337
2. M. Brack et.al., Phys.Rep.123(1985)275

HOT NUCLEAR MATTER WITH DENSITY DEPENDENT INTERACTIO

C.Das
Physics Department, Banki College, Banki, Cuttack, India
R.K.Tripathi
13 Natalie, DR, Hompton, VA 23660, USA
and
R.Sahu
Physics Department, Berhampur University,
Berhampur - 760007, India

Over the last few years, there has been an increased interest in the studies of excited nuclear matter because of the hope that such a hot and dense nuclear matter is likely to be produced during relativistic heavy-ion collisions. The studies of such matter under unusual conditions of densities and temperatures would also be useful in the understanding of stellar collapse, supernova explosions, neutron stars etc. Hence it would be quite interesting to calculate the equation of state, entropy and other thermodynamic variables of nuclear and neutron matter at different temperatures.

Recently we [1] have successfully explained the experimental observations regarding entropy production in heavy-ion collisions within a fully self consistent model. This model is a generalization of the Brueckner theory to low finite temperatures. However, in the above calculation, Sussex interaction has been used which gives insufficient binding by about 3 MeV per nucleon and does not saturate correctly in nuclear matter. Hence Tripathi et al. [2] have suggested the addition of a density dependent term to the original Sussex interaction matrix elements. The parameters of this density dependent term were fixed empirically by fitting the energies and and densities of nuclear matter and ^{16}O. We perform thecalculation using this effective interaction. The details of the model are given in ref.1. The single particle potential is calculated self-consistently. Because of this self-consistency, the scattering to intermediate states are taken into account properly through the pauli operator. The chemical potential is determined by the number density constraint. We restrict ourselves to symmetric nuclear matter and pure neutron matter.

We have calculated the single particle potential at densities varying from $\rho = 0.1$ fm^{-3} to $\rho = 0.4$ fm^{-3} and temperatures from T = 10 MeV to T = 30 MeV. We find that for a

given density, single particle potential curves corresponding to different temperatures almost meet at a point. Using the relation $\rho = 2k_F^3 / (3\pi^2)$, we find that this point almost corresponds to the Fermi momentum of the system. Below this point, the attractive mean field decreases as the temperatures increases. However, at higher momentum, reverse is the case. Baldo et al.[3] have studied the symmetrical nuclear matter at finite temperature in the frame work of the Brueckner- Hartree-Fock approximation. They also find the single particle potential graphs for T = 0,10,18 MeV meet at a point which almost corresponds to the Fermi momentum. However they find the depth of the potential to increase with temperature at low momentum. We have also calculated the single particle potential versus momentum for neutron matter at T = 10,20,30 MeV and ρ = 0.1,0.2 and 0.3 fm^{-3}. Since in neutron matter, only T = 1 part of the nuclear force operates, the single particle potential is more repulsive than the nuclear matter case. Otherwise, the behaviour of the curves is almost similar to the nuclear matter case.

We have also calculated the entropy per nucleon for nuclear and neutron matter. In ref. 1, we had calculated the entropy for nuclear matter taking only the Sussex interaction. Introduction of the density dependent term in the present calculation increases the entropy by about 5%. The results are still in agreement with experiment within the experimental errors. Without assuming breakup into two phases , our model is thus able to reproduce correctly the experimental value of entropy for nuclear matter.

We have also calculated the pressure versus density at different temperatures for nuclear and neutron matter. We find that phase transitions are absent for neutron matter. However, for nuclear matter, we observe a phase transition with the critical temperature T = 9 MeV. Our value of critical temperature is far below the values reported by other calculations. However Haar and Malfliet [4] had performed a fully self consistent DB calculation and found the critical temperature to be below 10 MeV.

We have also calculated free energy, energy per nucleon, effective mass and chemical potential for nuclear and neutron matter at different temperatures.

[1] C.Das et al., Phys. Rev. Lett. 56(1986)1663
[2] R.K.Tripathi et al., Nucl. Phys. A380(1982)483
[3] M.Baldo et al., Phys. Lett. B215(1988)19
[4] B.ter Haar and R.Malfliet, Phys. Rev. Lett. 56(1986)1237

MEAN SEPARATION BETWEEN NUCLEATION SITES AND COSMIC QUARK - HADRON PHASE TRANSITION

K. SAKTHI MURUGESAN, G. JANHVI, K. RAJA, AND P. R. SUBRAMANIAN
Department of Nuclear Physics, University of Madras, Guindy Campus, Madras 600 025.

Following an analysis of Kajantie and Kurki-Suonio [1] and Alcock et al. [2], the mean separation between the nucleation sites (phases) ℓ , after the nucleation had occured in the expansion of the Universe, is given by [2]

$$\ell = 0.3\, \sigma^{3/2}\ t\ /\ T_c^{1/2}\ L, \qquad (1)$$

where t is the age of the Universe, T_c is the phase transition temperature, L is the latent heat, and σ is the surface tension. This length ℓ will assume a greater significance in the calculations of the light element abundances of the early Universe using non-standard big bang theory [1-4].

Fuller et al. [3] have calculated the amount of latent heat released, during the quark - hadron phase transition, for different coexistence temperatures T_c. In their calculations, the latent heat L is fixed for a given T_c (see Table I of Ref. 3). To obtain the appropriate value of nucleation sites for PNS calculations, they have to change the value of T_c. But in our lowest order perturbative QCD model [5], we can calculate different values of L for a given T_c by adjusting the QCD scale fixing parameter Λ. Our calculated values of T_c, L and phase transition time Δt for different values of B and Λ are presented in Table I. The calculated values of latent heat released during the phase transition is always larger than that of Ref.6, this being due to the inclusion of the proper volume correction (Hagedorn) in the HRG phase. Addition of more and more hadronic resonances in the hadronic phase decreases the release of latent heat during the cosmic quark-hadron phase transition. Inclusion

of Hagedorn's correction, however, decreases the critical energy density. Our calculation presented in Table I may be useful to estimate the appropriate distance between nucleation sites [1-4] and to reproduce the correct values of the light element abundances using the non-standard big bang model.

Table I.

B (MeV/fm^3)	Λ (MeV)	T_c (MeV)	L (MeV^4)	Δt (us)
30	100	102	8.95×10^8	93
60	0	104	1.81×10^9	98
60	250	150	1.59×10^9	23
150	100	150	4.30×10^9	29
250	0	150	7.30×10^9	97

References:

1. K. Kajantie and H. Kuriki-Suonio, Phys. Rev. D34, 1719 (1986).
2. C. Alcock et al., Nucl. Phys. A498, 301 (1989).
3. G. M. Fuller et al., Phys. Rev. D37, 1380 (1988).
4. T. Kajino, Phys. Rev. Lett. 66, 125 (1991).
5. K. Sakthi Murugesan, G. Janahvi, and P. R. Subramanian, Phys. Rev. D41, 2384 (1990); D42, 3576 (1990).
6. H. Voss et al., J. Phys. G15, 561 (1989).

BARYON MASS SPECTRA

A.K. Gautam, Rajesh Gaur and A.K. Shiromani
Physics Department, R.B.S. College, AGRA.

With in last two decades attempts have been made to study the mass spectrum of the particles which are produced from various colliding beam experiments **(1)**. It is worth noting that hadrons are constituted from quarks. Three quarks or three antiquarks constitute a baryon while one quark and one antiquark constitute a meson.

The combination of coulombic potential, based on quark confinement and linear potential, based on asymptotic freedom provides the bases to study meson mass spectra. **(2)**. The use of the bag model has been found to be a good tool to study baryon mass spectra.

In this work we have used the bag model for the study of baryons constituted from uuc, udc and ddc. The mass of a baryon is given by **(3)**

$$E(R) = \sum_i N_i \left(m_i^2 + \frac{x_i^2}{R^2}\right)^{\frac{1}{2}} + B\,(4\pi R^3/3)$$

where
B is a bag paramenter which is calculated by minimizing the energy of a bag.

The particle masses so estimated with bag radii are shown in the figure and are found to be in good agreement with the results of other workers

References :-

(1) Schwitters R.F. and Strauch K. Ann. Rev. Nucl. Sci. 26, **89 (1979), Reports of DESY,** CERN, KEK,

(2) A.K. Gautam, Symposium on Nuclear Physics 32B (1989) P 74 A.K. Gautam and A.K. Shiromani DAE Symposium on Nuclear Physics 33B (1990) P 233.

(3) Chodos,A. et.al. Phys. Rev. D9 (1974) 3471

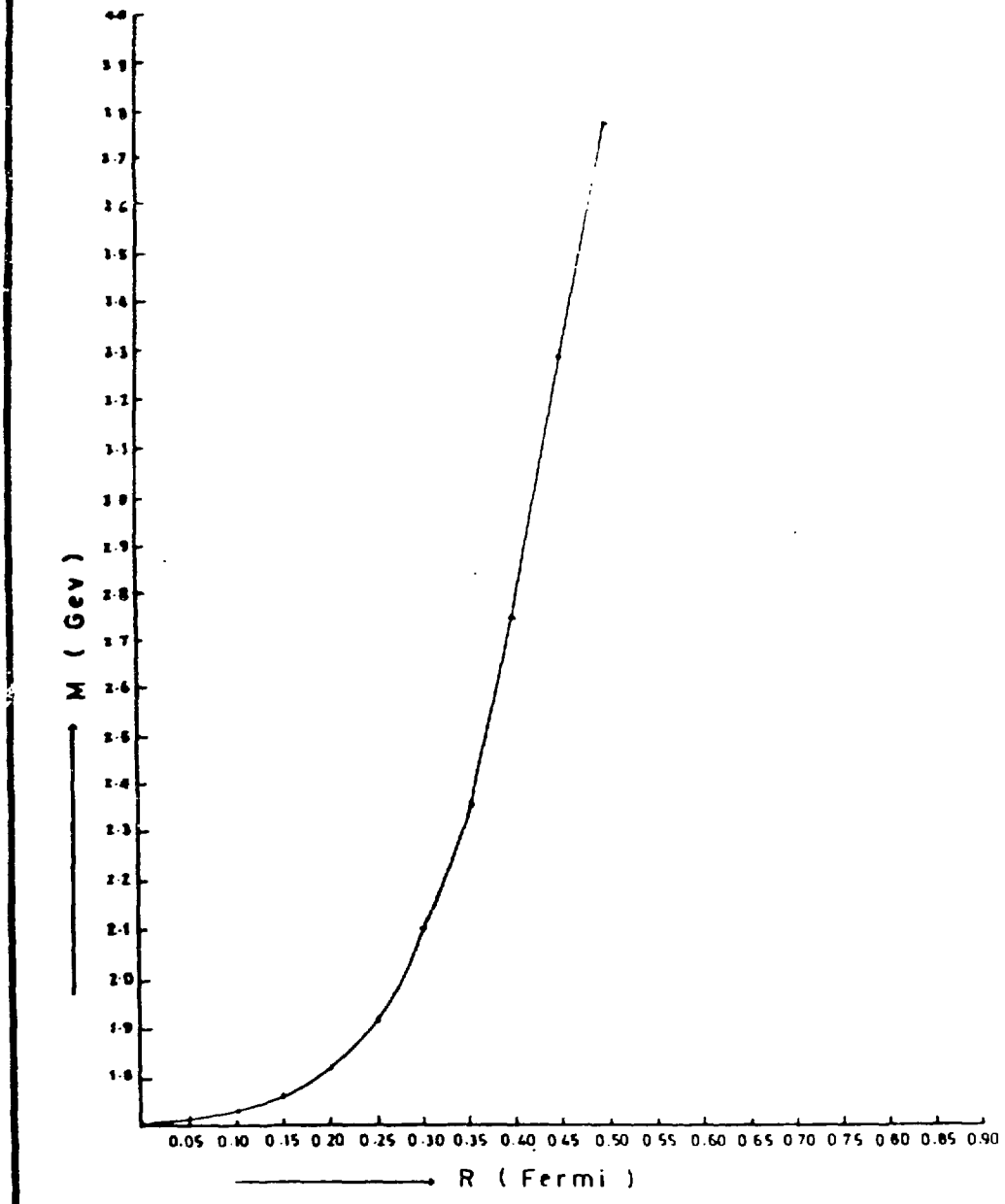

FIG. :VARIATION OF MASSES WITH BAG RADII FOR THREE QUARKS SYSTEM uuc udc ddc FOR LIMITED DATA.

FINITE TEMPERATURE NUCLEAR MATTER: A FIELD THEORETIC METHOD

H. Mishra, S.P. Misra, P.K. Panda
Institute of Physics, Bhubaneswar-751005, India.

B.K. Parida
Department of Physics
Regional College of Education, Bhubaneswar-751007, India.

The understanding of hot dense nuclear matter is an interesting problem in theoritical physics in the context of heavy ion collision experiments as well as big bang cosmology. We develop here a nonperturbative technique in field theory to study the properties of infinite nuclear matter at zero temperature as well as at finite temperatures. Here we dress the nuclear matter with off mass shell pion quanta [1]. This dressing with scalar isoscalar pion condensates simulate the effect of σ-mesons [2] of e.g. Walecka's model. The short distance repulsive interaction arises from composite structure of nucleons and/or through vector meson exchange. The method of thermofield dynamics [3] is used for finite temperature calculations besause here statistical average is done through an expectation value over a "thermal vacuum" in an extended Hilbert space.

The thermodynamic potential is calculated in a variational method and from it we calculate different thermodynamic quantities. We first plot the binding energy per nucleon as a function of baryon number density in fig. 1. for temperatures at zero MeV, 5 MeV , 10 MeV and 15 MeV. As the temperature increases the minimum shifts towards higher densities. We next plot pressure as a function of nucleon density in fig. 2. Vanishing of pocket in the same curve for temperature around 15 MeV may be noted which could be an effect of phase transition. Entropy density is plotted as function of nucleon density in fig. 3. at temperatures 50 MeV, 100 MeV, 150 MeV and 200 MeV. Finally in fig. 4. we plot the average number of pions per nucleon as a function of nucleon density. It is interesting to note that this results are effectively independent of temperature. Therefore only zero temperature graph is plotted.

Besides the aesthetic appeal of classical σ-fields arising out of pion dressing, this model may have experimental consequences. E.g. the off shell $\pi^+\pi^-$ pair as present through pion dressing may annihilate to hard photons with a probability in excess of what one may expect otherwise.

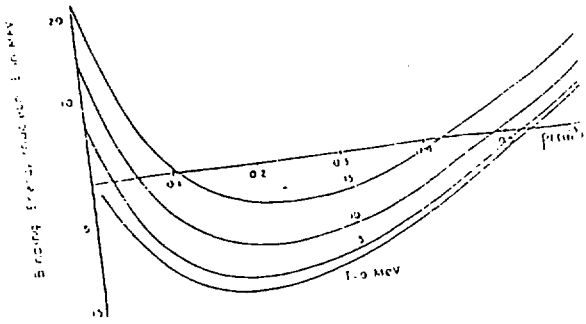

Fig. 1.

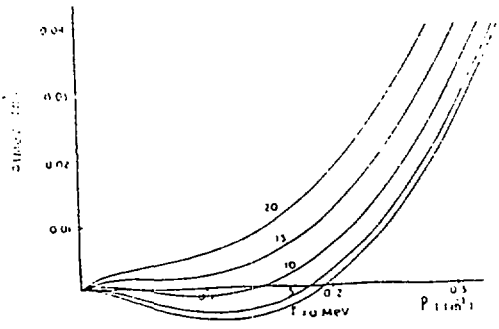

Fig. 2.

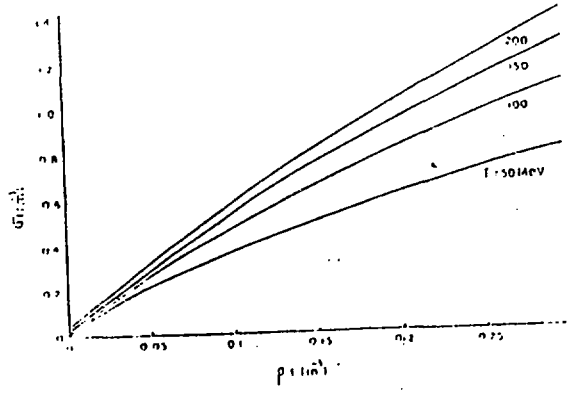

Fig. 3.

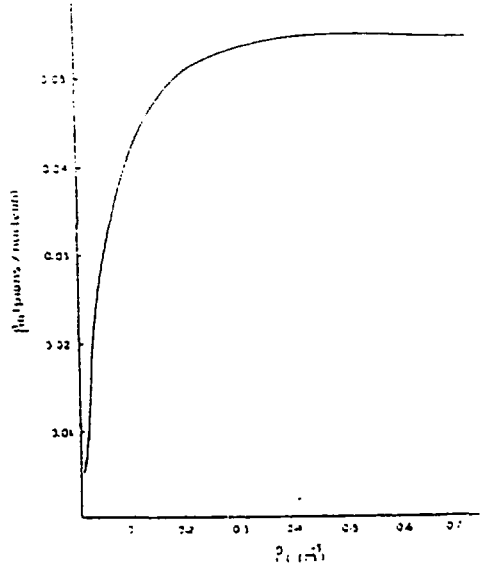

Fig. 4.

REFERENCES

[1]. A. Mishra, H.Mishra and S.P.Misra Int. J. Mod. Phys. A5 17 (1990) 3391.

[2]. J.D. Walecka, Ann. Phys. 83 (1974) 491.

[3]. H. Umezawa, H. matsumoto and Tachiki *Thermofield dynamics and condensed states* (North Holand, Amsterdam, 1982).

SOLAR NEUTRINO PROBLEM AND ASTROPHYSICAL S-FACTOR

PRATIBHA and V.K.SHARMA
Department of Physics, Institute of Advanced Studies
Meerut University, Meerut 250004, India

The radiative-capture cross sections $^3He(\alpha,\gamma)^7Be$ $^3H(\alpha,\gamma)^7Li$ are very important to understand the solar-neutrino problem, which is receiving massive theoretical and experimental attention at the present moment in nuclear astrophysics. For such studies the resonating group method (RGM) and the generator coordinate method (GCM) is widely used to calculate the zero energy cross section factor S(0) which is an important ingredient in solar-neutrino problem as well as in cosmology. Here we present the theoretical and experimental estimates of the S(0) factor by others (see Ref.) as well as with our GCM.

The radiative capture cross-section in the first order perturbation theory is given by

$$\sigma(E_{c.m.}) = \sum_{E\lambda,M\lambda} \frac{8\pi(\lambda+1)}{\lambda\{(2\lambda+1)!!\}^2} \frac{1}{\hbar}\left(\frac{\omega}{c}\right)^{2\lambda+1} \times \frac{1}{2S_i+1} \sum_{J_i L_i} \left| \langle (L_f S_f) J_f \| \mathcal{M}^{E(M)\lambda} \| (L_i S_i) J_i \rangle \right|^2 \qquad (1)$$

The S-factor is defined as (Ref. KAJINO 1984)

$$S(E_{c.m.}) = \sigma(E_{c.m}) E_{c.m.} \exp(2\pi\eta_c) \qquad (2)$$

where $\eta_c = Z_1 Z_2 e^2/\hbar v_i$ is the Sommerfeld parameter, and v_i is the relative velocity between the two incident nuclei. The astrophysical S-factor and references are shown in the Table I.

TABLE I

Reaction Rates for $^{3}H(\alpha,\gamma)^{7}Li$ and $^{3}He(\alpha,\gamma)^{7}Be$

Reaction		S(O)KeV barn	References
		$^{3}H(\alpha,\gamma)^{7}Li$	
Experiment		Ø.1ØØ ±Ø.Ø25	GRIFFITH et al.Can.J. Phys.39(1961)1937
Theory	RGM	Ø.1ØØ3	KAJINO and ARIMA.Phys.
		Ø.Ø981	Rev.Lett.,52(1984)739
	RGM	Ø.Ø98±Ø.ØØ6	KAJINO.Mich.St.Univ (1986)
	RGM	Ø.97Ø±Ø.Ø38	KAJINO.Mich.St.Univ (1987)
	RGM	Ø.1ØØ±Ø.Ø25	KAJINO et al.Phys.Lett. B2Ø2(1988)475
		$^{3}He(\alpha,\gamma)^{7}Be$	
Experiment		Ø.514 ±Ø.Ø54	Phys.Rev.131(1963)2578
		Ø.588 ±Ø.Ø71	Nucl.Phys.A128(1969)325
		Ø.322 ±Ø.Ø33	Z. Phys. A3Ø4(1982)3Ø7
		Ø.521 ±Ø.Ø3Ø	Phys.Rev.lettA8(1982)1164
		Ø.573 ±Ø.Ø5Ø	Osborne et al. (1982)
		Ø.66Ø ±Ø.Ø36	Phys.Rev.C27(1983)11
		Ø.56Ø ±Ø.Ø3Ø	Z.Phys. A31Ø(1983)91
Theory	RGM	Ø.511	KAJINO and ARIMA.Phys.
		Ø.5ØØ	Rev.Lett.52(1984)739
	RGM	Ø.598	WALLISER et al.,Nucl. Phys.A419(1984)133
	GCM	Ø.59Ø	V.K.SHARMA in Int.Sym. Heavy ion Phys and Nucl.Astr.(1988)Japan
	RGM	Ø.5Ø ±Ø.Ø3	KAJINO Mich.St.Univ. (1986)
	RGM	Ø.49 ±Ø.14	KAJINO Mich.St.Univ. (1987)
	RGM	Ø.56 ±Ø.Ø3	KAJINO et al Phys.Lett. B2Ø2(1988)475

NUCLEAR MATTER RESULTS FOR DENSITY-DEPENDENT M3Y INTERACTIONS

K C Panda
Post-Graduate Department of Physics
Sambalpur University, Jyoti Vihar,
Sambalpur - 768019

The M3Y interaction v(r) has been modified with various density-dependent forms (DDM3Y) so that the heavy-ion interaction potential obtained in the folding model from such modified interactions predict the elastic scattering cross sections accurately. When the folding model concept of calculating the potential of two interacting systems is transformed for one isolated system i.e. nuclear matter or finite nucleus, we obtain the following forms for DDM3Y interactions $v(r,\rho)$.

DDM3YI[1]:

$$v(r,\rho) = v(r)C(1+\alpha e^{-\beta\rho})$$

$$v(r) = 7999\,\frac{e^{-4r}}{4r} - 2134\,\frac{e^{-2.5r}}{2.5r} + J_{oo}\delta(r). \qquad (1)$$

DDM3YII[2]:

$$v(r,\rho) = v(r)D(1-x\rho^{2/3})^2. \qquad (2)$$

DDM3YIII[3]:

$$v(r,\rho) = v(r)[1-\omega\gamma\rho^3][1-(1-\omega)\gamma\rho^3]. \qquad (3)$$

J_{oo}, C, α, β, D, x, ω and γ are parameters of these interactions.

To investigate the consistency of the density-dependent component of M3Y interaction in nuclear matter, we calculate energy per particle $\mathcal{E}$, symmetry coefficient $\mathcal{E}_s$, incompressibility $\mathcal{K}$, rearrangement energy V_R and effective mass of nuclear matter using these interactions. For this purpose, we derive the energy density of $N \neq Z$ case considering the contribution of odd-even states of DDM3Y interactions properly. The density functionals are obtained analytically.

Our preliminary results of $\mathcal{E}(k_F=1.36\ fm^{-1})$ and $\mathcal{E}_S(k_F=1.36\ fm^{-1})$ and $\mathcal{X}(k_F=1.36\ fm^{-1})$ presented in a table show that the density-dependent component of DDM3Y interactions lead to a large difference of these results from those found in literature i.e. $\mathcal{E}$ = -16MeV, $\mathcal{E}_S$=60 MeV and $\mathcal{X}$ =279MeV.

	Interactions		
	DDM3YI	DDM3YII	DDM3YIII
$\mathcal{E}$(MeV)	-2.89	0.82	2.86
$\mathcal{E}_S$(MeV)	17.48	16.89	16.12
$\mathcal{X}$(MeV)	-407.80	156.05	1008.12

References :

1. A.M.Kobos et al Nucl.Phys. A425, 205 (1984).

2. A.K.Choudhuri Nucl. Phys. A459, 417 (1986).

3. H.J.Gills Nucl.Phys. A473, 111 (1987).

d. INTERMEDIATE ENERGY NUCLEAR REACTIONS AND NON-NUCLEONIC DEGREES OF FREEDOM.

COULOMB DISSOCIATION OF EXOTIC NUCLEI IN A DIRECT FRAGMENTATION MODEL

R. Shyam, P. Banerjee and G. Baur
Saha Institute of Nuclear Physics,
1/AF, Bidhan Nagar, Calcutta, India
Institut fur Kernphysik, KFA Julich,
D-5170 Julich, Germany

Recent experiments with beams of radioactive neutron-rich exotic nuclei like ^{11}Li and ^{11}Be revealed that they have rather unusually large root mean square radius [1,2] and strikingly large total reaction and break-up cross-sections [2,3]. The electromagnetic dissociation cross-sections for ^{11}Li, calculated by assuming a shell model type structure [4] for this nucleus, come out to be somewhat smaller than the experimental data. In the cluster type structure model [5] for ^{11}Li, a (bound) two-neutron system (di-neutron) is assumed to be loosely bound to a ^{9}Li core. This is supported by the fact that the rms radius of ^{9}Li core is much smaller than that of ^{11}Li. Similar is the case for ^{10}Be and ^{11}Be. Thus the last two(one) neutrons(neutron) are(is) responsible for the large increase in the matter radii of ^{11}Li and ^{11}Be and hence for the appearance of a "neutron halo" in these nuclei.

Based on the cluster model, we have calculated the Coulomb dissociation contribution to the two-neutron and one-neutron removal cross-section of ^{11}Li and ^{11}Be projectiles in a direct fragmentation model. The model is formulated within the framework of the post form distorted-wave Born approximation [6]. In this theory, the "post acceleration effect" of the ^{9}Li and ^{10}Be fragments (i.e. the extra Coulomb repulsion experienced by these fragments) in the final channel is accounted for properly. The Coulomb break-up can explain majority of the experimental 2n removal cross-section of ^{11}Li for the ^{197}Au target at the incident energy of 29 MeV/A. The behaviour of the cross-sections for the Coulomb break-up of ^{11}Be on ^{208}Pb target at the beam energy of 33 MeV/A is similar, although the absolute magnitude in this case is smaller. The beam energy dependence of the calculated cross-sections is in good agreement with the few

experimental points which are available upto now. The angular distributions of the ^{9}Li as well as of 2n system is found to be concentrated in the very forward angles.

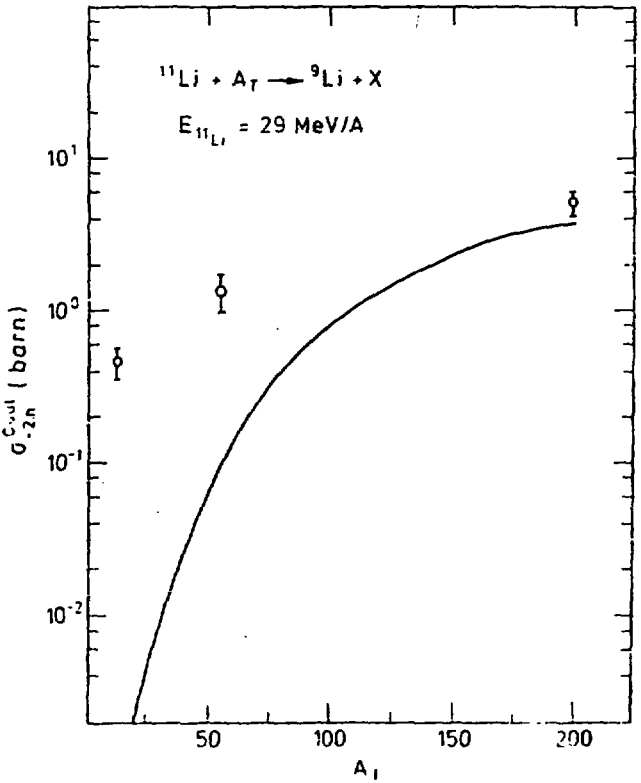

Coulomb part of the (^{11}Li , ^{9}Li) fragmentation cross-section for the beam energy of 29 MeV/A as a function of the target mass. The experimental points correspond to the total two-neutron removal cross-section of ^{11}Li.

References

1. I. Tanihata et al., Phys. Lett. B160(1985)380; Phys. Rev. Lett. 55(1985)2676; Phys. Lett. B206(1988)592.
2. T. Kobayashi et al., Phys. Rev. Lett. 60(1988)2599; Phys. Lett. B232(1989)51.
3. R. Anne et al., Phys. Lett. B250(1990)19.
4. G. Bertsch and J. Foxwell, Phys. Rev. C41(1990)1300.
5. P. G. Hansen and B. Jonson, Europhysics Lett. 4(1987)409.
6. G. Baur and D.Trautmann, Nucl. Phys. A191(1972)321.

DETERMINATION OF $^{12}C(p,p')^{12}C^{*}(1^{+})$ INELASTIC SCATTERING AMPLITUDES

A. Sudha Rao, K.S Mallesh, M.S. Vidya and
G. Ramachandran
University of Mysore, Mysore - 6

Abstract: We identify spin observables on $^{12}C(p,p'\gamma)^{12}C$ to supplement the differential cross sections and the seven existing spin measurements on the inelastic scattering so that a discrete ambiguity free empirical determination of the six inelastic scattering amplitudes is achieved. Sixteen such equivalent sets of spin observables (which do not demand measurement of photon polarization) are listed and numerical estimates presented to facilitate planning of the experiments.

Writing the reaction amplitude for $^{12}C(p,p'\gamma)^{12}C$ as

$$M = G(\theta,\phi)\ T \qquad (1)$$

Where T denotes the matrix for inelastic scattering and G the amplitude for the gamma decay with (θ,ϕ) being the polar angles of the emitted photon, we define the spin observables (when photon polarization is not measured) as

$$D_{ij}(\theta,\phi) = Tr(M\sigma_i M^{+}\sigma_j);\ i,j = 0,1,2,3\ldots \qquad (2)$$

where σ_0 denotes the unit 2X2 matrix and the others Pauli spin matrices. Since the overall phase of T is arbitrary, one can choose one out of the six inelastic amplitudes constituting T to be real and determine all the six of them without any discrete ambiguities by supplementing the existing measurements (viz., both the differential cross sections and seven spin measurements on inelastic scattering) with future measurements on a set of seven appropriately chosen spin observables viz., the D's as shown, for example, in Table 1.

We have identified sixteen such equivalent sets none of which demand photon polarization measurements. Numerical estimates of the proposed observables have also been obtained based on unpublished theoretical amplitudes [1].

Table 1: One set (Out of the suggested sixteen sets) of spin observables

$$D_{oo}(\theta,\phi) = (8\pi)^{-1} R\,[\,(|A|^2+|B|^2+|C|^2+|D|^2+|E|^2+|F|^2) + 0.25(3\cos^2\theta-1)(|A|^2-2|B|^2+|C|^2+|D|^2+2|E|^2+|F|^2) + 1.5\sin^2\theta\,\mathrm{Re}\{(AC^*-DF^*)\exp(2i\phi)\}]$$ with $\phi = 0$

$$D_{xo}(\theta,\phi) = (5.66\pi)^{-1} 3R\sin\theta\cos\theta\,\mathrm{Re}\{[(E^*A-BF^*) + (B^*D-EC^*)]\exp(i\phi)\}$$ with $\phi = 0$ and $\pi/2$

$$D_{yo}(\theta,\phi) = (5.66\pi)^{-1} 3R\sin\theta\cos\theta\,\mathrm{Im}\{[(E^*A-BF^*) + (B^*D-EC^*)]\exp(i\phi)\}$$ with $\phi = 0$ and $\pi/2$

$$D_{xx}(\theta,\phi) = (5.66\pi)^{-1} 3R\sin\theta\cos\theta\,\mathrm{Re}\{[(E^*A+BF^*) + (B^*D+EC^*)]\exp(i\phi)\}$$ with $\phi = 0$ and $\pi/2$

Here $A=\langle 1, 1/2|T|0,1/2\rangle$, $B=\langle 0,1/2|T|0,1/2\rangle$, $C=\langle 1, 1/2|T|0,1/2\rangle$, $D=\langle 1,1/2|T|0,-1/2\rangle$, $E=\langle 0, 1/2|T|0,-1/2\rangle$, and $F=\langle 1,1/2|T|0, 1/2\rangle$ are the matrix elements of the inelastic scattering matrix T and R is the branching ratio as given in [2].

We thank Professor Piekarewicz for making available the DREX and DW81 amplitudes and ASR thanks UGC for financial assistance.

References:

[1] J. Pierarewicz, Private Communication.
[2] J. Pierarewicz, E. Rost and J.R. Shepard, Phys. Rev. C 41 (1990), 2277.

NUCLEON PROPERTIES IN CHIRAL COLOR DIELECTRIC MODEL

Sarira Sahu and S.C. Phatak

Institute of Physics, Sachivalaya Marg, Bhubaneswar-751005

Color Dielectric Model (CDM) has a number of attractive features which make it interesting from nuclear physics point of view. For example, in CDM the interaction of the color dielectric (scalar) field with quarks and gluons is such that one obtains absolute confinement of quarks and gluons. Furthermore, unlike the bag models, the confinement in CDM is generated dynamically. Therefore it is possible to perform a dynamical calculation of multi-nucleon systems within CDM[1]. One of the shortcomming of the CDM is that it does not possess chiral invariance. However, chiral invariant versions of CDM (CCDM)[2] have developed and solutions using hedgehog ansatz obtained.

In the present work we are reporting a detailed investigation of the properties of light hadrons in CCDM[3]. In our calculation, we first solve the quark and scalar field equations self-consistently and construct bare (3 - quark) states for nucleon and delta. Using the quark wavefunctions and scalar field we calculate the gluonic[1] and pionic contributions to nucleon and delta masses perturbatively. To include pionic effect we construct the physical baryon state with one pion "in the air". The calculated nucleon and delta masses are then fitted by adjusting the glueball mass (mass of the scalar field) and strong coupling constant. Finally, the static properties of hadrons are calculated by using the nucleon and delta states thus constructed, over a wide range of parameters[3].

The CCDM has five parameters; the bag constant (B), (m_{GB}) the glueball mass, α the coefficient appearing in the scalar potential $U(\chi)$, the quark mass m_f and α_s. We have studied the color dielectric model of the baryon (nucleon and delta) incorporating the chiral symmetry by introducing a non-linear quark-pion coupling and treating the gluonic and pionic effects perturbatively. We find that the strong coupling constant is very sensitive to the quark and glueball masses and very small for single phase solutions. With the inclusion of pionic correction we have calculated the static properties of the nucleon over a wide range of parameters and compared these with the experimental values. It is observed that for small glueball masses the proton rms radius increases slowly as quark mass increases, whereas for large glueball masses first it decreases and then increases slowly. But the neutron rms radius remains almost constant (-.31 fermi) over the wide variation of quark and glueball masses and lies very close to the experimental value (-.35 fermi). Proton rms radius lies in the vicinity of the experimental value for small

m_{GB} (< 1100 MeV) and quark masses below 100 Mev. But for glueball mass below 700 MeV it becomes large. Our results show that the magnitude of the proton and neutron magnetic moments increases with increasing m_f and decreasing m_{GB}. For the best fitting parameter set the proton magnetic moment(2.66 μ_N) is 5% less then the experimental one (2.79 μ_N) and neutron magnetic moment (-1.90 μ_N) is almost same as the observed value (-1.91 μ_N). The calculated values of $f_{NN\pi}$ is almost independent of the parameters used and in excellent agreement with the observed value. There is practically no change in g_A due to the pion coupling. For wide range variation of parameters g_A lies inbetween 1.22 and 1.30, which is rather close to the experimental value 1.26. All the static properties are almost insensitive to the variation in $B^{\frac{1}{4}}$ and α. The proton magnetic moment is observed to be slightly smaller than the experimental one and it is not possible to improve the agreement further by simply varying parameters. The calculations also show that inclusion of quark self-energy decreases proton charge rms radius and nuclear magnetic moments, thus worsening the agreement with the corresponding experimental values.

References

1. S.C. Phatak, to appear in *Phys. Rev.* C.
2. H. Kitagawa, *Nucl. Phys.* **A487**, 544 (1988).
3. S. Sahu and S.C. Phatak, Priprint IP-BBSR-91/36

SPIN ORBIT $N-N$ INTERACTION FROM *COGEP*

S.B. Khadkikar and K.B. Vijayakumar
Physical Research Laboratory
Ahmedabad 380 009, India

We have investigated the effect of the spin orbit arising from the exchange of confined gluons on 3_P and 3_D phase shifts (PS). For the confinement of quarks we use the relativistic harmonic model (RHM) in which quarks are confined by a harmonic oscillator Lorentz scalar + vector potential. For the confinement of gluons we use the current confinement model (CCM) developed in the spirit of RHM. Making use of confined gluon propagator we have obtained confined one gluon exchange potential ($COGEP$). The $L.S$ part of $COGEP$ is given by

$$V_{ij}^{LS} = \frac{\alpha_s}{4}\frac{N^4}{(E+M)^2}\frac{\lambda_i \bullet \lambda_j}{2r} \otimes \left\{\left[\vec{r}\times\left(\hat{P}_i-\hat{P}_j\right)\bullet(\vec{\sigma}_i+\vec{\sigma}_j)\right]\left[D_o'(\vec{r})+2D_1'(\vec{r})\right] - \left[\vec{r}\times\left(\hat{P}_i+\hat{P}_j\right)\bullet(\vec{\sigma}_i-\vec{\sigma}_j)\right]\left[D_o'(\vec{r})-D_1'(\vec{r})\right]\right\}$$

Only spin-symmetric part contributes to scattering, PS are calculated using Kohn-Hulthen-Kato variational principle. We have plotted $^3P_0$ (Fig. 1) $^3P_1$ (Fig. 2) and $^3P_2$ (Fig. 3) (without $^3P_2$- $^3F_2$ coupling); $^3D_1$ (Fig. 4), $^3D_2$ (Fig. 5) and $^3D_3$ (Fig. 6) (without $^3D_3$- $^3G_3$ coupling) PS in comparison with the PS of Arndt.

We find, in general, there is little agreement between our phase-shifts and Arndt analysis, the latter being conditioned by $OPEP$ for all high partial waves. Since the phase-shifts are derived quantities only angular distribution can confirm the existence of a rather strong spin-orbit force which is required in nuclear structure also.

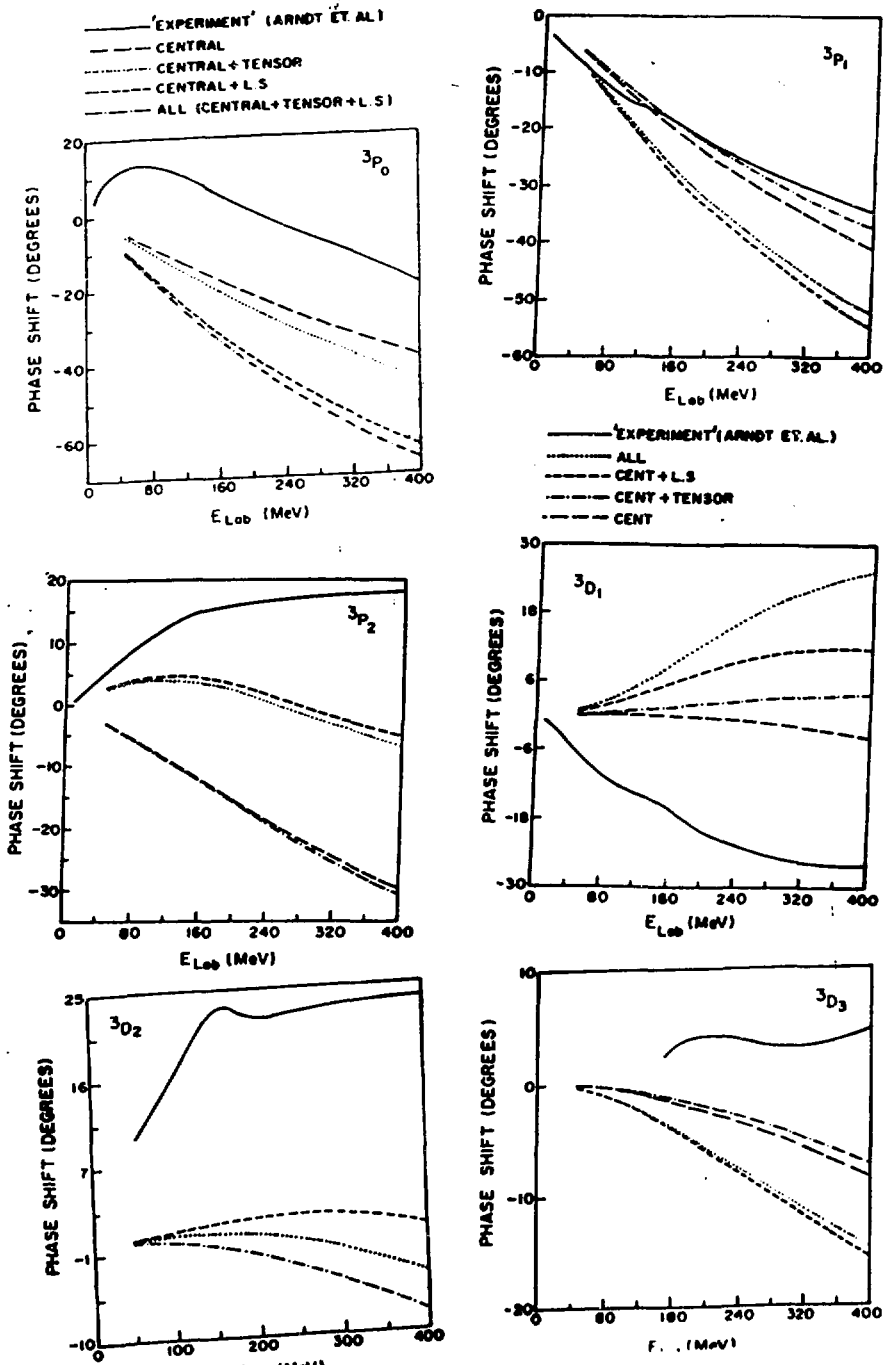
'EXPERIMENT' (ARNDT ET. AL.)
CENTRAL
CENTRAL + TENSOR
CENTRAL + L.S
ALL (CENTRAL + TENSOR + L.S)
$^3P_0$
$^3P_1$
$^3P_2$
$^3D_1$
$^3D_2$
$^3D_3$
PHASE SHIFT (DEGREES)
E_{Lab} (MeV)
'EXPERIMENT' (ARNDT ET. AL.)
ALL
CENT + L.S
CENT + TENSOR
CENT

MULTIPLICITIES OF THE EMITTED NEUTRON AND LIGHT CHARGED-PARTICLES IN MULTIFRAGMENTATION PROCESS

A.Das, L.Satpathy, M.Mishra and M.Satpathy*
Institute of Physics, Bhubaneswar-751005
*Utkal University, Bhubaneswar-751004

During the last few years, the study of the properties of hot nuclei has been an area of intense investigation. In particular, we have not yet acquired adequate knowledge regarding the decay modes of a very hot nucleus. A possible way of getting the information about the hot nuclei is to measure the multiplicities and energies of the emitted neutron, and other light charged-particles such as proton and alpha-particle. In this context, many measurements[1] are being carried out for heavy ion induced fission and fusion processes. However, in case of multifragmentation process, such measurements, at present are rather scanty. Recently, Gonin et. al.[1] have made such measurements for hot nuclei produced in heavy ion induced reaction and compared the experimental multiplicities obtained for neutron, proton and alpha-particle, with that of the statistical models like PACE2 and CASCADE. They found that these statistical model calculations underestimate the multiplicities of those particles, in particular of neutron by about a factor four compared to the experiment. This strikingly low neutron multiplicity of the statistical models has created a serious problem in this area of study. It has been generally felt[1] that the dynamical effects and the deformation degrees of freedom, are likely to play an important role in enhancing the multiplicities of the emitted light particles. Similar situation prevails in the multifragmentation process, which is also usually described in various statistical models. We feel the usual statistical models are inadequate to describe the process, because these do not include the nuclear interaction amongst the fragments. This area of study provides a good prospect for, not only, unraveling the mechanism of the process, but also, for testing the various presently available models.

To study this problem, we have used improved multifragmentation model based on grand canonical ensemble, proposed by us earlier[3], in which the nuclear mean field seen by a fragment in the assembly of interacting nuclear species, is calculated in addition to Coulomb mean field, following a statistical method. Using above model, we have calculated the multiplicities for neutron, proton, and alpha-particle as a function of temperature with nuclear plus Coulomb interaction and with only Coulomb interaction, in the $p + Ag$ reaction. The corresponding results are shown as solid and dashed curves for neutron(n) in Fig.1 and for proton(p) and alpha-particle(α) in Fig.2. It is indeed gratifying to find that, due to the inclusion of nuclear force, there is an enhancement of the neutron multiplicity by a factor about 10 at temperature 3 MeV.

This enhancement factor gradually decreases to 2.5 when the temperature increases to 6 MeV. The fall in the enhancement is due to the relative increase of the kinetic energy with respect to the potential energy with the rise of temperature. In case of proton and alpha-particle, the multiplicities are also substantially enhanced.

Thus in the frame work of statistical model, the multiplicities of the emitted neutron and charged-particles are very substancially enhanced without resorting to other mechanisms like dynamical and deformation effects etc.., but by taking into account interfragment nuclear interaction, which is an integral part of nuclear dynamics hitherto unaccounted.

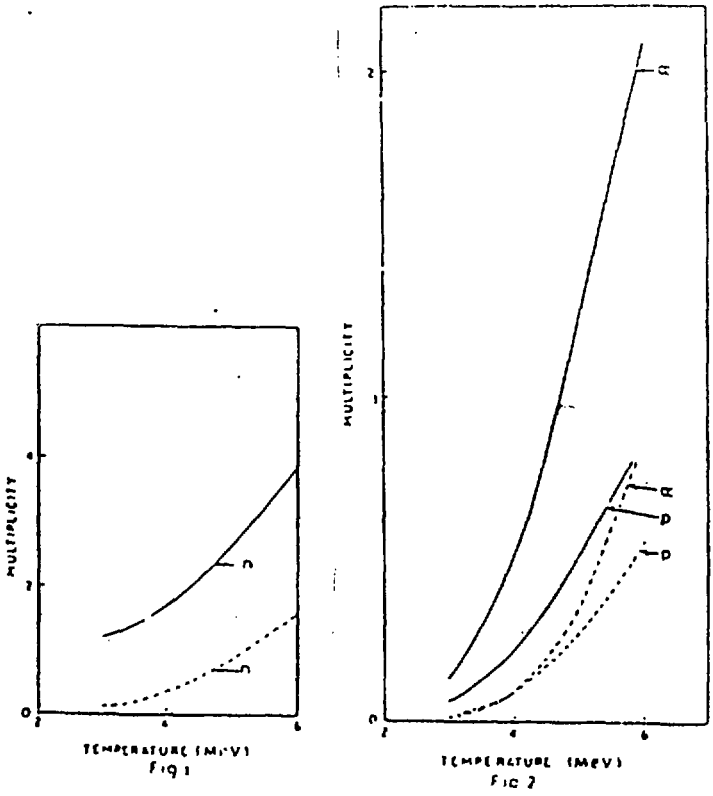

References:

1. M.Gonin et. al., Phys. Rev. C42, (1990), 2125; A.Gavron et. al., Phys. Rev. C35, (1987), 579; E.Holub et. al., Phys. Rev. C28, (1983), 252.
2. J.Aichelin et. al., Phys. Rev. C30, (1984), 107; X.Campi et. al., Phys. Lett. B142, (1984), 8.
3. L.Satpathy, M.Mishra, A.Das and M.Satpathy, Phys. Lett. B237, (1990), 181.

N-N INTERACTION IN CHIRAL COLOUR DIELECTRIC MODEL

Sanjay K. Ghosh
Institute of Physics
Bhubaneswar 751 005
INDIA

Colour Dielectric Model(CDM) which is based on the idea of Nelson and Patkos[1] generates the confinement of quarks and gluons dynamically through the interaction of these fields with scalar field. In the present work we have applied chiral extension of CDM to describe N-N interaction. The Lagrangian density of the nonlinear version of the chiral CDM is given by,

$$\mathcal{L}(x)=\bar{\psi}(x)\left[i\gamma^{\mu}\partial_{\mu}-\frac{m}{\chi(x)}\left\{\cos\left(\frac{\pi(x)}{f}\right)+i\gamma_5\vec{\tau}.\hat{\pi}(x)\sin\left(\frac{\pi(x)}{f}\right)\right\}\right.$$
$$\left.+\frac{g}{2}\gamma^{\mu}\lambda_a A^a_{\mu}(x)\right]\psi(x)+\frac{1}{2}(D_{\mu}\vec{\pi}(x))^2-\frac{1}{2}m_{\pi}^2\pi^2(x)-\frac{1}{4}\chi^4(x)(F^a_{\mu\nu}(x))$$
$$^2+\frac{1}{2}\sigma_v^2(\partial_{\mu}\chi(x))^2-U(\chi) \qquad (1)$$

where $\psi(x)$, $A_{\mu}(x)$, $\chi(x)$ and $\vec{\pi}(x)$ are quark, gluon. scalar (color dielectric) and pion fields respectively, The self-interaction of the scalar field is asumed to be of the form,

$$U(\chi)=\alpha B\chi^2(x)\left[1-2(1-2/\alpha)\chi(x)+(1-3/\alpha)\chi^2(x)\right], \quad (2)$$

so that $U(\chi)$ has an absolute minimum at $\chi=0$ and a secondary minimum at $\chi=1$.

To start with we assume that nucleon consist of 3(u & d) equal mass valence quarks. The quark wave functions are obtained by solving the quark and scalar field equation self consistently and treating pions and gluons perturbatively[2]. Nucleon states are constructed by taking combinatian of quark wave function. The N-N potential is calculated using the expression[3] $V(x)=-\frac{1}{(2\pi)^3}\int d^3k e^{ik.x}\,T^B_{fi}$, where T^B_{fi} is the Born approximation to the reduced matrix element T_{fi} for the elastic scattering of the

constituent particles.So we first calculate the scattering matrix element for the gluon as well as pion mediated elastic scattering of quarks. The interactions contributing to potential is shown in fig(1). The straight lines represents quarks and dashed lines represent gluons or pions. For gluons fig(a) vanishes identically where as for pions both (a) and (b) contribute.

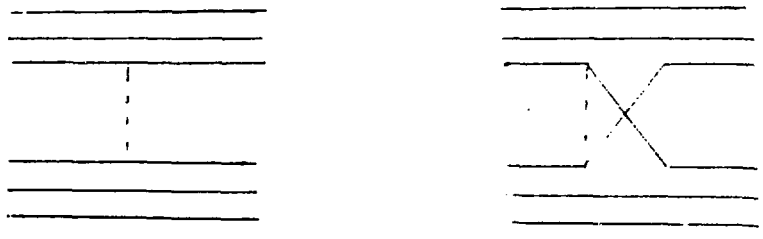

1(a) 1(b)

The quark coordinates are intregated out to get the potential as a function of internucleon distance. Finally we take matrix element of V between initial and final two nucleon system to get the potential V(R) in terms of two nucleon operators. The potential coming from both one gluon exchange and one pion exchange are of the same form which is given by

$V(R) = f_1(R) + f_2(R)(\sigma_1.\sigma_2) + f_3(R)(\tau_1.\tau_2) f_4(R)(\sigma_1.\sigma_2)(\tau_1.\tau_2) + f_5(R) T_2(\sigma_1.\sigma_2).C_2(\Omega_R) + f_5(R) T_2(\sigma_1.\sigma_2).C_2(\Omega_R)(\tau_1.\tau_2)$

where σ_1, σ_2 and τ_1, τ_2 are spin and isospin operators for nucleons. T_2 is the tensor of rank two and $C_2(\Omega_R)$ is the spherical harmonics. The final results are not yet available, but a rough estimate shows that OGE part of the potential gives a short range repulsion and OPEP partgives mainly attractive contribution.

REFERENCE:

1.H.B.Nielson and A.Patkos: Nucl.Phys.B197(1982) 139

2.S.C.Phatak: Phys.Rev.C

3.Wolfgang Lucha et.al.Phys.Rev.D44(1991)242

INCLUSIVE $(p,p'\pi^+)$ REACTION

Neelima G.Kelkar and B.K.Jain
Nuclear Physics Division, B.A.R.C., Bombay 400 085.

The Δ^{++} produced in the (p,Δ^{++}) reaction on a nucleus decays to a proton and pion in the final state. In an experiment to study the inclusive (p,Δ^{++}) reaction the outgoing proton and pion would be observed in coincidence. Hence we study the features of the $(p,p'\pi^+)$ reaction theoretically with Δ^{++} formed in the intermediate state. (see fig.1).

The cross section for this reaction in the lab. system is given as,

$$\frac{d^4\sigma}{d\Omega_{p'}d\Omega_\pi dE_{p'}dE_\pi} = \frac{k_{p'}k_\pi}{k_p}\frac{m_p^2}{2(2\pi)^5\hbar c}|V(\omega,q)|^2 D_\Delta^2 \times \sum_n \delta(\omega-\omega_n)\langle n|1|\tilde{\rho}_{no}(-q)|^2|0\rangle \quad \ldots(1)$$

where $\omega = E_p - E_{p'} - E_\pi$. $V(\omega,q)$ contains the spin-isospin interaction at the two $\pi N\Delta$ vertices and D_Δ is the mass propagator for the delta. The response function which involves a summation over the various possible excited states, 'n', of the nucleus is written in terms of the self-energy of the pion in the medium. Since our calculations involve large energy transfers we consider contributions to self-energy from nucleon-hole as well as delta-hole excitations.

We construct the outgoing proton spectrum $d^2\sigma/d\Omega_{p'}dE_{p'}$ from eq.(1) by integrating over the allowed range of energy and all angles of the outgoing pion. In fig.2 we plot $d^2\sigma/d\Omega_{p'}dE_{p'}$ as a function of $T_{p'}$, at various energies of incidence. At incident beam energies upto 1 GeV we see a single peak in the cross sections while at higher energies two distinct peaks appear. The range of ω increases with beam energy. Since integral over E_π implies an integral over a certain range of delta mass, this change in the peak structure in $d^2\sigma/d\Omega_{p'}dE_{p'}$ is a reflection of the response of the nucleus with the increase in the energy transfer, ω , to the nucleus. However, unlike in the case of the (p,p') reaction, here the nucleon and delta sectors in the response do not separate out.

In the (p,p') reaction one observes a peak in the outgoing proton spectrum due to quasifree nucleon-nucleon scattering and then another broad peak at higher $T_{p'}$ due to quasifree delta production.

The cross-sections in fig.2 are calculated using a completely relativistic formalism. In a non-relativistic calculation we observe only a single peak in the proton spectrum at all energies and the cross-sections are highly overestimated.

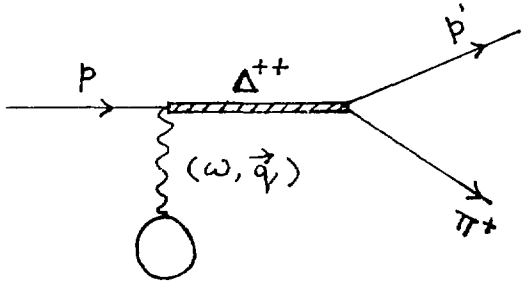

Fig. 1

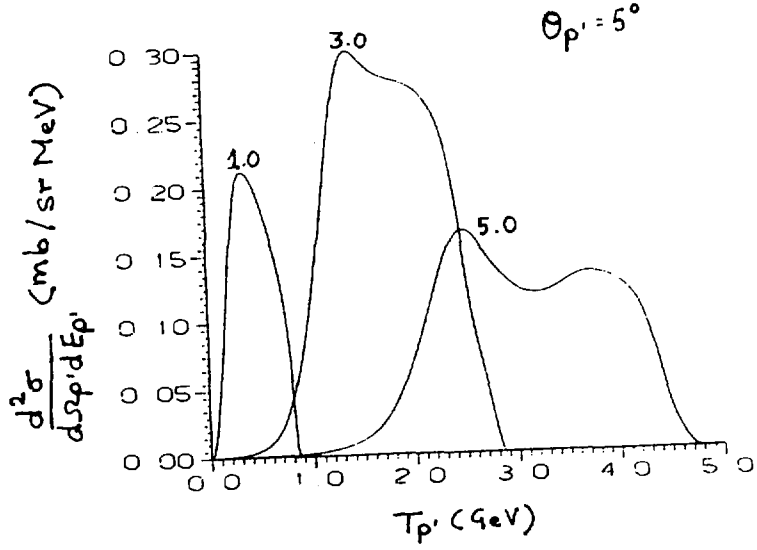

Fig. 2

K^+ PRODUCTION IN HEAVY ION COLLISION AT FAR SUBTHRESHOLD BEAM ENERGY

B. Ghosh
Institute of Physics, Bhubaneswar-751 005

In recent years there has been a lot of activities centered around the experimental and theoretical studies of the subthreshold and energetic particle emisson in intermediate energy nuclear collisions[1]. One of the latest additions to these activities is the measurement[2] of K^+ inclusive cross-section with a beam energy as low as 92 MeV/nucleon, the free N-N threshold energy for K^+ production being 1.58 GeV. Earlier K^+ production was measured at above-threshold beam energies[1]. Such high energy experimental data were studied in the framework of a hadrochemical model and also by relativistic and nonrelativistic transport theory aproach based on sequential independent baryon-baryon collisions. However, such models are suitable for beam energies around 500 MeV/nucleon and above[1,2]. On the other hand for the kaon production by a beam energy far below the threshold cooperative mechanisms and off-shell effects are likely to be important[1,2]. Therefore we have calculated here the inclusive K^+ production cross-sections for the collision $^{36}Ar+^{48}Ti$ at the beam energy of 92 MeV/nucleon, in the framework of a cooperative mechanism which has earlier been reasonably successful in explaining subthreshold pion[3] and energetic proton[4] emissions. In this formalism the Lorentz-invariant inclusive particle(λ) production cross-section is given by[3]

$$E_\lambda (d^3\sigma/d\,p_\lambda^3) = \sum_{MN} \sigma_{AB}(M,N) F_{MN}^{\lambda}(\vec{p}_\lambda) \qquad (1)$$

where, $\sigma_{AB}(M,N)$ is the formation cross-section and $F_{MN}^{\lambda}(\vec{p})$ gives the phase space distribution of the observed particle in the collision between the nuclei A and B. The sum is over groups (virtual clusters) of mutually interacting M projectile and N target nucleons.

As coulomb effects are likely to be important at this low energy regime we have included the coulomb final state interactions following a covariant formalism[5], in which the K^+ cross-section is given by

$$\sigma_+(\vec{p}) = \sigma_o(\vec{p}-\Delta\vec{p})D_+(\vec{p}) \qquad (2)$$

where, $\Delta\vec{p}$ is a momentum shift and $D(\vec{p})$ is the phase space distortion factor. σ_o is the cross-section of the corresponding neutral particle. In Fig.1 and Fig.2 we show the angle-integrated and energy-integrated cross-sections of K^+. It may be noted that the detailed energy distribution is not available experimentally. The total cross-section either from Fig.1 or Fig.2 is 162 pb with coulomb effects and 174 pb without coulomb effects whereas the experimental total cross-section for the same system is (240±150)pb[2]. Our calculated $\sigma_{K^+}/\sigma_{\pi^+}$ ratio is 8.6×10^{-7} which agrees with the experimental result 10^{-6} [2]. Thus, it appears to us that like other subthreshold particles[6] K^+ production also is governed mainly by phase space constraints at this beam energy regime.

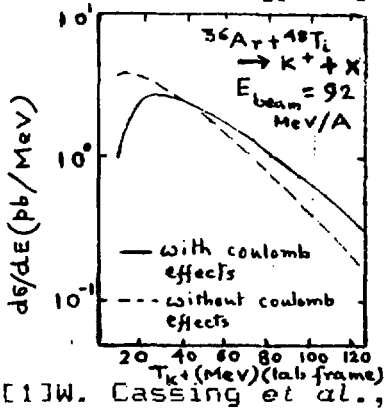

Fig.1

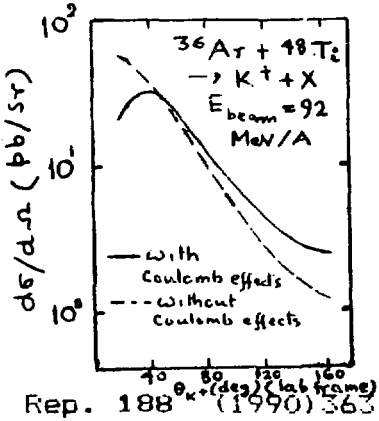

Fig.2

[1]W. Cassing *et al.*, Phys. Rep. 188 (1990)363 and references therein.
[2]J. Julien *et al.*, Phys. Lett. B 364 (1991)269.
[3]R. Shyam and J. Knoll, Nucl. Phys.A 426(1984)606.
[4]B. Ghosh and R. Shyam, Phys. Lett.B 234(1990)245.
[5]B. Ghosh, J. Phys. G (in press).
[6]A. Badala *et al.*, Europhys. Lett.15(1991)145.

BAG MODEL FORMULATION OF HADRON MASSES

Rajesh Gaur, A.K.Gautam and A.K.Shiromani
Physics Deptt., R.B.S.College, Agra.

Experimental investigations of the products of Lepton - Lepton (1) Hadron - Hadron (2)and Hadron nucleous interactions have yielded a number of the particles constituted from various families of particles. The mass spectrum of hadrons, so produced, has been studied theoritically on the bases of potential models, considering the concepts of quartk confinement and asymptotic freedom on the one side while on other side the particle has been assumed to be confined in a bag (3) based only on quark confinement. On the bases of Quantum Chromodynamics (Q C D) quarks are assumed to be interacting through a coulombic potential upto certain distance (Quark Confinement) and beyond a certain distance linear potential is said to exist (Asymptotic Freedom) (4) In this work we have used the bag model for the study of Baryon masses constituted by different quarks. The mass of a Baryon is given by

$$E(R) = N_i \sum_i \left(m_i^2 + \frac{X_i^2}{R^2}\right)^{\frac{1}{2}} + B\,(4\pi R^3/3)$$

Where

N_i, m_i, X_i, are the total number of quarks, mass of quark and monentum with flavour i respectively B is a constant, positive energy per unit volume, R is the bag radius in which quarks are confined.

The particle masses have been estimated for different bag radii and compared with other theoritical worker and Experimental results.

Reference:

1. Schwitterers.R.F. et.al. Ann.Rev.Nucl Sci.26,89 (1979).
2. Dorfan,J.M.Slac Report 4816(1979).
3. Chodos,A,et.al.Phys.Rev.D9(1974)3471.
4. A.K.Gautam,Sym.on Nucl.Phys.328P74(1989),ibid D.A.E.Sym.on nucl.phys.33B (1990)233.

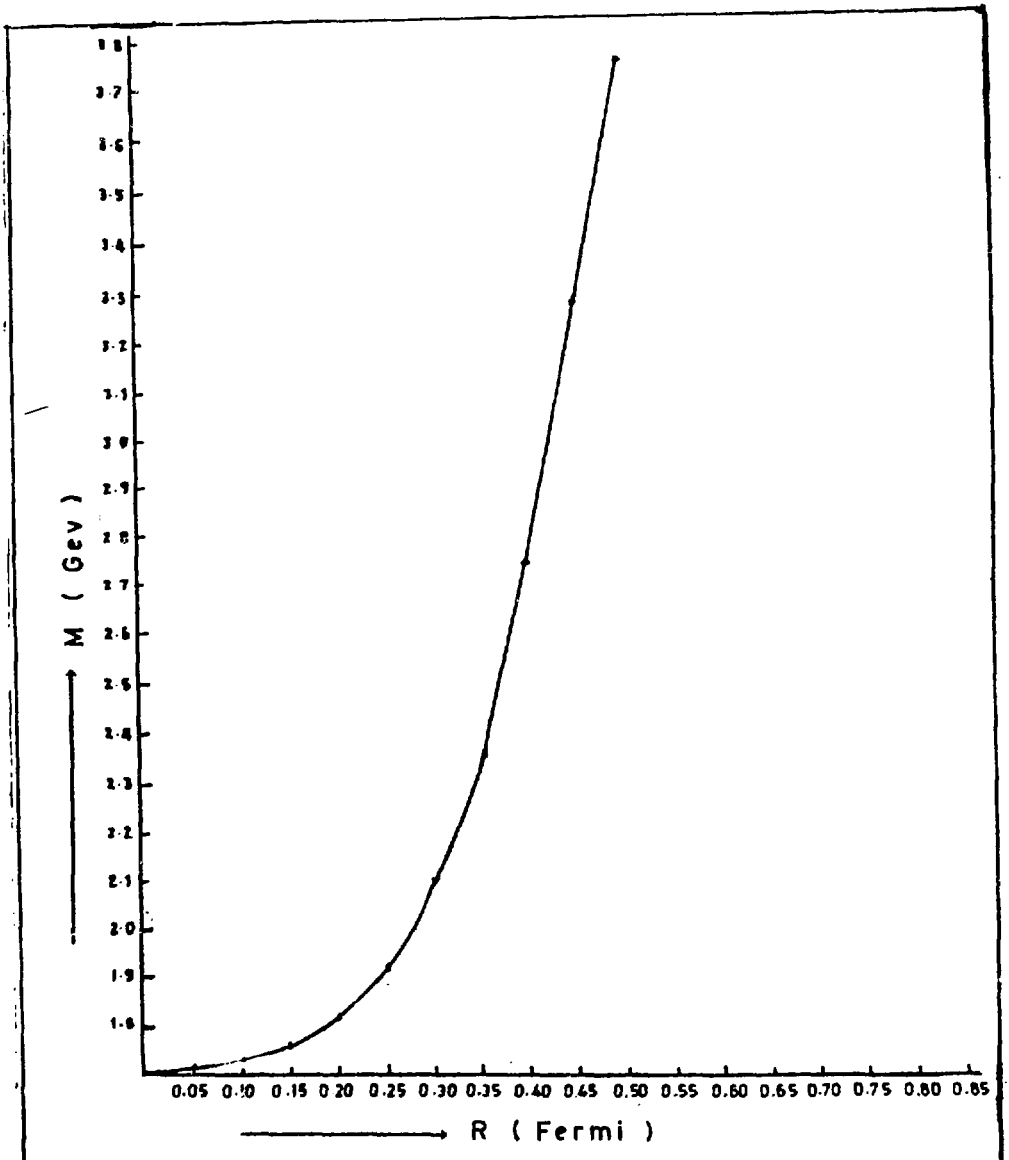

FIG. :VARIATION OF MASSES WITH BAG RADII FOR THREE QUARKS SYSTEM uuc udc ddc FOR LIMITED DATA.

ANNIHILATION RANGE, $\bar{P}P$ SCATTERING PARAMETERS AND COMPLEX POTENTIAL SCATTERING

A. V. Lagu
Physics Department, Banaras Hindu University

Using a generalized effective range (ER) expansion (which has been found to be easy to use and transparent) developed earlier /1,2/ in conjunction with good quality $\bar{p}p$ data at low energies/3/, we find the S-wave scattering parameters as: Scattering length = $A = a_r + ia_i = 0.7 - i0.8$ fm, and Effective range = $R = R_r + iR_i = 0.75 - i\ 1.01$ fm. These compare reasonably with a multichannel ER analysis /4-Fit.B/ giving $A = 0.7 - i\ 0.3$ fm and $R = 0.5 - i\ 1.1$ fm. A dispersion theoretic /5/ analysis gives $A = 0.84 - i\ 0.37$ fm and $R = -4.92 - i\ 3.86$ fm.

To understand the nature of the underlying potential leading to these values of scattering parameters and their physical significance we did an ER expansion for a complex square well potential $V_R + iV_I$ such that the range r_2 of the real part is different and greater than the range r_1 of the imaginary part of the potential. This turned out to be a very long affair and great caution had to be exercised so as to not miss any terms of correct order in k and finally led to exact analytic expressions for a_r, a_i, R_r and R_i (which are too long to be reproduced here). It was found that it was impossible to reproduce the scattering parameters of ref./4-Fit.B/ to better than ± 0.15 (in natural units). Within this bound, the potential parameter set turned out to be $V_R = 24.9$ MeV, $V_I = 95$ MeV, $r_2 = 1.67$ fm, $r_1 = 1.16$ fm. Without ambiguity, r_1 is now the annihilation range and turns out to be greater than 1 fm. This large value for annihilation range was suspected earlier but is clearly demonstrated in the present work.

The analytical expressions for scattering parameters turn out to be very useful because they lead to quite new insights into complex potential scattering. To give only one instance, using the potential parameters of Koch et al /6/ (where

$r_1 = r_2 = r_e = 4$fm and $V_I = 103.3$ MeV) we show in fig.1 the trajectory in the complex effective range plane which results when V_R increases. A new loop to the trajectory occurs when a level gets added due to the increasing real strength. Remarkably, the trajectory is very similar to the trajectory of the pole of the Koch model depicted in fig.9 of ref./7/ and also to the trajectory in the complex scattering length plane depicted in fig.4.5 of ref. /8/. The loops in complex plane lead us to suspect some connection with Berry's phase.

This work was supported in part by the DAE, Govt. of India through a project grant.

References

/1/ A.V.Lagu, in Physics at LEAR with Low Energy Antiproton, ed. C.Amsler et al (Harwood, 1988) p.251.
/2/ A.V.Lagu, Preprint IISc-CTS-4/90 and to be published.
/3/ T.A. Shibata, personal communication.
/4/ J.Mahalanabis et al, Nucl.Phys. A485 (1988) 546.
/5/ P.Kroll and W.Schweiger, Nucl.Phys. A503 (1989) 865.
/6/ J.H.Koch et al, Phys.Rev.Lett. 26 (1971) 1465.
/7/ L.P.Kok and H.van Haeringen, Ann. Phys. 131 (1981) 426.
/8/ A.M.Badalyan et al, Phys. Rep. 82 (1982) 31.

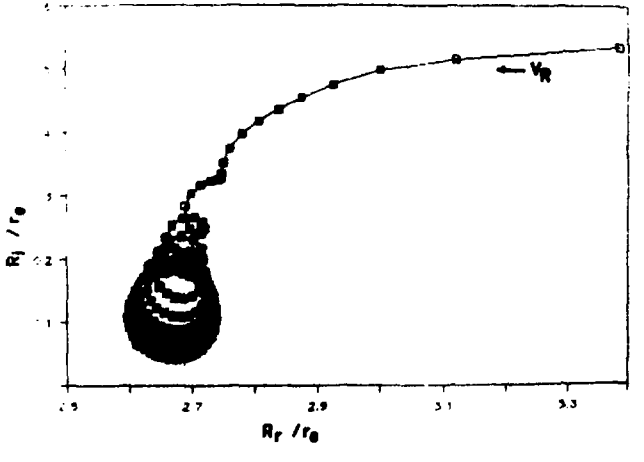

Fig. 1

DIELECTRIC FUNCTIONAL DEPENDENCE OF GLUONIC EFFECTS IN COLOR DIELECTRIC MODEL

Sarira Sahu
Institute of physics, Sachivalaya Marg, Bhubaneswar 751005

The Lagrangian density for the Color Dielectric Model (CDM)[1] is

$$\mathcal{L}(x) = \sum_f \overline{\psi}_f(x)(i\gamma^\mu\partial_\mu - \frac{m_f}{\chi(x)^\tau} - \frac{g_s}{2}\gamma^\mu\lambda_a A^a_\mu(x))\psi_f(x)$$

$$+\frac{1}{2}\sigma_v^2(\partial_\mu\chi(x))^2 - \frac{1}{4}K(\chi)F^a_{\mu\nu}(x)F^{\mu\nu}_a(x) - U(\chi)$$

where $\psi(x)$, $\chi(x)$ and $A^a_{\mu\nu}(x)$ are effective quark, scalar and the gluon fields. m_f is the quark mass and the summation is over all flavors. $F^a_{\mu\nu}$ is the color electromagnetic field tensor. Ptential

$$U(\chi) = B(\alpha\chi^2(x) - 2(\alpha-2)\chi^3(x) + (\alpha-3)\chi^4)$$

For $\alpha > 6$, $U(\chi)$ is such that it has a double well structure with an absolute minimum at χ=0, which corresponds to physical vacuum and a secondary minimum at χ=1 corresponds to perturbative vacuum. The energy density difference between the two minima measures the pressure of the physical vacuum; i.e. the bag constant B. The gluon field is coupled with the dielectric field through the dielectric functional $K(\chi)=\chi^\beta$ and it goes to 0 for physical vacuum and to 1 for perturbative vacuum. As $K(\chi)$ distinguishes the physical and the perturbative vacua, it can be treated as the order parameter. The scalar (color dielectric) field in the Lagrangian represents the non-perturbative features of the QCD vacuum. As χ goes to 0 for r > 1 fermi and goes to 1 for r goes to 0, the effective mass term $\frac{m}{\chi^\tau(x)}$ in the Lagrangian goes to infinity for $r > 1$ fermi and confines the system absolutely.

Recently Aoki and Hyuga[2,3] have shown that $\tau : \beta = 1 : 2$ (case I) is superior to $\tau : \beta = 1 : 4$ (case II) for nucleon and delta. In the present work the nucleon static properties as well as the baryon spectrum for Octat and decuplet for case I and Case II are calculated and compared with the experimental results and showed that in both the cases the results are in good agreement with the experimental values.

The CDM has five parameters ; the bag constant(B), σ_v,α the constant in the scalar potential , the light quark masses m_u (strange quark mass m_s for Ω^- mass fitting) and strong coupling constant α_s. For calculational convenience we have defined $m^2_{GB} = (\frac{2B\alpha}{\sigma_v^2})$ as an independent parameter. The quark and the color dielectric field equations

are solved in mean field approximation where as the gluonic effects are included perturbatively[2]. As the quarks interacts weakly in the asymptotic limit and also the dielectric field takes into account the long range order effects of the QCD vacuum, gluon can be treated perturbatively. In the first stage of the numerical calculation the parameters - B,α,m_{GB} and m_f are adjusted to fit the N, Δ masses and the strong coupling constant is calculated. The centre of mass correction has been included for mass calculation. The CDM has been extended to the strange baryonic sector. By fitting the observed value of Ω^- mass we have determined the strange quark mass and then all other strange baryon masses are calculated. For a wide range of parameters the masses and the static properties of nucleon are calculated.

For the best fitting parameter set it is observed that the gluonic contribution to the baryon masses for case I is greater then the case II and it is about 7 to 10%. For wide range variation of parameters the axial coupling constant varies inbetween 1.21 and 1.27 and lies in the vicinity of the experimental value (1.26). Similarly the proton charge rms radius is found to be .79 fermi for the above said parameter set which is also very close to the experimental value .83 fermi. But the magnetic moments of proton and neutron are found to be 1.82 μ_N and -1.22 μ_N respectively which are much below the observed values (2.79μ_N and -1.91μ_N). The strange quark mass is 152 MeV greater then the light quark mass. It is observed that the Σ mass for case I is about 5% less the then observed one and the Ξ mass is about 5% larger then the observed value for the case II. All other masses are in excellent agreement with the observed values. Thus the results show that for both the cases the baryon spectrum fitting as well as the proton rms radius and axial coupling constant are in good agreement with the observed values. Best fitting is obtained for m_{GB}= 2488 MeV, α= 20, m_u= 199 MeV and m_s= 352 MeV. The Baryon masses (in MeV) are given in the Table for case I and Case II for the above parameter set.

N	Λ	Σ	Ξ	Δ	Σ^*	Ξ^*	Ω^-	
938.	1125.	1151.	1326.	1232.	1388.	1533.	1672.	I
938.	1137.	1194.	1377.	1232.	1382.	1527.	1672.	II
938.	1116.	1193.	1318.	1232.	1385.	1531.	1672.	Expt

References :

1. S.Sahu and S.C. Phatak, Priprint IP-BBSR-91/36
2. N. Aoki and H. Hyuga, Nucl. Phys. **A 505** (1989) 525
3. N. Aoki and H. Hyuga, Nucl. Phys. **A 516** (1990) 496

DEPENDENCE OF THE CHARACTERISTICS OF CLUSTERS ON TARGET SIZE IN PARTICLE -EMULSION COLLISIONS

M.Saleem Khan, M.Khushnood and A.R.Ansari,
High Energy Physics Lab, Department of Physics,
Jamia Millia Islamia, New Delhi-110025.

To investigate the dependence of the angular characteristics of secondary particles on the energy and identity of the impinging hadron, random samples of 875 and 873 events having $N_h \geq 2$ respectively caused by 50 GeV negative pions and 400 GeV protons in nuclear emulsion were taken. Here N_h denotes the number of heavily ionizing tracks with $\beta \leq 0.7$. Furthermore, for studying the dependence of angular characteristics of secondary charged particles on the target size, the data at both the projectile energies have been divided in three different groups viz (i) $2 \leq N_h \leq 6$, (ii) $N_h \geq 7$ and (iii) $N_h \geq 2$. It is reported that (i) the events having $2 \leq N_h \leq 6$ are due to the light group (CNO) and disintegrations with $N_h \geq 7$ correspond to heavy nuclei (AgBr). The events with $N_h \geq 2$ represent the emulsion nuclei. Thus N_h is related to the atomic masses of the target nuclei.

Several workers (2) have reported that the final state charged shower particles are the decay product of clusters formed in the intermediate stage of high energy hadronic collisions. Thus the characteristics of clusters are investigated with the help of minimum rapidity gap, Δ_{min}, distributions between two adjecent charged shower particles. Δ_{min}- distributions for the three groups of N_h at both 50 and 400 GeV are shown in the figure. It may be noticed in the figure that clear peaks occur at the smallest value of Δ_{min} in each case. It may also be seen in the figure that Δ_{min}-distributions fall off very rapidly with increasing Δ_{min}. Furthermore, about 90% of the

number of gaps in each group of N_h at 400 GeV are observed to lie in the range of $\Delta_{min} \sim 0.1$ which is the probable space of η between two adjacent charged shower particles decaying from a single cluster. While this number comes out to be about 60% in each N_h interval at 50 GeV, the multiperepheral

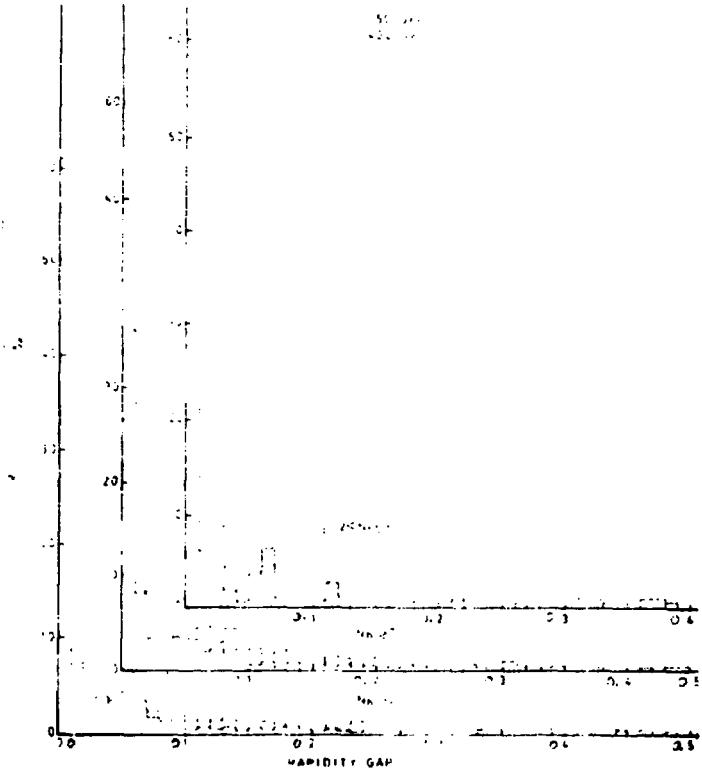

model (3) predicts that the probability of events having at least one cluster is about 90%. Thus our findings at 400 GeV are in nice agreement with the prediction of this model, while the results obtained at 50 GeV are in marked disagreement with the predicted value. The percentage of events having at least one single cluster strongly depends on the energy of the projectile. The results further reveal that this percentage of events does not depend on the size of the target nucleus.

REFERENCES:

1. M.Irfan et.al : Can.J.Phys. 62, 230 (1984)
2. A.Shakeel et.al :J.Phy.Soc.Jpn, 55, 3362 (1986); R.K.Shivpuri and C.Gupta: Phy.Rev. D15, 3332 (1977); M.Irfan et.al : Phys. Rev. D30, 218 (1984); H.Ahrar : Can.J.Phys. 68,253 (1990)
3. S.T.Jones and D.R.Snider: Phys. Rev. D9, 242 (1974)

THE SPIN ORBIT FORCE FROM *COGEP*

K.B. Vijayakumar and S.B. Khadkikar
Physical Research Laboratory
Ahmedabad 380 009, India

We wish to present the spin-orbit ($L.S$) potential arising out of the confined one gluon exchange among relativistically confined quarks in the nucleons. For this purpose we have plotted the diagonal kernels of ${}^3P_0$ (Fig. 1), ${}^3P_1$ (Fig. 2), ${}^3P_2$ (Fig. 3), ${}^3D_1$ (Fig. 4), ${}^3D_2$ (Fig. 5), ${}^3D_3$ (Fig. 6), of the adiabatic $N-N$ diagonal tensor and $L.S$ potentials against the relative distance (R) between the nucleons. The ratio of $L.S$ potentials for ${}^3P$ states are ${}^3P_2 : {}^3P_1 : {}^3P_0 : = 1 : -1 : -2$. Fig. 7 gives the intrinsic adiabatic potential for ${}^3P$ state. For ${}^3P$ state the $L.S$ potential is intrinsically attractive. The ratio of $L.S$ potentials for ${}^3D$ states are ${}^3D_1 : {}^3D_2 : {}^3D_3 = -\frac{1}{3} : -1 : \frac{1}{2}$. Fig. 8 gives the intrinsic adiabatic potentials for ${}^3D$ state. For ${}^3D$ state the $L.S.$ potential is intrinsically repulsive . The $L.S$ potential obtained from *COGEP* have the right sign and the right order of magnitude and are consistent with the phenomenological $L.S$ potential.

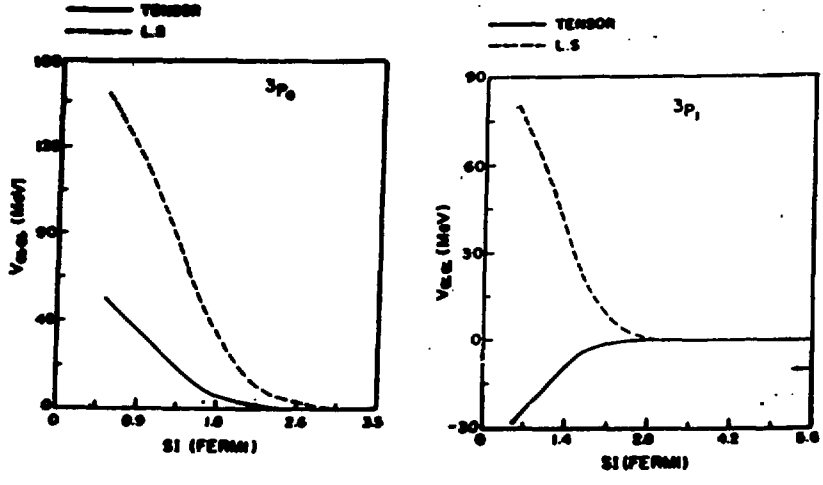

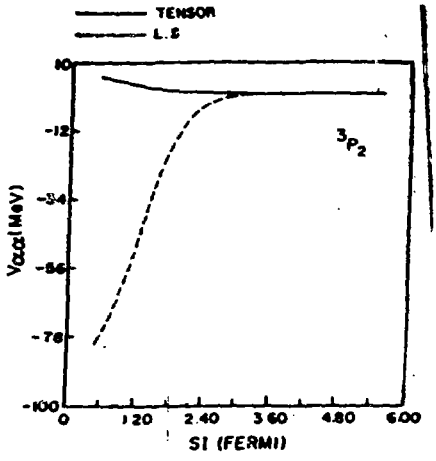
TENSOR
L.S
$^3P_2$
$V_{\alpha\alpha}$ (MeV)
SI (FERMI)

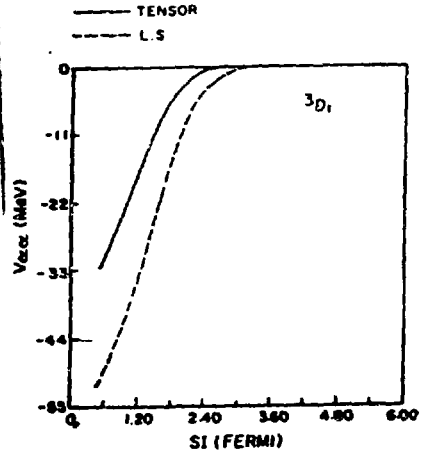
TENSOR
L.S
$^3D_1$
$V_{\alpha\alpha}$ (MeV)
SI (FERMI)

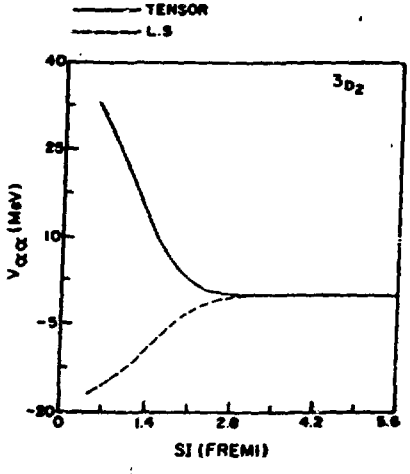
TENSOR
L.S
$^3D_2$
$V_{\alpha\alpha}$ (MeV)
SI (FREMI)

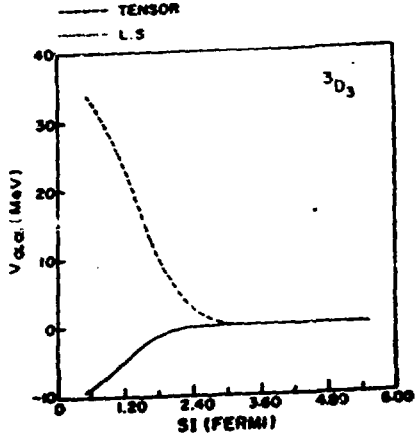
TENSOR
L.S
$^3D_3$
$V_{\alpha\alpha}$ (MeV)
SI (FERMI)

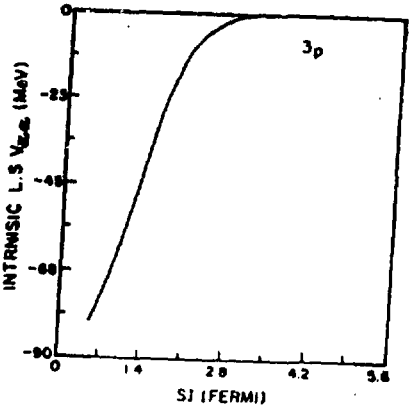
^3P
INTRINSIC L.S $V_{\alpha\alpha}$ (MeV)
SI (FERMI)

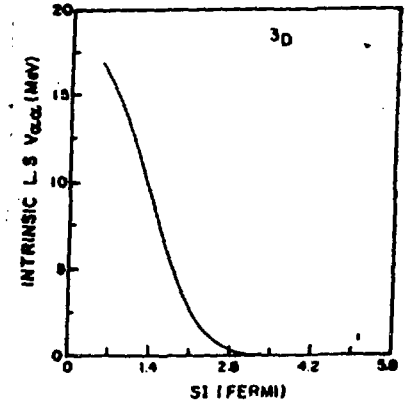
^3D
INTRINSIC L.S $V_{\alpha\alpha}$ (MeV)
SI (FERMI)

TENSOR $N-N$ INTERACTION FROM *COGEP*

K.B. Vijayakumar and S.B. Khadkikar
Physical Research Laboratory
Ahmedabad 380 009, India

We have investigated the effect of the tensor force arising from the exchange of confined gluons among relativistically confined quarks on the $^3S_1$ $^3D_1$ nucleon-nucleon ($N-N$) scattering phase-shifts (PS) using coupled channel resonating group formalism. For the quarks we use the relativistic Lorentz scalar plus vector harmonic confinement model (RHM)[1] which explains the properties of light hadrons. A similar confinement scheme for gluons, the current confinement model (CCM)[2] describing the glue-balls is employed to obtain[3] confined one gluon exchange potential ($COGEP$) using the propagators given by D_1, D_0.

The tensor part of $COGEP$ is

$$V_{ij}^{TEN}(\vec{r}) = -\frac{\alpha_s}{4}\frac{N^4}{(E+M)^2}\lambda_i\lambda_j\left[\frac{D_1''(r)}{3} - \frac{D_1'(r)}{3r}\right]S_{ij} \qquad (1)$$

where

$$S_{ij} = [3(\sigma_i.\hat{r})(\sigma_i.\hat{r}) - \sigma_i.\sigma_j] \qquad (2)$$

The PS are calculated using the Kohn-Hulthen-Kato[4] variational principle. Our calculated $^3S_1$ PS fall below the PS of Arndt et. al[5]. A measure of the strength of the tensor force is the mixing parameter ε which indicates the proportion of the $^3S_1$ and $^3D_1$ states in the triplet state. Our calculated ε have much greater D-state probability and hence give poorer fit to the mixing parameter data of Arndt et. al. But the overall strength of tensor force is weak. Fig. 2 shows the $^3S_1$ PS with enhanced strength ($\alpha_s = \alpha_s * 2.1$) for S-D coupling and without S-D coupling in comparison with Arndt et al. Here the α_s for the tensor force is doubled and the resultant calculation of $^3S_1$ PS are

slightly above the PS of Arndt. But the ϵ is much overestimated indicating a too strong a tensor component. Also there is an unpleasant hump in the PS at $E_{Lab} \approx 250$ MeV. Fig. 4 shows ${}^3S_1$ PS with $\alpha_s = 6.5$ which brings the final PS nearer to Arndt PS though ϵ remains overestimated. In conclusion, the tensor force arising from $COGEP$ is able to give enough additional attraction in ${}^3S_1$ PS state and a substantial mixing parameter ϵ. The calculation of deuteron bound state only will be able to fix the strength α_s uniquely.

1. Khadkikar S.B. and Gupta S.K., Phys. Lett. (1983) 124B 523.
2. Khadkikar S.B. and Vinodkumar P.C., Pramana (1987) 29 39.
3. Khadkikar S.B. and Vijayakumar K.B. (1991) Phys. Lett. 254B 320.
4. Kamimura K. (1977) Suppl. of Prog. of Theor. Phys. 62 236.
5. Arndt et. al. (1983) Phy. Rev. D28 97.

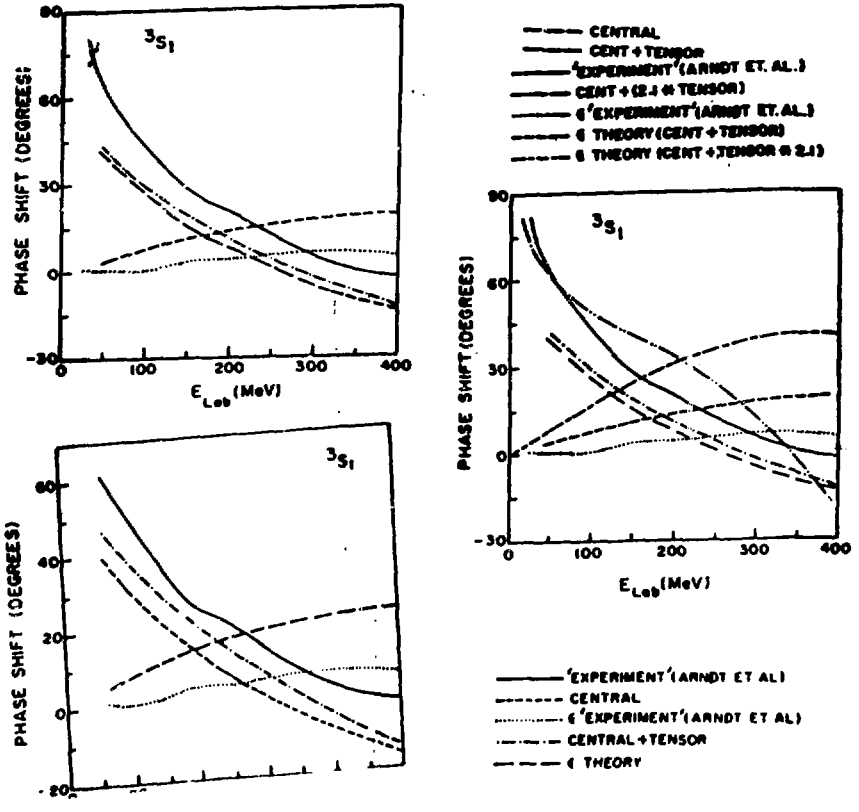

THE EFFECT OF CONFINEMENT OF GLUONS ON N-N SCATTERING:- P-P AND N-P DIFFERENTIAL CROSS SECTIONS

S.B.Khadkikar and K.B.VijayaKumar
Physical Research Lab. Ahmedabad-380009.

We have investigated the effect of confinement of gluons on nucleon-nucleon (N-N) scattering phase shifts (PS). The phenomenological models such as non-relativistic quark model or the relativistic M.I.T bag model though have incorporated the effect of confinement of quarks, the effect of confinement of gluons has not been taken into account. So, we have developed two models. For the confinement of quarks we use the relativistic harmonic model (RHM) /1/ in which quarks are confined by a harmonic oscillator lorentz scalar+vector potential. For the confinement of gluons we use the current confinement model (CCM) /2/ developed in the spirit of RHM. The confined gluon propagators (CGP) are derived in CCM. Making use of CGP we have obtained confined-one-gluon-exchange potential (COGEP) between quarks. With the COGEP we have investigated N-N interaction based on RHM, where we have employed the resonating group method to solve the scattering problem between two nucleon systems.

The following investigation have been carried out:
i) We have investigated the singlet N-N scattering PS using central part of COGEP.
ii) We have also investigated the effect of tensor and spin-orbit forces arising from COGEP on $^3S_1$-$^3D_1$ states and on tripet P and D states.
iii) We have also calculated proton-proton (P-P) and neutron-proton (N-P) differential cross section ($\sigma(\theta)$) using our PS upto angular momentum (L) = 2.

We obtain qualtatively good agreement with the experimental P-P and N-P $\sigma(\theta)$ with strong coupling constant (α_s)=6.5. Fig.1 gives the P-P $\sigma(\theta)$ vs scattering angle (θ). While calculating P-P $\sigma(\theta)$ we have not taken couloumb scattering into account. The important feature of isotropy of the P-P $\sigma(\theta)$ is reproduced at all eneriges. Fig.2 gives N-P $\sigma(\vartheta)$ vs scattering angle. In the energy range E_{LAB} - 200-400 MeV there is fairly a good agreement with the observed $\sigma(\theta)$ at $\theta=0^0$. But the dip in the calculated $\sigma(\theta)$ at $\theta=\pi/2$ (E_{LAB}=50 MeV) falls below the dip in the experimental $\sigma(\theta)$. The calculated $\sigma(\theta)$ using the single energy PS of Arndt et al /3/ do not give any dip in the cross section at low eneriges (Fig.3). This is due to the small p-wave PS at low eneriges. Though the dip in the $\sigma(\theta)$ increases with energy still the dip in the $\sigma(\theta)$ in the energy range 200-400 MeV is smaller then the experimental dip in the

cross section.

In conclusion we have obtained fairly a good agreement with the experimental P-P and N-P $\sigma(\theta)$ without meson exchanges but using confined gluon exchange between relativistically confined quarks, even though the higher L PS donot agree with Arndt et al.

/1/ Khadkikar S.B and Gupta S.K 1983 Phys.Lett. 254B 320
/2/ Khadkikar S.B. and Vinodkumar P.C. 1987 Pramana 29 39
/3/ Arndt et al 1983 Phys.Rev D28 97

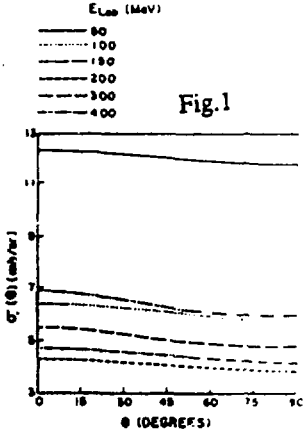

Fig.1

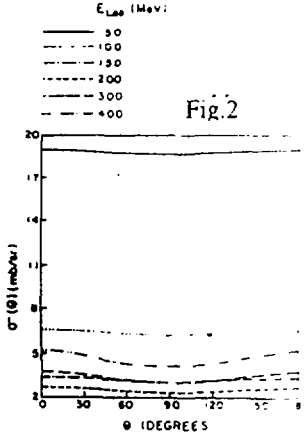

Fig.2

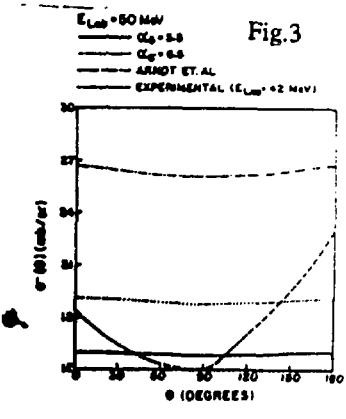

Fig.3

PARITY NON-CONSERVATION IN ATOMS DUE TO NEUTRAL WEAK CURRENTS AND THE NUCLEAR ANAPOLE MOMENT

Swati Bhagwat and B.P.Das
Department of Physics, I.I.T. Powai, Bombay-400 076

The two possible sources of parity non-conservation (PNC) in atoms are:

(i)The neutral weak current interaction between the nucleus and the electrons mediated by the intermediate vector boson Z_0 (1).

(ii)The electromagnetic interaction between the nuclear anapole moment and the electrons of the atom (2).

The first type of interaction can be represented as

$$H_{nw} = H^1_{nw} + H^2_{nw}$$

where, $H^1_{nw} = V^N \times A^e$ and $H^2_{nw} = V^e \times A^N$. $V^N(A^N)$ and $V^e(A^e)$ are the nuclear and the electron vector (axial vector) currents respectively.

For an atom with a nucleus consisting of Z protons and N neutrons, the neutral weak current hamiltonian can be written as (3)

$$H^1_{nw} = \frac{G_F}{2\sqrt{2}} Q_w \rho_N(r) \gamma_5$$

and

$$H^2_{nw} = \frac{G_F}{2\sqrt{2}} \frac{P_w}{I} \rho_N(r) \bar{\alpha}.\bar{I}$$

where $Q_w = (c_{1p}Z + c_{1n}N)$, $\rho_N(r)$ is the nuclear density and γ_5 is a pseudo-scalar $P_w = (c_{2p}Z + c_{2n}N)$, $\bar{\alpha}$ is the Dirac matrix and $\bar{I}$ is the nuclear spin c_{1p}/c_{2p} and c_{1n}/c_{2n} are the proton-electron and neutron-electron coupling constants. The Hamiltonian describing the interaction of nuclear anapole moment with the atomic electrons is given by (3)

$$H_{an} = \frac{G_F}{2\sqrt{2}I} a_n \rho_N(r) \bar{\alpha}.\bar{I}$$

where $a_n = \kappa_a 2\chi/(I+1)$. κ_a and χ are quantities which depend on nuclear parameters(4).

The experiments that are underway to detect PNC in atoms can discriminate between nuclear spin independent (NSI) and nuclear spin dependent (NSD) effects (5,6).Thus it is convenient to write the atomic PNC Hamiltonian as

$$H_{NSI} = \frac{G_F}{2\sqrt{2}} Q_w \rho_N(r) \gamma_5$$

and

$$H_{NSD} = \frac{G_F}{2\sqrt{2}I} \mu_w \rho_N(r) \bar{\alpha}.\bar{I}$$

where $\mu_w = P_w$ or a_n.

The physical quantity that is measured in the atomic PNC experiments can be related to an electric-dipole transition amplitude (E1PNC) which results from the mixing of opposite parity states due to the presence of H_{NSI}/H_{NSD}(5,6). We have carried out preliminary calculations of E1PNC for $6p_{1/2} \rightarrow 6p_{3/2}$ transition in atomic thallium using a relativistic many-body approach.Our calculations have taken into account the relativistic Hartree-Fock and some important core polarization effects.We present below the results of our calculations .

Transition $(F \rightarrow F')$	E1PNC^{NSI}	E1PNC^{NSD}
$0 \rightarrow 1$	-342.6199	643.8710
$1 \rightarrow 1$	-242.2689	-118.3536
$1 \rightarrow 2$	-541.7298	-512.0796

F and F' are the total angular momenta of the initial and final states of the atom. E1PNC^{NSI} and E1PNC^{NSD} are in units of $G_F Q_w/2\sqrt{2}$ and $G_F \mu_w/2\sqrt{2}$.

By combining the results of our calculation with those of the experiment it is possible to extract the values of Q_w and μ_w which can provide a check on the validity of several unification models of particle physics.It would be necessary to carry out calculations on Tl^{205} nucleus to determine whether the dominant contribution comes from the nuclear anapole moment or the neutral weak current interaction.

References

1.M.A.Bouchiat and C.C.Bouchiat Phys.Lett.B 48,111(1974)
2.E.M.Henley, W-Y.P.Hwang and G.N.Epstein Phys.Lett.B 88,349(1979)
3.E.R.Boston D.Phil. Thesis,Oxford (1990)
4.V.V.Flambaum and I.B.Khriplovich Sov.Phys.JETP 52,836(1980)
5.M.J.D.Macpherson, D.N.Stacey, P.E.G.Baird, J.P.Hoare, P.G.H.Sandars, K.M.J.Tregido and Wang Guowen Europhys.Lett. 4,811(1987)
6.T.Wolfendale,P.E.G.Baird and P.G.H.Sandars Europhys.Lett.(1991) (To be published)

BARYONIC MATTER IN THE NONLINEAR MESON FIELD THEORY

Safayet Karim Chowdhury [+] and Sasabindu Sarkar
Department of Theoretical Physics
Indian Association for the Cultivation of Science
Jadavpur, Calcutta 700 032, India.

In this work we utilise the freedom one has in choosing the four parameters of nonlinear meson field theory of nuclear matter[1] with self interactions, due to uncertainties in the nuclear bulk properties $m^*(\rho_0)$ and $K(\rho_0)$ at saturation density ρ_0 to investigate the changes in the behaviour of delta excited baryonic matter in various models with different sets of effective nucleon mass $m^*(\rho_0)$ and bulk modulus $K(\rho_0)$. In particular we study the influence of these two quantities on the occurrence of phase transitions in baryonic matter at some finite density or at somefinite temperature at zero baryon density. We also discuss the problem concerning occurrence and non-occurrence of negative effective nucleon mass in different cases when the two baryon (nucleon and delta) couplings with the scalar meson is taken to be equal or in the ratio of SU(6) mass splitting[2]. It is found that in the linear and nonlinear mean field theory the problem of negative effective nucleon mass does not occur in relativistic Hartree approximation. This observation confirms the fact that delta-meson coupling constants can not be definitely determined by meanfield theory. Instead one has to study the electromagnetic excitation of the delta baryon which takes place during quasielastic electron scattering[3]. We further investigate possible phase transition in nucleon antinucleon plasma and baryon antibaryon plasma considering the presence of delta particles also in the mean field theory[4,5] However we find that there is no sudden change in the effective nucleon mass in the plasma with temperature

when we use relativistic Hartree approximation. Relative abundance of nucleon and delta resonance in various models is also studied.

+ Permanent Address - Physics Department,
B.K.C. College,
Calcutta - 700035

References :

1. B.D. Serot and J.D. Walecka, Advances in Nuclear Physics (Plenum: Newyork, 1985)

2. P.Levai et al Phys. Lett.B 177 (1986) 5.

3. K.Wehrberger, C. Bedau and F.Beck, Nucl.Phys. A504(1989) 797.

4. J.Theis et al Phys. Rev. D28 (1983) 2286.

5. S.Sarkar, S.Niyogi and S.K. Chowdhury Phys. Rev. D32 (1985) 1823.

SUBNUCLEAR DEGREES OF FREEDOM IN THE DEUTERON

V.K.SHARMA
Department of Physics, Institute of Advanced Studies
Meerut University, Meerut 250004, India

In recent years our experimental and theoretical understanding in nuclear physics clearly indicates that the nucleons are made of quarks and gluons. The dynamics of quarks and gluons are responsible for the exchange of pions in N-N interaction. This aspect has been confirmed by electron disintegration experiments of the deuteron at Sacley[1]. Meson exchange picture does describe the asymptotic form of the N-N interaction when the internucleon distance is of order 1.8 fm and average nucleon size is 0.86 fm.

Recently the physical interpretation of the generator coordinate method (GCM)[2] for subnuclear description of six quarks suggests the coexistence of quark shell-model [3] and quark cluster aspects in deuteron. For a nucleon one can consider that three quarks in a bag obeys asymptotic freedom(shell-model aspect) equivalent to confinement(quark cluster aspect) due to SU(3) symmetry. The effects of antisymmetrization in deuteron give rise to quark exchange forces viz., when one quark exchange takes place between the two nucleons inside deuteron the incoming and outgoing quarks will behave as $q\bar{q}$ pair, in analogy to cooper pair formation in superconducting state, which give rise to one-pion exchange term. Similarly two quarks simultaneously exchanging between two nucleons give rise to two-pion exchange term , and for three quarks or no quark exchange give the three-pion exchange term in N-N interaction.

In the present investigation we propose the GCM for the subnuclear description of the deuteron in terms of quarks inside the nucleons. The two-nucleon wavefunction of deuteron in terms of (3q+3q)system is given by [4]

$$\Psi_{NN}(c=0,T=0,S=1)=\frac{1}{3}\{\psi([6]_0[222]_c[33]_{TS}T=0,S=1)+$$
$$+2\psi([42]_0[222]_c[33]_{TS}T=0,S=1)-$$
$$-2\psi([42]_0[222]_c[51]_{TS}T=0,S=1)\},(1)$$

with an antisymmetric wavefunction in orbital,color and spin-isospin spaces as per Young symmetry and which can be expended in terms of one-body fractional parentage coefficient.The system of six quarks is treated via the hamiltonian[4]

where $$H=\frac{-\hbar^2}{2m}\sum_{i=1}^{6}\nabla_i^2-T_G+\sum_{i=1}^{6}T_i'+\sum_{i<j}^{6}V_{ij}\ , \qquad (2)$$

$$V_{ij}=(\lambda_i\cdot\lambda_j)_c[f(\vec{r}_{ij})+(\vec{\sigma}_i\cdot\vec{\sigma}_j)_{TS}g(\vec{r}_{ij})]\ ; \qquad (3)$$

with T' is the v^2/c^2 correction to the quark kinetic energy with mass m about 330 MeV.

The GC amplitude satisfy the following equation,

$$4\pi\int_0^\infty S^2dS'\,[H_L(S,S')-EN_L(S,S')]f_L(S')=0\ ; \qquad (4)$$

and $$N_L(S,S')=e^{-\frac{3}{8}\beta(S^2+S'^2)}\left[\left\{1+(-)^L\right\}\left\{I_L\left(\frac{3}{4}\beta SS'\right)+\frac{1}{9}I_{2L}\left(\frac{\beta}{4}SS'\right)\right\}\right], \qquad (5)$$

$$H_L(S,S')=T_L^{(1)}(S,S')+T_L^{(2)}(S,S')+V_L(S,S')\ , \qquad (6)$$

with $$T_L^{(1)}(S,S')=N_L(S,S')\left[\frac{15}{4}\frac{\hbar^2\beta}{m}-\frac{3\hbar^2\beta^2}{16m}(S^2+S'^2)+\frac{\hbar^2\beta^2}{8m}(SS')\right.\cdot$$
$$\left.\times\sum_{\Lambda}\langle L0\,10|\Lambda0\rangle^2\left\{\frac{41}{27}N_\Lambda^{[51]}(S,S')+\frac{40}{27}N_\Lambda^{[33]}(S,S')\right\}\right]\cdot \qquad (7)$$

Similarly other terms are calculated.

It is noticed that in future we can be expected to increasingly deal with the nucleus as system of nucleons,mesons,deltas ...etc,and on the microscopic level,quarks and gluons.

REFERENCES

1. M. BERNHEIM et al.Phys.Rev.Lett.**46**(1981)2Ø1.
2. V.K. SHARMA.in Fifth Int.Conf.on Clustering Aspects in Nuclear and Subnuclear Systems, Kyoto,Japan(1988) p.32Ø Contributed papers
3. H.R.PETRY,Lecture Notes in Physics,Vol.197 (1983)Berlin.
4. M.HERVEY,Nucl.Phys.,**A352**(1981)3Ø1.

The p(p,p'π)n Reaction

A.B.Santra and B.K.Jain
Nuclear Physics Division
BARC, Bombay 400 085

In pp collision, one pion production process is the most dominant inelastic channel compared to others at intermediate energies. Therefore, the information on this simple reaction is useful to understand the pion production data on complex nuclei, as well as, to clarify conjectures about the dibaryonic resonances[1].

The Rice-Houston group[2], working at LAMPF, has measured the differential cross-section $d^5\sigma/dp_p d\Omega_p d\Omega_\pi$ for the $p + p \rightarrow p + \pi^+ + n$ reaction at 800 MeV in a kinematically complete experiment. They have measured the proton spectra at different angles, detecting simultaneously a π^+ at some other angle. Experimental data are available for various sets of proton and pion angles.

We assume that the production of pion occurs through the formation of an intermediate delta isobar. The transition matrix for this process can be written as the product of an isobar production amplitude, an isobar propagator, $G_\alpha(\mu)$, and an isobar decay amplitude.

$$\langle pn\pi^+|T|pp\rangle = \sum_{\alpha}\sum_{i} \langle \pi^+ N_{\underline{i}}|\alpha\rangle\, G_\alpha(\mu)\, \langle \alpha N_i|t|\mathcal{A}(pp)\rangle \qquad (1)$$

The sum over α includes both Δ^{++} and Δ^+ isobars. The label $\underline{i}$ is the compliment of i ;i.e., $\underline{i}$=2 when i=1 and vice-versa. N_1 and N_2 denote neutron and proton respectively. $\mathcal{A}$ denotes the antisymmetrization operator in the initial state. The $NN \rightarrow N\Delta$ transition t-matrix has been taken from our earlier model[3]

where by doing distorted wave analysis of $p(p,n)\Delta^{++}$ reaction, a parameterized form of such a t-matrix was obtained.

Using the T-matrix given in eq.(1), we have calculated $d^5\sigma/dp_p d\Omega_p d\Omega_\pi$ for various sets of proton and pion angles. In figs.(1) and (2), the outgoing proton spectra for (θ_p=14.5 , θ_π=21) and (θ_p=19 , θ_π=53) are shown along with the measured values. We see that our model describes the experimental data reasonbly well. The dominant contributions come from the proceses in which Δ^{++} is formed in the intermediate state. Due to a suppressing isospin factor, the contribution from the Δ^{+} term is much smaller. Inclusion of the exchange term reduces the cross-section. The relative phases of the direct and exchange terms as well as Δ^{++} and Δ^{+} terms are important.

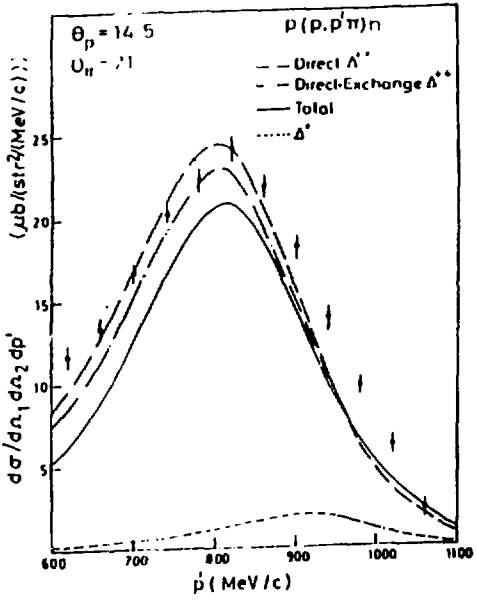

Fig(1)

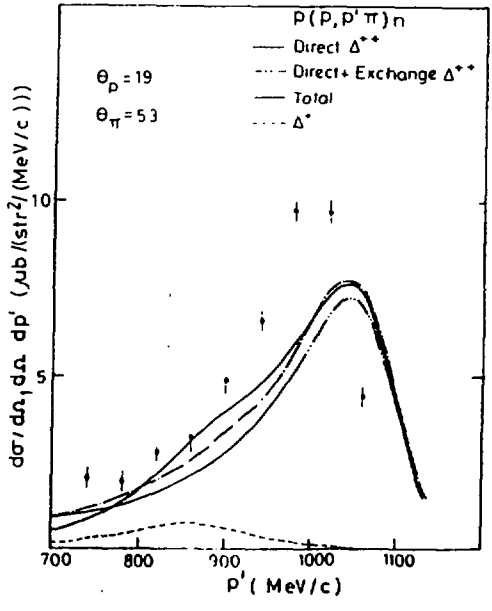

Fig(2)

1. R.Bhandari et al.,Phys.Rev.Lett.46(1981)1111
2. A.D.Hancock et al.,Phys.Rev.C27(1983)2742
3. A.B.Santra and B.K.Jain,DAE Nucl.Phys.Symp.(1989)

INCLUSIVE (P, Δ^{++}) REACTION

Neelima G.Kelkar and B.K. Jain
Nuclear Physics Division, B.A.R.C., Bombay-85.

In an inclusive (P, Δ^{++}) reaction, the nucleus is left in any state consistent with the kinematics. The cross-sections for this reaction depend on the interaction of the projectile with the nucleus and the spin-isospin response of the nucleus . In this paper we present the formalism for this reaction and study the features of the inclusive cross-sections.

For the incident proton being excited to Δ^{++} , the inclusive cross-section in c.m. is given as,

$$\frac{d^3\sigma}{d(\mu^2)d\Omega\, d\omega} = \frac{1}{(2\pi\hbar c)^2}\frac{E_A m_p m_\Delta}{E_c}\frac{k_\Delta}{k_p}\sum_n \delta(\omega-\omega_n)\frac{1}{g_i}\sum|T_{no}|^2\,\rho(\mu^2) \qquad \ldots\ldots(1)$$

where 'n' denotes the excited and '0' the ground state of the target nucleus. ω is energy transfered to the nucleus. Using one pion exchange transition potential, the transition amplitude T_{no} in (1) can be written as,

$$\frac{1}{g_i}\sum_n \delta(\omega-\omega_n)\sum_{\substack{\sigma_p\sigma_\Delta \\ m_\Delta}}|T_{no}|^2 = \frac{1}{2}|V(\omega,q)|^2\sum_n \delta(\omega-\omega_n)\langle n||\tilde{\rho}_{no}(-\underset{\sim}{q})|^2|0\rangle \qquad \ldots\ldots(2)$$

where $V(\omega,q)$ contains the spin-isospin interaction at the $\pi N\Delta$ vertex and $\tilde{\rho}_{no}(-\underset{\sim}{q})$ is the nuclear transition density defined as,

$$\tilde{\rho}_{no}(-\underset{\sim}{q}) = \int d\vec{r}\,\chi^{-*}_{\vec{k}_\Delta}(\vec{r})\langle n|\sum_j \delta(r-r_j)\vec{\sigma}(i).\hat{q}\,\tau_{-1}(i)|0\rangle\chi^{+}_{\vec{k}_p}(\vec{r}) \qquad \ldots\ldots(3)$$

Using plane waves for the continuum particles and replacing the target nucleus by a Fermi gas of the same density, $\tilde{\rho}_{no}(-\underset{\sim}{q})$ is given as,

$$\sum_n \delta(\omega-\omega_n)\langle|\tilde{\rho}_{no}(-\underset{\sim}{q})|^2\rangle = -\frac{1}{\pi}\frac{m_\pi^2}{f_\pi^2}\cdot\frac{1}{q^2}\,\mathrm{Im}\,\Pi(\omega,q)\cdot\frac{3\pi^2 A}{8k_F^3} \qquad \ldots\ldots(4)$$

where $\mathrm{Im}\,\Pi(\omega,q) = \mathrm{Im}\,\Pi_N(\omega,q) + \mathrm{Im}\,\Pi_\Delta(\omega,q)$
is the self-energy of pions in the nuclear medium[1]

Using kinematics of mass 16 nucleus and k_F=210 MeV/c in fig.1 we plot for incident energy 3 GeV, the double differential cross-section $d^2\sigma/d\Omega d\omega$ obtained from (1) as a function of energy transfered to the nucleus (ω) and angle of the outgoing delta. At forward angles 2 distinct peaks in the cross-section as a function of ω can be observed which merge into one at large angles. The two peaks appear due to the peaks in $I_m \pi_N(\omega, q)$. $I_m \pi_\Delta(\omega, q)$ enhances the second peak corresponding to large energy transfers. For incident beam energies upto 1 GeV we observe only a single peak due to much smaller range of ω.

We also construct the missing mass specturm $d\sigma/d(M^2)$ from (1) and is shown in fig.2 for various incident energies. The cross-section increases as a function of beam energy upto about 2 GeV and starts falling at higher energies which is a feature similar to exclusive (ρ, Δ^{++}) reaction.[2]

Finally it is important to mention that all calculations are done in a fully relativistic formalism. Non-relativistic approximations for the transition potential or the self-energies lead to incorrect conclusions.

1. B.K.Jain, J.T.Londergan, G.E.Walker, Phys.Rev.C37, 1564 (1988).
2. B.K.Jain, N.G.Kelkar, J.T.Londergan, Phys.Rev.C43, 271(1991).

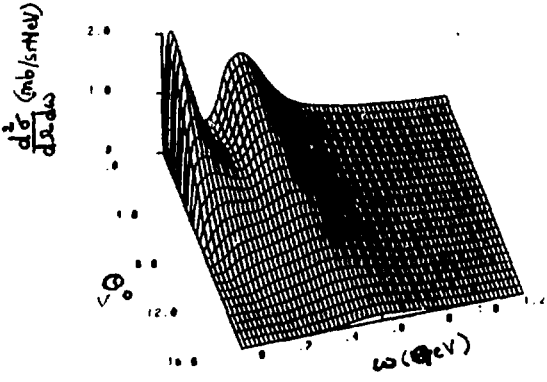

Fig.1

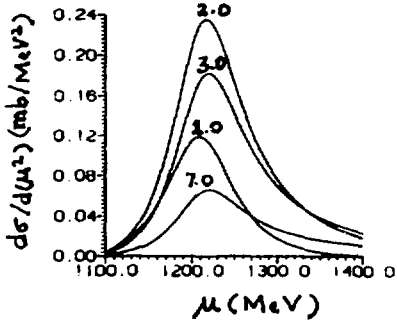

Fig.2

SOME CHARACTERISTICS OF PROJECTILE FRAGMENTS PRODUCED IN ^{28}Si-Em and ^{12}C-Em INTERACTIONS at 4.5 A GeV/c

M. Tariq, M. Zafar, S. Ahmad, A. Tufail, Tayyab, A.R. Khan and M. Shafi

Department of Physics,
A.M.U., Aligarh-202002

A study of fragmentation characteristics of ^{28}Si and ^{12}C nuclei in interactions with emulsion nuclei at 4.5 A GeV/c has been made. 701 events of ^{28}Si-Em and 844 events of ^{12}C-Em interactions have been analysed. The method of scanning, measurements, categorization of various tracks and relevant experimental details are as usually adopted in emulsion experiments. The mean multiplicities of relativistic singly and multiply-charged projectile fragments (PF's) have been estimated for both the projectiles (Table 1).

The effective number of projectile (or beam) nucleons, ν_B, interacting with target nucleus have been estimated by using the following relation: $\nu_B = A_B - (A_B/Z_B)Q$; where A_B and Z_B are respectively mass number and atomic number of beam nuclei and Q is the total charge of projectile fragments, i.e., $Q = \sum_f Z_f$, where Z_f is the charge of a fragment of f^{th} kind.

The probability distributions of projectile fragments with charge Z=1 are plotted in Fig. 1. We observe from the figure that the relative yield for lower values of $N_{(Z=1)}$ is more in case of ^{12}C-Em interactions as compared to ^{28}Si-Em collisions. However, the distribution extends upto larger values of $N_{(Z=1)}$ in ^{28}Si-Em interactions. Thus we may infer that probability distribution of singly charged fragments depends on the mass of the projectile. Furthermore, the variation of $\langle Q \rangle$ with $N_{(Z=1)}$ is shown in Fig.2. From this figure we may conclude that $\langle Q \rangle$ increases linearly with $N_{(Z=1)}$ and reaches to a saturation at higher values of $N_{(Z=1)}$.

The average multiplicities of shower particles per interacting nucleon of beam, i.e. $\langle N_s \rangle / \bar{\nu}_B$ have been calculated which comes out to be 1.08 ± 0.14 and 1.05 ± 0.12 respectively for ^{28}Si and ^{12}C projectiles. It is interesting to note that these values are close to the value $\langle N_s - \alpha_A \rangle$ of P-Em interactions at same energy per particle (i.e. 4.5 GeV). α_A in contribution of leading particle in P-Em collision. $\langle N_s \rangle$ and α_A are 1.63 ± 0.2 (1) and 0.67 (2) respectively. The variations $\langle N_x \rangle$ vs $\bar{\nu}_B$ and $\langle N_x \rangle / \bar{\nu}_B$ vs $\bar{\nu}_B$ where x stands for shower grey, black and heavy tracks have also been studied (Figure is not shown) and it has been found that $\langle N_x \rangle$ varies linearly with $\bar{\nu}_B$. These findings are in accordance with the predictions of participant and spectator picture of nucleus-nucleus collisions(3). The results suggest that the collision dynamics is the same in ^{12}C-Em and ^{28}Si-Em interactions.

Table-1.

Projectile	$\langle N_{Z=1} \rangle$	$\langle N_{Z=2} \rangle$	$\langle N_{Z=3} \rangle$	$\langle N_{Z=4} \rangle$	$\langle N_{Z \geq 5} \rangle$
^{28}Si	1.82 ± 0.05	0.24 ± 0.02	0.77 ± 0.03	0.16 ± 0.02	0.42 ± 0.03
^{12}C	0.62 ± 0.03	0.67 ± 0.03	0.11 ± 0.01	0.03 ± 0.01	0.03 ± 0.01

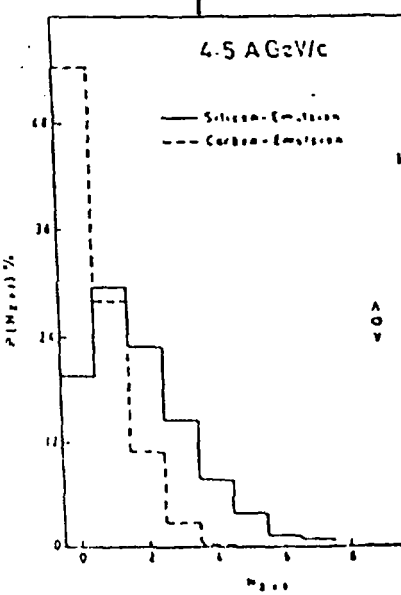

Fig.1

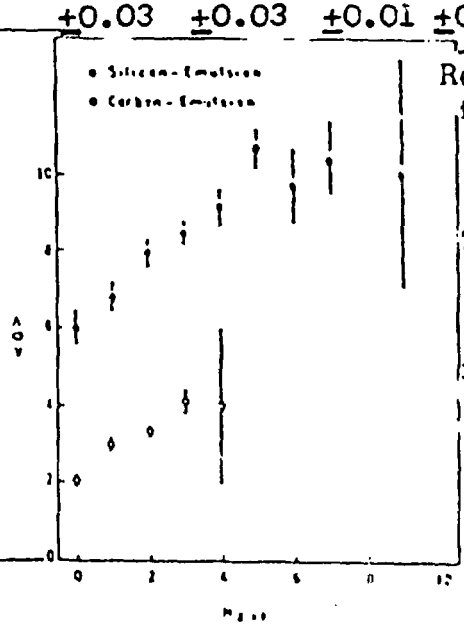

Fig.2

References:

1. R.P. Feynman; Phys. Rev Lett. 23, 1415 (1969).

2. V.I. Bubnov et al; Z. Phys. A302, 133 (1981).

3. T. Aziz et al; Ind. J. Pure Appl. Phys. 18, 778 (1980).

THE EFFECT OF DISPERSIVE ΛNN FORCES ON THE SPIN-DEPENDENCE OF ΛN POTENTIAL

Nasra Neelofer and *Mohammad Shoeb*,
Department of Physics, AMU, Aligarh-202002.

Recently, Bodner and Usmani [1] have made variarional Monte-Carlo (MC) analysis of B_Λ using Urbana type two-body ΛN potential consistent with Λp scattering along with three-body ΛNN forces. The inclusion of spin-dependent dispersive ΛNN force reduces the spin-dependence (V_σ) by ~ 1/3 of two-body ΛN force compared to the case where Wigner type ΛNN force is introduced.

Recently, Gal [2] derived the following form for dispersive ΛNN interaction :

$$V^{DS}_{\Lambda NN} = W\, Y(r_{\Lambda 1})Y(r_{\Lambda 2})\, \{Y(r_{\Lambda 1})T^2(r_{\Lambda 1})\, [T(r_{\Lambda 2})(3\cos^2\theta_{1\Lambda 2}-1)-1] + (1\longleftrightarrow 2)\}(1/9)\vec{\tau}_1.\vec{\tau}_2(\vec{\sigma}_1.\vec{\sigma}_2 + \vec{\sigma}_\Lambda.\vec{s}_{12}) \quad , ...(1)$$

where $\vec{s}_{12} = (\vec{\sigma}_1 + \vec{\sigma}_2)/2$, $Y(r) = (e^{-\mu r}/\mu r)(1-e^{-\hat{c}r^2})$, $T(r) = [1+(3/x)+(3/x^2)](1-e^{-\hat{c}r^2})$ and $x = \mu r$. The other symbols have their usual meaning.

In this brief note we report the preliminary results of the effect of $V^{DS}_{\Lambda NN}$(eq.1) on the V_σ of ΛN potential. The space-exchange ΛN force contribution to the energy is also included as its effect was found to be significant [3].The two-body and three-body correlations along with two-body NN potential are the same as given in ref. [1]. The preliminary results of s-shell hypernuclei, ${}^{3}_{\Lambda}H$, ${}^{4}_{\Lambda}H$ (${}^{4}_{\Lambda}H^{*}$), ${}^{4}_{\Lambda}He$ (${}^{4}_{\Lambda}He^{*}$) and ${}^{5}_{\Lambda}He$ are given in Table I. The multi-dimensional integrations involved in the calculations are performed by standard MC technique [1,3].The energy of the core nuclei is the same as in ref.[1]. The calculated mean values of $V_\sigma^{(3)}$, $V_\sigma^{(4)}$ and $V_\sigma^{(4,4^*)}$ are slightly lower than corresponding values given in Table 6b of ref. [1]. The behaviour of $V^{DS}_{\Lambda NN}$ is

repulsive for $^{5}_{\Lambda}$He, $^{4}_{\Lambda}$He, $^{4}_{\Lambda}$H but attractive for $^{3}_{\Lambda}$H and contributes ~ 15% to its energy. The core polarization energy and the contribution of space-exchange ΛN potential for these systems is almost the same as found in ref [4]. However, further calculations with different three-body ΛNN and space-exchange ΛN correlation functions needs to be done before we make any definite comment on the effect of $V^{DS}_{\Lambda NN}$ and V_{σ}.

This work is being done in collaboration with Prof. M. Z. Rahman Khan, AMU, Aligarh and Prof. Q. N. Usmani Jamia Millia Islamia, N. Delhi.

TABLE I

Variational MC results for energy of hypernuclei (in all cases W=0.09 MeV, s=1.0, μ=0.7fm^{-1}, $\hat{c}$ = 2.0 fm^{-2})

Hypernuclei	V_A MeV	$k_{\Lambda N}$ fm^{-1}	k_{NN} fm^{-1}	α	$\langle V^{DS}_{\Lambda NN}\rangle$ MeV	-E ± ΔE MeV	Points
$^{3}_{\Lambda}$H	-6.26	0.08	0.27	0.25	-0.02	2.36±0.02	60,000
$^{4}_{\Lambda}$H - $^{4}_{\Lambda}$He	-6.19	0.12	0.37	0.20	0.0	10.49±0.04	30,000
$^{4}_{\Lambda}$H* - $^{4}_{\Lambda}$He*	-6.13	0.09	0.31	0.10	0.38	9.34±0.04	30,000
$^{5}_{\Lambda}$He	-6.15	0.125	0.30	0.35	2.36	34.33±0.21	20,000

$V_{\sigma}^{(3)}$=0.22 MeV, $V_{\sigma}^{(4)}$=0.16 MeV, $V_{\sigma}^{(4,4^{*})}$=0.18 MeV.(due to lack of space the variational parameters are not quoted)

References :

1). A.R. Bodmer and Q.N. Usmani, Nucl. Phys., A477 (1988) 621,and references therein.
2). A. Gal, Invited talk at the Dalitz Conference, Oxford, 4-6 July 1990.
3). Mohd. Shoeb and Q.N. Usmani, DAE Symposium on Nucl. Phys., Vol.32B (1989) 022.
4). M. Shoeb and Q.N.Usmani, Private Communication.

e. RELATIVISTIC HEAVY-ION COLLISIONS AND QUARK-GLUON PHASE.

THE EFFECT OF DEFORMATION AND COLOUR SINGLETNESS ON QUARK-GLUON DECONFINEMENT PHASE TRANSITION IN THE BAG MODEL

M. G. Mustafa and A. Ansari
Institute of Physics , Bhubaneswar , India

In relativistic heavy ion collision , where hot and compressed matter zone is formed, it is likely that the intrinsic shape of the hadrons will get deformed. Also a temperature induced deformation can develop when quarks and gluons populate large angular momentum states during their intrinsic excitation. In fact even at zero temperature it is expected [1] that the intrinsic shape of the bag would be deformed due to the non-isotropic pressure of the gluons on the bag surface. The hypothesis of colour confinement demands the constraint of the colourless states (singlet of $SU(N_c)$ group) of quark-gluon system as a subsidary requirement in describing the thermodynamical behaviour [2].

Keeping those ideas in mind we have constructed the colour singlet partition function for a finite size deformable bag of speroidal shape, and the thermodynamic properties of massless quarks (two flavours) and gluons (Abelian) are studied with chemical potential $\mu \neq 0$ under the constraint that the baryon number, $b = 1$. The transition temperature, T_S in the large volume limit as well as the critical temperature , $T_C > T_S$, beyond which hadrons cease to exist, both are found to decrease with increase of deformation, α_2. The $\mu - T$ curve for the value of the deformation parameter $D(= \alpha_2 + 1) = 2$ (values of the μ and T at the boundary $P = 0$ where free energy F has extrema) shows that in the temperature range $T_S < T < T_C$ the μ is double valued for each T implies that two possible radii corresponding to two extrema in F. Thus, a region of superheated metastable state in the temperature range $T_S < T < T_C$ in $\mu - T$ plane exists with higher radius. The increase of T_C over T_S by about 20 Mev which is more or less deformation independent, arises entirely due to the restriction to colour singletness. Recently, Ellis and Olive [3] have studied the nature of boundary between the hadronic and QGP phase in the $\mu - T$ plane. They find a temperature T_C^G at which the gluon condensate disappears and a higher value T_X beyond which no hadron can exist. Thus, they get a $T_C^G - T_X$ band in the $\mu - T$ plane which may belong to superheated mixed hadron phase. To us there seems to be a parallel

between this $T_C^G - T_X$ band and our $T_S - T_C$ region with T_X equivalent to our T_C. In a very recent model calculation Brown et al [4], have shown that the hadron and qurak-gluon do not coexist at a common temperature.However,for the feasibility of phase transition they suggest the scenario of a phase jump through non-equilibrium processes. On hadronic side they get $T_H = 128$ Mev and on the QGP side $T_{QG} = 172$ Mev. In our calculation we predict a transition temperature. However, if the hadron temperature can rise to T_S (around point B in Fig.1) then it may absorb enough latent heat to reach the point A on the left. Depending upon the dynamical conditions, like in a nuclear fission, the quarks and gluons can become deconfined, and with a further deposit of energy their teperature can rise to T_C. In table 1,the variation of transition temperature as a function D is enumerated for colour unprojected as well as colour singlet case with superscript 'o'.There is a sizeable decrease in T_C for the values of D away from unity and at each value of D, $T_C^O > T_C$. Around $\alpha_2 \geq 2$ the rate of decrease of T_C becomes negligible.

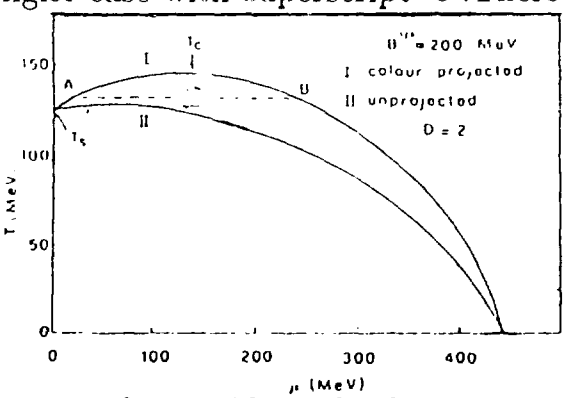

Fig.1: Plot of μ Vs T

Table 1 : The shape is oblate , spherical, or prolate, respectively as $1 \geq D > 1$.

$D =$	0.6	0.8	1.0	1.2	1.4	1.6	1.8	2.0
$T_C =$	139.0	145.0	146.0	145.0	142.0	137.0	132.5	129.0
$T_C^0 =$	157.0	163.5	165.0	163.5	160.0	155.0	150.	145.0

References:

1. R. D. Viollier and et al Nucl.Phys.A 407(1983) 269
2. A. Ansari and et al, Hadronic J. Suppl. 5 (1990) 233
3. J. Ellis and Keith A. Olive, Phys. Lett. B 260(1991) 173
4. G. E. Brown and et al, Phys. Lett.B 263(1991) 337

QUARK GLUON PLASMA EQUATION OF STATE IN A RELATIVISTIC HARMONIC CONFINEMENT MODEL

S.B. Khadkikar and J.C. Parikh
Physical Research Laboratory
Ahmedabad 380 009, India

The properties of hadrons and glue-balls have been determined quite successfully in relativistic harmonic models[1] for confinemnt of quarks and gluons. The same models have been able to obtain nucleon-nucleon phase-shifts[2] to explain nucleon-nucleon scattering data. It is therefore of interest to study the equation of state of quark gluon plasma (QGP) using these models and compare with those obtained through bag model and Monte Carlo simulation of QCD. The advantage of our models is the more realistic treatment of confinement. We also study the phase transition from pionic matter to QGP.

The EOS for non-interacting Bose and Fermi particles are given by

$$\frac{PV}{k_B T} = \begin{cases} -g_v g_I \sum_n g_n \log\left(1 - e^{-\beta\epsilon_n}\right) & \text{(Bose)} \\ g_v g_I \sum_n g_n \log\left(1 + e^{-\beta\epsilon_n}\right) & \text{(Fermi)} \end{cases}$$

where g_v, g_I and g_n are respectively the statistical weights corresponding to volume, internal degrees of freedom (spin, flavour, colour etc.) and degeneracy of the eigenvalue ϵ_n. In the hadronic phase $g_v = \frac{V}{(2\pi^3)} g_I = 3$ for pions and $g_n = 1$ with the summation over n replaced by the integral over the momentum. For the quarks and antiquarks in the deconfined phase, $g_v = \frac{VC_q^3}{(2\pi)^3}, g_I = 12$ (2 flavours) and $g_n = \frac{(n+1)(n+2)}{2}$ and for the gluons $g_v = \frac{VC_g^3}{(2\pi)^3}, g_I = 16$ and $g_n = \frac{(n+1)(n+2)}{2}$. Also, we take $\epsilon_n = \epsilon_p = \sqrt{\vec{p}^2 + M_i^2}$ with $M_1 = M_\pi = 139$ MeV for the hadronic phase and for quarks and gluons the energies are defined by $E^2 = M^2 + (2n+1)\Omega, M_{gl} = 0$. It is then a straightforward matter to evaluate

the sums and obtain the EOS. The result for the phase transition of a pion gas to a deconfined state of quarks and gluons is shown in Fig. 1.

In the present work, the temperature dependence of the pressure for QGP is found to be $P \sim T^7$ beyond $T_c = 177\,\text{MeV}$ with latent heat of 336 MeV/fm^3. The velocity of sound in QGP at T_c is found to be $\sim \sqrt{\frac{1}{6}}\,c$ and not $\sqrt{\frac{1}{3}}\,c$ found with T^4 dependence of the equation of state in other models. The difference is the result of overall confinement of the QGP with string-like energy-frequency relationship in harmonic confinement models. Further astrophysical implications of this model equation of state are currently being studied.

1. S.B. Khadkikar, Pramana - J. Phys. 24 (1985) 63 and references therein.
2. S.B. Khadkikar and K.B. Vijayakumar, Phys. Letts. B. 254 (1991) 330.

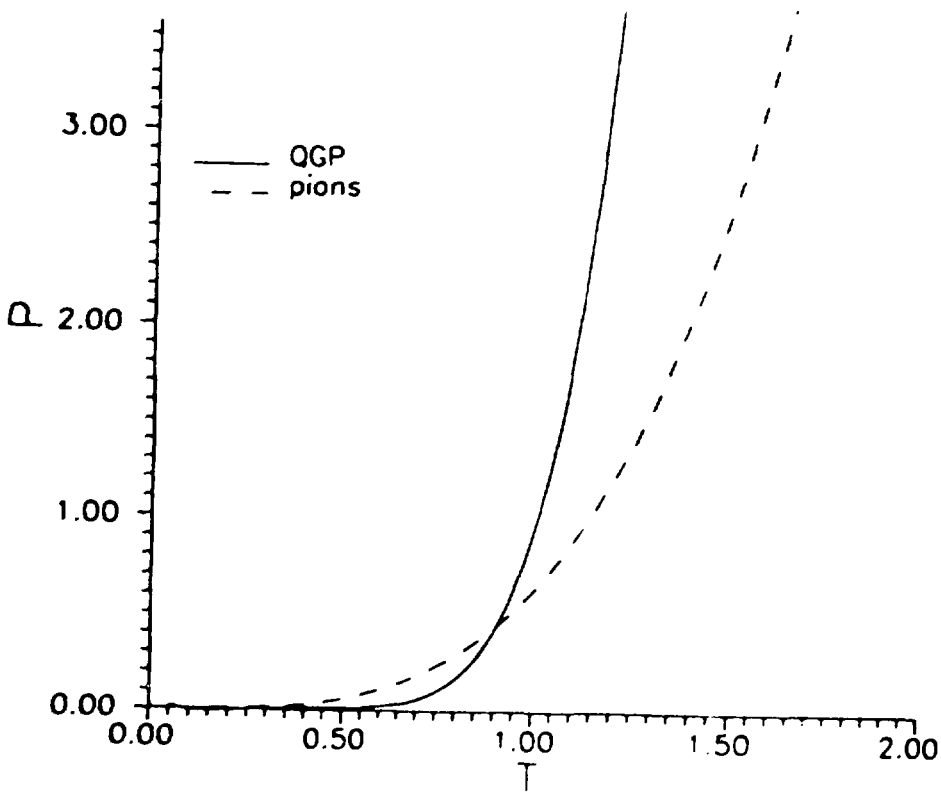

Figure 1 Pressure (in fm^{-4}) versus Temperature (in fm^{-1}) for pions and quark gluon plasma.

AN IMPROVED QGP MODEL FOR RELATIVISTIC HEAVY ION COLLISIONS - R.S. Kaushal(+) and Praveen Akhaury (++), Dept. of Physics & Astrophysics, University of Delhi, Delhi-110007; + UGC Research Scientist, ++ UGC Junior Research Fellow.

In recent years, while there has been considerable theoretical [1-6] interest in understanding the mechanism and the details of relativistic heavy ion collisions (RHIC), experimentalists have been trying [7-9] to look for an anomalous phenomenon which perhaps could be an indication of the formation of quark-gluon plasma (QGP) in the laboratory. The production of heavy quark flavours in RHIC is normally held responsible [6,7] for the formation of QGP. The J/ψ suppression observed [8,9] recently in O-U and S-U collisions at 200 GeV/nucleon energies turns out to be an interesting effect. Several authors have studied [3-5] the J/ψ suppression and in this case one calculates the survival probability (S) which is related to the probability of disintigration (P) by P=1-S=1-exp(-T), where T is the temperature. While Ftacnik et al [4] have studied the J/ψ suppression due to J/ψ- and χ-disintegration in a dense hadronic gas formed in RHIC, Karsch and Petronzio [3] (KP) study the E_T- and nuclear-size-dependence of J/ψ suppression within the framework of a hydrodynamical evolution model.

The temperature profile function considered by KP is $T(r)=T(o)[1-(r/R)^2]^{b/3}$, where R is the projectile radius and b is a parameter fixed by KP as 1/3. This form of T(r) accounts only for the radial dependence in a cylinderical volume at some initial time $t_i \approx 1$ fm/c. The z-dependence here is somehow ignored. In the present work, we introduce the concept of temperature density and, in general, consider the temperature function as $T(\vec{r})=T_0 T(r)f(z)$, with the normalization constant T_0 determined from $\int T(\vec{r})dV=1$. While for T(r) we use the form of KP, for the form of f(z) we decide to choose an exponential one $f(z)=\exp(-\beta z)$. Fourier transform of $T(\vec{r})$ w.r.t. z-coordinate turns out to be

$$|T(p_T)|=(\beta/\sinh \beta\ell/2)\,[\{\cosh(\beta\ell)-\cos(p_T\ell)\}/2(\beta^2+p_T^2)]^{\frac{1}{2}},$$

and the survival probability, S, as a function of p_T can be obtained. To obtain the E_T-dependence of S we use the expression for the energy density :
$\epsilon(\vec{r}) = \alpha\pi^2 T^4(\vec{r})/15$, and compute $\epsilon_T=|\epsilon(p_T)|$. The quantity

which is of experimental interest is $x(=\epsilon_T/\epsilon_{Tmax})$, which is found to be $x=|T(p_T)|^{\alpha}$(with β replaced by 4β).

In Figs.(1) and (2) we have shown S as a function of p_T and of x, respectively for two values of β alongwith the experimental and other theoretical results. It can be noticed that the modification to KP model, in general, not only leads to an improved agreement with experimental results on the J/ψ suppression, but also accommodates for the peaking tendencies if shown by the available data as a function of p_T.

References:

[1] L.Van Hove, CERN Preprint TH-5069/88; [2] J.Blaizot and J.V. Ollitrault, Phys. Lett. 199B (1987)499; [3] F. Karsch and R.Petronzio, Z. Phys. C37(1988)627; Phys. Lett. 212B (1988)255; [4] J.Ftacnik et al, Phys. Lett. 207B (1988) 257; CERN Preprint TH-5090/88; [5] K.Kajantie et al, Phys. Lett.223B (1989)213; T.Matsui and H.Satz Phys. Lett. 178B (1986)416; [6] P.Koch et al, Phys. Rep. 142 (1986) 167; [7] A. Bamberger et al, Phys. Lett. 184B (1987)271; [8] C.Baglin, in Proc. 3rd Int. Conf. on Nucleus-Nucleus collision Saint Malo, June 6-11, 1988; [9] C.Baglin et al, Phys. Lett. 220B (1989)471; ibid. 255B (1991)459.

Fig.1: S vs. p_T — present (β=0.9 fm/c); ..... present (β=1.1 fm/c); _.._.. Ref. [4]; ✚ Ref. [8].

Fig.2: S vs. x : — and .... same as in Fig.(1); -..-.. Ref.[3]; -.-. Ref.[4]; ✚ Ref.[9].

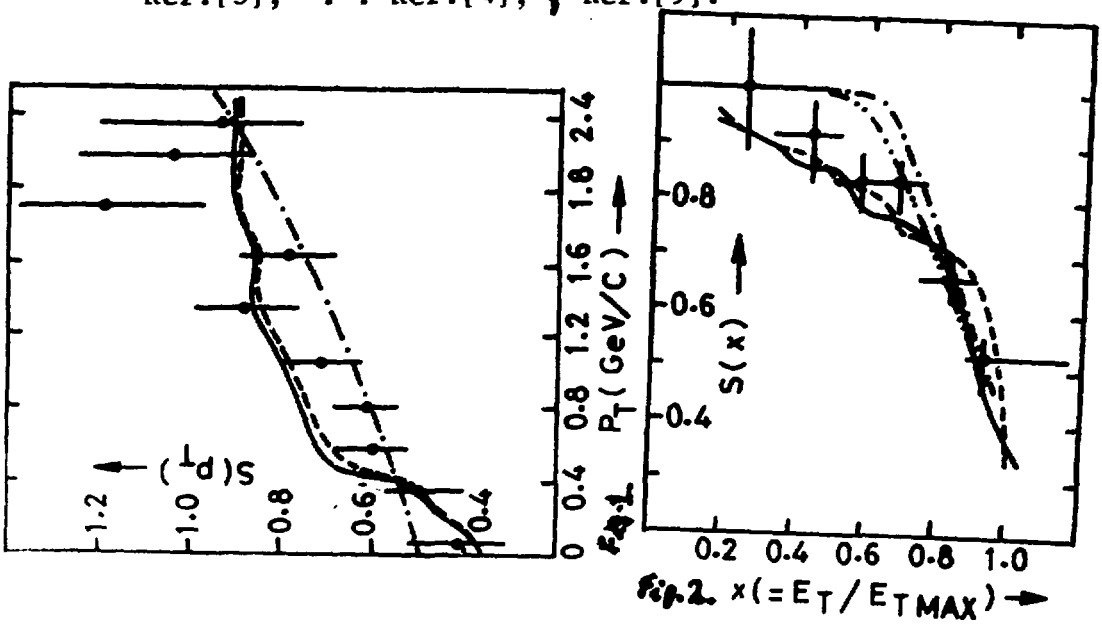

EQUATION OF STATE OF QUASI-FREE GLUON GAS

Somenath Chakrabarty[a], Debadesh Bandyopadhyay[b]
and Debapriya Syam[c]
(a) Saha Institute of Nuclear Physics, 1/AF Bidhan Nagar,
Calcutta 700 064
(b) Goethe-Institut, Steubenstrasse 44,D-6800 Mannheim 1,
Germany
(c) Physics Department, Krishnagar Government College
Krishnagar, West Bengal

In the past ten to fifteen years a lot of work has been done to unravel the characteristics of the state of matter known as the Quark-Gluon Plasma (QGP) [1]. A popular approach leads to the so called Bag model equation of state [2]. From an analysis of the dara for the energy density ϵ and the pressure P, generated by Monte-Carlo simulations on the lattice, Gorenstein and Mogilevsky have found that $\epsilon = \sigma T^4$ and $P = \frac{1}{3}\sigma T^4 - AT$ where σ is the Stefan-Boltzmann constant, while $A^{1/3} = 0.8T_c$ (for $SU(2)_c$ gauge theory and $= 1.5T_c$ for $SU(3)_c$, including two light dynamical quark flavours.

Recently, Lucha and Schöberl [3] have developed a relativistic version of the virial theorem. Here we shall extend this technique to a highly relativistic gas, namely to a system of gluons beyond the deconfinement temperature $T_c \approx 200$MeV. Since the gluons have only a small effective mass, they move with velocities close to that of light, and consequently we must consider "duynamic screening". In this case the screeneing length varies with direction. Additionally, we have imposed the requirement that the number of gluons in the region bounded by the screening length must be less than or about one, so that one can ignore three body interactions or correlations. We calculate the pressure and the energy density of the gluon gas, having chosen the parameters to satisfy the above constraint.

Following [3], we have the expression for pressure [4]

$$P \approx \frac{16}{6\pi^2}.4\pi.\int_0^\infty \frac{1}{(p^2+m_{\rm eff}^2)^{1/2}}.\left[exp\left((p^2+m_{\rm eff}^2)^{1/2}/T\right)-1\right]^{-1}p^4dp - \frac{1}{6}nA - B \qquad (1)$$

The energy density can be calculated in the same way to yield

$$\epsilon = \frac{16}{(2\pi)^3}.4\pi.\int_0^\infty (p^2+m_{\rm eff}^2)^{1/2}.\left[exp\left((p^2+m_{\rm eff}^2)^{1/2}/T\right)-1\right]^{-1}p^2dp - \frac{1}{2}nA + B \qquad (2)$$

where the term $-\frac{1}{2}nA$ represents the total potential energy of the system, the quantity A is given by

$$A \approx \frac{ng^3 g_{\text{eff}}^2}{4e} \int_0^{\pi} \frac{(r_D^2(\theta) - r_<^2) sin\theta d\theta}{(cos^2\theta + (1-v^2)sin^2\theta)^{1/2}} \qquad (3)$$

the screening length $r_D(\theta)$ can be defined in terms of the longitudinal component ϵ_L of the dielectric tensor [5], $e = 2.718...$, n is the number density, and is given by

$$n = \frac{8x2}{(2\pi)^3}.4\pi. \int_0^{\infty} [exp((p^2 + m_{\text{eff}}^2)^{1/2}/T) - 1]^{-1} p^2 dp \qquad (4)$$

To satisfy all the constraints, we set, rather arbitrarily $m_{\text{eff}} = 0.1T$, the other parameters $g \approx 2.3$ (which is consistent with the value of electric mass of gluon, $m_{el} = 2 - 3T$), and g_{eff} varies between 0.08 and 0.84.

We have seen from our results, that our model is more or less consistent with the recent lattice result of Ukawa [6]. Ukawa interprets the drop in the value of P/P_{pertb} near T_c as a signature of the presence of heavy hadrons (glueballs?). We have a more straight forward interpretation: the drop signifies the increasing importance of residual interactions in the vicinity of the critical temperature.

References:

[1] See for example Nucl. Phys. **A498** (1989), proc. QM'88.
[2] A. Chados et al, Phys. Rev. **D9** (1974) 3471.
[3] W. Lucha and F. F. Schöberl, Phys. Rev. Lett. **64** (1990) 2733; W. Lucha, Mod. Phys. Letts. **A5** (1990) 2473.
[4] S. Chakrabarty, D. Bandyopadhyay and D. Syam, to be published.
[6] A. Ukawa, in Ref. [1].

PHOTONS AND PIONS FROM QUARK-GLUON PLASMA AND HADRONIC MATTER

Subodha Mishra[1], Somenath Chakrabarty[2], Jan-e Alam[3], Dinesh K. Srivastava[3], and Bikash Sinha[3]

1 Institute of Physics, Sachivalya Marg, Bhubaneswar.
2 Saha Institute of Nuclear Physics, 1/AF Bidhan Nagar, Calcutta 700 064.
3 Variable Energy Cyclotron Centre, 1/AF Bidhan Nagar, Calcutta 700 064.

Ultra-relativistic heavy ion collisions offfer the possibility of creating Quark-Gluon Plasma (QGP) in the laboratory, which otherwise was formed in the early Universe, micro-second after Big Bang. Assuming that QGP is formed in such ● collisions and Bjorken's scaling law [1] is applicable for the space time evolution of the system, one can estimate the order of magnitude for the life time of the QGP bubble, which is found to be ~2-8 fm/c. Since the QGP phase is very short-lived, how then one can detect it experimentally? Since only hadrons, leptons, and photons are observed experimentally, more specifically how one can distinguish these two phases from the experimental ovservations. The basic process of QGP formation is: nucleus + nucleus → QGP → hadrons, leptons, and photons. If there is no phase transition, we have, nucleus + nucleus → hot and dense hadronic matter → hadrons, leptons, and photons.

In this article we shall discuss π^0 and photon emmissions from both hadronic matter and QGP. In the QGP sector we have massless quarks (up and down) and gluons. Here the processes for phton emission are Compton scattering ($q(\bar{q})g \rightarrow q(\bar{q})\gamma$) and pair annihilation ($q\bar{q} \rightarrow g\gamma$), both for pure QGP and QGP sector of mixed phase. We consider the leakage of π^0 from QGP surface by the fragmentation of quarks and gluons [2], both for QGP part of mixed phase and pure QGP phase.

In the case of pure hadronic case, the constituents are massive pions (π^+, π^-, π^0). The main sources of photons in this phase is the reaction ($\pi^+\pi^- \rightarrow \gamma\gamma$) and the decay ($\pi^0 \rightarrow \gamma\gamma$). All these photons have been counted both for hadronic part of mixed phase and pure hadronic phase. We also consider the π^0 coming out at the time of freeze out (after that the whole system breaks into free-streeming gas).

Integrating the rates of the above reactions, leakage, and decay over the space-time history, assuming the applicability of Bjorken's hydrodynamics [1] for both the QGP and hadronic phases and considering the variations of effective degrees of freedom in the hadronic phase with temperature, we evaluate the following ratios:

(1) γ's from QGP $/\pi^0$ leaking out from the QGP surface,

(2) γ's from hadronic phase$/\pi^0$ emmited at freeze out.

where we have taken the initial proper time $\tau_0 = 1 fm/c$, critical temperature T_c=160 and 200 MeV, initial temperature $T_i = 1.5T_c$ and $2T_c$ and freeze out temperature T_f=140 MeV.

We conclude that the ratio (1) saturates beyond a certain transverse momentum $(p_T) \geq 2.5$ GeV, but the ratio (2) does not. Therefore it can be a signal for quark-hadron phase transition.

References

[1] J. D. Bjorken, Phys. Rev. D27(1983)140.

[2] Sibaji Raha and Bikash Sinha, Int. Jour. Mod. Phys. A6 No.4(1991)517.

CAN THE HADRONIC GAS SHINE AS BRIGHT AS QUARK-GLUON PLASMA

Somenath Chakrabarty[1], Jan-e Alam[2],Dinesh K. Srivastava[2]
Bikash Sinha[2], and Sibaji Raha[3]
(1) Saha Institute of Nuclear Physics, 1/AF Bidhan Nagar, Calcutta 700 064
(2) Variable Energy Cyclotron Centre, 1/AF Bidhan Nagar Calcutta 700 064
(3) Bose Institute, 93/1 Acharya Prafulla Chandra Road, Calcutta 700 009

It is generally expected that at very high density and /or high temperature normal hadronic matter undergoes a colour deconfined phase transition to a new phase, known as Quark-Gluon Plasma (QGP). Such a state of matter is predicted to occur, from QCD considerations also. If QGP exists, its properties are expected to be drastically different from hadronic matter at corresponding energy densities. The QGP, if it is formed, exists only for a fraction of the total evolution time. Colour confinement clearly prevents free quarks or gluons from escaping from the 'firebal' and most of the detected hadrons escape the reaction volume at the freeze-out time. How can then one know if a QGP was at all formed? Does the QGP leaves any finger-prints, any signatures of its transient existence? Indeed, there are several suggestions in the literature as to how to put the QGP in evidence. Specially, we shall concentrate only on the emmission of photons. Experimental data necessarily correspond to the space time integrated history over the whole evolution and since photons interact very weakly with the QGP system, can retain the memory of the early time or the time when they are created in the system.

In this note we shall consider photon emission both from the hadronic and Quark Gluon Plasma. We shall consider all possible photon emission processes in hadronic matter, the reactions are: $\pi^+\pi^- \rightarrow \rho^0\gamma$, $\pi^+\pi^0 \rightarrow \rho^+\gamma$, $\pi^0\pi^- \rightarrow \rho^-\gamma$,$\pi^+\rho^0 \rightarrow \pi^+\gamma$, $\pi^-\rho^0 \rightarrow \pi^-\gamma$,$\pi^-\rho^+ \rightarrow \pi^0\gamma$, $\pi^+\rho^- \rightarrow \pi^0\gamma$,$\pi^0\rho^+ \rightarrow \pi^+\gamma$, $\pi^0\rho^- \rightarrow \pi^-\gamma$,$\pi^+\pi^- \rightarrow \eta\gamma$, $\pi^+\eta \rightarrow \pi^+\gamma$,$\pi^-\eta \rightarrow \pi^-\gamma$ and $\pi^+\pi^- \rightarrow \gamma\gamma$. Similarly there are some decay processes, they are: $\omega \rightarrow \pi^0\gamma$,$\rho^0 \rightarrow \pi^+\pi^-\gamma$, $\pi^0 \rightarrow \gamma\gamma$, and $\eta \rightarrow \gamma\gamma$

The photon emission processes from QGP are (i) Generalized Compton scattering ($q(\bar{q})g \rightarrow q(\bar{q})\gamma$) and (ii) Annihilation Process ($q\bar{q} \rightarrow g\gamma$).

Recently Kapusta et al [1] has shown that the rate of photon emission from QGP and Hadronic matter at a particular temperature, $T = 200$ MeV are same and they concluded that the hadron gas shines just as brightly as Quark-Gluon Plasma.

In our calculation we have re-investigated [2] Kapusta's work at $T = 160$ MeV and $T = 250$ MeV and obtain exactly the same result was obtained by Kapusta. In these calculations the space time evolution of the QGP and Hadronic system is not taken into account. These are instantaneous processes and from unit volume of the QGP or Hadronic system.

We have then investigated the total number of photons emitted from both QGP and Hadronic matter taking into account the space timeevolution of both the gases (rates/volume are integrated over space and time). Our starting point is pure QGP at initial temperature T_i (we have chosen two possible initial temperatures $1.5T_c$ and $2T_c$, where T_c is the critical temperature for quark-hadron phase transition). Initial proper time $\tau_i = 1fm$. As the system expands it cools according to Bjorken scaling law, and when the temperature drops to T_C, phase transition from pure QGP to hadronic phase sets in. If the phase transition is first order in nature, at $T = T_c$, we have a mixed phase of quark-gluon plasma and hadron gas. Then after some time τ_H, the whole Quark-matter is converted to hadronic matter and the temperature becomes less than T_c. The produced hadronic gas is again assumed to be a thermalized massive ideal gas, at some proper time τ_f, corresponds to the freeze-out temperature $T_f = 140MeV$, the whole system breaks into free-streaming gas.

We have seen that although the rates per unit volume from mixed phase are identical, the total number of photons emitted from QGP and hadronic phase are entirely different. For $T_c = 160MeV$ and $T_i = 2T_c$, the number of emited photons are more from QGP phase at very high photon transverse momentum $P_T > 3$ GeV. As the initial temperature is increased, the QGP phase dominates over hadronic phase more and more and for $T_c = 200MeV$, and $T_i = 2T_c$, there is a clear distinction between hadronic and QGP phase.

Since to distinguish QGP from Hadronic matter by the p_T distribution of emitted photons the initial temperature should be very high, therefore we can conclude that although this signature is not so conclusive for QGP formation in SPS energy, but at RHIC and LHC energies there should be clear distinction between QGP photons and Hadronic photons.

References:

[1] University of Minesota preprint, 1991.
[2] J. Alam, S. Chakrabarty, D. K. Srivastava, S. Raha and B. Sinha, to be published.

MODEL DEPENDENT PHASE TRANSITION FROM HADRONIC MATTER TO QUARK-GLUON PLASMA

K. Sakthi Murugesan, G. Janhavi, K. Raja, and P. R. Subramanian
Department of Nuclear Physics, University of Madras, Guindy Campus, Madras 600 025.

Ultrarelativistic Heavy-Ion Collisions are interesting tools to study the existence of quark gluon plasma (QGP). The location of the phase transition to QGP in hadronic matter can be found by an analysis of their equations of state (EOS). Present analysis of the QCD phase transition shows that the value of the bag constant B, which is used in the EOS, should be < 200 MeV/fm^3. Only then the theory may be useful to study both heavy ion collisions and cosmological problems [1]. In Ref. 2, it is reported that the critical energy density for deconfinement is nearly independent of the chemical potential μ_q and the baryon number density ρ_b (here $B > 200$ MeV/fm^3). For $B < 200$ MeV/fm^3, it is difficult to study [1] the dynamics of hadronization phase transition by using the model of Ref. 2. Following Ref. 3, we modify the above model by including the Hagedorn's correction only for the baryons and their resonances in the HRG phase: We exclude this correction for all mesons in the HRG phase. The resulting two phase coexistence region which separates the purely hadronic and QGP sectors in temperature - chemical potential plane is shown in Fig.1 for two cases. Using our modified model, the calculated values of critical energy densities for deconfinement depends strongly on μ_q and ρ_b and is shown in Figs. 2 & 3. The phase diagrams and the critical energy density for the complete deconfinement and onset of deconfinement for a softer EOS are investigated in detail using the modified model. The strong dependence of the critical energy density for deconfinement on μ_q and ρ_b may change the trend of the dynamics of the hadronization phase transition. Hence the modified model will be useful to study the phase transition for all values of the bag constant B.

References:

1. K. Sakthi Murugesan, Ph.D. Thesis (University of Madras, 1991).
2. P. R. Subramanian, H. Stocker, and W. Greiner, Phys. Lett. B173, 468 (1986).
3. H. Kouno and F. Takagi, Z. Phys. C42, 209 (1989).

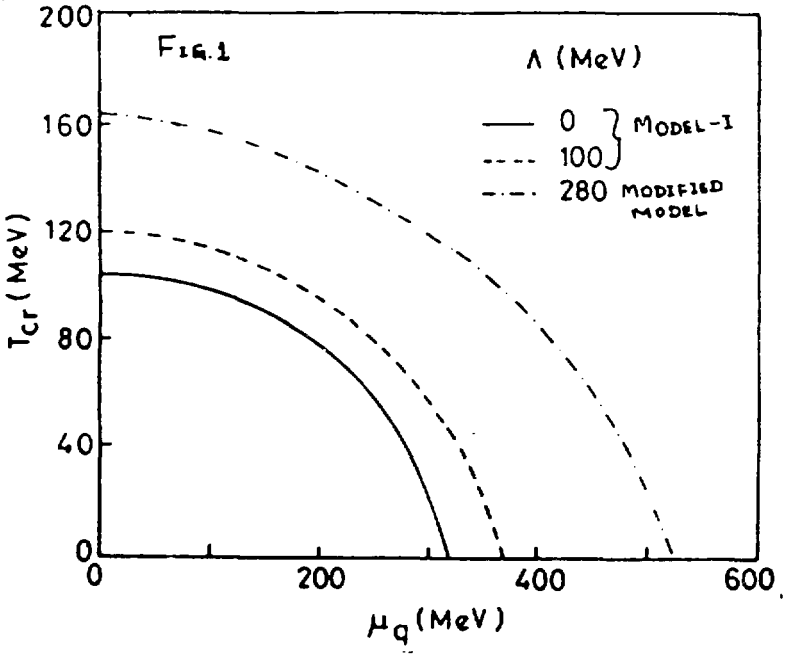

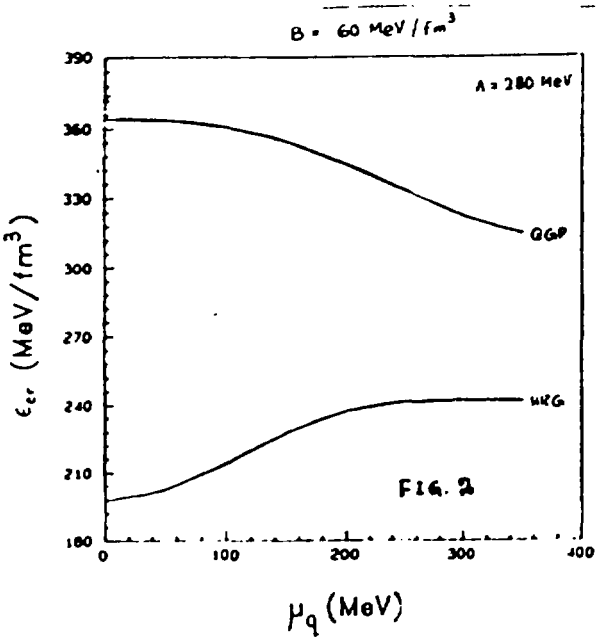

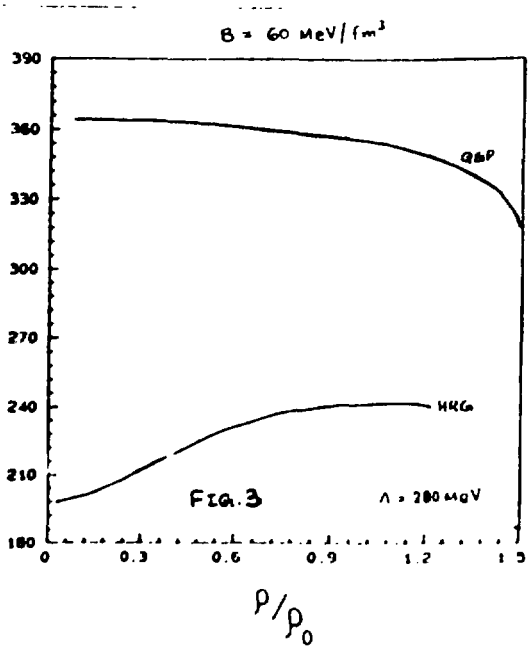

TEMPERATURE DEPENDENCE OF BAG CONSTANT USING CHROMOMAGNETISM

N. Meenakumari and M. Rajasekaran
Department of Nuclear Physics, University of Madras
Guindy Campus, Madras 600 - 025

Minimising the thermodynamic QCD vacuum energy with respect to the colour magnetic field, we determine the bag constant as a function of temperature. Our results are compared with the abelian bag model [1], which determines the bag constant in the perturbative vacuum region.

It is well known that the response of QCD vacuum to the colour magnetic field would reveal the true nature of QCD vacuum. Inside the hadron one sees a perturbative vacuum, while outside, the QCD vacuum which has a lower energy density. From Savvidy's model one can write the QCD vacuum energy density [2] as

$$E(H) = \frac{33}{96\pi^2}(gH)^2 \left(\ln \frac{gH}{\Lambda^2} - \frac{1}{2}\right) \qquad (1)$$

where H stands for the colour magnetic field, Λ is the Savvidy scale parameter and g is the QCD coupling constant. Eq. (1) shows that E(H) has two minima, the perturbative vacuum at H = 0 where the energy density is 0 and the QCD vacuum at H = Λ^2 /g. On identifying the energy difference between the two minima as an estimate of the bag constant B, one gets $B^{1/4} \approx 100$ MeV. This precisely brings the resemblance between the bag model and the QCD, since in the MIT bag model the QCD vacuum is lower in energy than the perturbative vacuum by the bag constant B per unit volume.

Now to obtain the finite temperature effects of vacuum energy, one has to examine the free energy

$$F = -T \ln Z$$

where the partition function

$$Z = \prod_{\alpha} \sum_{m} \exp\left[-(m+\tfrac{1}{2})\frac{\omega_\alpha}{T}\right]$$

Using this, we minimise the effective potential

$$V = F(gH,T) - F(0,T)$$

with respect to gH and on identifying the difference between the two minima as the bag constant, we determine B as a function of T. In the Fig., we plot the normalised value of $B^{1/4}$ as a function of temperature, which is independent of Λ. We compare it with the thermodynamic bag model where

$$\frac{B}{B_0} = 1 - \frac{T^4}{T_c^4}$$

It is found that our results obtained using rigorous QCD calculations agree well with the naive bag model. Also the relation between the critical temperature and the bag constant

$$T_c = k\, B^{1/4}$$

still holds good, though the value of k is increased in taking the interactions into account.

One of us (N. M) thanks the UGC for the award of SRF

References:

[1] F. Takagi, Z. Phys. C37 (1988) 259
[2] J. I. Kapusta, Nucl. Phys. B190 (1981) 425

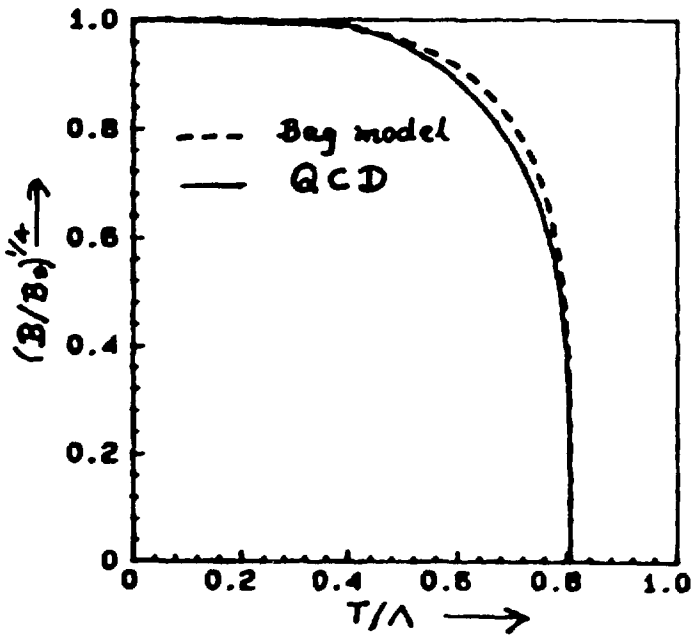

PION COHERENCE ZONE FOR 'HOT' AND 'COLD' EVENTS IN RELATIVISTIC HEAVY ION COLLISION

Dipak Ghosh, *Jaya Roy, Sharmila Sarkar and Ranjan Sengupta
Jadavpur University, Calcutta 700 032; *R. C. C., Calcutta

A new signature for quark matter formation in relativistic heavy ion collisions in terms of emission spectra in the fragmentation region was proposed by Raha et. al.[1]. According to them, during the separation of the spectators from the participants, due to excitation, there is some intercommunication, resulting the excitation of the spectators. This communication strongly depends whether or not the participants form a QGP. Therefore the energy imparted in terms of temperature to the spectators may carry characteristic information about the formation of a QGP in the participant region; so the observation of two distinctly different temperatures in the fragmentation region with a ratio of four among them was interpreted as a signal for QGP.

In our earlier work, a comparison of P_T distribution of the projectile alpha particles for ^{12}C-Em. interaction at 4.5A GeV/c with double Maxwell-Boltzmann distribution was done [2]. This yielded two temperatures in the projectile fragmentation region i.e., 10 MeV (cold) and 40 MeV (hot) with different reaction mechanisms; i.e. there exists two different class of events with these two temperatures. According to the Model of Raha et. al. [1] the 10 MeV temperature may belong to events where a QGP is formed in the participant region.

Here we have studied the pion production mechanism in these two classes of events. For the purpose of the present analysis, for both 'hot' and 'cold' group each event was divided into several pseudorapidity (η) bins : where pseudorapidity is defined as $\eta = -\ln \tan \theta/2$, θ being the emission angle. Each bin was treated as 'mini star' of multiplicity n_i where i denotes η bin then total multiplicity n_i of each event is $n = \sum n_i$.

Table I represents the χ^2/d.o.f. (degrees of freedom) values for Poisson and chaotic distributions for different bins for both 'hot' and 'cold' events. The observed multiplicity distribution in five intervals was compared with the Poisson and chaotic distribution for both groups. The Poission distribution is given by the relation –

$$P(n_i)=\text{Exp}(-\langle n_i\rangle)\ \frac{\langle n_i\rangle^{n_i}}{n_i!} \qquad .....(i)$$

and the chaotic distribution is represented by –

$$P(n_i) = \frac{1}{1+\langle n_i\rangle}\left[\frac{\langle n_i\rangle}{\langle n_i\rangle+1}\right]^{n_i} \cdots (ii)$$

corresponding to mean multiplicities $\langle n_i\rangle$.

Although the gap 1 shows the minimum of χ^2/d.o.f. in both cases of 'hot' and 'cold' events, we do not take this gap into consideration due to low statistics in that bin. From the table I one can conclude the following : the value of χ^2/d.o.f. when compared with the Poisson distribution, in the 4th rapidity bin is less than the other bin values in case of 'cold' events : which infers that the multiplicity distribution in the said bin is significantly Poisson-like. In this bin the distribution is tending towards chaotic for 'hot' events. The overall situation is quite different in case of 'hot' events, the most Poisson - like distribution appears in the 5th gap where for 'cold' events pion distribution is not at all Poisson-like and tend towards chaotic. This implies that in a specific pseudorapidity bin, pion production is coherent in case of 'cold' events, and incoherent in case of 'hot' events. Again in another specific pseudorapidity bin, pion production is coherent for 'hot' events but incoherent for 'cold' events.

TABLE I

χ^2/d.o.f. (degrees of freedom)

Distribution of	$-5<\eta<-3$ Gap 1	$-3<\eta<-1$ Gap 2	$-1<\eta<1$ Gap 3	$1<\eta<3$ Gap 4	$3<\eta<5$ Gap 5
Poisson hot	0·26	2·64	2·79	8·48	1·18
Chaotic	0·96	1·42	4·56	6·81	2·27
Poisson cold	0·31	2·23	4·07	1·54	4·41
Chaotic	0·24	1·37	3·83	2·73	1·31

REFERENCE :

1. S. Raha, R.M. Weiner and J. W. Wheeler – Phys. Rev. Lett. 53 (1984) 138
2. D. Ghosh, J. Roy and R. Sengupta – J. Phys. G. Nucl. Phys. 14 (1988) 711

EVIDENCE OF SELF-SIMILAR PROTON EMISSION IN NUCLEUS-NUCLEUS COLLISION

Dipak Ghosh, Argha Deb, Premomoy Ghosh ,
Biswanath Biswas & Jayanta Roychoudhury
Jadavpur University ,Cal-32

Recently a new method ,the "intermittency", based on calculation of scaled factorial moments in the limit of small phase-space intervals has been proposed by Bialas & Peschanski[1] to measure the dynamical fluctuation in pionization process without any bias of statistical fluctuation.But the origin of such signal has not yet been explained unambiguously .At this juncture,it is worth investigating not only the factorial moments, F_i, but also the fractal moments, G_i,[2] for better understanding of self-similar property of the process.

Attempts made to find the proper dynamics of multiparticle production process have mostly been confined to the domain of investigation of the relativistic shower particles, though the medium energy(30-400MeV) knocked out protons,which have same time-scale of emission as that of the shower particles, may also play an important role in this regard. The objective of this paper is to investigate the intermittent as well as the fractal behaviour of the medium energy protons,emitted in ^{16}O-Ag/Br and ^{24}Mg-Ag/Br interaction at 2.1 GeV/c and 4.5 GeV/c respectively.

The average scaled factorial moment $\langle F_i \rangle$ of order i for a sample of events with mean particle multiplicity $\langle N \rangle$ is defined as[1]

$$\langle F_i \rangle = M^{i-1} \langle \sum k_m (k_m-1) - \cdots - (k_m-i+1) / \langle N \rangle^i \rangle$$

where M is the no of $\delta(\cos\theta)$ bins(θ is the angle of emission), into which the total cos interval $\Delta(\cos\theta)$,has been divided. k_m in the above formula is the number of particles in the mth bin . Here $\langle\ \rangle$ sign denotes the average over the whole sample of events .

If the considered range of the phase space variable is divided into M_0 bins of width , of which M bins are non-empty, and k_j be the number of particles in the jth non-empty bin, the multifractal moment G_i is defined as $G_i = \sum p_j^i$ where $p_j = k_j/n$ with $n = k_1 + k_2 + \ldots + k_M$, i is any real number. If the process exhibits self-similar behaviour, the moments show a power law relation of the form $G_i \propto \delta^{\tau(i)}$. Once $\tau(i)$ is determined, the spectral function $f(\alpha)$ can be obtained by Legendre transform

$$f(\alpha) = i\alpha_i - \tau(i)$$

where $\alpha_i = d\tau(i)/di$

Factorial moments calculated for both type of interaction show intermittent behaviour of particle emission. Fractal analysis performed on the same data samples also reveals some interesting features. The generalised dimensions (D_0, D_1 & D_2) suggest multifractality in each type of interaction. The spectral functions $f(\alpha)$ as a function of α is shown in the figure and thus this data reveals the first ever evidence of intermittent as well as fractal behavior of medium energy proton emission in high energy interactions .

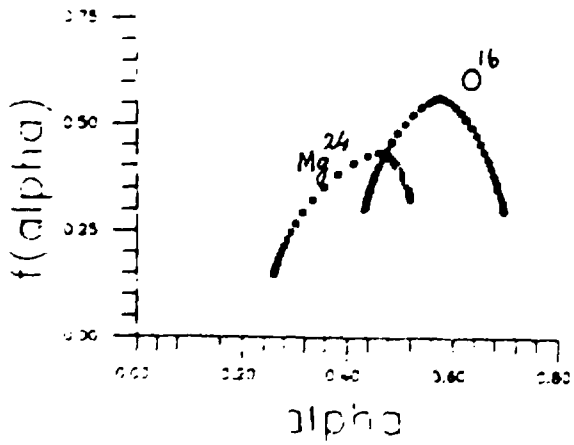

References:

1. Bialas A. et.al. Nucl. Phys. B273(1986)703
Nucl. Phys. B308(1988)857
2. Hwa R. C. Phys. Rev. D41(1990)1456

EFFECT OF TEMPERATURE ON COLLECTIVE BEHAVIOR

B.Singh, H.S. Palsania, V.Kumar, K.B.Bhalla and S.Lokanathan
Department of Physics, University of Rajasthan
JAIPUR-302004

It is well known that collective flow is the manifestation of high density and large correlation length. Several experimental evidences of collective effects in relativistic nuclear collision have been made available[1-4] in recent years. In order to understand collective effect models such as Hydrodynamical[5] and Modified Intra-Nuclear Cascade[6] have been proposed. The above mentioned models explain some of the bulk-characteristics like flow angle but are silent about the micro-characteristics such as fragment mass distribution and effect of temperature and density on the distribution. Quamtum statistical model [7] predicts that the conditions of low temperature and high density are more favorable to the production of heavier fragments.

We have divided the bounce-off events[8] in La^{139}+Ag(Br) collision at 1.1 A GeV primary energy into following three categories i) $1 \leq N_p \leq 3$, ii) $4 \leq N_p \leq 6$ and iii) $N_p \geq 7$ corresponding to small medium and large projectile spectator chunk in order to study the variation of collectiveness and the effect of temperature. In figure 1 strength of back to back (target-projectile) correlation in azimuthal plane ($\Delta\phi = |\phi_{TF} - \phi_{PF}|$) has been plotted. The effect shows a regular enhancement in going from category i) to iii).

The momentum width of nucleons in their fragmenting sources can be investigated by plotting[8] θ_{PF}(projected) onto a plane containing the principal vector of PF's. In figure 2 a),b) and c) θ(proj) has been plotted for alphas and fragments(PF's with $Z \geq 3$) for the three categories respectively. It may be noted that in all the categories width is narrower in case of fragments as compared to that in case of alphas. Also, the width of a distribution in category (i) is more that in the subsequent category of events.

The excitation energies of the bounce-off nuclei E^* have been computed using Quasi Elastic Scattering (QES) kinematics[9] and values of E^*, temperature T and $\overline{\Delta\phi}$ are given in table 1 for the three categories of data. The data shows that in the case of events of category (i) where participant chunk is bigger hence density should have been higher and because of temperature rise to a high degree collective effect is diluted.

Table 1: Excitation energy (E^*), temperature (T) and $\overline{\Delta\phi}$ for above mentioned categories.

	$1 \leq N_p \leq 3$	$4 \leq N_p \leq 6$	$N_p \geq 7$
E^*	6.6 GeV	4.5 GeV	3.3 GeV
T	30 MeV	20 MeV	17 Mev
$\overline{\Delta\phi}$	119.8°	125.9°	133.7°

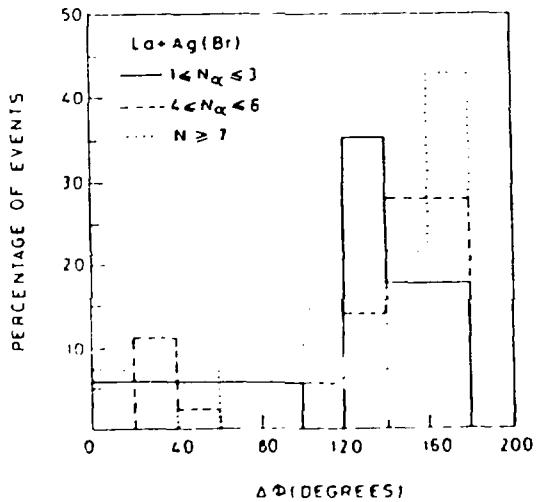

Fig 1

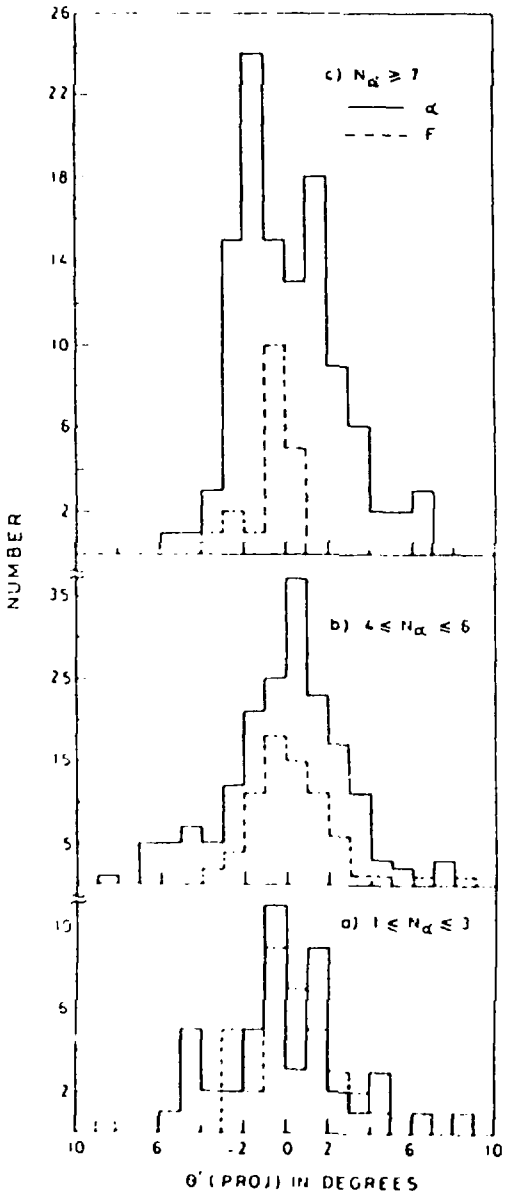

Fig 2

REFERENCES

1. Baumgardt, H. G., et. al., Z. Phys A237, 359 (1975).
2. H. A. Gustafsson, Phys. Rev. Lett. 52, 1590 (1984)
3. H. G. Ritter, Nucl. Phys. A447, 3C (1985).
4. Arora R. and Kumar V., et. al., Z. Phys A333, [illegible] (1989)
5. Schein D., et. al., Phys. Lett. 32, 741 (1974)
6. J. Cugnon and D. L'Hote, Nucl. Phys. A447, 27C (1985), J. Cugnon, et. al., Phys. Rev. C35, 861 (1987) and L. Braun and Z. Fraenkel,
7. H. Stocker et. al., Nucl. Phys. A400 (1983) 63C.
8. Paltania H. S., et. al., Modern Phys. Letters A, Vol. No. 6, No. 10 (1991) 2757-2765
9. H. H. Heckman, et. al., Phys. Rev. C34, 1333 (1986)

HIGH RESOLUTION STUDY OF HELIUM PROJECTILE FRAGMENTS EMITTED IN ^{32}S-EMULSION COLLISIONS AT 200 A GeV ENERGY

(EMU-01 COLLABORATIONN)
Reported By: Renu Arora, Physics Department,
Panjab University, Chandigarh-160014.

Study of angular distribution of Helium fragments, emitted in nucleus-nucleus collisions at relativistic energies, can yield information on the mechanism of projectile fragmentation, on the role played by the Fermi motion of nucleons and on the excitation energy received during collision by the spectator part of the projectile. A few experiments had been done several years on the emission of Helium fragments in heavy ion collisions at Bevatron energies. The EMU-01 collaboration studied the phenomenon in ^{16}O-Emulsion interactions at 200 A GeV [1]. This paper describes the first ever measurements on the angular distributions of helium fragments in ^{32}S-Emulsion collisions at 200 A GeV energy.

In this experiment we have used horizontally exposed emulsion plates and vertically exposed emulsion chambers. 463 minimum bias events have been examined in stacks and about 300 events in chambers. By making measurements relative to close-by beam tracks and using Koristka R4 microscope and Leitz ASM 68K system, we have been able to measure Helium emission angles with an unprecedented accuracy of 0.03 milliradians.

Fig.1 shows the experimentally measured Helium emission probability per interaction for events with one or more helium fragments.

Fig.2 depicts the correlation of number of Helium fragments emitted (N_α) with ln N_g, where N_g, the number of grey tracks emitted, is generally taken as a measure of the number of participant nucleons in the target. It is seen that N_α is inversely proportional to ln N_g.

Fig.3 depicts the projected angle distribution of Helium fragments. The distribution is gaussian with a dispersion, $\sigma(\theta)$=0.26 mrad. This dispersion is related to the Fermi momentum $\langle p_f \rangle$ of nucleons within the projectile. Acoording to Goldhaber [2]

$$p_f^2 = 5\sigma(p)^2 (A_p-1)/A_F(A_p-A_F)$$

where A_p = Mass no. of projectile, A_F = mass no. of fragment and $\sigma(p)$ is the dispersion in momenta of nucleons= $A_p A_F/\mathrm{Sin}\ \sigma(\theta)$.

$\sigma(p)$ is also related to the excitation energy (kT imparted to the spectator portion of the projectile through the following relation [2]:

$$kT=\sigma(p)^2 A_p/m_N A_F (A_p-A_F)$$

Where m_N = nucleon mass. Using $\sigma(\theta)$=Ø.26 mrad and the above relations we get the Fermi momentum, p_F = 2Ø4 MeV/c which compares well with the value 26Ø MeV/c obtained from electron scattering experiments with Fe target. The average value of excitation energy deduced from our experiment for the Sulphur-Emulsion collisions is 9.1±Ø.9 MeV which is of the order of the average binding energy per nucleon.

Fig.4 shows the space angle frequency histogram of Helium fragments. Following Aggarwal et al [3] we fitted a Maxwell-Boltzmann distribution to the data. We find that our experimental data is consistent with the emission of Helium fragments from a single source moving with a speed which is very slightly less than that of the projectile and having a temperature of about 9 MeV.

REFERENCES: 1. M.I.Adamovich et al., Phys. Rev. C4Ø (1989)66.
2. A.S.Goldhaber, Phys. Letts. (1974)3Ø6.
3. M.M.Aggarwal et al., Phys. Rev. C27 (1983)64Ø.

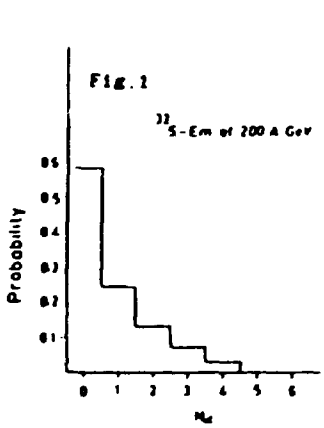

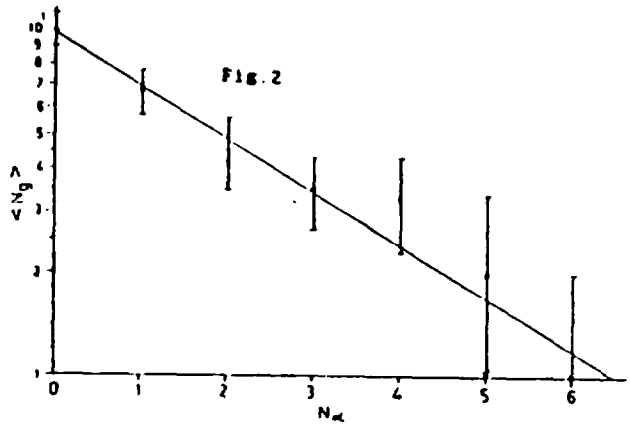

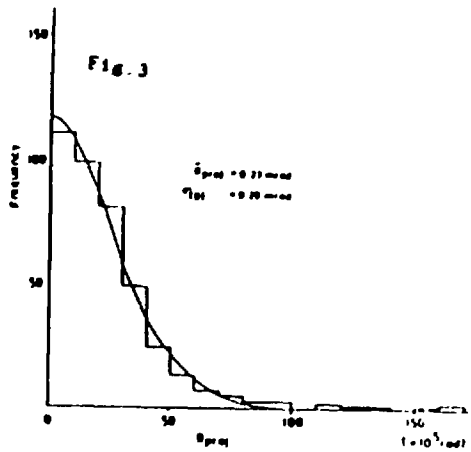

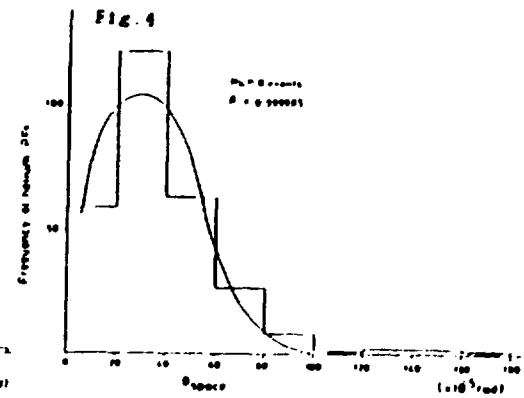

FORWARD BACKWARD CORRELATIONS

EMU - 01 Collaboration

Anju Bhasin, Physics Deptt., Univ. of Jammu, Jammu-180001.

Long range correlations in nucleus-nucleus collisions of O^{16} projectile at 200 and 15 A GeV with nuclear emulsions give the following conclusion. Table 1 summarizes information regarding particles in forward and backward hemispheres for the two energies. It is evident that the ratio of the particles produced in the two hemispheres is constant over the energy range.

TABLE 1

Energy	$\langle n_B \rangle$	$\langle n_f \rangle$	$\langle n_B \rangle / \langle n_f \rangle$	$\langle n_B \rangle / \langle N_s \rangle$	$\langle n_f \rangle / \langle N_s \rangle$
15	24.93±2.43	20.42±1.99	1.22±0.16	0.549±0.075	0.45±0.062
200	82.12±7.07	74.88±6.44	1.09±0.13	0.523±0.064	0.47±0.061
*	(84.478)	(65.8593)	(1.2827)	(0.56318)	(0.4390)

* Values calculated from the FRITIOF model

The tracks in the forward and backward hemispheres are parameterized by a relation:
$\langle n_B \rangle = a + b\, n_f$ and $\langle n_f \rangle = a + b\, n_B$

The slope b is the measure of the strength of long range correlation in the two hemispheres. A linear dependence of the above relation is shown in Fig 1(a,b).The value of slope parameter is shown in Table 2. . It is observed that 'b' is higher for $\langle n_B \rangle$ vs n_f as compared to $\langle n_f \rangle$ vs n_B thereby indicating strong correlation in the first case and weaker in the second case. The value of slope is also calculated using the following equation.
$b = d\langle n_B \rangle / dn_f = (\langle n_B n_f \rangle - \langle n_B \rangle \langle n_f \rangle) / (\langle n_f^2 \rangle - \langle n_f \rangle^2)$

The calculated values of slope are also given in Table 2(values in brackets) and they agree well with experimental values.

TABLE 2

Energy	slope b	
	$\langle n_B \rangle$ Vs n_f	$\langle n_B \rangle$ Vs n_f
15	1.1052±0.090 (1.03584)	0.3498±0.4219 (0.3755)
200	1.2149±0.0672 (1.20259)	0.5280±0.0358 (0.5144)

Strength of correlation increases with energy. In hadron-hadron interactions the strength of correlation is observed to be weak(b=0.15[1]),thus indicating a symmetric emission of particles. The strength of the correlation grows stronger as we move from hadron nucleus (b=0.86±0.07[2]) to nucleus-nucleus interactions(b=1.21±0.06),therby suggesting multiple collision of

excited nucleons inside the nucleus.

Correlations are also studied in limited η region. For $|\eta| \leq \eta_{cut}$ the correlation strength parameter first rises with η_{cut} upto 2 and then remains constant. This is true for both the energies (Fig2(a,b)). But with elimination of a central region and considering the particles in the region $|\eta| > \eta_{cut}$(Fig 3(a,b)) ,it is observed that b remains constant over whole of selected η_{cut} at 200 A GeV whereas at 15 A GeV the correlation strength falls from $\sim$ 1 for $\Delta\eta_{sf}$ = 0.25 to almost 0 for $\Delta\eta_{sf} > 3$, thus indicating that no correlation exists between pure target and pure projectile fragments.Results from FRITIOF code in general agree in trends with the experimental data but are quite different quantitatively. FRITIOF underestimates the number of particles in forward hemisphere(Table 1). These results are consistent with other experimental findings .

References:

1. S. Uhlig et al; Nucl Phys B 132 (1978) 15.
2. L.M.Barbier et al; Phys Rev. D 37 (1988) 1113.
3. G. Singh et al; Phys Rev. C 39 (1989) 1835.

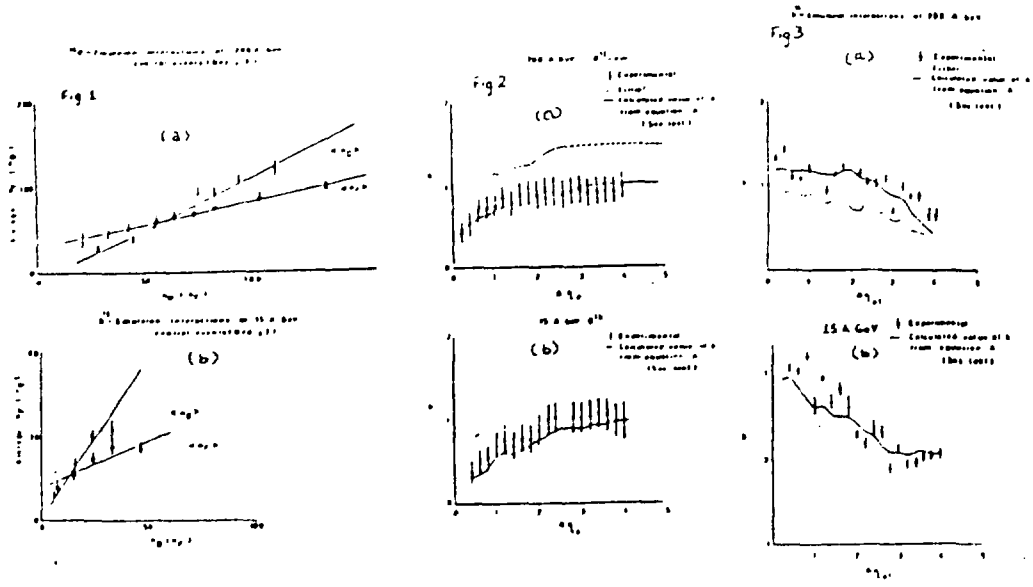

DIFFRACTION DISSOCIATION OF ^{12}C NUCLEI IN NUCLEAR EMULSION

M.S.Ahamad , K.A.Siddiqui and R.Hasan
Department of Physics, A.M.U. Aligarh-202002.

Fragmentation of relativistic projectile nuclei would give the information about the internal structure of nuclei under condition of small transfer of momentum and energy. However, the partner-nucleus in an inelasltic collisions is not a simple spectator of the fragmentation process as it is assumed in participant and spectator model. The dynamics of the inelastic collisions of high energy nuclei distorts the intranuclear characteristics of nucleons and nucleon clusters as a consequence of transverse motion of the fragmenting residual nuclei, the angular momentum, effects of intranuclear rescattering and so forth (1,2).

This makes it interesting to study those collisions channel of nuclei in which the effect of the partner-nucleus would be minimal. One should expect that we can assign reactions of this type those which are extremely peripheral,i.e., reaction of dissociation of the incident nucleus in the field of the target. In the present report we are going to study such type of events from ^{12}C-emulsion collisions at 4.5 A GeV/c.

Present experiment has been performed in a stack of BR-2 emulsion having 600 μm thickness exposed at Dubna Synchrophasotron to a beam of ^{12}C nuclei with momentum 4.5 A GeV/c. The mean free path of ^{12}C nuclei in emulsion have been found to 13.79+0.25 cm. 1250 inelastic collisions were selected, without any bias, for the final analysis. Details of experiment and technique used are already given in our earlier papers (3,4).

In the present report we discuss the diffraction dissociation of relativistic carbon nucleus into three ^4He fragments ($^{12}C \dashrightarrow 3\,^4He$) at 4.5 A GeV/c. In our sample of 1250 events , 26 belong to this category , which is 2.08% of the total inelastic collisions.

We assume that the momentum of each ^{4}He fragment emitted in a dissociated event is equal to one third of the projectile nucleus momentum P_0. Consequently, transverse momentum of each He fragment is given by

$$q_i = 1/3\ p_0 \sin\theta_i , \qquad (1)$$

where θ_i is the angle of emmission of the fragment. The vector sum of q_i in each event is equal to the transverse momentum transferred to the ^{12}C nucleus in the diffraction dissociation process. Therefore, to a first approximation, the transverse momentum of each ^{4}He particle

$$\vec{q}_i^{\,*} = \vec{q}_i - 1/3 \sum_{i=1}^{3} \vec{q}_i \qquad (2)$$

Figure (1) shows the transverse momentum distribution of ^{4}He particles inside the carbon projectile nucleus, q^*. In the case of diffraction dissociation events, it has been observed that in most of the events, two ^{4}He fragments are emitted within a very narrow angle along the beam direction, i.e., having low transverse momentum. The third ^{4}He fragment is emitted at relatively large angle, i.e., it has a relatively large transverse momentum, probably to compensate for the sum of transverse momenta of the other two ^{4}He particles. This indicates that the dissociation of ^{12}C to 3^{4}He goes through an intermediate ^{8}Be state.

From the investigation of diffraction dissociation events, we conclude that the percentage of such type of events are 2.08 of the total inelastic collisions. The study of such events also indicates that this reaction goes through an intermediate ^{8}Be state.

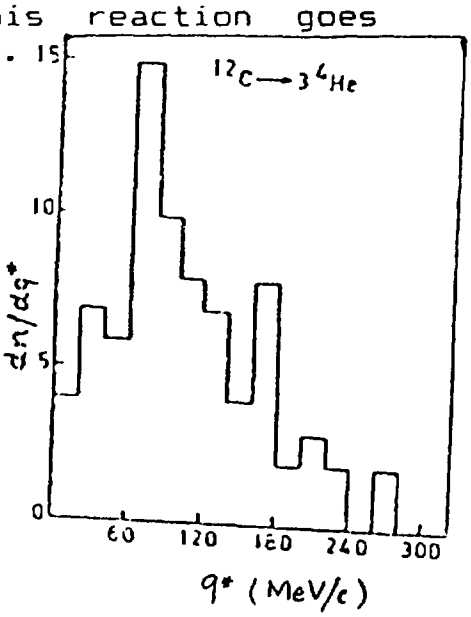

Fig.1. The transverse momentum distribution of ^{4}He particles inside the Carbon projectile nucleus.

References

1. K.G. Gulamov et al: Dokl. Akad. Nauk. Uzbek SSR, Nos 5,6,10(1983).
2. R.A. Bondarenko et al: Sov.J.Nucl. Phys. 38, 903(1983).
3. M.Q.R. Khan et al: Nuo. Cim. A99, 417(1988).
4. M.S.Ahmad et al : Nucl. Phys. A499, 82(1989).

EFFECT OF ELECTROWEAK EFFECT AND QCD ON RATIO R

A.K.Gautam, Rajesh Gaur, A.K.Shiromani
Physics Department R.B.S.College, Agra.

The ratio of production cross sections of hadrons and $\mu^+ \mu^-$ leptons following electron-Positron ($e^- e^+$) annihilation known as ration R, is quantity of fundamental importance as it provides a measure of the sum of squares of electric charges of quarks of which the hadrons are composite structure(1).

In this work we make use of the results of CELLO collaboration (2) regarding the value of the coupling constant to estimate the ratio R at 34 GeV Hoyer model and Lund model respectively. The value of R is likely to be affected by electroweak effects and quantum chromodynamic (QCD) corrections of the first order and second order and third order. Gautam and Goel (3) have studied the effects of QCD corrections upto second order and electroweakeffects. In this work we consider the influence of electroweak effect and QCD correction upto third order on the basis of the calculated values of the ratio R and their comparison with corresponding experimental results check efficacy of fragmentation model.

The production cross section of hadron from e^+ e^- annihilation is due to the decay of intermediate vector boson Z^0 is given by (4).

$$\sigma^{Z}_{had} = 12\ r_{QCD}\ \frac{k_s^2}{(S-M_Z^2)+s^2\Gamma_{tot}^2/M_Z}(V_e^2+a_e^2)\ (V_q^2+a_q^2)$$

Where V_e, V_q, a_e and a_q represent the vector and axial vector coupling constants of the electron and quark flavours, respectively, values of these constants, reviewed by Naroska(5), and r_{QCD} represents the contribution due to gluon radiation, which in the $\overline{MS}$ scheme is given by(6).

The average value of the ratio R for HM is $4.0325^{+0.0513}_{-0.0506}$ and for LM is $4.235^{+0.102}_{-0.106}$.

Zeroth order QCD value of R (= 3.67)

being lower than the value of R in this work provides evidence of QCD correction as well as for electroweak interference. Thus the calculate values of the ratio R for LM and HM are very close to the other calculated values and are in agreement with the corresponding experimental values of JADE and TASSO collaboration(7) and other theritical workers(3).

References:

1. N.Cabibbo, Parisi and G. Testa, Nuovo cimento. Lett. 4,35(1970).
2. H.J.Behrend et.al. DESY Report 8f2-061 (1982).
3. A.K.Gautam and S.P.Goel, Ind. J.Pure and Appl. Phys.25, 154 (1987), Ibid. Ind. J.Phys.62A 913 (1988), 62A,198(1988).
4. W.de Boer, Desy report 89-III(1989).
5. B.Naroska DESY Report 82-051(1982),85-090(1985) Electroweak efects at high Energies ed. Harvey B.Newman(New York: Plenum Press)P227(1985).
6. W.Celmaster and R.J.Gonsalves, Phys.Rev.Lett 44 560(1980).
7. P.Soding & G.Wolf Ann Rev. Nucl.Part Sci. 31, 231(1981).

Electron-Positron Annihilation into Hadrons

A.K.Gautam, Rajesh Gaur and A.K. Shiromani
Physics Department R.B.S. College, Agra.

During the past few years much attention has been focused on the analysis of the products of electron - positron annihilation (e^+e^-) experiments at high centre of mass energies because e^+e^- colliding beam experiments (1) provide an unique opportunity to study high energy systems of particles in a pure quantum state, having the quantum numbers of a photon. According to quark-parton model (2) hadron production from e^+e^- annihilation take place into two steps. In the first step, an intermediate pair of quark and antiquark ($q\bar{q}$) is produced and in the second step, the $q\bar{q}$ pair is fragmented to produce hadrons. The type of $q\bar{q}$ pair depends upon the colliding beam centre of mass energy.

In this work, we estimate the value of ratio R at 34 Gev. The results of CELLO collaboration (3) are used for this purpose. The QCD corrections upto third order are examined in the frame work of the ratio R for Lund, and Hoyer models.

The ratio of production cross section of hadrons (σ_{had}) and that of μ leptons (σ_μ) following in $\overline{MS}$ renormalization scheme (4) is reduced to

$$R = 3 \sum_f Q_f^2 \left[1 + \frac{\alpha_s}{\pi} + (1.986 - 0.115\, n_f) \left(\frac{\alpha_s}{\pi}\right)^2 + (70.985 - 1.2\, n_f - 0.005\, n_f^2 - 1.679 \frac{(\sum e_q)^2}{3\sum e_q^2}) \left(\frac{\alpha_s}{\pi}\right)^3 \right]$$

Where Q_f is the sum runs over the square of charge Q of a quark flavour 'f', f= u,d,s,c and b at the stated energy 34 Gev. and α_s is know as coupling constant which is actully not a constant but varies with energy both in QED and QCD, and is defined in renormalization scheme (5) as

$$\alpha_s = \frac{12}{(33-2n_f)\, \ln(s/\Lambda^2_{\overline{MS}}) + 6\left(\frac{153-19n_f}{32-2n_f}\right) \cdot \ln[\ln s/\Lambda^2_{\overline{MS}}}$$

The results of our calculations are presented in Table for Lund model (column 4) and for Hoyer model (column 6). The average value of the ratio R for the LM is $4.105^{+0.093}_{-0.110}$ and for the HM, is $3.924^{+0.062}_{-0.049}$. The value of ratio R for both th models are in good agreement with the exptimental values (6) of R . These corrections are is near agreement with the work of other workers (7).

References :-

1. Schwitters, R.F. and Strauch K. Ann. Rev. Nucl. Sci. 26 (1978) 889

2. Gellman, M.: Phys. Lett. 8 (1964) 214, Zweing. G CERN Report Th 401 & Th 412 (1964).

3. Behrend, H.J., Chen, C, Fenner, H. et.al.: DESY Report (1982), 82 - 061.

4. Boer (1989) DESU Report 89 - 111 and Brighton Conf. on Electroweak Radiative corrections.

5. Boer SLAC Report 4428 & Xth WARSAW Symp. on Elementary Particle Physics, Kazimierz Poland (1987).

6. Wolf, G.: J. Phys. 43C3 (1982), 525

7. Gautam A.K. & Goel S.P., Ind. J. Phys. A 62 (1988b) 913

Table

The [illegible] at 34 GeV for Jade and Hoyer Models

Sl. No.	Condition	Jade Model		Hoyer Model	
		α_s	R	α_s	R
1.	[illegible] $S, A<0.1$	0.2[illegible]$\pm$0.045	$4.2331^{+0.0391}_{-0.1332}$	0.190$\pm$0.030	$3.9[illegible]^{+0.0708}_{-0.0611}$
2.	$\square \geq 0.20$	0.26[illegible]$\pm$0.040	$4.1408^{+0.1307}_{-0.110}$	0.19[illegible]$\pm$0.020	$3.9[illegible]^{+0.0464}_{-0.0415}$
3.	$\square \geq 0.3$[illegible]	0.255$\pm$0.050	$4.140^{+0.1637}_{-0.1442}$	0.200$\pm$0.035	$3.952^{+0.068}_{-0.0733}$
4.	Fraction of three jet events	0.235$\pm$0.025	$4.070^{+0.0562}_{-0.0831}$	0.145$\pm$0.020	$3.870^{+0.0378}_{-0.0354}$
5.	Cluster Thrust	0.235$\pm$0.025	$4.070^{+0.0562}_{-0.0831}$	0.155$\pm$0.015	$3.8891^{+0.1454}_{-0.0488}$
6.	E.W.A.C.	0.2[illegible]$\pm$0.040	$4.0004^{+0.1135}_{-0.1051}$	0.150$\pm$0.020	$3.879[illegible]^{+0.033}_{-0.0354}$

[illegible] symbols used in Table are

S--------Sphericity

--------Aplanarity

$\square$ --------[illegible]ness

E.W.A.C.------- Energy weighted angular correlations.

NUCLEAR MASSES FROM QUARK SHELL MODEL

M. Rajasekaran, N. Meenakumari and V. Devanathan
Department Of Nuclear Physics, University of Madras
Guindy Campus, Madras 600 025

The statistical bag model of baryons proposed by us [1] had provided substantial support for the basic assumption of our theory in the region of 1 GeV or higher. Here we are interested in probing the low energy region, which is of main interest for the nuclear physicists.

We consider the nucleus as a bag of radius R, consisting of quarks and gluons [2], thus picturising the multi-nucleon system directly in terms of its basic QCD constituents. The single particle levels of MIT bag are taken as the input and the spin and isospin degrees of freedom are treated explicitly. For a system of non interacting particles, the energy of the many particle states is given by the sum of single particle energies and the energy arising from the collective rotations in spin and isospin spaces. Hence we write the energy of the nucleus as [1]

$$E = \sum_i \epsilon_i (n_i + \bar{n}_i) + \gamma \langle \tau \rangle + \delta \langle J \rangle + \epsilon_g + BV$$

where ϵ_g is the gluonic contribution, γ and δ are the Lagrangian multipliers to conserve the net isospin $\langle \tau \rangle$ and spin $\langle J \rangle$ of the nucleus, and n_i and $\bar{n}_i$ are the occupational probabilities of quarks and antiquarks. The level sequence used in this relativistic single particle model has the spin-orbit coupling inbuilt. With the above formalism we calculate the masses of a few ground state nuclei, which are compared with the experimental values in Table I. We have used T ≈ 0 MeV, at which we have only the valence quarks. Making use of single particle energy levels for massless quarks, which we have generated upto $\pm 13\hbar/2$ and assuming the mass of O^{17}, we have fixed B, which is used through out our calculations.

Following are the important results obtained in

our scheme.

(1) The radius of the nucleus still goes as $R = r_o A^{1/3}$,the value of r_o = 1.04 fm, being unique for all nuclei.
(2) The value of $B^{1/4}$ = 140.1 MeV, which is well in agreement with MIT data.
(3) The occupation probabilities of different single particle levels reveal that the net spin of the nuclei is still contributed by the three quarks corresponding to the unpaired nucleon.

Table I

Nucleus	R (fm)	Calculated Mass(MeV)	Experimental Mass(MeV)
12^C	2.381	11321.24	11177.23
13^C	2.445	12265.82	12111.79
14^N	2.506	13091.7	13042.97
16^O	2.621	14860.49	14898.26
17^O	2.674	input	15833.6
19^F	2.775	17721.37	17695.82
20^{Ne}	2.823	18640.6	18621.67

Though we have cited a few light nuclei only, the theory holds good even for heavy ions. For nuclei with non zero quadrupole moment, one can use the quark levels for a deformed bag, which are available in literature. Our model would enable one to deal with high spin states also, since the rotational energies have been accounted for.

One of us (N. M) acknowledges with thanks, the UGC for the award of SRF.

References:
[1] M. Rajasekaran, N. Meenakumari and V. Devanathan Mod. Phys. Lett., A5 (1990) 2537
[2] H. R. Petry et al.,Phys. Lett., 159B (1985) 363

FINITE SIZE NUCLEONIC EFFECTS IN THE NUCLEAR MEDIUM

M. Rajasekaran and N. Meenakumari
Department of Nuclear Physics, University of Madras
Guindy Campus, Madras 600 025, India

We investigate the finite size effects of nucleons inside a nucleus. This new approach is entirely different from Hagedorn's volume correction method [1] and is more rigorous. The size of the nucleon is varied and the magnitude of the hard-core potential is extracted by minimising the energy with respect to the nuclear radius. We also determine the effective mass of the nucleon as a function of the attractive potential well depth.

We start with the following expression for nuclear energy which takes into account the kinetic energy of the individual nucleons, the repulsive hard core contribution and the attractive potential energy.

$$E = \frac{3Ak_F^2}{10M} + \frac{V_R A(A-1)}{2}\frac{b^3}{R^3}\left(1 - \frac{9b}{16R} + \frac{b^3}{32R^3}\right) - AV_0 \quad (1)$$

We picture the nucleus as a Fermi gas of A nucleons moving in a potential well of depth $-V_0$, whose kinetic energy is given by the first term of Eq. 1. Taking the N-N repulsive forces into account, we sum over all pairs of nucleons and write the net hard-core energy as

$$E_R = \frac{A\ (A-1)\ P\ V_R}{2}$$

where V_R is the magnitude of the positive hard core potential which acts between $^AC_2$ pairs of nucleons, when they approach each other within a hard-core radius b, the macroscopic probability of finding a pair of nucleons closer to b being given by P. Combining all these to get the total energy of the nucleus, we find that the system is unstable since the minimum energy of the system occurs for very large values of R. To avoid this we add a "confining term" BV [2] where B gets fixed by the energy minimisation of the nucleus with respect to R.

Using the energy equation and assuming the nuclear radius and the binding energy per nucleon, we solve for the two unknowns V_R and B and find that the contribution from the hard-core energy and the confining part is appreciable. In the Fig., for some typical values of V_o we have plotted V_R against b. We find that V_R decreases as b increases and there is a steep rise in V_R for b < 0.4 fm. This correct behavior of hard-core potential justifies the way in which finite size effects are incorporated. Also V_R increases with the well depth which could be anticipated, as V_o increases the kinetic energy should increase to keep the equilibrium size intact. Now combining the first two terms of Eq. 1 as the kinetic energy arising from the nucleons of effective mass m^* we get $m^* \simeq 0.8m$, which any way would be a function of well depth. These observations prove that applying volume correction terms have no meaning as the particles are not billiard balls but fuzzy objects consisting of a quark core surrounded by a pion cloud, their interactions being different in different energy regions.

References:
[1] R. Hagedorn, Z. Phys. C17, 265 (1983)
[2] H. Hofestadt et. al., Z. Phys. A 326, 391 (1987)

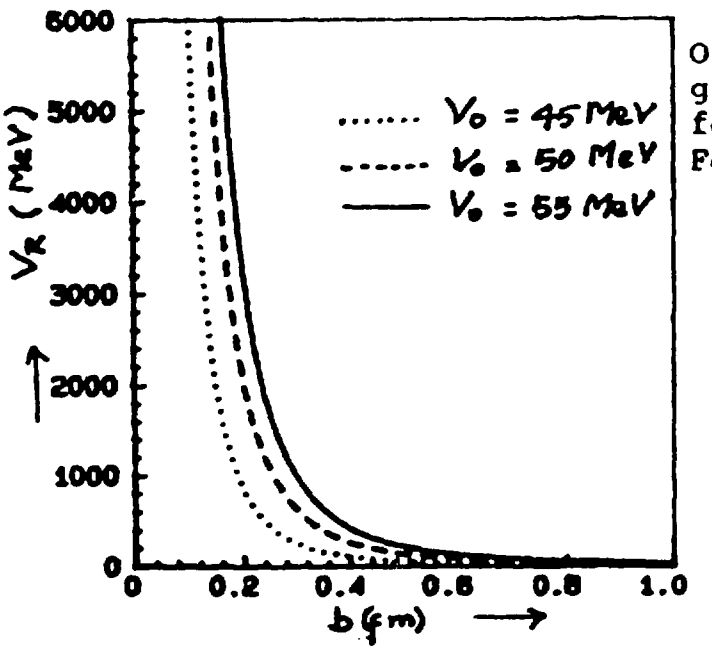

One of us (N. M) is grateful to U.G.C for the award of Fellowship.

BOOST NON-INVARIANT FLOW IN ULTRA RELATIVISTIC HEAVY ION COLLISIONS; AN APPROXIMATE METHOD

Jan-e Alam[a], Somenath Chakrabarty[b], Dinesh K. Srivastava[a], and Bikash Sinha[a]
(a) Variable Energy Cyclotron Centre, 1/AF Bidhan Nagar, Calcutta 700 064
(b) Saha Institute of Nuclear Physics, 1/AF Bidhan Nagar, Calcutta 700 064

Ultra-relativistic heavy ion collisions offer the possibility to study the nuclear matter at very high temperatures and/or high densities, where the individual nucleon looses their identity and subnucleonic degrees of freedom play a dominant role. The hadronic matter produced in these collisions is treated as a relativistic ideal fluid characterised by smothly varying fields, the four velocity $u^\mu(x)$, the pressure $P(x)$, the energy density $\epsilon(x)$, the temperature $T(x)$, etc.The themodynamical quantities are related by equations of states $P = P(\epsilon)$. The space-time evolution of the central rapidity region of the collisions is described by Bjorken's scaling solutions, in which it is assumed that there exists a central plateua structure in the rapidity distribution of secondary particles which gives rise to boost invariant initial conditions. But so far this plateau is not observed in case of heavy ion collions. In this work we attempt to relax the boost invariance of the initial conditions and solve the hydrodynamical equations for small deviation from similarity flow. The hydrodynamical equations to be solved for isentropic expansion of an ideal fluid are

$$\partial_\mu T^{\mu\nu} = 0 \quad \text{energy} - \text{momentum} \quad \text{conservation} \tag{1}$$

and

$$\partial_\mu s^\mu = 0 \quad \text{isentropic} \quad \text{expansion} \tag{2}$$

where

$$T^{\mu\nu} = (\epsilon + P)u^\mu u^\nu + g^{\mu\nu}P \tag{3},$$

$$s^\mu = su^\mu, \quad s \text{ is the entropy denisty} \tag{4}$$

$$g^{\mu\nu} = \text{diag}(+1, -1, -1, -1) \tag{5}$$

Introducing the new variables (τ, η), where

$$\tau = \sqrt{(t^2 - z^2)}, \quad \text{proper} \quad \text{time} \tag{6}$$

and

$$\eta = \frac{1}{2} ln \frac{t + z}{t - z} \tag{7}$$

the space time rapidity.

For (1+1) dimensional expansion of the fluid eqs.(1) and (2) give, in terms of new variables

$$\frac{\partial}{\partial\tau}(s\tau cosh(y-\eta)) + \frac{\partial}{\partial\eta}(s\ sinh(y-\eta)) = 0 \tag{8}$$

$$\frac{\partial}{\partial\tau}(T\tau sinh(y-\eta)) + \frac{\partial}{\partial\eta}(Tsinh(y-\eta)) = 0 \tag{9}$$

where $y = tanh^{-1}v$, called fluid rapidity.

From eqs. (8) and (9) it is clear that for $y = \eta$ (similarity flow) we get $s\tau$ =const. this is Bjorken's scaling solution [1]. Now one may ask what is the consequence of a small deviation from similarity flow? i.e. if $y = \eta + \Delta(\tau, \eta)$, where Δ is small. What is the rapidity distribution of secondary particles under this approximation?

For small Δ eqs. (8) and (9) become

$$\frac{\partial}{\partial\tau}(s\tau) + \frac{\partial}{\partial\eta}(s\Delta) = 0 \tag{10}$$

$$\frac{\partial}{\partial\tau}(T\tau\Delta) + \frac{\partial}{\partial\eta}(T) = 0 \tag{11}$$

respectively. The solution we get

$$s(\tau,\eta) = \frac{a}{\tau^{1+b/(1-c_s^2)}} e^{C/\tau^{1-c_s^2}} e^{-d(\eta+C_1/K)^2} \tag{12}$$

Some general observations can be made about the solutions immediately. For symmetric situation; A + A head collisions, it is expected that solutions should be symmetric around $y = 0$ and thus $C_1 = 0$ we also see that $K = 0$ gives Bjorken's scaling solution [1].

With the solution written above the rapidity distribution of the secondary particles at the freeze-out reads

$$\frac{dN}{d\eta} = C\pi R_A^2 \tau_f \left[\frac{A}{\tau^{1+b}} e^{-b\eta^2}\right] \tag{13}$$

here A, a, b, C_1, and K are constants. This distribution is gaussian in nature, which is true in SPS energy range; no central plateua structure is observed.

Reference:

[1] J. D. Bjorken, Phys. Rev. **D27** (1983) 140.

BOOST NON INVARIANT HYDRODYNAMICS IN ULTRA RELATIVISTIC HEAVY ION COLLISIONS-AN EXACT METHOD

Dinesh K. Srivastava[1], Jan-e Alam[1], Somenath Chakrabarty[2], Sibaji Raha[3], and Bikash Sinha[1]

(1)Variable Energy Cyclotron Centre, 1/AF Bidhan Nagar, Calcutta 700 064

(2)Saha Institute of Nuclear Physics, 1/AF Bidhan Nagar, Calcutta 700 064

(3)Bose Institute, 93/1 Acharya Prafulla Chandra Road, Calcutta 700 009

Ultrarelativistic heavy ion collisions are routinely studied using the Bjorken's boost invariant hydrodynamics [1]. Such a description would be rigourously justified only if a central rapidity plateau were observed in the particle rapidity density for $A-A$ collisions which in turn implies the boost invariance assumed in such studies. However, as such a plateau is not observed for $A-A$ collisions, at the presently available energies, boost invariance of initial boundary conditions may not be necessarily valid. This would then also raise questions about the accuracy of the energy density estimates and space time developments of the plasma used in most of the studies related to the signals of QGP. We have obtained analytical solutions of the boost non invariant hydrodynamical equations for a $(1+1)$ dimensional expansion of the plasma. For this we obtain [2] the potential 'χ' for the hydrodynamical flow of plasma, by using the energy-momentum and entropy conservations as

$$\frac{\partial^2\chi}{\partial y^2} = (1-c_s^2)\frac{\partial\chi}{\partial\omega} + c_s^2\frac{\partial^2\chi}{\partial\omega^2} \tag{1}$$

where $\omega = ln(T/T_0)$, and y is the fluid rapidity. The boost invariance assumed by Bjorken is now seen to arise by assuming indepdence of χ from y and yields

$$\chi = Be^{-2\omega} \tag{2}$$

which has its origin in the assumption $dz/dt = z/t$ and leads to the scaling $T^3\tau = \text{const}$, for $c_s^2 = 1/3$. Now if we put

$$\chi = \chi_1 e^{-\omega}, \quad p = (\omega^2 - c_s^2 y^2)^{1/2}, \quad q = \tanh^{-1}(c_s y/\omega) \tag{3}$$

equation (1) leads to

$$\frac{1}{p^2}\frac{\partial^2\chi_1}{\partial q^2} - \frac{\partial^2\chi_1}{\partial p^2} - \frac{1}{p}\frac{\partial\chi_1}{\partial p} + \chi_1 = 0 \tag{4}$$

The solutions of this equation assume a particularly simple form if we analogusly assume that the hydrodynamical flow is such that $d\omega/dy = \omega/y$, and we get a class of boost non-invariant solutions,

$$\chi = AI_0(p)e^{-\omega} \tag{5}$$

We can add (2) to (5) to get a more general solution. We show that for such a case the boost non-invariance provides a more rapid cooling of the plasma and leads to the particle rapidity density varying with rapidity as desired by experiments. Implications of these results for RHIC and LHC will be discussed.

References:
[1] J. D. Bjorken, Phys. Rev. **D27** (1983) 140.
[2] D. K. Srivastava, J. Alam, S. Chakrabarty, S. Raha and B. Sinha, to be published.

CURVATURE RADIATION AND (γ/π^0) SIGNAL OF QUARK-GLUON PLASMA

Somenath Chakrabarty[a], Sibaji Raha[b] and Bikash Sinha[c]
(a)Saha Institute of Nuclear Physics, 1/AF Bidhan Nagar, Calcutta 700 064
(b)Bose Institute, 93/1 Acharya Prafulla Chandra Road, Calcutta 700 009
(c)Variable Energy Cyclotron Centre, 1/AF Bidhan Nagar, Calcutta 700 064

Using the idea of curvature radiation from an accelerated charge in a magnetic field, the surface emissions of photons and pions from a confined quark-gluon plasma (QGP) is studied. It is expected that due to colour confining force a quark will be pulled back to QGP phase if it tries to escape from the boundary of QGP surface. Then this quark will follow a curved trajectory near the surface and as a consequence it can emit both photons and pions. These processes are analogous to that of the emission of electromagnetic radiation from an accelerated charge in a magnetic field (synchrotron radiation). Classically, the emission of pion is forbidden. Here we have also calculated the volume part of photon emission processes (annihilation + Compton) from QGP. We have seen that the surface contribution of photon emission is almost equal in magnitude as that of volume.

From some initial temperature T_i (we have chosen $T_i = 1.2T_c$, $1.5T_c$ and $2T_c$) corresponding to some initial proper time τ_i, to T_c, the critical temperature for quark-hadron phase transition ($= 160MeV$ in our calculation) corresponding proper time τ_c, the system is in a pure QGP phase. After τ_c the mixed phase (quark + hadron) starts (assuming first order phase transition). Photons and pions can be emitted from the mixed phase as well. We have included both the volume and surface processes for photon emission from the mixed phase. For QGP phase, pion emission is a surface phenomenon, where as in the case of hadronic component it is like black body radiation. We have discarded the possibility of photon emission from hadronic phase.

In the figure below we have shown the ratios of transverse momentum (p_T) distribution for photons and neutral pions (π^0) for a number of initial temperatures (indicated by the numbers). Solid curves indicate the emission from pure QGP phase, where as the dotted curves are for QGP plus mixed phases.

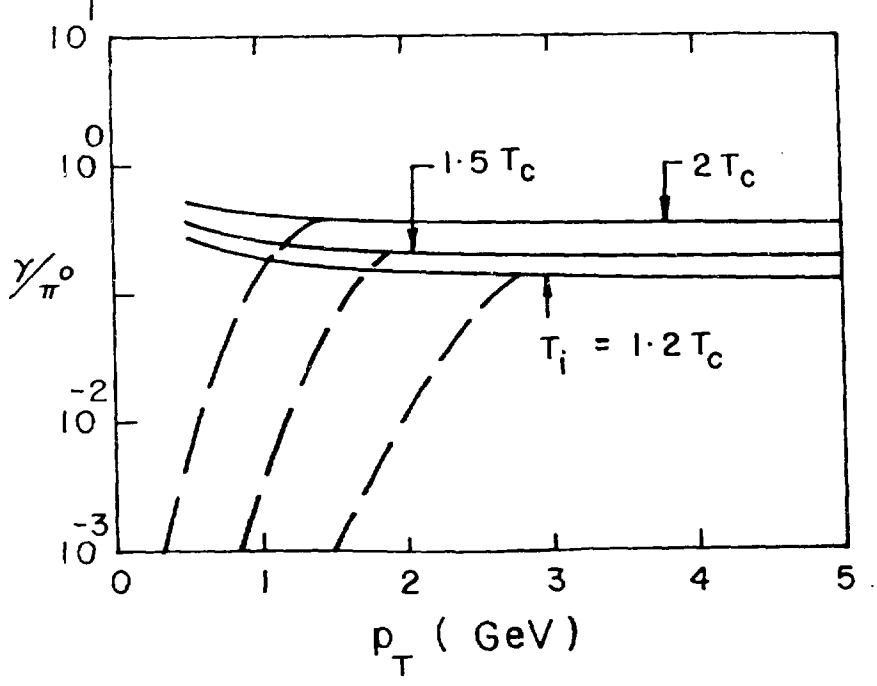

Fig. 1

Ratio of the p_T distributions of emitted photons and π^0 from QGP and QGP + Mixed phases. T_i indicates the initial temperature of the plasma. Solid curves indicate emission from pure QGP where as the dotted curves are for QGP + Mixed phases.

These curves show that the ratios saturate to a constant value for the range of p_T relevant for QGP diagnostics. The constant ratio is a function of T_i.

AN INVESTIGATION OF MANY PION DYNAMICAL CORRELATION IN HEAVY ION INTERACTION

Dipak Ghosh, Sanjib Sen, Madhumita Lahiri, Argha Deb, Biswanath Biswas , Jayanta Ray Choudhury (Jadavpur University) & Jaya Roy(RCC, Cal-32)

This paper deals with the study of many pion dynamical correlations in ^{24}Mg-AgBr interaction at 4.5 Gev/c per nucleuon using the cumulative rapidity gap distribution technique.

Correlations between produced particles have been investigated by styding the distribution of rap-gaps between particls when the rap-gaps are differtiated according to the no. of particles inside the gap. There is a basic difference in cases where two particles have a rapidity difference of Δy and where no other particles are found between them compared to the cases where one or more particles were distributed in this rapidity interval. For fixed multiplicity n, ${}_nG_k$ can be defined as the gap-length between two particles having (k-1) particles distributed in the interval between them. Now we can define the normalised semi-inclusive (ie for fixed multiplicity) rapidity-gap correlation function of order k as,

$$ {}_nR_K(G) = \frac{{}_nf_K(G)}{{}_n\tilde{f}_K(G)} - 1 $$

In ratio, the numerator represents the experimental distribution of rapidity-gaps and the denominator represents the corresponding distribution calculated from one dimensional density distribution where no correlations were present.

To avoid large statistical error, the function can be redefined, taking the contribution from different multiplicities like,

$$ F_K(G) = \frac{\sum_{n>K} \bar{n}(n)\,(n-K)\,{}_nf_K(G)}{\sum_{n>K} \bar{n}(n)\,(n-k)} \quad , \quad \& $$

$$ \tilde{F}_K(G) = \sum_{n>k} \bar{n}(n)\,(n-K)\,{}_n\tilde{f}_K(G) \Big/ \sum_{n>K} \bar{n}(n)\,(n-K) $$

where $\pi(n)$ is the experimentally determined multiplicity distribution and the corresponding correlation function is,

$$R_K(G) = [F_K(G) / \widetilde{F}_K(G)] - 1$$

The non-zero values of $R_K(G)$ ensures correlation.

Fig 1(a,b) shows the values of $F_k(G)$ & $\widetilde{F}_k(G)$ for k=1,2,3 (a) & k=1,2,3 (b). The data unambiguously speaks the form of many-particle dynamical correlation among pions produced in Mg-AgBr interaction at 4.5 Gev/c per nucleon.

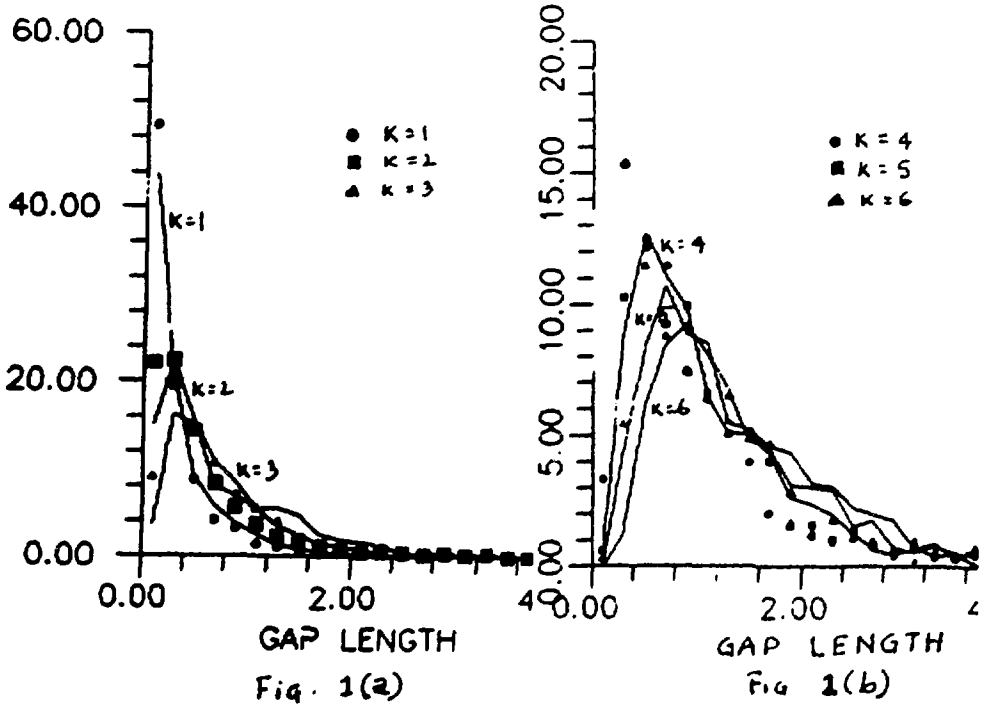

Fig. 1(a)

Fig 1(b)

MULTIPION PRODUCTION IN NUCLEAR COLLISION AND GENERALISED DIMENSION OF FRACTALITY.

Dipak Ghosh, Jaya Roy, Premomoy Ghosh, Argha Deb.
Jadavpur University, Cal-32, R.C.C., J.U., Cal-32.

Study of fractality in particle production in high energy interaction was first introduced as "Intermittency" in terms of normalised $q-1$ q F-moments, $F_q = M^{q} . \sum_{j=1}^{M} n_j (n_j-1)..(n_j-q+1)/\langle n \rangle^{q}$ ...(1). From the fundamental property of fractality, already developed in other branches of physics, Bialas and Peschanski[1] suggested the scaling behaviour $F_q \propto \delta\eta^{-a_q}$ ...(2), in case intermittency exists. Fialkowski[2] et al suggested correction of normalised factorial moments by $R_q = 1/M^{q} . \sum_{j=1}^{M} M^{q} . (\langle n_j \rangle / \langle n \rangle)^{q}$ .....(3) giving $\langle F_q \rangle = \langle F_q \rangle / R_q$, the reduced F-moments, for non-uniform shape of particle distribution in (pseudo)rapidity phase space. a_q in equation (2) are intermittency exponents being related to Generalised dimensions of fractality by $D_q = 1 - a_q/(q-1)$....(4) where $a_q/(q-1) = d_q$ are anomalus fractal dimensions. It is speculated that in case of transition from QGP to hadron phase in thermodynamic equilibrium, d_q are independent of q and if hadrnization takes place through cascading process, d_q is expected to be linear with q.

In order to extract multifractal structure in multiparticle production in terms of generalised dimensions, G-moments are another set of moments which are calculated by summing the probabilities p_j to find n_j particles in bin j, over non-empty bins M. G-moments being defined[3] as $G_q = \sum_{j=1}^{M} p_j^{q}$, for values of q. If the

fractality ispresent, $G_q \propto \delta\eta^{\tau(q)}$.....(5). In particle physics, in contrary to other branches of physics, the power law ..(5) does not hold at $\delta\eta \longrightarrow 0$, since the lowest n_j for nonempty bin is 1. $\tau(q)$ and then smooth spectral function $f(\alpha_q)$ is obtained for all the events by

$$\langle \ln G_q \rangle = 1/N.\sum_{i=1}^{N} \ln \sum_{j=1}^{M} p_{ij}^{q} \quad .....(6)$$

$\langle \tau(q) \rangle = \Delta\langle \ln G_q \rangle / (-\Delta \ln \delta\eta)$.....(7) and then through Lagendre transform,

$\langle f(\alpha_q) \rangle = q\langle \alpha_q \rangle - \langle \tau(q) \rangle$.....(8) where

$\langle \alpha_q \rangle = d\langle \tau(q) \rangle / dq$. If there is no fluctuation in pseudorapidity distribution, then $f(\alpha_q)=\alpha_q=1$ for all q. If there are fluctuations then $f(\alpha_q)$ is downward concave function and its spread is a measure of the size of them. From $f(\alpha_q)$, one gets the generalised dimensions at q=0, $D_0 = f(\alpha_q)$= the Fractal dimension, at q=1, $D_1 = f(\alpha_q)$=the Information dimension, at q=2, $D_2 = 2.\alpha_2 - f(\alpha_2)$= the correlation dimension. If $D_0 > D_1 > D_2$..... the fractal is uniform. We analyse ^{16}O-Ag/Br interaction data at 2.1 GeV/c in terms of F-moments and G-moments in pseudorapidity phase space $\Delta\eta=4$. F-moment analysis predicts cascading process of hadronization, while G-moments analysis indicates multifractality. However the generalised dimensions obtained from two sets of moments do not match, most likely due to different range of analysis. F-moment analysis was within $1 \geq \delta\eta \geq 0.1$ and D_q from G-moments were calculated at M=2 and 3 i.e. at $\delta\eta > 1$. Moreover F-moments are valid correlation functions while G-moments are dominated by single particle effect. Whatever be the reason, this difference in generalised dimensions still keeps open thequestion of fractality in multiparticle production.

Reference: [1] A.Bialas and R Peschanski, Nucl. Phys. B273(1986)703. [2] K.Fialkowski et al. Acta. Phys. Polo. B20(1989)639. [3] C.B.Chiu and R.C.Hwa, Phys.Rev.D42(1991)100.

COHERENT AND CHAOTIC PIONISATION IN RELATIVISTIC NUCLEAR COLLISION

Dipak Ghosh, Joya Roy, Biswanath Biswas, Jayanta Roychoudhury, Sadhan Naha, Dipak Banerjee, Madhumita Basu, Anuradha Bhattacharjee, Ranjan Sengupta, Tarit Guhathakurta, Anuradha Dutta, Anit Ghosh, Amitava Mukhopadhayaya, Argha Deb, Sarmila Sarkar, Niyanta Bose, Premomoy Ghosh, Atanu De, Sk. Anwar Hossain, Debasish Halder, Supriya Halder, Alokananda Ghosh, Sanjib Sen, Madhumita Lahiri, Susobhan Das, Krishnadas Purakait, Hiten Mukherjee, Rabin Roy, Manidipa Debbarma, Shibaprasad Ghosh.
Deparment of Physics, Jadavpur University

This paper presents an extensive study of coherent and chaotic pionisation process in asymmetric nuclear collision. The data includes O^{16}-CNO, C^{12}-CNO and Mg-AgBr at 2.1 and 4.5 GeV/c. In particular the multiplicity distributions of pion in different overlaping phase-spaces have been compared with Poisson distribution, chaotic distribution and also their superpotion. The poisson and chaotic distribution are represented by

$$P(n_i)=\exp(-\langle n_i\rangle)\langle n_i\rangle^{n_i}/n_i!$$

and $$P(n_i)=1/1+\langle n_i\rangle[\langle n_i\rangle/\langle n_i\rangle+1]^{n_i}$$

From a comparison of the multiplicity distribution P(n) in different overlapping napidity bins in O, Mg, C induced interaction with Poisson, chaotic and superposition of Poisson and chaotic it was observed chaoticity predominates as one goes from central to full phase space domain. The entropy content was also calculated using the relation

$S=\sum P(n)\ \ln P(n)$ and an analysis was performed in terms of new parameter defined as reduced entropy i.e, $S/\langle n\rangle$. The bin-wise reduced entropy values in three interactions reveals some very interesting features.

Reduced entropy			
	C^{12}-em	O^{16}-em	Mg^{24}-em
Bin 1	.67	.47	.53
Bin 2	.59	.36	.40
Bin 3	.48	.29	.33
Bin 4	.45	.27	.29
Bin 5	.44	.26	.27
Bin 6	.43	.25	.26
Bin 7	.42	.25	.25
Bin 8	.41	.24	.24

EVIDENCE OF SHORT MEAN FREE PATH AND FRACTALITY OF PROJECTILE FRAGMENTS IN HEAVY-ION INTERACTION

D.Ghosh, Jaya Roy*, D.Banerjee, Argha Deb, P.Ghosh
Jadavpur University, *RCC Calcutta

Experimental evidences concerning shortened mean free path effect and hence enhanced reaction cross section of Projectile fragments in high energy heavy ion interaction, continued to be of great importance as the phenomenon remains unexplained from a theoretical point of view and its supposed connection with the possible appearance of open colour states from quark-gluon matter. In this paper we report further evidence of SMFP of Z = 2 Projectile fragments produced in emulsion exposed to ^{24}Mg at 4.5 Gev/c/n for the first time. Mean free path measurement, following the much used method[1], shows that the MFP of Z = 2 Pf from ^{24}Mg - emulsion interaction is shorter than that of Primary alpha beam at the same momentum. Fig.1 shows the variation of the MFP with distance from interaction point, dashed line show the MFP of primary alpha beam. Fig.2 shows the excess of number of interactions observed over the expected value for the different distances ffrom the origin of Pf = 2. Fig.3 is the plot of F parameter, a test of anomaly which is insensitive to scanning efficiency. These plottings establishes SMFP effect for Z = 2 pf's from ^{24}Mg - emulsion interaction. The result was compared with the MFP measurements of alpha particles from ^{22}Ne[2], ^{12}C[3] at the same momentum and the relative abundance of "anomalons"[1] the proposed projectile fragment, supposed to have a very short MFP, being produced during the interaction and hence exhibiting the SMFP effect. Table - I shows the comparision. Assuming anomalons in Z = 2 pf's as ^{6}He formed during interaction in quasi molecular state[4] of MFP = 12.5 cm, the variation of MFP of Z = 2 pf from both ^{12}C & ^{24}Mg emulsion interaction results can be fairly interpreted considering a 50% admixture of ^{6}He with ^{4}He in pf Z=2, excepting for the first cm from the point of emission.

Further an investigation of fractality of secondary alpha particles was made with the help of factorial moment and fractal moment and the data indicates a positive signature as evident from Fig.4.

References

1. Friedlander E.M. etal Phy.Rev.c.vol.27P1489(1983)
2. El Nadi M. etal Proc. of 7th H.E. Heavy ion Study P618-648 GST DARMSTADT (1984)
3. Ghosh D. etal Phy.Rev.Lell.Vol 54,P.396(1985)
4. Bayman B.F. etal Phy.Rep.Vol.147.P.155-187(1997)

TABLE - I

Beam	Momenta	Alpha %	MFP
^{12}C	4.5 Gev/c/n	8	2cm
^{24}Mg	4.5 Gev/c/n	10	1.01 cm
^{22}Ne	4.5 Gev/c/n	6.3	2.5 cm

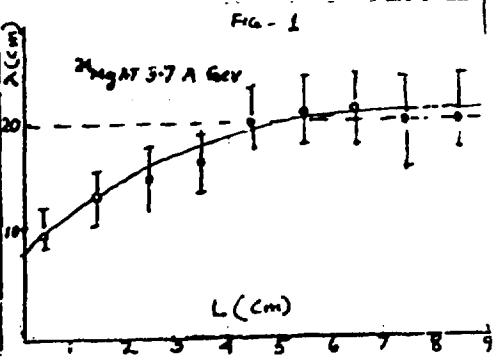

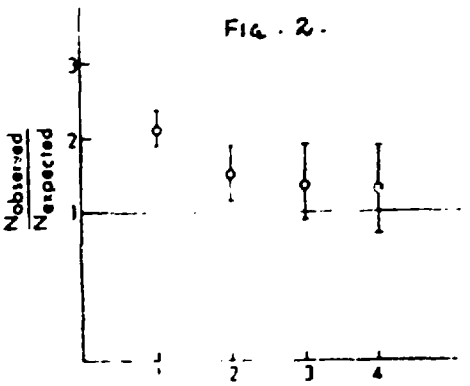

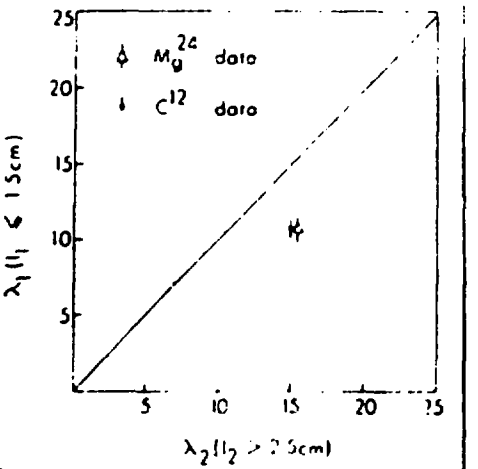

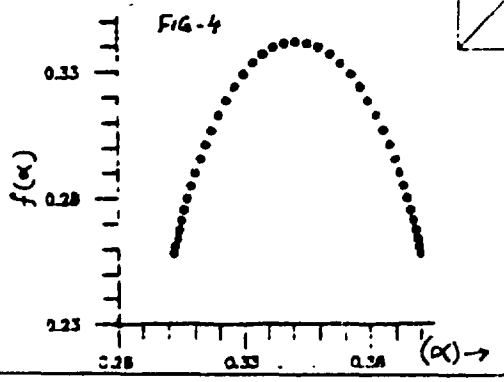

MULTIPLICITY DISTRIBUTIONS OF SECONDARY PARTICLES PRODUCED IN CARBON- AND SILICON-NUCLEUS INTERACTIONS AT 4.5A GeV/c

Tauseef Ahmad, M. Irfan and A.H. Naqvi
Department of Physics, A.M.U.; Aligarh-202002 (U.P.)

Interest in the study of high energy heavy-ion collisions has considerably grown during recent past. It is due to the possibility of appearance of collective properties of high energy nuclear matter at an extremely high density and temperature. The main aim of the present study is tc investigate the basic characteristics of the multiparticle production processes in the inelastic interactions of carbon and silicon nuclei at 4.5A GeV/c. For this purpose, random samples consisting of 852 and 1024 events produced in carbon- and silicon-nucleus collisions were collected for carrying out various measurements.

Multiplicity distributions of shower, grey, black and heavy tracks produced in carbon- and silicon-nucleus interactions are investigated. These distributions are compared with the corresponding distributions obtained for proton- and α-nucleus interactions[1-2] at the same beam momenta per nucleon. From the study of these distributions, it is noticed that multiplicity distributions of shower, grey and heavy tracks depend on projectile mass.

Mean multiplicities of charged secondary particles for both carbon- and silicon-nucleus interactions are listed in Table I, alongwith the results obtained by other workers[1-3]. It is interesting to note that the average multiplicity of shower tracks grows rapidly with increasing projectile mass. This behaviour incidentally is compatible with the predictions of the superposition models. The average multiplicity of grey tracks also increases with increasing projectile mass. This trend can be explained in terms of the predictions of the fireball model.

Variations of $\langle N_s \rangle$, $\langle N_g \rangle$ and $\langle N_b \rangle$ with projectile mass at 4.5A GeV/c are displayed in Fig.1.

Table I

Momentum A(GeV/c)	Projectile	$\langle N_g \rangle$	$\langle N_b \rangle$	$\langle N_s \rangle$
4.5	p	2.81±0.06	3.77±0.08	1.63±0.02
3.6	d	2.34±0.07	5.78±0.15	3.08±0.05
3.6	α	4.64±0.17	4.68±0.15	3.86±0.08
4.5	α	4.70±0.20	4.70±0.20	3.90±0.10
4.5	C	5.93±0.34	4.49±0.24	7.67±0.19
2.1	N	5.29±0.31	4.57±0.22	8.85±0.28
4.5	O	7.60±0.60	4.88±0.29	10.50±0.60
4.5	Si	8.59±0.26	4.69±0.23	11.26±0.03

The solid lines in the figure is determined by the following equation:

$$\langle N_x \rangle = \text{const. } A^{\alpha} \qquad (1)$$

where x represents shower or grey or black track. The best fitting values of α are 0.61±0.04, 0.33±0.02 and 0.06±0.02 respectively for the variations of the average number of shower, grey and black tracks with projectile mass. From these observations, it may be concluded that the larger the momenta of the secondary particles emitted in heavy-ion collisions, the stronger is the projectile mass dependence of the average particle multiplicities.

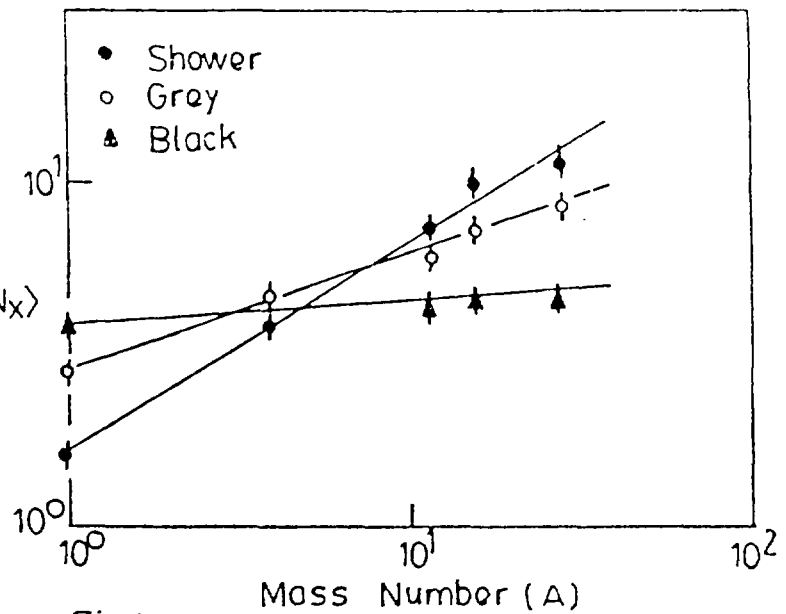

Fig.1.

References

[1] A-ABDDKLMTU collaboration:Z.Phys.A302 (1981) 133
[2] DGKLMTW Coll.:JINR Dubna comm., P1-8313 (1974)
[3] V.A.Antonchik et al:Sov.J.Nucl.Phys.39(1984) 774

HOT STABLE STRANGE QUARK MATTER IN THE EARLY UNIVERSE PHASE TRANSITION

K. Sakthi Murugesan and P. R. Subramanian
Department of Nuclear Physics, University of Madras, Guindy Campus, Madras 600 025.

Strange-Quark Matter (SQM) is a hypothetical stable phase of baryonic matter consisting of equal numbers of u, d and s quarks. The concept of SQM has been used to provide explanations for the missing dark matter in cosmology [1,2]. General theoretical arguments and recent model calculations suggest [1-3] that SQM could be the ground state of QCD at non-vanishing baryon-number, which may be existing in the inner core of neutron stars.

To form the stable strange quark matter in the early Universe QCD phase transition, the energy per baryon in the hadronic matter should be greater than that in the Quark-Gluon Plasma (QGP) phase. Otherwise SQM would be unstable [2].

We consider [4] the phase transition of a QGP consisting of u, d and s (sufficiently light) quarks and gluons into a hadron phase made up of all well established hadrons and their resonances with mass < 2 GeV. Our system has a very small chemical potential because of the small baryon - antibaryon assymmetry in the early Universe. We use the relativistic quantum statistics for particles in both the phases and include Hagedorn's correction for the finite size of the hadrons in the HRG phase. We also include the interaction between the quarks and gluons in the QGP phase via the running coupling constant. We calculate the energy density and baryon number density for both the phases on the basis of the Gibbs criteria for different values of the phase transition temperature. In Fig. 1, we present our results for energy per baryon as a function of the transition temperature T_c. We found that, during the early Universe QCD phase transition, the energy per baryon in the hadronic phase is greater than that of QGP phase for $T_c < 145$ MeV and hence SQM is stable. Hence there is a possibility for the formation of hot SQM in the early Universe phase transition at $T_c < 145$ MeV. This result is in favour of our earlier

work [4] in which we report that if T_c < 125 MeV, the non-SBB theory could not reproduce the light element abundances. Following our result, we conclude that if T_c < 145 MeV the SQM can be formed in the early Universe, paving the way for the formation of neutron stars and the dark matter out of SQM.

References:
1. E. Witten, Phys. Rev. D30, 272 (1984).
2. L. F. Abbott, Quark Matter '84, Lecture Notes in Physics Vol.221, p106 (Springer, Berlin, 1984).
3. J. Madsen and M. L. Olesen, Phys. Rev. D43, 1069 (1991).
4. K. Sakthi Murugesan, G. Janhavi, and P. R. Subramanian, Phys. Rev. D41, 2384 (1990); D42, 3576 (1990).

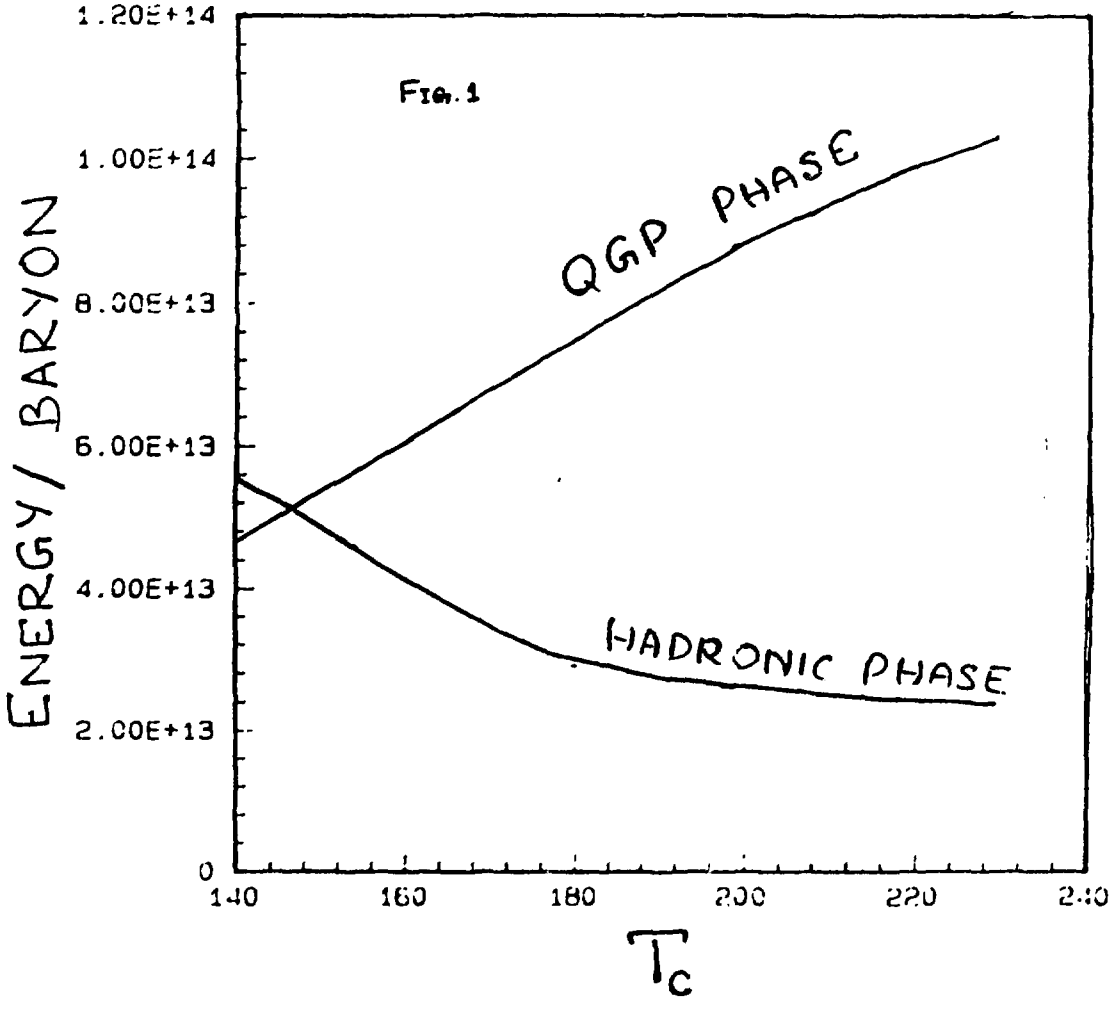

THE DECONFINEMENT CRITICAL ENERGY DENSITY DEPENDENCE ON THE HARD CORE RADIUS

S. Karthiyayini and V. Devanathan[$]
Department of Nuclear Physics, University of Madras, Madras
[$]Crystal Growth Centre, Anna University, Madras

In heavy ion collisions, a phase transition occurs between hadronic matter (H) and quark gluonic matter (QG). Such phase boundary curves in the temperature (T) - chemical potential (μ) plane is calculated by using different models [1-3]. The hadronic matter of thermodynamical model consists of non strange and strange, mesonic and baryonic resonances. Due to strong short range repulsion between the baryons, all the thermodynamic parameters, viz. the pressure, number density and energy density of H are modified to include the excluded volume effect [1]. Thus the available volume in a system of volume V with N hadrons of volume V_o ($=4\pi R^3/3$), is $V - NV_o$. The critical curves are drawn for the above described model considering various hard core radii R with a fixed bag constant $B^{1/4}$ = 200 MeV. The critical energy densities (ε_c) are calculated for both phases, for R = 1.0, 0.8 and 0.6 fm and are shown in figures 1, 2 and 3 respectively. In Fig. 3, the ε_c for H phase almost reaches that of QG phase and as it appears contrary to the generally considered physical solution [2], we omit the R = 0.6 case. Treating the actual picture of R divergence with increasing temperature [3] in the excluded volume correction, the ε_c are calculated for R(T). Comparison of this curve (shown in Fig. 2 as dashed curve) with Figs.1 and 2 makes us conclude that it is more appropriate to consider 0.8 fm as R. Thus we confirm that the hard core radius is not completely independent of the bag constant.

Fig. 1. R = 1.0 fm

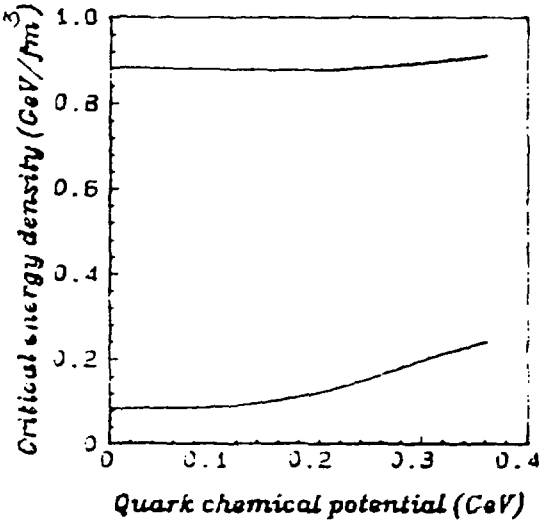

Fig. 2. R = 0.8 fm

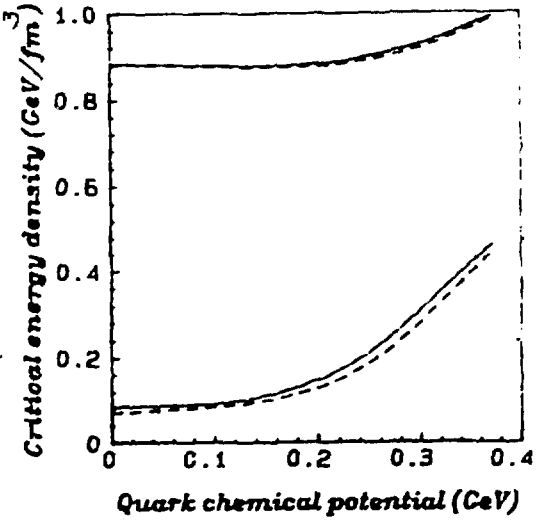

Fig. 3. R = 0.6 fm

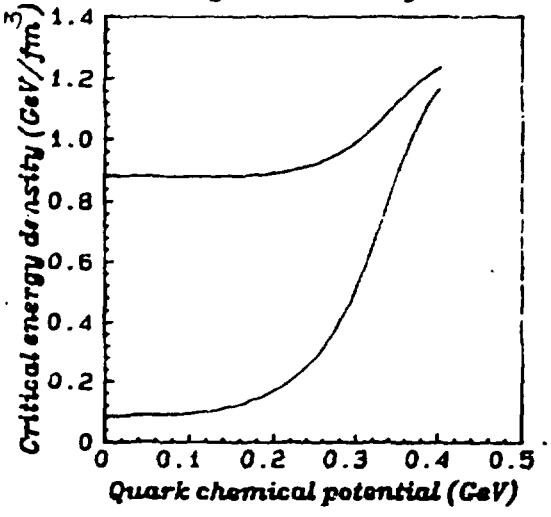

References:
1. J. Cleymans et al., Z. Phys. C33 (1986) 151
2. Dixit and Suhonen, Z. Phys. C18 (1983) 355
3. F. Takagi, Phys. Rev. D35 (1987) 2226

FRAGMENTATION STUDIES IN ^{40}Ar-EMULSION INTERACTIONS AT 1.8 A GeV

R.R. Joseph*, I.D. Ojha, B.K. Singh and S.K. Tuli
Department of Physics, Banaras Hindu University,
Varanasi-221005, India

Introduction: Relativistic heavy ion interactions may reveal new phenomena /1/ related to the phase transition of hadron gas to QGP phase. Detailed experimental information covering all aspects of particle production using different projectiles and energy is essential for such investigations. We present here an analysis of projectile fragments from ^{40}Ar-emulsion interactions at 1.8 A GeV. An event by event analysis was done for 730 interactions. Events with projectile fragments were divided into various reaction channels. There are indications that the projectile fragmentation properties are independent of target for peripheral collisions.

Results and Discussion: (A) We introduce a quantity Q which is related to the impact parameter and is a measure of the average total charge of projectile spectator fragments /2/

$$Q = \sum_{i=1}^{17} n_i Z_i$$

where n_i and Z_i are the number and charge of the projectile fragment. The average number of participating nucleons of the projectile nucleus, $\langle n_{int} \rangle$ is then related to Q as

$$\langle n_{int} \rangle = A - \frac{A}{Z} Q$$

where A and Z are the mass and charge numbers of projectile nucleus. In fig.1 we represent the variation of $\langle n_{int} \rangle$ with n_h. Since the emulsion used for this experiment is of low sensitivity, we had to correct our data by taking into account the Z=1 fragments going into the forward cone using the results of Ref./3/. Corrected values are also shown in the figure.

(B) Our data has been classified into the following reaction channels

(a) n He + Z 3 fragments + anything
(b) n He + anything
where n = 1,2,3,4. From a comparison of the situation in different He break-up channels, we found that O is minimum for 3 He reaction channel implying a greater forward collimation in this particular case. Also we observe that O and n are comparable for all channels within experimental uncertainty when we consider peripheral collisions. This supports the concept of factorization and limiting fragmentation for peripheral collisions only. Our results are compared with other experiments.

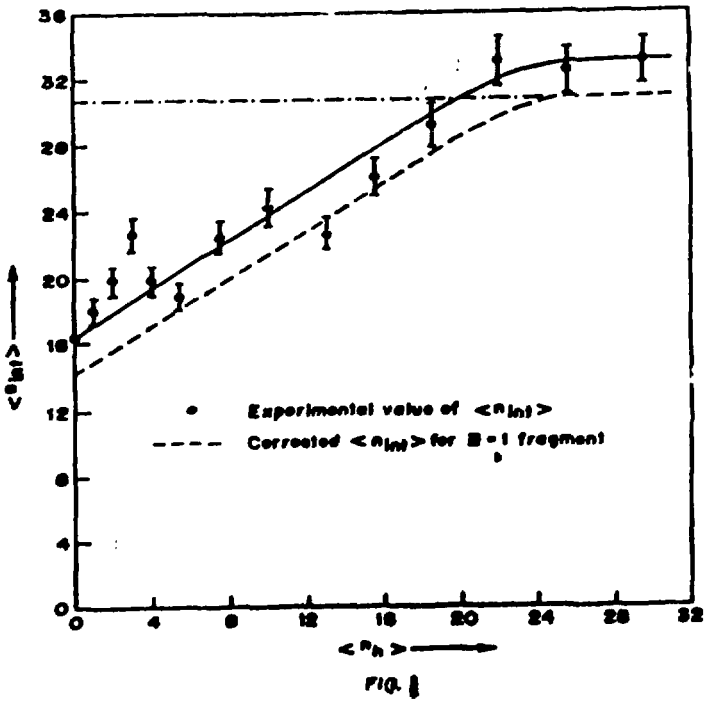

FIG. 1

References

/1/ Boguta J, 1982, Phys.Lett. 109B, 251.
/2/ Jakobsson B et al., 1974, Z.Phys. 268, 1.
/3/ Aleklett K. et al., 1988, Phys.Rev.C38, 1658
/4/ Bhanja R et al, 1983, Nucl.Phys.A411, 507.
/5/ Ahmad M.S. et al, 1989, Nucl.Phys.A499, 837.

*Present address: Department of Physics and Astrophysics, Delhi University, Delhi 110 007.

EMISSION OF LOW ENERGY PARTICLES IN ^{32}S-EMULSION INTERACTIONS AT 200 A GeV ENERGY

(EMU-01 COLLABORATION)
Reported By: V.S.Bhatia, Physics Department,
Panjab University, Chandigarh-160014.

Motivation for this work was provided by the paper of Schmidt et al [1] who found significant differences in target fragmentation behaviour in ^{16}O-nucleus and p-nucleus interactions at 200 A GeV energy. In the present experiment we have studied low energy particles emitted in ^{32}S-Emulsion interactions at 200 A GeV energy. Data on such particles emitted in nucleus-nucleus interactions is needed to determine the role of cascading during the collision process and to test the existing models of nucleus-nucleus collisions at ultra-relativistic energies.

A sample of 581 minimum bias inelastic events was collected by along the track scaning method in an emulsion stack exposed to Sulphur ions at the CERN SPS. Due to certain constraints , measurements could be done only on 463 events.The various tracks originating from the interaction vertex were classified into three types: (i) shower tracks having grain density (g.d.)$\leq$ 1.4g_o , where g_o = g.d. of a highly relativistic singly charged particle. Shower tracks are due to singly charged particles (mostly pions) of β>0.7 (ii) grey tracks having grain density >1.4g_o but residual range > 3mm (In the case of grey tracks caused by protons, this would imply proton energy of 30 MeV to 400 MeV); (iii) black tracks, having ranges less than 3mm. These are due to evaporation of the excited residual target nucleus. In our experiment, we determined the average number of black and grey tracks as $\langle N_b \rangle$= 4.7±3.2 and $\langle N_g \rangle$= 4.3±0.2, respectively. The main emphasis in this investigation is on the study of grey tracks because these are intimately related to the cascading processes. We have measured emission angles of all grey tracks. We have also identified 295 flat grey tracks by the standard methods of g.d. vs $p\beta$ and Range vs. $p\beta$. Out of 295 grey tracks, 27 have been identified as due to deutrons, 172 due to protons, 40 due to kaons and 56 due to pions. After applying geometrical correction [2] we find the yield per ^{32}S-Em interaction for deutrons, protons, kaons and pions as 0.38±0.11, 2.06±0.27, 0.28±0.10 and 1.01±0.20, respectively. The values of π/p, K/p and K/π are thus 0.38, 0.23 and 0.61, respectively. The corresponding values found in 400 GeV proton-Emulsion interactios are 0.19,0.06 and 0.34, respectively [3].

The asymmetry parameter, A[=(F-B)/(F+B)] is found to be 0.37,0.54, 0.57 and 0.31 for deutrons, protons, kaons and pions, respectively. Fig.1 shows the dependence of A on the grey track energy. It is seen that above 250 MeV energy the grey tracks are practically all emitted in the forward hemisphere in the lab frame. We have also measured the transverse momentum (p_t) and longitudinal momentum (p_l) of grey tracks. Fig.2 shows the correlation between $\langle p_l \rangle$ or $\langle p_t \rangle$ and N_h, (N_h=N_b+N_g). N_h is measure of degree of target excitation. It is seen that $\langle p_l \rangle$ and $\langle p_t \rangle$ are independent of N_h . Our values of $\langle p_l \rangle$ and $\langle p_t \rangle$ are 421±12 MeV/c and 257±7 MeV/c, respectively. These may be compared to the corresponding values of 470 MeV/c and 310 MeV/c,

measured by the WA80 collaboration in ^{16}O-nucleus collisions at 200 A GeV. On the other hand, the values obtained by WA80 for $\langle p_L \rangle$ and $\langle p_t \rangle$ in p-Ag collisions at 200 A GeV are 300 MeV/c and 125 MeV/c, which are significantly lower than those for ^{16}O-nucleus and ^{32}S-nucleus collisions. A successful theoretical model of nucleus-nucleus collisions should be able to explain this behaviour. Such a model should also explain the energy dependence of the asymmetry parameter A and the observed values of π/p, K/p and K/π ratios.

REFERENCES:
1. H.R.Schmidt et al (WA80 collaboration), Z.Phys. C38 (1988)109.
2. B.Jakobsson and R.Kulberg, Phys. Scripta 13 (1976)327.
3. Jasbir Singh, Ph.D Thesis, Panjab University (1979).

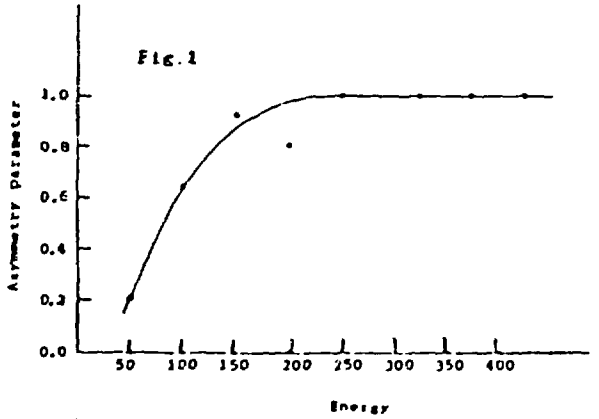

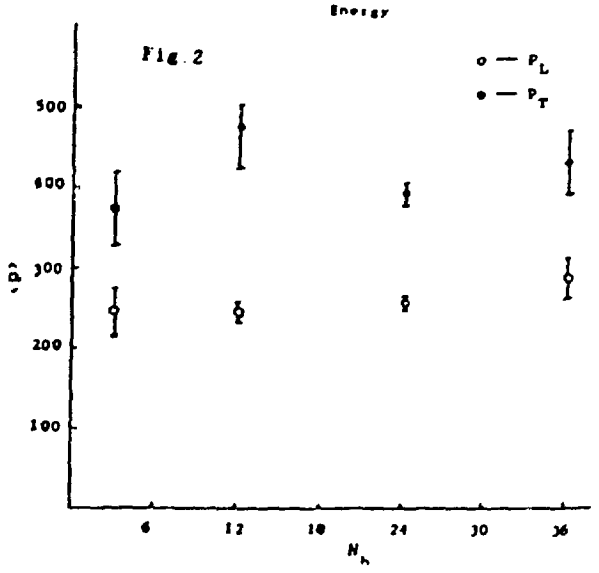

Non - Statistical Fluctuations in Relativistic Heavy-Ion Collisions

EMU - 01 Collaboration
Anju Bhasin, Physics Deptt., Univ. of Jammu, Jammu-180001.

Presented are the results on non-statistical fluctuation in relativistic heavy ion collisions on ^{16}O and ^{32}S induced interactions in nuclear emulsions at 200 A GeV. The analysis is based on scaled factorial moments as suggested by Bialas and Peschanki[1] . Two procedures of normalization of averages (over events and over different regions of phase space) namely 'horizontal' and 'vertical' averaging are used. Appropriate corrections as suggested by Fialkoswki[2] for horizontal procedure are also employed. The moments are studied as function of η -bin. The better resolution of chambers ($\delta\eta \sim 0.01$)allows us to study a region which is not normally accessible for other fixed target experiments. Fig.1 shows $\ln F_q$ versus $-\ln(\delta\eta)$ for the central O+em sample before and after the shape correction. For all moments,a linear behaviour is observed,characteristic of intermittency. Fig.2 shows the results of central S+Au and O+em data which are compared in Monte Carlo code FRITIOF on nucleus-nucleus collisions. For $\delta\eta \gtrsim 0.1$, the moments seem to increase with decreasing $\delta\eta$ but for smaller values of $\delta\eta$ (~ 0.2),the moments stay broadly constant. The rise for $\delta\eta > 0.1$ is consistent with other experimental findings[3]. The Fritiof model shows no variation with $\delta\eta$ as expected. Fig.3 shows results for central S+Au events . Consistency in the results is obtained for 'corrected horizontal' and 'vertical' averaging procedures. Predictions from α -model of Bialas and Peschanski[1] are also shown.

It is observed in all the above cases that the moments exibit the power law dependence on $\delta\eta$ for bin widths $\delta\eta \gtrsim 0.1$,however,their slopes roll off to approximately zero for $\delta\eta < 0.1$. This behaviour of the moments indicates that the particle production processes in ultra-relativistic nucleus-nucleus collisions produce non-statistical fluctuations which manifest themselves in the pseudorapidity distributions on scales down to $\sim$ 0.1 unit of pseudorapidity.

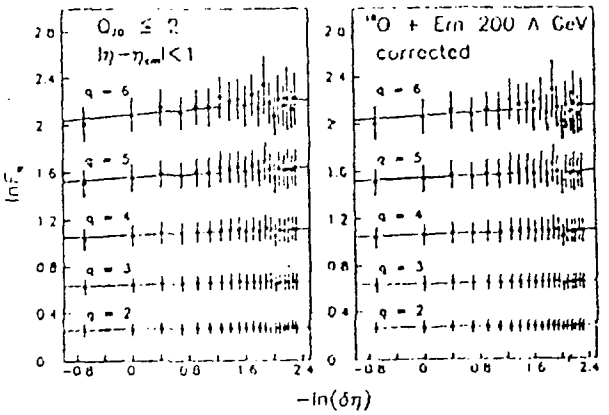

Fig 1. Scaled factorial moments for central ^{16}O+Em interactions at 200 A GeV. Left uncorrected and right Fialkowski corrected.

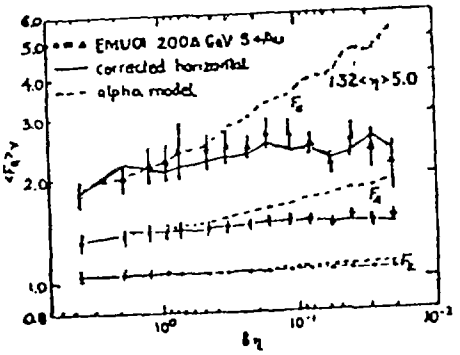

Fig 3. Scaled factorial moments calculated with two different metods and an MC-simulation using a model with built in intermittency.

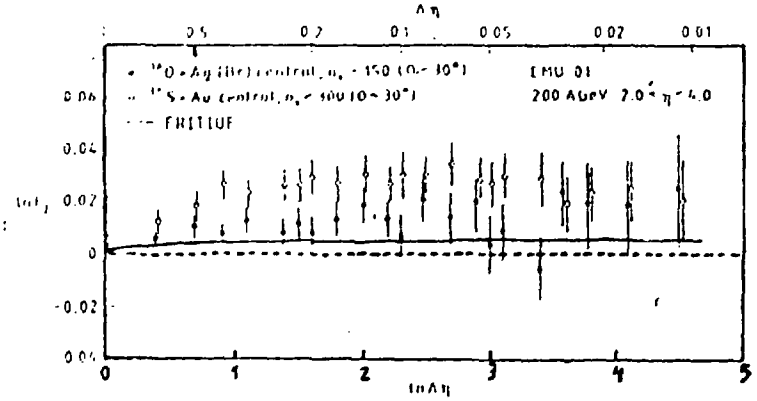

FIGURE 2

The normalized factorial moments F_2 of the multiplicity distribution as a function of bin width in pseudorapidity for $p = 2$ for the region $2.0 < \eta < 4.0$.

References:

1. A.Bialas and R.Peschanski, Nucl. Phys. B273 (1986)703; B308 (1988)857.
2. K.Fialkowski et al, Acta Physica Polonica B20 (1989)639.
3. R.Holynski et al,Phys.Rev.Lett. 62 (1989)733.

MULTIPLICITY CORRELATIONS IN NUCLEUS-NUCLEUS COLLISIONS.

K. A. Siddiqui, M. S. Ahmad and R. Hasan
Department of Physics A. M. U. Aligarh - 202002

It is well known that in the study of correlations of secondry charged particles produced in collisions of high energy hadrons with nuclei, it is possible to obtain extremely useful informations on the dynamic of collision and it allow us to discuss the mechanism of nucleus-nucleus (A-A) collisions. Several workers (1 - 4) have attempted to study the multiplicity correlations over widely different incident energies and using different projectile. An analysis of multiplicity correlations for p-nucleus collisions (5) showed that the inclination coefficient (n_i < n_j >) are monotonic and can reasonably be approximated by straight lines with positive slope. We have also studied the correlations among different multiplicity parameters with a view to ascertaining continuity from p-nucleus to A-A collision mechanism.

The present study is based on the data of 2550 inelastic collisions of ^{12}C nuclei at momentum 4.5 GeV/A. Details of stack and technique used have already been given in our eralier papers 6.7 .

The correlations of multiplicities $n_i = f(n_j)$ and their approximation by linear dependences $n_i = q + kn_j$ are given in fig. 1 & 2 for ^{12}C-Em and p-Em collisions respectively for the same incident momentum. The least square fits of experimental points have also been indicated in figures.

Similarty of correlations in ^{12}C nucleus and in hadron nucleus collisions shows that the correlations do not depend on the mass of the projectile and the contribution of the recoiling nucleus towards the excitation energy of the residual nucleus is approximately the same for p-nucleus and A-A collisions. The following conclusions from figs. 1, 2 and fitted data :

(a) In the case of p-Em collisions, the correlation between $\langle N_h \rangle$ and n_b is very strong , between $\langle n_g \rangle$ and n_b moderate and negative between $\langle n_s \rangle$ and n_b. In the case of ^{12}C-Em collisions the correlation between $\langle N_h \rangle$ and n_b is strong and moderate between ($\langle n_s \rangle$, $\langle n_g \rangle$) and n_b.

(b) There is negative correlation between n_g and $\langle n_s \rangle$ and very strong correlation between ($\langle n_b \rangle$, $\langle N_h \rangle$) and n_g in the case of p-Em collisions, whereas in the case of ^{12}C-Em collisions, there is strong correlation between $\langle N_h \rangle$ and n_g moderate correlation between ($\langle n_b \rangle$, $\langle n_s \rangle$) and n_g.

(c) For p-Em collisions, there is practically no dependence of $\langle n_g \rangle$, $\langle n_b \rangle$ and $\langle N_h \rangle$ on n_s, but in the case of ^{12}C-Em collisions this dependence is quite strong.

(d) For p-Em collisions, there is strong correlations between ($\langle n_b \rangle$, $\langle n_g \rangle$) and N_h and nagetive correlation between $\langle n_s \rangle$ and N_h whereas in the case of ^{12}C-Em collisions $\langle n_b \rangle$, $\langle n_g \rangle$ and $\langle n_s \rangle$ increase lenearly whith N_h.

(e) Correlations between multiplications of slow particles, i.e. between black and grey and heavy tracks seem to depend on the nature of the incident particle.

(f) The mean shower multiplicity $\langle n_s \rangle$ at fixed n_b, n_g and N_h is larger for ^{12}C-Em collisions than p-Em collisions.

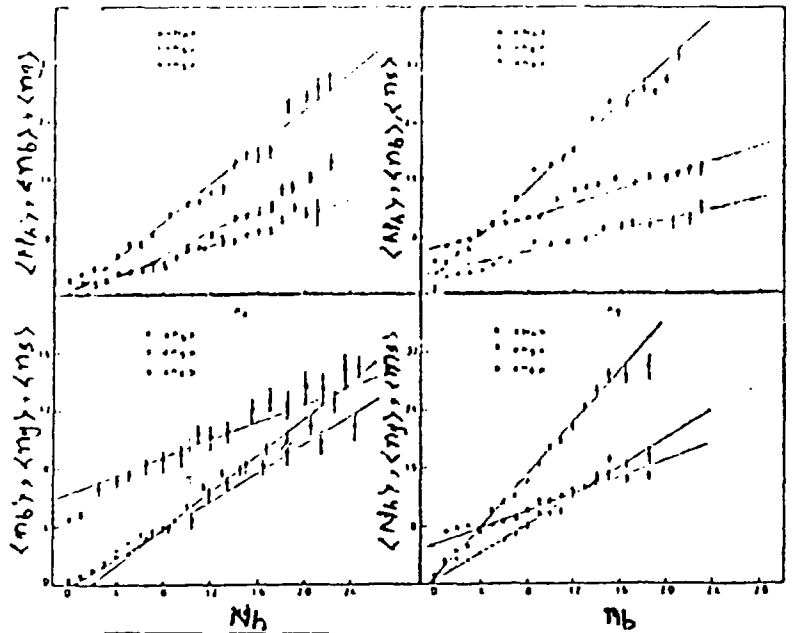

Fig.1: Multiplicity correlations $n_i = f(n_j)$ and their approximation by linear dependence $n_i = q + K n_j$ for Ne-Em collisions.

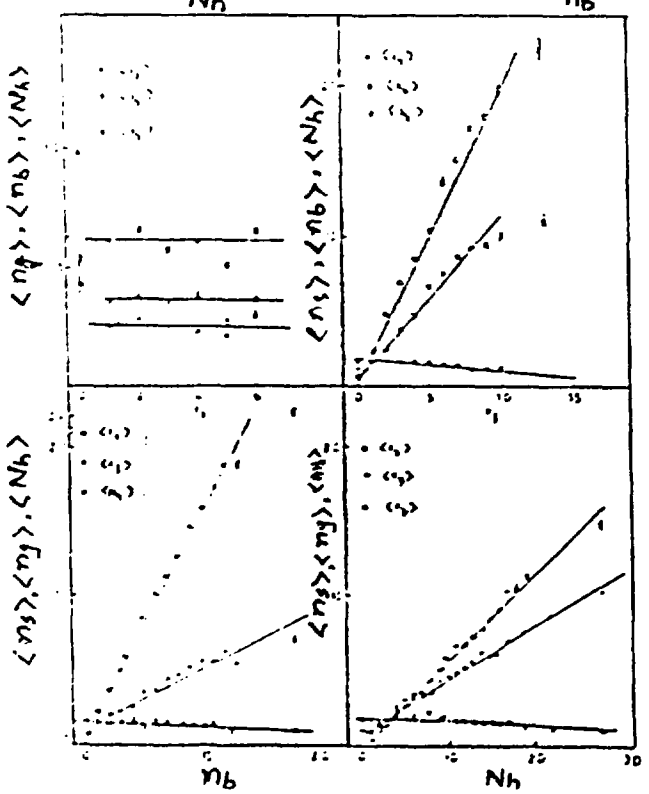

Fig.2. Multiplicity correlations $n_i = f(n_j)$ and their approximation by linear dependence $n_i = q + K n_j$ for p-Em collisions.

1. AAGMT collaboration; Nucl. Phys. B 129, 205 (1978)
2. I. otterlund et al; Nucl. Phys. B 142, 445 (1978)
3. AAGMT collaboration; Nucl. Phys. B 143, 232 (1978)
4. M. Ahrar et al; Cand. J. Phys. 62, 218 (1984)
5. S. A. Azimov et al; Sov. J. Nucl. Phys. 26, 180 (1977)
6. M. Q. R. Khan et al; Nuo. Cim. A99, 417 (1988)
7. M. S. Ahamad et al; Nucl. Phys. A 499, 82 (1989)

f. NUCLEAR INSTRUMENTATION AND EXPERIMENTAL TECHNIQUES.

PERFORMANCE OF THE ISOL ION-SOURCE IN THE ON-LINE: SOME NEW AND SURPRISING OBSERVATIONS

A. Chakrabarti, A. Banerjee, S. Chattopadhyay, A. Polley, V. Banerjee, S. Bhattacharya, T. Mukhopadhyay, A. Das, S. K. Pardhasaradhi and R. P. Sharma

Variable Energy Cyclotron Centre
1/AF Bidhan Nagar, Calcutta-700064

Introduction : The ISOL system at VECC has been commissioned recently [1]. Here we will report the results of the first on-line experiment at VECC to study the efficiency(η)of the system from the target chamber to a point about 1m downstream of the ion source, where the radioactive ion beam was collected on a catcher foil.

Experimental: Fig 1 shows the skimmer-ion source-extractor assembly. The ion-source was used in thermal ionisation (cavity ioniser) mode. Filament current of 24 A and cathode heating power (electron-bombardment) of 20 W were used. The capillary-skimmer distance was about 12 mm. In two separate expts., reaction products from ^{159}Tb(α,xn) and ^{232}Th(α,f) reactions were transported by He-jet. These were ionised in the ion source, extracted (7 kV potential) and allowed to deposit on the catcher foil. The γ-activities on the catcher were monitored using a 20% HpGe detector. For absolute η determination, the above activities were compared with those of catcher foils placed just after the target. A typical spectrum counted for 200 secs after a cooling time of about 7 min. is shown in fig.2 which gives an idea of yield obtained 1 m downstream of the ion-source for a total irradiation of 0.55 μamp-hr.

Results and discussion: We have obtained η of about 0.2% for ^{160}Ho and ^{159m}Ho. This is clearly an order of magnitude higher than the η obtained in the RAMA system[2]. In the fission reaction η obtained for ^{101,104}Tc, ^{107}Rh, ^{131}Te etc., is from 0.15% - 0.25%. The element Tc, Rh or their parents Mo, Ru could not so far be ionised with reasonable η in any on-line ISOL system. Very high η obtained in our system for these elements is an interesting observation from the view point of studying structures of n-rich isotopes and ion source development. Further detailed studies have been planned to understand the exact mechanism leading to high η for the above noble and

refractory metals.

References: 1. A. Chakrabarti, A. Banerjee, *et al* EMIS-12, Sendai, Japan; To be published in Nucl. Instr. & Meth.
2. D. M. Moltz, *et al* Nucl. Instr. & Meth. 172 (1980) 507.

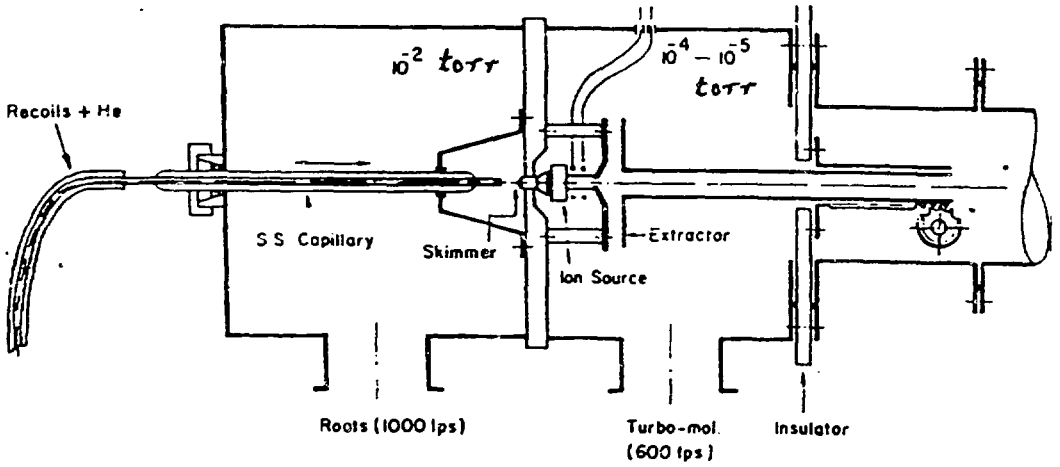

Fig. 1: Schematic Diagram of ISOL Ion-Source Region

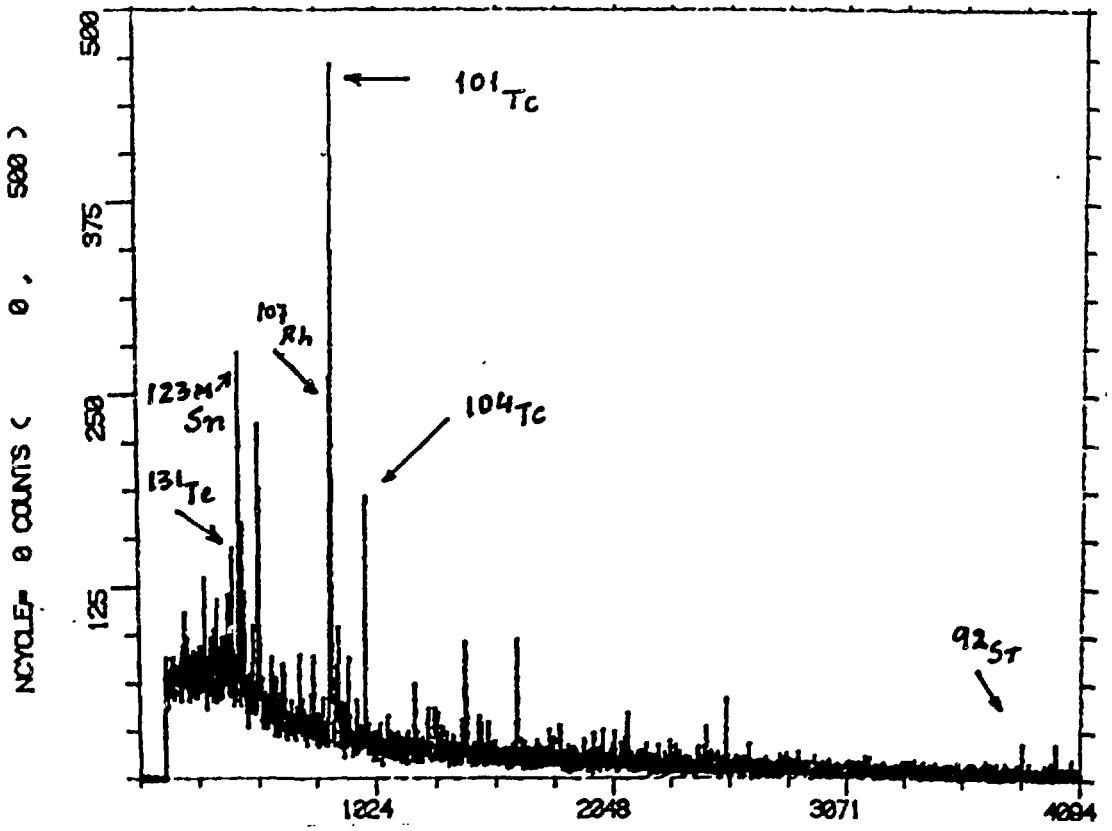

Fig. 2: A Typical γ-Spectrum of Fission Products Collected as Radioactive Ion Beams

AN ELECTROSTATIC DEFLECTOR FOR FUSION CROSS-SECTION MEASUREMENTS

M.L.Jhingan,H.C.Jain,S.Nagaraj,P.Singh*,Y.K.Agarwal,
M.G.Betigeri* and S.Saha,
Tata Institute of Fundamental Research,Bombay-400 005
* Bhabha Atomic Research Centre,Trombay,Bombay-40085

In heavy ion fusion reactions,the compound nucleus is formed in a highly excited state with high angular momentum and deexcites primarily by evaporation of low energy light particles. Since the light particles do not carry significant momentum, the evaporation residues (ERs) move in a forward cone. The detection of ERs is difficult in the presence of direct beam with 10^{10} to 10^{12} times relative intensity. It is,however, possible to separate the two with the help of an electric field applied perpendicular to the direction of motion since the deflection is proportional to E/q (where E is energy and q the charge state of the moving particle) which is nearly a factor of 2 to 3 different for the beam like particles and ERs. In this paper, we report the design, fabrication and testing of an electrostatic deflector /1/ for the measurement of the fusion cross section in medium heavy ion fusion reactions.

Fig.1 shows a schematic diagram of the experimental set up. In the test experiment, a ^{37}Cl beam with 115 Mev energy was bombarded on a self supporting ^{59}Co target with thickness 200 $\mu g/cm^2$ .The beam was monitored by detecting Rutherford scattered particles in a monitor detector (M) kept at an angle of 12° with respect to the beam direction.A collimator kept after the target restricts the entrance angle to the deflector

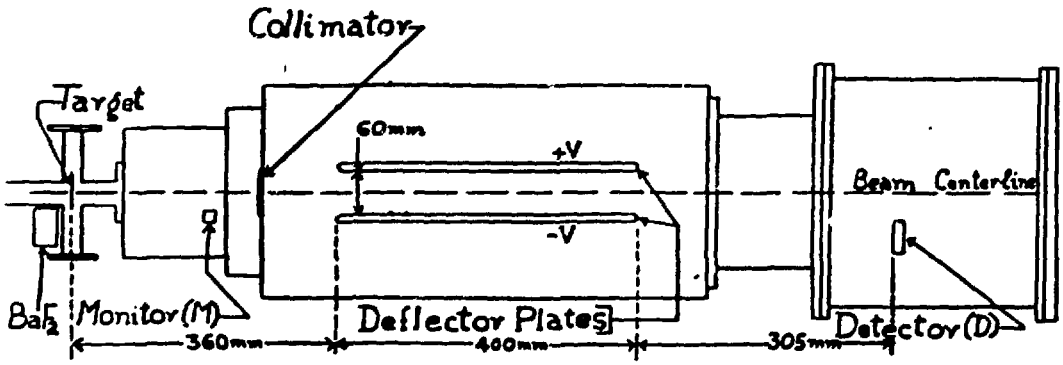

Fig.1 Schematic diagram of experimental set up

plates to 1°.The length of the deflector plates was 40 cm and gap was 6 cm.They were placed at a distance of 36 cm from the target position. The ERs travelled a further distance of 30.5 cm from the exit of the deflector plates before they were stopped in a surface barrier detector (D).The detector had an opening of 5 mm x 20 mm and was placed to accept the ERs undergoing a deflection of approximately 0.1 ± 0.2 degrees.In the present experiment, the deflector voltage on each plate was tuned (V~ 22 kV) through remote control to obtain maximum intensity of the ERs. The ER spectrum was further cleaned up from the beam like particles reaching the detector (D) due to slit scattering through time of flight measurement with respect to a fast detector placed close to the target and detecting gamma rays emitted in the fusion reaction. A 2-d spectrum with energy of the ERs along y-axis and time of flight along the x-axis was obtained with a PC based data acquisition system. Fig 2 shows a projection of the 2-d spectrum on the time axis.The peak with 40ns FWHM corresponds to the ERs produced in the $^{37}Cl+^{59}Co$ fusion reaction and reaching the detector after deflection.

Fig. 3 shows the projection on energy axis with a gate on time of flight peak in fig.2. The background under the peak was also subtracted. The projection shows a well defined energy peak of ERs. These measurements show that the present system can be effectively used to separate ERs from beam like particles, and to measure fusion cross sections, if the efficiency of the system is known. The efficiency can be obtained from Monte Carlo calculations/1/ and be checked through comparision of measured cross section with those obtained by γ ray technique/2/.

References:-

1. R.Schuber et al Nucl. Instr. Methods A269(1988) 585
2. M.Dasgupta et al Phys. Rev. Lett. 66(1991) 1414

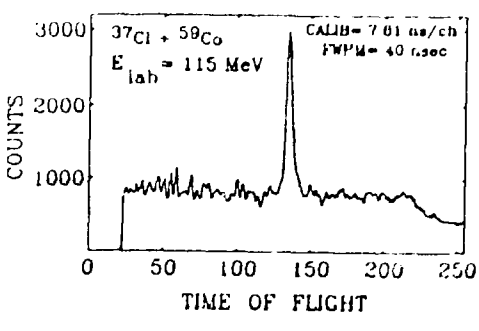

Fig.2 Time of flight spectrum

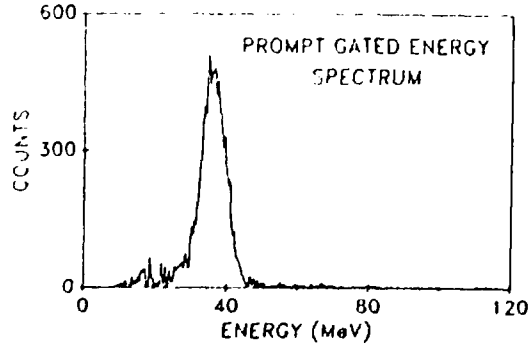

Fig.3 Energy Spectrum of ERs

BEAM PULSING SYSTEM FOR THE PELLETRON AT T.I.F.R

H.C. JAIN AND U.T. RAHEJA
TATA INSTITUTE OF FUNDAMENTAL RESEARCH, BOMBAY - 400005
P.J. BHALERAO, V.M. DATAR AND M.Y. VAZE
BHABHA ATOMIC RESEARCH CENTRE, BOMBAY - 400085

A beam pulsing system consisting of a double harmonic buncher /1/ at the low energy end and a rf-beam sweeper at the high energy end has been installed to obtain nano second pulsed beam from the 14-UD pelletron accelerator T.I.F.R. A schematic diagram of the system is shown in fig.1. The buncher consists of two sets of electrodes seperated by a drift space. The first set operates at a fundamental frequency f_1= 9.375 MHz whereas the second operates at twice the fundamental freqnecy f_2 = 18.75 MHz. The drift space provides the effect of a third harmonic. Thus, the entire system approximately simulates the effect of a saw tooth waveform. The beam sweeper has also been operated at 9.37 MHz in the present set up. The bunchers and the sweeper have been provided with independent amplitude and phase control for rf. They are phase locked with respect to a master oscillator with the help of an amplitude and phase control unit which picks up a signal containing amplitude and phase information of the rf voltage applied to the electrodes through a tank circuit. The signal modifies the amplitude and phase of the output through the master oscillator, a voltage controlled phase shifter and voltage controlled oscillator (VCO) in a closed loop. This output feeds the tank circuit in buncher/sweeper through an rf-power amplifier.

The above system has been tested for 70 MeV ^{16}O beam. The pulsed beam was monitored in a surface barrier detector through elastic scattering of ^{16}O ions at 15° from a thin 400 $\mu gm/cm^2$ ^{209}Bi target in the scattering chamber. The detector output was used as a start and the master oscillator signal as a stop for the time to amplitude converter(TAC). The amplitude and phases of f_1 and f_2 were tuned to obtain a minimum width for the time peak from the output of TAC. The width of peak was studied for injection voltages between 80 and 250KV. The width was found to decrease at the higher injection voltage. A typical bunched beam obtained from 70 MeV ^{16}O ions using 250 KV injection voltage is shown in fig 2. A width of ~ 2.0 ns was obtained in this measurement. The area under the peak showed nearly 60% efficiency for bunching.

The rf voltage on beam-sweeper electrodes was switched on after the bunched beam was obtained. The

amplitude and phase of the rf was adjusted to allow the bunched beam through 1.5 x 1.5 mm^2 slits after the sweeper while the dark current was cleaned up. The time peak corresponding to pulsed beam with sweeper-on is shown in fig.3.

Reference :

/1/ H.C. Jain et al, Symp. on Nucl. Phys. 28B(1985) C50.

ACKNOWLEDGEMENTS : Authors would like to acknowledge the help of the pelletron staff in the installation and alignment of the buncher-sweeper system.

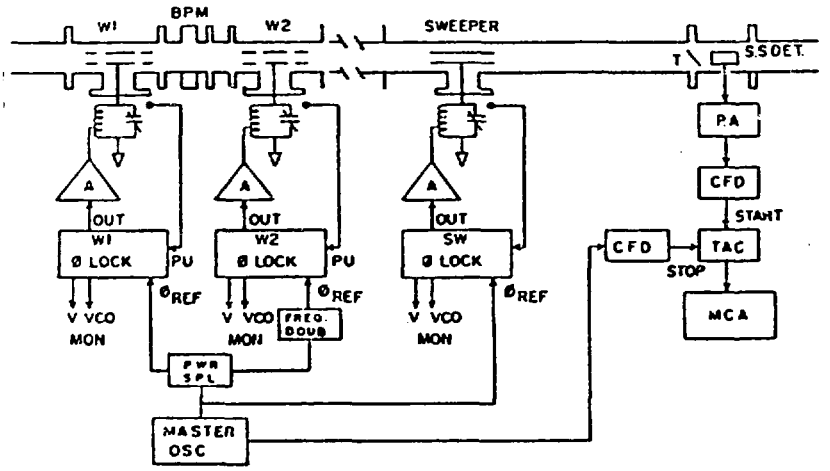

SCHEMATIC BLOCK DIAGRAM OF THE SYSTEM

Fig.-1

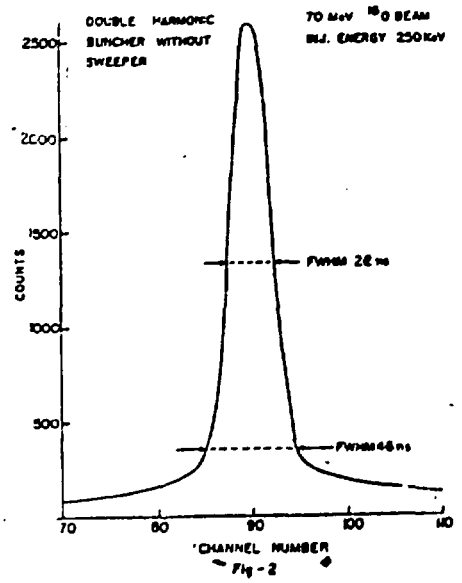

Fig.-2

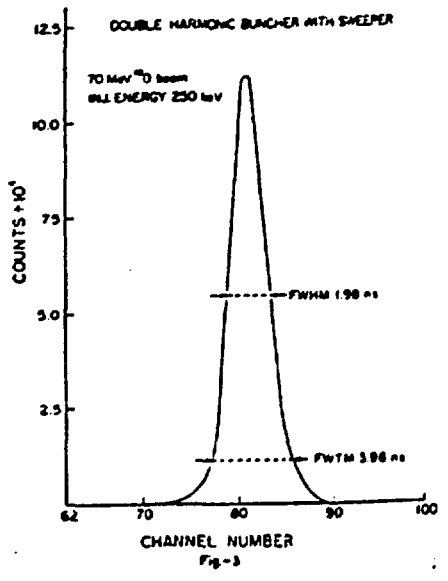

Fig.-3

POSITION SENSITIVE GAS DETECTORS

D. Kataria, J. Antony and E.T. Subramaniam
Nuclear Science Centre, JNU Campus, New Delhi 110067

A transmission type Position Sensitive Single Wire Proportional Counter (SWPC) with an active area of 85x14 mm^2 has been developed for use as a focal plane detector with the Heavy Ion Reaction Analyzer at NSC. A 176 ohm/cm resistive wire, 5 cm long, connected tc the centre pins of two connectors constitutes the anode and its Aluminium housing forms the cathode. There is provision for gas inlet and outlet on the housing. The entrance and exit foils are 1.5 micron aluminized mylar.

A transmission type, 45x45 mm^2 active area, Parallel Plate Avalanche Counter (PPAC) has also been developed. The two 'plates' of the PPAC are two wire grids of 25 micron gold plated Tungsten wires spaced 0.5 mm apart. A spacing of 1.6 mm between the 'plates' is achieved by soldering the two grids to the two faces of a double sided G10 pcb. One of the electrodes is kept at high voltage and the other is grounded through a 50 ohm resistor. The window foils are 2 micron thick mylar glued to Aluminium frames which also have provision for gas inlet-outlet and support wires for the pressure foils.

Gas is fed to the detectors using a fine needle valve and pumped out using a rotary pump through another needle valve. The pressure can be monitored using a 0-800 torr pressure transducer gauge. The needle valves can be set appropriately to maintain any desired gas pressure and flow.

A computer program written in Pascal for a CAMAC-based multiparameter data acquisition system was used to obtain the position spectrum for the SWPC by performing the charge division in software. The Program is user friendly & menu driven. It has features like scatter plot, contour plot and can display upto five software processed spectra. It can

handle upto 3.2 KHz count rates with a 16 Mhz PC AT 80386 computer in MS-DOS 3.2 environment.

The position resolution for 252Cf fission fragments was checked by masking the SWPC with two 1 mm wide slits, spaced 10 mm apart. The detector was maintained at a pressure of 200 torr P-10 gas and operated at 850 volts. The signals from the two ends of the anode were processed and fed to an ADC. Using the computer program described above the position resolution was determined to be 0.8 mm.

The PPAC was tested at 3-8 torr isobutane at voltages varying from 350 - 600 Volts. Signals were observed from both electrodes with rise times of the order of 3-5 ns. The PPAC in combination with a surface barrier detector gave time resolution of the order of 1 ns. The detector gives similar performance with fission fragments obtained by bombarding a Bismuth target with an Oxygen beam. It can handle count rates upto 10^4 /sec. The detector is so designed that it can be easily made position sensitive simply by replacing the pcb with another one where the wires can be connected to a resistor chain or to the taps of a chip delay line.

PULSE HEIGHT DEFECT OF BaF_2 SCINTILLATOR FOR LIGHT CHARGED PARTICLES

Bency V. John, N P D, B A R C, Bombay

The intrinsic BaF_2 scintillator is becoming popular as charged particle detector as well. Although the properties of BaF_2 to gamma radiation have been measured by several authors data on the response to charged particles are scarce. For scintillators it is commonly observed that the light output at a given particle energy decreases for heavier particle (pulse height defect). We have measured pulse height defect and the ratio of fast component to total light output for proton and alpha particles independently using Van De Graaff acclerator at Trombay. The BaF_2 scintillator used for the present measurement was grown at TP&PED BARC and has a size of 10 mm dia and 5 mm thickness.

Protons of energy ranging from 1.5 MeV to 2.5 MeV and alpha particles of energy 2 MeV were obtained from the acclerator. The particles elastically scattered from gold target (50 $\mu gm/cm^2$) were detected using BaF_2 to study its response using gated and normal amplifiers . Alphas from ^{241}Am and ^{229}Th were also used. Proton and alpha pulse heights(total) were comparable in this energy range. Since at low energies (<20 MeV) the scintillator response is linear, the measured ratio will hold good up to about 20 MeV and meaningful extrapolation can be made to find the energy region in which the detector can resolve the two particles.

Experimental setup

A vacuum chamber with a quartz window was used for the experiment.The gold target was mounted inside the chamber in beam line. The BaF_2 crystal was mounted inside the chamber on the window at an angle of 74° w.r.t beam direction and at a distance of 13.5 cms from the target. A collimator of 5 mm dia limits the solid angle to 1 mSr. Quartz window PMT EMI 9558 QB was mounted outside the chamber on the quartz window. The face of the crystal through which the scattered particle were entering has a very thin (1 μm) coating of aluminum. This coating acts as a reflector for scintillation light as well as a seal for ambient light.

Electronics

The anode signal was bifurcated. One part was fed to a variable width gate generator (5 ns to 100 ns, NE 4667). The gate of width 50 ns thus generated was used to activate a gated amplifier. The other part of the anode signal was suitably delayed and fed as the input to the gated amplifier which integrates the charge within the gate (NE 4695). The timing of the gate and anode signals are critically adjusted such that the gate reaches 15 nsec before the anode signal. The delay of charge pulse was required to permit coincidence and logical decision to be made. The total light output was measured using the dynode signal using ORTEC 572 amplifier with 2 μsec shaping time, separeatly.

Results

The energy of the scattered particle at an angle of 74°

was calculated and corrected for energy absorbed in the Al coating and target thickness effect. The $1/\sqrt{E}$ behaviour of energy resolution was checked (see table 2) The energy calibration for proton and alpha gives the pulse height defect as 1 : 0.45. The pulse height defect for electrons and alphas were obtained as 1 : 0.302 in another measurement using ^{137}Cs, ^{22}Na and ^{235}U sources and this value is in good agreement with reference 1.

Table 1. Pulse height defect of BaF_2

Relative pulse height	electron	proton	alpha
	1	.66	0.302

Table 2

Proton energy	Energy resolution %	$\sqrt{E}$ * en res
1.70 MeV	10.87	14.17
1.95 MeV	10.60	14.82
2.20 MeV	9.77	14.49
2.45 MeV	9.30	14.55

The relative ratios of fast component to total light output for proton and alpha particles are found to be 1: 0.5. The plot energy (MeV) vs fast component (arb unit) is given in fig 1.

Acknowledgement: The author is greatful to Dr.S.K.Kataria for the encouragement given and his keen interest in this work.

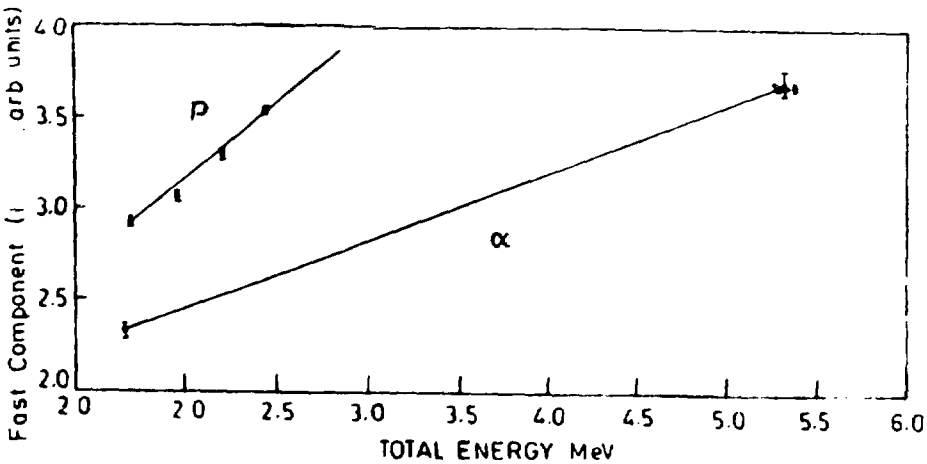

Fig1

Reference

1. S.Kubota, M. Suzuki,J.Ruan,F.Shiraiishi and Y.Takami Nucl Instr and Methods A(242) 291 (1986)

GROWTH AND CHARACTERISATION OF BISMUTH GERMANATE SCINTILLATOR

K.Hema Prasad, D.G.Desai, S.C.Karandikar, K.S.Keswani, M.N.Ahuja, Sangeeta and S.C.Sabharwal
Technical Physics & Prototype Engg. Division,
B.A.R.C., Bombay-85

Bismuth Germanate ($Bi_4Ge_3O_{12}$), usually abbreviated as BGO is an intrinsic scintillator having the best stopping power among the known materials. The growth of high quality and large size crystals of this material poses many problems. These are related to the starting material and the growth conditions. In this paper we discuss the growth of crystals upto 38 mm dia. single crystals have been grown by both Czochralski and Bridgman techniques, however the former technique is more commonly used as also in the present work. Crystals are pulled from a melt of stoichiometric composition in a platinium crucible under a mixed ambient of N_2 : O_2. A well prepared starting charge is prerequisite for the growth of high optical quality crystals. For this a mixture of the constiuent oxides is required to be subjected to repeated sinterings with intermediate grindings for sufficiently long durations at temperatures between 600-800° C. In case the mixture is directly heated to the melting temperature , preferential loss of Bi_2O_3 from the melt surface was observed to take place. The crystals grown in this case were of off stoichiometric composition and showed high optical absorption losses. A detailed spectroscopic analysis of the starting charge and the crystal ingots showed that the presence of certain transition metal divalent and tetravalent impurities have a detrimental effect on crystal transparency/coloration.

A growth disorder which is commonly observed in this material is the helical growth of the crystals. As shown in the table, the axial temperature gradients at the melt/solid surface was seen to be one of the important parameter governing the pitch of the helix. The other parameters such as the rotation and pull rates are also important to grow undistorted crystals.

The energy spectrum of Gamma-rays as detected by BGO crystal is shown in Fig.1.For the best crystals of 35mm dia.& 15mm long the energy resolution obtained was 16 % for 660 keV when used without any reflector.

Table

Shapes of BGO Crystals under Different Growth Conditions for a fixed Diameter of 18mm & Crucible Diameter of 50mm

Pull Rate mm/hr	Axial Gradient °C/cm	Crystal Shape
2	15	Helical, 10mm Pitch
3	15	Helical, 15mm Pitch
>5	15	Helical, >30mm Pitch
2	30	Twist Started at 50mm of length
3	30	Cylindrical
3	2	Irregular

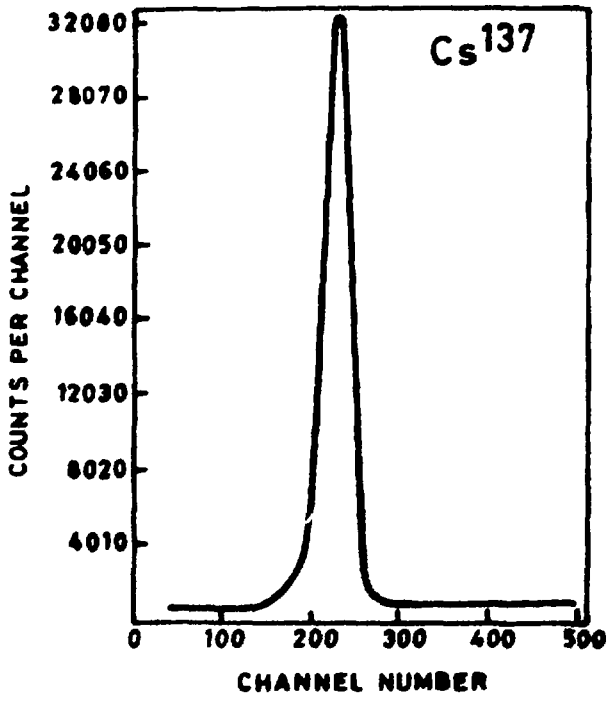

Fig.1 Gamma ray spectrum obtained with BGO crystal (a) Cs^{137} source

A CAMAC CRATE CONTROLLER FOR IBM PC/AT WITH 16 BIT DMA INTERFACE

P.S. Arvindakshan, Anita Behere,
M.D. Ghodgaonkar and B.R. Bairi.
Electronics Division, B. A. R. C. Bombay 400 085.

A CAMAC Crate Controller for IBM PC/AT has been designed for PC based Pelletron Control Instrumentation. This comprises of a General Purpose Crate Controller (GPCC) and a PC add-on-card (ATIFDMA) connected by 50 conductor Flat Ribbon Cable.

The GPCC as the name implies, is a general purpose controller in the sense that it can be interfaced to any computer using a Compatible Parallel Interface card. ATIFDMA is such an interface card for IBM PC/AT. The controller provides well buffered parallel bus which comprises of 16 bit wide bidirectional data and control and status signals necessary for the operation of the controller.

The GPCC fully conforms to the mechanical and signal standards of the CAMAC system. Auxiliary Controller Bus (ACB) logic is incorporated to enable operation of multiple controllers in a single CAMAC crate. Auxiliary Controllers (ACs) extend the capabilities and fields of applications of the CAMAC. ACs located in a CAMAC crate can provide the user with an extremely effective distributed processing capability. This capability is useful in both data acquisition and automatic control systems.

The GPCC has two modes of operation i.e, single mode and block mode. In single mode only one CAMAC cycle is generated by the GPCC on the initiation of GO command by the host computer, when its request is granted access. The GPCC will wait till it get its request granted.

In block mode operation it can perform the four standard block transfer algorithms defined in CAMAC standard viz. Qstop, Qrepeat, Qscan, and Stop on

TC. Qrepeat and Qscan modes are implemented at hardware level in GPCC using high speed CMOS Programmable Logic Devices (PLDs). The Stop on TC block transfer mode is implemented in ATIFDMA card. The Qstop mode, is implemented in software, synchronized with the Q status provided by the status register.

The ACB priority arbitration logic and CAMAC bus cycle logic is designed as a synchronous state machine and implemented through Registerd Bipolar PROMs. PC bus interface and DMA logic is implemented in PLDs on ATIFDMA to support both 16 bit and 24 bit CAMAC data transfer operations.

Both GPCC and ATIFDMA use open collector power driving TTL buffers for interfacing low impedance terminated line of length upto 10 metre. The propagation delays of the buffers and the cable delays necessiates slowing down of control and data signals. For this, additional wait states are introduced in the PC to GPCC bus operations. A software controlled wait state logic allows the GPCC to be interfaced with any computer of PC/AT family running at any frequency (including 486 EISA system).

Driver software for GPCC has been developed. The driver is written in Turbo C, to facilitate development of application software for data acquisition and control system. A diagnostic software with menu based user interface has also been developed for confirming reliable operation of the controller.

In addition to the buffered bus, a local bus is also provided to interface to an in-crate CAMAC CPU module for stand-alone applications.

The controller has been tested and its performance evaluated. In single mode, transfer rate of 56 KBps and in DMA block mode, transfer rate of over 500 KBps is observed over a cable length of 10 metre reliably.

One such controller with IBM PC/AT interface along with the driver and diagnostic software has been supplied to TIFR / Pelletron facility.

AN ONLINE DATA ACQUISION SYSTEM FOR VAX COMPUTER

R.K. Bhowmik, D.K. Goyal & S. Naithani
Nuclear Science Centre, JNU Campus, New Delhi 110 067

An on-line data acquisition system for a large installation should, along with high data throughput, support easy programmability for different experimental requirements and fail-safe operation in the case of a software or hardware crash. The above requirements have been kept in mind in transporting the existing PC-based data acquisition program [1,2] to the two online Micro-VAX computers at NSC running under VMS operating system and connected through ETHERNET.

The online Microvax computers, each having a memory of 9 MB, two disks of 159 MB capacity, 6250 BPI tape drive and a cartridge drive, are connected to CAMAC through the Q-bus compatible KS2922 interface card from Kinetic Systems, USA. Each card supports upto 8 CAMAC crates connected via a 40 wire ribbon cable with a DMA capability of 250 kilowords per sec. One of the crates housing the buffered singles ADCs is located in the data room while the others may be placed near the electronics setup in the beam hall.

The ONLINE program runs three separate sub-processes NSCTSK, SING-PROCESS and MULTI-PROCESS simultaneously from the same termial. The first one is used for communicating with the user through the keyboard, second for transferring buffered data from CAMAC to computer memory through DMA and the third for transferring the buffers to magtape and on-line analysis. The communication with the different sub-processes is done through shared memory and EVENT FLAGS. Since the operating systems maps the shared memory to a disk file, all the spectra along with the important parameters of the data base are retained even when the program exits. Two independent copies are retained by the two computers allowing two data acquisition systems to be used

simultaneously. Software interlock prevents two users from modifying the same data base.

The total experimental setup can be saved in three text files containing information about the data partition, CAMAC hardware and analysis algorithm. An I/O package TTSUBS allows the information to be entered interactively from the terminal or from a disk file. As a result, the software can be customised quickly for each user. The program supports upto eight buffered singles ADCs from different CAMAC crates and a multi-parameter buffer from all the modules in a single CAMAC crate. A simplified online program MCA is available where all commands can be entered through a cursor in the graphics display.

The multiparameter data can be saved block by block in magnetic tape with a maximum block size of 16384 bytes. A ZERO-SUPPRESSION algorithm has been incorporated in software by encoding a Pattern word from the non-zero ADCs. Software filtering of data is also possible resulting in a factor of 2-3 saving of tape. The histograms generated online are automatically dumped on tape at the end of a run. Due to the modular nature of the tape controller routine, both 6250 BPI and cartridge tape drives can be supported. In addition, through a remote tasking algorithm, the tape drive residing on the second VAX computer can also be accessed.

For fast graphics operation, a PC 386 computer with EGA card is used for text i/o and graphics using an RS-232 link to the VAX running at 19200 baud. A customised block-transfer algorithm is used for fast generation of histograms and two dimensional spectra. The spectrum files residing in VAX can also be transferred to PC and stored as binary files for offline analysis in PC by NSCSORT.

[1] R.K. Bhowmik et al, Proc. DAE Symp 31B(1988)P84
[2] R.K. Bhowmik et al, Proc. DAE Symp 32B(1989)O13

EFFECT OF CURING CYCLES ON ETCHING AND ANNEALING BEHAVIOUR OF CR-39 TRACK DETECTOR.

Anupam, S.K.Sharma, S.Kumar & N.Lal
DEPARTMENT OF PHYSICS, K.U.KURUKSHETRA - INDIA

CR-39, a detector of unique sensitivity, resolving power and having excellent optical properties was inducted into the family of track recorders in 1978 and its uses as particle track detector to accomplish numerous applications in a variety of scientific fields have proved its versatility in nuclear track research/1/.

The present work describes the results of relative track response of CR-39 (Pershore Mouldings) detectors reported to be manufactured in different cure cycles i.e. 8,32, and 96 hrs. A set of all these three types of detectors after exposure to 5.45MeV α-particles from ^{241}Am source in vacuum in an exposure unit was etched in 6.25N NaOH at 60°C. The bulketch rate, Vb and the ratio of track etch rate to bulketch rate, V were measured. It was found that Vb for detectors having cure cycle spread over longer time is less. It might be due to the relatively enhanced extent of cross-linking in the polymer detector. Etch rate ratio 'V' has been found to increase with increasing curing time. But this observation may not always hold, as a possible increase in cross-linking does not necessarily mean an increase in sensitivity, since the accumulation of the partially soluble etch product (Poly Allyl Alcohol) in the track cones could also manifest itself as a factor governing the sensitivity at highe extents of cross-linking/2/.

In order to investigate the effect of cure cycle on annealing, the pre and post α-irradiation annealing of samples was done in air at 80°, 95°, 100°C for five hours. The samples were then etched for 20 hours. The results of measurement of Vb are presented in the table. Similar behaviour was observed for annealing at fixed temp. (95°C) for different annealing times (5,10,15 hrs).

Detector Type	Percentage increase in Vb for samples annealed for 5 hrs at		
	80°C	95°C	110°C
CR-39(8 hrs)	21.15	31.73	51.92
CR-39(32 hrs)	18.48	28.26	51.09
CR-39(96 hrs)	17.28	25.93	48.15

As evident from the above results, the increasing tendency of Vb with Annealing temperature and time is more for detectors which are manufactured employing cure cycles spread over shorter spans. A possible explanation for this observation may be given as follows :

The energy gained by the polymer molecule can give rise to two processes namely (i) intrachain movement and (ii) mobility of the chain as a whole. The latter process is less probable as the macromolecule is rendered immovable in the three dimensional network structure of the polymer by the random cross-linking process unless high energies of the order to make the polymer a viscous liquid are reached. But annealing of the polymer to such temperatures is of no relevance in track detection. The intrachain mobility could be the mobility of the atoms and groups belonging to the (a) chain ends and (b) somewhere inside the chain. The movement of the chain ends is less restrictive than those of the groups inside the polymeric chain. As a result the increase in energy and hence Vb of the polymer during annealing is contributed more due to chain ends than due to the intrachain movement inside the chain. For a fixed monomer concentration, the polymer cured for less times have more chains and less average molecular weight as compared to those which have been cured for longer times. More number of chains means more chain ends which are more likely to contribute towards increasing the bulk etch rate.

Reference :

/1/ Cartwright et al Nucl.Inst. & Meth (1978), 153, 457-60.

/2/ Anupam et al. Nucl.Tracks & Radiat.Meas (1991), 18, 335-38.

SOME GAMMA DOSIMETRIC PROPERTIES OF CN-85 AND CR-39

S.L. Sharma, Physics Department, I.I.T. Kharagpur
Pin- 721 302(W.B)

Radiographic film badges, direct-current ionization chambers and thermoluminesence dosimeters are the common types of gamma dosimeters. These dosimeters show saturation in their response curves at high doses.

Experience shows that the etching characteristics of plastic track detectors are greatly affected when exposed to high doses of gamma or X-rays [1-3]. The exposure of plastic track detectors (polymers) to gamma radiation causes cross-linking and degradation (main chain scission). Both of these processes co-exist and either one may predominate depending upon the chemical structure of the polymer and environmental conditions under which the exposures to radiation are performed. Recent studies on the intrinsic viscosity [4] show that CN-85 and CR-39 plastic track detectors predominantly undergo degradation when exposed to high doses (>2Mrad) of gamma radiation. In fact, the mechanism of cross-linking contributes negligibly small beyond 2Mrad. Since the bulk etch rate and the track parameters (etched track diameter etc.) are directly influenced by the degradation of the bulk material, the gamma-dose dependence of the bulk etch rate as well as of the track parameters for CN-85 and CR-39 plastic track detectors are expected to provide an accurate estimation of unknown gamma-dose. Measurements have been carried out on (i) the gamma-dose dependence of V_B of CR-39 for various etching conditions in the dose range 2- 10Mrad, (ii) the gamma-dose dependence of the alpha track diameters in CR-39 and (iii) the gamma-dose dependence of V_B of CN-85 for various etching conditions in the dose range 2-20Mrad. Near linear relationship between V_B and gamma-dose for both CN-85 and CR-39 suggests their simple use as high gamma dosimeters.

Fig. 1 shows V_B versus gamma-dose for CN-85 at 50°C for various normality.

[1] Frank etal., Radiat. Eff. 2(1970)269.
[2] Akber etal., Nucl. Instr. Meth 173(1980)217.
[3] Zamani etal., Nucl. Tracks. 12(1986)141.
[4] Acierno etal., Radiat. Phys. Chem. 16(1980)95.

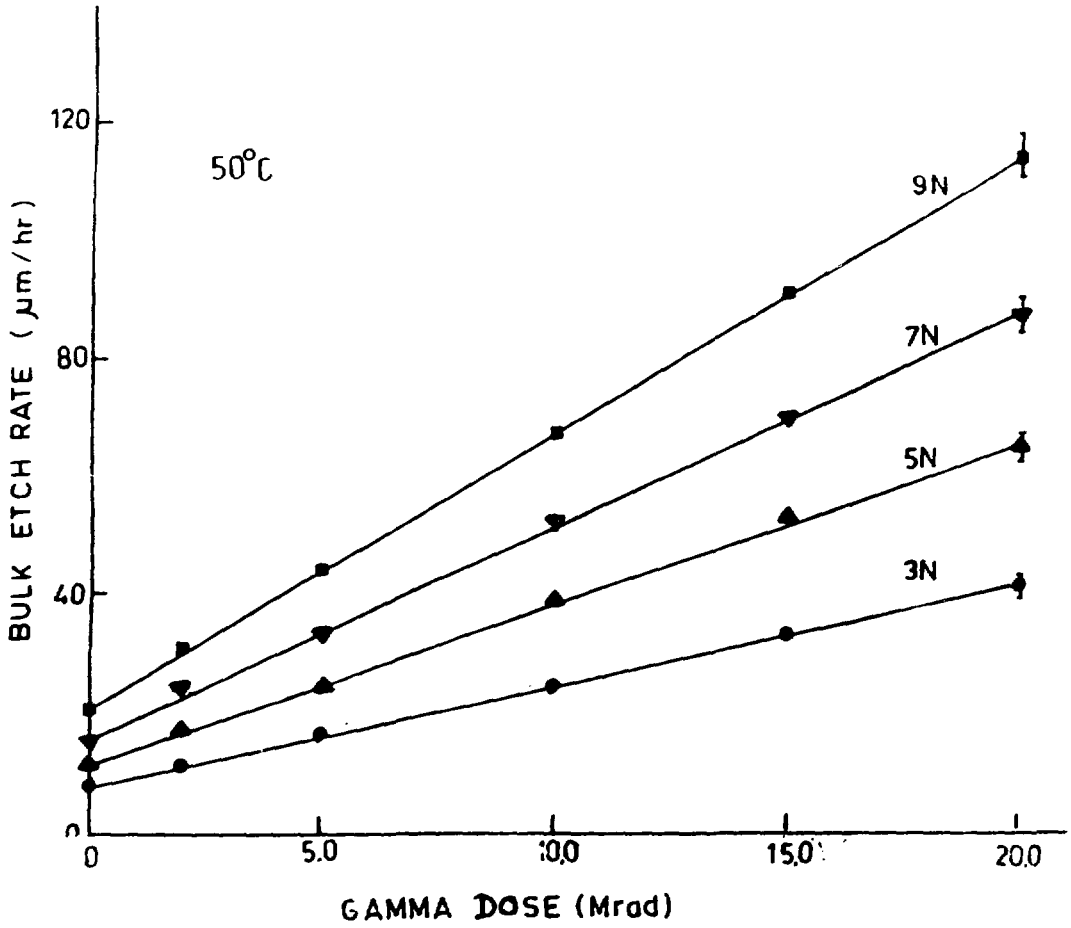

FIG. 1

^{136}Xe ION TRACK REGISTRATION IN MAKROFOL-KL POLYCARBONATE

Ashavani Kumar, P.J.Jojo and Rajendra Prasad
Department of Applied Physics, Z.H.College of Engg.& Tech.,
Aligarh Muslim University, Aligarh-202 002.

Solid State Nuclear Track Detectors (SSNTDs) are widely used for ion registration investigations. As the polycarbonate is insensitive to light charged particles, X and γ-rays, it is well suited for heavy ion work e.g. composition of cosmic rays, heavy ion nuclear reactions and exploration of extra heavy elements etc.[1,2] To identify heavy ions, the detector should be calibrated using some ions with known atomic number and energy under given etching conditions for the revelation of latent damage tracks in SSNTD. The bulk etch rate V_G and track etch rate V_T decide the geometrical shape of the etched track. Etching conditions and the radiation damage caused by the incident charged particle govern the etch rates and registration efficiency. Thus the optimum etch conditions can be decided for controlled calibration experiment. In the present study track registration parameters have been obtained for Makrofol-KL polycarbonate irradiated with ^{136}Xe ions at 45° Makrofol-KL is manufactured by Bayer Ltd., Germany. It contains a slight amount of a colour dye and is expected to have different characteristics from widely used other Makrofols (KG, E and N).

A stack of four Makrofol-KL circular (5cm diameter and 20um thick) sheets was irradiated with ^{136}Xe ion beam (11.56 MeV/n, 10^4-10^5 /cm^2) from the UNILAC, GSI Darmstadt, West Germany at an angle of 45°. The irradiated samples were etched in 6,25 N KOH at 55, 60, 65 and 70°C. The detector was fixed with temperature resistant adhesive (Araldite) on transparent glass slide to allow the etching from one surface only (because of penetrating latent tracks in the detector). V_G was measured by thickness measurement technique[3] using a microthickness dial guage while the track length measurements[2,4] were made with an optical microscope at 675 magnification.

Variation of track length vs the etching time at 60°C is shown in fig.1. The complete etching time t_c (the time

at which the cone length attains the maximum value) has been found to be 20,16,14 and 9 minutes at 55°,60°,65° and 70°C respectively. From V_G and V_T, the etching efficiency(η) at 55°,60°,65° and 70°C has been obtained. It is found to be almost independent of the etching temperature for ^{136}Xe ions incident on detector surface.

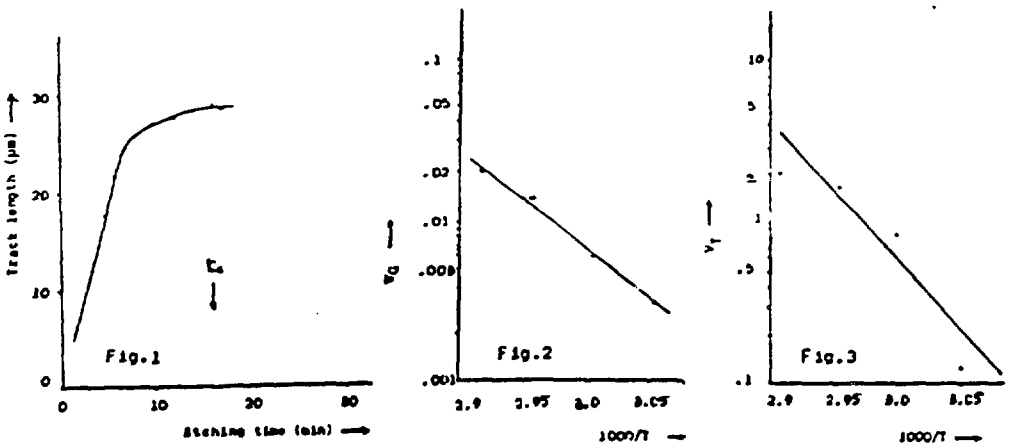

Figures 2&3 show the variation of V_G and V_T with reciprocal of temperature T°K. The straight lines represent the least square fits. Etching rates vs temperature follow Arrhenius equation

$$V_G \text{ or } V_T = \propto e^{-E/KT}$$

where $\propto$ is a constant, K is Boltzmann's constant and E is the activation energy for bulk or track etching. The values of activation energies for V_G and V_T have been found to be 1.24 eV and 1.71 eV from figures 2 and 3.

References:

1. Fleischer, R.L. et.al., Nuclear Tracks in Solids, University of California Press, Berkely (1975).

2. Durrani, S.A. and Bull, R.K., Solid State Nuclear Track Detection, Pergamon Press, U.K. (1987).

3. Enge, W. et.al., Nucl. Instrum. Meth. 127, 125-135 (1975).

4. Dwivedi, K.K. and Mukherji, S., Nucl Instrum Meth. 161, 317 (1979).

DEVELOPMENT OF 8K CHANNEL 100MHZ WILKINSON TYPE ADC

P.K. Mukhopadhyay and K.R. Marballi
Electronics Division, BARC, Bombay-85

Many experiments in nuclear energy spectroscopy are conducted at low count rates either deliberately (for good FWHM) or because of low source strength. Wilkinson type ADCs are preferred for such experiments where good differential non-linearity (DNL) is more important than fast conversion speed. Since a large number of such ADCs are imported every year we set out to design an ADC comparable to imported ones.

DESIGN ASPECTS AND PERFORMANCE:

The design of conventional Wilkinson ADCs is well known. We set out to improve DNL by incorporating digital sliding. In this method the starting digital offset of each conversion has a fixed and a variable part. At the end of conversion the variable offset is cancelled by adding its complement to the converted address. The method eliminates all periodic DNLs (induced by scaler transitions) leaving only the DNL of the peak stretcher. In one experimental run a DNL of +/-0.6% was observed over the top 99.5% of 8K range at a count level of >0.12 million/channel. The observed integral nonlinearity in the same run was 0.004% of range.

The long term stability was tested in our laboratory for 72 hours and found to be within one channel over 24 hours at constant ambient temperature (by noting peak position and room temperature at the same time of the day).

Four such ADC's have been constructed and delivered to Radiochemistry Division, BARC. In the acceptance test the FWHM (1.95 KeV) and FWTM (3.63 KeV) at 1332 KeV using one of the best HPGe detectors was found to be as good as those obtained with a SILENA 8K ADC in the same setup.

COINCIDENCE:

The ADC provides both prompt and late coinc./anticoinc. inputs. The prompt coincidence is tested at the instant when the analog input crosses a threshold (lower than LLD). The late

coincidence is tested at peak detect. A sampling mode for slowly varying signals is available. If this mode is used for normal pulses then the timing requirement of prompt coincidence is relaxed and a broad gate pulse extending upto peak detect is sufficient. The mode control switches have been placed on front panel for user convenience.

BASELINE RESTORER:

A gated wraparound BLR capable of working with both unipolar and bipolar pulses has been provided. This is useful when the pulse amplifier does not have a BLR or is situated at a distance.

INTERFACE AND CONSTRUCTION:

The ADC provides a 37 pin SILENA/ECIL compatible address interface. However it is possible to change control and address polarity to suit any other kind of interface. A spectrum stabilizer interface has been provided for gain and offset correction inputs from digital two peak stabilizers.

The ADC is constructed as a single width NIM module.

FUTURE DEVELOPMENT:

Work is underway to construct an improved model providing (1) late coincidence with adjustable delay and (2) a Lowes' livetime corrector[1] interface. The first feature will obviate the use of a delay amplifier in many experiments. The second feature will provide correct livetime for normal MCAs when pile-up-rejector is used (the livetime reckoning of normal MCAs is incorrect when PUR is used unless a Gedcke-Hale scheme of correction[1] is employed within the MCA).

ACKNOWLEDGEMENT:

Dr T. Dutta and Shri J.K. Samuel of Radiochemistry Division, BARC and Dr. R.K. Chowdhury of NPD, BARC have been very generous in allowing the use of their equipment. We also wish to thank Shri K.R. Gopalakrishnan, Head, Nuclear Instrumentation Section, Electronics Division, BARC and Shri B.R. Bairi, Head, Electronics Division, BARC for providing encouragement.

REFERENCES:

[1]. R. Jenkins, R.W. Gould and D. Gedcke, Quantitative X-ray Spectrometry, pp 265-271.

HEAVY ION REACTION ANALYZER AT NSC

A.K.Sinha, N.Madhavan, J.J.Das, P.Sugathan, E.T.Subramanian, Bishambar Kumar, Rajpal Sharma, D.O.Kataria and Jacob Chako
Nuclear Science Centre, P.O.Box 10502, New Delhi 67

The Heavy Ion Reaction Analyzer (HIRA) is set up at the Nuclear Science Centre, New Delhi in collaboration with the universities. The electromagnetic configuration selected for HIRA is QQ-ED-M-MD-ED-QQ and the entire system is mounted on a rotatable platform. In this paper, the current status of HIRA facility and some preliminary test results obtained using an alpha source are described.

The electromagnetic components have all been mounted on the platform, aligned and the corresponding vacuum chambers installed. A sliding seal vacuum chamber has been set up for target assembly. At the focal plane, a 38 cm diameter chamber is being used for detectors. The vacuum pumping is being done using two large cryopumps and three turbomolecular pumps. The vacuum achieved in the electrostatic deflector chambers and in the magnetic deflector chamber is of the order of 10^{-8} Torr while in the target chamber and the focal plane chamber the vacuum is of the order of 10^{-7} Torr when all the gate valves are open.

The electrostatic deflectors have been conditioned, one upto +/-225 KV and the other currently upto +/- 190 KV.

A ^{252}Cf alpha source was mounted in the target chamber and aligned with the optic axis of HIRA. The source size as seen by HIRA was selected to be 2 mm in diameter by using a proper aperture. At the focal plane, a 8mm x 27mm one-dimensional position senstive surface barrier detector was mounted.

Figs. 1 & 2 show the position spectrum of the alpha particles at the focal plane of HIRA for two settings of solid angle defining aperture at the target chamber. For the small solid angle of 1 msr, FWHM was found to be 1.7mm and FW1/10M was 3.6mm (Refer Fig.1). For the same electromagnetic settings, the 10 msr solid angle gave FWHM of 2.6mm and FW1/10M of 13mm (Refer Fig.2). The long tail (poor FW1/10M) in the 10msr case is as expected and is due to higher order angle related aberrations. The count rate seen at the focal plane showed that the transmission efficiency of HIRA is reasonably good. In the above tests no sextupole or octupole optimization was done and the quadrupole fields were selected to give a reasonable transmission and x-focus at the focal plane.

This facility is set up with contribution from several persons. In particular, guidance and help from Prof.G.K.Mehta is to be mentioned. We also appreciate the initial help from Prof.A.P.Patro, Dr.D.Kanjilal, Dr.A.Mandal and several other colleagues.

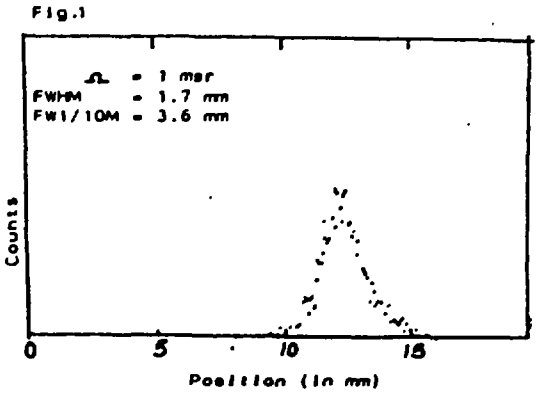

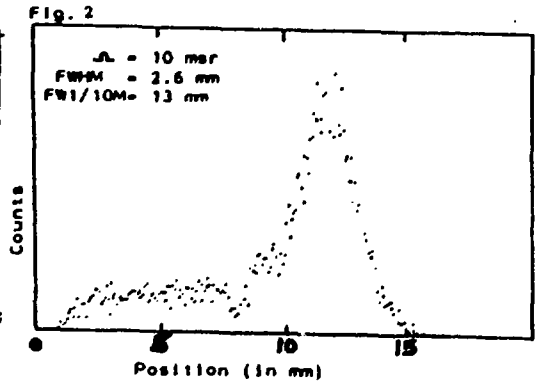

THE GENERAL PURPOSE SCATTERING CHAMBER AT THE NUCLEAR SCIENCE CENTRE

N.G. Puttaswamy, N.M. Badiger, and M. Raja Rao
Department of Physics, Bangalore University,
Bangalore 560 056.

AND

D.K. Avasthi, A. Tripathi, D. Kabiraj and
S. Venkataramanan
Nuclear Science Centre, JNU New Campus
Post Box No. 10502, New Delhi-110 067.

A 1.5-m diameter general purpose scattering chamber* has been installed at the Nuclear Science Centre, New Delhi, for studying charged particle reactions using the 15UD Pelletron accelerator. The scattering chamber made of stainless steel has diameter of 1.5 m and height of 0.6 m. The wall thickness of the chamber is 16 mm and the top/bottom plate has thickness of 32 mm. The beam entrance and exit ports are 4" in diameter. There are ten additional ports of diameter varying from 4" to 10"; however one 10" port is provided at 20^{o}. The chamber is pumped down by a 2000 lt/m (Alcatel) direct driven rotary pump and a 2000 lt/s (Edward's) diffstak pump mounted below the chamber. Eight targets can be mounted on a target ladder which is inserted from the centre of the bottom plate. Two independently movable detector arms have been provided. There is a provision to mount 5 ΔE-E telescopes on each arm at intervals of 6^{o}. The angle of detectors can be read with an accuracy of $\pm 0.05^{o}$ by using the scale and vernier provided on the index wheel attached to the detector-arm shafts. The targert ladder and detector arms can be moved independently by remote control.

* Built by Hind High Vacuum Co., Bangalore-560 058.

The rate of pressure rise has been determined to be 0.7 micron/h for the bare chamber and 3 micron/h when the accessories (viz., target ladder, detector arms, detector mounts, 22 lemo cables (RG 316), 4 SHV cables (RG 142) and the feed throughs) are kept in the chamber. The pump-down time to reach $2*10^{-6}$ mbar has been found to be 20 mins for the bare chamber and 5 hours for the chamber with accessories. The ultimate pressure reached has been found to be $3*10^{-7}$ mbar for the bare chamber and $5*10^{-7}$ mbar for the chamber with accessories.

A collimator arrangement has been provided at the entrance to the chamber with a provison to insert collimators of different sizes without disturbing the arrangement. A Faraday cup has been provided at a distance of 1.65 m away from the exit of the chamber.

In an experiment (using one collimator at the entrance to scattering chamber), elastic scattering of 80 MeV ^{16}O from ^{209}Bi has been studied on both sides of the beam. The offset angle of the detector measured in this experiment was found to be $+0.7^{o}\pm0.3^{o}$ as compared to $+0.3^{o}$ measured with a theodolite.

We are thankful to S. Gopal, University of Mysore, T.S. Mudhole, Karnatak University, and R.K. Bhowmik, Amit Roy and S.K. Dutta of Nuclear Science Centre for their help in the design of the chamber.

TARGETS OF EXPENSIVE MATERIALS

Jaipal, D.K.Avasthi, S.Gargari, J.Zacharias
Nuclear Science Centre, J.N.U.Campus
New Delhi - 110 067

Heavy ion sputtering[1,2] and Centrifuge machine[3] are quite useful for the preparation of target foils of expensive materials in small quantities. The present paper reports our experience in using these facilities for making the targets.

Heavy ion sputtering unit has been assembled and tested. A saddle field ion source B11W is used as a source of positive ions to sputter the target materials. Saddle Field ion source is chosen for the sputtering setup due to it's compact size, self focusing property and low cost. It has a design similar to that of Einzel Lens configuration. The source is mounted on a S.S. plate. The substrate holding arrangement as well as crucible for target material are also attached to the same plate with a tripod. There is a provision for varying the distance between the ion source and the target material. A thickness monitor FTM5 is mounted inside the beljar at about 45^0 to the ion beam direction facing the target material. Argon gas of 99.99% purity is passed in the ion source using a fine controlled leak valve. The vacuum in the chamber is maintained of the order of 10^{-6}mbar using a 280 l/s pumping station. The sputtered material is collected on glass slides in a close geometry. Ni target of thicknesses 63 $\mu g/cm^2$ was made as test cases. The ion current during the process was 100 μA at 7kV. The deposition rate for Ni at a distance of

70 mm was found to be 8 $\mu g/cm^2/h$. Since the substrate can be kept as close as 4 to 5 cm from the target material, the collection efficiency is high. The limitations of the set up is low deposition rate.

Arrangements are made to make thick targets of thickness 1 mg/cm^2 or above on mylar or on any other backing material using an centrifuge. Machanical fittings were made for 10 mm and 25mm diameter targets. The centrifuge tube is made of aluminium. The backing material is first fitted in between the aluminium cover plate and the centrifuge tube. The target material is added to ethyl acetate and kept in the centrifuge tube for about an hour. Liquid paraffine is added to this and kept in ultrasonic vibrator for about 1 hour so that a homogeneous suspension is made. The suspension is poured in the centrifuge tube and machine is set to run for 1 hour at a speed of 4000 RPM. The paraffine is sucked out of the tube and the tube is kept in vacuum oven for about 2-3 hours at a temperature of about 120^0.

This technique is found to be very useful for thick targets of powdered material.

REFERENCES:

1. G.Sletten and P.Kundsen , Nucl. Instr. and Meth. 102 (1971)459
2. A.H.F.Muggleton,"acuum ,Volume 37, Numbers 11/12 Pages 785-817
3. Isao Sugai Nucl. Instr. and Meth. 145(1977)409

DEVELOPMENT OF ETCHING AS A TECHNIQUE FOR NUCLEAR TARGETS

S.K.Pardha Saradhi, Md.Eqbal, and D.N.Rawat
Variable Energy Cyclotron Centre, Calcutta 700 064

Etching has often been employed as an auxiliary technique for surface treatment, pattern delineation, etc., in thin film technology. Occasionally, it is used for removal of backings of deposited films, too. We report here our studies in adapting chemical and electrochemical etching methods as a technique for fabrication of nuclear targets. By this, starting with a metal foil of a given thickness we can fabricate a target of any lower thickness.

Chemical Etching : In this method, the material being etched is first converted to a soluble higher oxidation state by a redox reaction. The bath may consist of a single component as in the case of V or more components as for the others. The starting foil is initially cleaned, annealed, and later degreased in a specially designed miniature Pyrex vapour degreaser (Fig.1) after which it is washed in methanol and deionized water. It is then etched to the required thickness in an appropriate mineral acid bath (Ref.1). A sufficiently large ratio of etchant to material is maintained and continuous stirring is employed to ensure an activation limited constant etching rate. In some cases, the etching is done in a special *angular etching unit* (Fig.2) to facilitate etching at 0°C.

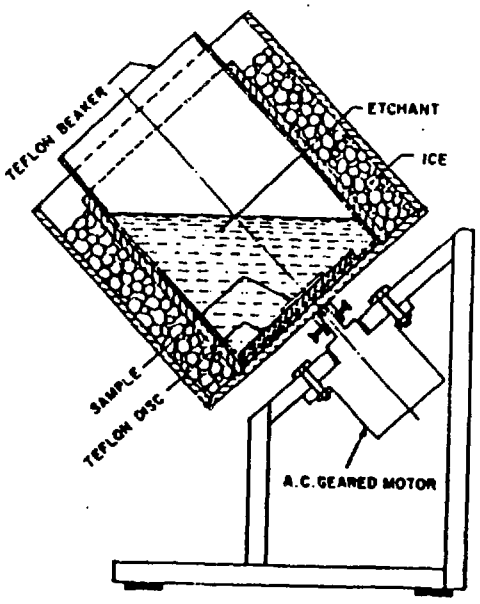

FIGURE 2: ANGULAR ETCHING

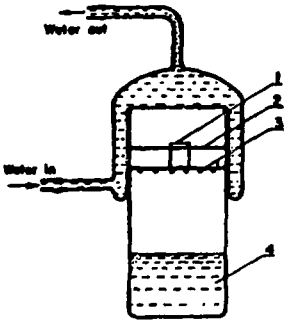

FIG.1. PYREX DEGREASER

Table-I

Matl.	Start t mg/cm^2	Etch-Rate (mg/cm^2)/mt	Target t mg/cm^2	Etch-Bath	Remarks
V	7.63	0.18	2.10	$HNO_3:H_2O::1:5$	
Ho	11.0	0.30	2.00	-do-	Surface preoxidized at 80°C
Si	35.0	0.23	1.05	$HF:HNO_3::1:20$	Angular etching at 0°C
Nb	10.7	0.58	2.0	$HF:HNO_3:H_2O$ (2:2:25)	Chem. etching
Nb	10.7	0.45	4.0	$HF:HNO_3:H_2O$ (2:2:50)	Electro-etching (J = 2mA/cm^2)
Ta	166.5	6.0	4.0	$HF:HNO_3:H_2O$ (1:1:5)	Chem. etching
Ta	166.5	1.80	4.0	$H_2SO_4:HF:H_2O$ (10:1:10)	Electro-etching (J = 2-3mA/cm^2) Etchant at 0°C

The reaction in the case of Silicon, for eg., is the following :

$$Si + 4HNO_3 \rightarrow SiO_2 + 4NO_2\uparrow + 2H_2O$$

$$SiO_2 + 6HF \rightarrow H_2SiF_6 + 2H_2O$$

The hydrofluoro-silicic acid formed in the process dissolves in water resulting in mass depletion.

Electrochemical Etching : In some cases, we resort to electrochemical etching where the etching rate can be control-led more accurately by adjusting the current density to obtain better suface finish for the target. The cell, which can accommodate a 35ml solution, is the same as was used by us for electrodepositions (Ref.2). Here, the starting foil is made as the anode whereas a 200-mesh Pt wire mesh acts as the cathode. The foil being etched is annealed in vacuum/Argon at regular intervals during reductions.

Details of the targets fabricated by these techniques are given in *Table-I*. These have been used several times in experiments with VEC.

Refrences : 1. Etching Processes, W. Kern & C. A. Deckert, p. 401 in *Thin Film Processes* AP (1978) & refs. therein.
2. S. K. Pardha Saradhi *et al*, DAE NP Symp. 32B 1989 p.O-14 .

THE MAXIMUM ENERGIES FOR MAKING THIN NUCLEAR TARGETS BY ION BEAM DEPOSITION

Arvind Jain
Nuclear Physics Division, BARC, Bombay-400 085

Thin films can be formed on a surface by ion beam deposition. Due to sputtering, the film will build up only if the self sputtering coefficient Y, or the number of atoms knocked out per incoming ion, is less than unity. For most of the elements the selfsputtering yield Y(E) is not available in the literature. A least square fit has been done to the available experimental sputtering yield data of nine elements viz. Al, Ni, Cr, Co, Cu, Sn, Ag, W and Au to the modified Sigmund equation /1//2/

$$Y(E)=0.42\alpha S_n[1-(E_{th}/E)^n]/U_s \qquad (1)$$

The parameters α, $E_{th}=K\,U_s$ and n have been kept as free parameters in the fit. U_s is the sublimation energy. S(E), the nuclear elastic crosssection, has been calculated at each energy using the average interatomic potential of Wilson et al./3/. The optimum parameters obtained from this global fit are $\alpha=0.1420$5, $E_{th}=11.485\ U_s$ and n= 1.5118. Using these constants, the energies have been calculated at which the sputtering yield becomes 0.25, 0.5, 0.75 and 1.0 respectively, for all the non gaseous elements in the periodic table and are given in Table 1. This information is useful for the preparation of nuclear targets by ion beam deposition. The calculated values of the energies for Y=1 using the fitted parameters are also compared alongside with the experimental values given by Almen and Bruce/4/.

El.	E(Y=1) calc.	E(Y=1) expt.
Ni	1100	1300
Cu	590	400
Ag	270	200
Sn	200	450

REFERENCES

/1/ P.Sigmund, Phys.Rev., 184(1969)383
/2/ N.Matsunami et al., Rad. Eff.Lett.57(1980)15
/3/ W.D.Wilson, L.G.Haggmark and J.B.Biersack, Phys.Rev. 15B(1977)2458.
/4/ O.Almen and G.Bruce, NIM 11(1961)287

TABLE 1

El.	E(eV)	E(eV)	E(eV)	E(eV)	EL.	E(eV)	E(eV)	E(eV)	E(eV)
For	Y=.25	Ø.5	.75	1.Ø		.25	.5	.75	1.Ø
Li	>1ØØØØ	1ØØØØ	1ØØØØ	1ØØØØ	Cd	19	27	37	52
Be	>1ØØØØ	1ØØØØ	1ØØØØ	1ØØØØ	In	46	75	13Ø	19Ø
B	>1ØØØØ	1ØØØØ	1ØØØØ	1ØØØØ	Sn	6Ø	11Ø	18Ø	28Ø
C	>1ØØØØ	1ØØØØ	1ØØØØ	1ØØØØ	Sb	5Ø	84	14Ø	22Ø
Na	25	5Ø	97	18Ø	Te	35	54	84	13Ø
Mg	37	81	17Ø	33Ø	Cs	13	17	22	29
Al	12Ø	37Ø	11ØØ	26ØØ	Ba	31	47	7Ø	11Ø
Si	19Ø	72Ø	24ØØ	1ØØØØ	La	57	9Ø	17Ø	29Ø
P	99	28Ø	69Ø	15ØØ	Ce	85	16Ø	27Ø	43Ø
S	79	21Ø	46Ø	955	Pr	72	13Ø	21Ø	33Ø
K	17	27	43	66	Nd	61	11Ø	17Ø	27Ø
Ca	39	74	14Ø	24Ø	Sm	37	56	85	13Ø
Sc	96	23Ø	48Ø	89Ø	Eu	31	45	67	96
Ti	15Ø	41Ø	955	19ØØ	Gd	67	12Ø	19Ø	29Ø
V	17Ø	46Ø	11ØØ	22ØØ	Tb	74	13Ø	22Ø	34Ø
Cr	12Ø	28Ø	6ØØ	12ØØ	Dy	52	83	13Ø	2ØØ
Mn	66	14Ø	27Ø	47Ø	Ho	55	89	14Ø	2ØØ
Fe	12Ø	28Ø	58Ø	11ØØ	Er	55	88	14Ø	22Ø
Co	12Ø	28Ø	58Ø	11ØØ	Tm	44	67	11Ø	16Ø
Ni	12Ø	27Ø	56Ø	11ØØ	Yb	29	41	58	82
Cu	81	18Ø	34Ø	59Ø	Lu	83	15Ø	24Ø	38Ø
Zn	24	38	59	9Ø	Hf	14Ø	26Ø	26Ø	75Ø
Ga	59	12Ø	21Ø	35Ø	Ta	19Ø	38Ø	71Ø	12ØØ
Ge	9Ø	19Ø	37Ø	64Ø	W	21Ø	43Ø	8ØØ	14ØØ
As	22	33	5Ø	75	Re	19Ø	38Ø	7ØØ	12ØØ
Se	41	7Ø	12Ø	19Ø	Os	19Ø	38Ø	7ØØ	12ØØ
Rb	27Ø	72Ø	16ØØ	31ØØ	Ir	15Ø	29Ø	52Ø	84Ø
Sr.	3Ø	48	75	12Ø	Pt	12Ø	22Ø	39Ø	62Ø
Y	96	2ØØ	37Ø	62Ø	Au	7Ø	12Ø	19Ø	28Ø
Zr	17Ø	38Ø	77Ø	14ØØ	Hg	14Ø	25Ø	44Ø	7ØØ
Nb	21Ø	52Ø	11ØØ	2ØØØ	Tl	31	43	62	86
Mo	18Ø	42Ø	85Ø	16ØØ	Pb	33	48	69	96
Tc	17Ø	39Ø	78Ø	14ØØ	Bi	36	52	75	11Ø
Ru	14Ø	3ØØ	58Ø	985	Po	24	32	44	6Ø
Pd	81	16Ø	28Ø	45Ø	Th	12Ø	21Ø	36Ø	56Ø
Ag	57	99	17Ø	27Ø	U	11Ø	19Ø	31Ø	47Ø
					Pu	71	12Ø	18Ø	27Ø

CANBERRA TO IBM PC INTERFACE FOR DATA ACQUISITION, ANALISIS, AND STORAGE.

S. K. Pal, A. Bandyopadhyay and S. K. De

Variable Energy Cyclotron Centre
1/AF, Bidhan Nagar, Calcutta - 700 064

At *VECC,* Calcutta, one CANBERRA SERIES-88 system is used for acquisition of experimental data and to record those data in a magnetic tape in-built with the system for off-line analysis. But the tape drive (PERTEC make) have been found to give frequent trouble. This type of magnetic tape is not manufactured now and the spare parts are also not available. For these complexities the following developments have been done to alleviate these problems.

Hardware : CANBERRA SERIES-88 System provides an EIA RS 232C compatible interface. The interface has a jumper socket at board location J1 which allows the RS 232C port to be configured as a Data set or a Terminal. As shipped, the interface will look like a Data set . This can be configured as a terminal by reversing the jumper plug [1]. This RS 232C port has been connected to the IBM PC Com1 port for the communication. There are two clock generators, one for TTY and one for EIA terminal. This EIA generator was set at 300 baud. With the existing hardware it can be increased upto 1200 baud only. But, by suitably modifying the hardware in the board level we have achieved the baud rate as 4800.

Software : An interrupt driven program has been developed in a user friendly way for transferring and storing data in both direction i.e from CANBERRA to IBM PC or from PC to CANBERRA. The entire code has been written in PASCAL language and it is menu driven. The serial interface is built around a Universal Asynchronous Receiver/Transmitter (UART) LSI circuit. When transmitting data to a device, the UART inserts the start bit before sending a character and inserts the stop bits following the character. When data is received the UART will synchronize to the start bit and check parity if any, for each received character [2]. The data can be transferred in both ASCII and BINARY mode. In ASCII mode the eighth bit is generated to give even parity for each character (byte). In BINARY mode

no parity is maintained but the Title and Header are as in ASCII mode. The ASCII character in the Title and Header have a zero in the eighth level (bit) of each byte.

In BINARY mode the time taken to transfer one 4K spectrum is about 45 seconds, whereas in ASCII mode it takes about 4 minutes. So to transfer Data we prefer BINARY mode. A program has been developed to convert BINARY data to its ASCII format such that one can get print out of the spectrum directly from BINARY data.

In order to analyse the data in IBM PC, a program has been developed which will convert the CANBERRA'S BINARY data to the required format of the Analysis program. Thus the acquisition of the experimental data in CANBERRA-88 and the analysis of the spectrum in IBM PC can be done parallely in on-line.

The data can be stored in the hard disk of the PC or in floppy disks by giving different file names for different spectrum. From these stored data off-line analysis can be done either in PC or in ND Computer. In the ND Computer the analysis program VECSORT is available. A SWAP program has been written to convert CANBERRA'S BINARY data to the required format that the VECSORT needs. With this facility one can get the plot of the spectrum either in Tektronix Plotter or in XY-Plotter.

The above modifications of hardware and the software which have been developed are working fine without giving any trouble. This development allows the user of CANBERRA MCA to dump his spectrums directly in IBM PC for further analysis in PC or ND computer simultaneously with acquistion.

References :-

[1] CANBERRA SERIES-88 schematics.
[2] IBM PC-XT Technical Reference Manual.

A CAMAC INTERFACE FOR SPECTROSCOPY ADCS

B.P. Ajith Kumar, S. Naithani, & R.K. Bhowmik
Nuclear Science Centre,JNU Campus, New Delhi 110 067

For high resolution work, spectroscopy ADCs with a resolution of 13 bit or more and fast conversion time are an essential component of the data acquisition sytem. Due to the highly noisy environment inside a CAMAC crate, CAMAC based high resolution ADCs are very expensive and have only recently been commercially available. It was therefore decided that the data acquisition system at the Nuclear Science Centre would be developed by interfacing NIM based Spectroscopy ADCs to the CAMAC crate. The interface should allow multi-singles data to be taken independently from each ADC in an uncorrelated single parameter mode or in succession from multiple ADCs in a Multiparameter mode. The present paper deals with the design features for an eight ADC interface for CANBERRA 8075 13 bit ADCs.

The ADC interface is divided into two parts, a single width CAMAC module for addressing upto eight ADCs and two double width NIM modules housed in NIM bins. Upto four ADCs can be connected to each NIM module. Two ribbon cables with 26 pin FRC connectors are used to connect the two NIM modules to the CAMAC module (fig 1).

The control lines of the eight ADCs are mapped to the subaddresses 0 - 7 of the CAMAC module. When an NAF instruction with F=0 is issued to the CAMAC module, an Enable Data signal is issued to the corresponding ADC through the NIM interface. The enable data signal causes the ADC to feed the 13 bit data onto its output lines. This data is buffered and passed through the FRC connector to the CAMAC module. It is possible to encode the unused bits 14-16 of the 16 bit data word with the A-information for a unique identification of the ADC being read.

At S2 time, a DATA ACCEPT signal is sent to the

ADC to reset it and enable a new conversion. A F10 clear signal from the CAMAC module also resets the ADC.

The conversion times for the 8075 ADCs depend on the pulse height, and for multiparameter mode of operation the readout is initiated by an external signal after all the ADCs having data have finished conversion. The CANBERRA 8075 ADC, after end of conversion, issues a Data Ready (RDY) signal. Absence of this signal causes zero data to be transferred to the CAMAC crate.

For single parameter mode of operation, the OR of the RDY signals from the ADCS can be used to generate a LAM and cause a readout of all the ADCS. Since each ADC is uniquely identified by the top three bits of the data, the software can generate separate histograms for each ADC. to reduce software overhead in processing zero data, absence of a RDY signal causes a VETO signal to be issued by the CAMAC module that suppresses data transfer. Each ADC can thus be scanned in the polling mode once in 8 us. Since CANBERRA ADCs have a double buffered data, no significant dead time is introduced by the scanning procedure.

ADC INTERFACE MODULE (NIM and CAMAC PARTS)

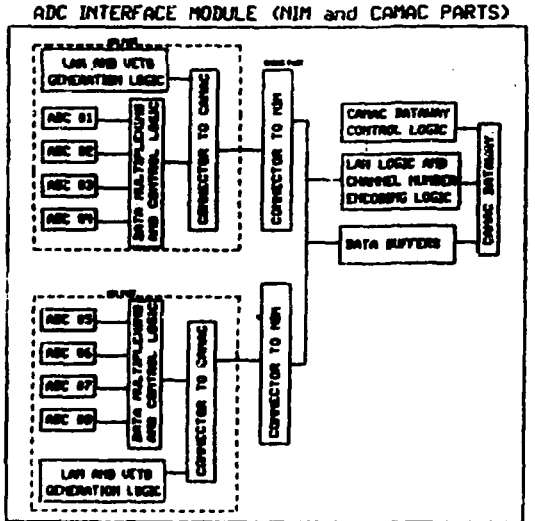

FIG. 5

A MULTIPLICITY FILTER ARRAY FOR GAMMA RAY SPECTROSCOPY

S.Muralithar, G.O.Rodrigues, R.P.Singh,
S.Venkatraman, S.Naithani and R.K. Bhowmik
Nuclear Science Centre,JNU Campus, New Delhi 110067

The compound nucleus produced in a fusion reaction undergoes particle decay and subsequently deexcites by emitting gamma rays. An estimate of the total angular momentum and energy carried away by photons can be done by surrounding the target by an array of detectors and detecting as many of the photons as possible. A crude selection of the entrance channel angular momentum can be done by insisting that a minimum number of photons be detected. This is the basic principle of a Multiplicity Filter array.

The Gamma Detector Array (GDA) facility at Nuclear Science Centre consists of six Compton suppressed 23% Ge detectors and fourteen BGO Multiplicity filter elements. The BGO elements have hexagonal shape with a face to face dimension of 38 mm and a length of 75 mm. They are arranged in two rings 40 mm above and below the target covering nearly 35% of the total solid angle. Details of the experimental arrangement is given in [1].

In a typical experiment, the Ge detectors have a count rate of 5 - 10 K/sec and BGO elements 50k - 100k/sec. The combined count rate of 500K-1000K/sec from the BGO ball requires a careful handling of the electronic signals. The special feactures of the electronics setup are reported in this paper.

The anode signal from the BGO elements are integrated over a 10K Ohm load and sent to the electronics setup through a homemade preamplifier. After suitable amplification they are shaped to a width of 200 ns by a Pole-Zero compensated shaper. Signals from the BGO elements are individually delayed by 150 ns by long cables and fed to two

Octal Constant Fraction Discriminators CF8000 from ORTEC,USA. The logic pulses from Discriminator are internally stretched to 50 ns width and the multiplicity output from each CF8000 is added together in a fast summing amplifier to get the multiplicity output. A fast discriminator is used to select the high multiplicity events.

Due to the extremely high count rate in the filter array and correspondingly large random coincidence rate with the Ge detectors, the basic system could not be used reliably. The CF8000 has a VETO input for a fast gating of the individual logic outputs with respect to an external gate. The timing outputs of the Ge detectors are stretched to 50 ns, ORed together and used to gate the CF8000 reducing the Ge-BGO random rate to an acceptable value. To obtain an analogue information about the Multiplicity and total energy, these signals are passed through a fast linear gate derived from the Ge-Ge coincidence logic, shaped by 0.5 us shaping amplifiers and recorded along with the Ge energy signals. An example of the Multiplicity distribution in the reaction 31P + 65Zn at 115 MeV is shown in fig 1.

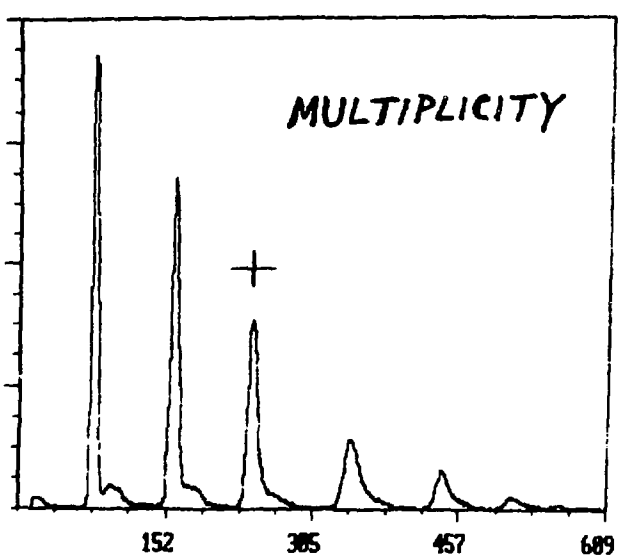

The generous help received from all the resident students and visiting faculty members in setting up and testing the facility is gratefully acknowledged.

[1] R.K. Bhowmik, Proc. DAE Symp 33A(1990)221

AN ANALYSIS PROGRAM FOR MULTI-DETECTOR ARRAY

R.K. Bhowmik, D.K. Goyal & S. Ghugre*
Nuclear Science Centre, JNU Campus, New Delhi 110 067

The gamma detector array (GDA) at NSC consists of six Compton suppressed high resolution germanium detectors and an array of fourteen multiplicity filter elements. For coincidence measurements, a Bit Pattern word identifying the detectors in coincidence, the energies of the corresponding gamma rays, and additional information like multiplicity, time difference etc are recorded event by event on magnetic tape by the ONLINE program. In the conventional mode of analysis, one dimensional histograms for each detector energy, gated by other detector energy are generated off-line. Since there are fifteen different combinations with each detector having separate calibration, the conventional method of data analysis is very inefficient and time consuming. The present paper describes the method used for an efficient analysis of multi-detector array data.

In the analysis program, the display and the sorting of mag tape are done by separate sub-processes running under VMS operating system. As a result, the processed data can be displayed while the sorting is in progress. The pulse heights in each detector are converted to keV by software gain matching and a large (1024 x 1024) data matrix is created with the energies of the two gamma rays along x & y direction. The large matrix can be saved as a disk file and susequently read back for a more detailed analysis.

As the Doppler shift of a level is dependent on angle and lifetime , all the detectors at a given angle are treated identically and data for a given angle pair combination are added together. Although most computers support large virtual arrays, random access to different segments of the virtual memory results in an undesirable amount of disk swapping.

The data are internally buffered in software before writing to the virtual memory resulting in an efficient sorting algorithm even for very large arrays (i.e. 4k x 4k). Even larger arrays may also be analysed by multiple passes through the data tapes.

Starting from the large matrix, one dimensional histograms for gamma energy at one angle gated by gamma energy at a different angle can be generated. Fig 1 shows an example of such analysis where the gamma rays produced in the reaction 30Si + 27Al at 85 MeV were analysed. By putting the gates on the 238 keV and 317 keV, the corresponding lines of 51Mn and 51Cr can be identified. By swapping the x & y gates, the Directional Correlation Ratio can also be calculated.

The program has additional features for analysing charged particle data. For example, Mass function and multiple BANANA GATES for charged particle telescopes and zero-suppression for sparse data are supported. A HELP file is available for explanation of each command.

* student, Bombay University

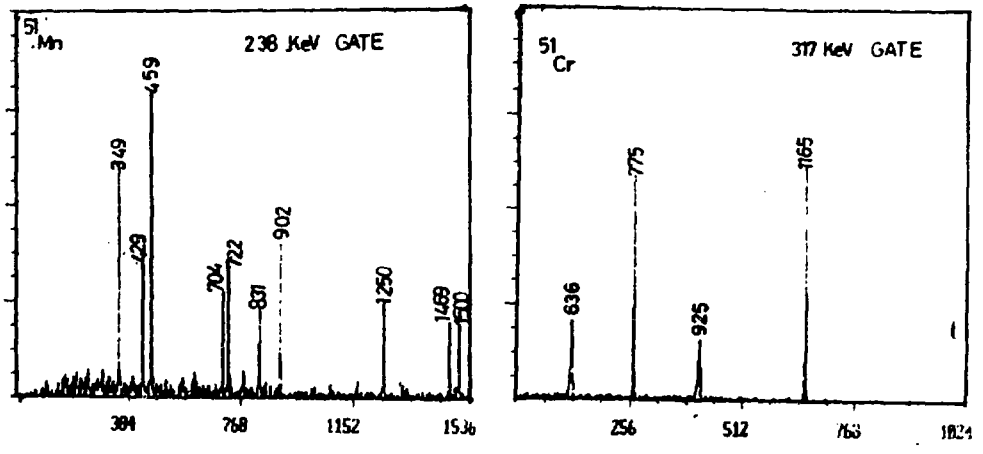

EFFICIENCY DETERMINATION OF Si(Li) X-RAY DETECTOR IN THE ENERGY RANGE 1-20 KeV

L.C. Tribedi And P.N.Tandon
Tata Institute of Fundamental Research,Bombay-5

Conventional method of using calibrated radioactive sources for determining the efficiency of an *X*-ray detector at very low energies $\leq$ 5 KeV is not common because of the non availability of convenient sources. In this energy range *PIXE* cross sections are increasingly being used with more confidence. The 'reference' cross sections generally used are derived from a large body of experimental data and theoretical calculation for ionization cross section [1]. We have determined the efficiency of our *X*-ray detector in the energy range 1-20 KeV and beyond by choosing suitable radioactive sources to cover the extended energy range. We have also measured *PIXE* cross section using 1 *MeV* proton beam to obtain many over-lapping data points for the efficiency curve in this energy range with an intention to test the suitability of these reference cross sections for efficiency determination particularly in the low energy region.

Carrier free 'point' sources of ^{54}Mn, ^{57}Co and ^{241}Am were used. They were mounted in the *PIXE* geometry on a holder inside the chamber. Both the source and the detector were in vacuum. The effect of self absorption was investigated by changing the angle between the source and the detector. The strength of the sources was determined by counting the photo peak of the high energy γ-rays in a well defined geometry with a standard integral $7.5cm \times 7.5cm$ *NaI(Tl)* detector. Additional counting was done for ^{241}Am source. The absolute efficiency was obtained using the known intensity of the emitted *X*-ray or gamma ray per nuclear decay[2] and is shown in fig. 1. It also shows efficiency data obtained by measuring *PIXE* cross section using thin targets of *NaCl,Mg,Al,Si,InP,KCl,*CaF_2*,Ti,Fe* and *Cu* and recording the spectra of the scattered particle along with the corresponding *X*-ray emitted simultaneously in a multichannel analyser.The agreement between the two sets of data is very good. The two sets of data corresponding to two different detectors, differs in there efficiency response curve particularly in the region 4-20 KeV. This difference in attributed to peripheral dead layer on one of the detectors.(fig. 2). The data was fitted to the usual expression for efficiency including various absorbers in the path of the *X*-rays upto active volume of the detector and the effect

of the dead layer. The reference cross section data as seen from the fitted curves could be relied upon for efficiency measurements also in the region $\leq$ 5 KeV

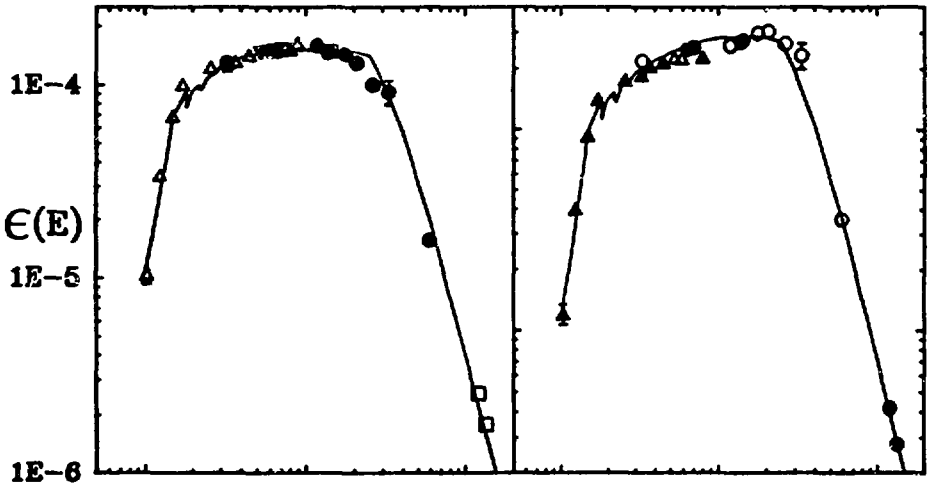

FIG . 1 FIG . 2

References:

1. H.Paul and J. Sacher Atomic Data and Nuclear Data tables 42(1989)106.
2. K.M.Barfoot et.al, NIM,85(1984),534.

DETERMINATION OF CARBON ON SURFACE BY PROTON RESONANCE SCATTERING

J. V. Ramana, Sanjivkumar, V. S. Raju, S. Gangadharan & S. Kailas*
Analytical Chemistry Division, B. A. R. C. BOMBAY - 400 085.
*Nuclear Physics Division, B. A. R. C. BOMBAY - 400 085.

INTRODUCTION: Non destructive determination of low Z elements, especially Carbon, has assumed considerable importance in many applications. (1,2) In recent years elastic backscattering by ^{4}He and ^{1}H ions is widely used for microanalysis in solids. (3)

A thorium sample of around 200 $\mu g/cm^2$. deposited on an aluminium backing had been used in Heavy ion reaction cross-section measurements at Pelletron Accelerator. This sample had a build up of carbon deposit on its surface due to ion beam cracking of vacuum system oil vapours. This had an effect on bombarding energy of incident beam and and also interferes with nuclear reactions from the target. The present work demonstrates a novel way to determine the carbon content on the surfaces by analysing the backscattered protons at about 165°, at the resonance energy of 1.73 MeV using the $^{12}C(p,p)^{12}C$ reaction. (4)

EXPERIMENTAL: The proton beam from the 5.5 MeV Van-de-Graff Accelerator at the Nuclear Physics Division is used in this work with a home made Silicon Surface barrier detector of 20 mm^2. active area for charged particle detection. The energy resolution of this detector is experimentally found to be <20 KeV. The measurements were carried out at a laboratory scattering angle θ=165° and E_p = 1.73 MeV with a resonance cross section of ≅930 mb with a width of ≅ 45 KeV.

Carbon films were generated by vacuum arc deposition (≅20$\mu g/cm^2$) and also by depositing a known amount of carbon on Al foils (16$\mu g/cm^2$ as measured using a micro balance) to be used as standards.

DATA ANALYSIS & RESULTS: The spectra are shown in fig. 1. The area under the peaks have been calculated and normalised with the standards. The carbon content is calculated to be 45 $\mu g/cm^2$ on target.

REFERENCES:

1. T. Nozaki etal. Journal of Rad. Anal. Chem, 19, (1974), 109
2. Y. Iton etal. Journal of Rad. Anal. Chem. 70, (1982) 329
3. W. K. Chu etal. Backscattering Spectrometry (AP) N. Y. 1977
4. E. Rauhala Nuclear Inst. & Meth. in Phy. Res. B12, (1985), 447

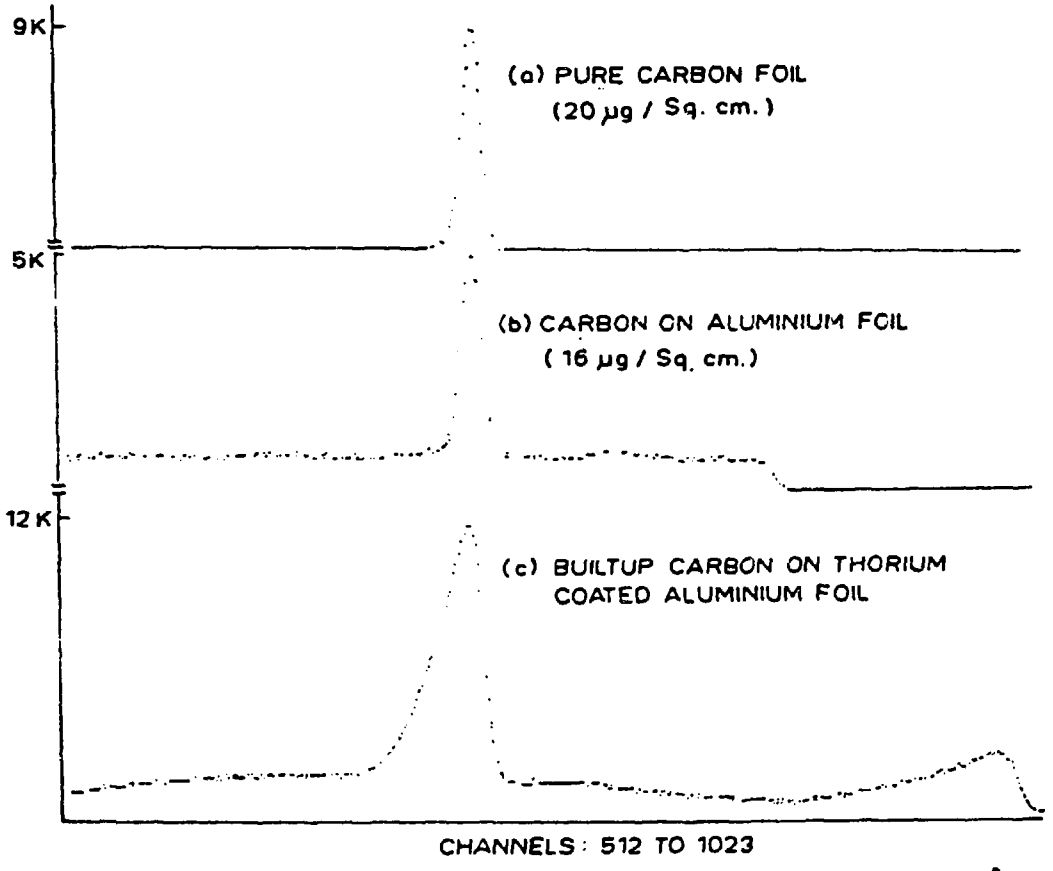

FIG. 1 PROTON BACKSCATTERED SPECTRA AT E_p = 1.73 MeV $\theta = 165^\circ$

NOVEL TECHNIQUES TO MEASURE ISOTOPE SHIFTS AND HYPERFINE STRUCTURE USING LASER SPECTROSCOPY

S. B. Dutta[a], Cyclotron Institute, Texas A&M University; D. L. Clark, Eastman Kodak Research Company, Rochester; T. U. Kuehl, GSI, Darmstadt, Germany; G. D. Sprouse, SUNY, Stony Brook.
[a] Present address: SUNY, Stony Brook.

Measurement of optical Isotope Shifts(IS) and Hyperfine Splitting(HFS) of natural and radioactive isotopes has been considered to be a sensitive method to study nuclear ground state properties viz., nuclear spins, moments and change in mean square charge radius. Large laser-atom interaction crosssection and high resolution obtained by tunable lasers make IS and HFS measurements quite important. New regions of nuclear deformations, shape transitions and shape coexistence have been revealed from these measurements. Current interest in this area is to develop techniques that can be used to study isotopes which are extremely short lived and available only in minute quantity. In the following section, a few different techniques will be described since each method is uniquely suitable to study a typical group of isotopes.

At the University of Rochester, NSRL, a very sensitive detection system was developed using photon burst technique that allows one to make measurements on as low as 50 atoms/sec crossing the laser beam. Heavy ion fusion evaporation reaction products were implanted in a tantalum oven which in turn was heated to form a collimated, thermal atomic beam. The atomic beam was intercepted by a laser beam in the perpendicular direction to avoid Doppler broadening and the correlated burst of photons were detected in a coincidence arrangement between two photo multiplier tubes. This method uses multiple excitation of a single atom which is basically limited to two level atoms and is not at all useful for atoms with complex atomic energy level structure.

Collinear laser spectroscopy have been used successfully by GSI, University of Mainz and ISOLDE collaboration to study long chains of isotopes. This method relies on efficient mass separation and is limited to life times of radioactive isotopes of the order of a few seconds. The photon detection efficiency being poor in the arrangement, one needs atleast 10^5 - 10^6 atoms/sec to be produced in the secondary ion source to make reliable measurements. In this method, mass separated radioactive isotopes are obtained as ions with energy about 50 keV. The fast ion beam is neutralised in an alkali charge exchange cell and normally transition is driven from a metastable state which is efficiently populated by charge exchange reaction. A collinear laser beam is overlapped with the fast beam and resonance fluorescence is detected by a photo multiplier tube situated perpendicular to the atomic and the laser beam directions. So far, this method proved to be the most universal one.

Another method was developed by GSI, Stony Brook collaboration to study the refractory elements which are inaccessible to the ISOLDE or GSI massseparator. Here, heavy ion fusion evaporation reaction products are implanted in an ultra pure cold argon gas cell. The projectile is separated out of the recoiling reaction products by mounting the gas cell at the end of the SHIP velocity filter at GSI, and this reduces any unwanted plasma formation in the gas cell. The reaction products are stopped and neutralised within a volume of approximately 1.5 cm^3 near the center of the cell. These atoms are illuminated with a laser beam and resonantly scattered photons are detected by an efficient light collection system placed in the perpendicular direction. The pressure broadening in the gas cell do not allow very high resolution measurement, but the method shows promise for measurements on isotopes with life times of the order of milliseconds and presence of 10^4 atoms/sec in the cell.

Results obtained in the above experiments will be discussed.

DETECTION OF ^{8}BE USING A SURFACE BARRIER DETECTOR TELESCOPE AND ITS DETECTION EFFICIENCY CALCULATION

Suresh Kumar, M. A. Eswaran, E.T. Mirgule
Nuclear Physics Division, B.A.R.C., Bombay-400085

As ^{8}Be nucleus even in its ground state is 92 keV unbound for decay into two alpha particles, the detection of ^{8}Be particle involves detection of its breakup α-particles in coincidence[1]. Here we report on a simple ΔE-E surface barrier detector telescope[2], which was employed to identify ^{8}Be besides other charged particles.

When the two α-particles of similar energy from the breakup of ^{8}Be, enter simultaneously into a conventional telescope it is identified as a ^{7}Li particle in the ΔE-E plot. This is because ΔE is proportional to $\sim mZ^2/E$ which is equal to 1/E, 16/E, 63/E and 64/E for protons, alphas, ^{7}Li and ^{8}Be of energy E. Though ^{7}Li and ^{8}Be are very close in ΔE-E plot, the Q-value corresponding to ^{8}Be exit channel is often more positive than the ^{7}Li exit channel. Hence upto ~15 MeV excitation range ^{8}Be can be detected without any interference from ^{7}Li.

In Fig.1(a) the velocity diagram is shown to illustrate the kinematic focusing of breakup alphas from a ^{8}Be of velocity V_8 (energy E_8), into a narrow cone of half angle $\beta_{max} = \sin^{-1}(\bar{v}/V_8) = \sin^{-1}\{(Q_8/E_8)^{1/2}\}$. Where Q_8 is the Q-value of ^{8}Be decay into two α-particles and $\bar{v}$ is corresponding c.m. velocity of each alpha particle. In Fig.1(b) the radial distribution of α-particles on detector corresponding to a given direction of ^{8}Be is illustrated, where $r_m = D \tan(\beta_{max})$ and R_d is the radius of the detector. As β_{max} is small (< 4 for $E_8 > 20$ MeV), the lab. angles β_1 and β_2 are approximately equal. With this approximation one can derive the fraction

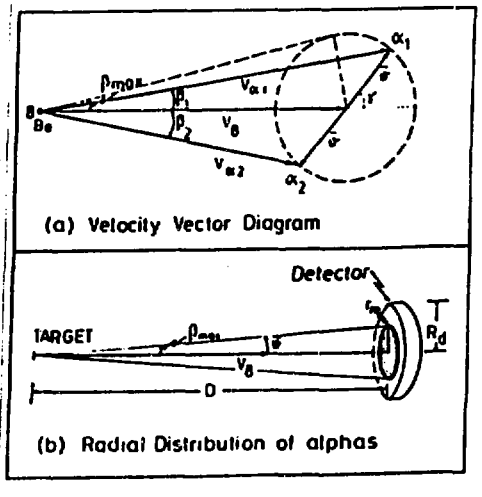

Fig.1

$F(r)$[1], for both breakup α-particles to fall in the annular region between r and r_m as $[1-(r/r_m)^2]^{1/2}$. If the ^{8}Be incident direction points close to perifery of the detector, only part of α-particles' cone will be intercepted by the detector and hence probability of ^{8}Be detection will accordingly be less than 1. By integrating the ^{8}Be detection probability over the entire area of the detector one can calculate the ^{8}Be detection efficiency. A computer program CEFFA is written to compute the ^{8}Be detection efficiency.

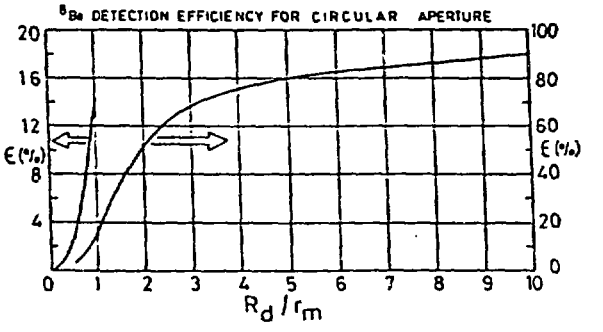

Fig.2

As the detection efficiency depends only on the dimension of the detector relative to r_m, the ^{8}Be detection efficiency, for circular aperture, plotted against (R_d/r_m) in Fig.2 which is applicable in general.

Such a telescope consisting of 30 μm ΔE and 2 mm E surface barrier detectors with radius R_d of 11 mm at a distance D of 13.4 cm was employed to study[2] the reactions $^{12}C(^{16}O,^8Be)^{20}Ne^*$ and $^{12}C(^{16}O,\alpha)^{24}Mg^*$ for ^{16}O beam energy from 60 to 90 MeV. The alpha and ^{8}Be spectrum were obtained using two dimensional gates on ΔE-E spectrum. An example of ^{8}Be spectrum obtained from the telescope at 63 MeV is shown in Fig.3, where the ^{8}Be peaks corresponding to low lying states of ^{20}Ne can be clearly identified. The efficiency of the telescope which varies with ^{8}Be energy is shown in the inset, where arrows indicate the position of the four marked ^{8}Be peaks in the spectrum.

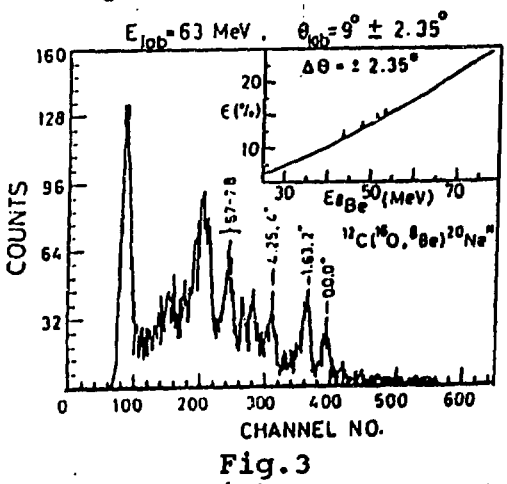

Fig.3

1) G.J.Wozniak et.al. Nucl.Inst.& Meth. 120 (1974) 29
2) Suresh Kumar et.al. NP Symp.(DAE) Madras (1990)103

POSITION SENSITIVE GASEOUS DETECTOR FOR HIRA

M.C.Radhakrishna, M.Raja Rao, N.G.Puttaswamy
Department of Physics, Bangalore University,
Bangalore 560 056
D.O.Kataria, A.Roy, A.K.Sinha
Nuclear Science Centre, New Delhi 110 067

Position sensitive gaseous single wire proportional counters of both stop-type as well as transmission-type, for use at the focal plane of the Heavy Ion Reaction Analyser at the NSC Pelletron have been fabricated and tested.

The body of the dectector is a single steel block 30cm X 5cm X 1Cm in which a rectangular slot 25cm X 2cm has been milled. A 0.001cm diameter nichrome anode wire of length 23.5cm and resistance about 4000 Ohms is streched along the axis of the slot, supported at each end by a vacuum-tight electrical feed-through bushings mounted on to a metal plate in the case of stop-type, and on to a window frame in the case of transmission type detector. One face of the counter is sealed by a 25cm X 3cm X 0.0006cm mylar window aluminized on the inner surface; the other surface is sealed either by a metal plate or else by a second window, when transmission of particles is desired. The seals are made with O-rings. A gas connection is provided at each end to permit the filling gas to flow continuously through the counter.

Testing of the detector was carried out by placing it within a vacuum chamber. A radioactive source ^{252}Cf is placed in front of the detector at about 20cm from it. A vacuum of 1m torr is maintained in vacuum chamber. The front face of the counter is covered with a aluminium foil with 10 slits of 0.2cm wide spaced 2cm apart. Electrical connections are made through the chamber walls to external modules via appropriate leads. Gas connections are also brought through the walls of the chamber.

The resistance of the anode wire being about 4000 Ohms, allows for effective use of the charge division method[1] of position determination. The two ends of the wire are connected to charge-sensitive preamplifiers. The outputs from the preamplifiers are connected to ADC units and an on-line computer through the main amplifiers. Also,

the strobe signal for the ADC is fed from one of the preamplifiers, properly shaped using timing filter amplifier, a constant fraction descriminator and a gate and delay generator.

A continuous flow of P10 Gas (90% Ar-10% CH_4 mixture) is maintained at a pressure of 80 torr in the counter. Each incoming fission fragment from the source produces a total current pulse I generated within a region along the wire around the position X from one end of the wire. The current devides and flows to ground through the pre-amplifiers, greater current flowing through the nearer one. If I1 and I2 are the currents from either ends of the wire, the computer calculates the implicit position X = (I1/I1+I2) for each event and uses these results to update the appropriate position spectrum created in the memory. A typical position spectrum obtained with this detector is shown in Fig.1. The position resolution thus obtained is better than 0.6mm.

The financial support for this work by UGC-NSC is gratefully acknowledged.

Reference:

1. G.L.Miller et.al., Nucl.Instr.& Meth.91 (1971) 389.

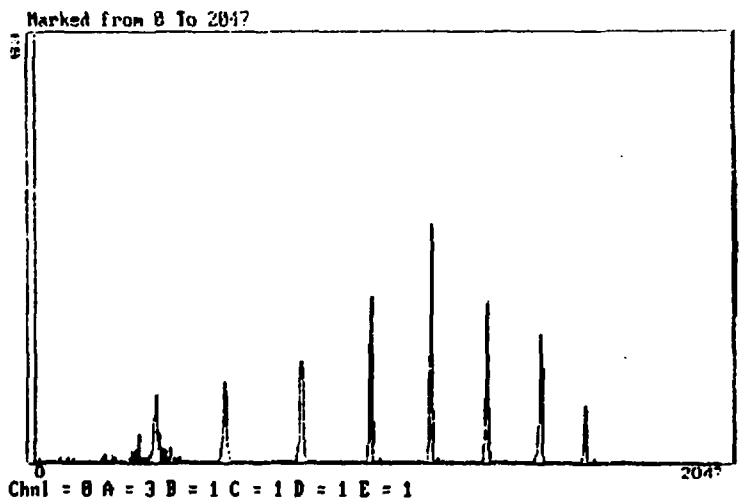

Figure 1. Position spectrum indicating (I1/I1+I2) along X-axis and the number of counts on the Y-axis. Peaks indicate the events as seen by the detector through the slits on the aluminium foil.

PERFORMANCE CHARACTERISTICS OF LARGE AREA POSITION SENSITIVE IONISATION CHAMBER

S.R.S.Murthy, V.S.Ambekar, D.C.Biswas, B.V.Dinesh, L.M.Pant and R.K.Choudhury.
Nuclear physics division, B.A.R.C, Bombay-400 085.

A large area position sensitive ionisation chamber has been developed for studying heavy ion induced nuclear reaction experiments using BARC-TIFR Pelletron facility. Using this detector, simultaneous measurement of energy, mass, charge and angle of emission of the reaction products are possible. The details about the design and other aspects of the detector has been reported earlier [1]. In this paper we present the results obtained from off-line tests using alpha particles from ^{241}Am-^{239}Pu sources and fission fragments from ^{252}Cf source. Collimated ^{241}Am+^{239}Pu sources were mounted in the detector and energy spectrum was obtained at various anodes(A_{1-4}). A typical energy spectrum measured from A_3 is shown in fig.1. The energy resolution (FWHM) was found to be 80 KeV for alpha particles at 200 mbar gas pressure. In order to obtain position resolution, a ^{252}Cf source was mounted in the target position inside the scattering chamber to simulate the in-beam experimental condition. The ionisation chamber and the scattering chamber were isolated by a 6 micron thick poly-propylene window and the detector was filled with P-10 gas of about 40 mbar pressure. The position information is obtained by delay-line method using anode pulses as start and pulses from θ-grid as stop signal. The θ-resolution was obtained by putting two vertical masks of about 3.5 deg each and the spectrum thus obtained is shown in fig 2. The FWHM is found to be 2 deg. The ϕ -information was obtained by electron drift time method and was measured by the time difference of cathode pulses and anode pulses. To measure the ϕ -resolution two horizontal masks covering 0.8 deg each was used and the spectrum is shown in fig.3.

The ϕ -resolution(FWHM) thus obtained was found to be 0.5 deg. Experiments are being planned to use the detector for heavy ion reaction studies using Pelletron accelerator.

FIG.1.

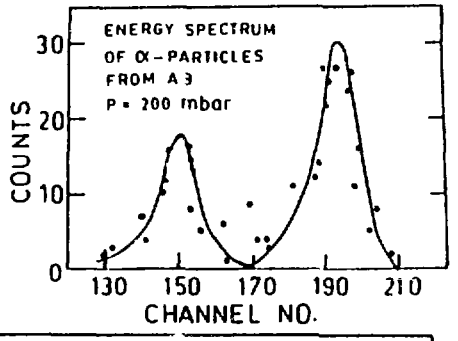

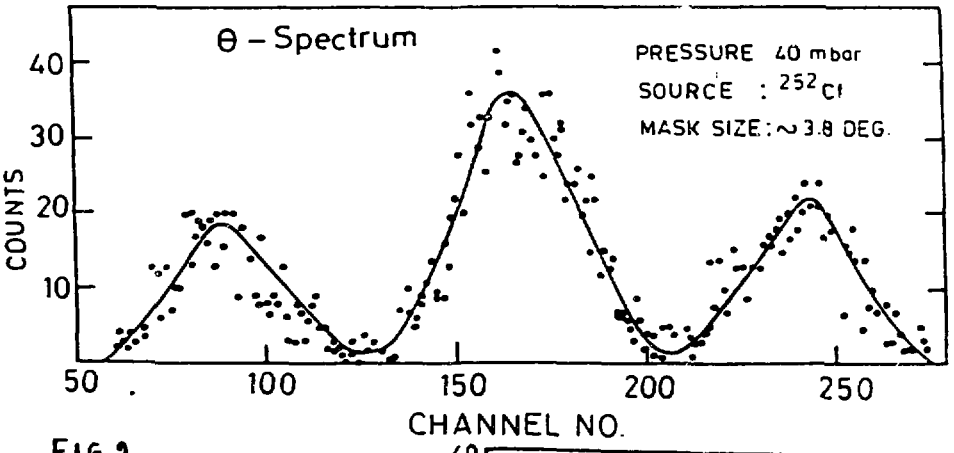

FIG.2.

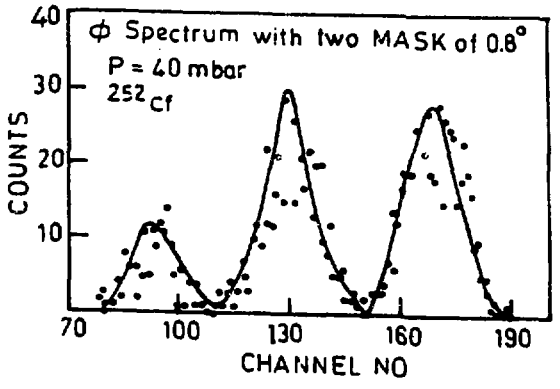

FIG.3.

Reference:

1) G.R.S Murthy, Invited Talk, Nucl. Symp. Dec.30A, P348, 1987, Bombay.

SIMULATION OF ATTENUATION EFFECTS IN THE SAMPLE

N. L. Singh and B. J. Patel
Physics Department, M.S.U. Baroda - 390 002

The exact magnitude of these effects are essential in the study of neutron activation cross section, specially in the case of (n,p) and (n,α) reaction, where the cross section are few tens of mb or less in magnitude. Actually in the neutron activation analysis, the samples and the solid angles are large to get good statistics, complex corrections have to be applied for the self scattering and self absorption effect in the target and pile-up effect in the detector. Taking special care of the above corrections experimentally by the " Simulation technique " /1/, which enables the exact magnitude of corrections to be known precisely.

The sample whose cross-section is to be measured is mixed uniformly with Al aluminium powder (monitor). This mixture is then pressed into a form of pellets of diameter 2 c.m. and thickness .2 - .3 cm each. Three or four such pellets comprise the cylindrical experimental target for neutron irradiation. Before irradiating however, relative efficiency measurements are made, for a predetermined target - detector geometry, using a thin uniform disc of standard Eu - 152 source, having same diameter as a target. This disc is then carefully kept between the pellets successivelly taking position between first and second, second and third and so on. At each position the standard Eu-152 spectrum is recorded. The respective position are designated as (0,3),(1,2), (2,1),(3,0), where the left hand side number in each bracket represents the number of absorber pellet standing between the detector and the disc source.

The average of the four spectra, so taken, would represent the spectrum of a " Simulated " cylindrical source of Eu-152 in which self

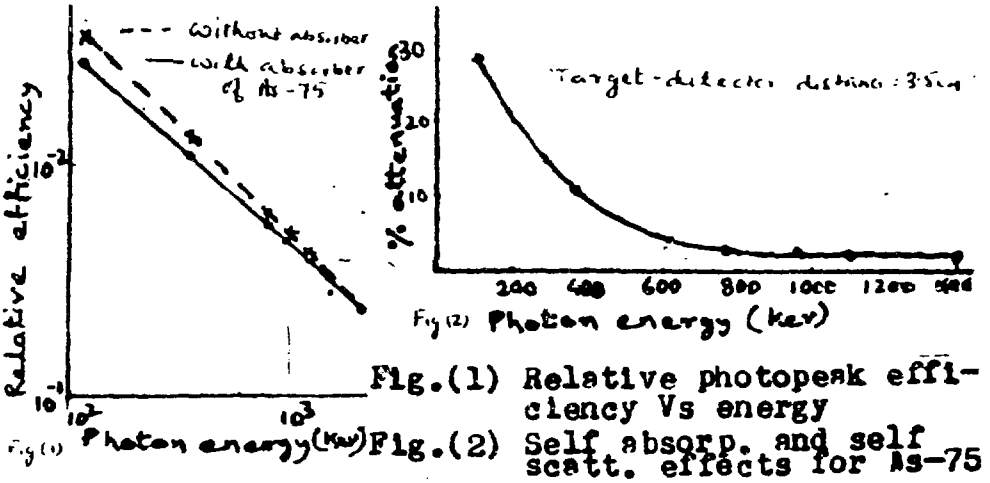

Fig.(1) Relative photopeak efficiency Vs energy

Fig.(2) Self absorp. and self scatt. effects for As-75

absorption and self scattering effects due to the target material are fully taken in to account, experimentally. To get an idea of the exten of attenuation for various photons energies, the above experiment is repeated with Eu-152 disc source alone in the above position without the absorber pellets.

The results are shown in figures for Arsenic (As-75) sample with three pellets. The relative photopeak efficiency Vs energy using Eu-152 source is shown in figure(1). The self absorption and self scattering effects is shown in figure (2).

The above in-situ efficiency measurement will give exact magnitude of error envolved in determination the cross - section which is to be corrected.

Ref :-

/1/J. Rama Rao et.al. Nucl. Instr. and Method B17 (1986) 368.

NUCLEAR INSTRUMENTATION FOR RAPID GRADATION OF COAL SEAMS BY NEUTRON ACTIVATION TECHNIQUE

N.Raja sekhar, Dr.S.V.S.Ramana Reddy, Dr.J.Ramachander Rao
Prof.M.Panduranga Rao
Regional Engineering College
Warangal-506 004
&
Mr.A.Venkatappaiah, Dr.Devaprathap
Exploration Division, Singareni Collieries Co.Ltd.Kothagudem

ABSTRACT

The useful heat value (U.H.V) of coal is a critical factor for the coal based industries. The conventional methods for this estimation consume considerable time which may not be total reflection of the bulk composition of coal. A rapid method to estimate U.H.V., using the sophisticated technique of neutron activation analysis is proposed.

INTRODUCTION

The conventional methods of coal analysis consume considerable time and energy, which may not be totally reflecting the bulk composition of coal. As the coal is highly heterogeneous in character and involves enormous quantities, it is very difficult to establish the representative sample. As such it is essential to increase the number of samples per day. To cope up with this task of analysing a large number of samples per day, the Neutron Activation Analysis has been contemplated.

The principle elements present in ash, namely, aluminium, and silicon are activated by the neutrons in the following way.

a) Slow neutron activation

$$^{27}_{13}Al + ^{1}_{0}n \longrightarrow ^{28*}_{13}Al + \gamma \quad \text{(prompt gamma ray)}$$

$$^{28*}_{13}Al \longrightarrow ^{28}_{14}Si + \gamma \quad \text{(delayed gamma ray) } 1.78 \text{ Mev}$$

b)Fast neutron activation

$$^{28}_{14}Si + ^{1}_{0}n \longrightarrow ^{28*}_{13}Al + ^{1}_{1}p$$

$$^{28*}_{13}Al \longrightarrow ^{28}_{14}Si + \gamma \quad \text{(delayed gamma ray) } 1.78 \text{ Mev}$$

The ^{28}Al in the exited state has a half-life of 138 seconds. The 1.78 Mev gamma rays are detected, counted, and gated for the number of counts in the region of interest.

Experimental set up

A 500 microgram Cf-252 neutron source with a half-life of 2.65 years and flux of the order of 1.15×10^9 neutrons per sec. is placed in a howitzer. The source is embedded by paraffin and then by concrete shielding. Samples are sent inside the howitzer by means of three channels placed at three sides. The plastic containers holding the coal samples after irradiation for 12 minutes are taken out and immediately set for counting. The counting facility consists of a 3" × 3" NaI(Tl) detector coupled to a microprocessor based multichannel analyser(MCA). The MCA has 2048 channels for storing data with each channel capable of storing $2^{20} - 1$ counts.

The 1.78 Mev gamma rays emmitted by the sample are sorted out and and stored in the MCA. The peak is gated and the number of counts(i.e: the intensity of gamma rays) present within these gates are alone printed and analysed.

Results and Observations

For all the standard samples that are studied, plots were drawn between the known U.H.V and the counts /100 sec./gm. The standard plot obtained is as shown in the Fig.1.

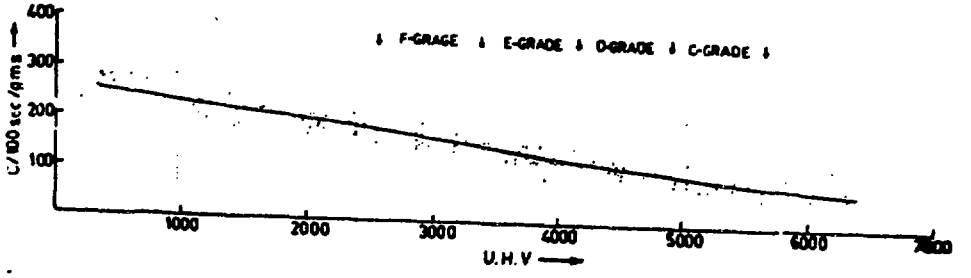

Fig-1

The U.H.V is more are less falling on these curves within the limits of experimental error.

The other constituents present in coal, namely, fixed carbon, moisture, volatile matter, and the remaining unaccounted elements in ash have been in proportionate concentration with Si and Al present in ash. A multiple regression analysis has been contemplated to study the correlation coefficients and the factors governing the constituents.

CONTINUOUS SLOWING DOWN APPROXIMATION RANGE OF LOW ENERGY ELECTRONS IN MATTER.

Manoranjan Agrawal, Km. Sarita, P.B.Pal*, D.K.Gupta and V.P.Varshney.
Deptt. of Physics, S.V.College, ALIGARH-202001

Continuous slowing down approximation (CSDA) range of monoenergetic electrons is defined as the total path length travelled by the electrons during transmission through the absorbers. The knowledge of electron range in matter is very important for its applications in nuclear physics, high energy physics, radiation technology and semi-conductor detectors.

A detailed study of CSDA range for electrons in high energy region has been done by many workers (1-5) but in the low energy region it is still less studied. Berger and Seltzer[6] calculated CSDA range by integrating the inverse of the total stopping power i.e.

$$R_{CSDA} = \int_{E}^{0} \left[-\frac{1}{\rho}\left(\frac{dE}{dx}\right)_{total} \right]^{-1} dE \qquad \text{——————(1)}$$

Recently we have calculated stopping power of electrons in energy region below 800keV [7] using the relation,

$$\left[-\frac{1}{\rho}\frac{dE}{dx} \right]_{total} = Q\frac{\gamma^{n+1}}{\sqrt{\gamma^2-1}} \qquad \text{——————(2)}$$

where $Q = C - D \ln Z$

E and γ are the total energy of electrons in keV and rest mass unit respectively, Z is the atomic number of elementary absorbers. In case of compounds, Z is replaced by Z eff.

In this paper, we are repoting CSDA range of electrons in matter (elements and compounds) in the energy region 1o-8oo keV, obtained by integrating the inverse of equation (2). The results thus obtained have been compared with the results of Berger and Seltzer [6] and are found in good agreement with in 7%.

Fig. described the comparison of present calculations with refrences[6] for three sample elements, viz. Aluminium (Al) Silver(Ag) and Uranium (U), in the energy region 1o-8oo keV. Present values are shown by solid lines and the values of ref. [6] are shown by solid circles. The values of constants C, D and n for electrons covering various range of atomic number (Z) and kinetic energy(T) are given in the table.

*Present address-Phys. Deptt., Ganjdundwara College, Ganjdundwara(ETAH).

is

The importance of our calculations in the use of a simplified emparical relation compared to rigorous calculations of previous workers .

Table

Kinetic energy (T), keV	Atomic Number (Z)	C	D	n
10 < T≤100	1≤Z≤30	4.2928	0.5151	-3.2627
	30≤Z≤92	5.1792	0.7551	-3.6600
100≤T≤800	1≤Z≤92	2.2126	0.2198	-0.2893

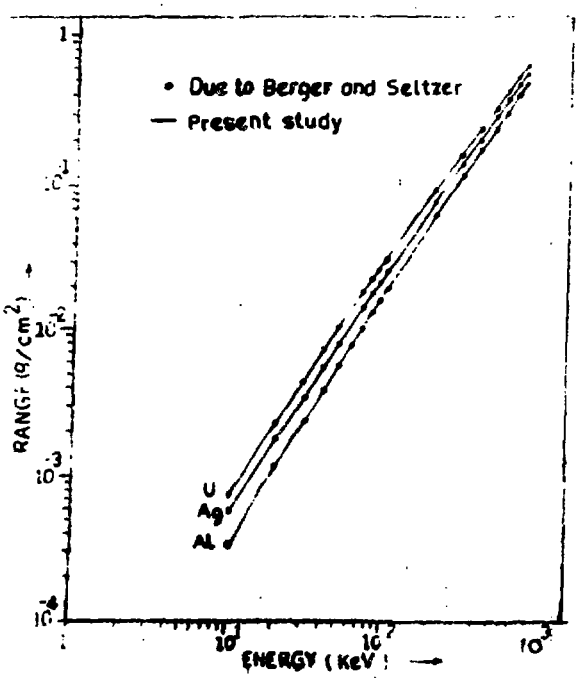

References-
1. R.R.Wilson; Phys. Rev. 84 (1951) 100.
2. T. Mukoyama ; Nucl. Inst. and methods 134(1976)125.
3. R.K.Batra; M.L.Sehgal; Phys.Rev. 23(1981)4448.
4. S.K.Gupta, D.K.Gupta; Comm. Appl. Phys. (U.S.A.) 52(1981)1175
5. P.B.Pal, V.P.Varshney; Ind. J. Pure and Appl.Phys 23(1985)24
6. M.J.Berzer, S.M. Seltzer ; Nat. Bur. Stand. Re.NO.NBS IR 82-2550-A(1983).
7. M. Agrawal, P.B.Pal, D.K.Gupta and V.P.Varshney; Ind.J. Pure and Appl. Phys. 29(1991)326.

CONTINUOUS SLOWING DOWN APPROXIMATION RANGE OF POSITRONS IN THE ENERGY REGION 10 - 900 KeV,

Manoranjan Agrawal, P.B.Pal*, D.K.Gupta & V.P.Varshney.
Physics Department, S.V. College, ALIGARH -202001 .

The knowledge of penetration of positrons is useful in semi conductor detection techiques, measurement of energy of positrons, nuclear physics, nuclear engineering a nd several other related fields. The concept of range of positrons is ambigious from the experimental as well as theoretical point of view. Theoretically[1], csda range is defined as, the total path length covered by the positrons from the point of entrance to the point where it comes at rest in matter. Mathematically, it is expressed as-

$$R_{CSDA} = \int_0^{E_0} \left[\left(-\frac{1}{\rho} \frac{dE}{dx} \right)_{tot} \right]^{-1} dE \quad -(1)$$

Where $\left(-\frac{1}{\rho}\frac{dE}{dx}\right)_{tot}$ is the sum of the total stopping power for positrons in absorber.

Recently, we have [2-4] calculated stopping power of electrons & positrons in low energy region using the relation,

$$\left[-\frac{1}{\rho} \frac{dE}{dx} \right]_{tot.} = \frac{Q \gamma^{n+1}}{\sqrt{\gamma^2 - 1}} \quad \text{——— (2)}$$

Where $Q = C - D \ln Z$

γ&E are the total energy of charge particles inrest mass and KeV units respectively. Z is the at. number of elemental absorber and for compounds Zeff is taken in place of Z.

In the paper, we are reporting csda range of positrons in matter (both element& compounds) in the energy region below 900 KeV in absorbers of at. number from Z - 1 to 92, obtained by integrating the inverse of eq.(2). The results thus obtained have been compared with the theoretical values reported by Berger & Seltzer[5] and are found in good a greement with in 7%.

The values of constants C, D & n for positrons covering various ranges of kinetic energy are given in the table . Fig. shows the comparison of present calculations with Berger & Seltzer[5] for three sample elements viz, C, Cu and Pb inthe energy region 10 - 900 KeV. Present values and Berger & Seltzer values are shown by solid-lines and solid circles respectively.

The study of higher energy region has been done by many workers [6-10] but the low energy region is still less studied. Our calculations are of much importance in the fabrication of semi-conductor detectors for low energy regions.

---

*Present Add. -Head of the Phys. Deptt., Ganjdundwara College, Ganjdundwara.

Table-

Kinetic Energy (T) KeV	n	C	D
$10 < T \leq 70$	- 4.71543	5.4682	0.77693
$70 \leq T \leq 400$	- 0.76864	3.0898	0.39358
$400 \leq T \leq 900$	- 0.11555	2.3288	0.30934

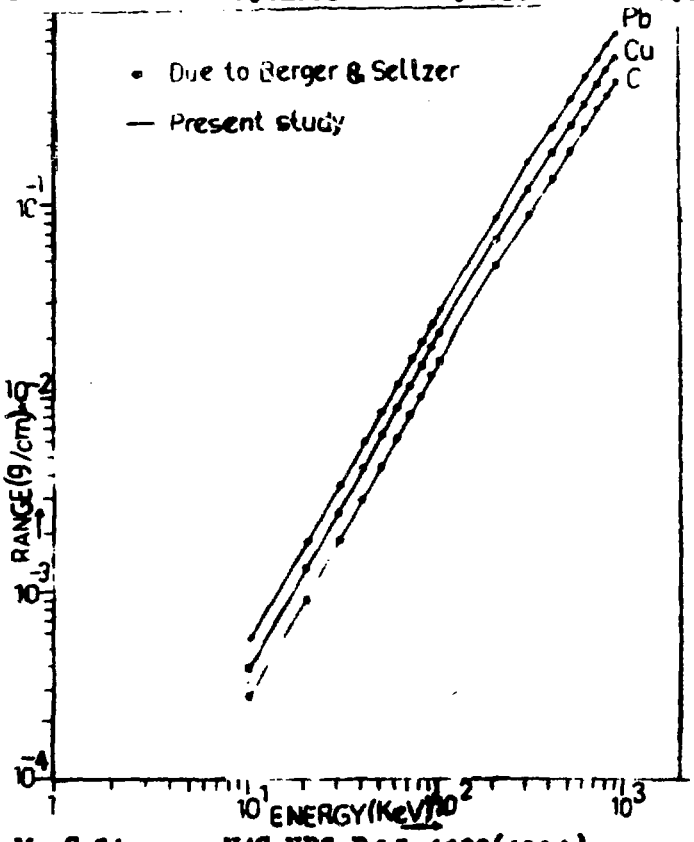

References-

1. M.J.Berger & S.M. Seltse r; NAS-NRC Publ.1133(1964).
2. M.Agrawal et a l; DAE Symps. Madras,33B(1990).333.
3. M. Agrawa l et al; Ind.J. Pure & Appl. Phys. 2 9(1991)326.
4. M. Agrawal et al; DAE Symps. Madras,33B(1990)335.
5. M.J.Berger & S.M.Seltzer; Nat.Bur.Stand.report No.NBSIR-82-2550 A(1 983).
6. R.R.Wilson;Phys.Rev. 84(1951).
7. J.Mukoyama;Nucl.Inst. & methods 134(1976)1 25.
8. R.K.Ba tra; M.L.Sehgal; Phys. Rev. 23 (1981) 4449.
9. S.K.Gupta & D.K.Gupta; J. Appl. Phys. USA 5 2 (1 981) 1175.
10. P.B.Pal e t a l .; Jap. J. Appl. Phys. 2 04 (1985).

AN EMPIRICAL STOPPING POWER EXPRESSION FOR 1-4 MeV LITHIUM IONS

Sarita , Manoranjan, P.B.Pal*, V.P.Varshney
Dept. of Physics ,S.V.College,Aligarh

Abstract. The stopping power data show its dependence on energy of interacting ion .An empirical stopping power energy dependence expression is presented for Lithium ions in energy range 1-4 MeV in eight elements The results are in good agrement with deviation less than 5%.

Introduction. The study of inelastic energy loss of charge particles ie electrons,positrons,protons and ions is an important task in nuclear physics to design of reactors and the ion-beam surface-layer analysis of materials. An extensive theoretical and experimental work[1-5] has been done so far.Areview on data[5] available reveals the stopping power of elements is dependent on energy.In present work an energy dependence empirical expression is presented for Lithium ion stopping power of C,Al,NI,Cu,Ag,In,Sn,and Au,

Description. The stopping power is expressed

$$S = A E^n$$

where A and n are parameters dependent on the atomic number Z of the target. E is energy in MeV of the colliding ion . S is the stopping power in KeV/(ug cm^{-2}) The stopping power - energy relation is fitted for the data available[5]. The best fit values of parameters A and n were calculated .

Results and Discussion. The computed values of A and n for Lithium ions in selected metal are listed in Table 1. The calculated results for the stopping power are

compared with the experimental results[5] tabulated in Table 2. and are in good agreement within 5% deviation .

Table 1. Values of parameters A and n .

Element	A	n
Carbon	4.3488	-0.3304
Aluminium	2.2991	-0.1524
Nickel	1.4666	-0.0659
Copper	1.1275	+0.0845
Silver	1.3109	-0.1562
Indium	0.9499	+0.0759
Tin	0.9738	+0.0282
Gold	0.5513	+0.1487

Table 2 Comparision between calculated and experimental stopping power.

E MeV	S_{ex}	S_{cal}	Dev %	E	S_{ex}	S_{cal}	Dev %
	Carbon				Aluminium		
1.75	3.56	3.61	+1.4	1.57	2.07	2.14	+3.4
2.15	3.47	3.38	-2.6	1.96	2.01	2.07	+3.0
2.55	3.35	3.19	-4.7	2.56	2.02	1.99	-1.5
2.95	3.00	3.04	+1.3	3.12	1.92	1.93	+0.5
3.35	2.98	2.92	-2.0	3.52	1.90	1.90	0.0
3.75	2.76	2.81	+1.8	3.92	1.81	1.87	3.3
3.95	2.64	2.76	+4.5				
	Silver				Gold		
2.12	1.18	1.16	-1.7	1.13	0.540	0.561	+3.9
2.51	1.12	1.13	+0.9	1.73	0.611	0.598	-2.1
2.95	1.11	1.11	0.0	2.32	0.657	0.625	-4.9
3.34	1.11	1.08	-2.7	2.91	0.690	0.646	-3.3
3.74	1.07	1.06	-0.93	3.51	0.670	0.664	-0.8
3.94	1.02	1.06	+3.92	3.91	0.660	0.675	+2.3

Acknowledgement. Authors are thankful to Dr D.K.Gupta Principal, S.V.College,Aligarh for providing research facilities and valuable suggestions.

References. 1. J.L.Fouyer et al ,Nucl.Inst.andMeth,140, 140(1977)305
2. D.C.Santry,R.D.Verner, Nucl.Inst.and Meth 115(1984)449
3. I.Nagy et al ,Nucl.Inst. and Meth,B12(1985) 34
4. I.Nagy et al ,Nucl.Inst.and Meth,B15(1986)8
5. H.H.Lin.et al.,Nucl.Inst.and Meth.B17(1986) 91

*Dept of Phy. Ganjdundwara COllege Ganjdundwara.Etah.U.P

***

g. ACCELERATORS AND ACCELERATOR BASED INTERDISCIPLINARY RESEARCH.

ECR HEAVY ION SOURCE OF VEC

D.K.Bose, G.S.Taki, B.Dasgupta, R.B.Mitra and R.K.Bhandari
VECC, 1/AF,Bidhan Nagar, CALCUTTA-700 064

The electron cyclotron resonance (ECR) heavy ion source which was under development, has been made operational from May 16, 1991. This source after coupling to the cyclotron shall open up new fields of research with varieties of heavy ions having high energy per nucleon.

The present source /1/ is a versatile compact room temperature two stage device enclosed in iron yoke cyclinder (Fig. 1). Both the stages have mirror type axial magnetic field configuration. In the second stage which is the main stripping stage has additional sextupolar radial magnetic field for generation of B-minimum field configuration. B-minimum field configuration is essential for plasma stabilisation and in turn production of high charge state ions. High charge state ions are produced by hot plasma electrons energised by microwave power through electron cyclotron resonance mechanism at 6.4 GHz frequency. Overall length of the sorce is 88 cm. Internal diameter of the copper main stage is 10.8 cm. The length, field diameter and pole tip field of the rare earth cobalt sextupole are 30.5 cm, 11.8 cm and 4 KGauss respectively. The source is pumped to 10^{-7} torr by diffstaks and the transport line better than 10^{-7} torr by cryopump.

Since middle of May the source is being tested using Argon-Oxygen mixture. Argon charge states upto 14 have been obtained as shown in Figure 2.

The development work for the injection line /2,3/ for the transport of the heavy ion beam into the cyclotron is underway. For charge analysis a 90 deg. magnet and for vertical bending an achromatic system comprising two 45 deg. magnets and three quadrupoles in between will be used. The beam will be bunched to improve intensity and will be finally inflected into the cyclotron by a mirror inflector.

The authors thank M.H. Rashid, C. Mallik, P.R. Sarma and N.K. Mukhopadhyay for their interest. The authors also thank Dr. B.C. Sinha, Director VECC for his constant encouragement.

References

/1/ D.K. Bose, G.S. Taki, J. Chawdhuri and R.K. Bhandari, 12th International Conference on Cyclotrons and their applications, May 1989.

/2/ R.K. Bhandari Proc. Nucl. Phys. Symp. DAE, 1988.

/3/G. Pal, C. Mallik, et. al.-Will be presented in this Symp.

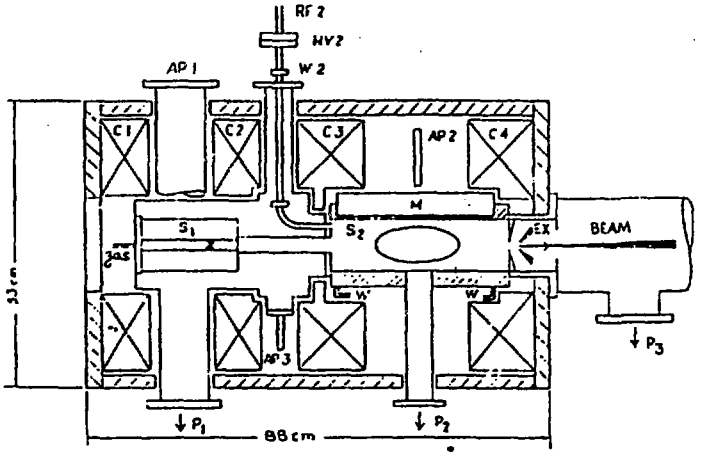

Fig. 1: Layout of the VEC ECR source. RF: microwave power feed, HV: high voltage isolators, W: microwave window, S1: stage 1, S2: stage 2, C: solenoid coil, H: sextupole magnet, AP: additional ports, P: pumping ports.

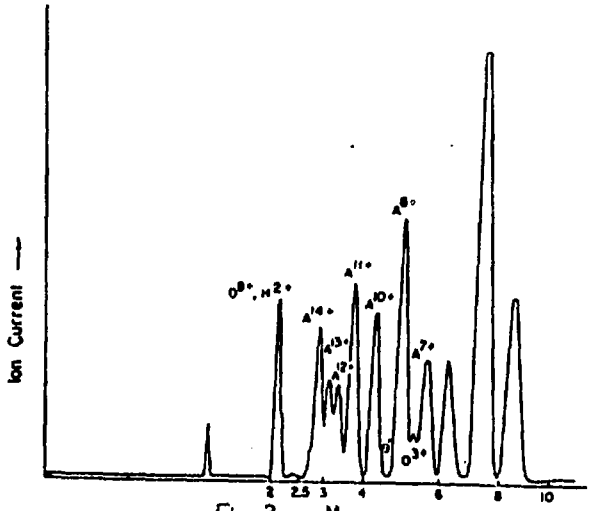

Fig 2.

TESTING OF NSC BEAM PULSING SYSTEM

D.k.Avasthi, Vandana Jha, R.Joshi, D.Kanjilal,
S.K.Datta, S.Chopra, M.M.Narayanan, A.Tripathi,
L.Senapati and A.Mandal

Nuclear Science Centre, JNU Campus, New Delhi 110067

The beam pulsing system installed in the pre-acceleration region of 15 UD Pelletron [1] at NSC consists of a chopper, travelling wave deflector, light ion buncher and heavy ion buncher. The chopper provides an ion beam width varying from 10 ns to 70 ns. Travelling wave deflector can change the repetition rate from 250 ns to 512 μs in steps of multiple of two. Light ion buncher, located 4.6m from the entrance of the accelerator tube, is used to bunch the ions of mass up to 80 amu. Heavy ion buncher, located 1m from the accelerator tube entrance is used for bunching the ions of mass above 80 amu. The experiments were conducted to test the performance of beam pulsing system for H, C, Ni and I beams. During the test of proton, a time of flight experiment was carried out to determine the beam energy.

The experimental set up had a BC400 plastic scintillator mounted on 8575 photomultiplier tube to detect the γ-rays originating due to the ion bunch hitting on the target. The target was a thick Al sheet at the end of Faraday cup. The anode signal was taken as start signal for time to amplitude converter. The RF from buncher was taken as the stop signal. The resolution of the detection system, measured using Co60 source and two plastic detectors, was found to be 0.5 ns. The width of ion bunches was determined from the FWHM of the timing peak in TAC spectrum. The pulse peak current was determined from the average DC current measured at the Faraday cup and repetition rate.

The measured FWHM for different ions is given in table 1. It has been shown earlier [2] that the analysing magnet is the major factor in causing the time spreads in the ion bunch. The time spread for various ions were estimated for a path difference of 39 mm in the analysing magnet corresponding to a 2.5 millirad divergence of the ion beam. The measured pulse widths of ion bunches is close to the estimated values.

A slow drift of the time peak, ~ 2 ns in 4 hours in the worst case, was observed. The shift is attributed to the instabilities in high voltage terminal and injector high voltage supply.

A TOF experiment was carried out in which the proton beam passed through a thin Al foil at the target position in the scattering chamber and finally stopped in a thick Al plate at the end of the Faraday cup. The γ - rays originating from the target and the Faraday cup were detected with a plastic scintillator. The difference between the two peaks in the TAC spectrum gave the time of flight of protons from the scattering chamber centre to the Faraday cup end. The measured beam energy, for a terminal voltage of 14 MV and injector voltage of 200 keV, was found to be 27.84 $\pm$ .15 MeV after correcting for the TOF of γ-rays, relativistic effect and energy loss in Al foil.

TABLE 1.

Ions	Energy	FWHM estimated	FWHM measured	Peak current
H	28 MeV	0.5 ns	0.6 ns	0.46 ma
C	85 MeV	1.1 ns	1.2 ns	0.42 pμa
Ni	85 MeV	2.1 ns	2.2 ns	3.8 pμa
I	105 MeV	3.1 ns	3.1 ns	3.2 pμa

The authors gratefully acknowledge valuable suggestions of Prof. A.P.Patro.

1.G.K.Mehta and A.P.Patro, NIM A268(1988)334.
2.D.K.Avasthi et al Indian J. Phys. 65A (1991)519.

MODIFICATIONS INCORPORATED IN THE 16 MV PELLETRON FOR BETTER PERFORMANCE

D.Kanjilal, S.Chopra and M.M.Narayanan
Nuclear Science Centre , Box 10502, New Delhi 67

During the installation, testing and running of the 16 MV Pelletron (1,2) at the Centre, we undertook various alterations and modifications for improving the performance of the machine. Some of these changes which may be interesting for various machines of this type are mentioned here.

The shorting rod connection at the nylon link broke down twice during conditioning. After opening the tank, the shorting rod drive mechanism was operated to simulate the breaking process. It was seen that the nylon rod got bent at the entry point at either end of the column. This problem was solved by putting shorting rod guides there.

Due to some of the sparks presumably travelling along the acelerator column one charging power resistor(50 k ohms, 110 W) inside the machine was getting blown up repeatedly. After putting a spark protection cover around the resistor we could eliminate this problem.

To illuminate inside the machine when it is running we have used two high pressure feedthrus at tank top and bottom to power two industrial light bulbs kept inside a glass cover and a steel frame. Now we see regularly the components and connections inside the machine without opening the tank.

While removing the terminal shells for getting access to the terminal for tests and maintenance we found that it was getting increasingly difficult to pull the lower shell up to the terminal level using the annular service platform (ASP) with two or more persons working standing on the ASP. This is so mainly due to the fact that the excess load of the dynamically varying unbalanced load of the effective extra lengths of

the four steel strings holding the ASP acts against the counterweight in this case. This problem is solved by correcting the variation of the load of the ASP at all points after connecting a chain at the bottom of the counterweight to vary the load of the counterweight accordingly.

To analyse the residual gases inside the machine we put initially only one residual gas analyser (RGA) at the tank top.After establishing a reasonably good vacuum in the range of 10^{-8} torr we found that the breakdown products of sulphur hexafluoride is quite prominent inside the machine. To find out the locations of the various points of small leaks we procured another RGA and put it at tank bottom. By simultaneously studying the two RGA spectra putting the six ion pumps from top to bottom of the tank ON or OFF at various combinations we could find the regions of leak inside the machine for detailed leak testing.

While running molecular TaSi beam thru the machine and anlysing the charge state distributions of Ta and Si the view port below the analyser magnet for vertical alignment got ruptured due to high energy heavy ion beam of Ta falling on it. So a magnetically operable tantalum beam stopper was put above the window which can be removed externally for alignment without breaking the vacuum.

We connected some of the getter and ion pumps to the emergency power line and the interlocks are modified accordingly so that after a power failure the pumps, vacuum gauges and valve controllers get power from the diesel generator; the gauges get on automatically, the vacuum level is checked and if found alright then the valves are opened to maintain high vacuum inside the injector and the machine during the power breakdown. Contributions of Leo R Parpart of EII are acknowledged.

1. G.K.Mehta and A.P.Patro, Nucl. Instr. and Meth., A268 (1988) 334
2. D. Kanjilal, SNEAP'90,(1990), pp33

LOW POWER RF TESTS ON THE RFQ ACCELERATOR

Kavitha Murthy, S.A.Mateen, V.T.Nimje, R.C.Sethi
Nuclear Physics Division, BARC, Bombay 400 085.
S.V.Sadawarte, M.V.Pande, R.D.Luktuke, A.N.Garud
TP & PE Division, BARC, Bombay 400 085.

An RFQ accelerator, capable of accelerating upto 20 mA (max.) of deuteron beam to a final energy of 150 keV, has been designed and built. This accelerator operates at a frequency of 45 MHz, at a voltage of 55 kV, requiring 30 kW of RF power.

Low power RF tests have been done to determine the three important parameters of the resonator, viz., resonant frequency, Q-value and shunt impedance.

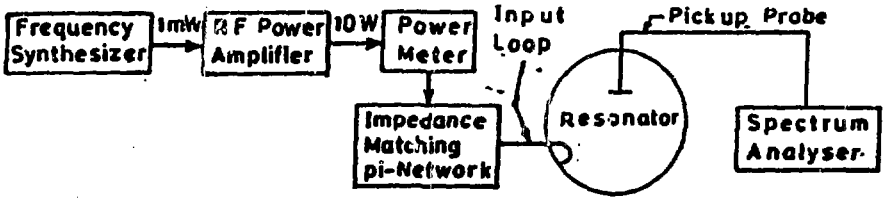

Fig.1

The schematic of the method used to determine the above parameters is shown in fig.1. Proper impedance matching is achieved by tuning the matching pi-network and varying the orientation of the inductive input loop, till the reverse power is reduced to zero. The output pickup probe is capacitive in nature.

The frequency was varied from 20 MHz to 70 MHz in convenient steps and the amplitude observed on a spectrum analyser, at each setting. A plot of frequency

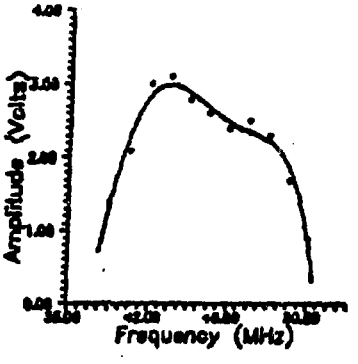

Fig.2

vs. amplitude was then plotted. As shown in fig.2, the resonant frequency f_o .is 43 MHz but the frequency response is not sharp, indicative of a low Q - value.

To obtain the Q - value, the 3-dB method was used. The amplitude V_o at the resonant frequency is observed on an oscilloscope. The frequency is then changed on either side of f_o till the amplitude is Ø.7Ø7 times V_o. The difference between the two frequencies gives Δf. The Q - value is then calculated using the relation: $Q = \frac{f_o}{\Delta f}$

In this case, Δf was found to be Ø.3 MHz. The Q value works out to be 142, which is very low. This is most probably due to the poor copper electroplating of the inner side of the tank. The low Q - value is also responsible for the broad frequency response seen in fig.2.

The perturbation method was used to determine the shunt impedance. A perturbing object (in this case, a metallic bead of 4 mm dia) is introduced into the resonator and the resulting frequency shift (δf) is noted. The shunt impedance R_p is calculated using the following relation: $R_p = \frac{2 * Q * \delta f}{\pi * f_o^2 * \delta C}$

where δC = capacitance of the bead = 1 pF. In this case, the frequency shift was found to be too small to measure, due to the low Q - value.

In addition to the above tests, the voltage distribution in the longitudinal direction was checked. It shows the required standing wave pattern. Efforts are being made to improve the electroplating of the resonator tank, in order to obtain the designed Q - value of 6ØØØ to 7ØØØ.

Acknowledgements:

The authors would like to thank Dr.S.S.Kapoor and Dr.M.A.Eswaran for their encouragement, Shri.R.S.Sardesai and Dr.N.M.Thakur for their help during the experiments.

K-X RAY EMISSION FROM HIGHLY STRIPPED ^{32}S IONS CHANNELED ALONG $< 100 >$ AXIS IN Si

Vandana Nanal, M.B.Kurup, P.N.Tandon and K.G.Prasad
Tata Institute of Fundamental Research, Bombay 5.

Recently it has been observed that for high energy ($\simeq$ 20 MeV/amu) hydrogen like heavy ions, the charge equillibration in a channeled direction is dominated by Radiative Electron Capture(REC)[1]. But for the low energy counterparts, the situation can be quite different and a study of the characteristic as well as the REC X-rays from the projectiles channeled in thin single crystals is useful to understand the process. We report here our first attempt to study projectile X-ray cross-sections of highly stripped ^{32}S ions channeled in Si crystal.

The experiments were carried out using ^{32}S beam of 120 MeV from pelletron accelerator on $0.2\mu m$ thick $< 100 >$ Si crystal. The different charge states($8^+, 9^+, 14^+, 15^+, 16^+$) were obtained using a post-stripper foil. A thin gold foil($800\mu g/cm^2$) was placed downstream after the target and elastically scattered ^{32}S from this gold foil was used for normalisation. Both the target and projectile X-rays were detected by a $Si(Li)$ detector kept at 20° to the beam direction.

Fig.1 shows the variation of the target as well as the projectile K X-ray yield as a function of angle (θ) between the beam and $< 100 >$ axis of Si. The quantity χ_{min} is defined as the ratio of the yield in the aligned direction to that in the random direction. For $^{32}S^{6+}$(no K vacancy), χ_{min} for target K X-ray is 16.8(0.5)% and that for projectile K X-ray is 27.6(0.3)%. The fact that projectile K X-ray emission shows weaker channeling indicates that the impact parameter involved in the process is large (by a factor of $\simeq \sqrt{2}$) as compared to that in the target K X-ray emission.

When incident projectile has a K vacancy($15^+, 16^+$), the overall projectile K X- ray intensity is same in random as well as aligned case though the intensity ratios of various components are different for 15^+ and 16^+. This is strikingly different from the lower charge states($8^+, 9^+, 14^+$- no K vacancy) where intensity of all the components of the projectile K X-ray is reduced by the same amount under the channeling condition.

Fig. 2 shows the X-ray spectrum for both the aligned and random directions for $^{32}S^{16+}$ The intensity of these hypersatellite lines (Ly_α-

2.618 keV and Ly_β-3.095 keV) is enhanced by a factor of 2 in aligned spectrum. This implies that under the channeling conditions, the initial charge state is retained over a longer path inside the cystal as electron capture/loss process is reduced. Also, the aligned spectrum shows significant increase in the intensity of the series limit lines viz. 3.19 keV and 3.46 keV. We have also observed that shifting the observation area to just beyond the target reduces the intensity of the hypersatellites drastically. This probably is an indication that lifetimes of these hypersatellite levels are small. Detailed investigation of these effects are in progress.

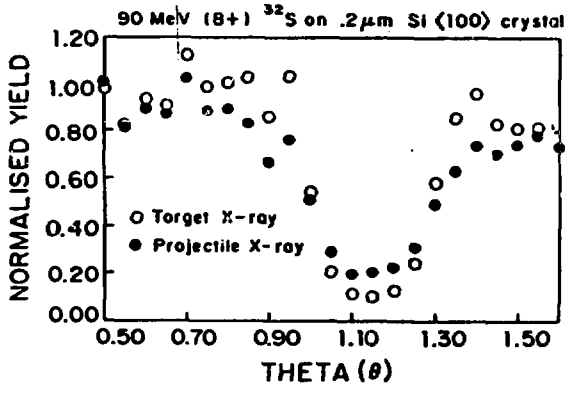

Fig. 1

Fig. 2 ↓

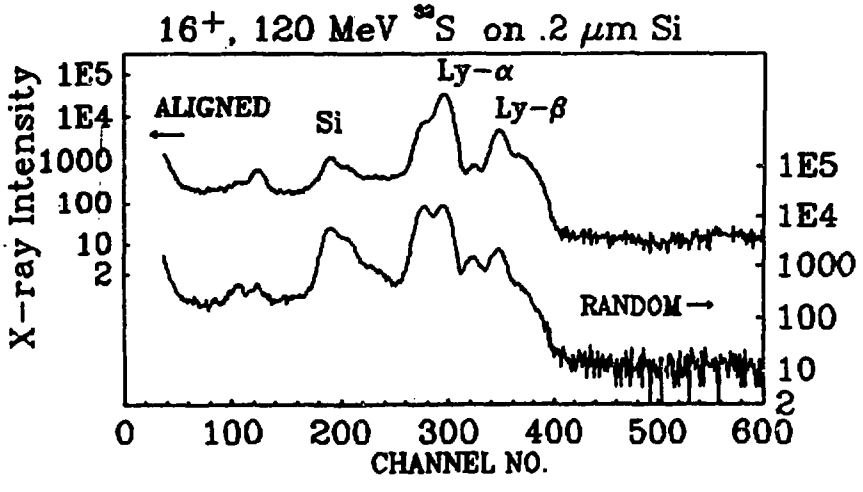

Reference:

1. S.Andriamonje et.al., Phys.Rev.Lett,59,2271(1987)

STUDY OF EXCITATION FUNCTION AND TRANSITION PROBABILITIES IN Ar IONS

Tapan Nandi, M.B.Kurup and K.G.Prasad
Tata Institute of Fundamental Research, Bombay-400005,
P.Saraswati, G.Krishnamurty, P.M.R.Rao and A.P.Mishra
Bhabha Atomic Research Centre, Bombay-400085

Reliable determination of atomic level life times in rare gas species of high ionisation state is important for a number of applications. Beam foil excitation technique is a convenient method to study these. Further, foil excitation can populate inner shell excited states and orbits with high angular momenta which are much less excited in most other light sources. Study of the excitation function for such levels is also very important. We have studied both excitation functions and life times for a number of atomic levels in different ionic states of ^{40}Ar using a 400 KV ion accelerator.

Ar^+ beam ($\simeq$ 100nA) in the range 176-336 KeV passing through 4-5 $\mu g/cm^2$ carbon foils was used to produce excitations in the projectile ions. The optical spectra were recorded at right angles to the flight path of the beam with a monochromator-photo-multiplier combination operating in the single photon counting mode. The spectral range of the system is 2500-5000$A°$. The observed spectra show many transitions in ArII and ArIII which were not earlier observed in beam foil excitation. We have also identified a number of lines of ArIV for the first time in such spectra. Excitation functions of few selected lines of ArII are shown in fig.1 and those for ArIII and ArIV in fig.2. It is clear that the overall population of ArII decreases while those of ArIII and ArIV increase as the beam energy is increased from 176 to 336 KeV. Further in ArIII and IV, the excitation seems to be independent of the electronic state of the concerned level. However in ArII, all the low lying states show a similar tendency,while the high lying state ($4d\ ^2D_{3/2}$) shows an excitation behaviour typical of ArIII or IV. The experimental data for ArIII, ArIV and the low lying states of ArII agree well with the calculated excitation function[1] also.

The life time (τ) of several levels were measured by the time of flight method. The post-foil beam velocity was calculated using energy loss in the foil estimated from TRIM-88. A multiexponential fit to the experimental data was carried out to extract the decay times. Transition probabilities were obtained from the measured mean lives by using the tabulated branching ratios in each case. They compare well with earlier reported values wherever available. As seen in table 1, we have reported these values for several transitions in ArII, ArIII and ArIV for the first time. An overall increase in the transition probabilities as the ionization state of the Ar ions increases is evident from table 1.

References

1. E. Veje et.al, Phys. Rev. A 14, 2077 (1976)
2. W.L.Wiese and G.A.Martin, 'Transition Probablities',NBS.(U.S)68,1980

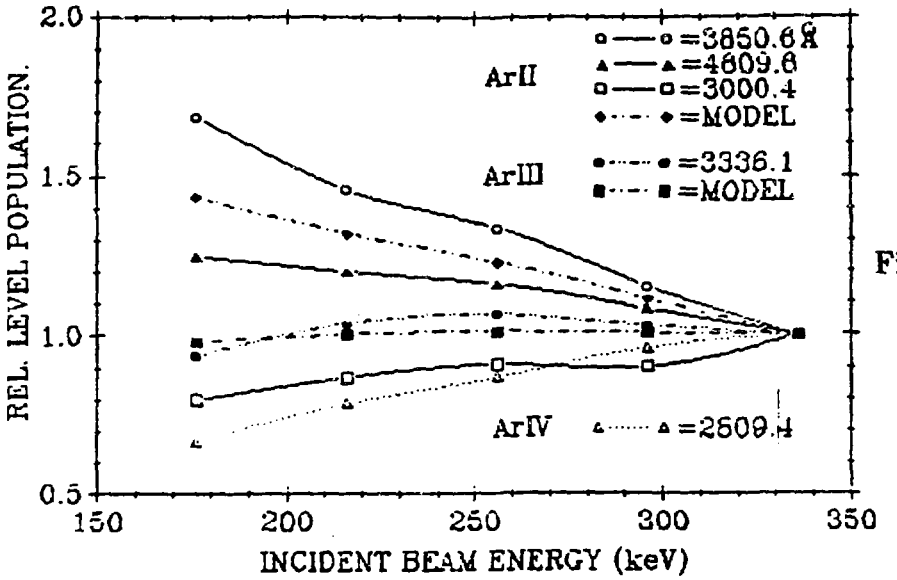

Fig. 1

TABLE. 1

Ionic state	Upper level	λ in Å	Brnchg. Ratio %	τ (ns)	Tr.Prob. 10^8/s Present	Others
ArII	$4p\ ^4P^\circ_{5/2}$	4806.07	60.3	7.12	0.85	0.79
	$4p\ ^4P^\circ_{1/2}$	4431.02	6.9	7.78	0.09	0.09
	$4p\ ^4D^\circ_{3/2}$	4331.25	42.0	7.71	0.54	0.56
	$4p\ ^4P^\circ_{3/2}$	4400.09	10.2	7.02	0.16	0.13
	$5s\ ^2P_{3/2}$	4103.91	blend.	4.13	----	----
	$5s\ ^4P_{5/2}$	4103.91			----	----
	$4d\ ^2D_{3/2}$	3000.44	32.1	2.51	1.28	----
ArIII	$4p'\ ^3P_0$	2842.88	23.3	2.04	1.14	----
	$4p'\ ^3P_1$	2855.29	17.4	1.95	0.89	----
	$4p'\ ^3P_2$	2884.12	21.4	1.92	1.12	----
	$4p''\ ^3D_3$	3024.05	37.5	2.73	1.37	2.60
	$4p''\ ^3D_2$	3054.54	26.5	2.35	1.11	1.90
	$4p\ ^5P_3$	3285.85	66.0	3.06	2.15	2.00
	$4p'\ ^3F_4$	3336.12	73.3	3.49	2.10	2.00
	$4p'\ ^3F_3$	3344.71	40.0	2.54	1.67	1.80
	$4p'\ ^3D_3$	3480.55	40.0	2.40	1.57	1.60
	$4p'\ ^3D_2$	3503.58	35.7	2.76	1.29	1.20
ArIV	$4p'\ ^2F^\circ_{7/2}$	2757.92	100	2.01	4.97	----
	$4p\ ^4D^\circ_{3/2}$	2776.26	76.9	2.37	3.25	----
	$4p\ ^4D^\circ_{1/2}$	2797.11	63.6	2.89	2.20	----
	$4p\ ^4D^\circ_{7/2}$	2809.44	100	2.09	2.78	----

K-SHELL VACANCIES AT 25 MeV OXYGEN IONS INSIDE Ti, Fe, Ni AND Gd HOSTS.

L.C.Tribedi, R.G.Pillay, K.G.Prasad and P.N.Tandon
Tata Institute of Fundamental Research, Bombay-5.

Transient magnetic fields[1] experienced by ions moving inside a polarized ferromagnetic medium are attributed to the polarization of bound s-electrons of the moving ion. For light ions these fields are directly correlated with the number of single K-shell vacancies. A measurement of these vacancy fractions is required to obtain accurately the average degree of polarization of the ions and hence to understand the polarization mechanism of the bound electron. We report here measurement of K-shell vacancies of *Oxygen* ions moving inside *Ti, Fe, Ni* and *Gd* hosts at a velocity of $7.9V_o$ using the probe layer technique. A thin layer of $SiO(1.8\mu g/cm^2)$ was used as probe for *Fe* and *Ni* while $Ti(1.4\mu g/cm^2)$ was used for *Gd* host. Measurements were done at the *BARC-TIFR* Pelletron accelerator at Bombay[2].

The measured sensitivity of the probes to the number of K-shell vacancies of the incident projectile ion is shown in fig.1. The dependence of the probe K X-ray cross section for various values of the host thickness was measured for several charge states of the incident ion. Figs. 2 and 3 show results obtained for *Fe* and *Ni* hosts. The data was fitted using a three component model[3] involving rate equations describing the state of the projectile having $F_j(x)$ K-vacancies (j=0,1,2) as a function of the host thickness x. The continuous lines through the data denote a simultaneous fit to all the incident charge states of the ion using the above model. From the fitted values of the parameter the fractions F_1 and F_2 could be obtained.

The values obtained for various hosts are

	Ti	*Fe*	*Ni*	*Gd*
$F_1(\%)$	40(2)	45(1)	44(2)	50(2)
$F_2(\%)$	8(1)	12(1)	12(1)	25(1)

The derived values of the polarization transferred to *Oxygen* ions from *Fe, Ni* and *Gd* hosts using the measured transient field precession are.[1]

	Fe	*Ni*	*Gd*
P_1,	0.13(2)	0.04(1)	0.25(3)

The implication of this result to the understanding of transient field phenomenon will be discussed.

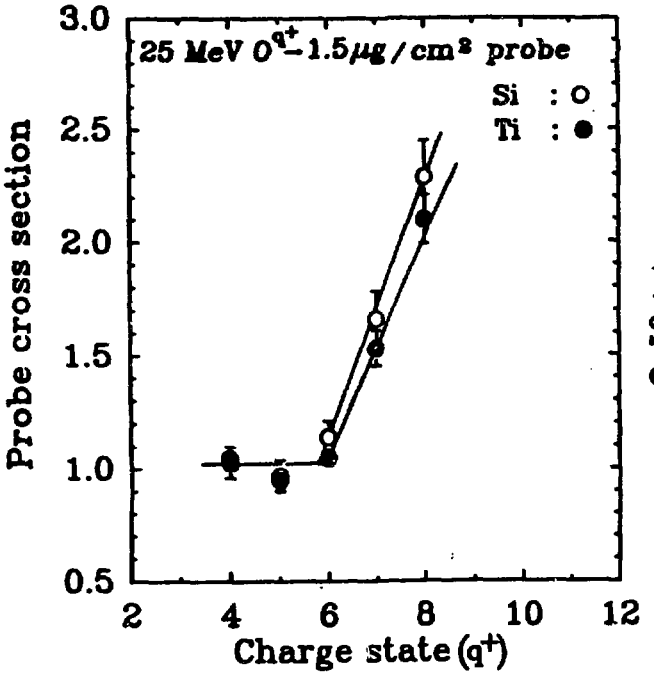

Fig . 1
Sensitivity of Si & Ti as probes

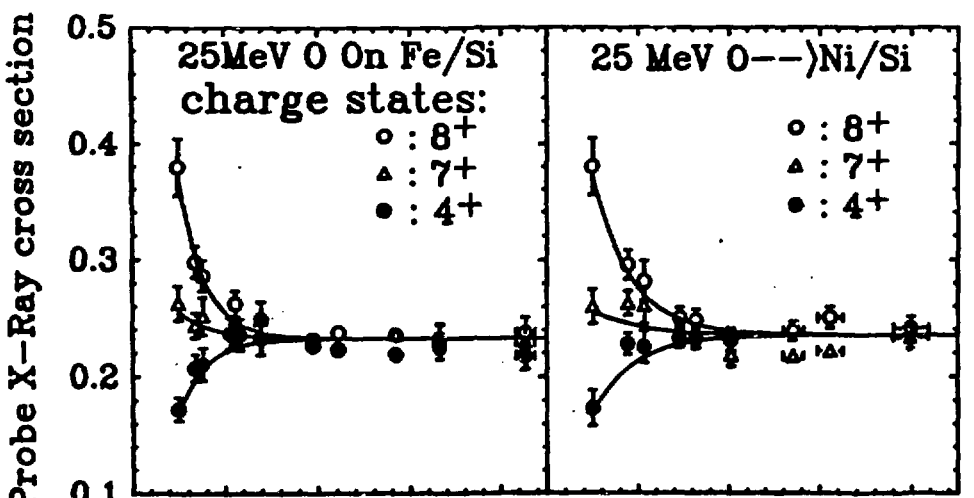

Fig . 2

Fig . 3

References:

1. K.H Speidal et.al, Z. Phys. D6(1987),43
2. Tribedi et.al Proc. of DAE Symp. in Nucl. Phy.,1990,O62.
3. K.Dybdal and N.Rud, Phys.Scripta 35(1987), 441

CHARGE STATE AND TARGET THICKNESS DEPENDENCE OF PROJECTILE X-RAYS FROM 120 MEV $^{32}S^{q+}$ IONS INCIDENT ON C TARGETS

L.C. Tribedi , K.G. Prasad and P.N. Tandon
Tata Institute of Fundamental Research, Bombay-5.

We have measured the projectile K X-rays from $^{32}S^{q+}$ ions ($q^+ = 10, 13, 15$ and 16) incident on self supporting C foils of thickness varying between $10 - 90 \mu gm/cm^2$ to understand the development of single and double K-shell vacancies of the projectile as it passes through the foil. The measurements were done using 120 MeV ^{32}S beam from the *BARC-TIFR* Pelletron accelerator. A post accelerator foil stripper was used to produce different charge states of the accelerated beam. The $Si(Li)$ X-ray detector was mounted outside the chamber at 90° to the incident beam direction and was isolated from the vacuum by a $25 \mu m Be$ window. A part of the X-ray spectrum obtained is shown in Fig.1 for different charge states of the incident beam. The X-rays originating from the projectile (200-380 chs.) were fitted to six gaussians of equal width and the intensities of the various components determined. The total K X-ray production cross-section for different charge states of the projectile is shown in Fig.2, demonstrating strong sensitivity to K-shell vacancies of the projectile. Fig.3 shows the normal and hyper satellite X-ray production data for projectile incident with no K-vacancies. The cross section for K X-rays associated with single vacancies (σ_x) decreases with target thickness while that corresponding to double vacancies (σ_x^h) increases. This variation in cross section is insensitive to incident charge state with having no K-shell vacancy. Similar data for incident charge state having one or two K-shell vacancies is shown in Fig. 4 where cross section for both components decrease with thickness of the target. The data is being quantitatively analyzed using the three component model and the importance of various cross sections governing the evolution of the projectile K-vacancies will be presented.

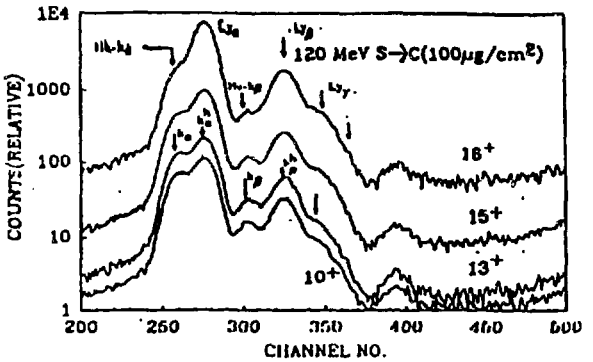

Fig.- 1

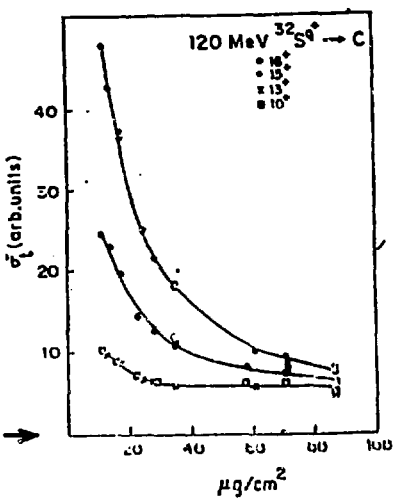

Fig : 2 →

Fig . 3

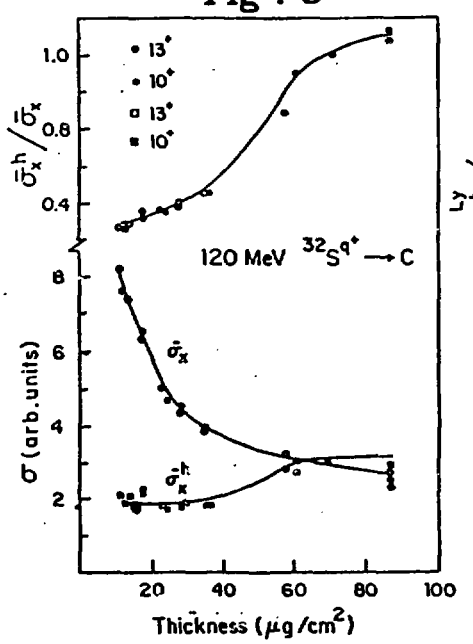

FIG. 4

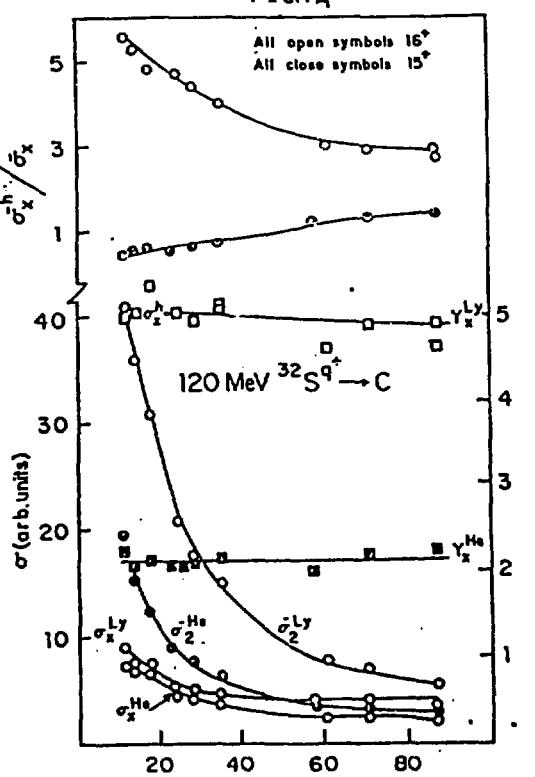

Acknowledgement

The authors would like to thank V.S.Nanal, T.Nandi and M.B.Kurup for their help during the experiment.

ENHANCED FOCUSING IN CYCLOTRONS BY RADIAL AND AZIMUTHAL VARIATION IN MAGNETIC FIELD

P.R. Sarma
Variable Energy Cyclotron Centre, Bidhan Nagar, Calcutta - 64

In high energy cyclotrons, the vertical focusing of the ions has to be very strong. This is achieved by using either separated sectors or highly spiral sectors. There is a limit of about 70° for the spiral angle because at higher angles the distance between the sectors and hence the flutter decreases. In separated sectors cyclotrons the average field is small and so the machine size is large.

Recently a new type of radially and azimuthally varying (RAVF) magnetic field was proposed [1] for very strong focusing in cyclotrons. In Thomas focusing as well as spiral focusing only azimuthal field variation is used (although a spiral produces radial field variation also). In the new scheme both radial as well as azimuthal field variation is there. The alternating field gradients in adjacent regions give rise to strong focusing. In the present paper we explore the possible geometries which can give the required radial field variation.

In RAVF scheme the hills and the valleys are divided into two regions each having the following field variations:

1) $B_{av} + B_o \sin(2\pi\omega r)$ 2) $B_{av} + B_o \cos(2\pi\omega r)$
2) $B_{av} - B_o \sin(2\pi\omega r)$ 3) $B_{av} - B_o \cos(2\pi\omega r)$

where ω = no. of oscillations in the field and B_{av} = average magnetic field. With such field variations the vertical betatron frequency ν_z has been calculated by the matrix method [2].

$$\nu_z = \frac{N}{2\pi} \cos^{-1}[.5\ \text{Trace(Trnasfer matrix)}]$$

Fig. 1 shows that stronger focusing can be obtained with RAVF for much smaller field variation.

Let us now see what type of pole face structure gives rise to radial sinusoidal field. It has been shown by Dunn et al. [4] that the following potential function gives rise to a sinusoidal field :

$$U = z + \delta \sin(x) \sinh(z)$$

The contour comes out to be similar to (but not exactly) atriangular one. Mechanically it is difficult to give such pole faace variation. Instead one can actually use separated

triangular pieces on the pole face. We have calculated the field due to such contours by Schwarz-Christoffel transformation and is given below.

$$B(r)=P(\mu^2+a^2)^{.5-\alpha}\ (\mu^2+1)^{\alpha-1}\ (\mu^2+b^2)^{-\alpha}$$

where μ is obtained from

$$r=\int_0^{\mu}(t^2+a^2)^{\alpha-1}\ (t^2+1)^{1-2\alpha}\ (t^2+b^2)^{\alpha}dt$$

The constants a,b and P are obtained from the pole geometry. Fig. 2 shows the geometry of the poles and Fig. 3 gives the field produced due to the triangular variation. It can be readily seen that a trapezoidal pole will give rise to a better sinusoidal variation.

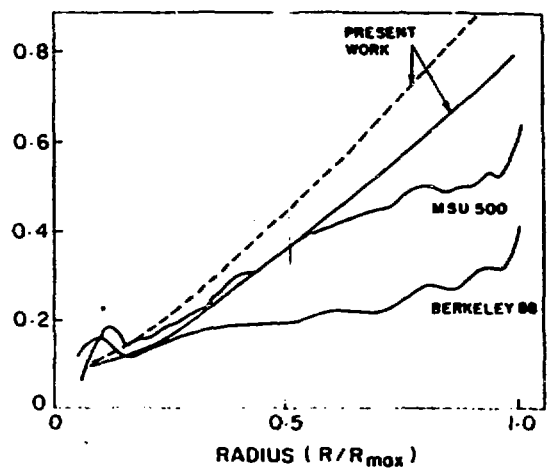

Fig.1. Continuous curve is for ω=5, Bav=18 kG, Bo=3 kG. Dotted one for ω=3, Bav=36 kG, Bo=7.5 kG

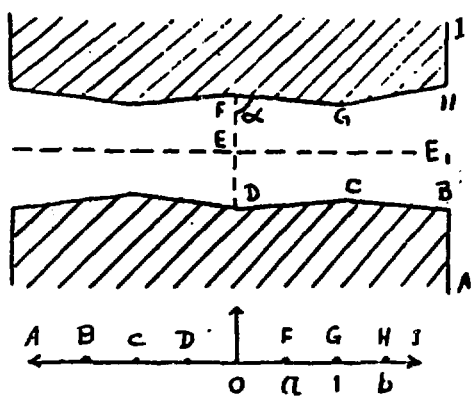

Fig.2. Triangular pole face

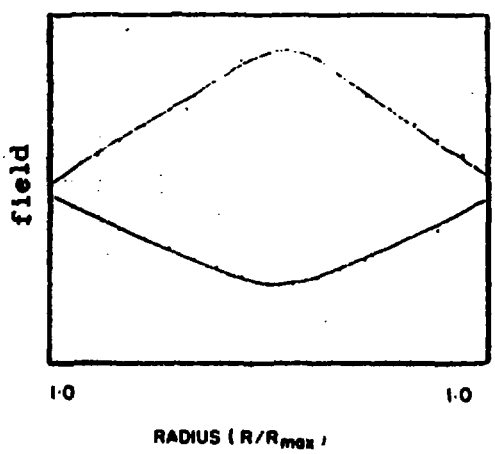

Fig.3. Field due to triangular pole with α=.4933 and α=.5067.

Reference

1) P.R.Sarma, Nucl. Instr. and Meth. A305, 10 (1991).
2) G.schatz, Nucl. Instr. and Meth. 67, 103 (1969).
3) P.D.Dunn, L.B.Mullet, T.G.Pickavance, W.Walkinshaw and J.J.Wilkins, CERN Accelerator Conf. 1956, p.9.

AN ANALYTICAL STUDY OF BEAM TRANSMISSION THROUGH HOLE LENS OF VEC MAIN MAGNET

Jane Alam, V.S. Pandit and P.R. Sarma

Variable Energy Cyclotron Centre
Bidhan Nagar, Calcutta - 700 064

In order to accelerate heavy ions with VEC an ECR ion source has been developed. The ion beam from the ECR ion source will be injected axially in the central region of the cyclotron. In order to improve the axial injection system a knowledge of the motion of injected particles through the magnetic field in the hole is necessary. Present work describes an analytical approach to study the behaviour of charged particle in the hole.

The magnetic field inside the axial hole of the upper pole of the main magnet has been calculated using the POISSON code. The axial magnetic field has been fitted to the Glaser model [1]. The equations of motion of the charged particle in cylindrical coordinate can be simplified to give the following differential equation for the radial motion

$$\frac{d^2y}{dx^2} + \frac{K^2y}{(1+x^2)^2} = \frac{C}{y^3} \qquad (1)$$

where

$$y=r/a, \quad x=z/a, \quad K^2=qB^2a^2/8mV_0, \quad W^2=1+K^2$$

$$C = (mr_0^4/2qVa^2)[\theta_0 - qB(z_0)/2m]^2$$

It is very interesting to note that the term on the right hand side of equation (1) dropped off in standard discussion of short magnetic lenses [1] but it becomes very important here near the axis. The solution of the nonlinear ordinary differential equation (1) is given by [2]

$$r(z) = a[Au^2(z)+Bv^2(z)+Du(z)v(z)]^{1/2} \qquad (2)$$

provided

$$AB - D^2/4 = C/WR^2 \qquad (3)$$

Where WR is the Wronskian of the two fundamental solutions u(z) and v(z) of the equation (1) with right hand side equals

zero. Here

$$u(z)=\sin W\phi/\sin\phi \ , \quad v(z)=\cos W\phi/\sin\phi, \quad \phi=\mathrm{Cot}^{-1}(z/a)$$

A single Glaser type of magnetic field does not fit the entire length of hole. So we have tried to fit the Glaser model

$$B(z) = B_0/(1+z^2/a^2) \quad \text{for} \quad 0 \leq z \leq 7 \quad \text{(in cm)}$$

and another model with the centre displaced by an amount b for the remaining part of the hole.

The constants A, B, D can be found out by using equations (2) and (3) and setting the required values of radial displacement r_0 and divergence r_0' at the median plane. Fig. 1 below shows the radial displacement r as a function of z for 10 keV deuteron , B_0= 13.7 KG , r_0=1mm, r_0'=10 mrad.

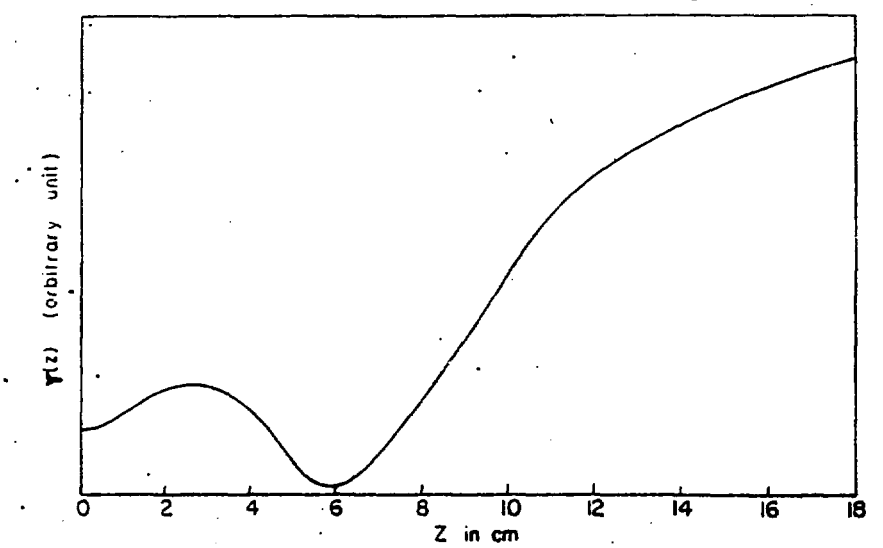

Fig.1. Radial displacement vs. z

In this paper we have presented only preliminary results and detailed calculations are in progress. Lot of computations can be avoided by using this analytical method. Once the analytical expression for r(z) is obtained, one can easily get the angle of rotation and other physical quantities.

Reference:

[1] A.B.EL-Kareh and J.C.J.EL-Kareh, Electron Beams, Lenses and Optics; Vol.1, Academic Press (1970).

[2] W.F. Ames, Nonlinear Ordinary Differential Equations in Transport Processes, Academic Press (1968).

PC BASED ACCELERATOR CONTROL SYSTEM

B.P.Ajith Kumar, J.Kannaiyan, D.Kanjilal & R.K.Bhowmik
Nuclear Science Centre, JNU Campus, New Delhi 110 067

Operation of a complex machine like the 15 UD Pelletron Accelerator involves the monitoring and controlling of a few hundred parameters and can be done most efficiently by using a computer. This paper explains the Control System Software PELCON developed at NSC. An earlier version with limited capabilities was reported in [1].

The Hardware for the accelerator control consists of a main CAMAC crate connected to a PC-AT 386 computer through a home made Crate Controller supporting the ACB. This, in principle, allows the accelerator to be controlled simultaneously by more than one computer. A Serial Highway Driver module located in this Crate interfaces three serial crates placed at various locations in the Pelletron tower. All the modules needed for the operation of the Pelletron are plugged in the three serial crates.

The Software, written entirely in C language, is DATABASE oriented and is highly modular in nature. It provides an integrated environment with MENU selectable DATABASE EDITOR, PAGE EDITOR, DATABASE LISTER and ONLINE CONTROL options. The various parameters of the machine are continuously scanned at the rate of more than 10 times per sec and displayed in a 43 line EGA monitor. Suitable choice of colour in the display allows the status of the machine to be reviewed at a glance.

For the control of the machine components, assignable Shaft Encoders and a "DO-IT" button is provided. A movable highlighter on the screen is used for assigning. The assigned parameters are scanned at a rate exceeding 200 times/sec providing a nearly instantaneous response. An ONLINE HELP facility is provided.

A large number of new features have been added to the software for efficient operation. The entire setup can be saved in a data file for a future run. After a power failure, the parameter values can be restored automatically eliminating the need of an uninterrupted power supply.

A number of useful parameters like the most probable charge state and the magnetic field of the Analysing magnet for a given energy and charge state of the ion can also be calculated online.

It is possible to define the desirable range of Minimum and Maximum values for any variable to be controlled. A logical output is generated if the current value is outside a predefined window. This feature is used for implementing software interlocks and a diagramatic display. The software interlock is used to provide active control of the accelerator (i.e. to shut down a gate valve if the pressure rises or the pump trips off). Upto eight parameters can be assigned to analogue outputs through DAC converters and be continuously monitored through the eight channel chart recorder.

A DIAGRAMATIC DISPLAY of the machine status is provided at the Console showing the status of all critical components like magnets, pumps & gate valves. This is driven by the Database software through output registers in the CAMAC crate. The Display is configured by using a text file. A separate relay driven SAFETY INTERLOCK MONITOR is provided at the Console displaying the Door interlocks and Radiation levels inside the Accelerator tower and in the beam hall.

[1] B.P. A.Kumar et al, Proc. DAE Symp 31B(1988)P83

DESIGN OF HIGH RESOLUTION LINES FOR VECC

C. Mallik, N. K. Mukhopadhyaya, B. B. Bhattacharya
VARIABLE ENERGY CYCLOTRON CENTRE
I/AF, Bidhan Nagar, Calcutta-700 064

To augment the facilities for experimentalists at VECC, new high resolutions have been designed and are currently being installed. With the procurement of two 120 degrees magnets major modifications in the high resolution lines have been incorporated. While the 160 degree magnet will operate in achromatic and dispersive mode the new lines will provide clean and better resolved beams.

The design goals have been to obtain (1)a modular approach(2) as few parameters as possible (3)telescopic transport and (4) UNanalysed beams with ease i.e flexibility. The new lines comprise of160 degreesbend section, matching section, monochromator section and beam guidance section.

(a)The 160 degree bend section provides an analysed beam of $\Delta p/p$ =1/1000 (for beam half width =3 mm). For achromatic transport mirror symmetry with QQDQQ configuration is utilised with two parameters.

(b)The matching section is composed of three doublets. Since three doublets allow transport with cross-mirror or cross-translational property maximum three parameters are required. Looking at the acceptance of the monochromator section and the requirement to have beams of different sizes four parameters will be needed. The intermediate doublet will provide two parameters. Magnifications in the horizontal plane are obtained from 0.4 to 2 keeping the vertical plane magnification at unity. This should be adequate for matching to monochromator and the target stations downstream.

(c)This section is composed of two 120 degree dipoles and 4 quadrupole doublets arranged as QQDQQQQDQQ having anti-mirror symmetry. The section provides dispersed as well as achromatic beam. The transfer matrix are for

dispersed beam

$$\begin{bmatrix} 1. & 0. & 16.88 & & \\ 0. & 1. & 0. & & \\ & & & -1. & 0. \\ & & & 0. & -1. \end{bmatrix}$$

achromatic beam

$$\begin{bmatrix} 1. & 0. & 0. & & \\ 34. & 1. & 0. & & \\ & & & -1. & 0. \\ & & & 0. & -1. \end{bmatrix}$$

(Standard TRANSPORT units and notations are used) Hence this choice of the optics gives (1)good control in the

vertical plane (magnet gap=4.3 cm)(2)telescopic transport and symmetry properties minimize aberrations (3)spatial and angular dispersion vanishes for achromatic beams (4)zero angular dispersion for analysed beams and (5)two parameters for quadrupoles.

The transmission for a 2x5sq.mm beam spot at the target location and a resolution of 15 kev for 50 Mev alpha beam will be 1.6% of the beam coming out of the cyclotron. The major aberration is aperture aberration but we have decided not to place any correcting element as the effect is small. Even half section of the monochromator can be used to obtain beams for a target station. Fig. 1 shows the beam envelope in horizontal (x) and vertical plane (y) from the virtual source of the cyclotron to the monochromator image point for tranport of achromatic beam. Fig. 2 shows the beam envelope in the monochromator section for analysed beam.

From the image point of the monochromator beams are guided by telescopic transfer using 4 quadrupoles and two parameters.

We acknowledge support given by S.K.Das, P.R.Sarma, M.H.Rashid, C.V.S.Rao, and D.P.Hazra. We are grateful for the encouragement given by Dr.B.Sinha.

Fig. 1

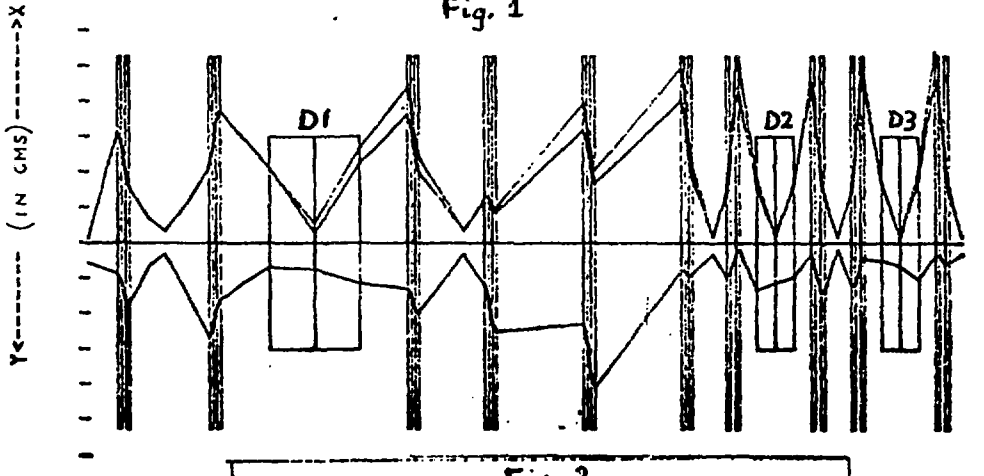

Fig. 2

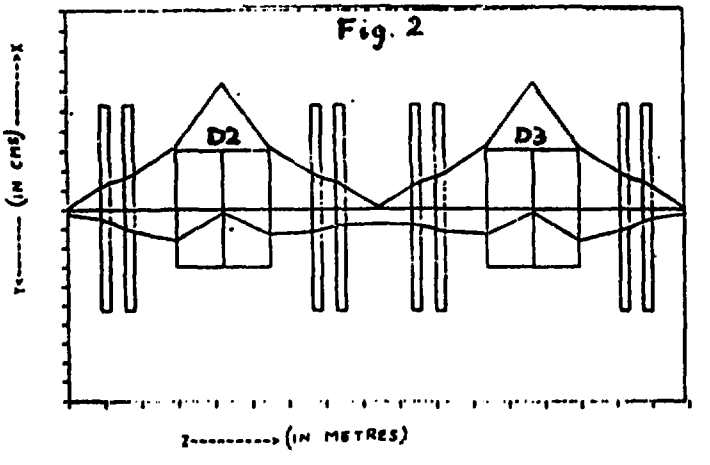

DEVELOPMENT OF AXIAL INJECTION SYSTEM AT VECC

G.Pal, C.Mallik, M.H.Rashid, J.Alam,
G.S.Taki, D.K.Bose and R.K.Bhandari
VECC, 1/AF, Bidhan Nagar, Calcutta-700 064

At VECC, an ECR ion source has been developed to obtain heavy ion beams. These heavy ion beams will be guided in the external axial injection line into the cyclotron. The components for this system are being fabricated. Design philosophy has been discussed elsewhere /1/. The beam line from the ion source to the charge analysing section has already been laid out, and tested. In the present paper we sketch the beam line design and present calculations regarding hole lens-inflector combination.

The beam from the extraction aperture of the ion source travels in the falling fringing field of the solenoidal field of the ECR ion source. It is imaged at the object slit of the analysing magnet with magnification equal to 2 using two Glaser lenses. The analysing section consists of a 90 deg. dipole magnet (at present 2x45 deg. dipoles) which has a pole face rotation of 30 deg. to provide vertical focussing and double focussing at the image slit. A charge resolution of 1 in 40 is achieved for 20 mm image size. The analysed beam then traverses 4 quadrupoles to match the beam to the cyclotron. It is followed by a DQQQD system which bends the beam by 90 deg. for injecting in the cyclotron. In the vertical line 4 Glaser lenses are used along with a solenoid lens for transporting and rotating the beam. There is provision for steering the beam using 4 coils in the belly of the Glaser lenses. Beam is monitored using 4 jaw collimators. A buncher is placed above the yoke of the cyclotron.

Beam at the entry of the cyclotron in the yoke encounters the axial field of the cyclotron which has a focussing action. This has been calculated using POISSON code. The geometry of the hole lens is shown in the figure 1(inset), where the field profile is also shown. Mh is the transfer matrix for the hole lens in the standard TRANSPORT units.

Beam in the constant magnetic field now traverses a mirror inflector which bends the beam by 90 deg. and places it in the acceleration cycle properly. The choice of mirror inflector is governed by the ease of fabrication. Voltage applied to the gridded inflector corresponds to theaccelerating voltage which has been restricted to 10 kV. The gap has been fixed at 11.7 mm. The action of the

inflector is represented by Mi the first order transfer matrix.

As is obvious from the above calculations, there exists coupling between the transverse subspaces resulting in the growth in beam-emittance in either plane at the expense of the other. This has resulted because we have considered in the fixed frame of reference while there is rotation of the beam in the axial magnetic field.. As optimization calculation have shown, by placing a beam rotator (a solenoid lens) downstream compensates this rotation to obtain approximate matched beam at the exit of the inflector. With a variable beam rotator trading in emittances can be accomplished to advantage. For total matching, however, four quadrupoles are used.

We acknowledge support given by B.Dasgupta, R.B.Mitra, P.R.Sarma, S.K.Das and N.K.Mukhopadhyay. We are grateful to Dr.B.Sinha for constant encouragement.

$$Mh=\begin{bmatrix} 1.25 & 0.0099 & 0.12 & -0.0018 \\ -170.1 & -0.15 & 171.9 & 1.55 \\ -0.12 & 0.018 & 1.25 & 0.0099 \\ -171.9 & -1.55 & -170.1 & -0.15 \end{bmatrix} \quad Mi=\begin{bmatrix} 0.98 & 0.0 & 0.19 & 0.0 \\ -126.53 & 0.94 & 658.0 & 0.0 \\ 0.0 & 0.0 & -1.0 & 0.0 \\ 0.0 & -0.19 & 0.0 & -0.99 \end{bmatrix}$$

References:
/1/Bhandari R.K.et.al.,10th Intl.Conf.on Cyclotrons and their Applications,East Lansing,(1984).

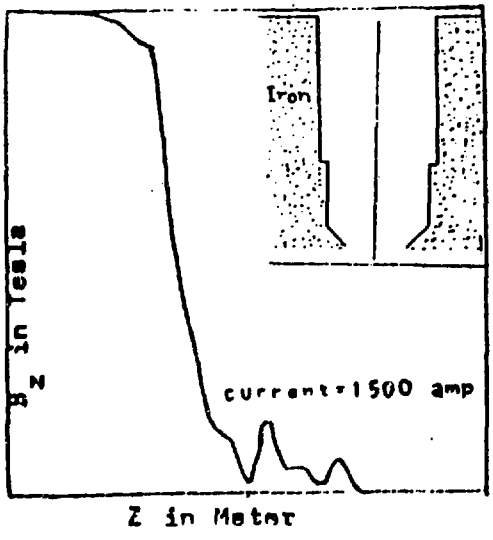

Fig.1 Plot of Axial Magnetic field as a function of distance from median plane.

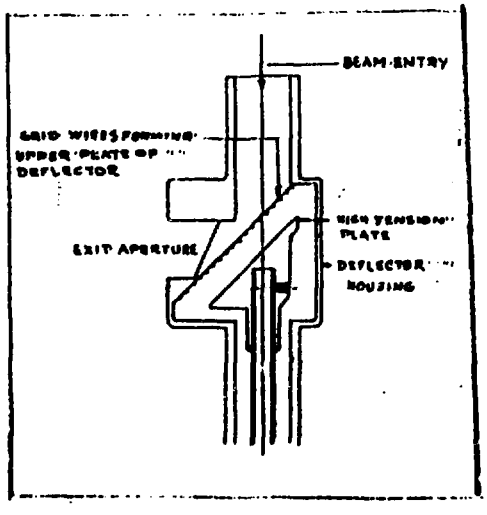

Fig.2 Sketch of electrostatic mirror inflector.

DESIGN OF HIGH POWER DIRECTIONAL COUPLER

S.A.Mateen, NPD, BARC, Bombay 400 085.

INTRODUCTION

A directional coupler is a device that couples a secondary system to a wave travelling in a particular direction on a primary line and entirely ignores the wave travelling in the opposite direction. In our application, the directional coupler is used to measure the power fed to the RFQ accelerator from the RF power amplifier.The set up is depicted in fig 1.

DESIGN

The specifications of the high power directional coupler are as follows:

1) Input power = 30kW 2) Frequency = 45MHz
3) Coupling ratio = 60dB

The design of the high power directional coupler is done in two independent steps. First, the dimensions of the outer and inner conductors are optimised to obtain a 50 ohm characteristic impedance (fig 2). The outer and inner conductor diameters of 1 5/8" and 0.706" respectively, are taken with air as dielectric. The gap between the outer and inner conductors is sufficient to withstand 30kW of power at 45MHz. The inner conductor is supported by teflon rings.

The loop is introduced into the assembly through a circular hole on the outer conductor. The resistive loop, designed for 60dB coupling, is shown in fig 3. The output voltage is

$$e_o = (jwM/z_o)2E_f$$

where E_f is the forward voltage, w is the operating frequency and M is the mutual inductance between the loop and the centre conductor.

The two stringent conditions which the loop has to satisfy are as follows:

a) $R \ll X_a$ b) $CR = M/Z_o$

The loop is provided with an arrangement to

move up and down as well as in the clockwise and anticlockwise directions. Loop coupling is dependent on the area of the loop and the angle of orientation. The value of M and C have to be realized physically to satisfy condition (b). The above relation must simultaneously satisfy the condition $R \ll X_c$, so that the voltage across the capacitance is more than that developed across R. The loop position is adjusted in such a way that the loop is sensitive to the signal in one direction only. The fabrication of the directional coupler is in the process.

ACKNOWLEDGEMENT:

The author thanks Dr.S.S.Kapoor, Dr.M.A.Eswaran and Dr.R.C.Sethi for their support and guidance and Kum.Kavitha Murthy for her keen interest and valuable suggestions.

REFERENCES

1) W.L.Firestone, Analysis of transmission line directional couplers, Proc IRE, October 1954, p1529-1538.
2) D.L.Hollway, The comparison reflectometer, IEEE Trans on MTT vol MTT-15, No 4, Apr 1967 p250-259

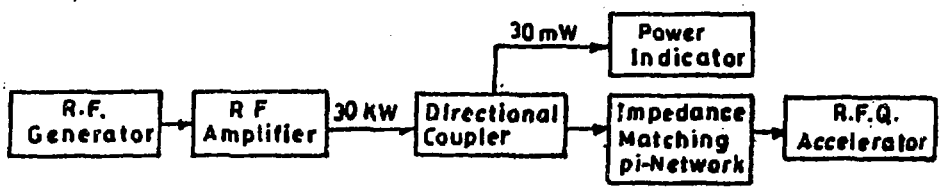

FIG.1

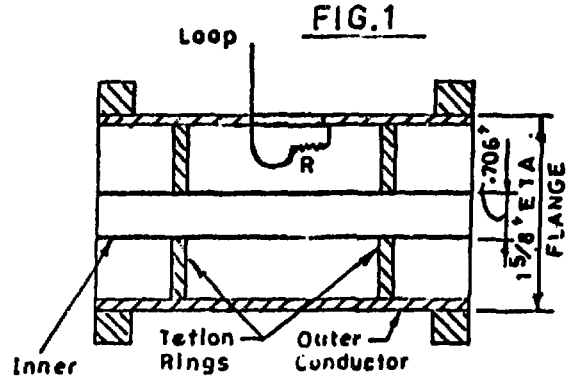

FIG.2

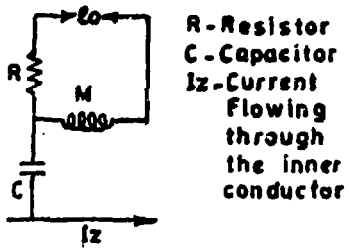

FIG.3

RELATIVISTIC-QUANTUM PARTICLES FOR BOUND-STATES AND SCATTERED-STATES WAVE SOLUTIONS- SUITABLE FOR HIGH-ENERGY-PARTICLE-ACCELERATORS :

J.N.MOHANTY AND C.B. SAMANTARAY.
P.G. DEPARTMENT OF PHYSICS,
RAVENSHAW COLLEGE, CUTTACK-753003
ORISSA

ABSTRACTS :-

We propose here to solve the Dirac equation[1] for electromagnetic potentials viz. Vector potential and Scalar potential. The Vector potential in our model is of the type $A = -\frac{H_0 \exp[k(y-y_0)]}{\gamma}$ suitable for synchrotron- radiation[2,3,4] of high energy particles and in accelerators and in fission - reactors as well.

INTRODUCTION :-

The exact magnetic field solutions of Dirac equation depend upon the asymptotic space-co-ordinate and spin-angular-momentum as distinct from pauli-spin representation. (Pynmann-Gelmann-1958)[5] Reducing the Dirac equation to one dimentional schroedinger one with $\epsilon, \lambda, \nu^2+\nu_0^2$ etc, We derivethe wave-function which includes wave-particle interactions for high-energy range. For both bound-states $\psi_s \propto \exp(-\epsilon y)$, $\psi_s \sim \hat{y}$ at $y=0$ in terms of series and coulomb scattered-states (ψ_s at $y \to \pm\infty$), and in terms of whittaker, functions and confluent hypergeometric-series.

THEORY AND EXACT SOLUTIONS :-

Here we employ the Dirac relativistic wave equation and solve it for exponentially varied magnetic vector potential.

Contd....

The relativistically invariant two-component equation for an electron in the external magnetic field is given as.

$$\left[(P + eA)^2 + m^2 + e^2 \sigma . (H + iE) \right] \psi = (W + eV)^2 \psi \quad \ldots\ldots (1)$$

Which, for vector potential $A = -\frac{H_0 \exp[-\alpha(y-y_0)^2]}{\gamma}$ reduces to

$$\left[\frac{d^2}{dy^2} - \epsilon^2 + 2\nu_N^2 - \frac{\lambda_N(\lambda_N - 1)}{y^2} \right] \psi_s = 0 \qquad (2)$$

Putting $\psi_s \sim (y-y_0)^{\lambda_N} \exp\{-\epsilon(y-y_0)\} f_s(y-y_0)$ in (2) we obtain

$$z f_s''(z) + f_s'(z)(2\lambda_N - z) + \left[\frac{(\nu^2 + \nu_i^2)}{\epsilon} e^{-\alpha y_0^2} - \lambda_N \right] f_s(z) = 0 \qquad (3)$$

where $f_s(z) = z^{-\lambda_N} \exp(-\frac{z}{2}) F_s(z)$ Substitution leads to usual Whittaker form

$$F_s''(z) + \left[-\frac{1}{4} + \frac{k'}{z} + \frac{\frac{1}{4} - \mu'^2}{z^2} \right] F_s(z) = 0 \text{ whose solutions are}$$

(1) For bound states $\psi_s(y-y_0) = (y-y_0)^{\{\lambda_N - \left(\frac{\nu^2 + \nu_i^2}{\epsilon}\right)\}} \exp(-\alpha y_0^2) \; (2\epsilon)^{-\frac{(\nu^2+\nu_i^2)}{\epsilon}} \exp(-\alpha y_0^2)$

$$\cdot \frac{2\mu'!}{(\mu' - k' - \frac{1}{2})!} \left\{ 1 + \frac{(\frac{1}{2} - \mu' + k') \cdot (\frac{1}{2} + \mu' + k')}{z} + \; \right\}$$

(2) Asymptotic wave solutions (scattered states)

$$\psi_s(y-y_0)\big|_{y \to \infty} = (y-y_0)^{\{\lambda_N + \frac{\nu^2+\nu_i^2}{i\eta}\}} e^{-\alpha y_0^2} \cdot (-2i\eta)^{\frac{(\nu^2+\nu_i^2)}{i\eta}} e^{-\alpha y_0^2}$$

$$\left[\frac{2\mu'!}{(\mu' - k' - \frac{1}{2})!} \right]$$

DISCUSSION :-

Here we get three types of wave solutions like bound-states, scattered-state, and pure imaginary values. The wave function is exponentially falls with increasing value of α only but varies with other values of $\nu^2 + \nu_0^2, \lambda_N$. This suggests an Oscillating type of wave function with centred of gaussian-type potential. The scattered states wave solution is utilised for high-energy particle accelerators, hence for fission-reactors.

REFERENCES :-

1. Dirac PAM 1928 Proc. R.Soc (London) AII7 610
2. Rander J et al 1970 Phys. Rev. Lett 24 283
3. Occhionero F. and Demianski M. 1969 Phys. Rev. Lett. 23 1128
4. Datlowe D. and Meyer P. 1970 Bull A m Phys. Soc. 15 611
5. Fynmann R. P. and Gell-mann M 1958 Phys. Review 109 193

K-SHELL IONIZATION CROSS SECTIONS FOR LOW Z ELEMENTS ($1 \leq Z \leq 22$) BY PROTONS IN THE ENERGY RANGE 0.5 TO 2.5 MeV

L.C.Tribedi and P.N.Tandon
Tata Institute of Fundamental Research,Bombay-5

Proton induced X-ray emission ($PIXE$) cross sections are now increasingly being used with confidence in calibrating the efficiency of $Si(Li)$ X-ray detectors, particularly in the low energy region $\leq$ 5 keV, where convenient standard radioactive sources are not available. For such purpose 'reference' cross sections[1] have been generated from the measured and the theoretically calculated cross sections. However, most accurate and abundant experimental data for $21 \leq Z \leq 30$ has been used for generating these 'reference' cross sections in the low Z region due to scarcity of experimental data. We report here proton induced K X-ray production cross section measurements for $Na, Mg, Al, Si, Cl, K, Ca$ and Ti in the energy range 0.5 to 2.5 MeV using proton beams from the Van de Graaff accelerator at Trombay. The X-ray and the particle detectors were mounted in vacuum inside a SS chamber. A triple axis multiple target holder was used which could accommodate twenty seven targets at a time. The cross sections were evaluated from the measured K X-ray peak intensity (N_x) and the simultaneously detected scattered protons peak intensity (N_p) from the thin targets used with the help of the relation

$$\sigma_K(E) = \frac{N_x}{N_p} \frac{\sigma_R(E)\Omega}{f\omega_K\epsilon(E)}$$

where Ω is the solid angle subtended by the particle detector, σ_R is the Rutherford scattering cross section and ϵ is the absolute photo peak detection efficiency of the detector. The efficiency of the detector was measured independently. The cross section values obtained are shown in fig. 1. The ionization cross sections obtained, using fluorescence yield tables of Krause[2], are compared with the $PWBA$ theory corrected for Binding energy and Coulomb deflection and energy loss in perturbed stationary state approach[3]. The agreement between the experimental data with theory is remarkable. We have also compared the data with various other theories like Binary Encounter Approximation, Semi Classical Approximation.

Fig . 1

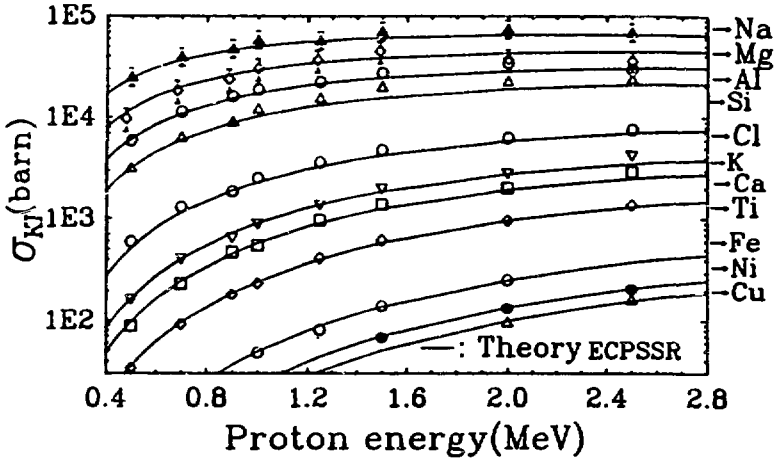

Fig . 2
Reduced cross section vs. reduced proton-energy

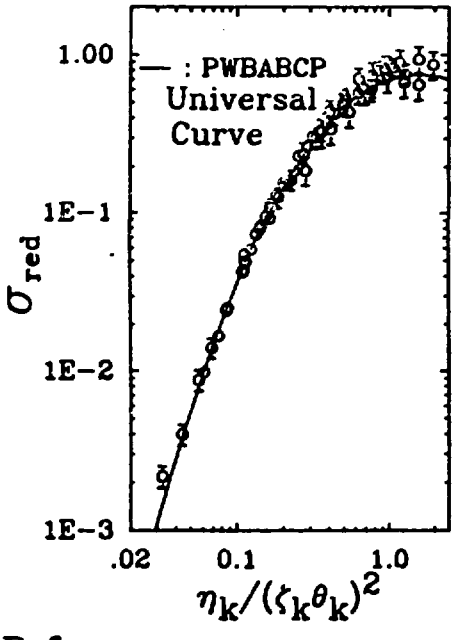

Fig . 3
Classical approximation

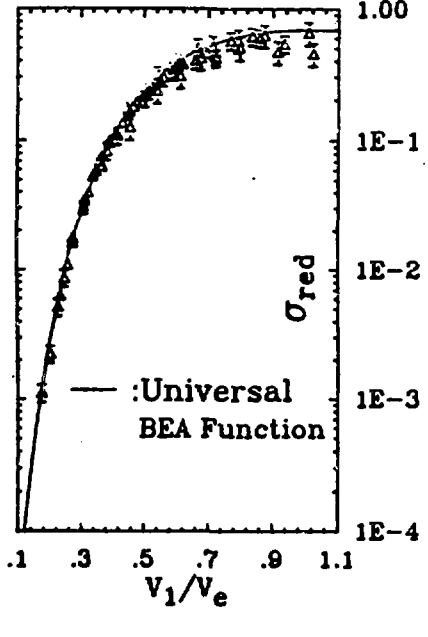

References:

1. H.Paul and J. Sacher
   Atomic Data and Nuclear Data Tables 42(1989)106
2. M.O.Krause, J. Phys. Chem Ref. Data 8(1979)307
3. G.Basbas et.al, Phys.Rev A,17(1978),1655

PROTON INDUCED K-IONIZATION CROSS SECTION MEASUREMENTS FOR LOW Z ELEMENTS USING A 400 KeV ION ACCELERATOR

L.C.Tribedi, M.B.Kurup, K.G.Prasad and P.N.Tandon
Tata Institute of Fundamental Research,Bombay -5.

The 400 KeV accelerator has been used mostly as an ion implanter for many years now. It is also a useful source of low energy beams for ion atom collision investigations. For a quantitative comparison with theoretical models the energy of the beam should be accurately known. We have used some low energy proton resonance reactions at three different energies to calibrate this machine. In addition K-shell X-ray production cross section for $11 \leq Z \leq 20$ induced by protons of energy between 100 to 320 KeV have been measured and the results compared with theoretical models.

The 340.5 and 223.9 KeV resonance[1] in the reaction $^{19}F(p,\alpha)^{16}O$ and the $^{11}B(p,\alpha)^{8}Be \rightarrow 2\alpha$ reaction at a resonance of 162.5 KeV with varying extracting voltages from the machine were used for calibration. Thick target of ^{19}F on Ta backing were used and the 6.13 MeV gamma-ray from ^{16}O recorded in a 6" hexagonal 10" long $NaI(Tl)$ detector. Typical yield curve for the 340.5 KeV resonance is shown in fig.1. A thin target of ^{11}B was used for the second reaction and α-particle yield was measured. Using these resonances we know the energy of the machine to an accuracy of 1 KeV in the region of interest.

The proton induced cross sections were measured using thin targets of *NaCl, Mg, Al, Si, InP, KCl* and *Ca* deposited on thin carbon backing. The scattered particle and the emitted X-ray spectra were recorded simultaneously. For normalisation of the X-ray spectra, the current integration was done collecting the charge from the entire chamber which was electrically isolated. The measured X-ray yield at 319 keV was normalised to the accurately known cross section[2] and the derived normalisation constant was used to calculate the cross sections at lower energies. The K-shell ionization values derived using single vacancy fluorescence yields are shown in fig.2. The solid line through the data points are *PWBA* calculations based on Perturbed stationary states taking into account corrections due to Coulomb deflection, binding energy and relativistic effects(*ECPSSR*) The agreement between the theory and experiment is remarkable.

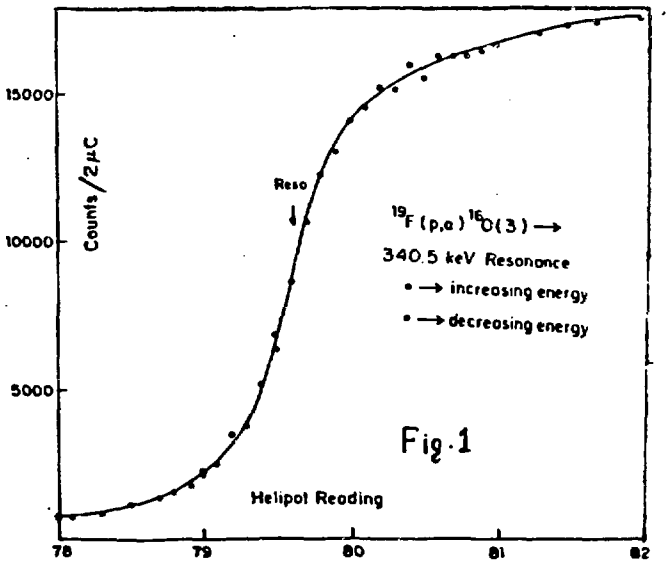

Fig.1

Fig. 2 ↓

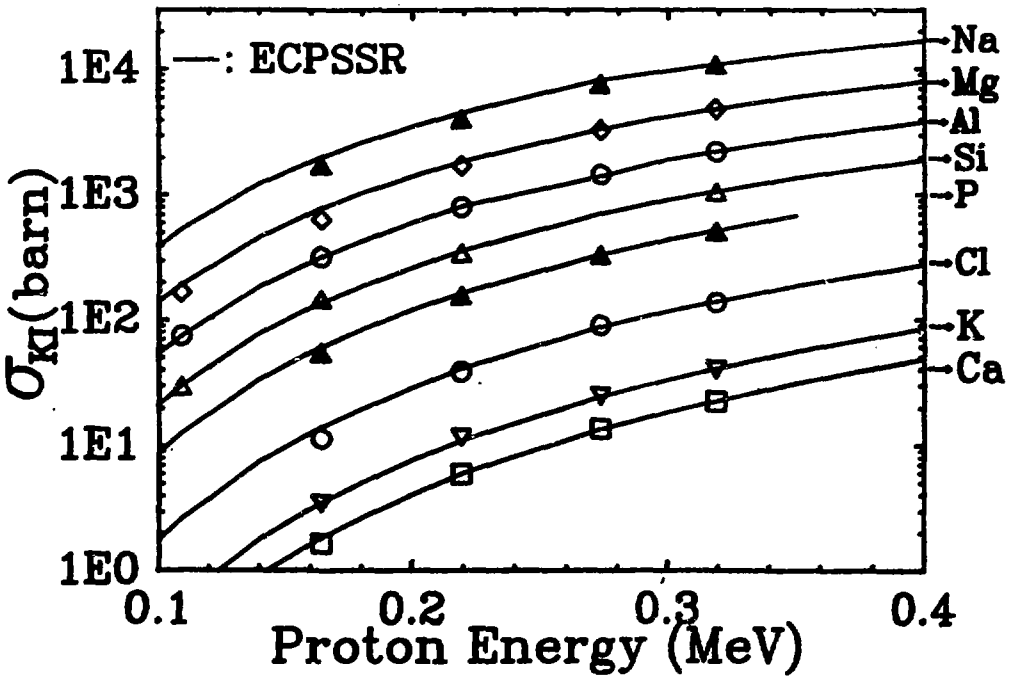

Reference:

1. T.Freye et.al, Z. Phys. A281,211(1977)
2. H.Paul and J.Sacher, Atomic and Nucl.Data tables,42(1989)106

EFFECT OF 100 MeV ^{16}O ION IRRADIATION ON Pb-DOPED Bi-BASED SUPERCONDUCTORS

S.A. Agnihotry, R.H. Bhawalkar, S. Chandra
National Physical Laboratory
Dr.K.S.Krishnan Road, New Delhi-110012
L. Senapati, D. Kanjilal, G.K. Mehta
Nuclear Science Centre, New Delhi-110067

Results of preliminary investigations of the effect of oxygen ion irradiation on the Bi-based high temperature superconductors are reported in this paper. Bar shaped specimens of Pb-doped Bi-Sr-Ca-Cu-O system of dimensions 10x5xo.5 mm^3 were irradiated by 100 MeV ^{16}O ions in the fluence range of 1.5×10^{12} to 3.5×10^{15} ions/cm^2 at room temperature. During irradiation the temperature of the specimens did not change appreciably, due to the use of low ion beam of 1 pnA.

Five bar shaped specimens were cut from a single pellet, obtained by conventional solid state diffusion reaction with the starting nominal composition $Bi_1Pb_1Sr_3Ca_3Cu_4O_y$ at 840°C for 132 hrs in air followed by furnace cooling. The specimens as characterized by XRD analysis had $Bi_2Sr_2Ca_1Cu_2O_y$ (2212) as the predominent phase and the high Tc phase $Bi_2Sr_2Ca_2Cu_3O_y$ (2223) was either absent or present as a minor phase (< 25% as estimated from the intensities of the 002 peaks in the XRD pattern). The resistance at room temperature-R_{RT} for the specimens was in the range 15 to 16 mΩ, with the zero resistance temperature-Tc° between 93 to 103 K.

Irradiation has been found to induce changes in both the normal state and the superconducting properties depending upon the fluence as also the quality of the specimen e.g. relative proportion of the two phases 2212 and 2223. R_{RT} has been observed to be more sensitive to irradiation than Tc°. The observed changes in R_{RT} as illustrated in the figure and Tc° clearly reveal that there exists a "critical fluence" of about 2.7×10^{14}

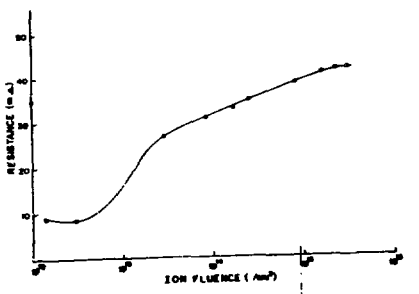

ions/cm^2. At fluence less than the critical fluence R_{RT} decreased without detectable changes in Tc° and the XRD pattern. However, at fluences exceeding the critical fluence R_{RT} increased and Tc° decreased. Correspondingly the XRD analysis exhibited decrease/deterioration of the 2223 phase. These observations are similar to our earlier ones /1/ with annealing time exceeding the optimum annealing time-resulting in maximum Tc° and also volume fraction of the 2223 phase and minimum R_{RT}. To understand the mechanism bringing about the observed decrease in R_{RT} at lower fluence without detectable changes in Tc° and the XRD pattern, further detailed investigations are planned.

We thank NSC pelletron staff for making available high quality ^{16}O ion beam to us and for help in the experiment.

References

/1/ S. Chandra, S.A. Agnihotry, P.Asthana, K.C. Nagpal, K.K. Saini, Chander Kant, C.P. Sharma, S.N. Ekbote - Phys. Stat. Sol(a). 123,269 (1991)

MEASUREMENT OF THE BREMSSTRAHLUNG RADIATION FROM ELECTRON - ATOM / MOLECULE COLLISIONS

R.Shanker
Atomic Physics Laboratory, Department of Physics,
B.H.U., Varanasi - 221005, INDIA

and

R.Hippler
Fakultaet fur Physik, Universitat Bielefeld,
4800 - Bielefeld 1 , GERMANY

The energy spectra of the electron bremsstrahlung have been measured for electron impact with Argon and SF_6 targets with various incident energies ranging from 2.5 keV to 15.0 keV. The scaled cross sections (arb. units) have been determined and compared with the available theory. The additivity hypothesis of the molecular targets has been considered and applied to the present data.Agreement between the experiment and the theory is found to be satisfactory. More details of the experimental set up and the results (see, eg. fig.1) will be presented and discussed.

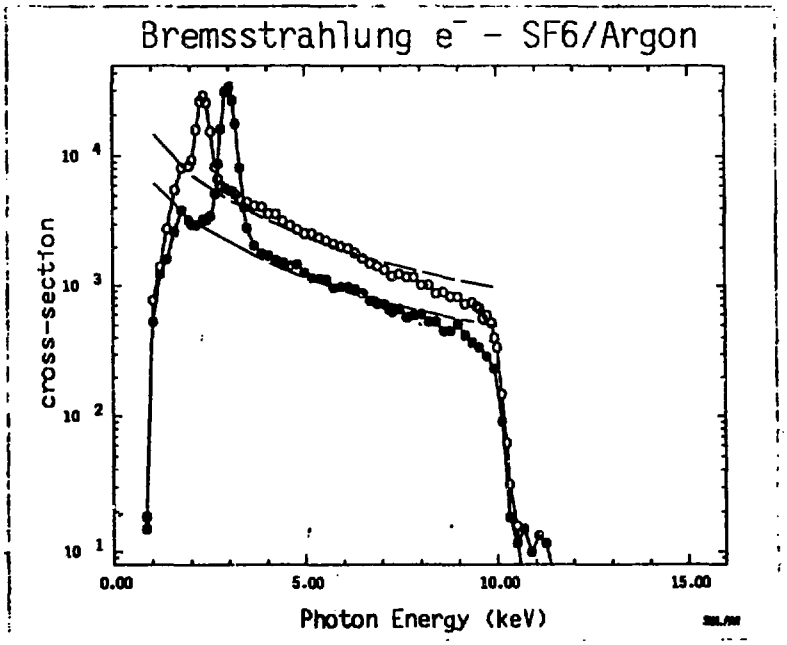

Figure 1: Scaled bremsstrahlung cross sections (arb. units) for 10.0 keV electron-Ar/SF collisions.
6
• present data for Ar target: o data for SF : -- theory (Ref. 1)
6

Reference:

(1) R.H.Pratt, H.K.Tseng, C.M.Lee and L.Kissel Atomic Data and Nucl.Data Tables 20, 175 (1977).

MEASUREMENT OF ARGON - RECOIL ION CHARGE STATE DISTRIBUTIONS IN 60-70 MeV $O^{5+,6+}$ - Ar COLLISIONS.

M.J.Singh,S.K.Goel & R.Shanker.

Atomic Physics Laboratory,Physics Department,
Banaras Hindu University, Varanasi-221005.

&

D.O.Kataria,N.Madhavan & A.K.Sinha

Nuclear Science Centre,J.N.U. Campus,New-Delhi.

The first Atomic Physics experiment on the production of highly charged slow moving argon-recoil ions from 60-70 MeV O^{n+} ($n=5+,6+$) pulsed ion beam impact on Argon gas target has been performed by using the 15UD Pelletron machine at Nuclear Science Centre, New Delhi. The preliminary data on the Argon-recoil ion charge state distributions as a function of projectile's energy and its charge state have been obtained. A typical spectrum of the Argon - recoil ion charge state distributions for 60 MeV O^{5+} - Ar collisions is shown in Fig.1. The experimental setup, methodology and spectra will be presented and discussed in light of the recoil ion data of Cocke(1) for 34 MeV Cl^{9+} - Ar collisions.

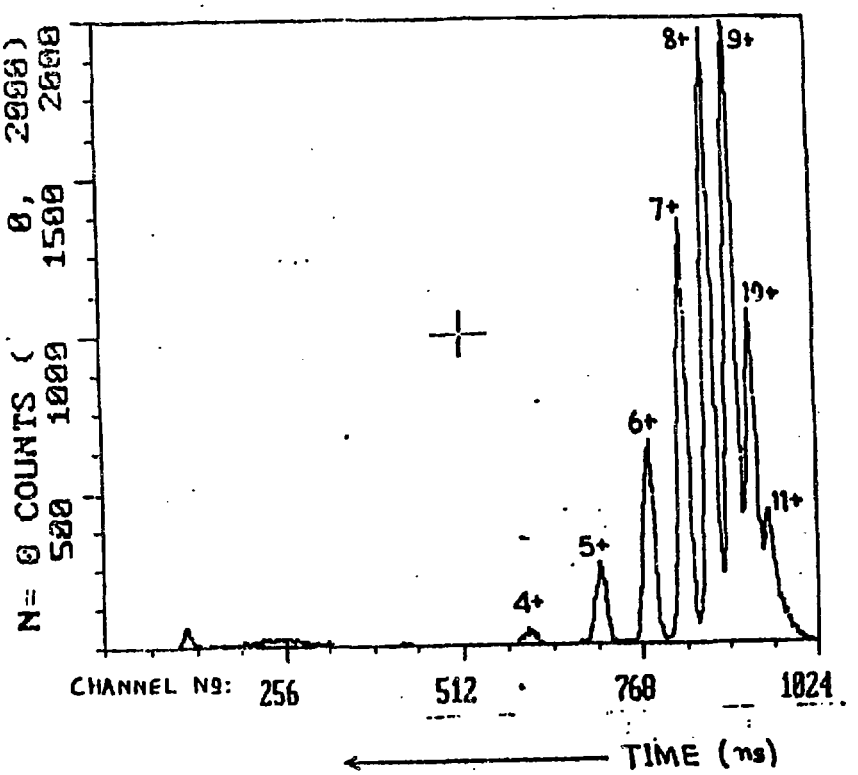

Fig 1: Time of flight spectrum of Argon - recoil ions produced by beam of 60 MeV O^{5+}.

We are thankful to Prof.G.K.Mehta, Director (N.S.C.) for his continuous support and encouragement in the above work. The cooperation received from the scattering chamber group and the personnels of Pelletron machine in carrying out the experiment is very much appreciated.

Reference:

1) C.L.Cocke, Phys. Rev. A20, 749(1979).

MICROTRONS AND THEIR APPLICATIONS

H.C. SONI & S.S. RAMAMURTHI
Centre for Advanced Technology, Indore

1.0 INTRODUCTION

The "Microtron" - an electron accelerator is very powerful tool for research, medical and industrial applications which need electron beam in energy range of few tens of MeV. In research these machines are used for photon and neutron activation analysis, electron channelling experiments, study of radiation damage, radiolysis studies and for construction of free electron lasers. The microtrons are used for radiotherapy in treatment of malignant (cancerous) tumours. They are also used for x-ray radiography of thick components in nuclear power, heavy ship building, armament and space industries where thickness of material to be radiographed quite often reaches to equivalent steel thickness of 250mm. Excellent beam quality, in terms of energy spread and emittance, of electron beam from microtron, makes it suitable for injection into bigger circular machines.

2.0 PROGRAMME AT CAT

After considering vast usability of this machine, Centre for Advanced Technology, DAE, Indore has taken up a programme for development and construction of microtrons for various applications as shown in Table-1 during phase 1 and for higher energy and higher current microtrons suitable for FEL and some activation analysis experiments during phase 2. As such the 20 MeV injector microtron is suitable for many activation analysis experiments. One 20 meV, 30mA microtron (as shown in fig-1) suitable for injection of electron beam into 700 MeV booster synchrotron of SRS facility is in advanced stages of assembly and testing at CAT. This machine will be commissioned by January 1992. It is a 22 orbit microtron having 2.0 tonn magnet assembly with diameter of 1.4 meters mounted in vertical orientation. RF cavity of the microtron is powered by 5 MW, 2856 MHZ klystron. Personal computer based control system is used for this microtron. Two more microtrons; one of 20 MeV, 30mA for activation analysis and the other of 8 MeV, 50mA for radiochemistry applications are under fabrication.

Table 1

Specifications of microtrons required for various applications

Applications	Injector	Radiotherapy	X-ray radiography
Specifications			
Energy(MeV)	20	4 - 20	4 - 10
Beam pulse current(mA)	30	15	30
Energy spread (FWHM)	0.2%	—	—
Emittance(m.rad) horizontal : vertical :	$1\pi\times10^{-6}$ $3\pi\times10^{-6}$	— —	— —
Pulse repetition rate (Hz)	1 - 3	30	300
Pulse duration (μs)	1 - 2	2	2
Beam size(max.) (mm x mm)	3 x 5	3 x 5	3 x 5
Av. beam power -Upper Limit (Watt)	3.6	18	180
x-ray intensity (Gy/min) at 1 m dist. from tungsten target		0.3-3.8	3.0-6.8

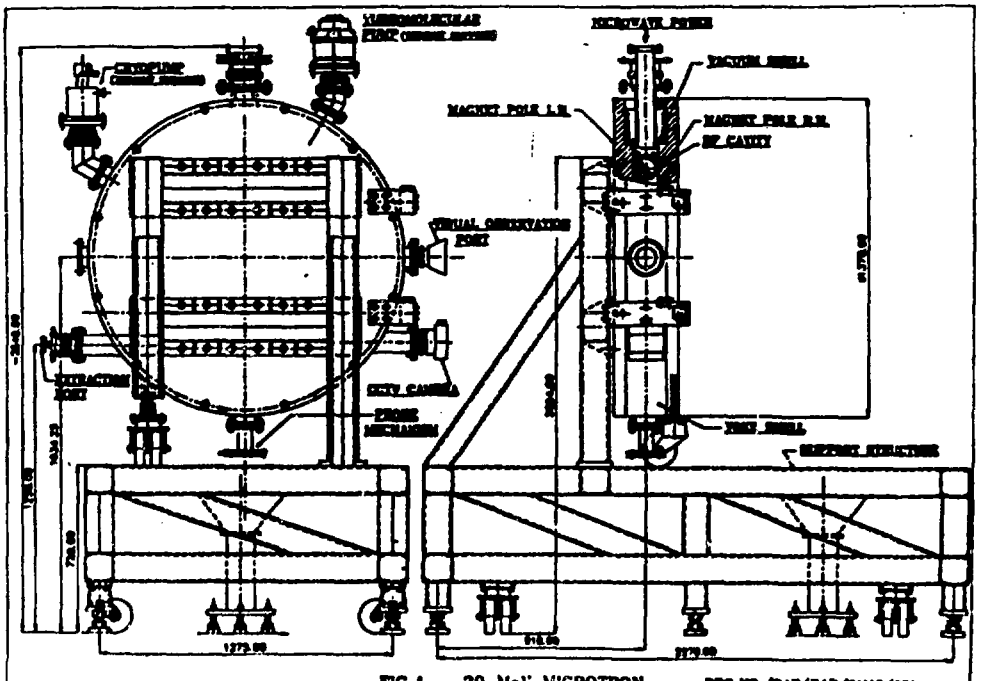

FIG. 1 – 20 MeV MICROTRON DRG.NO./CAT/EAP/91110/001

CHARACTERISTICS of INDUS–1 and INDUS–2

G.Singh, G.K.Sahoo, A.D.Ghodke & S.S.Ramamurthi
Centre for Advanced Technology, Indore–452 013, India.

INDUS–1 & INDUS–2 are the two synchrotron radiation sources under construction at CAT. INDUS–1 will provide VUV radiation and INDUS–2 mainly x–rays. Both these sources will have a common injector system consisting of a synchrotron with the maximum beam energy of 700 MeV and a 20 MeV microtron.

INDUS–1, a 450 MeV electron storage ring, is an advanced stage of construction. This storage ring will have four unit cells each consisting of a 90° bending magnet and two doublets of quadrupoles. The ring will have a provision for insertion of a 3Tesla superconducting wiggler in one of the straight sections. The critical wavelength[λ_c] of radiation from bending magnets will be 61Å and from the wiggler 30Å. The machine has been designed to operate in two modes for providing different emittances. The basic parameters of the storage ring are given in Table–1. The flux and brightness as a function of wavelength are plotted in Fig.1(a & b). The figures show that sufficiently high flux and brightness of radiation will be available to users at wavelengths down to 30Å from bending magnets and to 15Å from the wiggler. Like other storage rings, INDUS–1 will also provide a highly polarized radiation. The percentage of parallel polarization integrated over the vertical emission angle is expected to be nearly 88% at $\lambda=\lambda_c$, 100% for $\lambda<\lambda_c/100$ and 75% for $\lambda>100\lambda_c$.

TABLE–1

Energy	: 450 MeV
Current	: 100 mA
Bending field	: 1.5 Tesla
Critical wavelength	: 61.38Å (BM)
Circumference	: 18.96 m
Flux[λ_c]	: 7.2×10^{11}
Tune 1. ν_x,ν_z	: 1.88,1.22
ϵ_x	: 7.1×10^{-8}m.rad
Brightness[λ_c]	: 3.2×10^{12}(BM)
Beam lifetime	: 1.8 Hours
Tune 2. ν_x,ν_z	: 1.55,1.56
ϵ_x	: 2.1×10^{-8}m.rad
Brightness[λ_c]	: 6.5×10^{11}(BM)
Beam lifetime	: 3.6 Hours
Energy spread	: 3.85×10^{-4}
Revolution Frequ.	: 15.82 MHz
RF	: 31.64 MHz
Harmonic number	: 2
Power loss	: 0.36 kW (BM)
	: 0.05 KW (3T W)

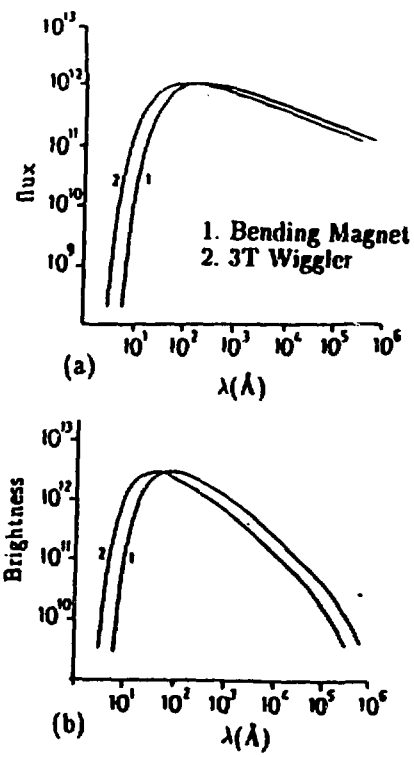

Fig.1 a) Flux vs. wavelength &
b) Brightness vs. wavelength

INDUS–2, a 2 GeV electron storage ring, is presently in a design stage. This ring is being designed to provide a small beam emittance as well as to provide five long straight sections each of 4.5m long with zero dispersion for insertion devices. A DBA(Double Bend Achromat) type of lattice with 8 unit cells is presently under consideration. The critical wavelength of radiation from the bending magnets will be 3.87Å. The basic parameters of the storage ring are given in Table–2. Presently, two insertion devices are proposed to be installed in the ring. A 5Tesla two period superconducting wiggler will provide radiation with the critical wavelength of 0.93Å. The second insertion device is a 1.8Tesla multipole wiggler with 11 poles. This device will provide radiation with the critical wavelength of 2.6Å. The flux and brightness as a function of wavelength are plotted in Fig.2(a & b). As evident from these figures, INDUS–2 will provide intense x–rays down to 0.5Å.

TABLE–2

Energy	: 2 GeV
Current	: 300 mA
Bending field	: 1.2 Tesla
Critical wavelength	: 3.87Å (BM)
	: 0.93Å (5T W)
	: 2.59Å (1.8T W)
Circumference	: 173.8 m
Typical tune point:	
ν_x, ν_z	: 9.2, 6.2
ϵ_x	: 4.0×10^{-8} m.rad
Flux[λ_c]	: 9.6×10^{12} (BM)
Brightness[λ_c]	: 5.35×10^{13} (BM)
Energy spread	: 7.22×10^{-4}
Revolution Frequ.	: 1.726 MHz
RF	: 189.8 MHz
Harmonic number	: 110
Power loss	: 76.3 kW (BM)
	: 7.6 kW (5T W)
	: 5.2 kW (1.8T W)

Brightness in Photons/s/mm^2/mrad^2/0.1% BW
Flux in Photons/s/mrad Horz./0.1% BW

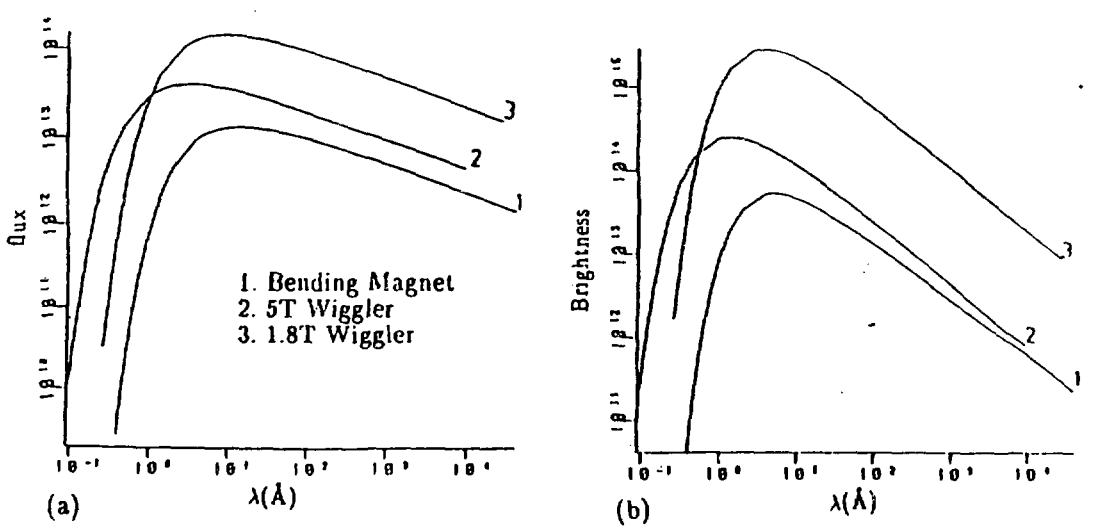

Fig.2 a) Flux vs. wavelength & b) Brightness vs. wavelength

MAGNET FABRICATION TECHNIQUES FOR SYNCHROTRON RADIATION SOURCE

S.S.Prabhu, A.M.Puntambekar, K.Sreeramulu, K.A.Hussain,
S.S.Ramamurthi
ACCELERATOR PROGRAMME,
CENTRE FOR ADVANCED TECHNOLOGY, INDORE - 452 013

The booster dipole magnets are constructed from CRGO Si steel stampings of 0.35 mm thickness. The booster ring magnets are laminated because of eddy current losses, as magnetic field will be increased from 370 gauss (20 Mev) to 13000 gauss (700 Mev). The field should be uniform to ± 5×10^{-4} during this ramping operation. This uniformity is possible if the permeability of material is as high as possible so CRGO Si steel material has been selected. The field uniformity also calls for pole gap uniformity of 50 micron. The accuracy of 50 micron only possible if we control inaccuracies due to Die punch clearances, Die & punch design, Jigs & fixtures design, Assembly process used.
The pole gap was 51 mm which was punch within ± 10 micron and overall size within ± 20 microns. To get sector type of shape each block has also been made in sector type having outer arc length of 78 mm at 1900R & inner arc length 55 mm at 1330 mm. To get sector type of shape 4 cut type of stamping are used in ratio of 10:4. The bonding is done by room temperature epoxy of Dr.Beck's Co. The block after stacking, with epoxy in between two lamination, has been kept under 20 Ton pressure and cured at 80°C for 4 Hrs and afterwards 16-18 hrs at room temp. Such 4 blocks again assembled with epoxy to get one main block. Such six main block will give us booster dipole magnet. The entry & exit block has provided with cosine countour to get hard edge approximation. The pole gap accuracies after complete fabrication shows that 85% blocks are within 40 micron and balance 15% blocks within 50 micron. These blocks are firmly held in position by using number of outer brackets inner radius brackets and end plates.

All these dipole magnets are at present in assembly stage and one dipole magnet has been completely field mapped and has given field uniformity much better than ± 3×10^{-4} over good field region of 9 cm.

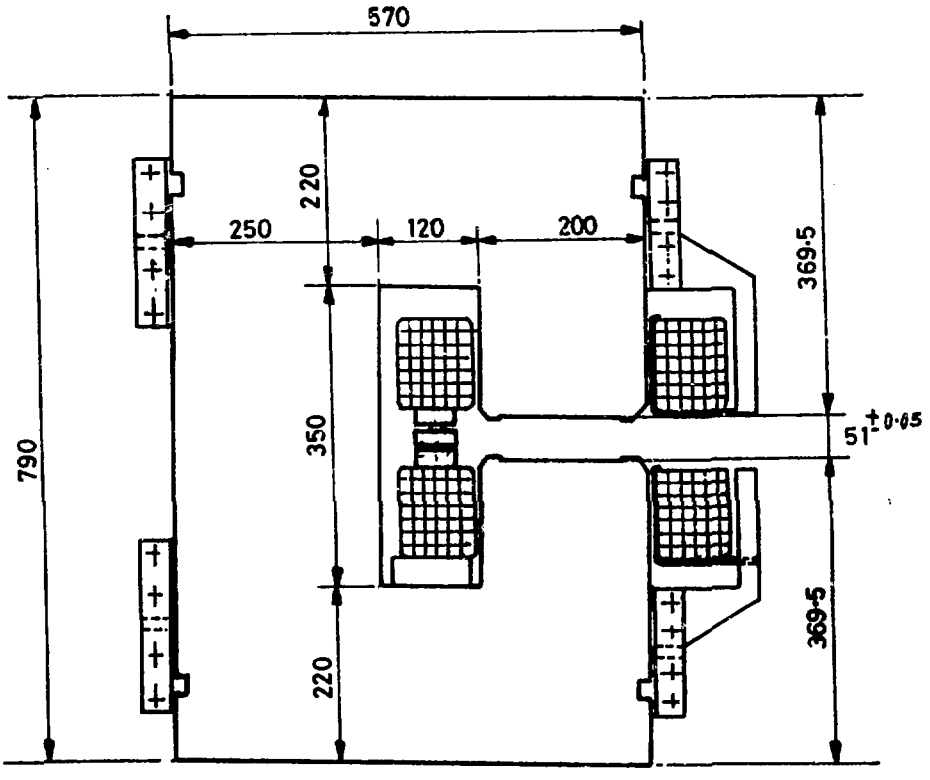

Booster Dipole Magnet

Fig. 1

A COMPACT VERSATILE MAGNETIC BEAM STEERER FOR NSC PELLETRON

G.O. Rodrigues and A. Mandal
Nuclear Science Centre,JNU CAmpus, New Delhi 110 067

A compact and easily mountable beam steerer has been fabricated following the design of Williams et al [1] and tested for guiding the beam from NSC pelletron. It is capable of beam positioning, beam shuttering and homogenous irradiation of targets.

The steering magnet (fig 1) consists of four identical rectangular shaped coils, each with 708 turns using 19SWG wire. Each coil is wound over a steel core (MS-37) of size 150mm * 130mm * 12mm. The four cores are joined together making a square gap of 138mm. Two parallel coils are in series for each of the X and Y directions. They can be powered independently from two separate power supplies. When the vertical coils are powered, the yokes in the horizontal plane act as poles and vice-versa. Each coil is cooled indirectly by water and its temperature is sensed by a thermal sensor which cuts off the coil current when its temperature rises above 80^{o}C. A Dual bipolar power supply of rating 30 V 3 A is required for energising the beam steerer.

The field produced at the centre of the steerer was measured using a Group-3 Hall probe. The variation of the field with current is shown in fig 2. The field obtained at 2 Amperes was 127 $\pm$ 2 Gauss, which agrees with the calculated value of 128.9 Gauss. The excitation curve is linear, and the hysteresis loss is very small. The field homogenity calculated using POISSON code is compared with the measured values in fig 3. Inhomogenity around 2 cm from the centre was found to be 2 %.

The authors wish to thank Prof.A.P.Patro and Prof.G.K.Mehta for their constant inspiration to this work.

REFERENCES:

(1) M.F.Williams,A.F.Zeller and J.A.Nolen,MSU Annual Report,MSU-86-223,p.172.

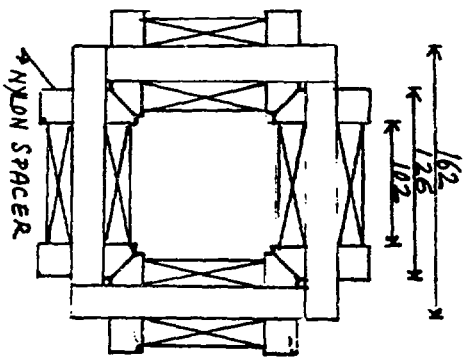

FIG.1 SCHEMATIC DIAGRAM OF BEAM STEERER

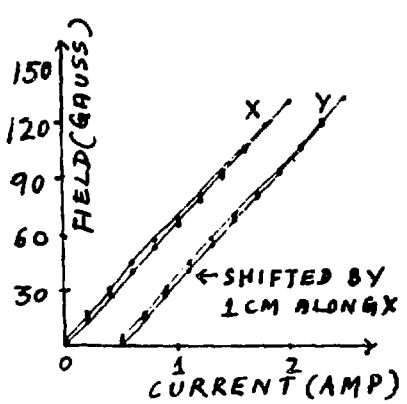

FIG.2 EXCITATION CURVE

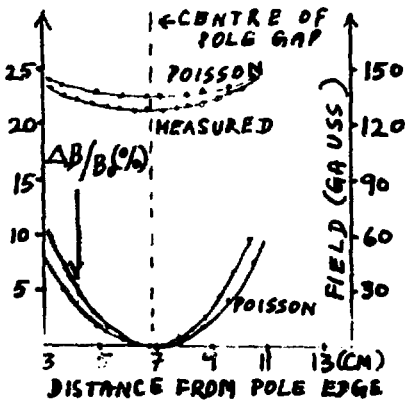

FIG.3 THE FIELD VARIATION (2A) INX-PLANE IS COMPARED WITH POISSON

MOLECULAR BEAMS AND ISOTOPIC BEAMS USING THE NSC 16MV PELLETRON

I.S.Iyer and D.Kanjilal
Nuclear Science Centre, Post Box 10502, New Delhi 110067

In addition to accelerating elemental ions of the natural isotopes of H,He,C,O,Si,P,Ni,I etc., we have developed, accelerated and analysed elements of very low (or negative) electron affinities by injecting molecular negative ions into our Pelletron[1,2].Also, we have attempted to produce and accelerate the rarer isotopes of C,O and Si using natural elements or their compounds. The negative ion source used for all these beams was the EII supplied SNICS II. The results of these attempts are discussed.

MOLECULAR BEAMS

Since only negative ions can be injected into a Tandem Accelerator, it is difficult to accelerate elements having low electron affinities. In such cases, a suitable molecular ion of the desired element is injected. The molecular ion dissociates at the stripper in the high voltage terminal.The stripped positive ions are then further accelerated and analysed to obtain the various charge states of the desired element.

^{14}N: Nitrogen has a negative electron affinity and so the only method of accelerating it in a Tandem Accelerator is by injecting a molecular ion. We injected the CN- ion into our Pelletron and could obtain upto 2pnA of Nitrogen beam of energy 77.7MeV. The currents obtained and beam energies are summarized in table 1.

^{181}Ta: Since we could not obtain appreciable negative ion currents of the tantalum elemental ion, TaSi- ion was injected into the Pelletron. The charge state distribution and beam intensities obtained are listed in table 1.

ISOTOPIC BEAMS FROM NATURAL ELEMENTS

^{13}C: (^{12}C:98.89%; ^{13}C:1.11%): We were very successful with this beam and could deliver beam intensities of upto 4pnA on target of charge state +5. A Gamma ray spectroscopy experiment was performed using this beam by a group from SINP, Calcutta. The beam current requirement for this experiment was less than 0.5pnA and so we could deliver the required intensity without taxing the source much. The currents obtained are summarized in table 2.

^{30}Si:(^{28}Si:92.23%, ^{29}Si:4.67%, ^{30}Si:3.10%):This beam was also obtained without much difficulty and is used often by the Bombay University group for Gamma ray spectroscopy experiments. Substantial amounts of ^{29}Si were also obtained from the source.The beam currents obtained are listed in table 2.

^{18}O:(^{16}O:99.76%, ^{17}O:0.037%, ^{18}O:0.20%): We have not got much success with this beam using natural oxides and are still in the process of developing it.

TABLE 1

BEAM TYPE	MOLECULAR ION INJECTED	BEAM CURRENT ON TARGET (pnA)	CHARGE STATE	BEAM ENERGY (MeV)	SNICS CATHODE MATERIAL
^{14}N	CN^-	2 pnA	+5	77.7 MeV	TiN + C
		0.6	+6	91.7	"
		0.5	+4	63.7	"
^{181}Ta	Ta Si^-	10 pnA	+8	144.5	Ta Si + Al
		4	+9	160.8	"
		1.3	+10	177.1	"
		0.5	+11	93.4	"

TABLE 2

BEAM TYPE	NEGATIVE ION BEAM INTENSITY (nA)	BEAM CURRENT ON TARGET (pnA)	CHARGE STATE	BEAM ENERGY (MeV)	SNICS CATHODE MATERIAL
^{13}C	110 nA	4 pnA	+5	77 MeV	Graphite Powder
		1.6	+6	90	"
		1.3	+4	64	"
^{30}Si	95 nA	3.5 pnA	+7	89 MeV	Silicon Crystals
		3	+8	100	"
		1	+9	111	"
		0.8	+6	78	"

References:
1.G.K.Mehta and A.P.Patro, NIM A268(1988)334
2.D.Kanjilal, SNEAP'90 (1990)33

MULTIELEMENTAL ANALYSIS OF PANTNAGAR SOIL BY FAST NEUTRON ACTIVATION ANALYSIS

G.C. JOSHI and H.M. AGARWAL*
Department of Physics
G.B. Pant University, PANTNAGAR 263 145

Multielemental analysis of soil samples has been intense during the last 2-3 decades, highlighted by increasing demands for fertilizer, pesticides and environmental pollution.

The concentration of various elements in the soil is largely dependent on that of the rocks from which the soil parent material was derived; the human activities and climate, however, may effect the elemental concentrations in the soil. Moreover, soil is the ultimate and the most important sink of trace elements in the environment. Some of the trace elements are required for the growth of plants while some are toxic to the plant, animal and human being. Therefore, time to time multielemental analysis of soil is required.

Analytical methods of high precision, accuracy and sensitivity are required for the determination of low levels of several elements in soil samples. FNAA (Fast Neutron Activation Analysis) technique is particularly suitable for this purpose. The advantages of FNAA are well known.

For the first time, soil samples from five fields of major crops (Soya, Maize, Paddy, Urd and Arhar) located in Crop Research Centre, Pantnagar were collected. The samples were irradiated at the KORONA generator of GKSS Research Centre, West Germany. KORONA/1/ consists of high intensity, concentric, sealed neutron tube with a compact arrangement of an annular ion source, a cylindrical target and the irradiated terminal of a fast sample transport device. Cyclic activation and measurement are possible with a minimum

cycle period of 5 sec. The activated samples were analysed using the detection system described in ref /2/

The average concentration of major elements in five fields is not much different except in the case of calcium (Ca) which shows deficiency in soil of soya, maize, urd and arhar fields. No contamination of As ($<$ 15 ppm), Cd ($<$1 ppm), Pb ($<$50 ppm), Hg ($<$1 ppm) and radioactive isotopes Th ($<$8 ppm) and U ($<$ 3ppm) has been found at an alarming level. For the first time, this kind of soil analysis has been performed and thus it provides the base data of elemental concentrations for future multielemental analysis of soil samples of Pantnagar crop fields.

High flux multielemental FNAA is unquestionably a reliable and accurate method of analysis. Further application of this technique for multielemental analysis of soil of Pantnagar crop fields will depend on economic factor and the availability of intense 14 MeV neutron source.

References

/1/ H.U. Fanger et al., J. Radioanal. Chem. 61, (1981) 147

/2/ H.M. Agarwal, DAE Symposium on Nuclear Physics 33B (1990) 151.

* It is a great pleasure for us to thank Dr. R. Pepelnik (GKSS Research Centre, West Germany) for his keen interest throughout this work.

HARDENING OF CHROMIUM FILMS BY HIGH ENERGY NICKEL ION IRRADIATION

Amitabh Jain and S Loganathan, IIT Delhi, New Delhi 110016, and L Senapati, Jaipal, D Kanjilal and G K Mehta, NSC, Post Box 10502, New Delhi 110067

An energetic ion incident on a metal surface slows down through electronic energy loss and nuclear energy loss mechanisms. Electronic excitation dominates at high energies and has been thought only to result in heating (1). However an understanding of the relaxation process is too inadequate to rule out the possibility of phenomena that might result in microstructural changes.

We carried out 75 MeV nickel ion irradiation at a dose of $10^{15} cm^{-2}$ (using the 15UD Pelletron at the Nuclear Science Centre) into 1 micron thick chromium films deposited on stainless steel substrates held at $150^{0}C$ and measured Knoop microhardness inorder to obtain an indication of any microstructural change. This irradiation is calculated to result in an electronic energy loss of 1.6 keV/angstrom in the film (fig. 1) and negligible nuclear energy loss. The samples registered a hardness increase of 100%, following irradiation, for small indentaion depths that are confined to the film (fig. 2). There are no hardness changes felt when the indentation depth is several times the film thickness and approximately equal to the ion range or the position of the maximum in the nuclear energy loss. We therefore clearly see an effect of the electronic energy loss.

The hardness of (unirradiated) films is limited by the loose columnar structure characteristic of the low substrate temperature used during film deposition (2,3). A possible strengthening mechanism is the fusion of these grains.

We acknowledge the help extended by Dr S K Datta and others in the Pelletron group.

References:

1. S A Durrani and R K Bull, Solid State Nuclear Track Detection, Pergamon, 1987.
2. K Reichelt and X Jiang, Vacuum, 42 (1991) 171.
3. G Thurner and R Abermann, Thin Solid Films, 192 (1990) 277

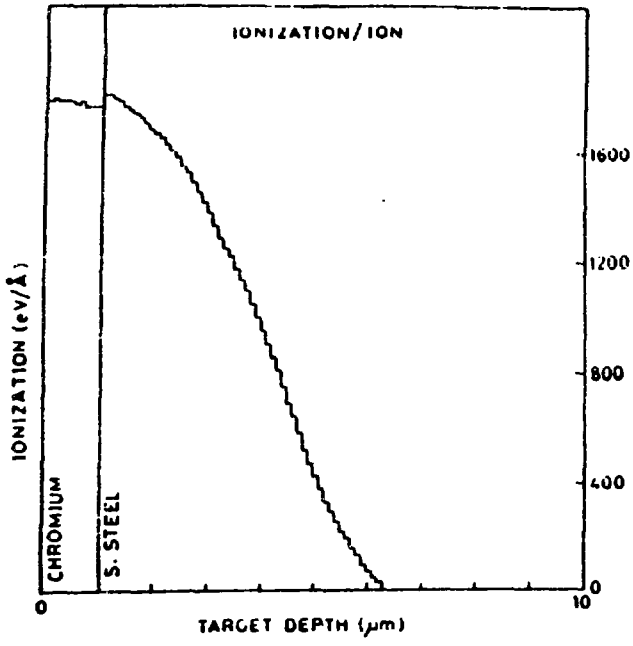

Fig.1. Electonic energy loss as a function of depth for 75 MeV Ni ions incident on a 1 μm chromium film on stainless steel.

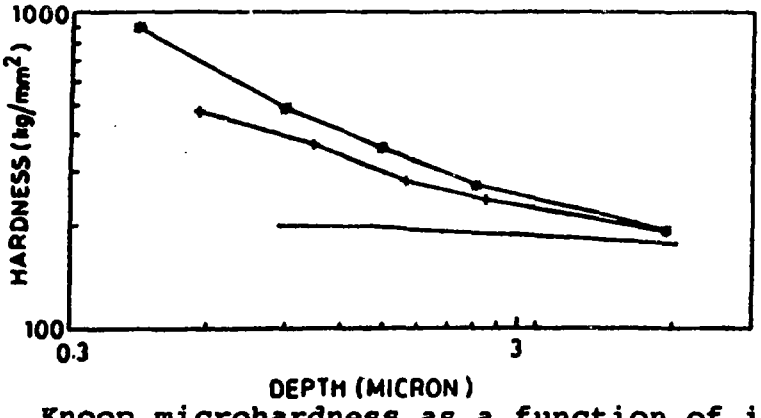

Fig.2. Knoop microhardness as a function of indentation depth. The curves in ascending order pertain to an uncoated stainless steel substrate, a substrate with chromium film of thickness 1 μm and the film-substrate system after irradiation with 75 MeV Ni ions to a dose of $10^{15}cm^{-2}$.

SURFACE BEHAVIOUR OF N_2^+ ION IMPLANTED AUSTENITIC 302 AND 310 STAINLESS STEELS

S. Aggarwal, A.K. Goel, R.K. Mohindra, P.K. Ghosh*, M.C. Bhatnagar+ and Ami Chand+, Physics Department, Kurukshetra University, Kurukshetra-132 119, *WRL, Department of Mech. & Indus. Engg., University of Roorkee, Roorkee-247664, +I.I.T., New Delhi-110016.

The investigations of high dose N_2^+ ion implantation are presented here on near surface hardness of austenitic-302 and -310 stainless steels (SS), having different surface conditions such as strain induced (produced by mechanical polishing) and extra strain free (due to chemical etching of mechanically polished samples). Samples were taken of 302 & 310 SS having compositions (Cr-18.48, Ni-8.32, C-0.15, Mn-1.86, Si-0.59, Fe-base) and (Cr-25.78, Ni-18.2, C-0.08, Mn-1.63, Si-1.12, Fe-base) respectively. The specimens were implanted with N_2^+ ions of 130 keV at a dose of 2.5×10^{17} ions/cm^2 under a vacuum of 2×10^{-6} Torr. The temperature during implantation was 300°C and was measured using a thermocouple. Surface microhardening was studied using Knoop microhardness tester for an indentation time of 10 sec. The compound formation studies in the implanted layer were carried out with X-ray photoelectron spectroscopy (XPS) combined with Ar^+ sputtering.

The depth of implanted N_2^+ ions at the same energy & dose in stainless steel is of the order of 400 nm /1/. The XPS spectra was recorded for N(1s), Ni(2p), Fe(2p) and Cr(2p) in case of both the stainless steels at a depth of 80 nm. Formation of iron nitrides and cromium nitrides along with iron oxide & Nickel oxide in case of N_2^+ implanted 302 & 310 SS have been distinctly observed. Fig. shows the relative KHN measurements at different loads resulting into different depths of penetration (The five different points on each

curve correspond to 2,5,10,25 & 50 gf respectively). From curves a & b in figure we observe that N_2^+ implantation increases microhardness at 2 gf by 950 KHN & by 830 KHN in case of mechanically polished 310 SS & 302 SS samples respectively. The corresponding increase at the same load for etched samples is by 780 KHN and 660 KHN (curves c and d) respectively. As the load increases the probe depth of the indenter exceeds the depth of implanted layer, resulting in large contribution of the substrate to apparent hardness. As evident from figure the increase in KHN is more in case of mechanically polished and etched 310 SS implanted samples than 302 SS (under same condition) which may be due to the fact that microhardness will increase with increase in Cr content in the materials /2/. Moreover additional strengthening mechanisms can be associated with the formation of iron nitride /1,3/ and cromium nitride /1,3/ precipitates in the implanted layers in both materials as observed by XPS.

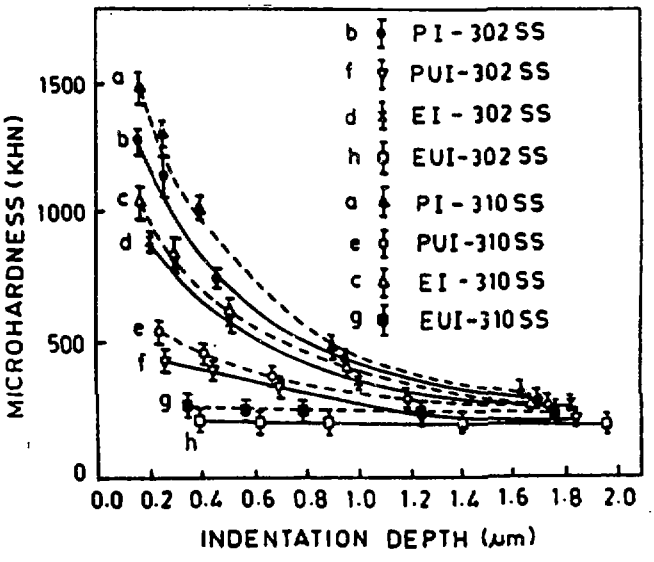

References

1. A.K. Goel et al., Ind. J. Phys., 64A(1990)444.
2. J. Sasaki et al., Thin Solid Films, 201(1991) 39.
3. W.M. Bone et al., J. Vac. Sci. Tech. A2(1984) 788.

UHV for Synchrotron Radiation Source - Indus-1

M.G. Karmarkar & S.S. Ramamurthi
Centre for Advanced Technology (CAT)
Indore - 452013, INDIA

ABSTRACT

A 450 MeV Synchrotron Radiation Source Indus-1, under construction will have a 20 MeV microtron pre-injector, 450/700 MeV Booster Synchrotron and a 450 MeV electron Storage Ring. Ultra High Vacuum (UHV) system is designed to maintain pressure of $< 1 \times 10^{-9}$ mbar in beam envelope. The beam envelope is an all metal bakable system fabricated out of stainless steel material. Fabricated components are thoroughly preconditioned to get clean (hydrocarbon free) vacuum Turbomolecular pumps are used for initial pumping (from atmospheric pressure down to 10^{-5} mbar) and bakeout, whereas triode sputter ion pump (SIP) and titanium Sublimation Pumps (TiSP) are used for maintaining UHV. Distributed ion pumps are also installed in bending magnet vacuum chambers, where they will pump gases produced by interaction of synchrotron radiation with chamber walls. To minimise distortion of magnetic field due to eddy current set up in booster dipole chamber wall during field rapping, specially designed thin wall SS corrugated vacuum chambers are used. The microtron uses 500 l/s TMP and cryopump to take care of desorption of water vapour from microtron magnet prefaces, which forms a part of vacuum chamber. Details of UHV system of Indus-1 are presented.

MAGNETIC FIELD ANALYSIS FOR SYNCHROTRON MAGNETS

S.P. Bhaskar, R.K. Mishra, R.S. Shinde, Sivakotaiah
Y.R.C. Murthi, V. Tomar
Centre for Advanced Technology (CAT)
Indore - 452013, INDIA

ABSTRACT

Results of the field mapping of the dipole magnets 700 MeV Booster Synchrotron in the Synchrotron Radiation Facility at CAT are presented in this paper. Based on some preliminary measurements of these magnets, some changes were made in the pole tip profile of the magnet and entry exit blocks of the magnet. Results of the magnetic field measurement after these changes will also be discussed. Multipole analysis of the integrated field pattern of these magnets will be discussed in this paper.

ALPHA INDUCED K-SHELL X-RAY PRODUCTION CROSS-SECTIONS FOR SOME LOW Z ELEMENTS ($8 \leq Z \leq 31$)

Anita Rani and N. Nath
Physics Department, Kurukshetra University,
Kurukshetra-132 119.

The K X-ray production cross-sections (relative to Ti) on thin targets in the range $8 \leq Z \leq 31$ have been measured at the mean alpha energies of 2.8 and 4.2 MeV. A windowless, retractable Kevex Si(Li) detector system having energy resolution of 146 eV at 6.4 keV was used for the detection of the characteristic K X-rays. The measurements were performed using thin film samples made out of respective elements. An annular Pu^{238} alpha-radioisotope with appropriate thin nickle absorbing covers was used as the excitor. A clean high vacuum chamber maintained at a pressure of $\sim 10^{-7}$ torr contained both excitor source and sample. Cross-sections were evaluated using the ECPSSR theory. Measured and calculated X-ray fluorescence cross-sections agreed well within reasonable limit of experimental errors.

AUTHOR INDEX

Name	Page No.
Agarwal, Neelam	85
Agarwal, H.M	233,493
Agarwal, Y.K.	3,381
Aggarwal, S.	497
Aggrawal, Meenakshi	107,109
Agnihotry, S.A.	477
Agrawal, B.K.	19,33,105,243
Agrawal, Manoranjan	437,439,441
Ahamad, M.S.	341,377
Ahmad, S.	311
Ahmad, Tauseef	365
Ahmed, Zafar	179
Ahuja, M.N.	389
Akbar, A. Mohamed	57,59
Akhaury, Praveen	319
Alam, Jane	323,325,351,353,461,467
Ambekar, V.S.	127,225,227,431
Anand, R.P.	135,231
Ansari, A.	19,105,243,315
Ansari, M.A.	LC3
Ansari, A.R.	293
Antony, J.	385
Anupam	395
Anwar, Sk. Hossain	361
Arora, Renu	337
Arulmozhi, G.	81
Arunachalam, N.	57,59
Arvindakshan, P.S.	391
Avasthi, D.K.	405,407,445
Badiger, N.M.	405
Bairi, B.R.	391
Bandyopadhyay, A.	413
Bandyopadhyay, Debadesh	321
Banerjee, Dipak	361,363
Banerjee, A.	379
Banerjee, V.	379
Banerjee, P.	5,271
Banerjee, S.R.	143
Banik, D.	13
Bansal, S.L.	253
Basu, Madhumita	361
Basu, Somapriya	13
Basu, S.K.	55
Batra, J.S.	83

Baur, G. 271
Behere, Anita 391
Bera, P.K. 245
Betigeri, M.G. 129,139,159,381
Bhagwat, Swati 301
Bhalla, K.B. 335
Bhalerao, P.J. 383
Bhandari, R.K. 443,467
Bharti, A. 93
Bhardwaj, H.D. 203
Bhardwaj, M.K. 205
Bhasin, Anju 339,375
Bhattacharjee, Anuradha 361
Bhatia, V.S. 373
Bhattacharya, R. 77
Bhattacharya, B.B. 465
Bhatnagar, M.C. 497
Bhattacharya, S. 151,199,379
Bhatnagar, P.K. 171
Bhattacharya, C. 199
Bhavalkar, R.H. 477
Bhowmik, R.K. 9,141,209,393,415,
417,419,463
Biswas, Debabrata 117
Biswas, D.C. 127,221,225,227,431
Biswas, Biswanath 333,357,361
Bose, Niyanta 361
Bose, D.K. 443,467
Burte, P.P. 133
Chakrabarty, Somenath 321,323,325,351,353,35
Chakrabarty, D.R. 125
Chakravarty, N. 201
Chakrabarti, A. 379
Chand, B. 9
Chandra, S. 477
Chand, Ami 497
Charagi, S.K. 159,161
Chatterjee, A. 135,163,221,223
Chattopadhyay, S. 3,379
Chattopadhyay, S. 55
Chatterjee, J.M. 13
Chattopadhyay, R.K. 5,13
Chattopadhyay, Rakhi 113
Chaudhuri, A.K. 29,117
Chaubey, A.K. 205
Chikara, B.K. 107,109
Chintalapudi, S.N. 73,143
Chopra, S. 445,447

Choudhury, R.K. 127,135,227,231,431
Chowdhury, S.Karim 303
Clark, D.L. 425
Coffin, J.P. 151
Dange, S.P. 215,217
Darshan, V.P. 145
Das, Susobhan 361
Das, A. 279
Das, A. 379
Das, J.J. 403
Das, S.K. 133,219
Das, S.P. 177
Das, C. 259
Das, B.P. 301
Dasgupta, B. 443
Dasgupta, S.S. 211
Datar, V.M. 125,383
Datta, S.K. 445
Datta, T. 215,217
De, Atanu 361
De, S.K. 413
Deb, Argha 333,357,359,361,363
Debbarma, Manidipa 361
Desai, D.G. 389
Devanathan, V. 347,369
Devaprathap 435
Devare, H.G. 9
Devi, Y.D. 15,45,47
Devi, Usha A.R. 239
Dey, C.C. 77
Dhiman, S.K. 103
Dinesh, B.V. 127,225,227,431
Dutta, Anuradha 361
Dutta, S.B. 425
Dutta, D. 147
Dutta, S. 177
Eqbal, Md. 409
Eswaran, M.A. 125,427
Eswaraiah, K. 169,171
Fernandez, C.V. 139,159
Gambhir, Y.K. 27,147
Gangadharan, S. 423
Garg, U. 127
Gargari, S. 407
Garg, S.B. 247,249
Garud, A.N. 449
Gaur, Rajesh 263,287,343,345
Gautam, A.K. 263,287,343,345

Ghodgaonkar, M.D. 391
Ghosh, P.K. 497
Ghosh, Dipak 331,333,357,359,
361,363
Ghosh, Premomoy 333,359,361,363
Ghosh, Anit 361
Ghosh, Alokananda 361
Ghosh, Shibaprasad 361
Ghosh, Sanjay.K 281
Ghosh, B. 285
Ghugre, S. 141,419
Godiyal, Ravi Datt 169,171
Goel, S.K. 481
Goel, A.K. 497
Goel, Alpana 17,101
Goswamy, A. 55,133,219
Goswami, Ranjana 5
Goswamy, J. 9
Goyal, D.K. 393,419
Guhathakurta, Tarit 361
Gupta, D.K. 61,63,437,439
Gupta, J.B. 11,51,53
Gupta, K.K. 61,63
Gupta, Raj K. 83
Gupta, Rakesh Kumar 93
Gupta, S.K. 139,159,161
Haider, W. 255
Halder, Debasish 361
Halder, Supriya 361
Hasan, R. 341,377
Hippler, R. 479
Hussain, K.A. 487
Irfan, M. 365
Iyer, R.H. 131,213
Iyer, I.S. 491
Ismail, M. 207
Jacob Chako 403
Jain, Arun K. 153,209,235
Jain, H.M. 251
Jain, B.K. 283,307,309
Jain, H.C. 3,55,381,383
Jain, Arvind 411
Jain, Amitabh 495
Jain, Kiran 17,101
Jain, A.K. 17,101
Jaipal 407,495
Jana, A.K. 157
Janhavi, G. 155,261,327

Jena, S. 177
Jha, Vandana 445
Jhingan, M.L. 3,139,381
John, B.V. 163,221,229,387
Jojo, P.J. 399
Joseph, R.R. 371
Joshi, R. 445
Joshi, G.C. 493
Jyrwa,B.M. 189
Kabiraj, D. 405
Kailas, S. 149,163,185,221,
223,229,423
Kalpana Sankar 81
Kalsi, P.C. 131,213
Kanjilal, D. 445,463,477,491,495,447
Kannaiyan, J. 463
Kapoor, S.S. 135,163,221,223,229,231
Kar, K. 13
Karandikar, S.C. 389
Karmarkar, M.G. 499
Karnik, Alka 221,223
Karthiyayini, S. 369
Kataria, D. 177,385
Kataria, D.O. 403,429,481
Kataria, S.K. 163
Kataria, S.K. 181,183,229
Kaur, Arvinder 95
Kaushal, R.S. 319
Kavathekar, A.K. 53
Kelkar, N.G. 283,309
Kerekatte, S.S. 221
Keswani, K.S. 389
Khadkikar, S.B. 277,295,297,299,317
Khan, M.Saleem 293
Khan, A.R. 311
Khosa, S.K. 89,91,93
Khushnood, H. 293
Kota, V.K.B. 15,23,45,47,49
Krishan, K. 151,199
Krishnamurthy, G. 453
Kuehl, T.U. 425
Kuldeep 159
Kulkarni, R.J. 241
Kumar, V. 335
Kumar, S. 395
Kumar, Ashavani 399
Kumar, Bishambar 403
Kumar, Ajith B.P. 415,463

Kumar, Ashok 169,171,173,175
Kumar, Sunita 171
Kumar, K. 153,229
Kumar, V. 335
Kumar, Sanjiv 423
Kumar, Suresh 125,427
Kurup, M.B. 137,451,453,475
Lahiri, Madhumita 357,361
Lal, N. 395
Loganathan, S. 495
Lokanathan, S. 335
Luktuke, R.D. 449
Lagu, A.V. 289
Madhavan, N. 177,403,481
Maharana, J.P. 27
Majumdar, D. 23,49
Majumdar, Ramen 35
Mallik, C. 465,467
Mallesh, K.S. 273
Mandal, A. 445,489
Mandal, S. 211
Manohar, S.B. 133,219
Marballi, K.R. 401
Mateen, S.A. 449,469
Mathur, Tripti 75,97
Mattu, P.K. 89,91
Meenakumari, N. 329,347,349
Mehta, G.K. 477,495
Mehta, D. 9
Mhaskar, S.P. 500
Mirgule, E.T. 125,427
Mishra, A.P. 453
Mishra, R.K. 500
Mishra, H. 265
Mishra, M. 279
Mishra, Subodha 323
Misra, R.C. 169,173,175
Misra, S.P. 31,265
Mitra, R.B. 443
Mohanty, J.N. 471
Mohanty, A.K. 149,163,181,183,229
Mohindra, R.K. 253,497
Mukhopadhyaya, N.K. 465
Mukhopadhyayaya, Amitava 361
Mukherjee, Hiten 361
Mukhopadhyay, T. 379
Mukhopadhyay, P.K. 401
Mukherjee, Shanker 75,97

Mukherjee, I. 129
Mukherjee, P. 129
Muralithar, S. 141,417
Murthy, Kavitha 449
Murthy, S.R.S. 431
Murti, Sivakotaiah Y.R.C. 500
Murty, G.S.K. 73
Murugesan, K.Sakthi 155,261,327,367
Mustafa, M.G. 315
Mythili, S. 129,209
Nadkarni, D.M. 135,223,225,227,231
Nagaraj, S. 381
Naha, Sadhan 361
Naik, H. 215,217
Naithani, S. 393,415,417
Nanal, Vandana 137,451
Nandi, Tapan 453
Naqvi, A.H. 365
Narayanan, M.M. 445,447
Nair, A.G.C. 219
Narsale, A.M. 141
Nath, N. 501
Navin, A. 221
Nayak, B.K. 127,135,227
Neelofer, Nasra 313
Nijasure, A. 163,221,229
Nimje, V.T. 449
Ojha, I.D. 371
Ostrowski, A. 167
Padmini, M.D. 193
Pai, V.N. 241
Pal, J. 157
Pal, Santanu 29,117
Pal, U.K. 125
Pal, S.K. 413
Pal, P.B. 437,439,441
Pal, G. 467
Palsania, H.S. 335
Panda, K.C. 195,197,269
Panda, P.K. 31,265
Pandey, A.K. 131,213
Pande, M.V. 449
Pandit, V.S. 461
Pandya, S.P. 1
Pant, L.M. 127,135,227,431
Pardhasaradhi, S.K. 13,379,409
Parida, B.K. 265
Parikh, J.C. 87,317

Patel, S.B.	141
Patel, B.J.	433
Patra, T.	195,197
Patra, S.K.	25,41,43
Phatak, S.C.	275
Pillay, R.G.	9,455
Polley, A.	379
Prabhu, S.S.	487
Praharaj, C.R.	7,25,39,41,43
Prasad, R.	63,203
Prasad, N.V.S. Vara	73
Prasad, K.Hema	389
Prasad, Rajendra	167,399
Prasad, K.G.	137,451,453,455,457,475
Pratibha	267
Premanand, R.	21,65,67,69,71,187
Pujari, P.K.	215
Puntambekar, A.M.	487
Purakait Krishnadas	361
Puttaswamy, N.G.	145,405,429
Radhakrishna, M.C.	429
Raghwa, A.S.	103
Ragoowansi, N.L.	125
Raha, Sibaji	325,353,355,
Raheja, U.T.	383
Raina, P.K.	103
Raj, D.Caleb Chanthi	21,65,67,69,71,187
Raj, S.I.A.Philomin	115
Raja, K.	155,261,327
Rajasekaran, M.	21,65,67,69,71 187,329,347,349
Rajasekaran, T.R.	79
Raju, V.S.	423
Ramachandran, G.	237,239,273
Ramamurthi, S.S.	483,485,487,499
Ramamurthi, K.	81
Ramamurthy, V.S.	163,177,257
Raman, J.V.	423
Ramaswamy, C.R.	79,145
Rami, F.	151
Rani, Anita	501
Rao, Ramachander J.	435
Rao, Panduranga M.	435
Rao, P.M.R.	453
Rao, Raja M.	405,429
Rao, Sudha A.	239,273
Rao, M.V.S.Chandrasekhar	73
Rao, V.Raghunatha	143

Rashid, M.H. 467
Rath, A.K. 7,39
Rattan, S. 201
Raviprasad, G.V. 177
Rawat, D.N. 409
Reddy, Ramana S.V.S. 435
Reddy, A.V.R. 133,219
Rizvi, I.A. 205
Rodrigues, G. 141,417,489
Roy, A. 177,209,429
Roy, Jaya 331,357,359.361,363
Roy, Rabin 361
Roy, B.J. 129,139
Roychoudhury, Jayanta 333,357,461
Sabharwal, S.C. 389
Sadawarte, S.V. 449
Saha, Asok 37
Saha, S.K. 55
Saha, S. 381
Sahu, B. 189
Sahu, R. 1,31,259
Sahu, Sarira 275,291
Saliem, S.M. 255
Salvi, V.P. 141
Samant, M.S. 135,231
Samantaray, C.B. 471
Sangeeta 389
Sankaracharyulu, M.G.V. 203
Santra, A.B. 307
Sarangi, P. 191
Sarangi, Subrata 87
Saraswati, P 453
Sarita 437,441
Sarkar, Sasabindu 303
Sarkar, Sharmila 331,361
Sarma, A. 143
Sarma, P.R. 459,461
Sastry, D.L. 73
Sathyavathiamma, M.P. 79,145
Satpathy, L. 177,191,257,279
Satpathy, M. 177,279
Satya Prakash 133,219
Satyanarayana, G. 73
Saxena, Alok 135,163,223,225,229
Sekhar, Raja N. 435
Sen, K.S. 119,121,123
Sen, P. 129
Sen, Sanjib 357,361

Sen, S. 177
Senapati, L. 445,477,495
Sengupta, Ranjan 331,361
Seth, Madhup 169,171
Sethi, B. 5,129
Sethi, R.C. 449
Shafi, M. 311
Shanker, R. 479,481
Shanmugam, G. 81,115,193
Sharan, S.R. 111
Sharma, R.C. 131
Sharma, Ashok Kumar 173,175
Sharma, A. 9
Sharma, R.P. 13,379
Sharma, S.D. 95
Sharma, Arvind 95
Sharma, V.K. 107,109,267,305
Sharma, S. 119,121,123
Sharma, R.C. 213
Sharma, S.K. 395
Sharma, S.L. 397
Sharma, Rajpal 403
Shastry, C.S. 189
Sheikh, J.A. 3,27,39
Shinde, R.S. 500
Shiromani, A.K. 263,287,343,345
Shoeb, Mohammad 313
Shyam, R. 271
Siddiqui, K.A. 341,377
Singh, R. 143
Singh, Yash Pal 165
Singh, B.P. 203
Singh, N. 9
Singh, A.J. 103
Singh, P. 149,163,221,229,381
Singh, B. 335
Singh, B.K. 371
Singh, R.P. 417
Singh, N.L. 433
Singh, M.J. 481
Singh, G. 485
Sinha, A. 177
Sinha, B.K. 77
Sinha, Bikash 323,325,351,353,355
Sinha, A.K. 403,429,481
Sinhg, Pragya 9
Sivakumar, P. 67
Soni, M.L. 99

Soni, H.C. 483
Sprouse, G.D. 425
Sreeramulu, K. 487
Srivastava, B.B. 85,169
Srivastava, Dinesh K. 323,325,351,353
Subramanian, P.R. 155,261,327,367
Subramaniam, E.T. 385,403
Sud, S.P. 61,63,119,121,123
Sudarshan, M. 143
Sugathan, P. 403
Suryanarayan, S.V. 127,135,181,227
Susan, P. 189
Syam, Debapriya 321
Taki, G.S. 443,467
Talukdar, B. 157,245
Tandon, P.N. 421,451,455,457,473,475
Tariq, M. 311
Tayyab 311
Tomar, B.S. 55,133,219
Tomar, V. 500
Trehan, P.N. 9
Tribedi, L.C. 421,455,457,473,475
Tripathi, A. 405
Tripathi, R.K. 259
Tripathi, A. 445
Tufail, A. 311
Tuli, S.K. 371
Tyagi, R.K. 63
Uma Maheswari, V.S. 257
Varshney, A.K. 61,63
Varshney, V.P. 61,437,439,441
Vaze, M.Y. 383
Veeraraghavan, S. 57,59
Venkataramanan, S. 405,417
Venkatappaiah, A. 435
Verma, S.P. 111
Verma, S.R. 169
Vidya, M.S. 237,273
Vijayakumar, K.B. 277,295,297,299
Voit, H. 167
Wagner, P. 151
Yadav, R.K. 177
Zachrias, J. 407
Zafar, M. 311